THE MECHANICS OF ULTRASONIC STRIP DRAWING

BY

Keith Andrew McQueen, M.Sc.

Submitted in part fulfilment of the requirements

for the Degree of Doctor of Philosophy

The University of Aston in Birmingham

June 1979

THE MECHANICS OF ULTRASONIC STRIP DRAWING

KEITH ANDREW McQUEEN M.Sc

A thesis submitted to the University of Aston in Birmingham for the Degree of Doctor of Philosophy.

July 1979

SUMMARY

In this thesis the application of power ultrasonics to metal processing, along with the mechanisms operating during such processes, is reviewed. The various techniques used to analyse metal forming processes are also reviewed.

A detailed description of the apparatus and instrumentation is given with the experimental procedure.

An upper-bound technique is used to analyse the combined strip-drawing and swaging process. The analysis shows that modified frictional conditions are a feature of this process.

It is shown that the drawing process, when augmented by swaging, reduces the draw force and that this reduction increases with decreasing draw speed. The swaging effect becomes more pronounced with an increase in die-semi-angle and decreases with an increase in die land length. By taking advantage in the reduction in draw force, reductions in area of 80% were achieved.

KEY WORDS: PLASTICITY, ULTRASONICS, STRIP-DRAWING, POWER UPPER-BOUND

NOMENCLATURE

μ = coefficient of Coulomb friction

α = die semi-angle

σ = stress

σ_1, σ_f = draw stress

σ_2 = back tension

σ_o = uni-axial flow stress

r = fractional reduction of area

h = strip thickness

$\dot{\Sigma}$ = strain rate

τ = shear stress

ΔV = velocity difference across a velocity discontinuity

m = friction factor

t_o = initial strip thickness

t_f = final strip thickness

V_o = initial velocity

V_f = final velocity

V_c = mean draw speed

$\dot{\xi}$ = instantaneous die velocity

$\dot{\xi}_p$ = instantaneous plug velocity

ω = angular frequency rad/sec

ϕ = die-to-plug phase angle

b = strip width

Γ = shear surface

CONTENTS

CHAPTER 1. INTRODUCTION

In a conventional strip, wire or tube drawing operation the drawn material, under ideal steady state conditions, is subject to a steady state of stress. This stress, within the capacity of the draw bench, is dependent upon die profile; frictional conditions; reduction of area; back tension; yield stress at inlet and the work hardening characteristic of the metal being drawn. The limiting reduction of area is reached when the draw stress causes tensile instability in the drawn stock.

Under conditions of homogeneous deformation, in the absence of friction or work-hardening, the limiting reduction of area is approximately 63%[1]. Work carried out under experimental conditions has led to reductions of area, in mild steel, of almost 50%[2]. This work was carried out at low draw speeds using a soap lubricant deposited on a grit blasted surface. The close attention which must be paid to lubrication, and the inherent instability of the process at these high levels of reduction, lead to lower reductions of area being generally used in industry; a typical compromise between the possible and the economically viable, for fixed plug tube drawing, is 30-35%.

The limiting reduction of area can be maximised by optimising the process with respect to die angle and reduction of area[7], [14], thus minimising the energy expended on die wall friction and redundant deformation.

Whilst some improvements in lubrication have led to increases in reduction of area under industrial conditions, the main increases in productivity have been achieved by using higher draw speeds, and by developing machines which are capable of processing larger coils of wire[3]. The use of high draw speeds imply the use of bull block machines and the use of large coils imply the production of stock on a fairly large scale. These innovations reduce the time spent, per unit length of finished product, on any element of a draw schedule, and/or

increase the ratio of productive to non-productive time in a production route. Such innovations are inappropriate for, say, batch production of tube or rod on chain benches and cup ironing in the absence of high efficiency transfer machines. Under these conditions an industrially usable increase in reduction of area is the only practicable means of improving productivity since, in this manner, the number of elements in a draw schedule can be significantly reduced.

It is clear that a significant increase in the reduction of area can be achieved only by a fundamental modification to the drawing process. Such a modification must be compatible with the relatively low speeds, and short cycle times, associated with drawing on chain benches or ironing on hydraulic presses. Augmentation of the drawing process was attempted as long ago as 1930 when, according to Biddell and Sansome[29], Nell filed a patent for a hydraulically operated 'percussive machine' which swaged stock through a longitudinally excited die. They also report that Simmonds, in 1940, filed a patent for a strip-drawing machine, that used a pair of dies which were reciprocated laterally, in antiphase, by mechanical means. Both of these processes were low frequency applications of vibratory metal-working; the earliest high-frequency applications, according to Biddell and Sansome[29], being that of Vang, in 1942, who used a resonant system of tooling which was found to give an increased depth of draw in the production of tubular components.

The real spur to the development of vibratory metal-working processes came, however, in 1955, when Blaha and Langenecker[6] published the results of work carried out on the effect of high frequency vibrations on the yield stress of zinc monocrystals during a tensile test, which indicated a reduction in yield stress when the vibrations were applied. Similar reductions in front tension were observed when vibrations were applied, in various forms, to the wire and tube drawing

processes, though it soon became evident that at least part of this reduction was due to the instrumentation recording the mean value of a cyclic stress. That is, the peak stress and therefore the true load reduction were unknown. Measurement of the cyclic stress in the drawn stock showed that a real load reduction was occurring under certain conditions, and that it should be possible, therefore, with the use of ultrasonically activated tools to increase the reduction of area. Continuing development has resulted in ultrasonically activated drawing dies (radial and axial mode), blank holders for the deep drawing of cups and axially vibrated plugs for tube drawing, as well as ultrasonically activated rolls; the value of the resulting increases in reduction of area is exemplified[4] by a ten pass, six anneal schedule which was reduced to a six pass, four anneal schedule for the production of brass tubes by drawing and ironing. This was achieved by replacing the ironing dies with an ultrasonically activated radial mode die set, that significantly increased the reduction of area per pass.

The addition of ultrasonic apparatus to conventional metal forming machine tools may critically affect their operation. For instance, radial mode dies and their supports are deeper than a conventional die and therefore reduce the daylight when mounted in a conventional press[18]. The addition of similar apparatus to bull blocks has little effect on the operation of the machine[17], though the effect on chain or hydraulic benches, because of the limited draw length, requires further consideration.

Conventional drawing on chain or hydraulic benches, under industrial conditions, as already stated, is carried out at reductions of area of approximately 30% to 35% during the intermediate stages of the draw schedule. The maximum increase in stock length is therefore between 43% and 54%. Considering, specifically, fixed plug tube drawing on a chain bench, and assuming that the plug bar to chain length ratio is related to the maximum elongation of the tube, then any increase in reduction of

area reduces the maximum length of tube that could be loaded onto the plug bar.

If the initial passes in a draw schedule were arranged to give full utilisation of the chain length, the tube would have to be cut before the next stage of the schedule could be carried out. In practice, with reductions in area of 30% to 35%, two passes of steel tube are generally possible before the tube needs to be cut again, though this will clearly result in only part of the chain length being utilised on the first of these passes. If a 50% or 66.7% reduction of area were possible under industrial conditions, full chain length would be utilised when drawing tubes of, respectively, half or one-third of the chain length, though such tubes would have to be cut after each pass. These reductions of area would, however, minimise the non-productive time per unit length of finished product. Any significant increase in reduction of area would result in a reduction in the number of passes required for the larger schedules based on conventional limit reductions. It may be, therefore, that reductions of area resulting in non-integer increases in tube length would prove to be sub-optimal, since this would result in decrease in the ratio between the productive and non-productive portions of the production cycle. This could only be realistically checked by comparing the costs of the whole production route based on both maximum reduction of area and integer length increase.

The foregoing parameters outline the use, and likely impact, of power ultrasonic technology in the metal forming industry. These developments have been based upon research carried out in the U.K., U.S.A., U.S.S.R., West Germany, Japan, Austria and Rumania; the results of which have been collated in various general articles and reviews[23-33]. This work has led to the identification of a number of mechanisms which operate during ultrasonic processing.

1) Superposition:

Pure superposition, in a tensile stress, is illustrated in Figure (1.1). It can be seen that the peak stress is equal to that of the steady-state flow stress.

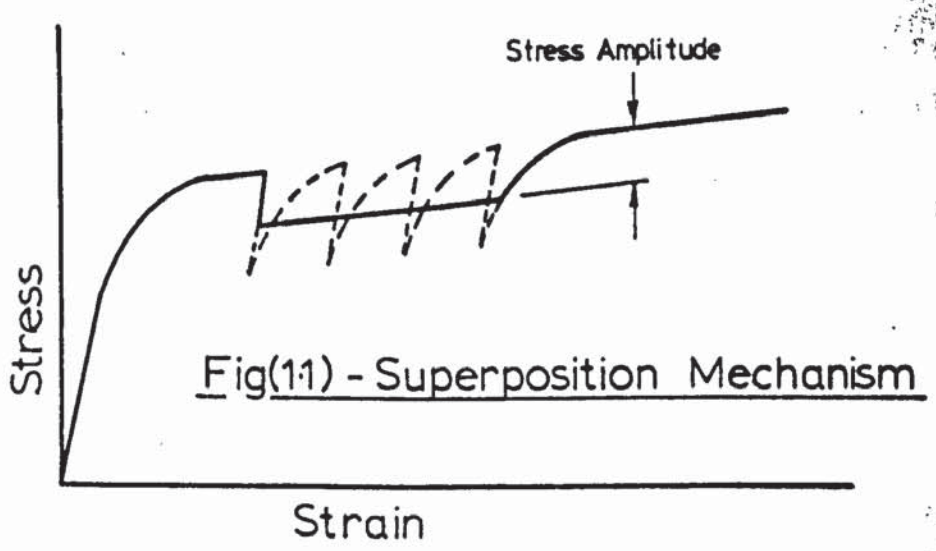

Fig(1.1) - Superposition Mechanism

If the load is monitored on an instrument which has a frequency response appreciably lower than that of the cyclic stress, the mean load will be measured, giving an apparent reduction in flow stress. There is now general agreement that superposition was the dominant mechanism observed by Blaha and Langehecker[6], though they initially attributed this apparent load reduction to a totally different mechanism..

The superposition mechanism, and those listed below, are discussed further in section 2.2.

2) Heating:

Temperature rises do occur during some oscillatory metal working operations[25,50] which result in a genuine reduction in material flow stress, though the efficiency compared with conventional techniques, is low.

3) Friction Vector

The friction force between two surfaces in relative motion will always act in opposition to the relative velocity. The friction vector is therefore reversed, when the peak tool velocity is greater than that of the deforming metal. This mechanism has been used to good effect in cup drawing[18][22][23] and fixed plug tube drawing[12][21].

4) Reduction of Friction

The vibrating tools can cause a reduction in coefficient of friction which has been attributed to[25] pumping of lubricant and chemical activation, separation of surfaces and softening or melting of asperities.

5) Metallurgical Effects

It is still not clear whether the application of ultrasound to metal deformation causes metallurgical changes in the absence of temperature rise.

6) Swaging Effect

This mechanism is operative when the non-zero component of the tool velocities is normal to the stock, as in tube or wire drawing with a radially vibrating die. The swaging effect is so-called, not surprisingly, because its operation is similar to that of the swaging process, which is widely used for pointing tubes and rod prior to drawing, as well as for the production of finished tubular products.

Most of the work reviewed in references (25-34) has been concerned with identification of the above mechanisms and the effects of power ultrasonics on deformation loads, particularly the drawing process. Little work, however, has been reported to show the extent to which a real reduction in front tension can be translated into an increase in

reduction of area and that which does exist does not give data in a very coherent form.

Dragan[21] states that an increase in 'elongation coefficient' of 30% to 75% was obtained with the use of an ultrasonically activated plug when cold drawing mild steel tube of 12.25 cm (one must assume that 'cm' should read 'mm') outer diameter and 0.3-2.2 mm wall thickness. The increase in 'elongation coefficient' implies a reduction of area, based upon 30%, of 46% to 60%.

If similar data are to be obtained for radially vibrating dies a very wide range of dies would be required, since account must be taken of changes in draw force with reduction of area, die angle and the vibrational amplitude of the die. It was to overcome this problem, and thus to further investigate the swaging effect, that an analogue of the above process was devised; the axisymmetric case was replaced by strip drawing. The radial resonator was replaced with a pair of axial mode wave guides which had the drawing dies mounted at their tips. The reduction of area could thus be varied, at will, by inserting shim steel at the mounting point of the wave guides. These tools are fully described in chapter 4.

Strip drawing has been used widely for experimental and analytical research into the mechanics of drawing. The strip drawing process is of little commercial importance in comparison with the wire and tube drawing processes, therefore, this work has been used essentially as an analogue of the axi-symmetric case. The published work relevant to strip drawing and its extension to wire and tube drawing is reviewed in section 2.1.

The use of a plane strain analogue also has the advantage that a theoretical analysis can be more readily attempted because there are only two non-zero, principal strain components rather than the three components generally present in drawing operations. The application

of ultrasonically vibrating tooling to a conventional metal forming process results in a change from a steady-state to a cyclic process. Any attempt to understand such a process, must therefore involve at least a qualitative analysis of a single cycle of the vibrating tools and their effect on the stress/strain/displacement system. The analysis cannot be confined to the deformation zone, as is generally the case in steady-state metal forming operations, since the drawn metal will form part of the vibrating system.

The aim in this thesis; therefore, is to examine analytically and experimentally the following processes:

(a) strip drawing through laterally vibrating dies. Thus the principal objective was to determine the effect on the process of die angle and land length, reduction of area, die amplitude and draw speed, in order to establish the process loads and limiting reduction of area for a given set of conditions.

(b) A subsidiary objective was to investigate a plane strain analogue of tube-drawing by vibrating the die in a 'radial' mode and axially vibrating a fixed 'plug'; the phase angle between the plug and dies to be variable.

The object of this work is to determine the optimum phase angle between die and plug.

The object of part (a) was largely completed though the experimental section of part (b) was not carried out. It was intended also to investigate the mechanics of bi-metal strip drawing through vibrating dies. The additional equipment required for these tests was designed and part of it was manufactured; the details are given in appendix (2).

CHAPTER 2 - LITERATURE SURVEY

In the introductory chapter, the limitations imposed upon the drawing process by the tensile deformation mode were briefly discussed. The likely impact of power ultrasonics on metal forming processes was also discussed, as was the mechanisms operating during such processes.

It is the intention in this chapter to review the literature relevent to the plane strain drawing of tube and strip with special emphasis on the techniques used to analysè these and related processes in order that their application to cyclic processes may be assessed. Finally, the development of research into ultrasonic metal forming, and the associated mechanisms, is reviewed from an historical standpoint, concentrating initially upon the mechanisms operating under ultrasonic action and followed by the applications to metal forming processes.

2.1. A REVIEW OF LITERATURE CONCERNED WITH CONVENTIONAL DRAWING OF WIRE, TUBE AND, ESPECIALLY, STRIP

The primary reason for investigating the strip drawing process, as already stated in Chapter 1, is not because of its commercial importance but because of its importance as an analogue of wire and tube drawing, since the analytical and experimental treatment of the plane strain analogue is simpler than the axisymmetric case. This is especially true in the case of close pass drawing of thin walled tubes since the deformation mode barely differs from that of the drawing of wide strip: wide strip is defined as strip whose width is greater than six times its undeformed thickness; this ensures that spread during drawing is confined to the edges of the strip because of transverse frictional constraint, and may, therefore, be ignored. The use of the plane strain analogue also allows the formulation of exact, though idealised analytical solutions[73].

The work which led to these solutions was reviewed by Green[72] in a paper published in 1960 which consolidated the work carried out by

various authors, mainly over the previous twenty years, though the work of Sachs dated from 1927; a detailed review of earlier work, including that of Sachs, due to MacLellan[84] was published in 1948.

Analytical work carried out since then has centred on the use of bounding techniques[76-82] and numerical methods[91-93]; these techniques being especially important where redundant shear is of a high order, as in the extrusion process.

General reviews of the wire drawing process have been published by Wistreich [83] in 1958 and, more recently, by Rowe[3]. These reviews deal, to a greater or lesser extent, not only with the analytical and experimental assessment of the process forces in wire drawing but also with die wear, friction, lubrication, temperature, surface finish and sizing. The primary importance of the latter work was the comparisons that were made between strip and wire drawing, and the demonstration of the variation of draw force with die angle and reduction of area, showing that optimum die angle increases with reduction of area. This interdependence had already been established by Hill and Tupper[85] for strip drawing; this will be discussed in greater detail later.

The experimental and theoretical work presented in the following chapters is concerned primarily with the assessment of process forces for a given set of conditions and to therefore establish values for limiting reduction of area. It is for this reason, therefore, that the following literature survey is not concerned with the problems of scheduling or producing a product to a given size and surface condition with specified mechanical properties.

It is convenient now to review the literature in terms of their analytical or experimental approach rather than the process type since this enables comparisons to be made more easily.

2.1.1. Equilibrium Analyses

In this type of analysis no attention is paid to the theories associated with plastically deforming metals, beyond the use of a suitable yield criterion. This technique has been used to analyse all the basic metal forming processes[1]; the primary advantage being analytical simplicity, though this very simplicity allows the technique to be used on the more complex metal forming processes, such as the complete analysis of deep drawing[87], or in analysing the effect of tool geometry[88].

An early, and typical, example of this type of analysis, which is relevant to the work shown in Chapter 3, is that due to Sachs, for strip drawing. This work has been widely reported in the standard texts on metal forming and was included in the review by MacLellan[84]. An expression for draw stress, which is generally normalised with respect to yield stress is given by:

$$\frac{\sigma_x}{2K} \doteq \frac{1+B}{B}\left[1-\left(\frac{h_a}{h_b}\right)^B\right] \qquad \text{(See Figure (2.1.))}$$

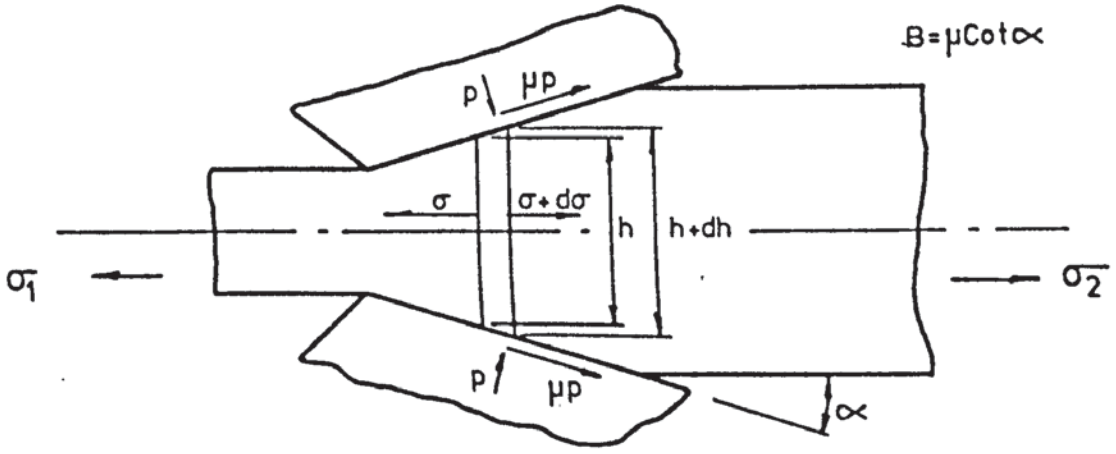

Fig(2.1)-Equilibrium Forces In Strip Drawing

A basic assumption made in this type of analysis is that deformation is homogeneous, that is, no direct account is taken of redundant deformation, though semi-empirical additions have been made to take account of the effect of tool geometry.

The primary advantage of this method of analysis is its relative simplicity when compared with methods rooted in the theory of plasticity; the effects of friction can be readily estimated where conditions of continuous boundary lubrication prevail. Experimental work tends to justify μ as a model for friction in cold, well lubricated metal forming processes. The work of Lancaster and Rowe[2] has demonstrated this when drawing strip; Young[22] obtained very good correlation between theory and experimental results when investigating friction vector reversal in deep drawing; Rothman and Sansome[89] and Chia[90] have also obtained good correlation between theory and experiment when using μ as a frictional model in rotating die experiments. This technique therefore accounts for work done against friction as well as making allowance for the homogeneous deformation of the metal. The accuracy associated with this method, therefore, relies upon there being low levels of redundant deformation; the equilibrium method is not, and makes no pretence to be, an accurate model of the deformation process and is therefore generally applied only to cold drawing and rolling of metals where die and draft angles are low and lubrication is good. The reduction of area should not be too low since this causes departure from the near ideal deformation mode associated with higher reductions of area; this phenomenon is discussed further in section (2.1.2). Work hardening can be accounted for[1] provided that the flow stress can be expressed as a suitable function of plastic strain, though this of course, complicates the solution of the equilibrium equation.

2.1.2. SLIPLINE FIELDS

The use of slip line field solutions to metal forming problems has been reviewed by Hill[73] and others[75,76]. The application of these analyses is confined to problems in plane strain since their solution is dependent upon being able to determine the stress and velocity fields from equations which have the property of mutual orthogonality; such equations are only known to exist in two dimensions, that is, logarithmic spirals in an axi-symmetric plane[74] and the more generally used cycloids for the construction of slip line field solutions in a Cartesian plane. Numerical methods of solution are possible[73, 74], though most solutions have been obtained from geometric construction. The constructions have utilised either tool / stock configurations which lead to simple feasible solutions, that is, solutions consisting of straight lines, sometimes with circular arcs, or a general method of construction due to Prager (Reference 75, Chapter 30).

The slip line field technique has been used by Hill and Tupper[85] to analyse the strip drawing process, again as an analogue of the more important tube and wire drawing processes. This work, for frictionless conditions showed that one of three modes of deformation will occur dependent upon the relationship between die angle and reduction of area.

The two most important modes, from a practical point of view are shown in Figures (2.2), (2.3) and (2.4); Figure (2.3) represents the limiting condition of Figure (2.2) and occurs when

$r = \frac{2 \sin\alpha}{1+2 \sin\alpha}$; at reductions of area less than this the deformation zones associated with each die meets at a point on the axis of symmetry, whilst at greater reductions of area the deformation zone spreads over a finite length of the axis of symmetry.

The third type of deformation mode, Figure (2.5), is in evidence at low reductions of area and is consistent with the mode of deformation that occurs when indenting a semi-infinite block[76], that is, the slip

Slip Line Field Configurations In Strip Drawing

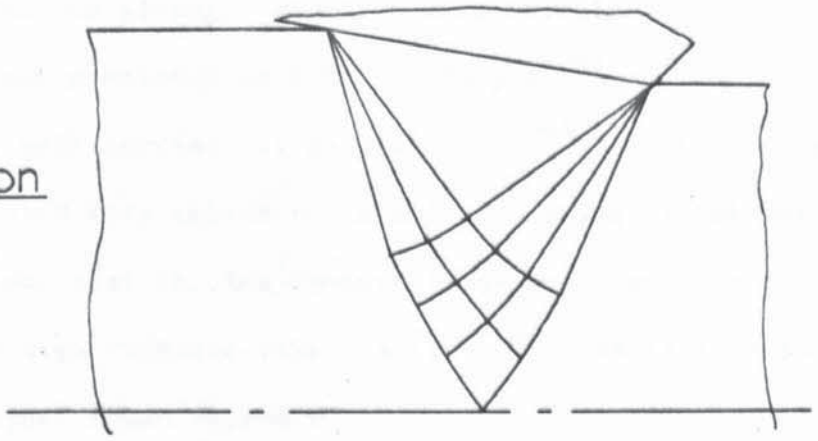

Fig(2.2) - Low Reduction Of Area

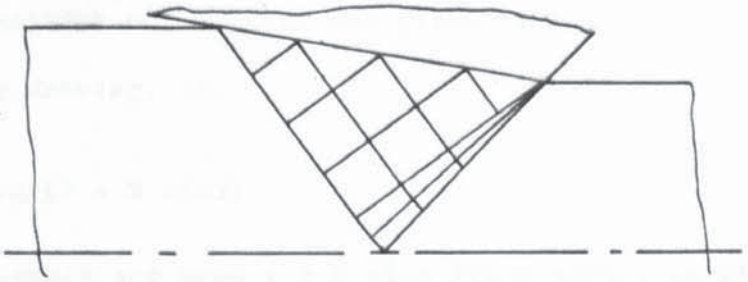

Fig(2.3) - Special Case At $r = \frac{2 \sin \alpha}{1 + 2 \sin \alpha}$

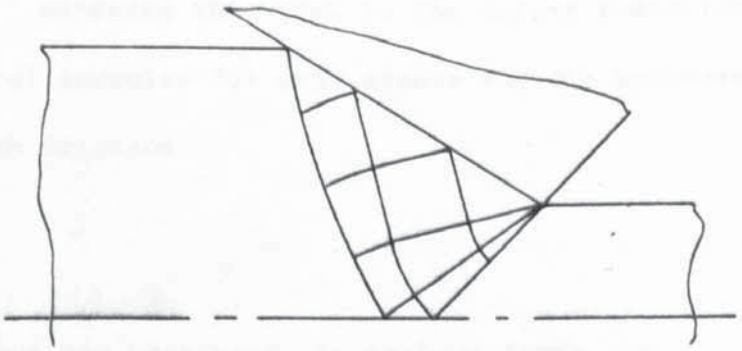

Fig(2.4) - High Reduction Of Area

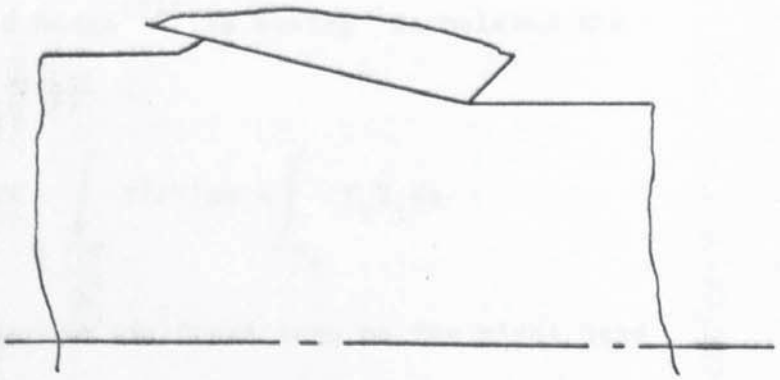

Fig(2.5) - Bulging

line field associated with the two dies separate and the deformation zones spread up-stream of the die giving a standing wave, or bulge, of metal. This phenomenon has been predicted by Hill and Tupper[85] and shown to exist in experimental work carried out by Wistreich[83]. This mode of deformation is associated with excessive localised working of the material and also chip formation, that is, the process tends to become one of machining with a very high negative rake. Avitzur[14] has treated this phenomenon using an upper bound approach.

The most important deformation modes, however, are carried out at reductions of area in excess of that which causes bulging. The range over which the primary deformation modes occur are given by Hill and Tupper[85], for frictionless drawing, as:

$$\alpha\,(0.230 + \frac{\alpha}{9}) \leqslant r \leqslant 2\sin\alpha/(1 + 2\sin\alpha)$$

when $r \leqslant 6.23 + \frac{\alpha}{9})$ bulging occurs and when $r \geqslant 2\sin\alpha/(1+2\sin\alpha)$, as already stated, the deformation zone extends over a finite length of the axis of symmetry. Green and Hill[86] extended this work to the larger reductions of area, giving also empirical formulae for draw stress and die pressure which took account of Coulomb friction.

2.1.3) UPPER BOUNDS

The upper bound technique has been used, in various forms, by Johnson and others[76], Avitzur[14] and others, Westwood and Wallace[82], and Halling and Mitchell[77-79].

Avitzur[14] cites Prager and Hodge[81] as having "formulated the upper bound theorem", as:

$$J^* = \frac{2}{\sqrt{3}}\sigma_o \int_V \sqrt{\frac{1}{2}\dot{\varepsilon}ij\,\dot{\varepsilon}ij}\; dV + \int_{s_t} \tau|\Delta V|ds - \int_{s_t} T_i V_i ds$$

where J^* is the upper bound on power; the first term on the right hand side represents the internal power of deformation; the second term

represents power loss at velocity discontinuities which may be within the metal or at a surface traction; the final term represents power supplied to the system in addition to that given by J*, for example, front tension in rolling.

Haddow[80], Halling and Mitchell[80], and Westwood and Wallace[82] cite Hill as the source of the expression:

$$\int_{su} T_i U_i ds \leq \int_v \sigma_{ij}^* \, e_{ij}^* \, dV + \sum \int_{sd^*} K \, [U^*] dS_d^* - \int_{st} T_i U_i^* ds$$

This is rather confusing, though the two expressions are, in essence, the same. The expression cited by Avitzur[14] with reference to page 237 of Prager and Hodge[81] is actually given as:

$$J^* = K\sqrt{2} \int_v \sqrt{\dot{\Sigma}_{ij} \dot{\Sigma}_{ij}} \, dV - \int_{s_t} T_i V_i^* ds$$

in the edition of reference (81), in the possession of the author. There is no reference to any of Hill's work in the relevant chapter of Prager and Hodge[81]; also, Avitzur[14] credits reference (81) to a different publisher from that which is in the possession of the author. This is clarified by Johnson and Mellor[76] (page 286) which states:

> "Drucker, Greenberg and Prager (1951) stated three limit theorems from which the formulae for obtaining bounds can be obtained. The theorems were, however, deducible from certain work principles published by Hill (1950)",

hence the confusion in sources!

A primary advantage of the upper bound technique is that only the velocity boundary conditions need to be satisfied, unlike the slip line field solutions which require that equilibrium conditions are maintained throughout the deformation zone, for a rigid-plastic material. The upper bound technique can also be applied to the axi-symmetric state.

Hill has proposed also a general method of solution of metal forming

processes which has been used by Lahoti and Kobayashi[94] to analyse open die forging that includes barreling, non-plane-strain Steckel rolling and tube sinking.

The approach to the upper bound technique used by Avitzur[14] and his co-workers differs from that of other workers in that it is essentially analytical rather than graphical and treats the total power of deformation as being the summation of the 'ideal internal power of deformation' defined by:

$$\text{a)} \quad W_i = \frac{2\sigma_o}{\sqrt{3}} \int_v \sqrt{\frac{1}{2}\dot{\Sigma}_{ij}\dot{\Sigma}_{ij}}\, dV$$

where σ_o is the uni-axial flow stress.

$\frac{1}{2}\dot{\Sigma}_{ij}\dot{\Sigma}_{ij}$ is the effective strain rate which, for a Mises material is given by:

$$\frac{1}{2}\dot{\Sigma}_{ij}\dot{\Sigma}_{ij} = \frac{1}{2}\left|\dot{\Sigma}_{11}^2 + \dot{\Sigma}_{22}^2 + \dot{\Sigma}_{33}^2\right| + \dot{\Sigma}_{12}^2 + \dot{\Sigma}_{23}^2 + \dot{\Sigma}_{31}^2 \qquad (21)$$

i and j can be defined in any suitable coordinate system.

The square root of the effective strain rate must be integrated with respect to the volume of the deformation zone.

b) Power loss at velocity discontinuities due either to shear or friction, given by:

$$\dot{W}_f = \int_{sr} \tau|\Delta v|\, ds$$

where τ is the shear stress at the velocity discontinuity.

At a frictional velcoity discontinuity τ is defined by:

$\tau = \frac{m\sigma_o}{\sqrt{3}}$; m is the frictional factor; this is a scalar the value of which is between 0 and 1; $\sigma_o/\sqrt{3}$ is the shear stress for a Mises material.

ds defines an element of the velocity discontinuity and $|\Delta v|$ the

absolute value of the velocity change across the discontinuity. The power loss at an internal velocity discontinuity is given by:

$W_{S_i} = \int_{r_i} \tau|\Delta V| ds$; this is similar to the expression for frictional power loss except that 'm' is effectively unity.

c) Any power input, such as back tension in drawing, must be accounted for, either in an absolute sense or as a proportion of the unknown input power.

The analysis for strip drawing given by Avitzur[14] is shown below.

It is first necessary to define a velocity field. The geometry of the strip drawing process lends itself to the use of the cylindrical polar coordinate system as shown in Figure (2.6).

Fig(2·6) - Kinematically Admissible Velocity Field For Strip Drawing (ref(14))

The velocity field is described by:

$\dot{U}_r = V = -Vf\, rf \frac{\cos\theta}{r}$, $\dot{U}y = \dot{U}_\theta = 0$

Also[14] $\dot{\Sigma}_{rr} = \partial \dot{U}_r, \quad \dot{\Sigma}_{\theta_\theta} = \frac{\dot{U}_r}{r} + \frac{1}{r} \frac{\partial \dot{U}_\theta}{\partial \theta}$

$$\dot{\Sigma}_{yy} = \frac{\partial \dot{U}_y}{\partial_y}$$

$$\dot{\Sigma}_{r_\theta} = \frac{1}{2} \left(\frac{1}{r} \frac{\partial \dot{U}_r}{\partial_\theta} + \frac{\partial \dot{U}_\theta}{\partial_r} - \frac{\dot{U}_\theta}{r}\right)$$

$$\dot{\Sigma}_{\theta y} = \frac{1}{2}\left(\frac{\partial U_\theta}{\partial y} + \frac{1}{r} \frac{\partial \dot{U}_y}{\partial_\theta}\right)$$

$$\dot{\Sigma}_{y_r} = \frac{1}{2} \left(\frac{\partial \dot{U}_r}{\partial_y} + \frac{\partial \dot{U}_y}{\partial_r}\right)$$

$\therefore \dot{\Sigma}_{ry} = \dot{\Sigma}_{y\theta} = 0$, and $\dot{\Sigma}_{yy} = 0$; from the assumption of plane strain, therefore:

$$\dot{\Sigma}_{rr} = -\dot{\Sigma}_{\theta\theta}$$

and

$$\dot{\Sigma}_{r_\theta} = \frac{1}{2} V_f r_f \frac{\sin\theta}{r^2}$$

This enables the evaluation of $\frac{1}{2} \dot{\Sigma}_{ij} \dot{\Sigma}_{ij}$ and hence:

$$w_i = \frac{2}{\sqrt{3}} \sigma_o V_f t_f \frac{E(\sqrt{3}/2, \alpha)}{\sin\alpha} \ln \left(\frac{t_o}{t_f}\right)$$

where $E(\sqrt{3}/2, \alpha)$ is an elliptic integral of the second kind; for small α the above expression simplifies to

$$w_i = \frac{2}{\sqrt{3}} \sigma_o V_f t_f \ln \left(\frac{t_o}{t_f}\right)$$

The power lost in shear at r_1 and r_2 is given by:

$$W_{S_1} = \frac{2}{\sqrt{3}} \sigma_o V_f r_f (1-\cos\alpha)$$

and, also:

$$W_{s_2} = \frac{2}{\sqrt{3}} \sigma_o V_f r_f (1-\cos\alpha)$$

The power loss at the die/strip interface is given by:

$$W_{s_3} = \frac{2}{\sqrt{3}} m\sigma_o V_f t_f \cot\alpha \ln \left(\frac{t_o}{t_f}\right)$$

and $J^* = V_f t_f \sigma_f$, therefore in a simpler form than that given by Avitzur[14].

$$\frac{\sigma_{x_f}}{\frac{2\sigma_o}{\sqrt{3}}} = \frac{E(\sqrt{3}/2,\alpha)}{\sin\alpha} \ln \left(\frac{t_o}{t_t}\right) + \frac{1-\cos\alpha}{\sin\alpha}$$

$$+ \frac{m}{2} \cot\alpha \ln \left(\frac{t_o}{t_f}\right)$$

This analytical technique has certain advantages; some account is taken of redundant shear in the inlet and outlet of the deformation zone; friction can be accounted for in terms of constant shear, Coulomb friction and hydrodynamic lubrication, though the latter two models lead to increasing analytical complexity. The whole expression can be minimised with respect to J^* where appropriate[103], though velocity fields tend to be dictated by the geometry of the deforming solid and the coordinate system employed in the analysis; the velocity discontinuity at the inlet of the deformation zone of the strip drawing analysis shown above is certainly unrealistic. Basily and Sansome[104] have overcome the difficulty by using a numerical method, in conjunction with the basic procedure laid down by Avitzur, when drawing rod to section.

The technique employed by Johnson[76] and his co-workers is a graphical method which plots the change in velocity of the metal as it passes through a series of prescribed velocity discontinuities, the object being to determine a series of discontinuities which

minimise the total power expended upon deforming the metal. Simple patterns of discontinuities can be expressed in terms, usually, of a single variable which may be minimised directly, giving a least upper bound for the proposed velocity discontinuity pattern. More complex patterns of velocity discontinuity have to be minimised graphically by trial and error or by numerical methods; not surprisingly the minimum upper bound is found when the system of velocity discontinuities closely approximates to the appropriate slip line field solution. The only frictional conditions that can be accounted for directly are sticking friction, zero-friction and the intermediate cases involving friction factor. The use of μ does not give an upper bound[76]. Oxley[95] has proposed a method for taking account of friction by adding terms which involve the friction angle.

Halling and Mitchell have used this technique to analyse plane-strain extrusion[73] and axi-symmetric extrusion[78] with an approximation[80] for work hardening.

Westwood and Wallace[82] proposed a method of analysing the force equilibrium on a prescribed system of shear planes, in plane strain, which was followed by Halling and Mitchell[79] for the analysis of axi-symmetric extrusion.

2.1.4. Numerical Methods

As already stated, Basily and Sansome[103] applied numerical techniques to the general approach used by Avitzur and slip-line fields can be defined numerically. Most of the numerical work, however, has centred upon the extension of the finite element technique from the study of fluid flow, vibration and elastic stresses. Gordon and Weinstein[91] have analysed the strip drawing process using the finite element technique, for an elastic-plastic, linear work-hardening, material. This analysis also took account of Coulomb friction and appears to give a good account of

the behaviour of real metals, showing the short-comings in the Sachs theory at low reduction of area and giving plastic zones similar to that obtained from slip-line field analyses.

2.2. A REVIEW OF THE LITERATURE RELEVANT TO VIBRATORY METAL DEFORMATION

The bulk of the work which has been published on the vibratory working of metals was prompted by the early work of Blaha and Langenecker[6] which indicated that, under the action of ultrasound, there was a reduction in the flow stress during a tensile test. This work was carried out on zinc mono-crystals which were vibrated at 800 kHz by interposing between the test machine crosshead and the test piece, a magnetostrictive ultrasonic drive. The early work on such tensile tests has been reviewed by Winsper and Sansome[24]: further work was carried out by Langenecker and co-workers on mono-crystals of aluminium and cadmium and with polycrystalline specimens of zinc, aluminium, cadmium, beryllium, tungsten and 18-8 stainless steel in the frequency range 15-25 kHz. It was observed that the stress reduction was dependent upon vibrational amplitude and independent of frequency within this range. Similar work at frequencies up to 1 MHz confirmed the above results; Langenecker, noting that the shape of the stress/strain curve changed, with increasing levels of ultrasound, in a similar manner to that observed with increasing temperature. The work of Neville and Brotzen was also discussed in reference(24). This work confirmed the results of Langenecker andhis co-workers; showing that the reduction in flow stress was independent of frequency, within the range 15-800 kHz, directly proportional to stress amplitude, and, for low carbon steel, independent of temperature within the range 30-500°C. The importance of the work of Nevill and Brotzen lies not in its confirmation of the earlier work, but in the alternative explanation of the underlying

mechanism. Langenecker had proposed models based upon the interaction of acoustic stress waves and dislocations[66], whereas Nevill and Brotzen noted that the dynamic stress amplitude was equal to the apparent reduction in flow stress (Figure (1.1)). In tensile tests carried out by Langenecker et al[58], very high temperatures were reached after very short exposure to ultrasonic energy, in fact the generation of significant temperature rise seems to be a feature of the work of Langenecker and his co-workers, though they claim that the efficiency of generating heat in this manner is greater than that of heat which is applied by more conventional methods; it is claimed that acoustic energy is absorbed, preferentially, at dislocations in such a manner that their movement through the bulk of the metal is eased[65,66]. Samples of steel[50] which were vibrated axially during a tensile test resulted in a typical ductile fracture whilst a similar sample, vibrated for only two seconds during the test, resulted in a fracture normal to the principal stress axis. This fracture occurred away from the centre of the heat affected zone that was generated at the stress antinode; Langenecker and Jones[50] attributed this to 'hardening by sound at the heated region'. Fracture of the boundary of the heat affected zone is a common mode of failure in welded joints; welding temperatures were certainly reached during these tests, therefore the failure was more likely to be due to mis-match at the boundary of the freshly annealed metal and worked metal in the test piece. The conclusion that 'ultrasonic hardening' had occurred could only be justified if this had been found as a result of a hardness survey across the undeformed heat affected zone.

The work of Nevill and Brotzen has been directly confirmed by other workers[64] and indirectly confirmed during the examination of metal forming processes which have been augmented by ultrasonic oscillations. Lehfeldt[64] has investigated the tensile test and bending test with superposed ultrasonic oscillations in order to establish the relationship between the applied oscillatory energy and its effect upon flow stress.

In both cases it was found that the indicated decrease in flow stress was equal to the dynamic stress amplitude. The interpretation given by Langenecker has never been fully explained since the essential mechanism of preferential absorbtion of acoustic energy is not clear; resonance has been generally rejected as a mechanism since the flow stress reduction appears to be frequency independent and the vibrational frequency of dislocations is some three orders of magnitude higher than the frequencies used in these tests[31]. This type of reduction in mean flow stress was called the "Blaha" effect by Langenecker though it is now generally considered to be a combination of the superposition and heating effects. This type of reduction, real or apparent, is present to a greater or lesser extent in most vibratory metal forming operations.

The combined phenomena of superposition and heating, under the action of ultrasound has been termed the 'volume effect' since they affect, or seemingly affect, the bulk of the metal. Other phenomena are treated as a group, termed the 'surface effect'. Winsper et al[27] cite five possible mechanisms, namely, surface separation, friction vector reversal, heating of surface asperities, pumping of lubricants, and cleaning of surfaces.

Surface separation, which may occur during strain relaxation in an ultrasonic metal forming operation, may lead to improvement of the lubrication, in a similar manner to the pumping of lubricant. Cleaning of surfaces has been noted when drawing wire through dies which were immersed in an ultrasonically activated oil bath[27], which could similarly improve lubrication, whilst heating of surface asperities may lead to localised softening. These mechanisms all lead to a reduction in the magnitude of the interfacial shear stress, thus reducing the magnitude of the frictional force. Friction vector reversal is a quite distinct mechanism, in fact, the reduction of friction force reduces the effectiveness of the reversed friction vectors. Friction vector reversal

occurs when the tool velocity, in magnitude and sense, is greater than the velocity of the deforming metal, which, under the action of ultrasound is a cyclic process, unlike the mandrel drawing of tube. This phenomenon is primarily in evidence in the drawing of tube with an ultrasonically activated fixed plug[42] and in deep drawing with a radially vibrated blank holder[22] [23] [39]. The deformation process, therefore, proceeds in a cyclic manner; when the friction vector acts in the direction of deformation the metal will deform at a load lower than that necessary under conventional conditions; as the friction vector is reversed the deformation will cease until the strain take-up down-stream of the deformation zone reaches that necessary to re-establish plastic deformation. In order to gain any real reduction in draw load it is therefore necessary to totally suppress plastic deformation when conventional friction conditions apply. The effectiveness of the friction vector reversal mechanism is therefore heavily dependent upon the peak tool velocity in relation to the steady state deformationspeed. This mechanism is discussed further in sections (2.2.2) and (2.2.4) when reviewing, respectively, the tube drawing and deep drawing processes under the action of ultrasound.

The other major mechanism is the swaging effect. This phenonenon is in evidence when there is a non-zero component of tool velocity normal to the surface of the deforming metal. Provided that this motion does not cause ejection of the deforming metal from the tools, the addition of such a velocity component introduces a higher compressive stress on one or two of the principal stress axes, which therefore reduces the most tensile principal stress. This mechanism would thereforebe of primary importance in processes relying upon high tensile principal stresses, such as wire drawing and tube drawing, draw ironing of cans, and rolling under conditions of high front or back tension.

These mechanisms are discussed further in the following section in

relation to their application to metal forming processes.

2.2.1. Strip Drawing

Severdenko et al[53] and Rozner[54,55] have investigated the drawing of strip through ultrasonically activated dies. Severdenko used a pair of axial resonators symmetrically disposed about the strip axis at an angle of 45°; cylindrical dies were used with dry soap as a lubricant, a draw speed of 0.08 m/sec and an oscillatory amplitude of 0.012 mm. No details were given of the applied frequency; nor was any mention made of the method of measuring die amplitude or process forces. Experiments were carried out on annealed copper strip (2mm x 20 mm) for which a maximum reduction of area of 71.4% was obtained, and aluminium strip (1.75 x 30 mm) which was reduced by 87.8%. This was achieved when the concentrations were driven in 'anti-phase', giving a hammering effect; these figures were reduced to 60% and 64% respectively when the concentrators were driven 'in-phase', giving a bending effect. When one concentrator was driven maximum reductions in area of 65.5% and 75% were obtained. The highest reductions of area have been attributed to what has become known as the swaging effect and a reduction in coefficient friction; indeed all three vibrational modes resulted in reductions of area in excess of that possible under conventional drawing conditions, that is, 56.5% for the copper and 58% for aluminium. Since Severdenko et al present their data in terms of limit reduction of area, the improvements are real and even in the worst case of 'in-phase' oscillations of the die were reasonably significant with improvements of 3.5% and 6% respectively. Friction vector reversal was unlikely to be in evidence under these conditions; it is probable, therefore that this reduction was caused by friction reduction due to breaking of surface contact. The results obtained when only driving one die are consistent with the remainder of the results in that they lie between those of the

'anti-phase' and 'in-phase' tests; there is likely to be some swaging effect in evidence though the exact vibrational mode of the dies is unlikely to be as stated since there is probably a sympathetic vibration induced in the 'static' die.

Rozner[54,55] used tooling which could be adjusted and enabled tests to be carried out with die semi-angles over the range 6°-30°. The equipment was mounted in a tensile testing machine; drawing was carried out at speeds of up to 50 cm/min (8.33 mm/sec) with die amplitudes of up to 0.03 cm at 20 kHz. Tests were carried out on annealed high-conductivity copper, annealed mild steel and annealed 70/30 brass. The strip was drawn dry or with paraffin or SAE 20 oil; steady state draw conditions were established before the wave guides were energised. No attempt was made to draw the strip beyond 30% reduction of area and experimental results were recorded on an x-y plotter.

The 'coefficient of fricton' was determined by force equilibrium from the expression:

$$\mu = \frac{(T/2Q) - \tan\alpha}{1+(T/2Q)\tan\alpha}$$

where T is the tag load and

Q is the transverse force.

Rozner was therefore taking the closure of the polygon of forces as being a measure of the coefficient of friction, which tended to reduce with reduction of area and also when the dies were energised. Die pressure varies in a similar manner and no draw speed dependance, within the range 5 cm/min to 50 cm/min, was detected. Microstructure was found to be unaffected by ultrasound.

The tooling configuration used by Rozner was similar to that used by the author, except that Rozner supported the 'active' end of the wave guides in needle roller bearings. This must have resulted in significant loss of acoustic energy to the machine frame and could well have accounted for the very low efficiency of transfer of acoustic energy reported by

Rozner (approx. 7.5%), that is, by providing a parallel path for energy transference. Whilst the presence of superposed stress is acknowledged by Rozner[54] the whole of the apparent die and tag load reduction is attributed to reduction in coefficient of friction; no attempt was made to measure dynamic load on the dies or strip and no mention was made of the effect of swaging on the strip, though there was clearly a significant swaging component in the process.

2.2.2. Tube Drawing and Wire Drawing

Winsper and Sansome have investigated the drawing of wire with longitudinally vibrating dies. Experiments were carried out over a low frequency range[40] and at 18.7 kHz[41]. The low frequency tests were carried out on a bull-block machine with the die mounted in an electro-hydraulically oscillated die plate. It was found that the mean draw force decreased when the die was vibrated and that this reduction was independent of frequency. The oscillatory amplitude was measured and found to be consistently higher than the apparent load reduction; this was attributed to increased friction forces due to disturbance of steady-state conditions. Winsper and Sansome therefore concluded that the load reduction was due wholly to stress superposition. No changes in mechanical properties of the drawn metal were detected. The process was shown to be critically affected by draw speed; stress amplitude decreased with draw speed and the mean draw load tended towards its non-oscillatory value. This was due to the reduced strain release during the down stream stroke of the die and the more rapid strain take-up on the up-stream stroke.

Later work by Winsper and Sansome[41] carried out at a frequency of

18.7 kHz utilised a multi-die arrangement which resulted in a genuine reduction in draw force, whilst single tests carried out at the same frequency resulted in a reduction in mean draw force that was due wholly to superposition. Similar work has been carried out by Samann[49], Inoue and Mori[48] and Vatrushin[47], again using dies excited in a longitudinal mode.

When the ultrasonically activated die was mounted between two fixed dies a reduction in total mean draw force of approximately twice the oscillatory force amplitude was achieved; with one fixed die the total mean draw force reduction was approximately 50% higher than the oscillatory force amplitude.

Severdenko et al[44] have investigated the sinking of brass tube under various modes of ultrasonic excitation, as shown in Figure (2.7). Four methods of drawing are shown in relation to the ultrasonic displacement wave, Figure (2.7)(a), (b) and (c) show drawing with the die set

Fig(2·7)- Tooling Used By Severdenko et al.[44]

co-axially with respect to the wave guide; Figure (2.7)(a) at a displacement antinode; Figure (2.7)(b) at a stress anti-node and Figure (2.7)(c) with two dies, one at each anti-node. In Figure (2.7)(d) and (e) the dies are set

normal to the wave guide axis, again, respectively at a displacement antinode, and at a stress antinode. A reduction of area of 23.4% was used throughout and draw speed ranged from 0.05m/sec to 0.4m/sec with an oscillatory amplitude of 0.01 μm.

Method (a) gives a reduction of mean draw force which shows a marked draw speed dependence; the reduction of mean draw force is probably wholly due to superposition and is consistent with the work of Winsper and Sansome[40, 41], Samann[49] and Pohlman and Lehfeldt[51], although Severdenko et al make no mention of superposition. Method (b) was not critically affected by draw speed; the die was placed at a displacement node, and should, therefore, have been unaffected by superposition. Severdenko et al attributed this reduction in draw force to what has become known as the swaging effect. They concluded it was due to the Poisson component of strain which was maximal at the stress anti-node. Method (c) gave results which were draw speed dependent, though not to such a great extent as in method (a). Two effects were in evidence in this case, both of which are draw speed dependent. The die mounted at the stress antinode imparted a swaging effect on the wire. The tube passing through the die mounted at the displacement antinode was therefore subject to a superposition effect, with back-tension due to the draw force required for the up-stream die. Method (d) must also have generated stress superposition due to transverse oscillatory displacement of the tube; the apparent load reduction was of a low order in comparison with that obtained in method (a), though it was still critically affected by draw speed. Similarly, method (e) gave results comparable to method (b), that is, the load reduction was sensibly independent of draw speed and the load reduction was somewhat lower than in method (b). Severdenko et al concluded that this was due to the difference in vibrational mode at the die orifice, that is, method (b) would, ideally, give a pure radial mode

of vibration whereas method (e) would yield an elliptical mode of vibration; no mention was made by Severdenko et al of stress superposition or the possibility of changes in frictional conditions. The choice of tube sinking is rather unfortunate in this connection since it is, even under steady state conditions, a difficult process to quantify as the thinning or thickening of the tube wall is affected by friction, die angle and reduction of area; no mention was made of how the different modes of die mounting affected wall thickness.

Later work carried out by Severdenko and co-workers concentrated upon wire drawing[44, 45] using the die/waveguide configuration shown in Figure (2.7)(d) and (e) with the addition of 'reflectors'. That is, dies giving a light reduction of area, positioned up-stream and down-stream of the main die in order to set up a standing acoustic wave in the wire.

Greater reduction of the mean draw force was obtained when the die was set at a stress antinode, though excessive temperature rise occurred in the deformation zone, necessitating cooling of the wire and die. This did not occur when the die was set at a displacement anti-node, and the load reduction was attributed, predominantly, to frictional changes[45]. Similar work was carried out on the drawing of titanium wires[43]; load reduction was reported though no attempt was made to increase reduction of area. Vatruskin[47] also reported load reduction in the drawing of wire whilst making no attempt to increase reduction of area; improvements would be marginal in this case as longitudinal die oscillation was employed.

Pohlman and Lehfeldt[51] have also made a comparative study of the various wave guide/die configurations when drawing wire, as shown in Figure (2.8).

Figure (2.8)(a), (b) and (c) correspond, respectively to Figure (2.7) (a), (b) and (e). Pohlman and Lehfeldt[51] obtained similar effects to Severdenko et al[44] though their investigation was more thorough

Fig(2·8)- Tooling Configurations Used By Pohlman And Lehfeldt (ref(51))

showing that the configuration in Figure (2.8) (a) resulted in a reduction in mean draw stress and that, in all cases, this reduction was equal to the dynamic stress amplitude. Swaging, due to Poisson strain at the stress antinode, Figure (2.8)(b) and (c), was shown to yield genuine reduction in draw force. Positioning of the die, transversely, at a displacement anti-node as in Figure (2.8) (d) resulted in a mean load reduction due to stress superposition; Pohlman and Lehfeldt showed that the peak bending stress induced in the wire by the transverse vibration was very close to the measured peak stress amplitude. The swaging effect was found to be in evidence when wire was drawn through the split dies shown in Figure (2.8(e) and (f) in which one half of the die was vibrated whilst the other half was set into a rigid block. The tooling configuration shown in Figure (2.8)(f) appeared to give a higher reduction in draw stress than the configuration shown in Figure (2.8(e). Changing the angle of inclination of the wave guide from the vertical to 45^{o} could change frictional conditions, both in magnitude and by inducing a reversal in the friction vector; there is also likely to be an increased level of stress superposition. Stress amplitude does not appear to have been measured by Pohlman and Lehfeldt[51] in this instance, which prevents a valid comparison to be made between the two tooling configurations.

Langenecker and Jones[50] also have investigated wire drawing through a longitudinally vibrating die. They state that 95% reduction in area of 1.5 mm copper wire in a five pass schedule was reduced to a two pass schedule - assuming equal reductions per pass, this would yield a change from a 5 x 45% schedule to a 2 x 77% schedule, without changing the final strength of the wire. It is not clear whether the die was sited at a stress antinode or a displacement antinode, though the former case would certainly account for the very high temperatures that were evidently generated during drawing. This heating effect was utilised directly in tube bending experiments[50] though it was claimed that the heating resulting from ultrasonic irradiation acted preferentially at dislocations and grain boundaries and was therefore considered to be more efficient, with respect to softening of the metal, than conventionally applied heat.

Atanasin[52] has presented an analysis of wire drawing through an axially vibrating die using the type of upper bound technique favoured by Avitzur[14]. The assumption was made that the metal flows as a visco-plastic material, which implied working of the metal at elevated temperatures. The flow stress of the metal, and also the coefficient of friction, was assumed to be modified by the intensity of ultrasonic irradiation. The flow stress equation, for copper and duralumin, was determined experimentally from tensile tests. There must have been considerable stress superposition, and probably significant temperature rise, though Atanasin accounted for the reduction in flow stress wholly in terms of acoustic field intensity, $I W/cm^2$, in an equation of the form:

$$\sigma_y(I) = \sigma_{yo} \exp a(I_o - I)$$

At very low draw speeds, treated mathematically as zero, the stress was shown to be virtually independent of die angles above 4^o, marginally

dependent upon frictional changes and heavily dependent upon reduction of area and ultrasonic intensity.

Similar trends were shown to exist when drawing at 5m/sec except that the draw force was affected by die angle to a greater extent; a clear optimum die angle was shown to exist for a specific drawing condition. Atanasin claims that the graphs obtained from the analytically derived expression for draw stress showed good agreement with experimental data, though no such data, or its source, was given in reference (52).

The various modes of die excitation have been discussed in this section; for fixed plug tube drawing, however, another common method of applying ultrasonic energy is to excite the plug into longitudinal resonance by means of a tuned plug bar and wave guide driven from a suitable H.F. source; this has been the primary commercial application of power ultrasonics in the metal forming industry to date. Real reductions in draw force can be obtained primarily by virtue of friction vector reversal. Winsper and Sansome[42] have investigated this process using a 0.5 in, 12° die, with a 0.476 in diameter plug. It was shown that the die, tag, and plug loads were reduced in direct proportion to plug amplitude and that the stress superposition, whilst varying with drawntube length, accounted for between 40% and 10% of the total indicated load reduction. When drawing at constant speed the load reduction was independent of reduction of area in the range 5% to 24.3%. It was also shown that plug oscillation improved surface finish on the inner and outer surfaces of the tube. Ultrasonic activation of the plug therefore results in a genuine reduction of draw force which could therefore be translated into an increase in reduction of area. Dragan[21], as already stated in the introductory chapter, has used this technique to give an increase in reduction of area under industrial conditions.

Cristescu and Dragan[102] have analysed the drawing of tube on an ultrasonically activated plug assuming that the material flow stress is

modified by the ultrasonic field intensity. This relationship was used also by Atanasin[52], that is, it was assumed that the effect of the ultrasound on the material was analogous to that of heating and that it was, therefore, viscoplastic. In this flow stress relationship:

$$\sigma(I) = \sigma(I_o) \exp \left[a(I_o - I)\right],$$

the constant, a, was stated to be a material constant, for a particular ultrasonic field intensity[52,102]. This constant was determined from tensile tests[52], though the method of applying the energy to the deformation zone varied widely from process to process and in relation to the tensile test; no account was taken directly of superposition or the manner in which the ultrasonic energy manifested itself in the volume, surface and swaging effects. No account was taken of friction vector reversal, which must be a predominant effect in the work of Critescu and Dragan[102]. The friction factor was asssumed to be subject to a 'global' reduction of 20%.

Dawson[70] has investigated the wire drawing and floating plug tube drawing processes when using a radially vibrating die.

A lower bound analysis of wire drawing was carried out by Dawson which was based upon the volume continuity expression.

Volume flow rate into the die = Volume flow rate out of the die - rate of decrease of the deformation zone.

which was used in conjunction with an equilibrium analysis. This analysis is discussed further in Appendix 4.

2.2.3. Extrusion

Little work has been carried out on the extrusion process, probably because of the relatively high reductions of area common in the industrial applications of extrusion and, therefore, the high levels of ultrasonic energy that would be required to surpplant the conventionally applied

power.

Spiers et al[35] have investigated the direct extrusion process when applying low frequency vibrations to the ram. Reduction in mean load was obtained in a similar manner to work on wire drawing through a die vibrated axially at low frequency[40], that is, the load reduction was found to be equal to the dynamic load amplitude; the load reduction was accounted for wholly in terms of stress superposition.

Investigations made by Petrukov et al into extrusion under the action of ultrasound have shown that the deformation mode was improved when ultrasonic vibrations were applied to the tooling in an axial mode, that is, frictional conditions were improved. This again is consistant with work carried out on wire drawing in which ultrasonic axial oscillations were applied to a die[41]. Further work carried out by Petrukov[69] on the application of radial oscillations of the die in extrusion; genuine reduction in extrusion load was obtained, along with reduction in redundant deformation; swaging was likely to be the predominant.

2.2.4. Deep drawing and draw ironing

Deep drawing and draw ironing are of interest, from an industrial point of view, because these processes are carried out at relatively low speeds, therefore the loss of effectiveness of the ultrasonic energy at high speeds is not too great a disadvantage.

Radial mode vibrations applied to the blank holder is the primary method of applying ultrasound to the deep drawing process; the main mechanisms are superposition in the drawn section of the cup and friction reduction and friction vector reversal at the blank/blankholder interface, though in the case of draw ironing the radial mode oscillations also result in load reduction due to swaging. Young[22] and Smith[23] have investigated an analogue of this process which involved drawing specimens through a pair of wedge shaped dies. Punch oscillations[38]

resulted in mean load reduction due to superposition whereas die oscillation resulted in increased draw ratio. In tests carried out by Biddell and Sansome[39] using a radially oscillating die, depth of draw was increased when deep drawing small cans on a mandrel. At low draw speed the radial resonator, powered through ceramic stacks, resulted in the whole of the deformation power being supplied from the ultrasonic generator, that is, no external steady state force was applied. The process was therefore converted from one of ironing to high frequency swaging; giving, in this case, a reduction of area of 40%.

2.2.5. Rolling

Little work has been done on the rolling of metal aided by ultrasound, again probably because of the large energy levels needed to improve the process significantly, under industrial conditions. Some work has been done in the U.S.S.R[57,58] in which the rolls were vibrated longitudinally at 20 kHz. This work resulted in a reduction in process forces, though it is not clear how these loads were measured and, therefore, the extent to which superposition was a factor in the load reduction. Improvement in surface finish was obtained[57] and residual stresses were reduced[56].

CHAPTER 3 - THEORY

In the previous chapter the analytical techniques used to analyse metal forming processes were reviewed. The preliminary reason for this was to establish the technique which was most applicable to the process under investigation, that is, strip drawing through vibrating dies. The use of slip line fields was not considered because of the need to determine the velocity boundary conditions prior to the construction of the stress and velocity fields; this problem was encountered by Dawson[70] when using a graphical upper bound technique, of the type used by Halling and Mitchell, to analyse the drawing of wire through radially vibrating dies.

An equilibrium analysis was also attempted by Dawson[70] which did not take account of the increase in the volume of the deformation zone. This is discussed further in appendix 4. Numerical methods also require a knowledge of the velocity boundary conditions and were not therefore considered.

The type of analysis favoured by Avitzur[14] suggested the route most likely to reach a solution since the velocity components within the deformation zone, due to swaging and drawing, could be treated separately and superposed; this approach is shown in the following sections. A further advantage of an analytical solution is that direct calculations, at any stage during the die penetration cycle, could be made, provided, of course, that a suitable expression could be obtained. Such a solution allows the effect of an individual parameter to be established.

The object in this chapter is to analyse the drawing of strip through vibrating dies and to extend the analysis to an analogue of the tube-drawing process in which metal is schematically drawn through a radially vibrating die with an axially vibrating fixed plug. Diagrams of the strip drawing process and tube drawing analogue are shown in Figure (3.1) and Figure (3.2) respectively.

Fig[3·1] - Diagram Of Strip Drawing Through Vibrating Dies

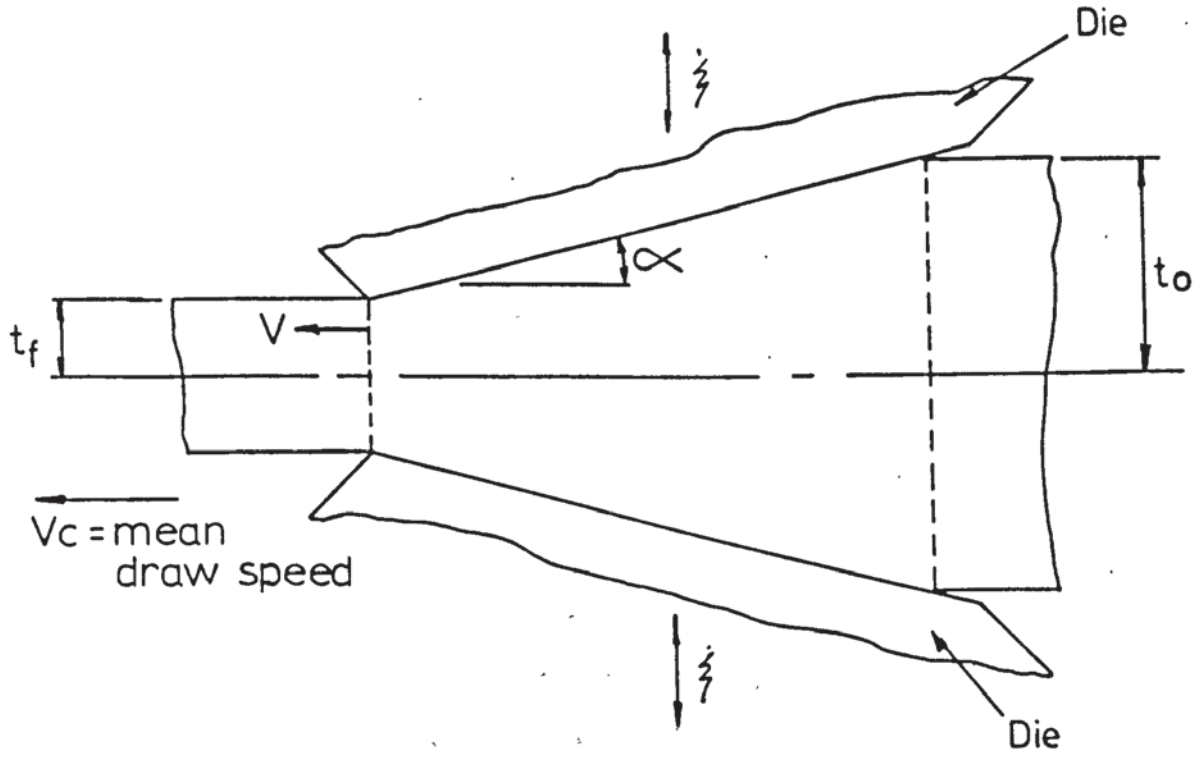

Fig[3·2] - Diagram Of The Tube Drawing Analogue

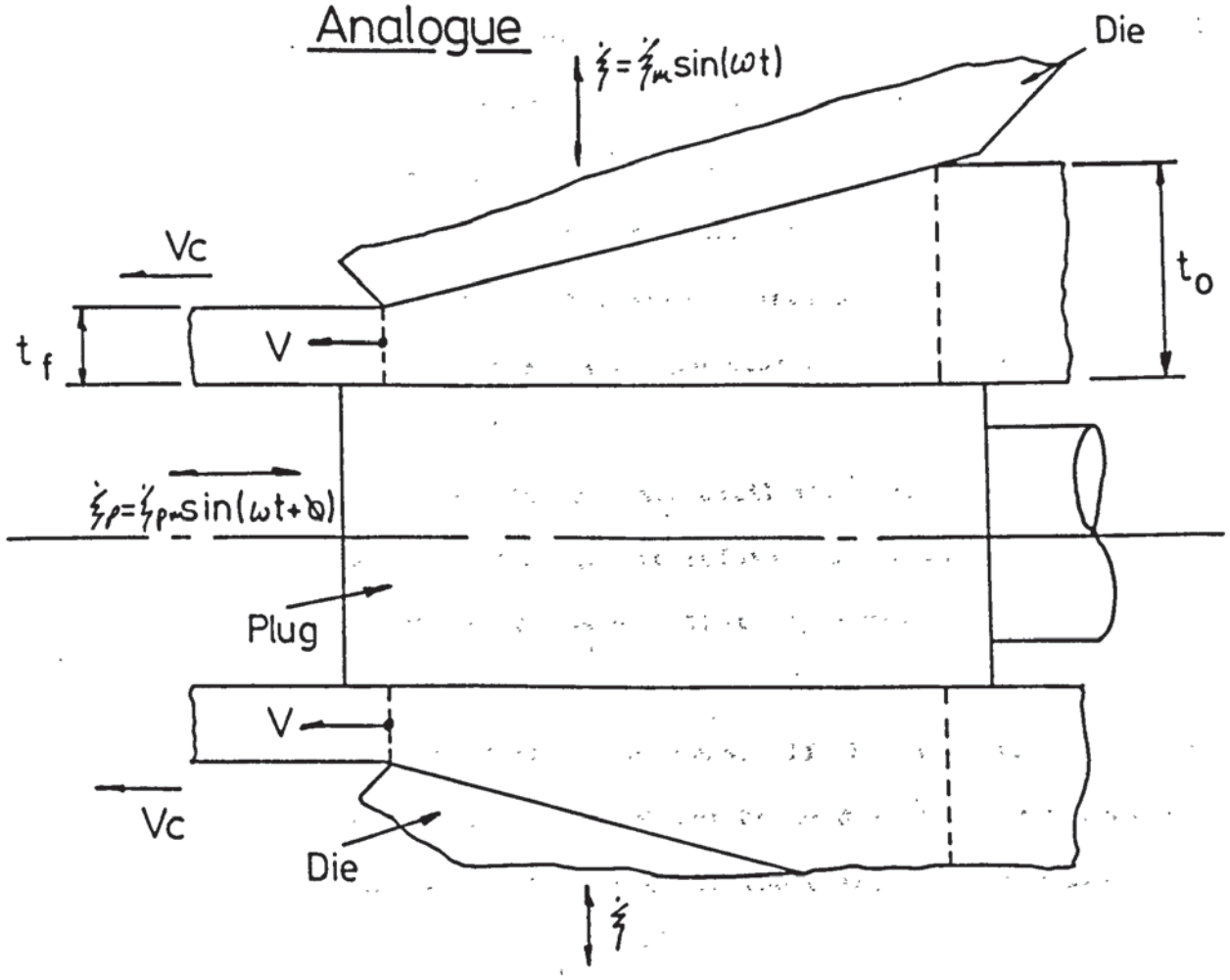

Strip drawing will be considered initially and any necessary modification made to the theory to give an analysis of the tube drawing analogue.

3.1. Velocity Conditions During Drawing Through Vibrating Dies

Is is essential to consider the process occurring in two phases, namely die indentation and die retraction. During the indentation phase the process combines drawing and swaging the predominance of either component being determined by some function of the velocities of the strip and die. It is therefore necessary to obtain a velocity field for drawing and swaging in order that the deformation power, or the equilibrium conditions, can be determined by superposition.

3.1.1. Velocity Field for Swaging a Wide Wedge

Consider a wide wedge of rigid - perfectly plastic material which is compressed between a pair of symmetrically inclined platens. The shape of the wedge is taken to be the same as that of the deformation zone which is assumed to exist when analysing the strip drawing process on either a Cartesian coordinate system or a cylindrical polar coordinate system. The sectional elevation of the wedge is either a symmetric trapezium, as shown in Figure (3.3) and Figure (3.4), or an annular sector, as shown in Figure (3.5). Two possible conditions exist, dependent upon the relationship between the angle of inclination of the platens and the frictional constraint present at the platen/wedge interface. These conditions are:

a) The wedge is held under the platens until the point of yielding is reached. In the plastic state, therefore, the metal will flow away from a neutral plane within the wedge. That is, a state of bi-directional flow, away from a zero velocity plane would exist.

b) The wedge is rejected from the platens. If this condition is to result in plastic deformation the wedge must be held in the platens by an additional constraint. In this state the metal will flow away from the

Fig[3·3]- Swaging Of A Wide Wedge

$(X_n < X_f)$

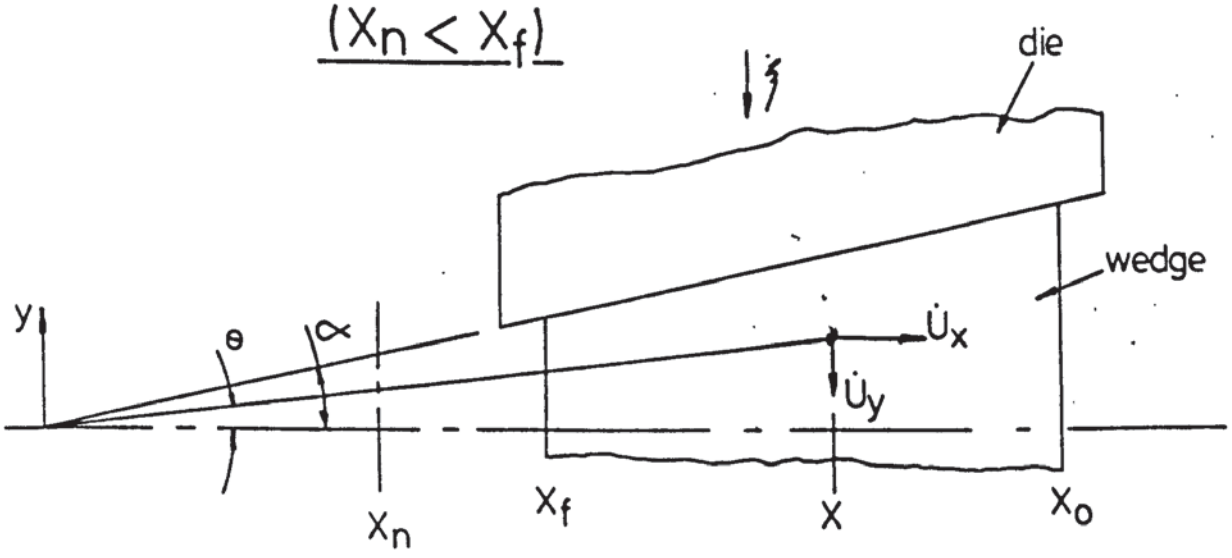

Fig[3·4]- Swaging Of A Wide Wedge

$(X_n \epsilon [X_f, X_o])$

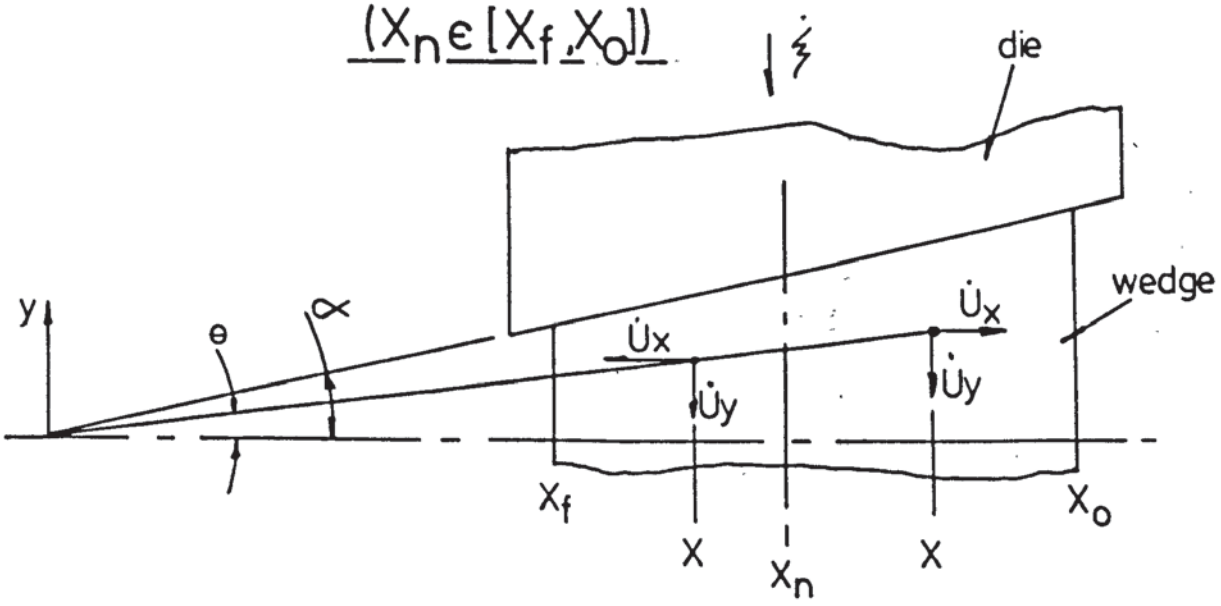

Fig(3·5)-Swaging Of An Annular Wedge With Rotating Dies

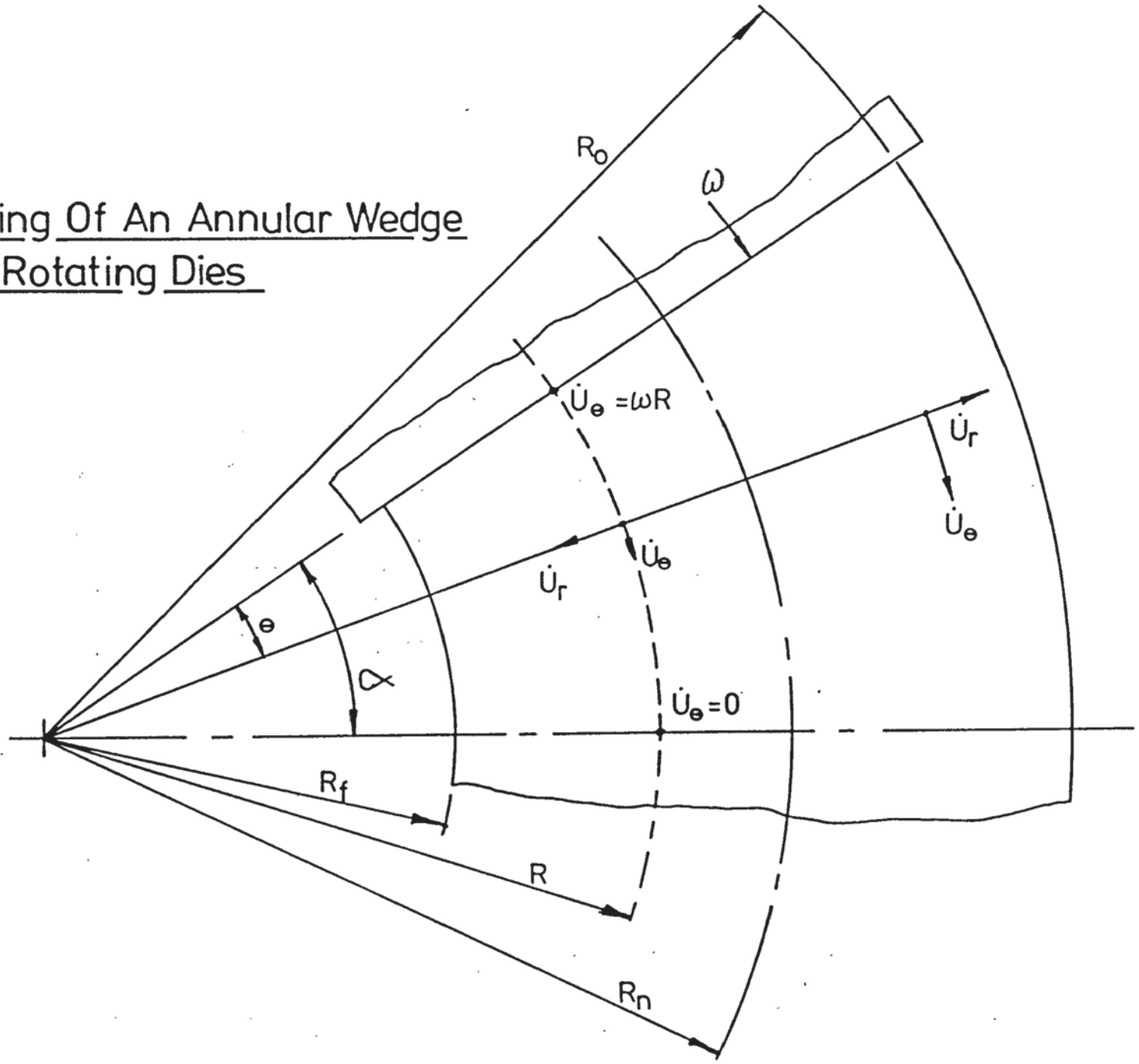

virtual apex of the platens.

The following sections model the swaging of a wide wedge using Cartesian and cylindrical polar coordinate systems.

3.1.2. Cartesian Coordinate System

Figure (3.3) shows the swaging of a wide wedge with axially vibrating dies for the unidirectional flow case. A neutral velocity plane, X_n, is assumed to exist between the origin of the coordinate system and the wedge. This implies that the two boundaries at the upstream and downstream ends of the deformation zone are moving in the same direction and that X_n is the position of an imaginary plane extrapolated from the velocity functions. The wedge is held so that plastic deformation is taking place, with velocity components $\dot{U}_x$ and $\dot{U}_y$. The $\dot{U}_z$ velocity component is zero, that is, a condition of plane strain exists.

It is convenient to define the distance of a point in the xy plane from the x-axis in terms of x and the angle, θ, of a line passing through the point and the origin of the coordinate system.

$$\therefore \quad y(\theta,x) = x \tan\theta \tag{3.1}$$

The vertical distance from a point, x, on the x-axis to the platen surface is given by

$$y(\alpha,x) = x \tan\alpha \tag{3.2}$$

The resolved velocity, V_θ, along a line acting through the virtual apex is given by:

$$V_\theta = \dot{U}_x \cos\theta + \dot{U}_y \sin\theta \tag{3.3}$$

The velocity discontinuity at the die surface is therefore given by:

$$V_\alpha = \dot{U}_x \cos\alpha + \dot{U}_y \sin\alpha \tag{3.4}$$

Equation (3.3) and equation (3.4) are equally valid for the condition shown in Figure (3.4), which shows the neutral plane within the wedge, provided correct attention is paid to the sign of $\dot{U}_x$.

It remains to be shown that $\dot{U}_x$ and $\dot{U}_y$ can be expressed as a kinematically admissible velocity field. The following shows that the two obvious approaches are not successful:

a) Volume Continuity

The volume displaced in the y direction per unit time between x and x_n is given by:

$$b\,|x - x_n|\,|\dot{\xi}| \tag{3.5}$$

The volume displaced in the x-direction per unit time, assuming constant velocity in any yz plane is given by:

$$|\dot{U}_x|\,b\,y(\alpha,x) \tag{3.6}$$

$\therefore$ For volume continuity, Eqn. (3.5) = Eqn. (3.6).

$\therefore\ b|x-x_n|\,|\dot{\xi}| = |\dot{U}x|\ b\ y(\alpha,x)$, for positive α,

$$\therefore\ |\dot{U}_x| = |\dot{\xi}||x-x_n|\,\frac{\cot\alpha}{x}$$

Since $\dot{U}_x > 0$ when $x > x_n$ and $\dot{U}_x < 0$ when $x < x_n$ $\therefore \dot{U}_x = |\xi|\cot\alpha\left[1-\frac{x_n}{x}\right]$ (3.7)

The strain rate in the x-direction is given by:

$$\Sigma_{xx} = \frac{\delta U_x}{\delta_x} = |\dot{\xi}|\,\cot\alpha\,\frac{x_n}{x^2}$$

From volume continuity and the plane strain assumption:

$$\dot{\Sigma}_{yy} \triangleq -\Sigma_{xx} = -\,|\dot{\xi}|\,\mathrm{Cot}\alpha\,\frac{x_n}{x^2} = \frac{\delta \dot{U}y}{\delta y}$$

$$\therefore\ \dot{U}y = -|\dot{\xi}|\,\cos\alpha\,\frac{x_n}{x^2}\,y(\theta,x) + B(y(\theta,x))$$

from symmetry $\dot{U}y = 0$ at $\Theta = 0$

$$\therefore\ B(y(\theta,x)) = 0$$

$$\therefore\ \dot{U}y = -|\dot{\xi}|\ \mathrm{Cot}\alpha\,\frac{x_n}{x^2}\ y(\theta, x)$$

at $\theta = \alpha$, from eqn. (3.2)

$$\dot{U}y = = |\dot{\xi}| \cot\alpha \frac{x_n}{x^2} \times \tan\alpha$$

$$= - |\dot{\xi}| \frac{x_n}{x}$$

which, in general, violates the boundary condition:

$$\dot{U}y = \pm \dot{\xi} \quad \text{at } \theta = \mp \alpha$$

The velocity field derived from volume continuity is therefore inadmissible.

b) Prescribed velocity

By assuming that $\dot{U}y$ varies as the distance of y (θ,x) from $(x,0)$ a velocity can be prescribed.

$$\dot{U}y = - |\dot{\xi}| \cot\alpha \frac{y(\theta,x)}{x} \tag{3.8}$$

$$\therefore \dot{\Sigma}yy = \frac{\delta \dot{U}y}{\delta y} = - |\dot{\xi}| \frac{\cot\alpha}{x}$$

$$\therefore \dot{\Sigma}xx = - \dot{\Sigma}yy = |\dot{\xi}| \frac{\cot\alpha}{x} = \frac{\delta \dot{U}x}{\delta x}$$

$$\therefore \dot{U}_x = |\dot{\xi}| \cot\alpha \ \ln x + B(x) \tag{3.9}$$

When $x = x_n$, $\dot{U}x = 0$

$$\therefore B(x) = - |\dot{\xi}| \cot\alpha \ln x_n$$

$$\therefore \dot{U}_x = |\dot{\xi}| \cot\alpha \ln\left(\frac{x}{x_n}\right) \tag{3.10}$$

It can be seen that $\dot{U}_x < 0$ when $x < x_n$ as expected. The velocity field:

$$\dot{U}y = -|\dot{\xi}| \cot\alpha \frac{y(\theta,x)}{x}$$

$\dot{U}x = |\dot{\xi}|\cot\alpha \ln(\frac{x}{x_n})$ is, therefore, kinematically admissible.

The optimal position of x_n can be determined by minimising the power supplied through the platens, J*, with respect to x_n. This assumes that any additional constraint required to hold the wedge between the platens plays no part in the plastic deformation and, therefore, has no effect on the velocity field.

Referring to Avitzur[14] the internal power of deformation is given by:

$$W_i = \frac{2}{\sqrt{3}} \sigma_o \int_V \sqrt{\frac{1}{2} \dot{\Sigma}_{ij} \dot{\Sigma}_{ij}} \; dV$$

and the frictional power loss is given by:

$$W_t = \int_S \tau |\Delta V| \; ds$$

(see Section (2.1.3))

The total power of deformation is given by

$$J^* = W_i + W_f \qquad (3.11)$$

and

$$dV = 2b \; dx \; dy$$

From Eqn. (2.1):

$$\frac{1}{2} \dot{\Sigma}_{ij} \dot{\Sigma}_{ij} = \frac{1}{2}(\dot{\Sigma}^2_{xx} + \dot{\Sigma}^2_{yy} + \dot{\Sigma}^2_{zz}) + \dot{\Sigma}^2_{xy} + \dot{\Sigma}^2_{yz} + \dot{\Sigma}^2_{zx}$$

Now $\dot{\Sigma}_{zz} = \dot{\Sigma}_{yz} = \dot{\Sigma}_{zx} = 0$, since no strain occurs in the Z-direction.

$\therefore$ Eqn. (2.1) becomes:

$$\frac{1}{2} \dot{\Sigma}_{ij} \dot{\Sigma}_{ij} = \dot{\Sigma}^2_{xx} + \dot{\Sigma}^2_{xy}$$

since $\dot{\Sigma}_{xx}^{.2} = \dot{\Sigma}_{yy}^{.2}$

Now:

$$\dot{\Sigma}_{xy} = \frac{1}{2}\left(\frac{\delta\dot{U}x}{\delta u} + \frac{\delta\dot{U}y}{\delta x}\right)$$

$$= \frac{|\dot{\xi}|\cot\alpha}{2x^2} \qquad y(\theta,x), \text{ from}$$

Eqn. (3.8) and Eqn (3.10).

$$\therefore \quad W_i = \frac{4\sigma_o b}{\sqrt{3}} \int_y \int_x \sqrt{\frac{1}{2}\,\dot{\Sigma}_{ij}\dot{\Sigma}_{ij}}\; dx\, dy \qquad (3.12)$$

and $W_f = \int_s \tau|\Delta V|ds$

τ is the shear stress between the platen/wedge interface and is taken to be a constant proportion of the plane strain yield stress of the wedge. Avitzur[14] used this method of accounting for interfacial friction rather than Coulomb friction; this was primarily a matter of analytical convenience since it avoids the introduction of a second, unknown, principal stress into the power equation. This method of accounting for friction is used in the velocity fields to be superposed for both swaging and drawing, without the need to account for the different pressure distributions across the platen.

$$\therefore \quad \tau = \frac{m\sigma_o}{\sqrt{3}}$$

and $ds = \frac{2b\,dx}{\cos\alpha}$

$$\Delta V = V_\alpha = \dot{U}_x\cos\alpha + \dot{U}_y \sin\alpha$$

$$= |\dot{\xi}|\cot\alpha\left[\cos\alpha \ln\left(\frac{x}{x_n}\right) - \tan\alpha \sin\alpha\right]$$

$$\therefore \quad W_f = \frac{m\sigma_o}{\sqrt{3}} \int_x \left| |\dot{\xi}| \text{Cos}\alpha \left[\text{Cot}\alpha \ln\left(\frac{x}{x_n}\right) - \text{Tan}\alpha \, \text{Sin}\alpha \right] \right| \frac{2b \, dx}{\cos\alpha}$$

$$= \frac{2m\sigma_o}{\sqrt{3}} |\dot{\xi}| \text{Cot}\alpha b \int_x \left| \ln\left(\frac{x}{x_n}\right) - \text{Tan}^2\alpha \right| \, dx \qquad (3.13)$$

Since W_i is independent of X_n, it is only necessary to minimise W_f with respect to x_n in order to minimise J*.

Now, since $\frac{dW_t}{dx_n} = 0$, is independent of m it is reasonable to expect x_n to be a strong function of α and m as well as the reduction of area. This approach to the problem is therefore rejected.

3.1.3) Cylindrical coordinate system

The annular wedge shown in Figure (3.5) has a half angle, α, inner and outer radii R_f and R_o, with width, b.

A zero velocity RZ plane lies at an angle, α, from the instantaneous position of a rotating plate. It is assumed that the geometric form of the wedge during deformation remains that of an annular wedge. This implies that the radial velocity in any θZ plane is constant. The radius, R_N, is the position of a cylindrical plane where the radial velocity of the deforming material is zero.

$$\therefore \text{ when } R_N < R, \; \dot{U}_R << 0$$

$$\text{and } R_N > R, \; \dot{U}_R > 0.$$

It is further assumed that the deformation is in plane strain and occurs without block slip away from the origin of the coordinate system.

A vector, radius R, rotating about a fixed point at ω rad/sec generates an area of revolution in the Rθ plane at the rate

$$\frac{\omega R^2}{2}$$

The volume displaced in the θ direction per unit time between R and R_N is given by:

$$\frac{b}{2}\,\omega\left|R^2 - R_N^{\,2}\right|$$

Also the volume displaced in the R direction per unit time is given by:

$$b\left|\dot{U}_R\right| R\alpha$$

From the assumptions of incompressibility and plane strain these volume flow rates must be equal.

$$\therefore \left|\dot{U}_R\right| = \frac{\omega}{2R\alpha}\left|R^2 - R_N^{\,2}\right|$$

$$\therefore \dot{U}_R = \frac{\omega R}{2\alpha}\left[1 - \left(\frac{R_N}{R}\right)^2\right]$$

The RR strain rate is given by:

$$\dot{\Sigma}_{RR} = \frac{\delta \dot{U}_R}{\delta R} = \frac{\omega}{2\alpha}\left[1+\left(\frac{R_N}{R}\right)^2\right] \quad \text{and} \quad \dot{\Sigma}_\theta = \dot{\Sigma}_{RR} = \frac{\dot{U}_R}{R} + \frac{1}{R}\frac{\delta \dot{U}_\theta}{\delta \theta}$$

$$\frac{-\omega}{2\alpha}\left[1+\left(\frac{R_N}{R}\right)^2\right] = \frac{\omega}{2\alpha}\left[1-\left(\frac{R_N}{R}\right)^2\right] + \frac{1}{R}\frac{\delta \dot{U}_\theta}{\delta \theta}$$

$$\therefore \frac{\delta \dot{U}_\theta}{\delta \theta} = -\frac{\omega R}{\alpha}$$

$$\therefore \dot{U}_\theta = -\frac{\omega R}{\alpha} + B(\theta)$$

when $\theta = 0$, $\dot{U}_\theta = \omega R$

$$\therefore B(\theta) = \omega R$$

and $\dot{U}_\theta = \omega R\left\{1-\frac{\theta}{\alpha}\right\}$, which also satisfies the boundary conditions.

$\dot{U}_\theta = 0$ at $\theta = \alpha$ and $\dot{U}_\theta = \omega R$ at $\theta = 0$

Thus a kinematically admissible velocity field for wedge compression is given by:

$$\dot{U}_R = \frac{\omega R}{2\alpha}\left[1 - \left(\frac{R_N}{R}\right)^2\right] \qquad (3.14)$$

$$\dot{U}_\theta = \omega R \left[1 - \frac{\theta}{\alpha}\right] \qquad (3.15)$$

The optimal neutral radius position may be determined by minimising the total deformation power, J*, with respect to R_N.

The internal deformation power is given by:

$$W_i = \frac{2\sigma_o}{\sqrt{3}} \int_v \sqrt{\frac{1}{2}\dot{\Sigma}_{ij}\,\dot{\Sigma}_{ij}}\; dv$$

where:

$$\frac{1}{2}\,\dot{\Sigma}_{ij}\,\dot{\Sigma}_{ij} = \frac{1}{2}\left(\dot{\Sigma}^2_{RR} + \dot{\Sigma}^2_{\theta\theta} + \dot{\Sigma}^2_{zz}\right) + \dot{\Sigma}^2_{RZ} + \dot{\Sigma}^2_{Z\theta} + \dot{\Sigma}^2_{\theta R}$$

Now: $\dot{\Sigma}^2_{RR} = \dot{\Sigma}^2_{\theta\theta}$ and $\dot{\Sigma}_{ZZ} = \dot{\Sigma}_{RZ} = \dot{\Sigma}_{\theta R} = 0$

$$\therefore \sqrt{\frac{1}{2}\,\dot{\Sigma}_{ij}\,\dot{\Sigma}_{ij}} = \dot{\Sigma}_{RR}$$

and $dV = 2bRd\theta dR$

$$\therefore \dot{W}_i = \frac{2}{\sqrt{3}}\,\sigma_o \int_\theta \int_R \dot{\Sigma}_{RR}\, 2bRd\theta dR$$

$$= \frac{2\sigma_o\, b\omega}{\alpha\sqrt{3}} \int_\theta \int_R \left[R + \frac{R_N^2}{R}\right] dRd\theta$$

The two modes of deformation are defined by:

a) $R_N \in [R_f, R_o]$

and b) $R_N \leq R_f$

Since $\left[R + \frac{R_N^2}{R}\right]$ is continuous in the interval $[R_f, R_o]$ the internal power term will be the same for conditions (a) and (b) above, thus for half of the wedge :

$$W_i = \frac{2\sigma_o b\omega}{\sqrt{3}\,\alpha} \left[\frac{1}{2}(R_o^2 - R_f^2) + R_N^2 \ln\left(\frac{R_o}{R_f}\right)\right]_o^\alpha$$

$$\therefore = \frac{2\sigma_o b\omega}{\sqrt{3}} \left[\frac{R_o^2}{2}(1-(1-r)^2) + R_N^2 \ln\left(\frac{1}{1-r}\right)\right]$$

Frictional power loss at the die surface is given by:

$$W_f = \int \tau |\Delta V| dS$$

$\tau = \frac{m\sigma_o}{\sqrt{3}}$ as before and $ds = 2b\,dR$

$$|\Delta V| = |\dot{U}_R|\Big|_{\theta=\alpha} = \left|\frac{\omega R}{2\alpha}\left[1 - \left(\frac{R_N^2}{R}\right)\right]\right|$$

when $R_N \leq R_f$, $U_R \geq 0$

$$\therefore W_f = \frac{m\sigma_o}{\sqrt{3}} \int_{R_f}^{R_o} \frac{\omega R}{2\alpha}\left(1-\left(\frac{R_N^2}{R}\right)\right) 2b\, dR$$

$$= \frac{m\sigma_o \omega b}{\sqrt{3}\,\alpha}\left[\frac{R_o^2(1-(1-r)^2)}{2} - R_N^2 \ln\left(\frac{1}{1-r}\right)\right]$$

When $R_N \in [R_f, R_o]$, $|\dot{U}_R|$ is discontinuous at $R = R_N$.

$$\therefore W_f = \frac{bm\sigma_o \omega}{\sqrt{3}\,\alpha}\left\{\int_{R_N}^{R_o}\left[R - \frac{R_N^2}{R}\right] dR + \int_{R_n}^{R_f}\left[R - \frac{R_N}{R}\right] dR\right\}$$

$$= \frac{bm\sigma_o \omega}{\sqrt{3}\alpha}\left\{\frac{R_o^2}{2}(1+(1-r)^2) - R_N^2 + R_N^2 \ln\left(\frac{R_N^2}{R_o^2(1-r)}\right)\right\}$$

$\therefore$ when $R_n \leq R_f$

$$\frac{J^*}{2} = W_i + W_f$$

$$J^* = \frac{2\sigma_o\, b\omega}{\sqrt{3}} \left\{ \frac{R_o^2}{2} \left(1 - (1-r)^2\right) + R_N^2 \ln \left(\frac{1}{1-r}\right) \right\}$$

$$+ \frac{bm\, \sigma_o \omega}{\sqrt{3}\alpha} \left\{ \frac{R_o^2 (1-(1-r)^2)}{2} - R_N^2 \ln \left(\frac{1}{1-r}\right) \right\}$$

$$= \frac{2\sigma_o\, b\, \omega}{\sqrt{3}} \left\{ \frac{R_o^2}{2} (1-(1-r)^2) + R_N^2 \ln \left(\frac{1}{1-r}\right) + \right.$$

$$\left. \frac{m}{2\alpha} \left(\frac{R_o^2 (1-(1-r)^2)}{2} - R_N^2 \ln \left(\frac{1}{1-r}\right) \right) \right\}$$

$$\therefore \frac{dJ^*}{dR_N} = 0 = 2R_N \ln \left(\frac{1}{1-r}\right) \left\{1 - \frac{m}{\alpha}\right\}$$

Since $\ln \left(\frac{1}{1-r}\right) \neq 0$, $R_N = 0$ or $m = 2\alpha$

When $R \in \{R_f, R_o\}$

$$\frac{J^*}{2} = W_i + W_f$$

$$= \frac{2\sigma_o b\omega}{\sqrt{3}} \left\{ \frac{R_o^2}{2} (1- (1-r)^2) + R_N^2 \ln \left(\frac{1}{1-r}\right) \right\}$$

$$+ \frac{bm\sigma_o\, \omega}{\sqrt{3}\alpha} \left\{ \frac{R_o^2}{2} (1+(1-r)^2) - R_N^2 + R_N^2 \ln \left(\frac{R_N^2}{R_o^2 (1-r)} \right) \right\}$$

$$\therefore \frac{dJ^*}{dR_N} = 0 = 2R_N \ln \left(\frac{1}{1-r}\right) + \frac{m}{2\alpha} \left[- 2R_N + 2R_N \ln \left(\frac{R_N^2}{R_o^2 (1-r)} \right) + 2R_N \right]$$

$$\therefore \ln (1-r) = \frac{m}{\alpha} \ln \left(\frac{R_N^2}{R_o^2 (1-r)} \right)$$

$$\therefore R_N^2 = R_o^2 (1-r)^{\frac{m+2\alpha}{2m}}$$

Let $\beta = \frac{m + 2\alpha}{2m}$

$$\therefore R_N = R_o (1-r)^{\beta}$$

$\therefore$ When $R_N \leqslant R_f$, $R_N = 0$ or $m = 2\alpha$ (3.16)

and when $R_N \in [R_f, R_o]$, $R_N = R_o(1-r)^{\beta}$ (3.17)

The condition:

$R_N = R_f = R_o (1-r)^{\beta} \Rightarrow \beta = 1$

since $R_f = R_o (1-r)$

$\therefore \quad \beta = \frac{m+2\alpha}{2m} = 1 \Rightarrow \quad m = 2\alpha$

which is one of the conditions for the solution of:

$$\frac{dJ^*}{dR_N} = 0, \text{ when } R_N \leqslant R_f$$

Also $\lim_{\alpha \to 0} \beta = \frac{1}{2} \qquad [R_N \in [R_f, R_o], \ m \neq 0]$

It would appear, though not proven, that the above conditions imply

when $m < 2\alpha$, $R_N = 0$

and $m \geqslant 2\alpha$, $R_N = R_o(1-r)^{\beta}$

Referring to Figure (3.6), the conditions one might expect when bi-directional flow conditions apply are to be found, that is, high friction and low die angle.

The velocity field may therefore be written as:

$$\dot{U}_R = \frac{\omega R}{2\alpha} \quad (m<2\alpha) \tag{3.18}$$

$$\dot{U}_R = \frac{\omega R}{2\alpha} \left[1 - \left(\frac{R_o(1-r)^{\beta}}{R}\right)^2\right] (m > 2\alpha) \tag{3.19}$$

$$\dot{U}_\theta = \omega R \left|1 - \frac{\theta}{\alpha}\right| \tag{3.20}$$

Fig(3.6)-Effect Of Die Semi-Angle And Friction Upon The Flow Conditions In The Wedge

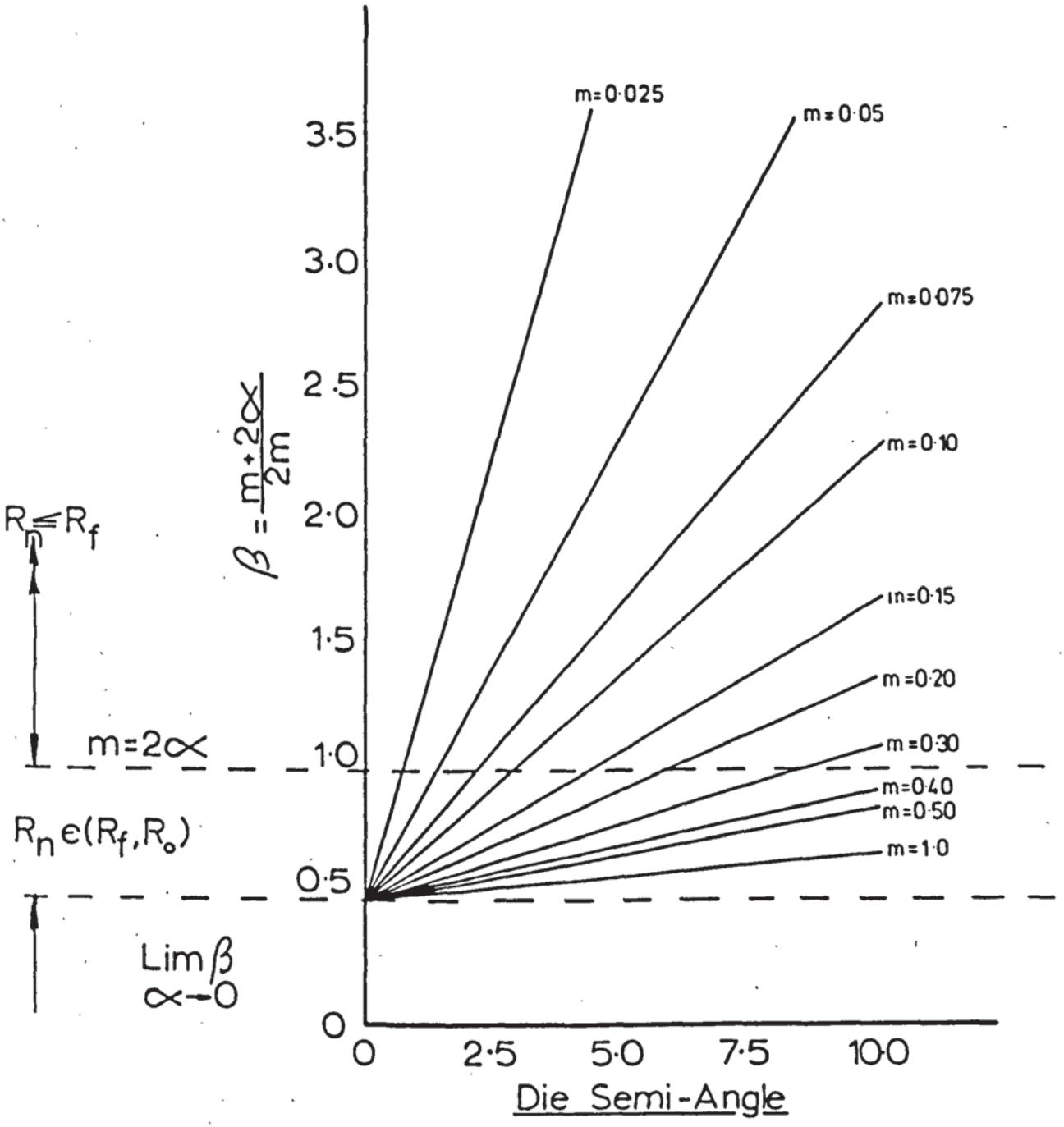

3.2) SWAGING OF PREFORMED STRIP

The preceding sections were concerned with finding a suitable velocity field for the swaging of a wide wedge. The swaging of a preformed strip takes this analysis one stage further, and uses the velocity field based upon the cylindrical polar coordinate system given in Eqn (3.18), Eqn (3.19) and Eqn (3.20). This implies that the deformation zone takes the form of an annular sector and that the terms for internal deformation power, W_i, and frictional power loss at the die surface, W_f, are the same as those for wedge compression.

It is assumed that, upon leaving the deformation zone, the metal flows parallel to the strip centre line, therefore, velocity discontinuities exist at the upstream and downstream boundaries of the deformation zone. These boundaries are denoted by S_1 and S_2 in Figure (3.7) and the associated power loss is given by:

$$W_{s_i} = \int_s \tau |\Delta V| dS \qquad (i = 1, 2)$$

$\tau = \frac{\sigma_o}{\sqrt{3}}$, $dS = Rbd\theta$, where R is the radius at the velocity discontinuity ΔV. When $R_N < R$ the velocity components, shown in Figure (3.8), $\dot{U}_R \text{ Tan } (\alpha-\theta)$ and $\dot{U}_\theta$, both act in the same direction and when $R_N > R$,

$\dot{U}_R \text{ Tan}(\alpha-\theta)$ and $\dot{U}_\theta$ oppose, as shown in Figure (3.9)

Therefore:

$$\dot{\Delta V} = \dot{U}_\theta + \dot{U}_R \text{ Tan } (\alpha-\theta)$$

$$= \omega R \left[1 - \frac{\theta}{\alpha}\right] + \frac{\omega R}{2\alpha}\left[1 - \left(\frac{R_N}{R}\right)^2\right] \tan(\alpha-\theta)$$

and

$$W_s \doteq \frac{\sigma_o}{\sqrt{3}} \int_\theta \left|\omega R\left[1 - \frac{\theta}{\alpha}\right] + \frac{\omega R}{2\alpha}\left[1-\left(\frac{R_N}{R}\right)^2\right] \tan(\alpha-\theta)\right| Rbd\theta$$

Fig(3.7)- Swaging Of Preformed Strip

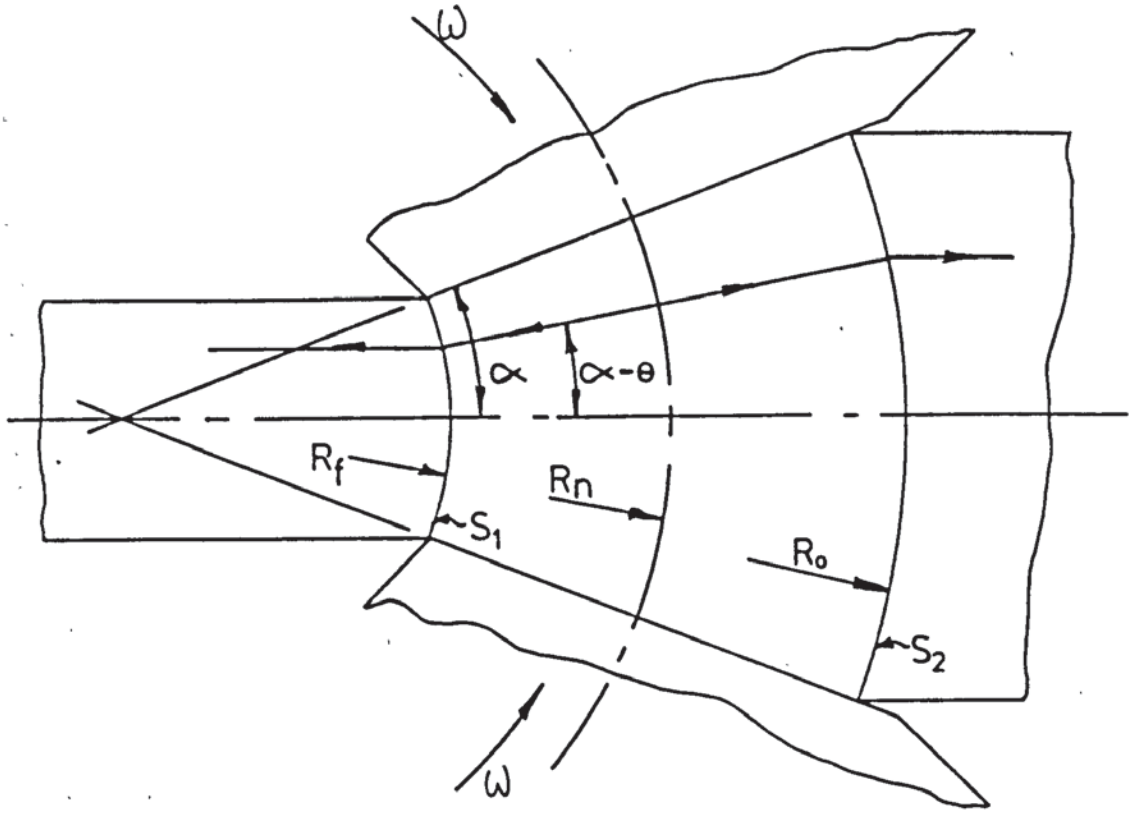

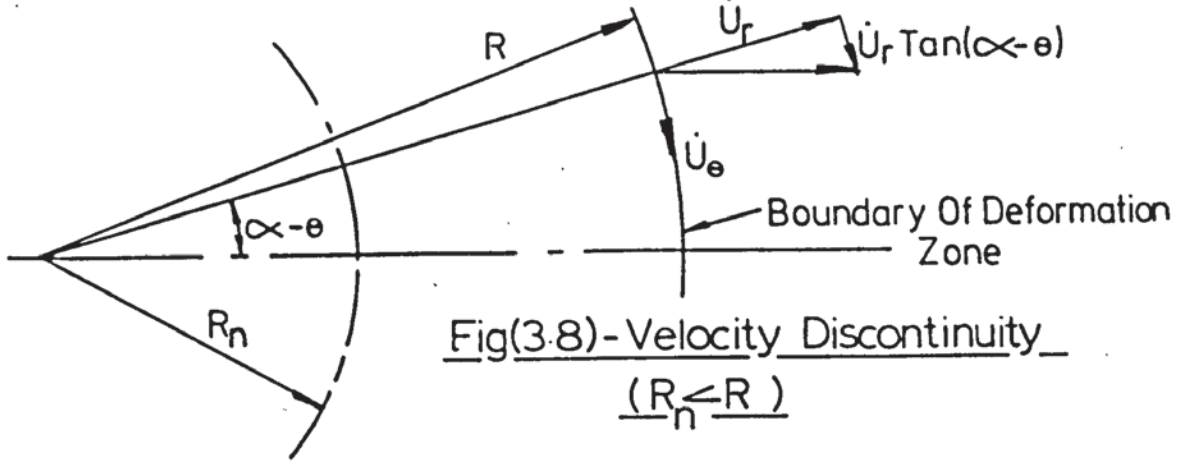

Fig(3.8)- Velocity Discontinuity
($R_n < R$)

Fig(3.9)- Velocity Discontinuity
($R_n > R$)

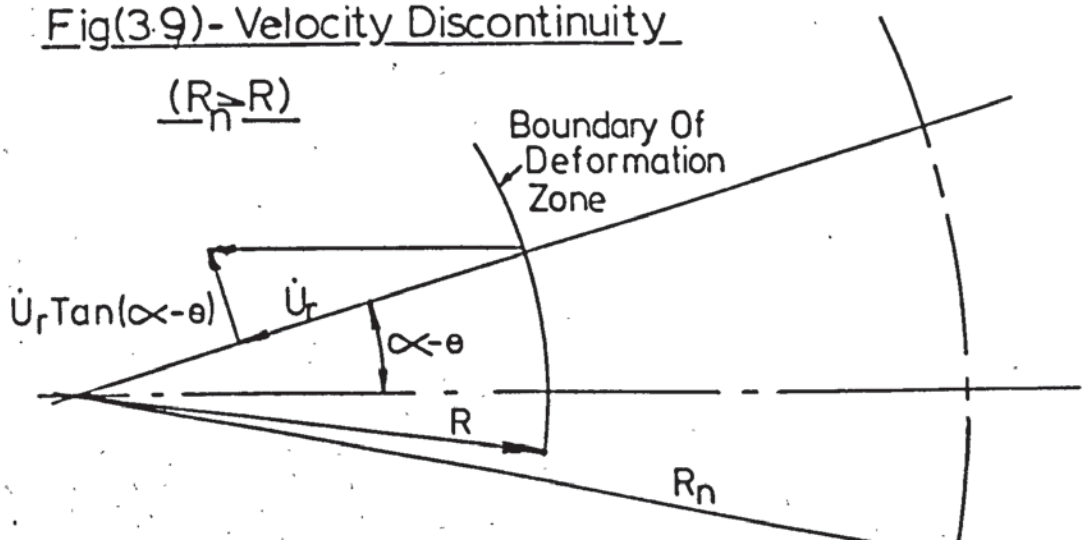

$$= \frac{\sigma_o R^2 b\omega}{\sqrt{3}} \int_{\theta=0}^{\alpha} \left| 1 - \frac{\theta}{\alpha} + \frac{\mathrm{Tan}(\alpha-\theta)}{2\alpha} \left[1 - \left(\frac{R_N}{R}\right)^2 \right] \right| d\theta \qquad (3.21)$$

Now $\theta < \alpha \lesssim 10^o$ $\therefore$ $\mathrm{Tan}(\alpha-\theta) \simeq (\alpha-\theta)$

$$\therefore W_s = \frac{\sigma_o R^2 b\omega}{\sqrt{3}} \int_{\theta=0}^{\alpha} \left| 1 - \frac{\theta}{\alpha} + \frac{(\alpha-\theta)}{2\alpha} \left[1 - \left(\frac{R_N}{R}\right)^2 \right] \right| d\theta \qquad (3.22)$$

$$\therefore W_{s2} = \frac{\sigma_o \omega R_o^2 b}{\sqrt{3}} \int_{0}^{\alpha} \left| 1 - \frac{\theta}{\alpha} + \frac{(\alpha-\theta)}{2\alpha} \left[1 - \left(\frac{R_N}{R_o}\right)^2 \right] \right| d\theta$$

$$= \frac{\sigma_o \omega R_o^2 b}{\sqrt{3}.2\alpha} \int_{o}^{\alpha} \left[2\alpha - 2\theta + (\alpha-\theta) \left[1 - \left(\frac{R_N}{R_o}\right)^2 \right] \right] d\theta$$

$$= \frac{\sigma_o \omega R_o^2 b}{\sqrt{3}.2\alpha} \left\{ 2\alpha\theta - \theta^2 + (\alpha\theta - \theta^2/2) \left[1 - \left(\frac{R_N}{R_o}\right)^2 \right] \right\}_o^{\alpha}$$

$$= \frac{\sigma_o \omega R_o^2 b}{\sqrt{3}.2\alpha} \{2\alpha^2 - \alpha^2 + (\alpha^2 - \alpha^2/2) \left[1 - \left(\frac{R_N}{R_o}\right)^2 \right]\}$$

$$= \frac{\sigma_o \omega R_o^2 b\alpha}{4\sqrt{3}} \{3 - \left(\frac{R_N}{R_o}\right)^2\} \qquad (3.23)$$

When $R < R_N$ the sign of ΔV can be positive or negative but cannot change sign in the interval $\theta \in (0,\alpha)$

$$\therefore W_{s_1} = \frac{\sigma_o \omega R_f^2 b\alpha}{4\sqrt{3}} \left| 3 - \left(\frac{R_N}{R_f}\right)^2 \right|$$

$$= \frac{\sigma_o \omega R_o^2 (1-r)^2 b\alpha}{4\sqrt{3}} \left| 3 - \left(\frac{R_N}{R_o(1-r)}\right)^2 \right| \qquad (3.24)$$

The total deformation power is given by:

$$J^* = 2(W_i + W_f + W_{s1} + W_{s2})$$

$$= \frac{4\sigma_o b\omega}{\sqrt{3}} \left[\frac{R_o^2}{2}(1-(1-r)^2) + R_N^2 \ln\left(\frac{1}{1-r}\right)\right]$$

$$+ \frac{2m\sigma_o \omega b}{\sqrt{3}\ \alpha} \left[\left(\frac{R_o^2(1-(1-r)^2)}{2} - R_N^2 \ln\left(\frac{1}{1-r}\right)\right) V\right.$$

$$\left.\left(\frac{R_o^2}{2}(1+(1-r)^2 - R_N^2\left[1 + \ln\left(\frac{R_N^2}{R_o^2(1-r)}\right)\right]\right)\right]$$

$$+ \frac{\sigma_o \omega R_o^2 b\alpha}{2\sqrt{3}} \left\{3 - \left(\frac{R_N}{R_o}\right)^2 + \left|3(1-r)^2 - \left(\frac{R_N}{R_o}\right)^2\right|\right\}$$

Let $x = \frac{R_N}{R_o}$

$$J^* = \frac{\sigma_o b\omega R_o^2}{\sqrt{3}} \left\{2(1-(1-r)^2) + 4x^2 \ln\left(\frac{1}{1-r}\right)\right.$$

$$+ \frac{m}{\alpha}\left[(1-(1-r)^2 - 2x^2 \ln\left(\frac{1}{1-r}\right)) V (1 + (1-r)^2 - 2x^2\left[1+\ln\left(\frac{x^2}{1-r}\right)\right])\right]$$

$$\left. + \frac{\alpha}{2}\left[3 - x^2 + \left|3(1-r)^2 - x^2\right|\right]\right\} \qquad (3.25)$$

The logical "OR" statement and the term with the modulus bracket in Eqn. (3.25) lead to the four possible conditions:

a) $3(1-r)^2 > x^2 \wedge R_N < R_f$

b) $3(1-r)^2 < x^2 \wedge R_N < R_f$

c) $3(1-r)^2 > x^2 \wedge R_N > R_f$

d) $3(1-r)^2 < x^2 \wedge R_N > R_f$

Only those terms in Eqn. (3.25) containing x will play any part in the minimisation of J*. Let these terms be denoted by:

$$K = 4x^2 \ln\left(\frac{1}{1-r}\right) - \frac{m}{\alpha}\left[2x^2\ln\left(\frac{1}{1-r}\right) \vee 2x^2\left[1+\ln\left(\frac{x^2}{1-r}\right)\right]\right]$$

$$+ \frac{\alpha}{2}\left[\,|3(1-r)^2 - x^2| - \dot{x}^2\right] \qquad (3.26)$$

Condition a) $\quad 3(1-r)^2 > x^2 \wedge R_N < R_f$

$$K_a = 4x^2\ln\left(\frac{1}{1-r}\right) - \frac{m}{\alpha}.2x^2\ln\left(\frac{1}{1-r}\right) + \frac{\alpha}{2}\left[3(1-r)^2 - 2x^2\right]$$

$$\frac{dK_a}{dx} = 8x\ln\left(\frac{1}{1-r}\right) - \frac{4mx}{\alpha}\ln\left(\frac{1}{1-r}\right) - 2x\alpha = 0$$

$\therefore$ $x = 0$ as expected since $R_N < R_f$

Now $3(1-r)^2 > x^2 \quad \wedge R_N < R_f$

$\Rightarrow \sqrt{3}(1-r) > x \wedge x < (1-r)$, which

is simply an overdefined form of

$$x < (1-r)$$

Condition b) $\quad 3(1-r)^2 < x^2 \wedge R_N < R_f$

This constraint system can be rewritten as:

$\sqrt{3}\,(1-r) < x \wedge x < (1-r)$, which is an invalid combination.

Condition c) $\quad 3(1-r)^2 > x^2 \wedge R_N > R_f$

$$K_c = 4x^2\ln\left(\frac{1}{1-r}\right) - \frac{2m}{\alpha}x^2\left[1 + \ln\left(\frac{x^2}{1-r}\right)\right] + \frac{\alpha}{2}\left[3(1-r)^2 - 2x^2\right]$$

$$\frac{dK_c}{dx} = 8x\ln\left(\frac{1}{1-r}\right) - \frac{4mx}{\alpha}\left[2 + \ln\left(\frac{x^2}{1-r}\right)\right] - 2x\alpha = 0$$

$$\therefore\ 4\ln\left(\frac{1}{1-r}\right) - \frac{2m}{\alpha}\left[2 + \ln\left(\frac{x^2}{1-r}\right)\right] - \alpha = 0$$

$$\therefore\ x^2 = (1-r)\exp\left\{\frac{2\alpha}{m}\left(\ln\left(\frac{1}{1-r}\right) - \frac{\alpha}{4}\right) - 2\right\}$$

$$\therefore\ x = (1-r)^{1/2}\exp\left\{\frac{\alpha}{m}\left(\ln\left(\frac{1}{1-r}\right) - \frac{\alpha}{4}\right) - 1\right\}$$

$$\therefore\ R_N = R_o(1-r)^{1/2}\exp\left\{\frac{\alpha}{m}\left(\ln\left(\frac{1}{1-r}\right) - \frac{\alpha}{4}\right) - 1\right\} \qquad (3.27)$$

Now:

$$3(1-r)^2 > x^2$$

$$\Rightarrow 3(1-r)^2 > (1-r)\exp\left\{\frac{2\alpha}{m}\left(\ln\left(\frac{1}{1-r}\right) - \frac{\alpha}{4}\right) - 2\right\}$$

$$= \frac{2 + \ln(3(1-r))}{2\left[\ln\left(\frac{1}{1-r}\right) - \frac{\alpha}{4}\right]} > \frac{\alpha}{m} \qquad (3.28)$$

and

$$R_N > R_f$$

$$\Rightarrow x > (1-r)$$

$$\Rightarrow (1-r)^{1/2}\exp\left\{\frac{\alpha}{m}\left(\ln\left(\frac{1}{1-r}\right) - \frac{\alpha}{4}\right) - 1\right\} > (1-r)$$

$$\Rightarrow \frac{\alpha}{m} > \frac{1/2\ln(1-r) + 1}{\ln\left(\frac{1}{1-r}\right) - \alpha/4} \qquad (3.29)$$

$$\therefore\ \frac{2 + \ln(3(1-r))}{2\ln\left(\frac{1}{1-r}\right) - \alpha/2} > \frac{\alpha}{m} > \frac{2 + \ln(1-r)}{2\ln\left(\frac{1}{1-r}\right) - \alpha/2} \qquad (3.30)$$

It can be seen that this constraint system is valid since:

$$\ln(3(1-r)) > \ln(1-r)$$

Condition d) $\quad 3(1-r)^2 < x^2 \wedge R_n > R_f$

$$K_d = 4x^2 \ln\left(\frac{1}{1-r}\right) - \frac{2mx^2}{\alpha}\left[1 + \ln\left(\frac{x^2}{1-r}\right)\right] + \frac{3\alpha(1-r)^2}{2}$$

$$\frac{dK_d}{dx} = 8x \ln\left(\frac{1}{1-r}\right) - \frac{4mx}{\alpha}\left[2 + \ln\left(\frac{x^2}{1-4}\right)\right] = 0$$

$$\therefore 2 \ln\left(\frac{1}{1-r}\right) = \frac{m}{\alpha}\left[2 + \ln\left(\frac{x^2}{1-r}\right)\right]$$

$$x^2 = (1-r) \exp\left\{\frac{2\alpha}{m} \ln\left(\frac{1}{1-r}\right) - 2\right\}$$

$$x = (1-r)^{1/2} \exp\left\{\frac{\alpha}{m} \ln\left(\frac{1}{1-r}\right) - 1\right\} \qquad (3.31)$$

$$\therefore R_N = R_o(1-r)^{1/2} \exp\left\{\frac{\alpha}{m} \ln\left(\frac{1}{1-r}\right) - 1\right\} \qquad (3.32)$$

Now:

$$3(1-r)^2 < x^2$$

$$=> 3(1-r)^2 < (1-r) \exp\left\{(2\ \alpha/m) \ln\left(\frac{1}{1-r}\right) - 2\right\}$$

$$=> \frac{2 + \ln(3(1-r))}{2 \ln\left(\frac{1}{1-r}\right)} < \frac{\alpha}{m} \qquad (3.33)$$

and: $\quad x > (1-r)$

$$=> (1-r)^{1/2} \exp\left\{\frac{\alpha}{m} \ln\ (1/1-r) - 1\right\} > (1-r)$$

$$=> \frac{\alpha}{m} \ln\left(\frac{1}{1-r}\right) - 1 > \frac{1}{2} \ln\ (1-r)$$

$$=> \frac{\alpha}{m} > \frac{2 + \ln\ (1-r)}{2 \ln\left(\frac{1}{1-r}\right)} \qquad (3.34)$$

The constraint system defined by relationships (3.33) and (3.34) is valid though (3.34) is redundant since:

$$\frac{\alpha}{m} > \frac{2 + \ln (3(1-r))}{2 \ln (1/1-r)} > \frac{2 + \ln (1-r)}{2 + \ln (1/1-r)}$$

The only relevant constraint is therefore defined by relationship (3.33).

3.3) Combined Drawing and Swaging

A kinematically admissible velocity field for the drawing of strip through inclined plates is given by Avitzur[14] as:

$$\dot{U}_R = \frac{-V_f R_f \cos \theta}{R}$$

$$\dot{U}_\theta = 0, \quad \text{as shown in Figure (3.10)}$$

where V_f is the draw speed. In this chapter V_f is used to denote the strip speed at the exit of the deformation zone, therefore the above velocity field will be defined in terms of the coiler velocity, V_c.

That is:

$$\dot{U}_R = - \frac{V_c R_f \cos\theta}{R} \qquad (3.29)$$

$$\dot{U}_\theta = 0 \qquad (3.30)$$

It is not possible simply to add the velocity fields for pure drawing and wedge compression to give the combined case, as this would yield:

$$\dot{U}_R = \frac{- V_c R_f \cos\theta}{R} + \frac{\omega R}{2a} \left\{1 - (R_N/R_f)^2\right\} \qquad (3.31)$$

which gives an instantaneous outlet velocity:

$$V_f = \dot{U}_R \sec\theta$$

Fig(3.10) - Kinematically Admissible Velocity Field for Strip Drawing[14]

$$= - V_c + \frac{\omega R_f}{2\alpha} \left\{1 - (R_N/R_f)^2\right\} \text{Sec}\theta$$

Since V_f is a function of θ, rigid body motion cannot prevail outside the deformation zone. The wedge compression velocity component of $\dot{U}_r$ must be proportional to $\text{Cos}\theta$ if this boundary condition is to be satisfied. A suitable velocity expression is given by:

$$\dot{U}_R = \frac{\omega R}{2\alpha} \left\{1 - (R_N/R)^2\right\} \text{Cos}\theta$$

$$\therefore \quad \dot{\Sigma}_{RR} = \frac{\delta \dot{U}_R}{\delta R} = \frac{\omega}{2\alpha} \left\{1 + (R_N/R)^2\right\} \cos\theta$$

and:

$$\dot{\Sigma}_{\theta\theta} = - \dot{\Sigma}_{RR} = \frac{\dot{U}_R}{R} + \frac{1}{R} \frac{\delta \dot{U}_\theta}{\delta \theta}$$

$$\therefore \quad - \frac{W}{2\alpha} \left\{1 + (R_N/R)^2\right\} \text{Cos}\theta = \frac{\omega \text{Cos}\theta}{2\alpha} \left\{1 - (R_N/R)^2\right\} + \frac{1}{R} \frac{\delta \dot{U}_\theta}{\delta \theta}$$

$$\therefore \quad \frac{\delta \dot{U}_\theta}{\delta \theta} = - \frac{\omega \text{Cos}\theta R}{\alpha}$$

$$\therefore \quad \dot{U}_\theta = - \frac{\omega \text{Sin}\theta R}{\alpha} + B(\theta)$$

$$\dot{U}_\theta = \omega R \text{ at } \theta = 0 \quad \therefore B(\theta) = \omega R$$

$$\therefore \dot{U}_\theta = \omega R \left\{1 - (\sin\theta/\alpha)\right\}$$

This equation violates the boundary condition $\dot{U}_\theta = 0$ at $\theta = \alpha$, though the small angle approximation can be applied, which yields:

$$\dot{U}_R = - V_c \frac{R_f}{R} + \frac{\omega R}{2\alpha} \left\{1 - (R_N/R)^2\right\} \qquad (3.32)$$

and $\dot{U}_\theta = \omega R\left\{1 - (\theta/\alpha)\right\}$ (3.33)

If this general superposition approach is to be used, in the absence of truly compatible velocity fields, one must either accept the violation of the boundary condition $\dot{U}_\theta = 0$ at $\theta = \alpha$, or, violation of the rigid body motion condition. The latter assumption leaves $\dot{U}_R$ independent of θ, thus eliminating the θR strain rate component which greatly simplifies the effective strain rate term, $1/2\dot{\Sigma}_{ij}\,\dot{\Sigma}_{ij}$.

It is for the sake of analytical simplicity that the velocity field given in equations (3.32) and (3.33) have been used in the following theoretical examination of the combined drawing and swaging of strip.

The terms for the individual components of power dissipation in combined drawing and swaging are

a) Internal Power of Deformation

$$W_i = \frac{2\sigma_o}{\sqrt{3}} \int_V \sqrt{\frac{1}{2}\,\Sigma_{ij}\,\Sigma_{ij}}\; dV$$

$$\frac{1}{2}\,\dot{\Sigma}_{ij}\,\dot{\Sigma}_{ij} = \tfrac{1}{2}(\dot{\Sigma}_{RR}^{\,2} + \Sigma_{\theta\theta}^2 + \Sigma_{zz}^2) + \dot{\Sigma}_{R\theta}^{\,2} + \dot{\Sigma}_{\theta z}^{\,2} + \dot{\Sigma}_{ZR}^2$$

$$\dot{\Sigma}_{RR} = \frac{\delta \dot{U}_R}{\delta R} = \frac{V_c\, R_f}{R^2} + \frac{\omega}{2\alpha}\left\{1 + (R_N/R)^2\right\}$$

From eqn (3.32)

$$\dot{\Sigma}_{\theta\theta} = \frac{\dot{U}_R}{R} + \frac{1}{R}\frac{\delta \dot{U}_\theta}{\delta \theta} = -\dot{\Sigma}_{RR} = -\left[\frac{V_c\, R_f}{R^2} + \frac{\omega}{2\alpha}\left\{1 + (R_N/R)^2\right\}\right]$$

These are the only non-zero strain rate components

$$\therefore \sqrt{\tfrac{1}{2}\dot{\Sigma}_{ij}\dot{\Sigma}_{ij}} = \dot{\Sigma}_{RR}$$

and $dV = bRdRd\theta$

$$\therefore W_i = \frac{2\sigma_o}{\sqrt{3}} \int_\theta \int_R \left\{ \frac{V_c R_f}{R^2} + \frac{\omega}{2\alpha} \left\{ 1 + (R_N/R)^2 \right\} \right\} b R dR d\theta$$

$$= \frac{2\sigma_o b}{\sqrt{3}} \int_\theta \int_R \left\{ \frac{V_c R_f}{R} + \frac{\omega}{2\alpha} \left\{ R + (R_N^2/R) \right\} \right\} dR d\theta$$

$$= \frac{2\sigma_o b}{\sqrt{3}} \int_{-\alpha}^{\alpha} \left\{ V_c R_f \ln R + \frac{\omega}{2\alpha} \left\{ R^2/2 + R_N^2 \ln R \right\} \right\}_{R_f}^{R_o} d\theta$$

$$= \frac{4\sigma o b \alpha}{\sqrt{3}} \left\{ V_c R_o (1-r) \ln\left(\frac{1}{1-r}\right) + \frac{\omega}{2\alpha} \left\{ R_o^2 r(2-r)/2 + R_N^2 \ln \left(\frac{1}{1-r}\right) \right\} \right\}$$

In order that a comparison can be made between the theoretical model and physical situation, the instantaneous angular velocity of the dies, ω, must be approximated from the axial displacement of the dies, $\dot{\xi}$

It is assumed that the die velocity, $\dot{\xi}$, is equal to the lateral, i.e. vertical component of the mean velocity $\bar{\dot{U}}_\theta\Big|_{\theta=0}$, that is:

$$\bar{\dot{U}}_\theta\Big|_{\theta=0} \cos\alpha = \frac{\omega(R_o + R_f)\cos\alpha}{\alpha} = \dot{\xi}$$

$$\therefore \dot{\xi} = \frac{\omega R_o (2-r)\cos\alpha}{2}$$

$$\therefore \dot{\omega} \simeq \frac{2\dot{\xi}}{R_o(2-r)} \qquad (3.34)$$

$\therefore$ the internal power of deformation becomes:

$$W_i = \frac{4\sigma o b \alpha}{\sqrt{3}} \left\{ V_c R_o (1-r) \ln\left(\frac{1}{1-r}\right) + \frac{\dot{\xi}}{R_o(2-r)\alpha} \left\{ \frac{R_o^2 r(2-r)}{2} + R_N^2 \ln \left(\frac{1}{1-r}\right) \right\} \right\}$$

$$= \frac{4\sigma_o b\alpha R_o}{\sqrt{3}} \left\{ V_c(1-r) \ln\left(\frac{1}{1-r}\right) + \frac{\dot{\xi}}{(2-r)\alpha} \left\{ \frac{r(2-r)}{2} + \left(\frac{R_N}{R_o}\right)^2 \ln\left(\frac{1}{1-r}\right) \right\} \right\} \quad (3.35)$$

b) Frictional Power Dissipated at the Die-Strip Interface

The frictional power dissipated at the die surface is given by:

$$W_f = \int_s \tau |\Delta V| ds$$

$$\tau = \frac{m\sigma_o}{\sqrt{3}} \quad \text{and} \quad ds = bdR$$

From Eqn (3.32)

$$\Delta V = \dot{U}_R = \frac{\omega R}{2\alpha} \left\{ 1 - (R_N/R)^2 \right\} - V_c \frac{R_f}{R}$$

From (3.34):

$$\Delta V = \dot{U}_R = \frac{\dot{\xi} R}{R_o(2-r)\alpha} \left\{ 1 - (R_N/R)^2 \right\} - \frac{V_c R_f}{R}$$

$$= \frac{\dot{\xi}\{R - R_N^2/R\}}{R_o(2-r)\alpha} - \frac{V_c R_f}{R}$$

$$W_f = \int_R \frac{m\sigma_o}{\sqrt{3}} \left| \frac{\dot{\xi}\{R - R_N^2/R\}}{R_o(2-r)\alpha} - \frac{V_c R_f}{R} \right| bdR$$

$$= \frac{bm\sigma_o}{\sqrt{3}} \int_R \left| \frac{\dot{\xi}\{R - R_N^2/R\}}{R_o(2-r)\alpha} - \frac{V_c R_f}{R} \right| dR \quad (3.36)$$

When the term inside the modulus bracket is equal to zero the integral is discontinuous, which occurs at the neutral radius, R_N^*, for the combined drawing and swaging case. That is:

$$\frac{\dot{\xi}\{R_N^* - R_N^2/R_N^*\}}{R_o(2-r)\alpha} = \frac{V_c R_f}{R_N^*}$$

$$\therefore R_N^* = \left\{ V_c R_o^2 (2-r)(1-r)\alpha/\dot{\xi} + R_N^2 \right\}^{\frac{1}{2}} \qquad (3.37)$$

or, dividing throughout by R_o:

$$\frac{R_N^*}{R_o} = \left\{ V_c (2-r)(1-r)\alpha/\dot{\xi} + x^2 \right\}^{\frac{1}{2}} \qquad (3.38)$$

The addition of a negative drawing velocity to the wedge compression velocity field may move the neutral radius to $R_N^* > R_o$. There are, therefore, three possible frictional conditions dependent upon the relative value of R_N^*, that is:

$$R_N^* < R_f$$

$$R_f < R_N^* < R_o$$

$$R_N^* > R_o$$

For $R_N^* > R_o$ and $R_N^* < R_f$, Eqn. (3.36) becomes:

$$W_f = \frac{bm\sigma o}{\sqrt{3}} \int_{R_f}^{R_o} \left| \frac{\dot{\xi} \left\{ R - R_N^2/R \right\}}{R_o (2-r)\alpha} - \frac{V_c R_f}{R} \right| dR$$

$$= \frac{bm\sigma o}{\sqrt{3}} \left\{ \left| \frac{\dot{\xi} \left\{ \tfrac{1}{2}R^2 - R_N^2 \ln R \right\}}{R_o (2-r)\alpha} - V_c R_f \ln R \right| \right\}_{R_f}^{R_o}$$

$$= \frac{bm\sigma o}{\sqrt{3}} \left\{ \left| \frac{\dot{\xi} \left\{ \tfrac{1}{2}(R_o^2 - R_f^2) - R_N^2 \ln \left(\frac{R_o}{R_f}\right) \right\}}{R_o (2-r)\alpha} - V_c R_o (1-r) \ln \left(\frac{R_o}{R_f}\right) \right| \right\}$$

$$= \frac{bm\sigma o\, R_o}{\sqrt{3}} \left\{ \left| \frac{\dot{\xi} \left\{ \tfrac{1}{2}r(2-r) - x^2 \ln \left(\frac{1}{1-r}\right) \right\}}{(2-r)\alpha} - V_c (1-r) \ln \left(\frac{1}{1-r}\right) \right| \right\} \qquad (3.39)$$

For $R_f < R_N^* < R_o$ Eqn (3.36) becomes:

$$W_f = \frac{bm\sigma o}{\sqrt{3}} \left[\int_{R_N^*}^{R_o} \left\{ \frac{\dot{\xi} \left\{ R - R_N^2/R \right\}}{R_o (2-r)\alpha} - \frac{V_c R_o (1-r)}{R} \right\} dR \right.$$

$$+\int_{R_N^*}^{R_f}\left\{\frac{\dot{\xi}\{R-R_N^2/R\}}{R_o(2-r)\alpha} - \frac{V_o R_o(1-r)}{R}\right\} dR\Bigg]$$

$$= \frac{bm\sigma o}{\sqrt{3}}\Bigg[\left[\frac{\dot{\xi}\{\frac{1}{2}R^2-R_N^2 \ln R\}}{R_o(2-r)\alpha} - V_c \dot{R_o}(1-r)\ln R\right]_{R_N^*}^{R_o}$$

$$+\left[\frac{\dot{\xi}\{\frac{1}{2}R^2-R_N^2 \ln R\}}{R_o(2-r)\alpha} - V_c R_o(1-r)\ln R\right]_{R_N^*}^{R_f}\Bigg]$$

$$= \frac{bm\sigma o}{\sqrt{3}}\Bigg[\frac{\dot{\xi}\{\frac{1}{2}(R_o^2-R_N^{*2}) - R_N^2 \ln(\frac{R_o}{R_N^*})\}}{R_o(2-r)\alpha} - V_c R_o(1-r)\ln(\frac{R_o}{R_N^*})$$

$$+\frac{\dot{\xi}\{\frac{1}{2}(R_f^2 - R_N^{*2}) - R_N^2 \ln(\frac{R_f}{R_N^*})\}}{R_o(2-r)\alpha} - V_c R_o(1-r)\ln(\frac{R_f}{R_N^*})\Bigg]$$

Substituting for R_N^* and extracting R_o with

$P = V_c(2-r)(1-r)\alpha/\dot{\xi}$ so that

$$\frac{R_N^*}{R_o} = [P+x]^{\frac{1}{2}} \qquad (3.40)$$

$$\therefore W_f = \frac{bm\sigma_o R_o}{\sqrt{3}}\Bigg[\frac{\dot{\xi}\{\frac{1}{2}(1-(P+x)) - x^2 \ln\frac{1}{\sqrt{(P+x)}}\}}{(2-r)\alpha} - V_c(1-r)\ln\frac{1}{\sqrt{(P+x)}}$$

$$+\frac{\dot{\xi}\{\frac{1}{2}((1-r)^2-(P+x)) - x^2\ln(\frac{1-r}{\sqrt{(P+x)}})\}}{(2-r)\alpha} - V_c(1-r)\ln(\frac{1-r}{\sqrt{(P+x)}})\Bigg] \qquad (3.41)$$

which applies for $R_f < R_N^* < R_o$

Eqns. (3.39) and (3.41) therefore represent the three possible conditions for the frictional power loss at the strip/die interface. These equations can be combined and further simplified in terms of the parameters P and x.

$$W_f = \frac{bm\sigma_o R_o \dot{\xi}}{\sqrt{3}\,(2-r)\alpha}\left\{\left|\tfrac{1}{2}r(2-r) - x^2\ln\left(\frac{1}{1-r}\right) - P\ln\left(\frac{1}{1-r}\right)\right| V \cdot \right.$$

$$\left[\tfrac{1}{2}(1-(P+x)) - x^2\ln\left(\frac{1}{\sqrt{(P+x)}}\right) - P\ln\left(\frac{1}{\sqrt{(P+x)}}\right)\right.$$

$$\left.\left. + \tfrac{1}{2}\left((1-r)^2 - (P+x)\right) - x^2\ln\left(\frac{1-r}{\sqrt{(P+x)}}\right) - P\ln\left(\frac{1-r}{\sqrt{(P+x)}}\right)\right]\right\}$$

$$\therefore W_f = \frac{bm\sigma_o R_o \dot{\xi}}{\sqrt{3}(2-r)\alpha}\left\{\left|\tfrac{1}{2}\,r(2-r) - (x^2 + P)\ln\left(\frac{1}{1-r}\right)\right|\right.$$

$$\left. V\left[(x^2 + P)\ln\left(\frac{P+x}{1-r}\right) - \tfrac{1}{2}\left\{2(P+x) + r(2-r)\right\}\right]\right\} \qquad (3.42)$$

d) Power loss at the Inlet and Outlet of the Deformation Zone

The power loss at each of the velocity discontinuities that bound the entry and outlet of the deformation zone is given, in general, by:

$$W_s = \int_s \xi|\Delta V|ds, \text{ where}$$

$\xi = \frac{\sigma_o}{\sqrt{3}}$ and $ds = bRsd\theta$, R_s being the radius at the velocity discontinuity in question. Since R_N* can be greater than R_o, the sign of the tangential velocity discontinuity at the inlet or outlet of the deformation zone can be positive or negative.

Now, $\Delta V = \dot{U}_\theta + U_R \,\mathrm{Tan}(\alpha-\theta)$

$$= \omega R_s \left\{1 - \frac{\theta}{\alpha}\right\} + \left[\frac{\omega R_s}{2\alpha} \left[1 - \left(\frac{R_N}{R_S}\right)^2\right] - V_c \frac{R_o(1-r)}{R_s}\right] \tan(\alpha-\theta)$$

Substituting from equation (3.34)

$$\therefore \Delta V = \frac{2\dot{\xi} R_s}{R_o(2-r)} \left[1 - \frac{\theta}{\alpha}\right] + \left[\frac{\dot{\xi} R_s}{R_o(2-r)\alpha} \left[1 - \left(\frac{R_N}{R_s}\right)^2\right] - \frac{V_c R_o(1-r)}{R_S}\right] \text{Tan}(\alpha-\theta)$$

For small θ, $\text{Tan}(\alpha-\theta) \Omega (\alpha-\theta)$

$$\therefore \Delta V = \frac{\dot{\xi}\,\alpha}{R_o(2-r)} \left\{\frac{2R_s}{\alpha} \left\{1 - \frac{\theta}{\alpha}\right\} + \left[\frac{R_S}{\alpha} \left[1 - (R_N/R_S)^2\right] - \frac{PR_o^2}{R_S}\right] (\alpha-\theta)\right\}$$

$$\therefore W_s = \frac{\dot{\sigma}_o}{\sqrt{3}} \int_\theta \frac{\dot{\xi}\alpha}{R_o(2-r)} \left|\frac{2R_s}{\alpha} \left\{1 - \frac{\theta}{\alpha}\right\} + \left[\frac{R_S}{\alpha} \left\{1 - \left(\frac{R_N}{R_S}\right)^2\right\} - \frac{PR_o^2}{R_S}\right] (\alpha-\theta)\right| bR_s d\theta$$

$$\therefore W_s = \frac{\sigma s\, \dot{\xi}\alpha\, bR_s}{\sqrt{3}\, R_o(2-r)} \int_\theta \left| \frac{2R_s}{\alpha} \left\{1 - \frac{\theta}{\alpha}\right\} + \left[\frac{R_s}{\alpha} \left\{1 - \left(\frac{R_N}{R_S}\right)^2\right\} - \frac{PR_o^2}{R_s}\right] (\alpha-\theta)\right| d\theta$$

$$= \frac{2\sigma o \dot{\xi}\alpha b\, R_s}{\sqrt{3}\, R_o(2-r)} \left[\left|\frac{2\, R_s}{\alpha} \left[\theta - \frac{\theta^2}{2\alpha}\right] + \left[\frac{R_s}{\alpha} \left\{1 - \left(\frac{R_N}{R_s}\right)^2\right\} - \frac{P\, R_o}{R_s}\right] \left(\alpha\theta - \frac{\theta^2}{2}\right)\right|\right]_o^\alpha$$

$$= \frac{2\sigma o \dot{\xi}\alpha\, b\, R_s^2}{\sqrt{3}\ R_o(2-r)} \left|1 + \frac{\alpha}{2} \left\{1 - (R_N/R_s)^2\right\} - \frac{\alpha^2 P\, R_o^2}{2\, R_s^2}\right| \qquad (3.42)$$

$\therefore$ For $R_s = R_o$

$$W_{s_2} = \frac{2\sigma o \dot{\xi}\alpha b\, R_o}{\sqrt{3}\ (2-r)} \left| 1 + \frac{\alpha}{2} \left\{1 - x^2\right\} - \frac{\alpha^2 P}{2}\right| \qquad (3.43)$$

and for $R_s = R_f$

$$W_{s_1} = \frac{2\sigma_o \dot{\xi} \alpha b \, R_o (1-r)^2}{\sqrt{3} \quad (2-r)} \left| 1 + \frac{\alpha}{2} \left[1 - \frac{x^2}{(1-r)^2} \right] - \frac{\alpha^2 P}{2(1-r)^2} \right| \qquad (3.44)$$

The total deformation power, $\dot{J}^*$, for combined drawing and swaging can be expressed both in terms of the power required to deform the metal and in terms of the power supplied to the system.

The power supplied to the system is given by:

$\dot{J}^* = \sum$ (Instantaneous functions for velocity x material yield stress) for the tag load and die pressure.

$$= 2(\sigma_f b t_f \dot{U}_R \Big|_{R=R_f} \sec(\alpha-\theta)$$

$$+ \sigma_\theta b (R_o - R_f \dot{\xi}) \qquad (3.45)$$

Assuming that σ_f and σ_θ are principal stresses then, using the von Mises yield criterion:

$$\sigma_\theta = \frac{2\sigma_o}{\sqrt{3}} - \sigma_f$$

From equations (3.45) and (3.32) at $R = R_f$.

$$\dot{J}^* = 2 \left\{ \sigma_f b t_f \left\{ \frac{\omega R_t}{2\alpha} \left(1 - \left(\frac{R_N}{R_f}\right)^2\right) - V_c \right\} \right.$$

$$\left. + \left(\frac{2\sigma_o}{\sqrt{3}} - \sigma_f\right) b \, (R_o - R_f) \, \dot{\xi} \right\}$$

$$= 2\left\{\sigma_f b t_f \left[\frac{\dot{\xi} R_f}{R_o (2-r)\alpha} \left(1 - \left(\frac{R_N}{R_f}\right)^2\right) - V_c \right]\right.$$

$$+ \frac{2\sigma_o}{\sqrt{3}} \; b\,(R_o - R_f)\,\dot{\xi} - \sigma_f b(R_o - R_f)\dot{\xi}\,\}$$

$$\therefore\; J^* = 2\sigma_f b\, R_o \left\{(1-r)\alpha \left[\frac{\dot{\xi}(1-r)}{(2-r)\alpha}\left(1 - \left(\frac{R_N}{R_f}\right)^2\right) - V_c\right]\right.$$

$$\left. - r\dot{\xi}\right\} + \frac{4\sigma_o}{\sqrt{3}}\; b\, R_o r\, \dot{\xi}\,. \qquad (3.46)$$

The deformation power is also given by:

$$J^* = W_i + 2\,(W_f + W_{sR_o} + W_{sR_f}) \qquad (3.47)$$

By equating the two expressions for J* the instantaneous draw stress, normalised with respect to draw stress, can be determined.

From equation (3.47)

$$J^* = \frac{4\sigma_o b\alpha\, R_o}{\sqrt{3}} \left\{V_c(1-r)\,\ln\left(\frac{1}{1-r}\right) + \frac{\dot{\xi}}{(2-r)\alpha}\left[\frac{r\,(2-r)}{} + \left(\frac{R_N}{R_o}\right)^2 \ln\left(\frac{1}{1-r}\right)\right]\right\}$$

$$+ 2\left\{\frac{bm\sigma_o R_o \dot{\xi}}{\sqrt{3}(2-r)\alpha}\left[\left|\tfrac{1}{2}r(2-r) - (x^2 - P)\,\ln\left(\frac{1}{1-r}\right)\right|\right.\right.$$

$$\left.\left. V\left\{x^2 + P)\,\ln\left(\frac{P+x}{1-r}\right) - \tfrac{1}{2}\;2(P+x) + r(2-r)\right\}\right]\right\}$$

$$+ \frac{2\sigma_o \dot{\xi}\alpha b\, R_o}{\sqrt{3}(2-r)}\left|1 + \frac{\alpha}{2}\left\{1 - x^2\right\} - \frac{\alpha^2 P}{2}\right|$$

$$+ \frac{2\sigma_o\, \dot{\xi}\alpha b\, R_o(1-r)^2}{\sqrt{3}\,(2-r)}\left|1 + \frac{\alpha}{2}\left(1 - \frac{x^2}{(1-r)^2}\right) - \frac{\alpha^2 P}{2(1-r)^2}\right|\Bigg\} \qquad (3.48)$$

Equating (3.46) and (3.48):

$$J^* = 2\sigma_f b\, R_o \left\{(1-r)\alpha \left[\frac{\dot{\xi}(1-r)}{(2-r)\alpha}\left(1 - \left(\frac{R_N}{R_f}\right)^2\right) - V_c\right] - r\dot{\xi}\right\} + \frac{4\sigma_o}{\sqrt{3}}\, b\, R_o r\, \dot{\xi}$$

$$\frac{\sigma_f}{\sigma_o/\sqrt{3}} = \left\{2\left\{\alpha V_c(1-r)\ln\left(\frac{1}{1-r}\right) + \frac{\dot{\xi}}{(2-r)}\left[\frac{r\,(2-r)}{2} + \left(\frac{R_N}{R_o}\right)^2 \ln\left(\frac{1}{1-r}\right)\right]\right\}\right.$$

$$+ \frac{m\,\dot{\xi}}{(2-r)\alpha}\left\{\left|\tfrac{1}{2}r\,(2-r) - (x^2+P)\ln\left(\frac{1}{1-r}\right)\right|V\left\{(x^2+P)\ln\left(\frac{P+x}{1-r}\right)\right.\right.$$

$$\left.\left. - \tfrac{1}{2}\left(2(P+x) + r\,(2-r)\right)\right\}\right\|$$

$$+ \frac{\dot{2\xi}\alpha}{(2-r)}\left|1 + \frac{\alpha}{2}\left\{1 - x^2\right\} - \frac{\alpha^2 P}{2}\right| + \frac{2\dot{\xi}\alpha(1-r)^2}{(2-r)}\left|1 + \frac{\alpha}{2}\left\{1 - \frac{x^2}{(1-r)^2}\right\}\right.$$

$$\left. - \frac{\alpha^2 P}{2(1-r)^2}\right| + 4r\dot{\xi}\Bigg\} \cdot \frac{1}{(1-r)\alpha\left\{\frac{\dot{\xi}(1-r)}{(2-r)\alpha}\left(1 - \left(\frac{R_N}{R_f}\right)^2\right) - V_c\right\}} \qquad (3.49)$$

3.4. Tube Drawing Analogue

The configuration of the tooling for the tube drawing analogue is shown in Figure (3.11); it is assumed that the velocity field is similar to that for strip drawing through vibrating dies. It is further assumed that the frictional constraint at the plug/strip interface does not affect metal flow.

Fig(3.11)-Tube Drawing Analogue

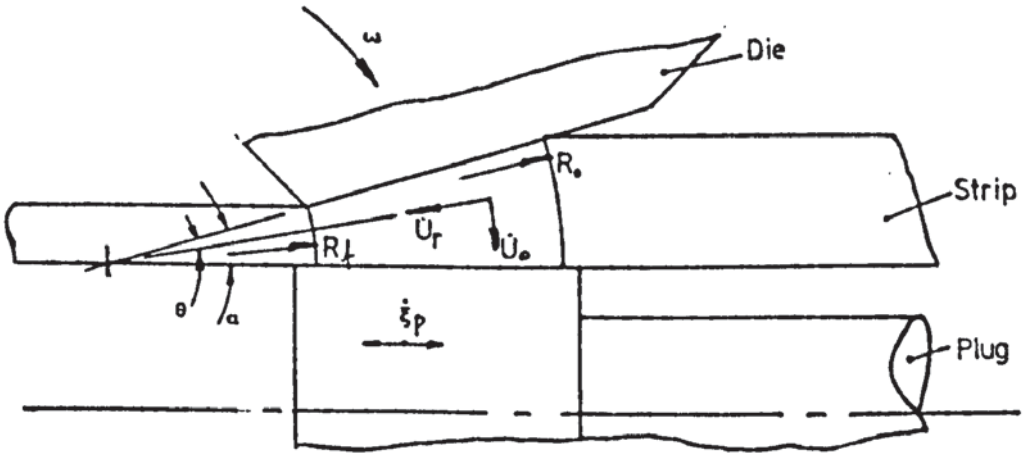

Now, restating the approximation for ω(Eqn.(3.34))

$$\omega \simeq \frac{2\dot{\xi}}{R_o(2-r)}$$

$$\text{also } \dot{U}_R = \frac{\omega R}{2\alpha}\left[1 - \left(\frac{R_N}{R}\right)^2\right] - V_c\,\frac{R_o(1-r)}{R}$$

$\dot{\xi}_p = \dot{\xi}_{p\,max}\,\text{Cos}(wt + \phi)$, the instantaneous plug velocity.

ϕ = Displacement phase angle between the die and plug.

The velocity discontinuity at the strip/plug interface is given by:

$$\Delta V = \frac{\omega R}{2\alpha}\left[1 - \left(\frac{R_N}{R}\right)^2\right] - \frac{V_c\,R_o(1-r)}{R} - \dot{\xi}_p$$

$$\simeq \frac{2\dot{\xi}}{R_o(2-r)} \cdot \frac{R}{2\alpha}\left[1 - \left(\frac{R_N}{R}\right)^2\right] - \frac{V_c R_o (1-r)}{R} - \dot{\xi}p$$

$$= \frac{R\dot{\xi}}{R_o(2-r)}\left[1 - \left(\frac{R_N}{R}\right)^2\right] - \frac{V_c R_o (1-r)}{R} - \dot{\xi}p \qquad (3.50)$$

The frictional power loss at the strip/plug interface is therefore given by:

$$W_{f_p} = \frac{m\sigma_o}{\sqrt{3}} \int_S |\Delta V| ds \qquad (3.51)$$

Substituting equation (3.50) into (3.51):

$$\therefore \quad W_{f_p} = \frac{m\sigma_o b}{\sqrt{3}} \int_R \left| \frac{R\dot{\xi}}{R_o(2-r)\alpha}\left[1 - \left(\frac{R_N}{R}\right)^2\right] - \frac{V_c R_o(1-r)}{R} - \dot{\xi}p \right| dR$$

This integral is discontinuous at $R = R^*_{N_p}$, the point of zero velocity when taking account of plug velocity.

$\therefore$ When $\Delta V = 0$, $R = R^*_{N_p}$

$$\therefore \quad \frac{\dot{\xi}}{R_o(2-r)\alpha}\left[\frac{R^*_{N_p} - R_N^2}{R^*_{N_p}}\right] - \frac{V_c R_o(1-r)}{R^*_{N_p}} - \dot{\xi}p = 0$$

$$\therefore \quad \frac{\dot{\xi}}{R_o(2-r)\alpha} R^{*2}_{N_p} - \dot{\xi}p R^*_{N_p} - \left[\frac{\dot{\xi} R_N^2}{R_o(2-r)\alpha} + V_c R_o(1-r)\right] = 0$$

$$\therefore \quad R^*_{N_p} = \frac{\dot{\xi}p \pm \sqrt{\dot{\xi}p^2 + \frac{4\dot{\xi}}{R_o(2-r)\alpha}\left[\frac{\dot{\xi} R_N^2}{R_o(2-r)\alpha} + V_c R_o(1-r)\right]}}{\frac{2\dot{\xi}}{R_o(2-r)\alpha}} \qquad (3.52)$$

The frictional power dissipated at the strip/plug interface is therefore given by:

$$W_{fp} = \frac{bm\sigma_o}{\sqrt{3}} \int_{R^*_{N_p}}^{R_o} \left\{ \frac{\dot{\xi}}{R_o(2-r)\alpha} \left[R - \frac{R_N^2}{R} \right] - \frac{V_c R_o (1-r)}{R} - \dot{\xi}_p \right\} dR$$

$$+ \frac{bm\,\sigma_o}{\sqrt{3}} \int_{R^*_{N_p}}^{R_f} \left\{ \frac{\dot{\xi}}{(R_o(2-r)\alpha} \left[R - \frac{R_N^2}{R} \right] - \frac{V_c R_o (1-r)}{R} - \dot{\xi}_p \right\} dR$$

$$= \frac{bm\sigma_o}{\sqrt{3}} \left[\frac{\dot{\xi}}{R_o(2-r)\alpha} \left[\frac{R^2}{2} - R_N^2 \ln R \right] - V_c R_o (1-r) \ln R - \dot{\xi}_p R \right]_{R^*_{N_p}}^{R_o}$$

$$+ \frac{bm\sigma_o}{\sqrt{3}} \left[\frac{\dot{\xi}}{R_o(2-r)\alpha} \left\{ R - R_N^2 \ln R \right\} - V_c R_o (1-r) \ln R - \dot{\xi}_p R \right]_{R^*_{N_p}}^{R_f}$$

$$W_{fp} = \frac{bm\sigma_o}{\sqrt{3}} \left[\frac{\dot{\xi}}{R_o(2-r)\alpha} \left[\frac{(R_o^2 - R^{*2}_{N_p})}{2} - R_N^2 \ln \left(\frac{R_o}{R^*_{N_p}} \right) \right] \right.$$

$$- V_c R_o (1-r) \ln \left(\frac{R_o}{R^*_{N_p}} \right) - \dot{\xi}_p (R_o - R^*_{N_p})$$

$$+ \frac{\dot{\xi}}{R_o(2-r)\alpha} \left[\frac{(R_f^2 - R^*_{N_p})}{2} - R_N^2 \ln \left(\frac{R_f}{R^*_{N_p}} \right) \right]$$

$$\left. - V_c R_o (1-r) \ln \left(\frac{R_f}{R^*_{N_p}} \right) - \dot{\xi}_p (R_f - R^*_{N_p}) \right]$$

$$W_{fp} = \frac{bm\,\sigma_o}{\sqrt{3}} \left[\frac{\dot{\xi}}{R_o(2-r)\alpha} \left[\frac{R_o^2 + R_f^2 - 2R_{N_p}^{*2}}{2} - R_N^2 \ln \left(\frac{R_o^2(1-r)}{R_{N_p}^{*2}} \right) \right] \right.$$

$$\left. - V_c R_o(1-r) \ln \left(\frac{R_o^2(1-r)}{R_{N_p}^{*2}} \right) - \dot{\xi}_p \left(R_o(2-r) + 2 R_{N_p}^{*} \right) \right]$$

$$W_{f_r} = \frac{bm\,\sigma_o R_o}{\sqrt{3}} \left[\frac{\dot{\xi}}{R_o^2(2-r)\alpha} \left[\frac{(R_o^2 + R_f^2 - 2 R_{N_p}^{*2})}{2} - R_N^2 \ln \left(\frac{R_o^2(1-r)}{R_{N_p}^{*2}} \right) \right] \right.$$

$$\left. - V_c (1-r) \ln \left(\frac{R_o^2(1-r)}{R_{N_p}^{*2}} \right) - \dot{\xi}_p \left((2-r) + \frac{2 R_{N_p}^{*}}{R_o} \right) \right]$$

$$W_{f_p} = \frac{bm\sigma_o R_o}{\sqrt{3}} \left[\frac{\dot{\xi}}{(2-r)\alpha} \left[\frac{(1+(1-r)^2 - 2(\frac{R_{N_p}^{*}}{R_o})^2)}{2} - (\frac{R_N}{R_o})^2 \ln \left(R_o^2 \frac{(1-1)}{R_{o\,p}^{*2}} \right) \right] \right.$$

$$\left. - V_c(1-r) \ln \left(\frac{R_o^2(1-r)}{R_{N_p}^{*2}} \right) - \dot{\xi}_p \left(2-r + \frac{2R_{N_p}^{*}}{R_o} \right) \right] \qquad (3.53)$$

The total power supplied to the system is given by the summation of the pressure x velocity terms for the coiler, dies and plug, that is:

$$J^* = 2 \{ \sigma_f\, b\, t_f\, \dot{U}_R \Big|_{R=R_f} + \sigma_\theta\, b(R_o - R_f)\, \dot{\xi}$$

$$+ m\, \tau \dot{\xi}_p\, b\, (R_o - R_f) \} \qquad (3.54)$$

$$J^* = 2\{ \sigma_f\, bt_f \left[\frac{\omega R_f}{2\alpha} \left(1 - (\frac{R_N}{R_f})^2\right) - V_c \right]$$

$$+ \left(\frac{2\sigma_o}{\sqrt{3}} - \sigma_f \right) b(R_o - R_f) \dot{\xi}$$

$$+ m \tau \dot{\xi} pb (R_o - R_f)\}$$

$$= 2\{\sigma_f bR_o(1-r)\alpha\left[\frac{2\dot{\xi}R_o(1-r)}{R_o(2-r)2\alpha}\left(1 - \left(\frac{R_N}{R_f}\right)^2\right) - V_c\right]$$

$$+ \frac{2\sigma_o}{\sqrt{3}} bR_o r\dot{\xi} - \sigma_f bR_o r\dot{\xi}\}$$

$$= 2bR_o\left\{\sigma_f\left[(1-r)\alpha\left(\frac{\dot{\xi}(1-r)}{(2-r)\alpha}\left(1-\left(\frac{R_N}{R_f}\right)^2\right) - V_c\right) - r\dot{\xi}\right]\right.$$

$$\left. + \frac{\sigma_o}{\sqrt{3}}\left\{2r\dot{\xi} + rm\dot{\xi}p\right\}\right\} \qquad (3.55)$$

The expression for determining the power requirement for the tube drawing analogue is similar to equation (3.47) with the addition of the term for friction at the strip/plug interface, that is, Eqn. (3.47) + Eqn (3.53):

$$J^* = W_1 + 2\,(W_f + W_{sR_o} + W_{sR_f} + W_{fp}) \qquad (3.56)$$

$$= \frac{4\sigma_o b\alpha R_o}{\sqrt{3}}\left\{V_c(1-r)\ln\left(\frac{1}{1-r}\right) + \frac{\dot{\xi}}{(2-r)\alpha}\left[\frac{r(2-r)}{2} + \left(\frac{R_N}{R_o}\right)^2 \ln\left(\frac{1}{1-r}\right)\right]\right\}$$

$$+ 2\left\{\frac{bm\sigma_o R_o\dot{\xi}}{\sqrt{3}(2-r)\alpha}\left[\left|\tfrac{1}{2}r(2-r) - (x^2+P)\ln\left(\frac{1}{1-r}\right)\right|\right.\right.$$

$$\left.\left. V\left[(x^2+P)\ln\left(\frac{P+x}{1-r}\right) - \tfrac{1}{2}\left[2(P+x) + r(2-r)\right]\right]\right]$$

$$\left. + \frac{2\sigma_o\dot{\xi}\alpha b R_o}{\sqrt{3}(3-r)}\right| 1 + \frac{\alpha}{2}\left\{1 - x^2\right\} - \frac{\alpha^2 P}{2}\left|\right.$$

$$+\frac{2\sigma_o \dot{\xi}\alpha b R_o(1-r)^2}{\sqrt{3}\,(2-r)}\left|1+\frac{\alpha}{2}\left[1-\frac{x^2}{(1-r)^2}\right]-\frac{\alpha^2 P}{2(1-r)^2}\right|$$

$$+\frac{bm\sigma_o R_o}{\sqrt{3}}\left[\frac{\dot{\xi}}{(2-r)\alpha}\left[\frac{1+(1-r)^2-2\left(\frac{R^*_{Np}}{R_o}\right)^2}{2}-\left(\frac{R_N}{R_o}\right)^2\ln\left(\frac{R_o^2(1-r)}{R^{*2}_{Np}}\right)\right]\right.$$

$$\left.-V_c(1-r)\ln\left(\frac{R_o^2(1-r)}{R^{*2}_{Np}}\right)+\dot{\xi}p\left(2-r+\frac{2R^*_{Np}}{R_o}\right)\right]\}$$

$$=\frac{2\sigma_o bR_o}{\sqrt{3}}\{\;2\alpha\;\{V_c(1-r)\ln\left(\frac{1}{1-r}\right)+\frac{\dot{\xi}}{(2-r)\alpha}\left[\frac{r(2-r)}{2}\right.\right.$$

$$\left.\left.+\left(\frac{R_N}{R_o}\right)^2\ln\left(\frac{1}{1-r}\right)\right]\}\;+\frac{m\dot{\xi}}{(2-r)\alpha}\left[\left|\tfrac{1}{2}r(2-r)-(x^2+P)\ln\left(\frac{1}{1-r}\right)\right|\right.$$

$$V\left[(x^2+P)\ln\left(\frac{P+x}{1-r}\right)\right.$$

$$\left.\left.-\tfrac{1}{2}\left[2(P+x)+r(2-r)\right]\right]\right]+\frac{2\dot{\xi}\alpha}{(2-r)}\left|1+\frac{\alpha}{2}\left\{1-x^2\right\}-\frac{\alpha^2 P}{2}\right|$$

$$+\frac{2\dot{\xi}\alpha(1-r)^2}{(2-r)}\left|1+\frac{\alpha}{2}\left[1-\frac{x^2}{(1-r)^2}\right]-\frac{\alpha^2 P}{2(1-r)^2}\right|$$

$$+m\left[\frac{\dot{\xi}}{(2-r)\alpha}\left[\frac{(1+(1-r)^2-2\left(\frac{R^*_{NP}}{R_o}\right)^2)}{2}-\left(\frac{R_N}{R_o}\right)^2\ln\left(\frac{R_o^2(1-r)}{R^{*2}_{Np}}\right)\right]\right.$$

$$\left.-V_c(1-r)\ln\left(\frac{R_o^2(1-r)}{R^{*2}_{Np}}\right)-\dot{\xi}p\left(2-r+\frac{2R^*_{Np}}{R_o}\right)\right]\}$$

$$= \frac{2\sigma_o b R_o}{\sqrt{3}} \{f(\alpha, V_c, r, \dot{\xi}, m, \dot{\xi}p, x, \phi)\} \qquad (3.56)$$

An expression for instantaneous draw stress can now be obtained by equating expressions (3.55) and (3.56):

$$2bR_o \left\{ \dot{\sigma}_f \left\{ (1-r)\alpha \left(\frac{\dot{\xi}(1-r)}{(2-r)\alpha} \cdot \left(1 - \left(\frac{R_N}{R_f}\right)^2\right) - V_c \right\} - r\dot{\xi} \right\} \right.$$

$$\left. + \frac{\sigma_o}{\sqrt{3}} \left\{ 2_r\dot{\xi} + rm\,\dot{\xi}p \right\} \right\}$$

$$= \frac{2\sigma_o b R_o}{\sqrt{3}} \quad f(\alpha, V_c, r, \dot{\xi}, m, \dot{\xi}p, x)$$

$$\therefore \frac{\sigma_f}{\frac{\sigma_o}{\sqrt{3}}} = \frac{f(\alpha, V_c, r, \dot{\xi}, m, \dot{\xi}p, x, \phi) - \left\{2r\dot{\xi} + rm\dot{\xi}p\right\}}{(1-r)\alpha \left\{ \frac{\dot{\xi}(1-r)}{(2-r)\alpha} \left(1 - \left(\frac{R_N}{R_f}\right)^2\right) - V_c \right\} - r\dot{\xi}} \qquad (3.57)$$

3.5. General Theoretical Considerations

The preceding sections in this chapter have been concerned with the behaviour of the metal as it is being plastically deformed under the converging platens; the draw stress determined in this manner should really be considered as a required draw stress, since the strain in the strip may not be compatible with this stress. That is, the strain take-up onto the coiler must allow sufficient front tension for plastic deformation to take place.

It is convenient to consider two separate phases:

a) Die Retraction Phase:

As the dies retract from their position of maximum penetration into the deformation zone, the coiler speed is initially greater than the horizontal component of the lateral die movement. This implies that conventional drawing conditions apply with an instantaneous draw speed of $(V_c - \dot{\xi}\cot\alpha)$, as shown in Figure (3.12).

Fig(3·12)-Velocity Conditions During Die Retraction

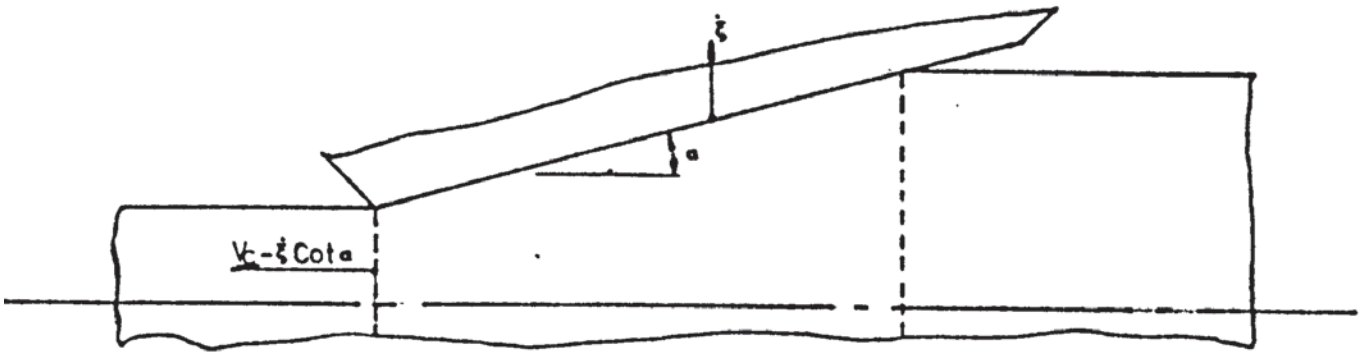

This condition would also imply that no advantage could be derived from the process at this stage unless there was:

a) A reduction in the magnitude of the friction force, and/or

b) The level of strain relaxation developed during the indentation phase was sufficient to prevent the front tension reaching the steady state draw stress, or failing at the U.T.S. of the drawn material.

Any major improvement to the process would therefore require that the "conventional draw" phase of the die retraction phase should be suppressed.

When $V_c < \dot{\xi}\text{Cos}\alpha$ plastic deformation cannot take place; the system is elastodynamic in nature and can be modeled, as shown in Figure (3.13), overleaf.

Strip Spring Constant, $K = \frac{\text{STRIP AREA}}{\text{STRIP LENGTH}} \times E$

$$= \frac{2\, t_o b(1-r)E}{L}$$

The change in σ_f is given by:

$$\Delta\sigma_f = K\,\Delta e$$

where Δe is the change in strain.

The transition from the conventional draw state to the elasto-dynamic condition occurs when:

Fig(3.13)-Model Of Die Retraction Phase

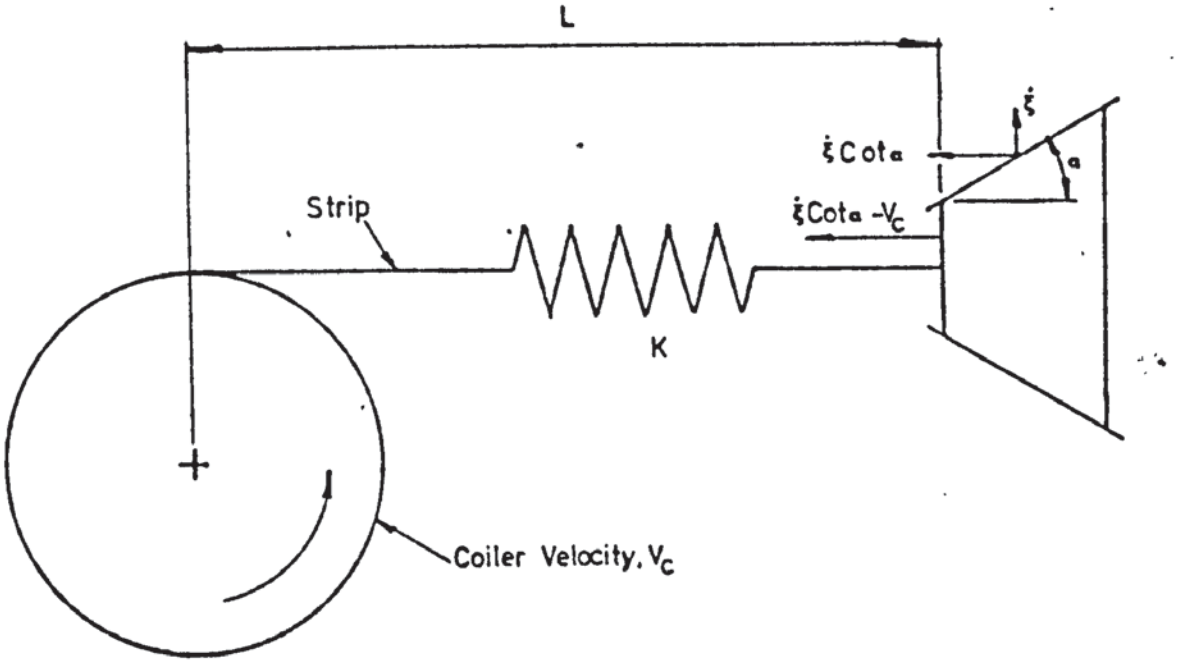

$$V_c = \dot{\xi}\cot\alpha \quad \text{at } t = t^*$$

that is, $V_c = \omega\xi_{max} \cos(\omega t^*) \cot\alpha$

and, therefore:

$$t^* = \frac{1}{\omega} \cos^{-1}\left[\frac{V_c}{\omega\xi_{max}\cos\alpha}\right]$$

The rate of change of Δe is given by:

$$\frac{d\Delta e}{dt} = -\frac{(\dot{\xi}\cot\alpha - V_c)}{L}$$

$$\therefore \Delta e = \frac{V_c t}{L} - \frac{\omega\xi_{max}\cot\alpha}{L} - \frac{\sin\omega t}{\omega} + A$$

when $\Delta e = 0$, $t = t^*$

$$\therefore A = -\frac{1}{L}\left(V_c t^* - \dot{\xi}_{max}\cot\alpha \sin\omega t^*\right)$$

$$\therefore \Delta e = \frac{1}{L}\left\{V_c\{t-t^*\} - \dot{\xi}_{max}\cot\alpha \{\sin\omega t - \sin\omega t^*\}\right\}$$

Although this does not indicate the mean value of draw stress it does show that, as might be expected, increasing coiler velocity will decrease the rate of stress reduction whilst increasing die velocity has the reverse effect.

b) Indentation Phase

As already stated, there are two possible flow conditions dependent upon the relative values of the measure of friction (m or μ) and the die semi-angle, α. This relationship between the friction angle and die angle determines, under conditions of zero front tension, whether the wedge in the deformation zone is compressed or rejected from the die throat.

The velocity field within the deformation zone is dependent upon the die velocity and the coiler velocity. Since the die velocity, in a single cycle, will vary from zero to, in general, a value greater than that of the coiler speed the dominance of each velocity term during the cycle is likely to change. At the start of the indentation phase the die velocity is zero, but the conventional drawing condition should not apply; the strain relaxation developed during the die retraction phase will have to be taken-up before drawing can occur. Thus, the difference between the mean draw speed and peak die velocity should reach as high a value as possible to give the maximum possible strain relaxation.

The effect of these two phenomena is illustrated diagramatically in Figure (3.14).

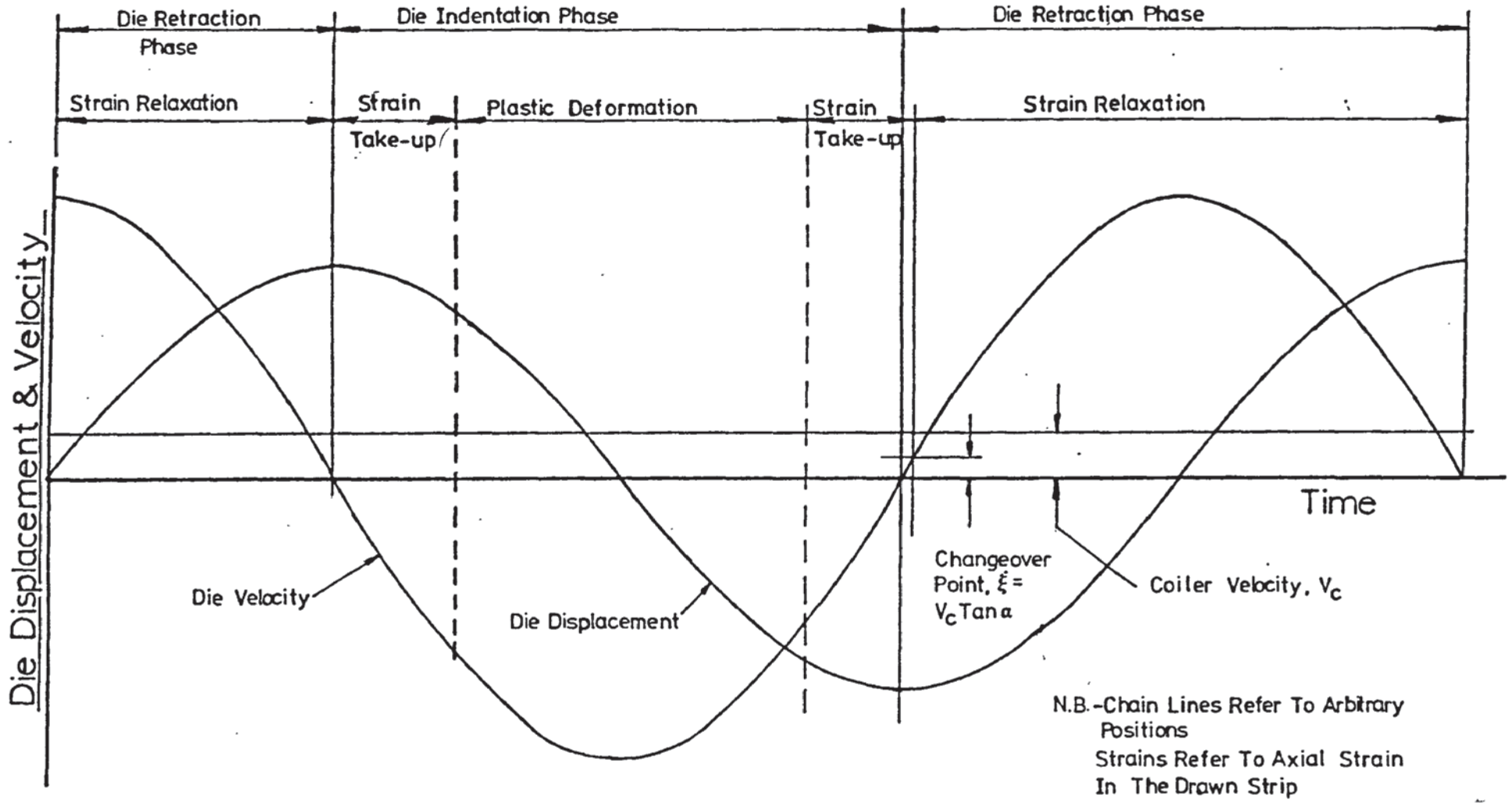

Fig(3·14)- Variation Of The Strain State In The Drawn Strip

In conventional steady-state drawing processes the stress and strain in the drawn stock are directly related to the draw load required to cause plastic deformation. It has been shown that this is not the case when such processes are augmented with vibrating dies.

Equations (3.49) and (3.57) are expressions for instantaneous draw stress and are therefore functions of time. Whether or not this stress can be attained is dependent upon the state of strain down stream of the die, which is also time dependent. It is, therefore, necessary to determine the interval in the deformation cycle over which the draw stress equation applies. This could only be achieved by plotting the strain take-up as the indentation phase proceeds and checking its compatibility with the appropriate draw stress equation.

It would be necessary to assume a point in the cycle at which plastic deformation is occurring. This should then be checked, incrementally, for compatibility of the draw stress equation with the state of strain, taking into account strain take-up and strain relaxation.

A substantial amount of further work would be required to obtain a complete analysis of the stress-strain cycle for die indentation and die retraction. Lack of time prevented the completion of this theoretical analysis.

CHAPTER 4. APPARATUS

4.1. GENERAL DESCRIPTION OF THE DRAW BENCH

The draw bench used in these tests was a welded structure designed upon the bull-block principle; strip was drawn through a pair of dies from a stock coil onto a driven coil. A bench of this type has the advantage that long pieces of strip can be drawn on relatively compact equipment thus allowing a greater amount of data to be collected, during a single test, than would be feasible on a chain-type bench. The former configuration also allows sustained drawing at speeds that would not be possible, under laboratory conditions, on a chain type bench.

General views of the draw bench are shown in plates 1 and 2 and a sectional diagram of the arrangement of the wave guides and guide rolls is shown in Figure (4.1).

Stock coils were mounted at the rear of the bench on shafts which ran in pillow block bearings. A light braking torque was applied through a rope brake, wound around the shaft, to prevent the strip from uncoiling. This did not apply any appreciable back tension and was, therefore, not taken into account when analysing the test results.

It can be seen in Figure (4.1) that the strip was passed from the stock coils into a pair of guide rolls. These rolls were shaped to take two pieces of strip whilst allowing sufficient clearance for a plug bar, and were free to rotate about the axis of a bolt by means of a rolling element bearing. The bolts were clamped into slots in a base plate, as shown in Figure (4.2), thus allowing the strip to be positioned correctly with respect to the die throat. The guide rolls were of the utmost importance when drawing under conditions of low draw speed, low reduction of area and high die velocity, that is, when front tension was very low. These factors are discussed in Chapter 8.

The strip was passed between the dies which were bolted to the ends of a matched pair of stepped wave guides. These wave guides were bolted

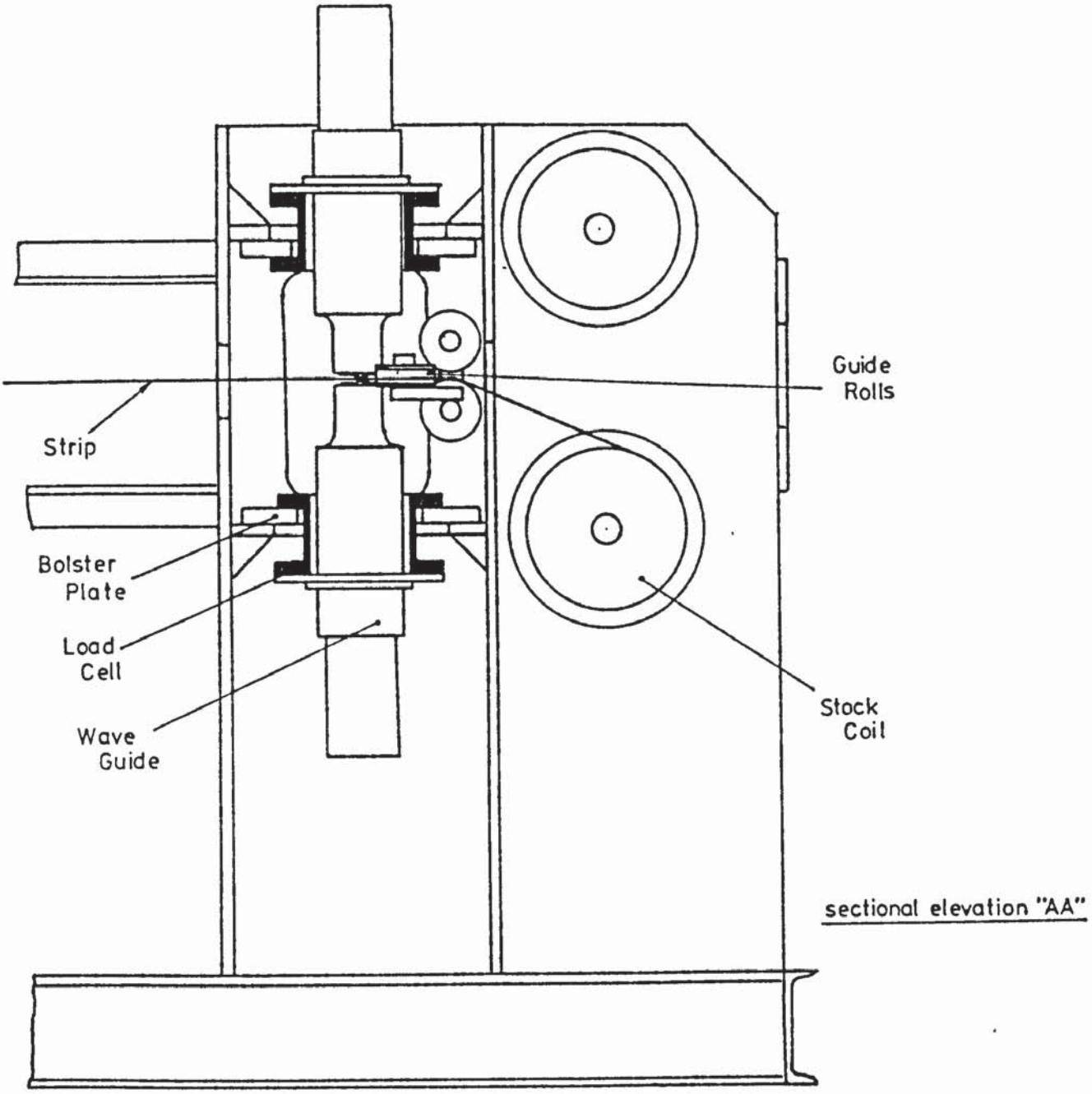

Fig(4.1) - General Arrangement Of The Rear Of The Draw Bench

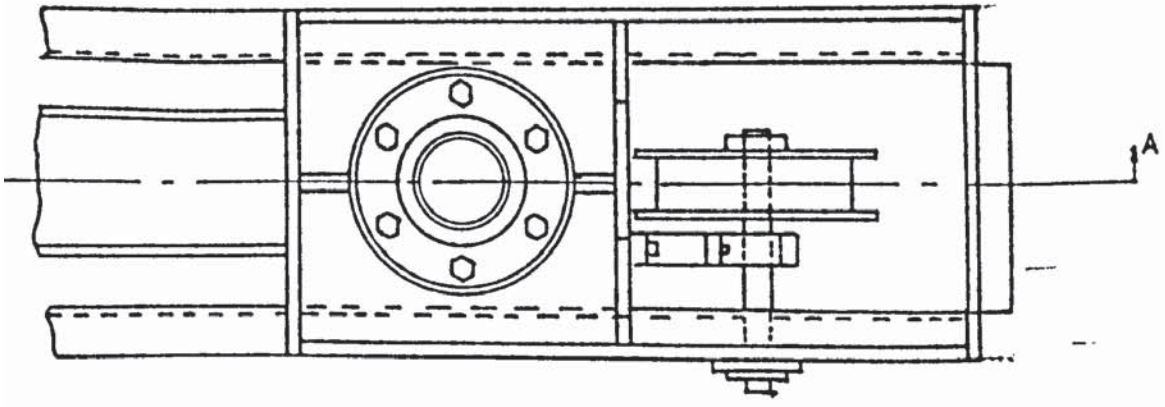

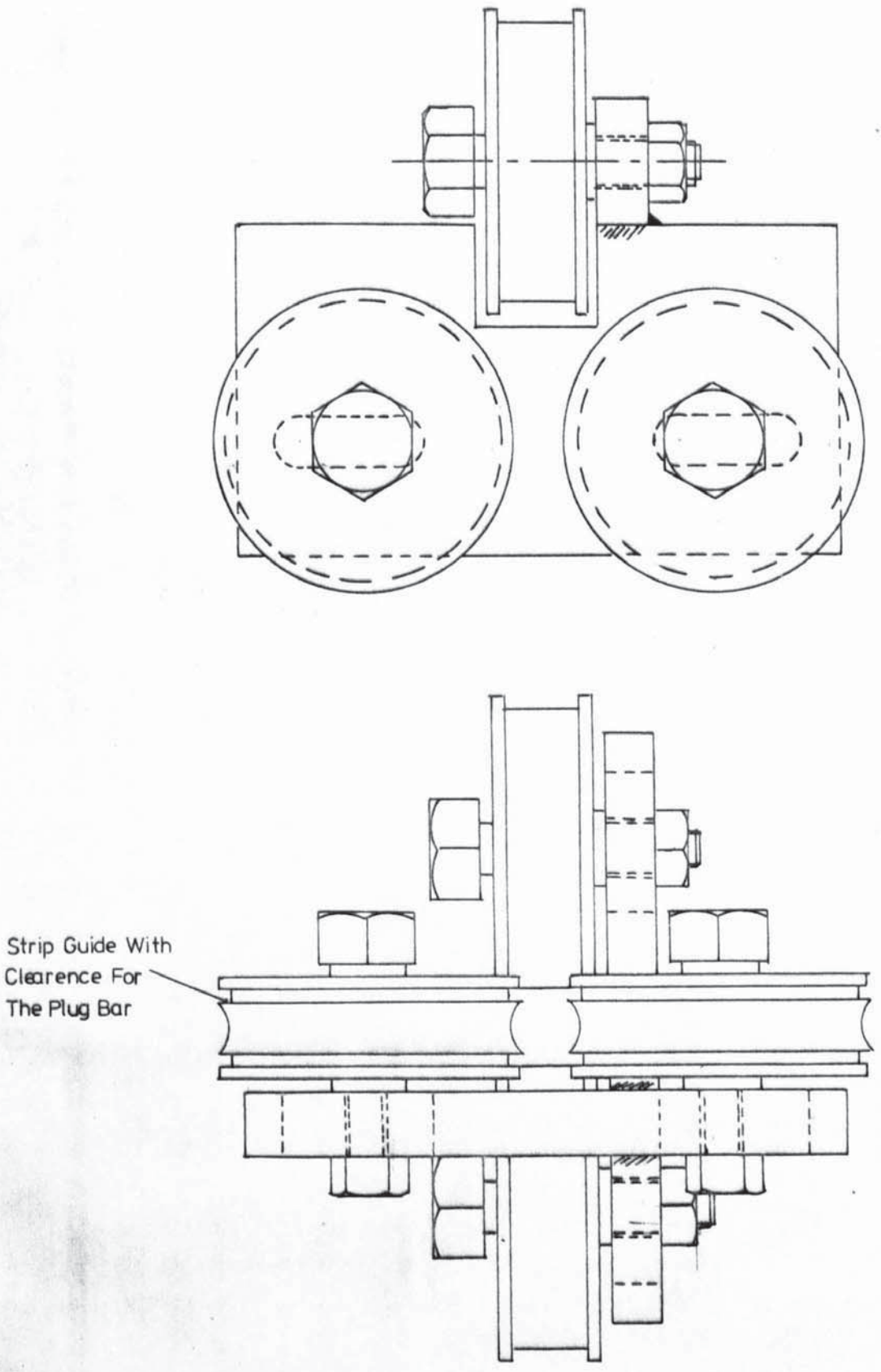

Fig(4.2)-Guide Roll Assembly

onto annular load cells which were, in turn, bolted to a bolster plate and thence to the machine frame. This assembly is shown in Figure (4.3) and details of the wave guide and load cell are shown in Figures (4.4) and (4.5) respectively.

It can be seen in Figure (4.3) that the bolster plate could be adjusted with the aid of set screws located in the machine frame. This permitted fine adjustment of the upper die relative to the lower die; any required movement was preset by adjusting the set pins against feeler gauges, unbolting the bolster plate and pushing the whole assembly against the set pins. The main weight of the assembly was carried by a small hydraulically operated mobile crane connected to an eye bolt in the wave guide; the bolster plate was clamped into its new position. The crane was also used for lifting the upper wave guide, when it was detached from the load cell, so that the strip could be positioned between the dies.

When carrying out the strip drawing tests, the die gap was set by inserting shim steel between the upper wave guide and the load cell. The shim steel was used also to set the dies parallel by inserting between the machine frame and the upper bolster, a series of 0.05 mm (0.002 in) leaves a shim steel of incrementally varying width. This, effectively, gave a wedge that compensated for the inaccuracies due to distortion of the welded structure and general build-up of manufacturing errors. The design of the wave guide is discussed fully in section (4.3) and further details of the associated load cell are given in Section (5.1.1).

After passing through the dies the strip ran over the appropriate tag load cell. The angle of contact of the strip on the tag load cell was held constant by a guide roll sited down stream of the cell, as shown in plate 3. The arm of the tag load cell restrained a grooved roll, which guided the strip. Referring to Figure (4.6) which shows the tag load cell it can be seen that the cantilevered arms were fixed to the square section of a shaft. The shaft was mounted in a pair of blocks. One end of the

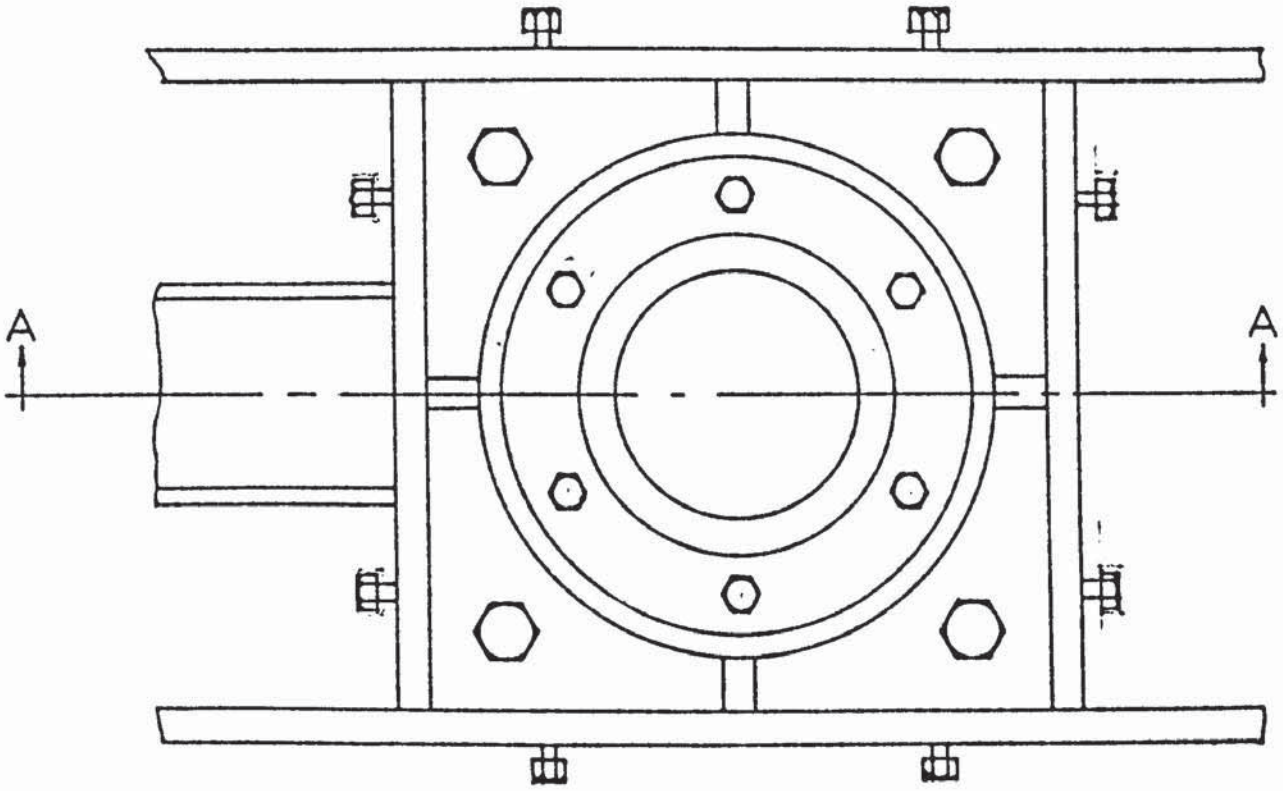

Fig(4.3) - Detail Of Waveguide Assembly_

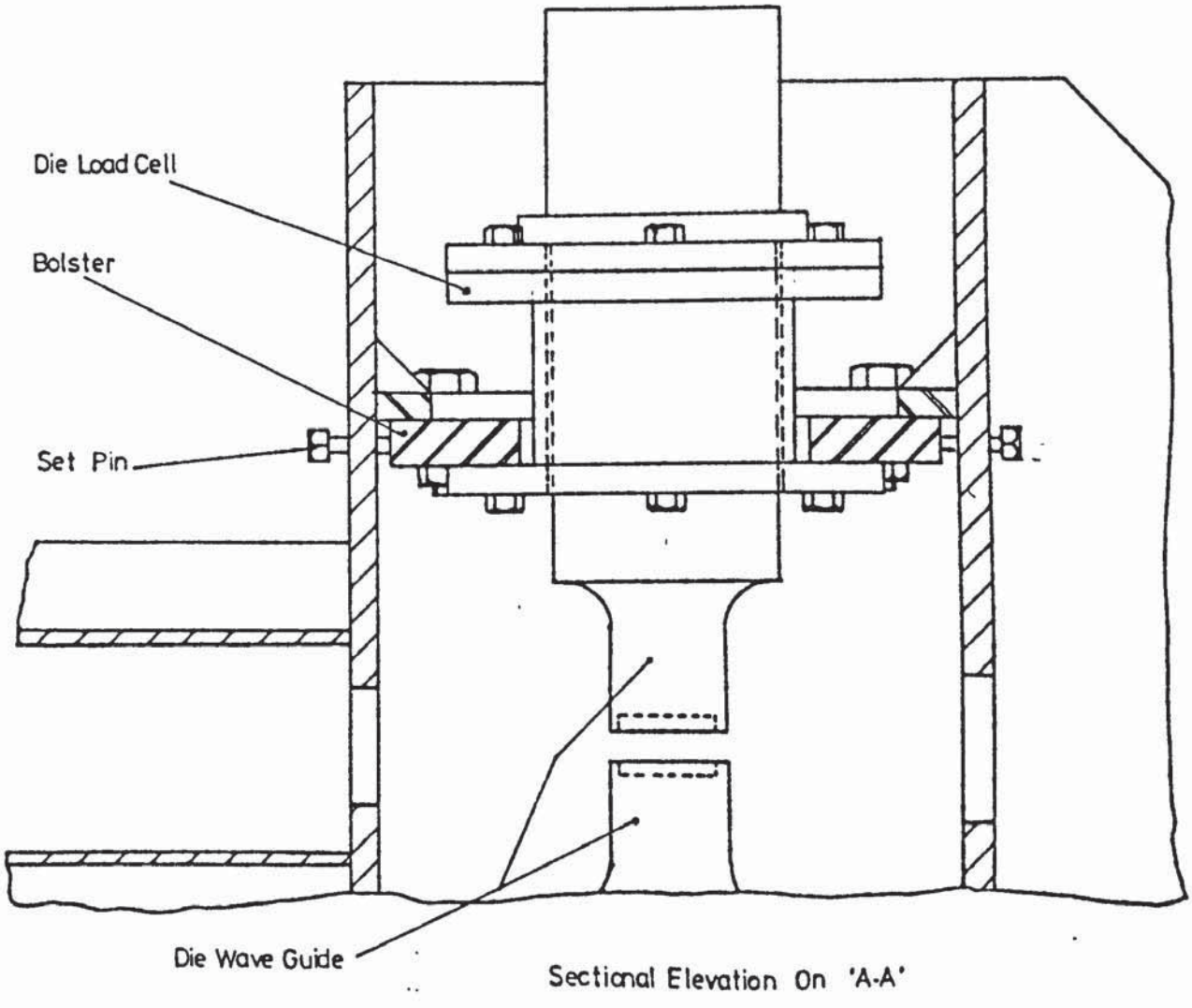

Fig(4.4) - Die Wave Guide

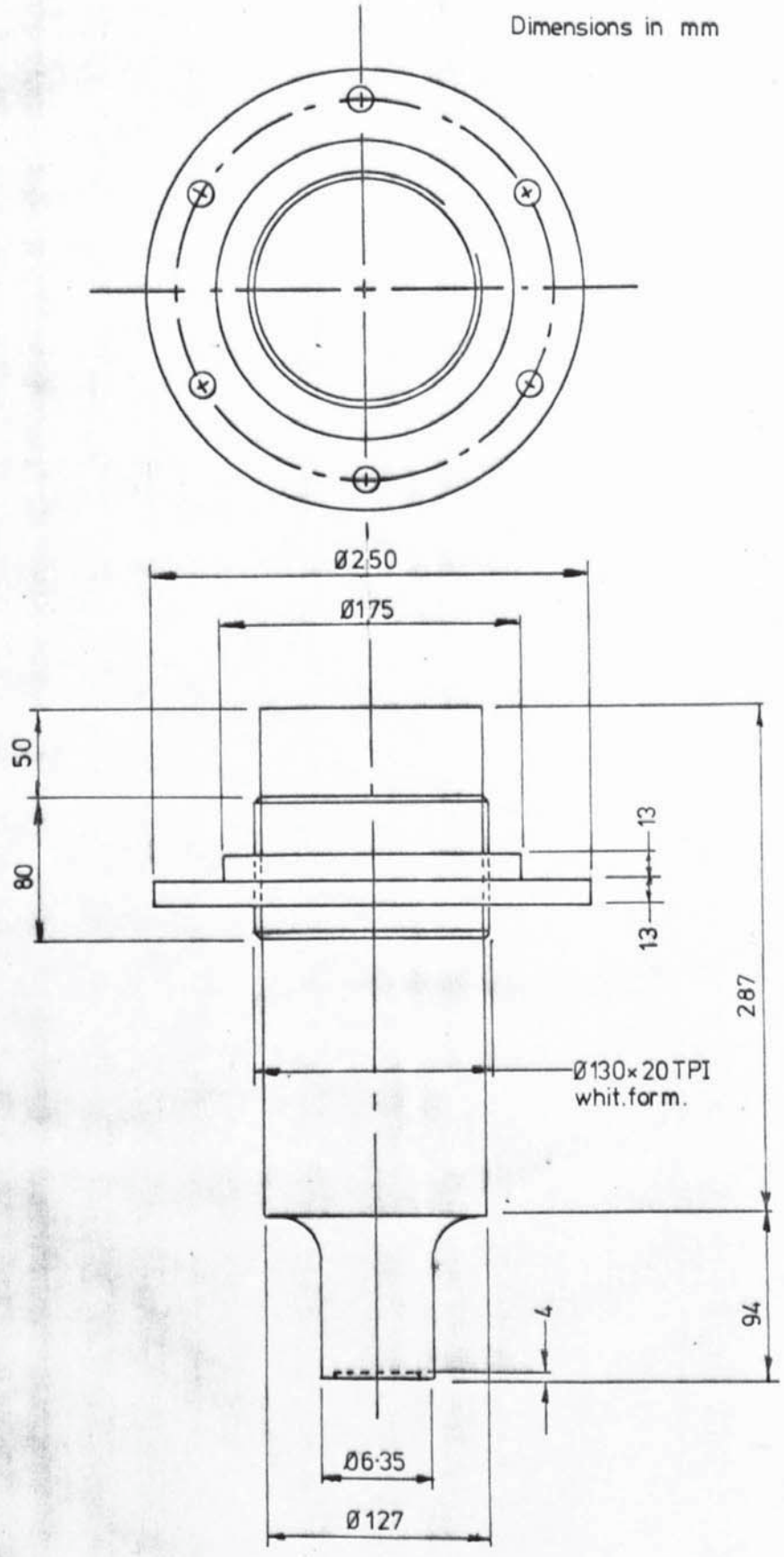

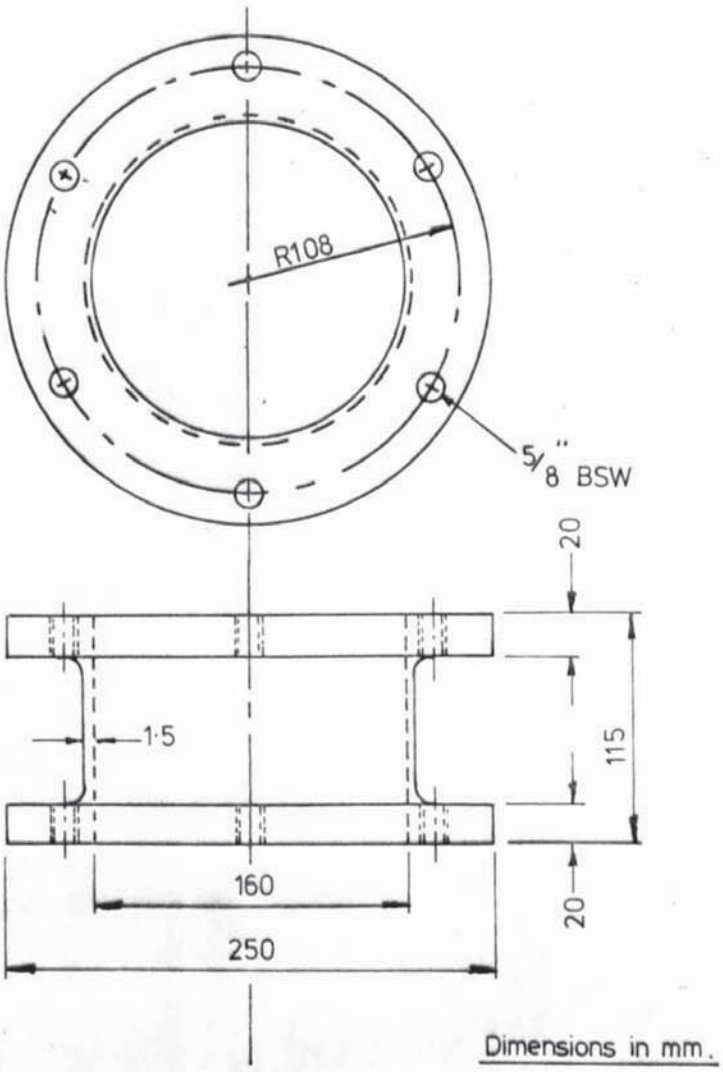

Fig(4.5)- Die Load Cell

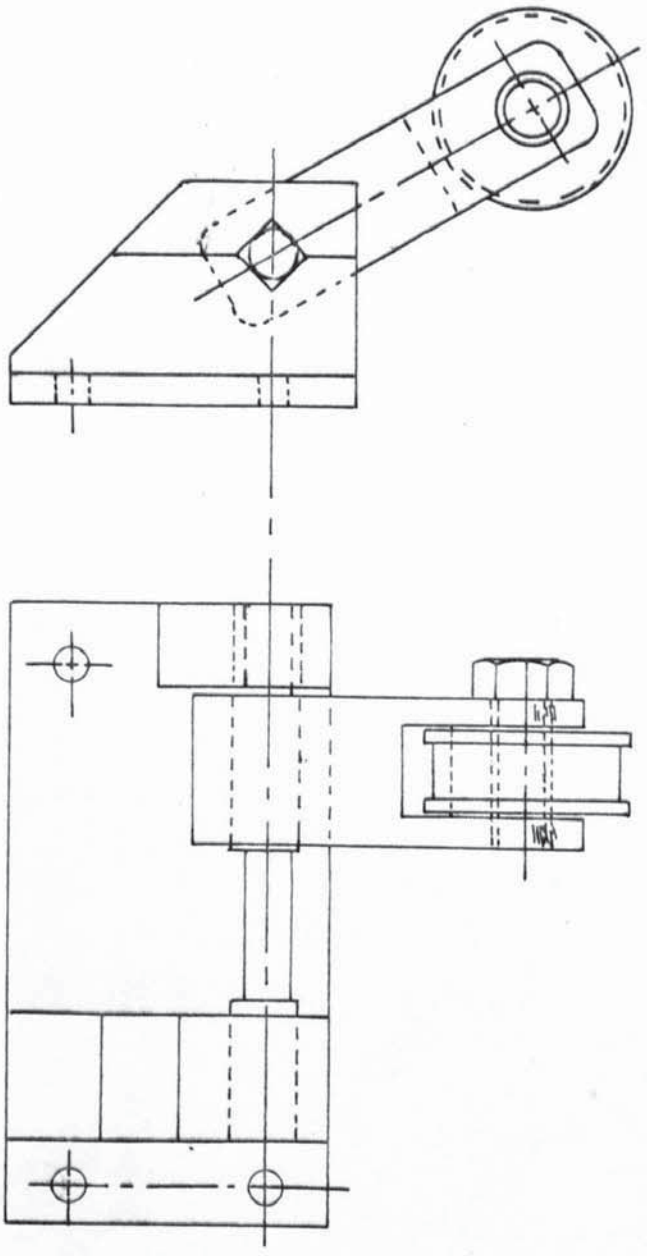

Fig(4.6)- Tag Load Cell

shaft was fixed and the other end was free to rotate in needle bearing. Thus the shaft, being the active element of the load cell was subject to torsion. Chevron strain gauges were bonded to the circular section of the shaft between the cantilever and the fixed end of the shaft.

The tag load was therefore measured by monitoring the torsional stress induced in the shaft. Further details of the tag load cell are given in section (5.1.2).

The strip passed to one of the coilers which were synchronously driven, through a chain drive, from a variable speed motor/gear box unit. The arrangement of the coilers and drive is shown in plate 2.

The method of holding the strip onto the coiler is shown in Figure (4.7).

Modification of the draw bench for the tube drawing analogue was achieved by packing out the wave guides to allow for the insertion of a square plug, details of which are given in section (4.4.2). A conical wave guide was mounted on tie bars at the rear of the bench. The plug bar was attached to the wave guide, which could be rotated in order that the plug faces could be set parallel to the dies. Axial position of the plug was achieved by adjusting the tie bars. The plug bar wave guide is shown in plate 5 and the whole of the plug bar assembly is shown, schematically, in Figure (4.8).

4.2. TRANSDUCERS AND GENERATORS

There are two methods of converting high frequency electrical energy into mechanical energy of the same frequency, both of which are based upon resonant systems. The earliest type of drive unit consisted of a rod, manufactured from laminated nickel sheet bonded together with enamel, around which was wound a coil of copper wire; the coil was energised by an H.F. generator. Later types of drive transducer consisted of a pair of piezo-ceramic discs held in compression between metal cylinders or cones. These end pieces are generally made of different metals, usually steel and

Fig(4.7) - Method Of Clamping The Strip Onto The Stock Coils

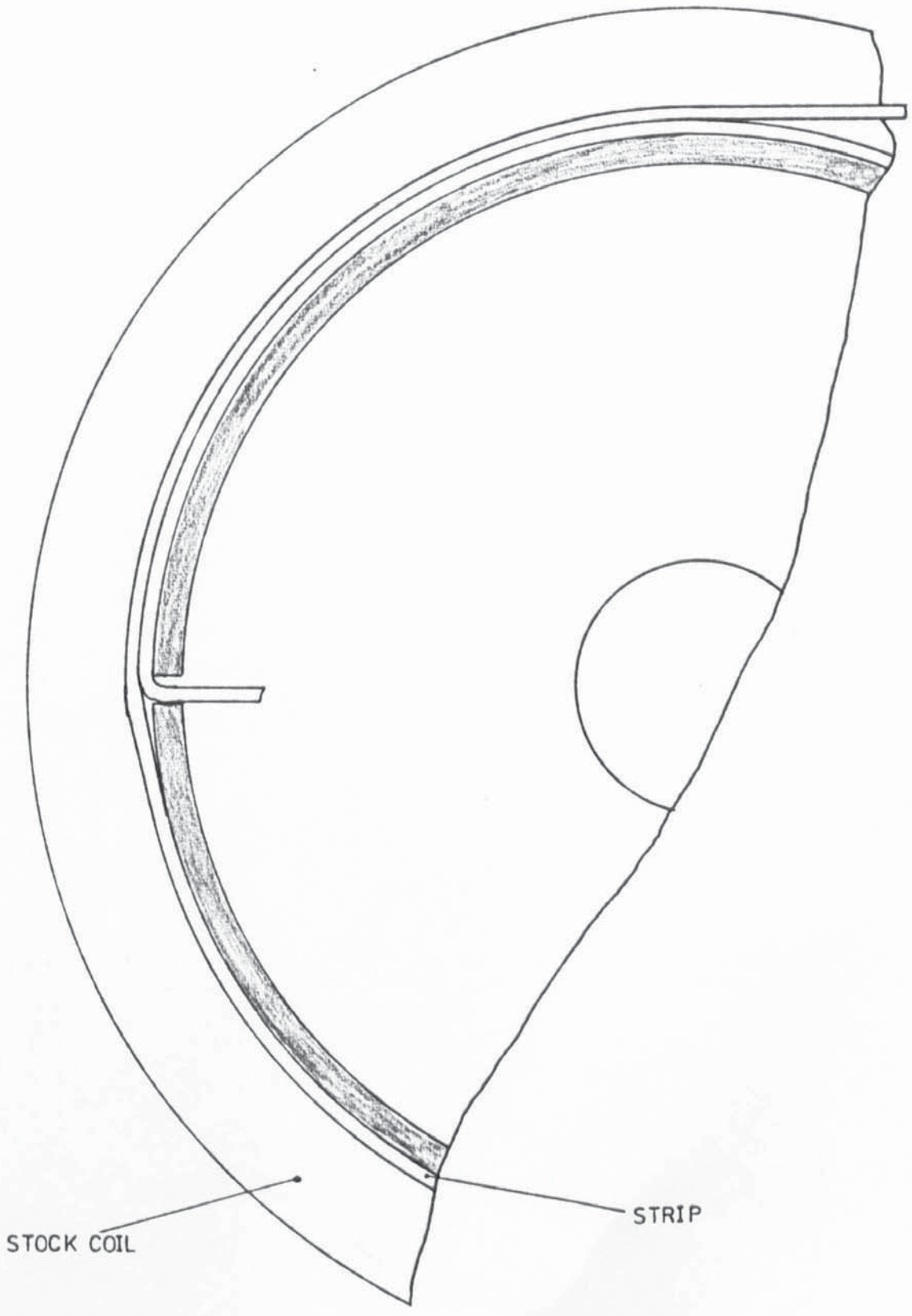

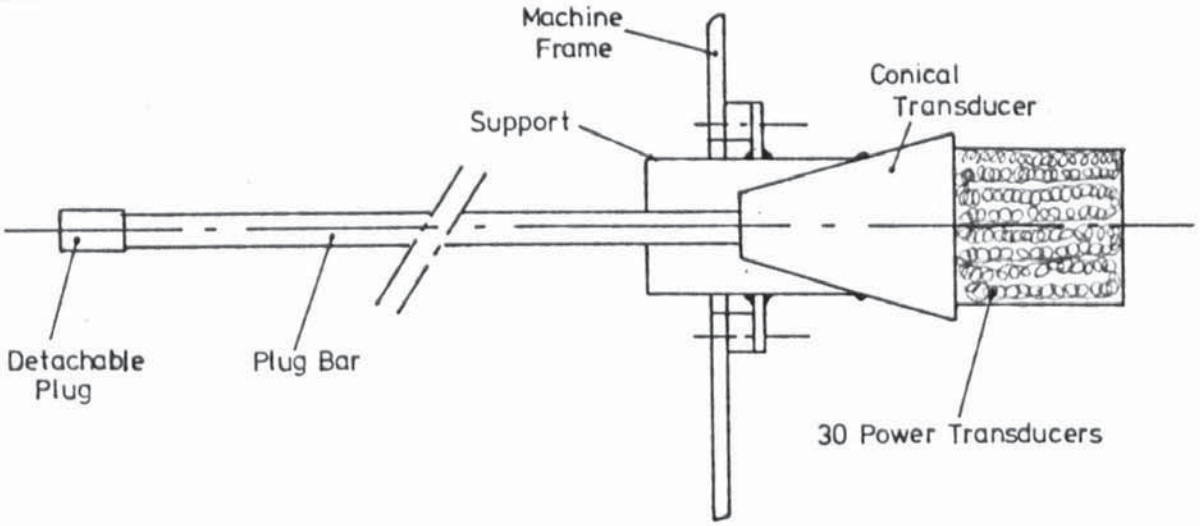

Fig(4.8) - Plug Bar Assembly

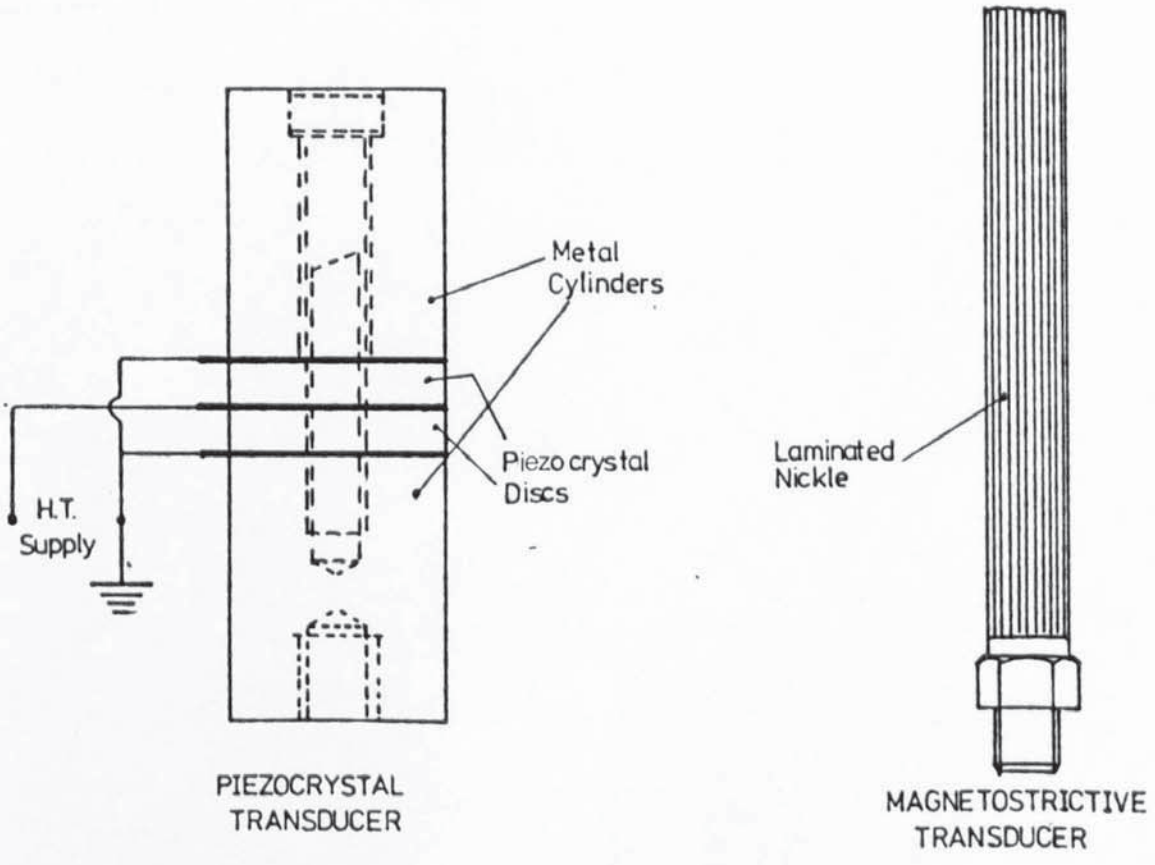

Fig(4.9)- Power Ultrasonic Transducers

aluminium. Because of the difference in their densities, and therefore consequent acoustic impedance mismatch a higher displacement amplitude is induced in the less dense metal. The piezoceramic discs are used in pairs and, to effect isolation of the H.T. connection, it is sandwiched between the discs.

The effective overall length of both types of stack is equal to a half wave length at the required frequency. Typical examples are shown, diagramatically, in Figure (4.9).

Piezo-ceramic stacks are attaining predominance for use in the metal forming applications of power ultrasonics. This is primarily because of their improved energy conversion efficiency with respect to magnetostrictive devices, though their operating bandwidth is lower necessitating, in certain cases, the use of automatic frequency control.

Power generators have, similarly, been subject to change over the past few years. The earliest type used thermionic valves. These units were generally rated at between one and three kilowatts and were therefore rather large and expensive. The overall efficiency of the units, used in conjunction with magnetostrictive transducers, was low. Later types of generator utilised switched thyristors which were not directly suited to use in conjunction with piezo-ceramic transducers because of the capacitive load they provide. Transistorised power generators now exist which are suited to use with capacitive devices and can supply H.F. power at relatively low cost.

4.2.1. Power Generators and Associated Equipment

The power generators used for these tests utilised switched thyristors and were manufactured by Ultrasonics Ltd. with a maximum power input of 1.2 kW. Three of these generators were used to drive, independently, the two die wave guides and the plug bar wave guide. Each of these generators was used to drive a set of magnetostrictive trans-

ducers of the type shown in Figure (4.9).

A block diagram of the H.F. power supply to the wave guides is shown in Figure (4.10). The die wave guides were synchronously driven from a master oscillator which drove the oscillators in the H.F. generators. The same master signal was passed through a phase shifter and another oscillator to drive the plug bar wave guide.

The H.F. power output of each power amplifier could be varied by adjusting the mains voltage with a variable transformer.

The above equipment is shown in Plate 6.

4.3. WAVE GUIDES, SUPPORTS AND TOOLS

In order to transfer the high frequency vibrational energy, supplied by the generators and transducers, into useful work it is necessary to guide the acoustic wave to the tool/product interface.

The simplest form of wave guide consists of one or more transducers attached to the end of a cylinder. The length of the cylinder is equal to an integer multiple of a half wave length. This configuration does not amplify the input and is therefore of little practical importance except when used in conjunction with an amplifying wave guide for plug bars.

The simplest usable wave guide consists of a cylinder which is stepped at a displacement antinode, as shown in Figure (4.11). The amplification factor is derived from the assumption of continuity of transmission of strain energy per unit time from the input to the output of the wave guide. That is, ignoring the sign of the velocities,

$$V_1 \pi R_1^2 = V_2 \pi R_2^2, \text{ see Figure (4.11)}$$

$$\therefore \frac{V_1}{V_2} = \left(\frac{R_2}{R_1}\right)^2$$

Thus a 2:1 relationship between R_1 and R_2 gives a x4 velocity transformation. The main disadvantage of this type of concentrator is the high stress peak developed at the step.

Fig(4.10) - Diagram Of The H.F. Power Supply To The Wave Guides

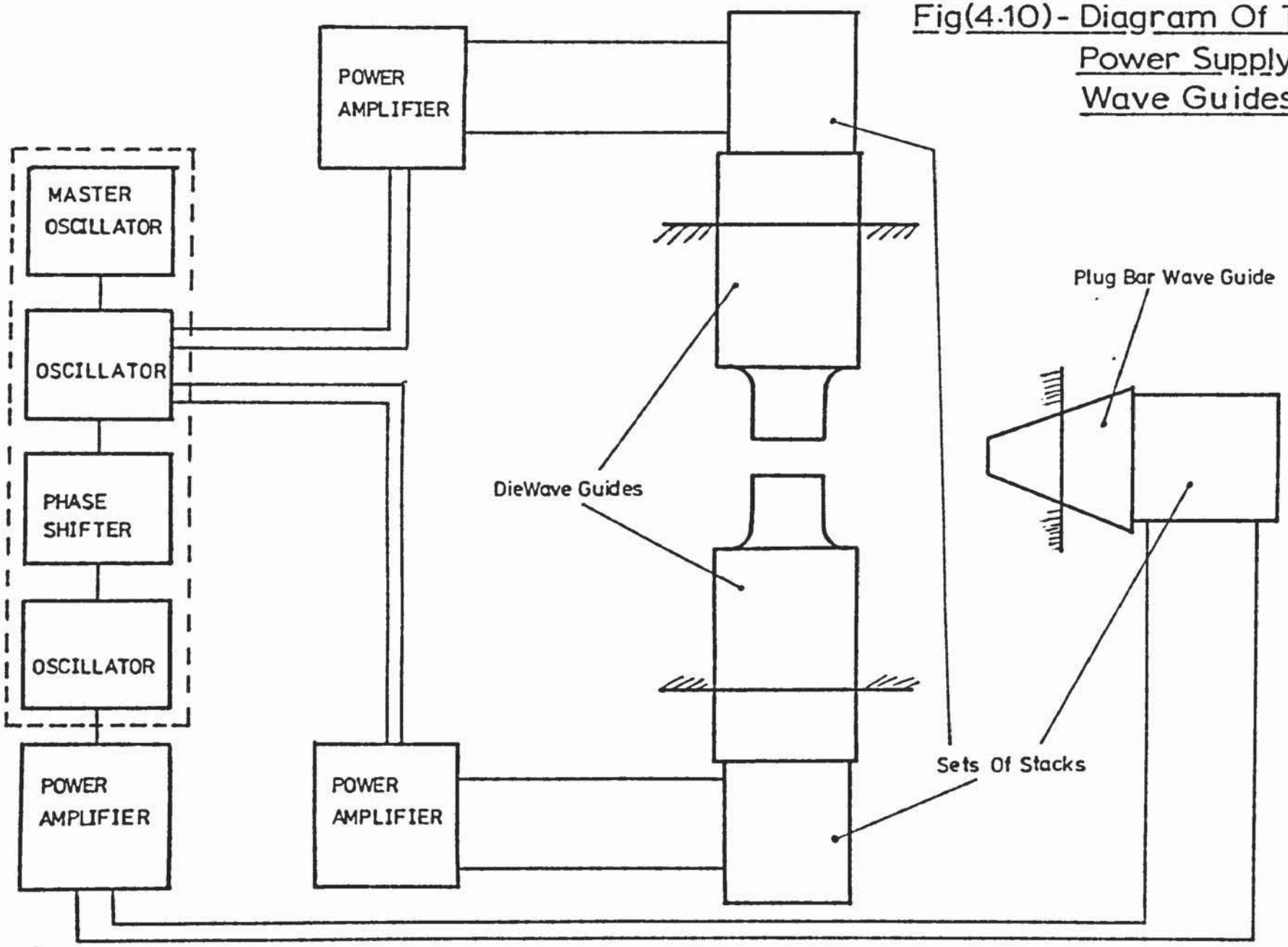

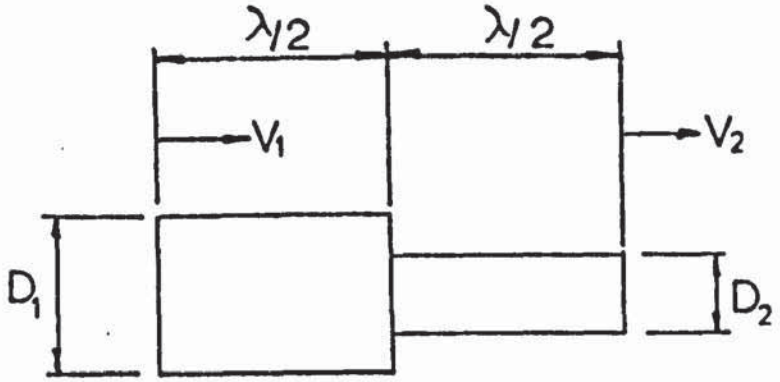

Fig(4·11) - Stepped Wave Guide

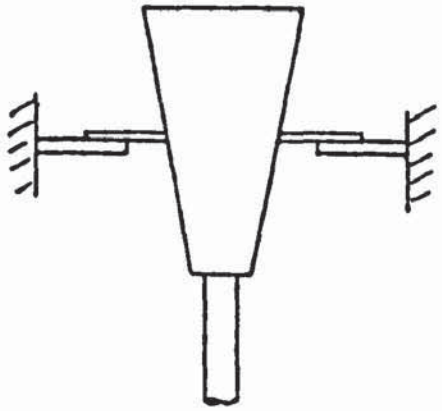

Fig(4·12) - Nodal Support

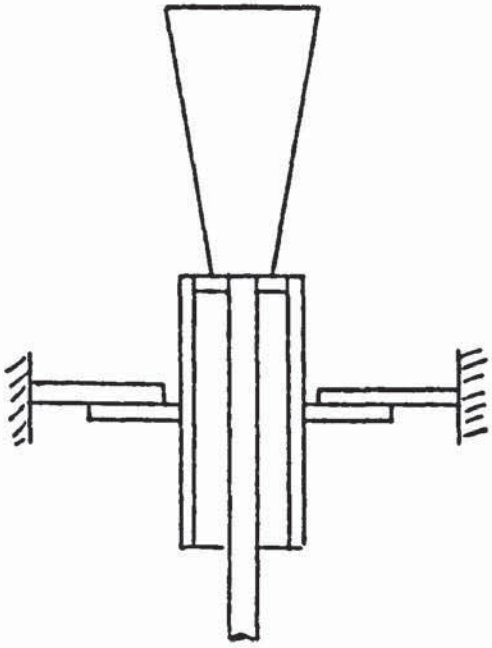

Fig(4·13) - Half-Wave Support

Other types of waveguide give a better energy transfer; conical wave guides are widely used though their maximum amplification is relatively low, that is, approximately x2.6. Other curves are used in the design of concentrators, for example, exponentials, catenaries and Gaussian curves.

Correct support of the wave guide is crucial to its performance since there must be minimal energy loss to the machine frame. There are essentially, two types of support; nodal and half wave. It can be seen in Figure (4.12) that the nodal support consists of a mounting plate located at a displacement node on the wave guide, which, in theory, prevents oscillatory energy passing to the machine frame. The main problem with this design is that, under load, the tuned frequency tends to change due to damping[33]. Under the correct operating conditions a better method of supporting the waveguide is by use of a 'half wave' support. This type of support is shown in Figure (4.13) and consists of a half wave length of tube, the end of which is attached to the wave guide at a displacement anti-node; the support is then attached to the machine frame at a displacement node on the support. The nodal point is invarient with respect to a small frequency shift. This type of support was used, initially, for the die wave guides. However, the diameter of the support was a substantial proportion of its length. This caused radial and flexural vibrations to be induced in the half wave support when the wave guide was energised and almost complete loss of acoustic energy to the machine from through the support; the die amplitude was therefore very low.

4.3.1. DIE WAVE GUIDES AND DRAWING DIES

A diagram of the die wave guide is shown in Figure (4.4). The overall length of the wave guide is equal to one full wave length with a step machined at one-quarter of a wave-length from the die seat. The wave guide was threaded over a nodal portion one-guarter wave-length from

the stacks; the nodal support was positioned, whilst the wave guides were energised, and locked into position with the locking collar. The two wave guides were manufactured to a close tolerance on their overall length giving tuned frequencies which differed by less than 50 Hz.

Three pairs of drawing dies were designed[15] and manufactured from a 20% Cr, 2.0% C cold working die steel (Uddenholm Sverka 3), hardened to 62 Rockwell 'C' scale. Various lubricants were used with these dies including soap, rape oil and molybdenum disulphide paste with little success, very severe pickup being a problem encountered with each of the lubricants, especially when the dies were vibrated. Subsequent hard chromium plating of the working surfaces improved the performance of the dies though pickup, under the action of the vibrating dies, was still unacceptably high. These dies were therefore replaced with the tools, shown in Figure (4.14), consisting of a tungsten carbide bricket brazed into a carbon steel (EN 8D) base. The working surfaces of the dies were ground to the required profile then lapped with diamond paste to a surface finish of approximately 0.05 μm. These tools along with the lubrication procedure are discussed further in section (6.2).

4.3.2. PLUG BAR

A diagram of the whole plug bar assembly is shown in Figure (4.8) and the plug bar wave guide and support is shown in plate 5. The conical wave guide was driven by thirty stacks linked to a 1200 W H.F. generator. A half wave support was utilised to isolate the vibrating system from the machine frame. The nodal mount on the half-wave collar allowed the whole assembly to be rotated about its axis permitting alignment of the square plug. The plug bar assembly was attached to the machine frame with tie bars, each using two nuts and two pairs of spherical washers allowing further adjustment of the position of the plug bar.

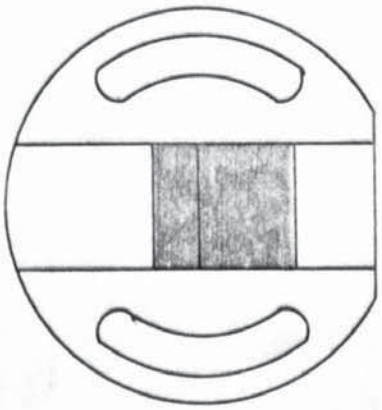

Plan View Of The Dies

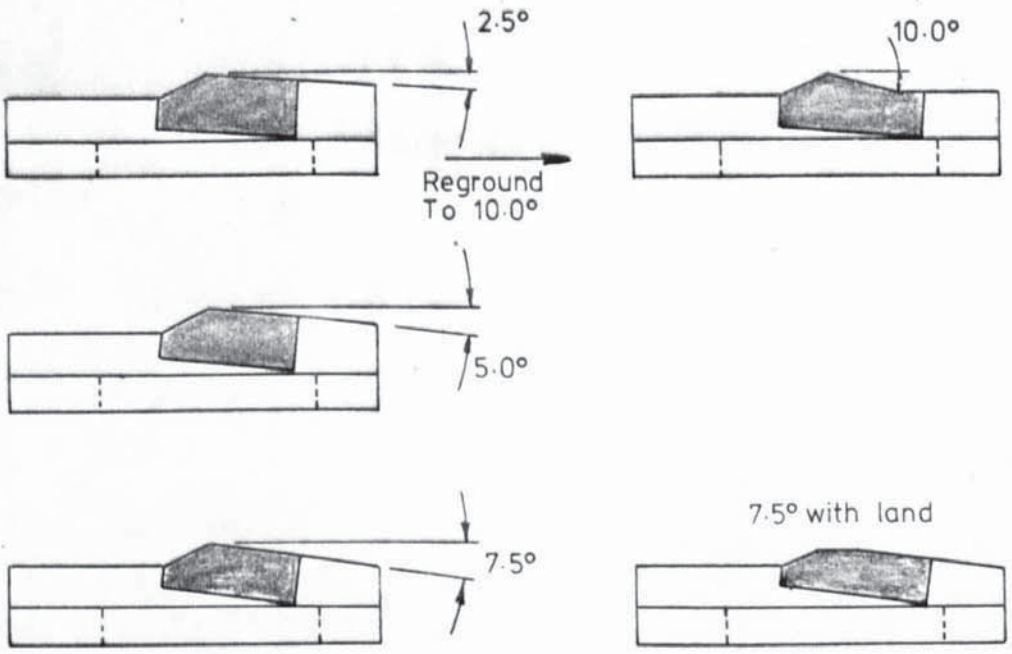

Side Elevation Of The Dies

DIE BASE MATERIAL - CARBON STEEL (EN8D)
INSERT MATERIAL - TUNGSTEN CARBIDE (WIMET ULTIMET W12)

Fig(4.14) - Details Of The Drawing Dies

The plug bar was made from drawn rod to the end of which was attached a plug. The whole of the plug bar assembly was tuned, under load, to the same frequency as the dies. Unfortunately, the shift in frequency of the die wave guides and plug bar wave guide under load would have necessitated tuning of the plug for each condition: the plug bar wave guide had previously been used by Waterhouse[12], in static die experiments, with good effect.

The plug was made from Uddenholm Sverka 3 - a cold drawing die steel (2% C, 20% Cr), hardened to 62 Rockwell 'C' and hard chromium plated.

CHAPTER 5: INSTRUMENTATION AND CALIBRATION

5.1) Measurement of the Non-Oscillatory Component of Tag and Die Load

It is evident from the literature reviewed in section 2.2 that a cyclic stress will be induced into the drawn product, irrespective of the vibrational mode of the tools. The frequency used in the following tests was approximately 13 kHz, whilst the flat frequency response of the galvanometers employed to record tag and die loads was less than 1 kHz. This implies therefore, that the recorded output of each load cell is a measure of mean rather than peak load. These load cells and their associated calibration procedure are described below.

5.1.1.) Die Load

Two components of die load were measured by monitoring the axial and bending load on the annular wave guide supports. It was not possible[15] to design the load cell on the basis of expected full load since it was necessary to maintain the die/ strip geometry whilst under load. The die load cell was therefore capable of carrying a far higher direct load than was needed for the experimental work.

The strain gauge bridge used for monitoring the axial force consisted of a full wave, 16 gauge, bridge wired to give compensation for temperature changes and to be insensitive to bending. The strain gauge bridge used to monitor the bending load on the cell consisted of a full wave, 4 gauge, bridge mounted so that the bending load in the direction of drawing could be measured. The layout of the strain gauges and the associated circuit diagrams are shown in Figure (5.1) and Figure (5.2).

Each signal was amplified with a Fylde FE-154-ABS/C bridge amplifier. These units consisted of a bridge supply, amplifier power supply, differential d.c. amplifier and current amplifier. The supply voltage to each bridge could be set individually, with the option of either a high or low current output. In the state supplied by the manufacturer, the amplifiers produced an unacceptable amount of high frequency and low frequency

Fig(5.1) - Layout Of Strain Gauges On The Die Load Cell

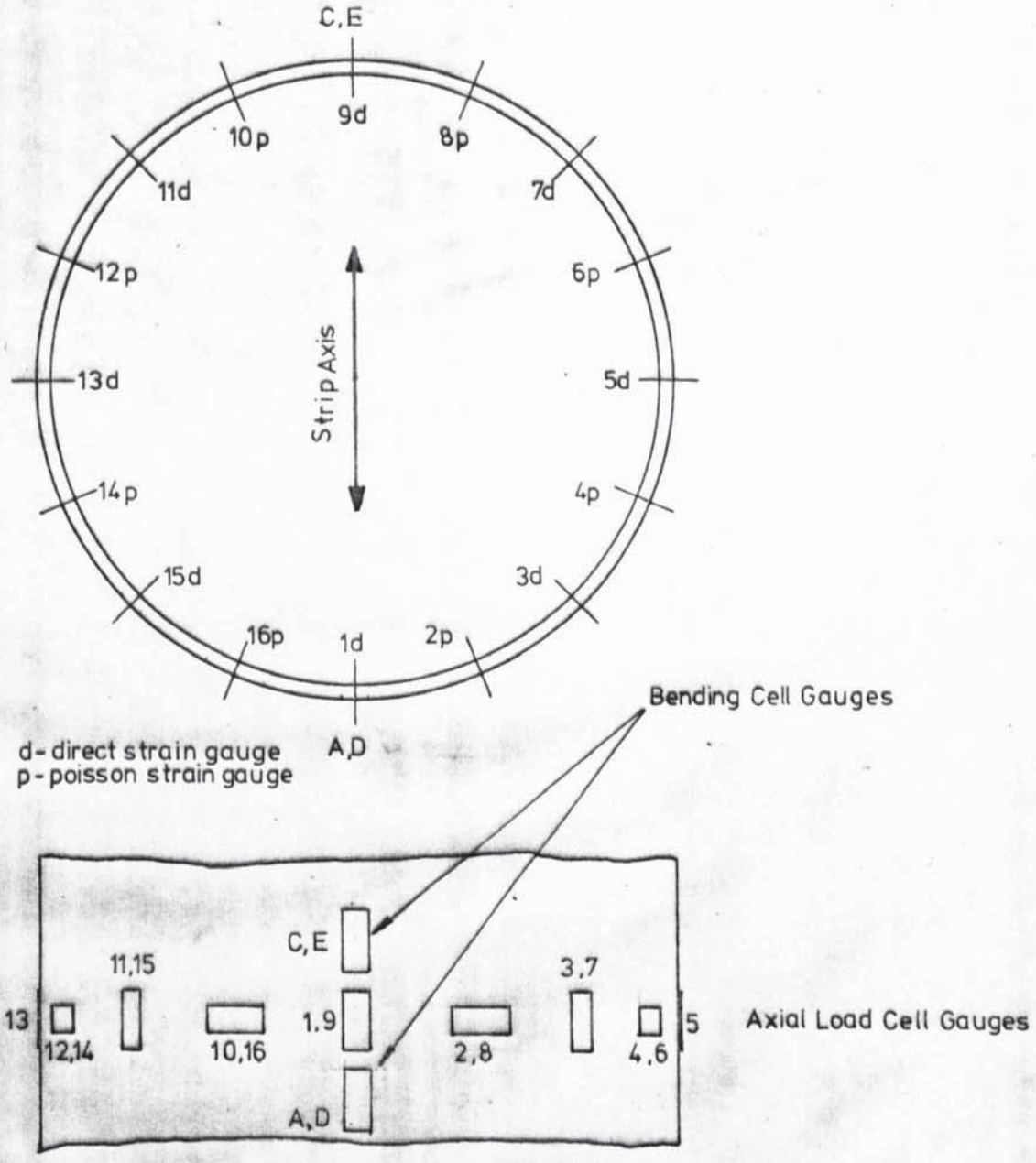

Fig(5.2)- Circuit Diagram For The Die Load Cell

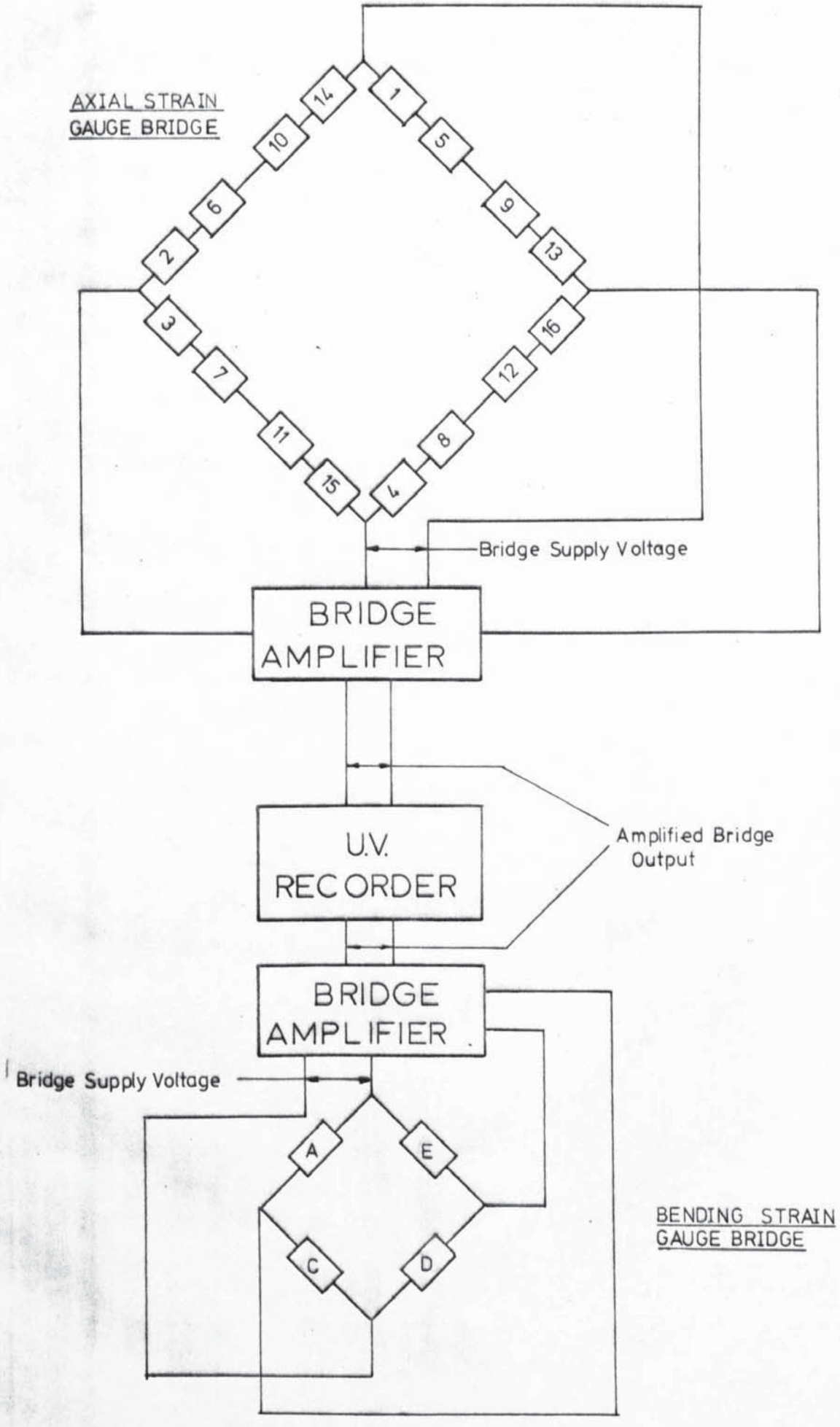

electrical noise. The high frequency component was removed by earthing each amplifier to a common point. The low frequency component could not be removed without the use of a filter between the output of the d.c. amplifier and the input to the current amplifier. In this configuration the amplifiers are only suitable for use with d.c. or very low frequency signals. As only the non-oscillatory components of force were measured by this system, the amplification was considered to be adequate.

Each amplifier gain and galvanometer was checked by applying to the d.c. amplifier input a series of voltages from a calibrated d.c. milli-volt supply. The amplifier output was monitored on a digital voltmeter and also on a U.V. recorder, through the appropriate galvanometer; the amplifier was driven, incrementally, to its limiting voltage of approximately 6.5v. The x10 gain was badly non-linear on all the amplifiers, though, as this gain was not used in the tests it was of no great significance. All other gains gave a linear output.

5.1.2) Tag Load

The tag load cell is shown in Figure (4.6) and Plate 3 and the associated circuit diagram is shown in Figure(5.3). It consists of a roller mounted at the end of a cantilever which is, in turn, mounted on a shaft. This shaft is fixed at one end and free to rotate in a bearing at the other. The strip is passed over the roller as it is being drawn, thus inducing a torsional stress in the shaft which is proportional to tag load. Two pairs of chevron strain gauges were mounted between the cantilever and the fixed end of the shaft, and wired to measure torsional stress. A stabilised power supply giving a 4v output was used to supply the bridge. No amplification was required.

5.1.3) Calibration of the Axial Load Cell

Each load cell was calibrated on a Mohr and Federhaff Universal testing

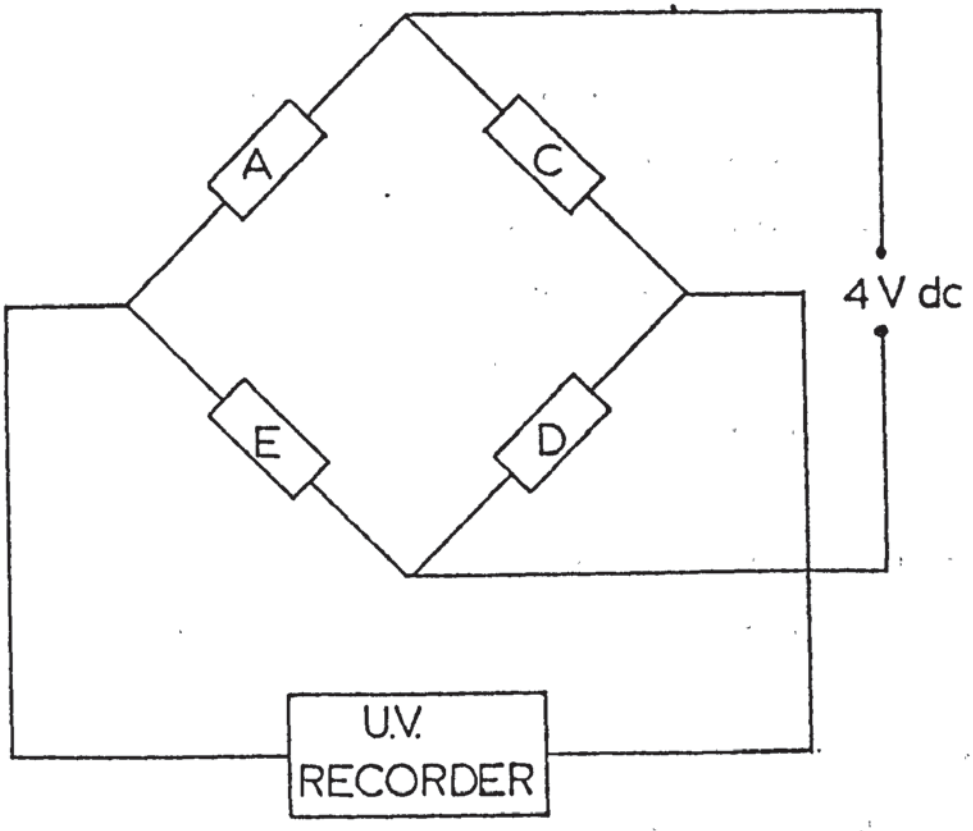

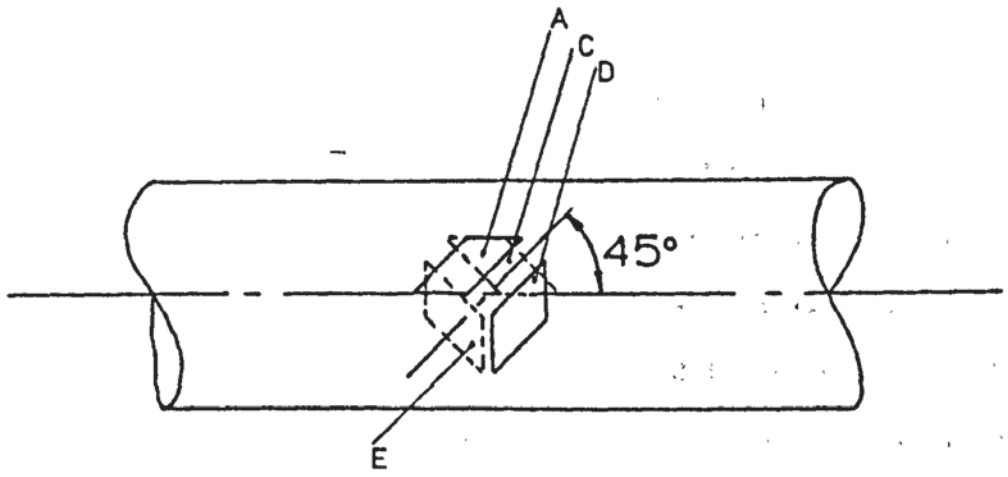

Fig(5·3)- Layout Of Strain Gauges And Circuit Diagram For The Tag Load Cell

machine. The load cell was loaded in tension through a pair of universal joints having a maximum capacity of 20 kN. This eliminates any possibility of applying a bending load to the cell and also enables any cross-sensitivity from a direct load to the bending load cell to be detected.

The load cell in the testing machine was first zeroed according to the instructions in the manufacturer's handbook. The bridge amplifiers that were connected to the direct load cell and its associated bending load cell were also zeroed for the required gain; the operation had to be repeated for each gain setting. The bridge zero and bridge supply voltage did not drift provided that the amplifiers were allowed to stabilise. This process took several hours, therefore the bridge amplifiers were run continuously for the duration of any series of tests.

The load cell was initially loaded and unloaded a number of times to ensure that there was no zero drift, and to test that the strain gauges were correctly bonded to the cell.

Calibration of the die load cells was carried out at nominal gains of 5000, 2000, 1000, 500 and 200, with the output from the bending load cell being monitored at gains of up to 2000. The results of these tests are shown in Figures (5.4), (5.5), (5.6) and (5.7).

5.1.4) Calibration of Bending and Tag Load Cells

The bending and tag load cells were calibrated in situ by simulating the true loading condition, as shown in Figure (5.8). It can be seen that the strip was clamped to the wave guide in such a way that the strip could be passed over the die. The clamping method is shown in detail in Figure (5.9). A proving ring was connected to the strip and suspended on cords to prevent its weight affecting the strip tension or bending load. Another piece of strip was connected to the proving ring and passed over the tag load cell, guide roll and coiler with the free end attached to a hydraulic ram which was activated with a hand pump. It was found necessary to

Fig(5.4) - Axial Load Cell Calibration

Axial Load v. Galvanometer Deflection

(Upper Axial Load Cell)

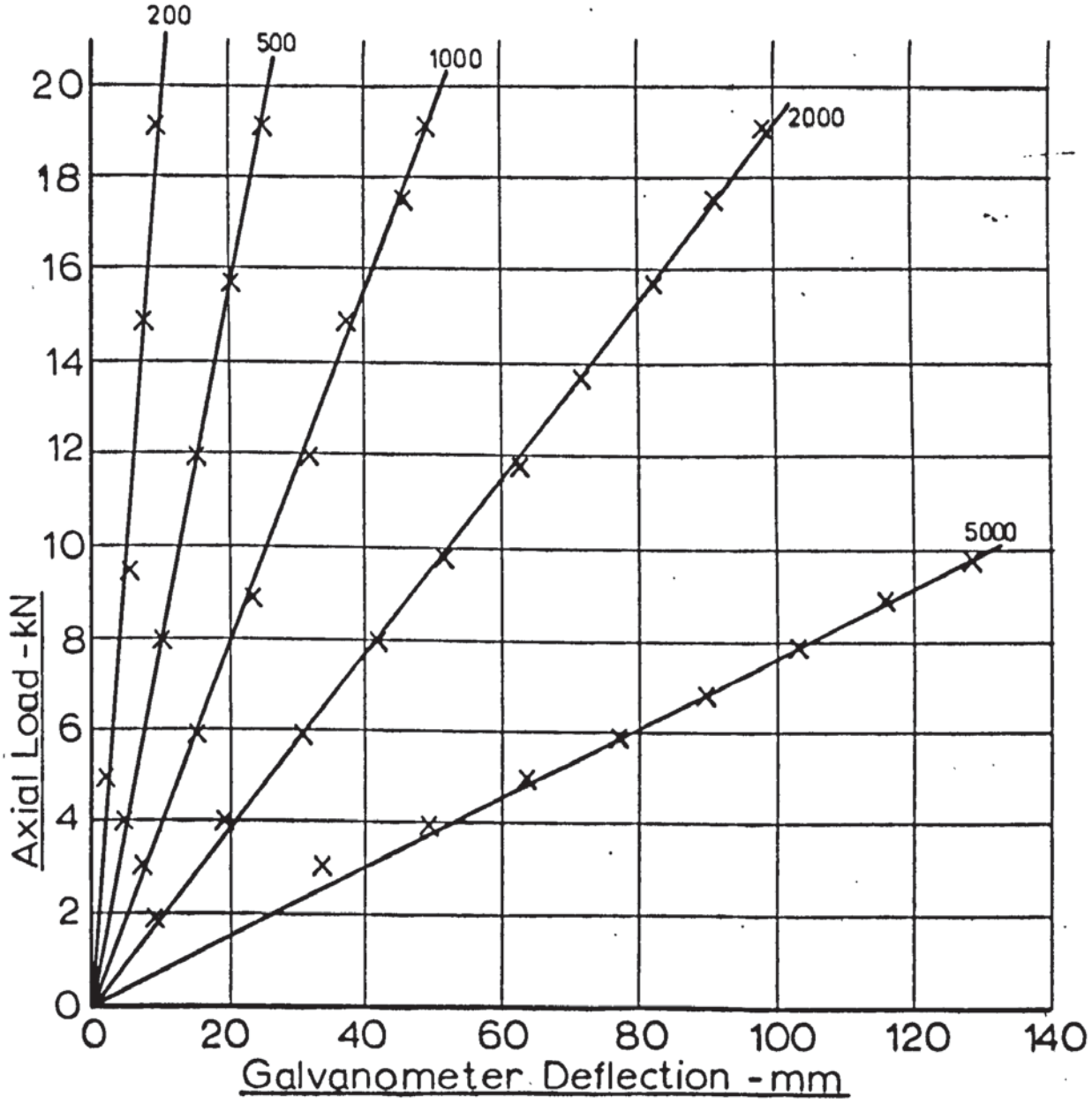

GALVANOMETER - A1000
SERIAL NO. - 2-289
BRIDGE VOLTAGE - 12V

Load Cell Constants

Gain		kN/mm
5000	—	0.073
2000	—	0.194
1000	—	0.392
500	—	0.644
200	—	2.210

Fig(5.5) - Bending Load Cell Output Due To Axial Load

Axial Load v. Galvanometer Deflection (Upper Load Cell)

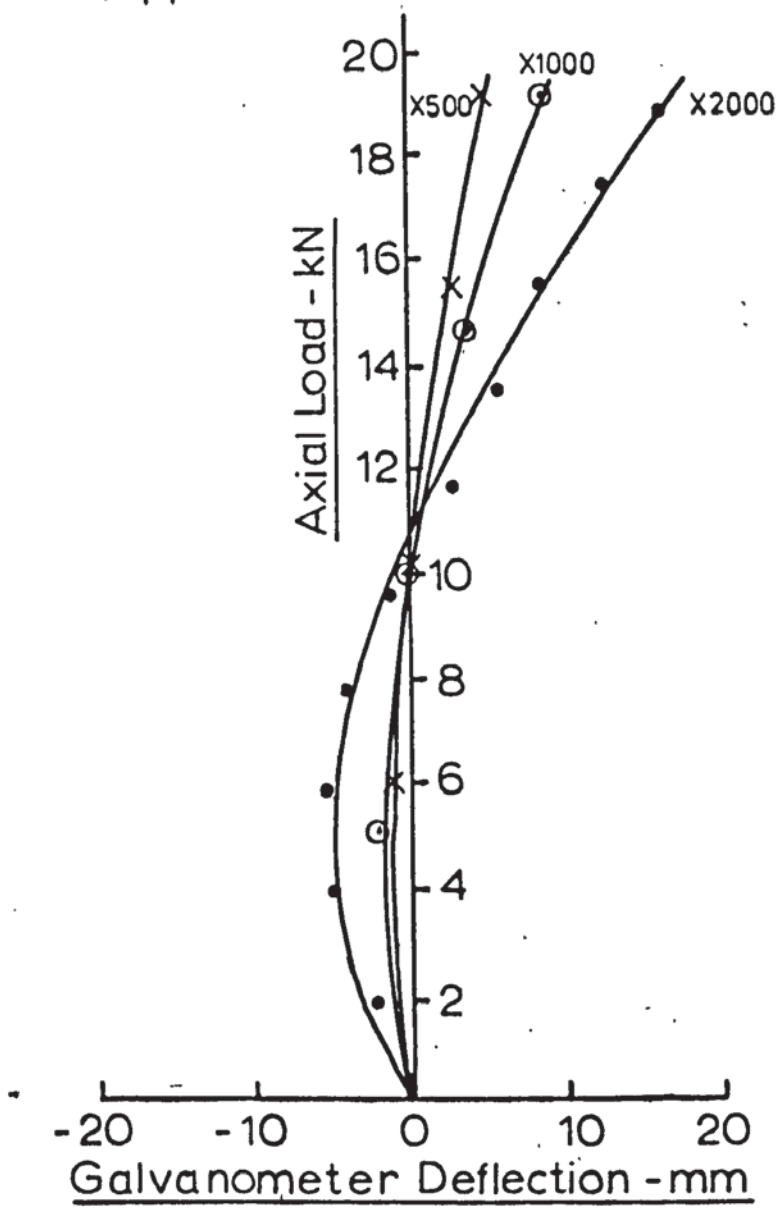

[Bending Load Cell Output At Gains Below 500 Was Negligible]

Fig(5.6) - Axial Load Cell Calibration

Axial Load v. Galvanometer Deflection

(Lower Axial Load Cell)

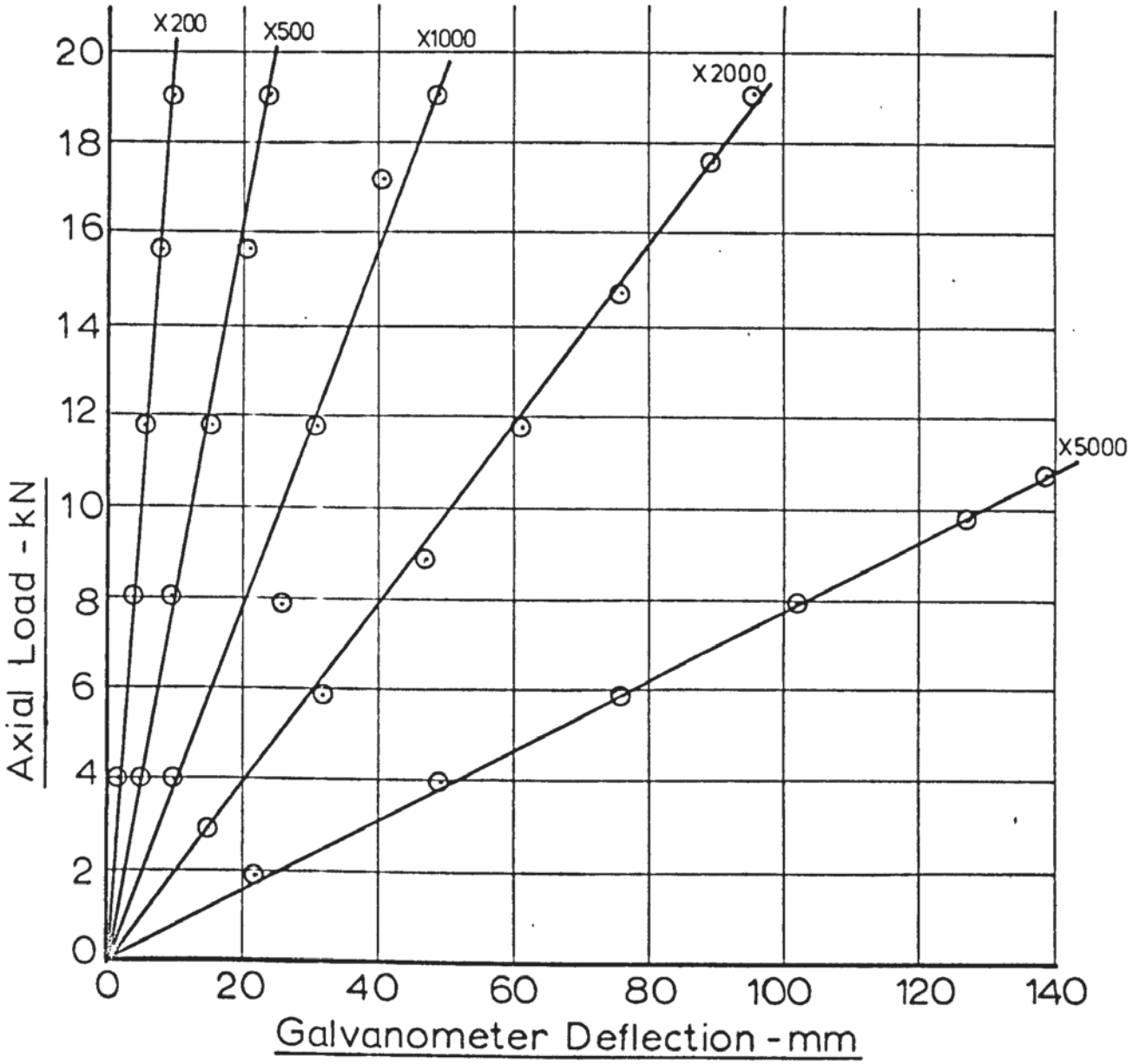

GALVANOMETER - A1000
SERIAL NO. - 4-10
BRIDGE VOLTAGE - 12V

Load Cell Constants

Gain	kN/mm
5000	0.073
2000	0.191
1000	0.397
500	0.760
200	1.550

Fig(5.7) - Bending Load Cell Output Due To Axial Load

Axial Load v. Galvanometer Deflection

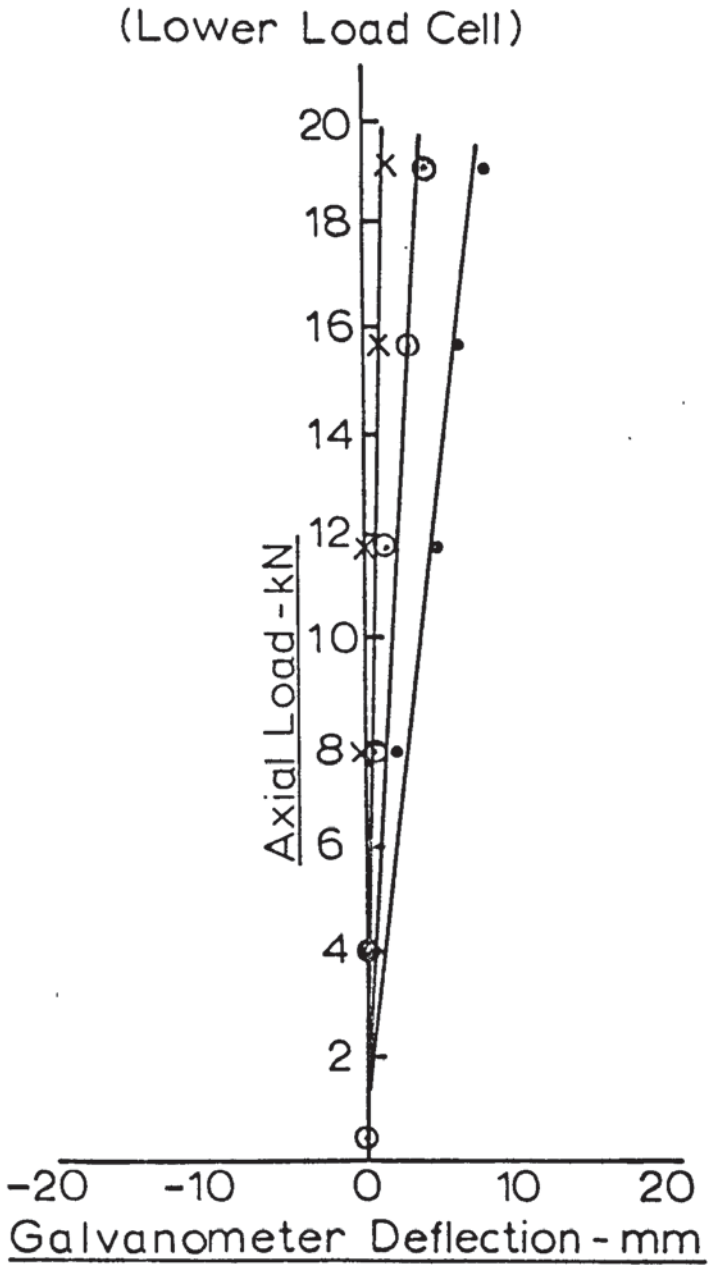

Fig(5.8) - Diagrammatic Arrangement Of Apparatus For Calibration Of Bending And Tag Load Cells

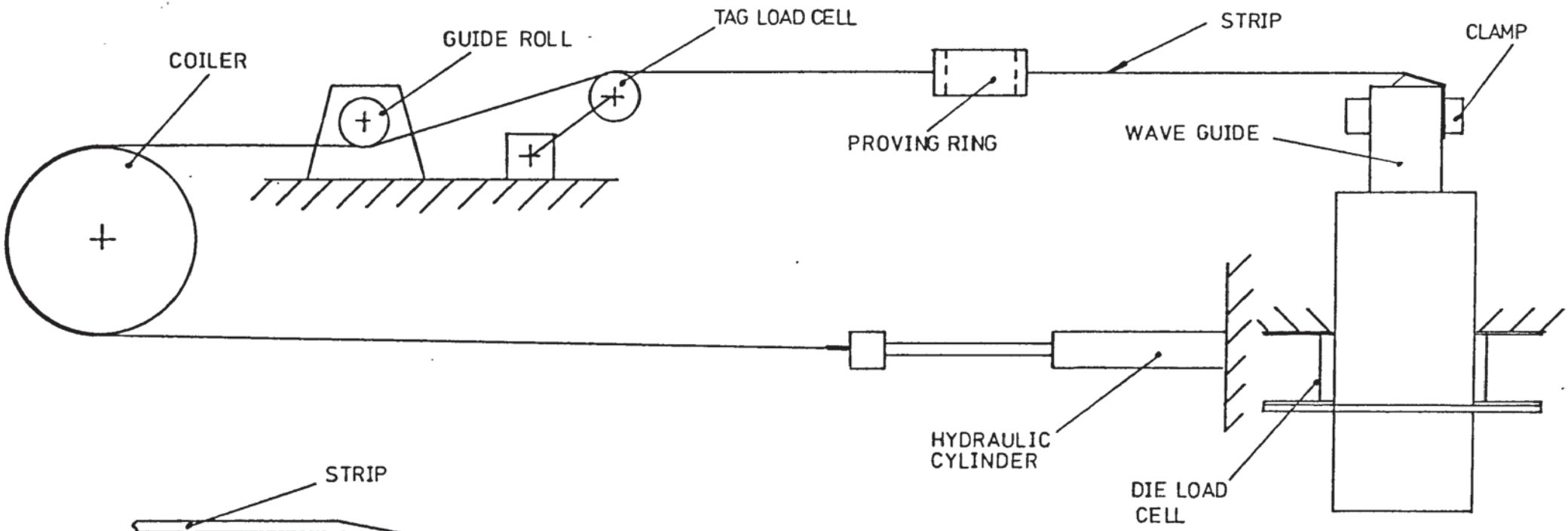

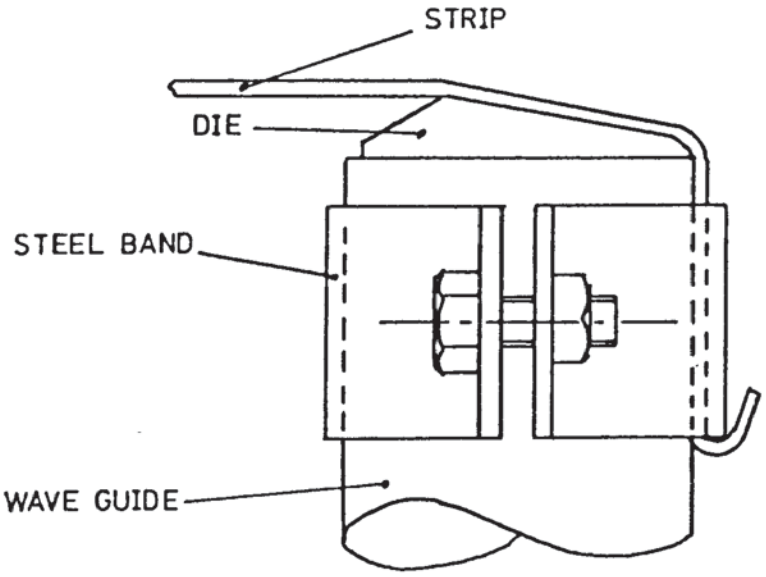

Fig(5.9) - Method Of Clamping Strip To Wave Guide

Fig(5·9) - Method Of Clamping The Strip To The Wave Guides When Calibrating The Bending And Tag Load Cells

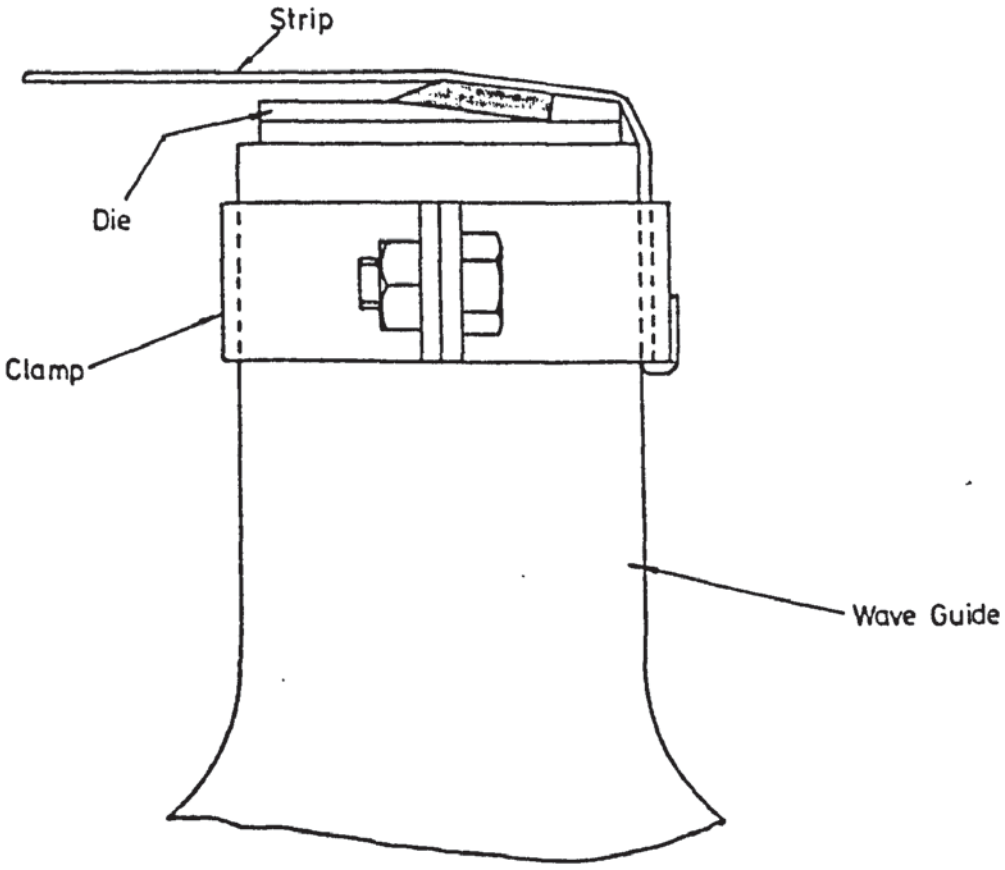

lubricate the coiler surface to allow maximum transmission of the hydraulic ram load past the coiler to the load cells.

The strip was loaded incrementally to give the required reading on the proving ring dial gauge, with the corresponding output from the load cell or cells being monitored on the U.V. recorder. The results of these tests are shown in Figures (5.10), (5.11) and (5.12).

Axial load cell output was also monitored during these tests but was found to be of a very low order. It can be concluded, therefore, that there was no cross sensitivity from the bending load to the axial load cell.

Fig(5.10) - Tag Load Cell Calibration

Tag Load v. Galvanometer Deflection

(Upper Tag Load Cell)

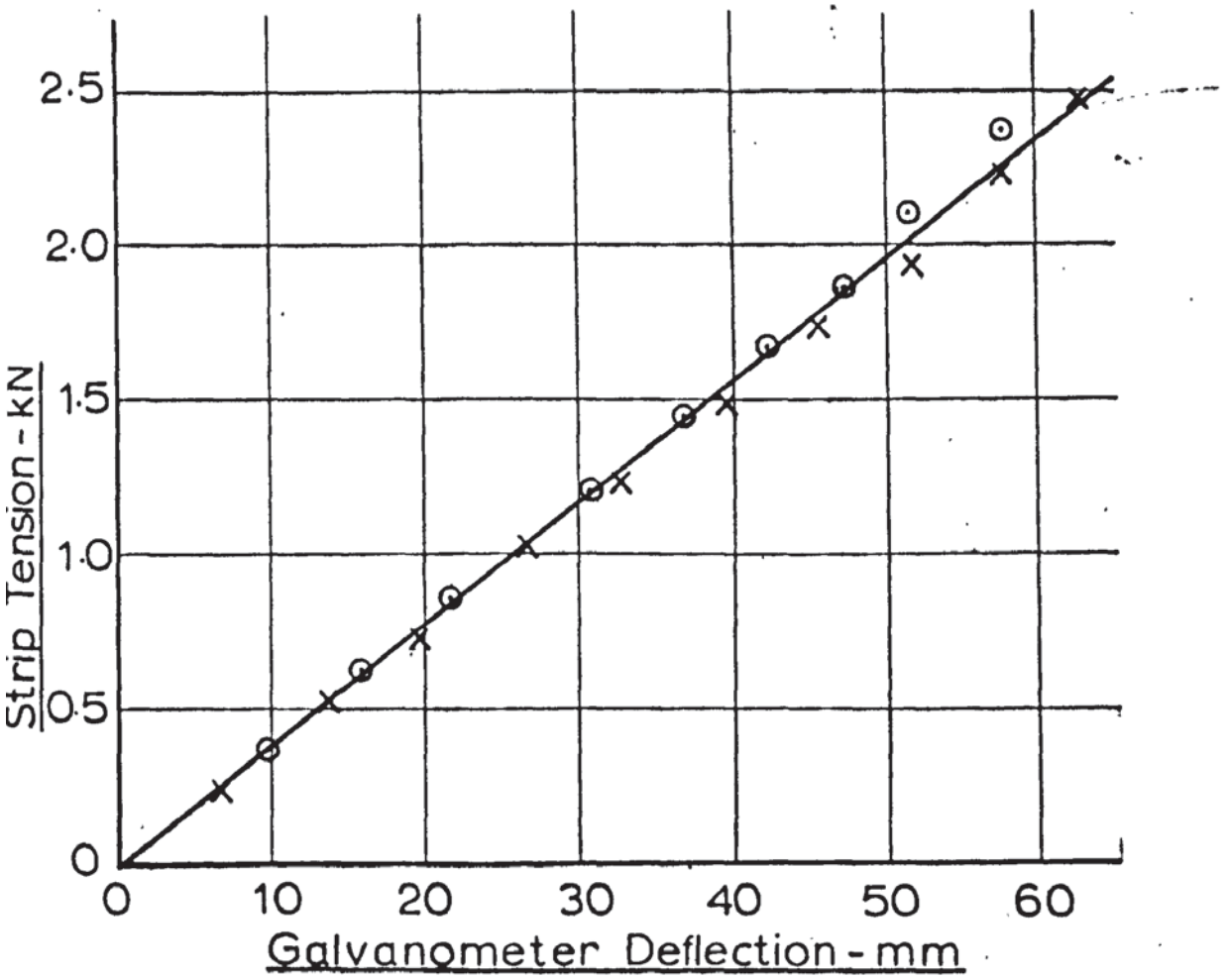

x - Loading
⊙ - Unloading

GALVAOMETER - B100
SERIAL NO. - 9091
BRIDGE VOLTAGE - 4V
PROVING RING CONSTANT - 0·0124 kN/DIV

Load Cell Constant - 0·0402 kN/mm

Fig(5.11) - Tag Load Cell Calibration

Tag Load v. Galvanometer Deflection

(Lower Tag Load Cell)

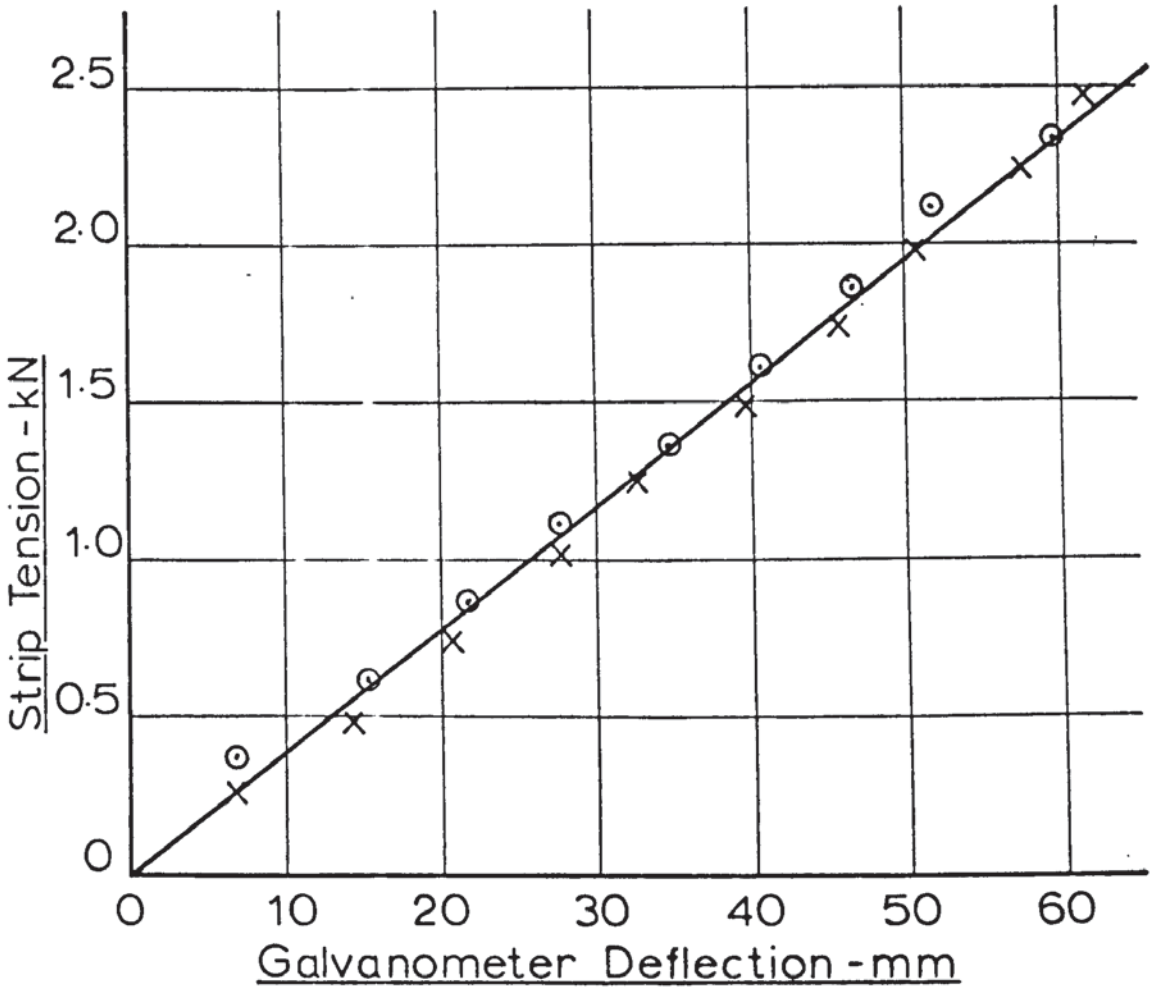

x - Loading

⊙ - Unloading

GALVANOMETER - M100
SERIAL NO. - 9658
BRIDGE VOLTAGE - 4V
PROVING RING CONSTANT - 0·0124 kN/DIV

Load Cell Constant - 0·0402 kN/mm

Fig(5.12) - Bending Load Cell Calibration

Bending Load v. Galvanometer Deflection

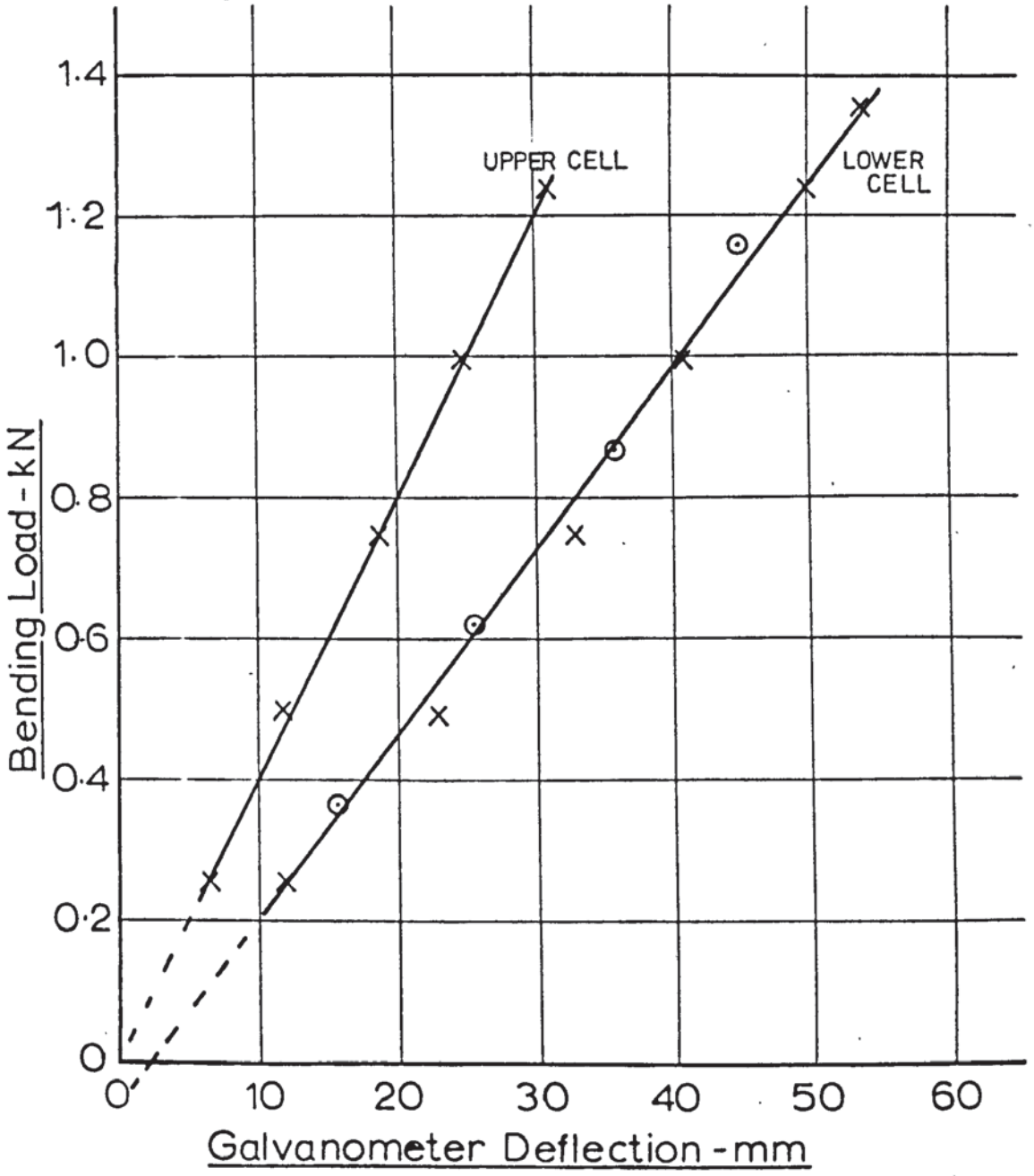

x - Loading
⊙ - Unloading

PROVING RING CONSTANT - 0·0124 kN/DIV

Upper Cell

GALVANOMETER - B450
SERIAL NO. - 3-6840
BRIDGE VOLTAGE - 4V

Cell Constant - 0·040 kN/mm

Lower Cell

GALVANOMETER - B450
SERIAL NO. - 3-6890
BRIDGE VOLTAGE - 5V

Cell Constant - 0·026 kN/mm

5.2) Measurement of Oscillatory Amplitude and Dynamic Strain

A number of methods of measuring strain and displacement at high frequencies have been employed by workers in the field of ultrasonic metal deformation. These methods usually fall into one of the following groups.

1. Piezoelectric accelerometers,
2. Eddy current detectors,
3. Magnetostrictive probes,
4. Strain gauges, and
5. Direct observation through a microscope

These methods are discussed in detail in this section, special reference being made to their application to the strip drawing tests.

5.2.1) Piezoelectric Accelerometers

Discs made from a piezoelectric material have been used extensively by members of the metal deformation research group at the University of Aston. The discs may be mounted directly onto a vibrating surface, though it is necessary to isolate the disc on a base if the surface is stressed.

As a first attempt to measure die amplitude, piezoelectric discs were bonded to the dies. Piezocrystal discs are supplied with a silver coating on each face giving a low resistance contact to which wires can be easily soldered. The discs are supplied with the coating either wholly covering each face or with contacts from both faces on one side of the disc, as shown in Figure (5.13). The former type of disc is used in commercially manufactured accelerometers in the form shown in Figure (5.14). These discs are generally soldered or clamped to a magnetic or screw base with a seismic mass mounted on top of the disc. The electrical output is taken from the base and the seismic mass[16]. The latter type of disc can be neatly bonded to a flat surface with the soldered contacts running from the top surface of the disc, as shown in Figure (5.15).

It was found necessary to shield the discs with aluminium foil. This prevented mutual interference from the electric fields generated by the

Fig(5.13) - Two Basic Forms Of Piezocrystal Discs

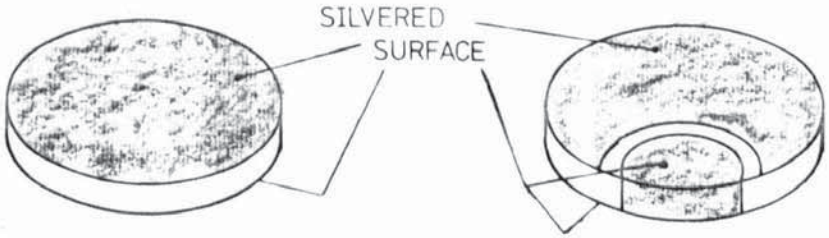

Fig(5.14) - Piezo Accelerometer

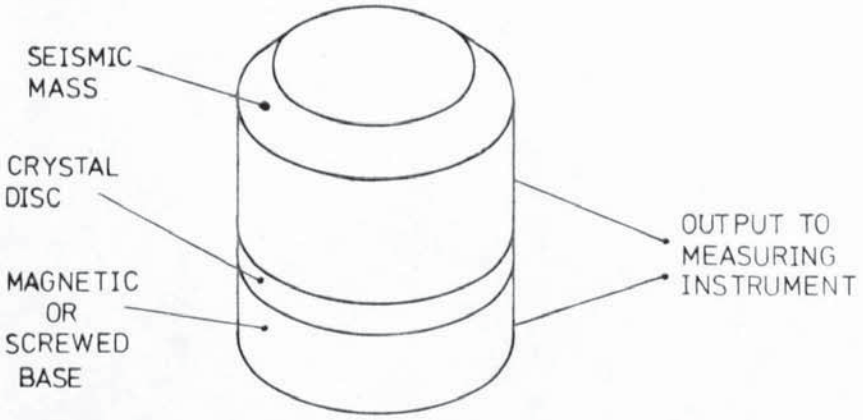

Fig(5.15) - Arrangement Of Piezocystal Discs For Measurement Of Die Amplitude

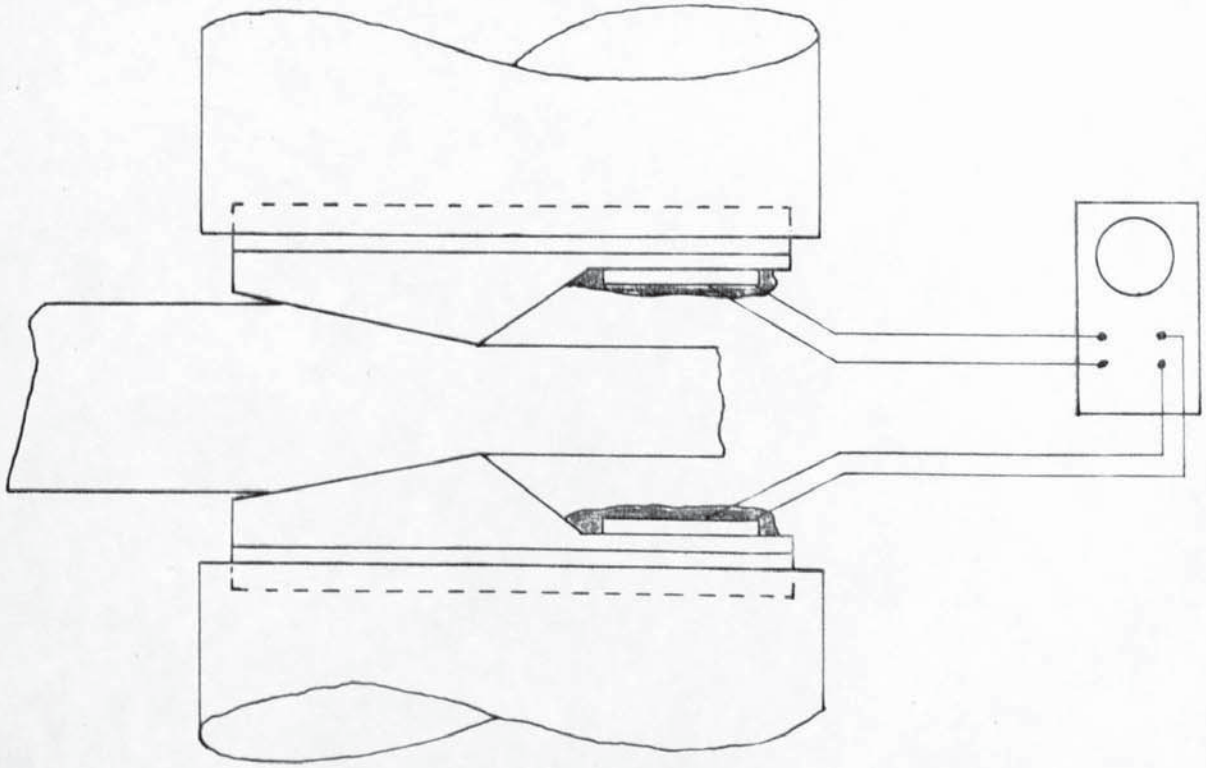

piezocrystals when the dies were vibrating. The arrangement shown in Figure (5.15) is not satisfactory since the disc is subjected to the transverse stresses generated in the die surface when the strip is being drawn. Such stresses generate a voltage in the piezocrystal disc in addition to the voltage generated as a result of the inertia force. The narrow gap between the dies did not allow the discs to be mounted on an isolating base. Any increase in temperature in the die would cause a drift in sensitivity if the temperature/output characteristic of the piezoelectric material was non-linear.

5.2.2) Eddy Current Detectors

A) "Distec"

The "Distec"is a non-contact displacement measuring instrument manufactured in the U.S.A. by the Helm Instrument Co. It consists of a probe, which is positioned close to a conducting surface, and a "signal conditioning unit", the output of which is fed to an oscilloscope or digital voltmeter, as shown in Figure (5.16). The manufacturers claim a flat output, within 1%, for frequencies in the range 0-50 kHz.

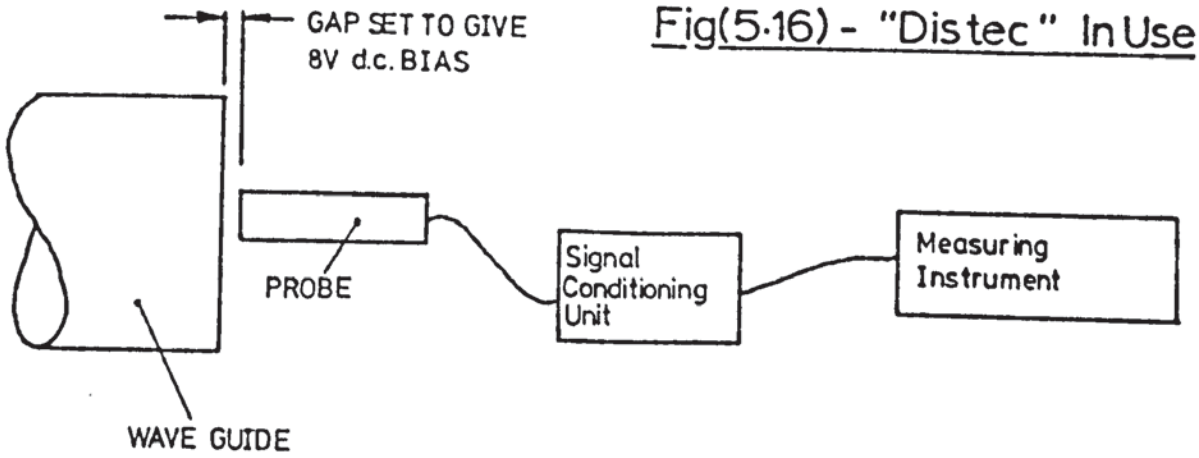

Fig(5.16) - "Distec" In Use

When calibrating the "Distec" the probe is mounted on a vernier height gauge, with the output from the signal conditioning unit being monitored on a digital voltmeter. The gap between the probe and the waveguide was increased incrementally until a saturation point is reached at an output of approximately 13v. Corresponding values of output voltage and height gauge reaching were noted. Figure (5.17) shows such a calibration curve for the lower die concentrator. It can be seen that the curve is linear within the range 4-10v, giving a calibration constant of 0.168 μm/mV. Since the frequency response of the "Distec" is flat over the required range the calibration constant can be used when the waveguide is vibrating, thus requiring the output to be monitored on an oscilloscope. The static output of the signal conditioning unit was initially set at approximately 8v to ensure that the transducer was operating on a linear part of its output characteristic.

The "Distec" has been used primarily as a means of calibrating other instruments which generally, are more robust and compact, and can be fixed permanently without the necessity for regular checks on the bias voltage required by the "Distec". Limitations on space usually render the use of the "Distec" impracticable for direct measurement during experimetal work.

B) Electro dynamic transducers

Transducers using a multi-turn coil positioned between the poles of a horseshoe magnet have been used by Herbertz[8] and Galan et al[9] to measure the amplitude of vibration of vibrating rods. The author used a similar device to measure die amplitude during the strip drawing tests. The transducer was bonded to the end of the waveguide using a silicone rubber adhesive, which withstood the severe fatigue conditions far better than rigid adhesives such as "Araldite". A diagram of the transducer attached to the wave guide is shown in Figure (5.18).

Fig(5.17) - "Distec" Calibration

Output Voltage v. Change In Gap Between Probe And Wave Guide

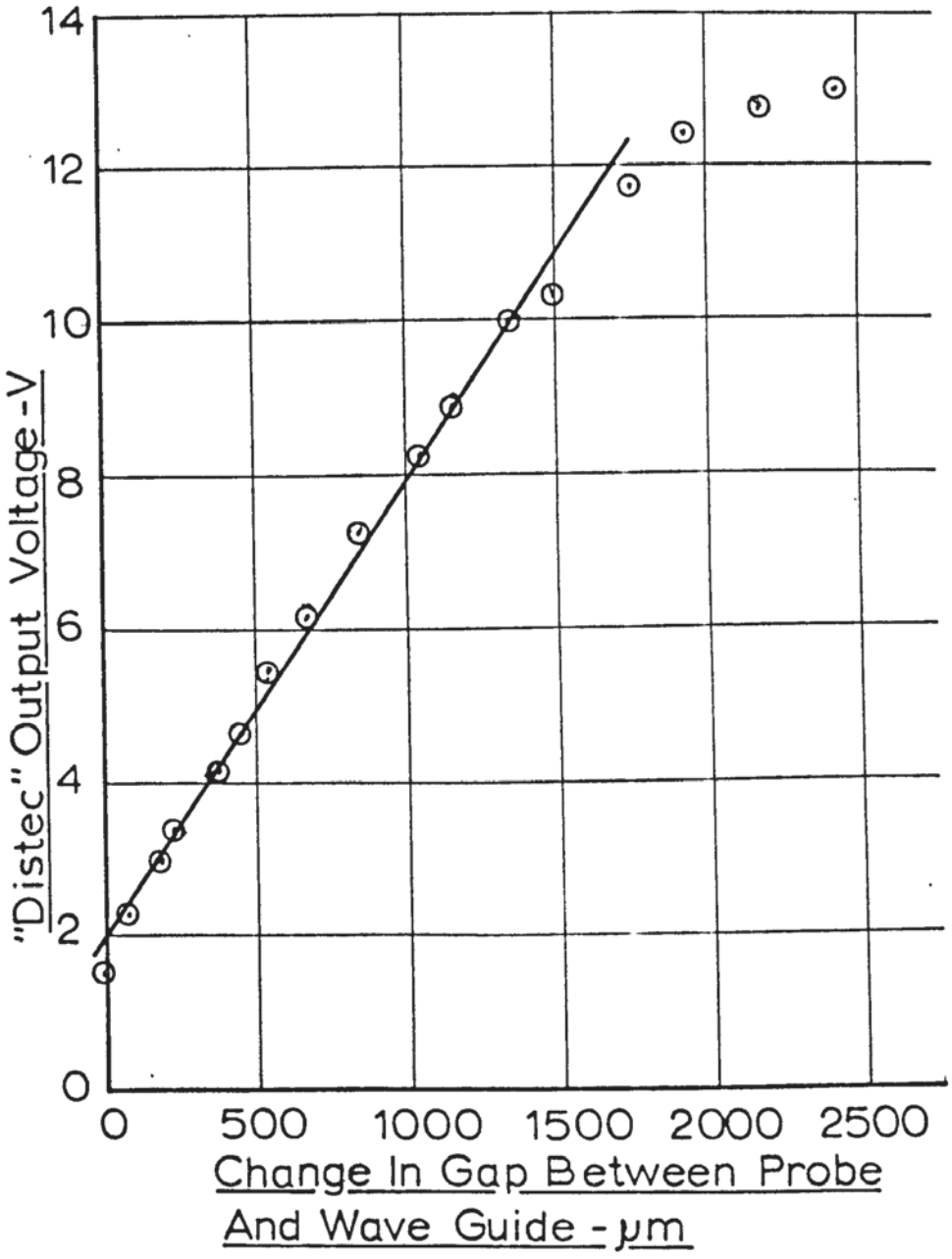

Calibration Constant - 0.168 μm/mV

"Distec" Serial No. - 16332 (Long Probe)

Fig(5.18) - Horseshoe Magnet Transducer Attached To Wave Guide

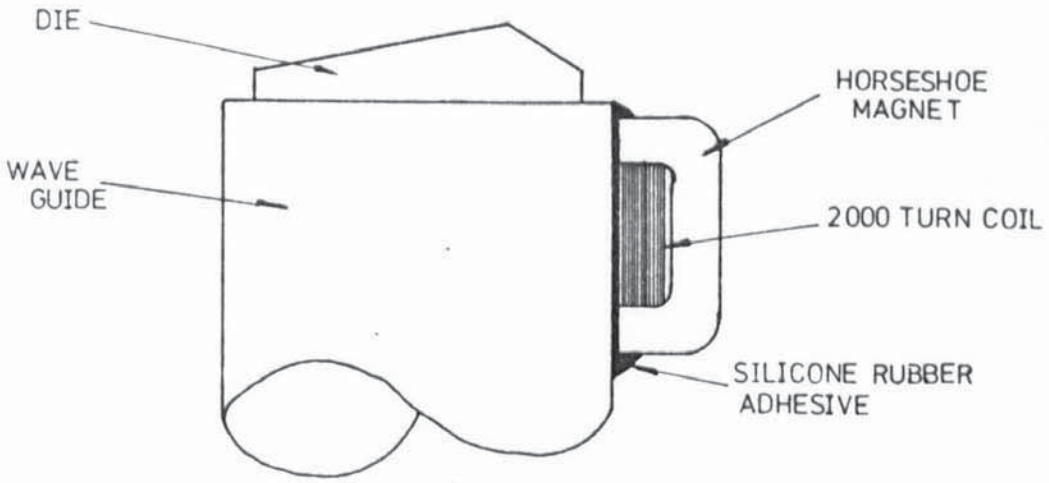

The transducers for the upper and lower wave guides were calibrated against a perviously calibrated "Distec". It can be seen in Figure (5.19) and Figure (5.20) that the output of the coil varied linearly with die amplitude. The first calibration test was carried out when the magnets were new, that is, they had been stored with their keeper plates in position. After several weeks it was noticed that the coil output for a given power input had dropped markedly. The calibration constant was checked by repeating the calibration test and it was found that the coil sensitivity had decreased by approximately 33%. The calibration constant was checked again several weeks later and was found to be unchanged. The loss of sensitiviey was probably due to deterioration in the magnet. No attempt was made to tune the transducer since a "clean" sinusoidal output of adequate strength could be obtained in its untuned state.

Kleesattel[10] has proposed designs for coil/magnet instruments which allow specific components of a vibration to be measured, that is, the instrument's sensitivity is directional.

A device of the type proposed by Kleesattel for measuring longitudinal vibrational amplitudes was constructed by the author. A diagram of this device is shown in Figure (5.21).

Fig(5·19) - Calibration Of Horseshoe Magnet Coil (Upper Wave Guide)

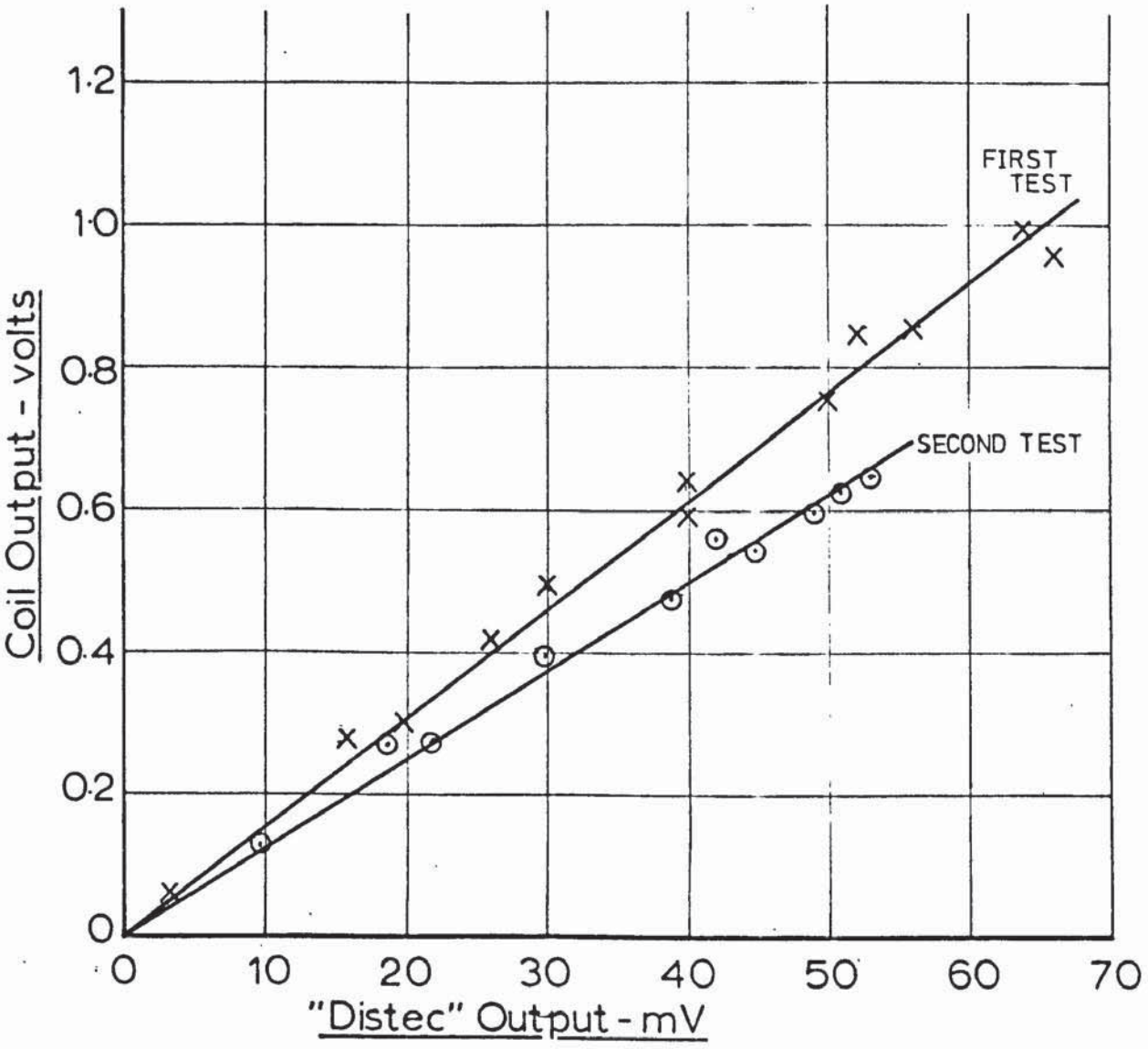

Fig(5.20) - Calibration Of Horseshoe Magnet Coil (Lower Wave Guide)

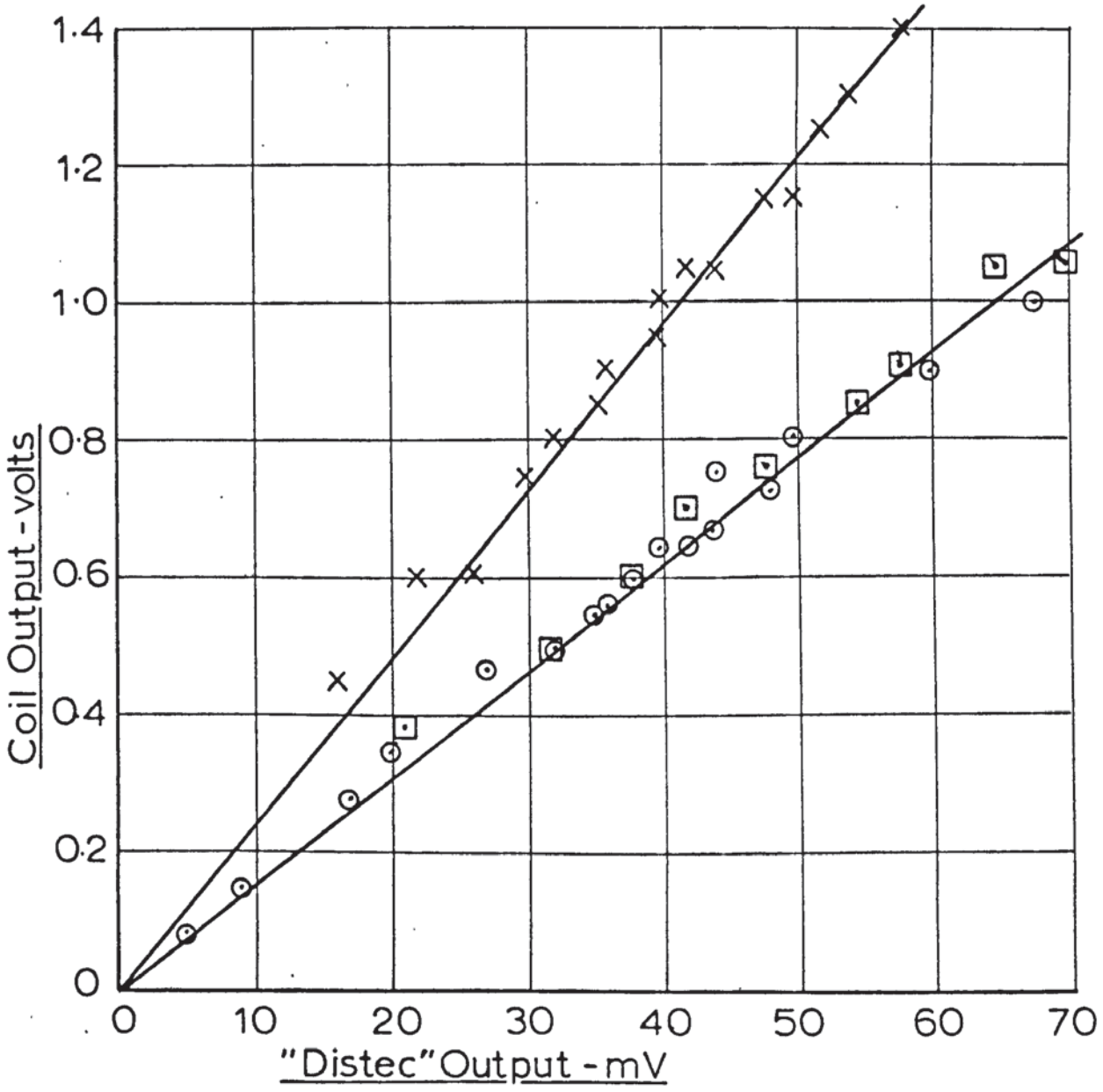

x - First Test
⊙ - Second Test
⊡ - Third Test

Fig(5.21) - Kleesattel Type Transducer

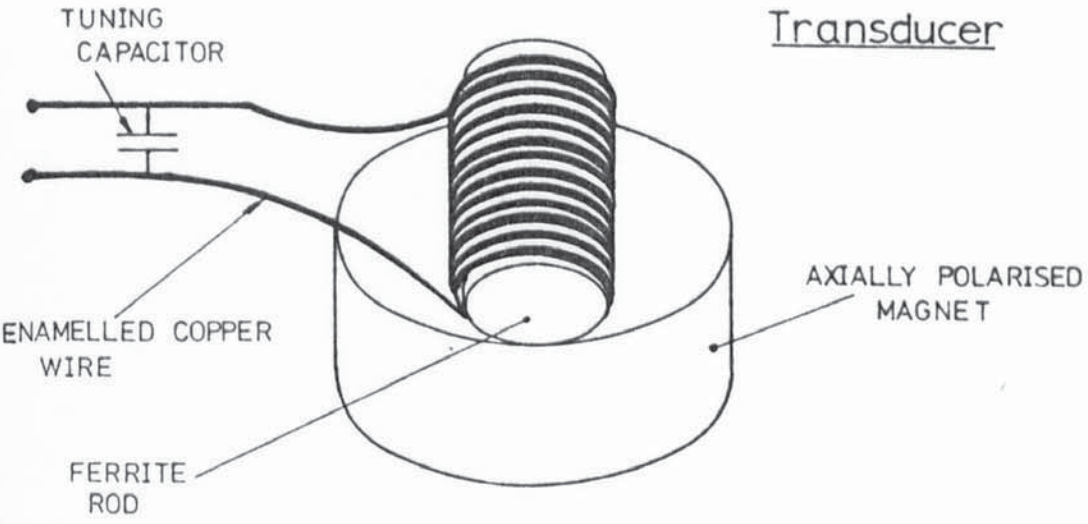

N.B. - THE WHOLE ASSEMBLY SHOULD BE ENCASED IN EPOXY RESIN. THE CAPACITOR MUST ALSO BE SEALED TO PREVENT DISCHARGE.

The transducer consists of a single coil of enamelled copper wire wound round a ferrite rod, the magnetic field being supplied by a high quality axially polarised permanent magnet. Kleesattel[10] states that the length of the coil should be no greater than one-tenth of a wavelength, in order that the instrument may accurately describe the vibrational mode at a specific point. The instrument constructed by the author used a coil length of approximately one-twentieth of a wavelength.

Ideally, a ceramic magnet should be used to supply the magnetic field thus avoiding the eddy current losses which occur in conducting magnets. A conducting magnet was employed in the above device, which gave a satisfactory performance. The transducer was tuned to 13 kHz by measuring its inductance on an inductance bridge. A capacitor, having the same inductive reactance as the transducer, was then wired in parallel with the transducer, thus maximising its output.

It was intended to use this type of transducer to measure the dynamic strain in the strip during drawing. In order to calibrate the transducer a length of predrawn strip was brazed to a stub which was screwed to the plug bar waveguide. The strip was passed over the tag load cell and guide roll

and wound onto the coiler. The coiler was driven to take-up the strip and develop an arbitrary level of pre-tension. Figure (5.22) shows the calibration set-up with the strain gauge bridge mounted at a stress antinode.

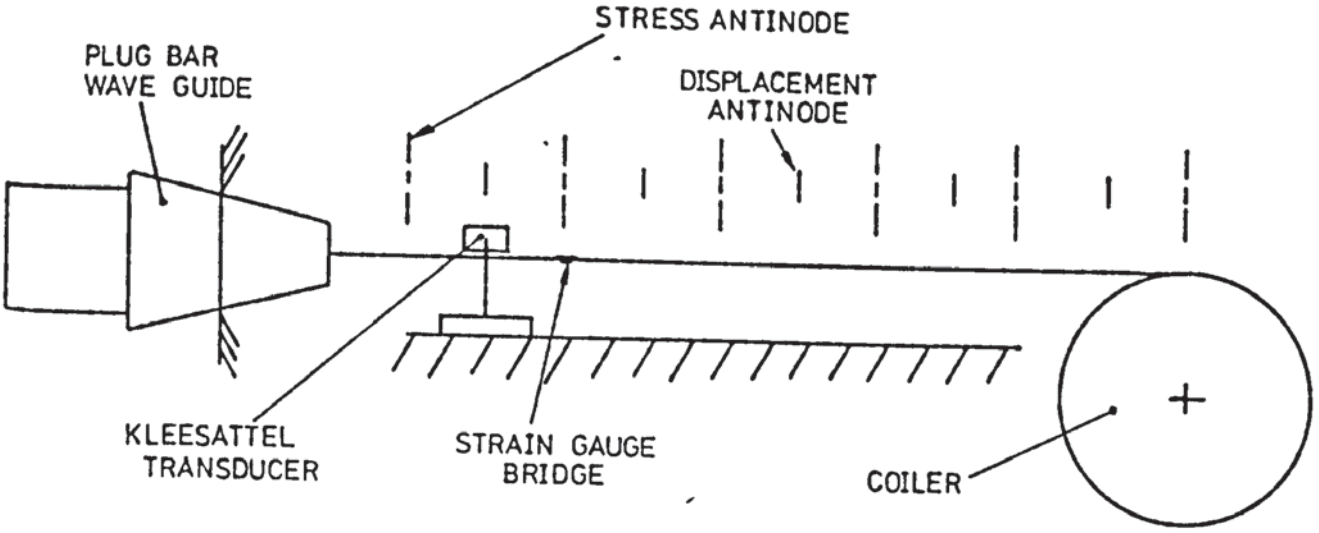

Fig(5.22)- Setup For Calibration Of Kleesattel Transducer

The exact position of the stress antinode was determined by utilising the directional properties of the transducer and also the fact that this type of instrument is sensitive to both stress and displacement waves. A peak output from the transducer was obtained at four equi-spaced points in a single wavelength, that is, at positions of peak stress and peak displacement. The difference between a stress and displacement antinodes can be determined by positioning the transducer across the strip. At a stress antinode the Poisson component of the stress wave can be detected. At a displacement antinode a similar operation produces a zero output, since the stress is zero and there is no transverse displacement.

The output from the strain gauge bridge was fed to the guarded differential input of a Bradley type 155 oscilloscope and the output from transducer was monitored on the other channel of the same oscilloscope.

The strip was vibrated, via the plug bar wave guide, at various amplitudes, first with the transducer positioned over a displacement antinode, then over a stress antinode. The results of these tests are shown in Figure (5.23).

Fig(5·23) - Calibration Of "Kleesattel" Coil

Bridge Output v. Transducer Output

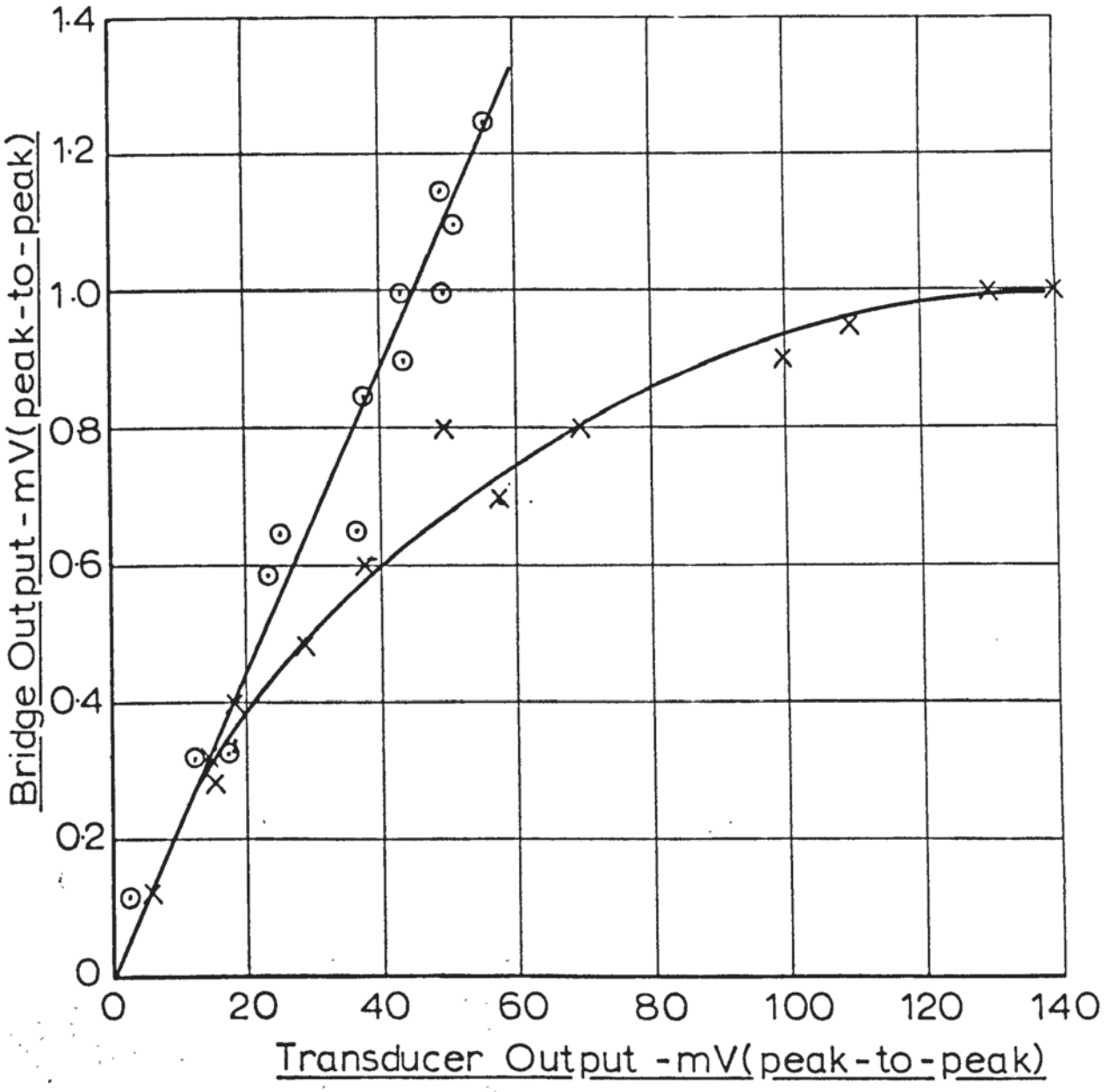

× - COIL PLACED OVER DISPLACEMENT ANTINODE

⊙ - COIL PLACED OVER STRESS ANTINODE

STRIP THICKNESS - 0·5mm
FREQUENCY - 13·89kHz
BRIDGE VOLTAGE - 4V
GAUGE FACTOR - 2·15
GAUGE RESISTANCE - 120Ω

It can be seen that the characteristics derived from these tests differ markedly. Referring to Figure (5.24), at a stress antinode the rate of change of velocity is maximal. Similarly, at a displacement antinode the stress differential is maximal. Thus at a stress antinode the eddy currents, caused by the rapid change in strip velocity, will be responsible for the transducer output. At a displacement antinode the stress gradient causes a permeability differential, which results in the magnetic field disturbance necessary to give an output from the transducer. The reduction of transducer sensitivity is therefore probably due to the magnetic saturation of the strip and/or non-linearities in its stress-permeability characteristic.

The transducer which used the horseshoe magnet operates in a similar manner to the latter case , though it gave a linear calibration curve. This implies that the bulk of the wave guides was sufficient to prevent magnetic saturation.

In order to obtain calibration constants for the whole range of strip reductions, it would be necessary to repeat the above procedure using a suitable range of pre-drawn strip. When the strip was being drawn the signal from the transducer was corrupted by transverse, and bending mode vibrations at 13 kHz and also by high amplitude, low frequency vibrations due to bending of the die wave guides. This rendered the signal unusable and the additional tests, required to extract a full set of calibration data, were not carried out.

A similar type of transducer has been used by Waterhouse[12] when drawing thin walled tube. These tests were carried out at low speed and low die amplitudes. This, along with the greater geometric stability of the tube when compared with strip, and the ridigity of the solid die, resulted in satisfactory performance from the transducer.

The main advantage of this device is that it is sensitive only to vibrations parallel to the axis of the ferrite core, and can therefore be

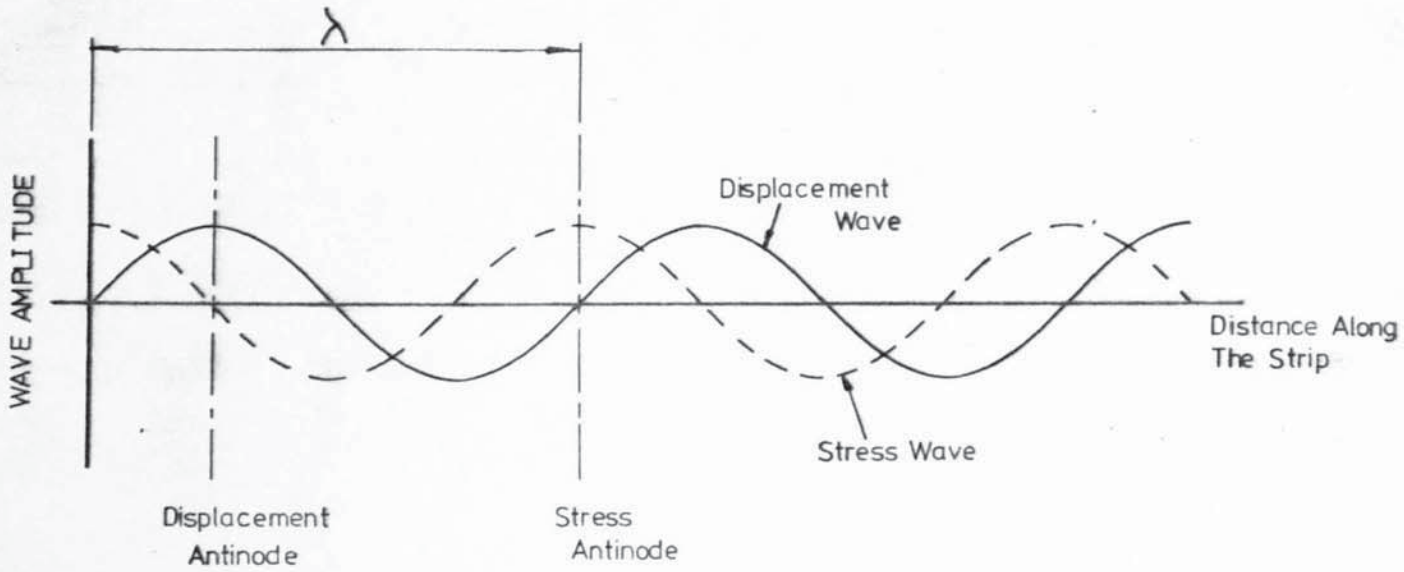

Fig(5.24) - Stress And Displacement Waves In A Vibrating Strip

used as a probe to determine vibrational modes and the position of nodes, as well as its use as a displacement transducer.

5.2.3) Magnetostrictive Probes

The "Macdonald" probe is a magnetostrictive device which was originally developed in the Department of Electrical Engineering at the University of Aston for the measurement of very low amplitude vibrations. This device, in the form used for the low amplitude work, is shown in Figure (5.25). The magneto-strictive wire is placed in contact with the vibrating surface which causes a signal to be generated in the coil. The coil should be of the same length as the magnet, though its actual length is unimportant since the wire as a whole is displaced by the vibration. That is, the "Macdonald" probe is a non-resonant device and for this reason the wire is mounted in a compliant material to prevent the development of a standing wave. The probe was tuned to the required frequency as before. Tuning is of far greater importance with this device than it is in the coil/magnet instruments.

A more robust version of this device was constructed by the author, as shown in Figure (5.26), which has a thicker wire to improve bending resistance, and the whole of the case was filled with silicone rubber to damp flexural vibrations and longitudinal standing waves. This version of the probe was calibrated against the horseshoe magnet transducer, the results of which are shown in Figure (5.27). These results show that the probe may give a low reading. It is therefore necessary to be experienced in the use of this probe before it can be used for quantitative work, though fairly good repeatability can be achieved with practice. The maximum amplitude of vibration generated in the die wave guides under no load conditions is at the limit of the usable range of this device.

The primary use of this instrument is as a probe for determining vibrational modes and for locating displacement nodes on wave guides prior

Fig(5·25) - "Macdonald" Probe For Low Amplitude Measurement

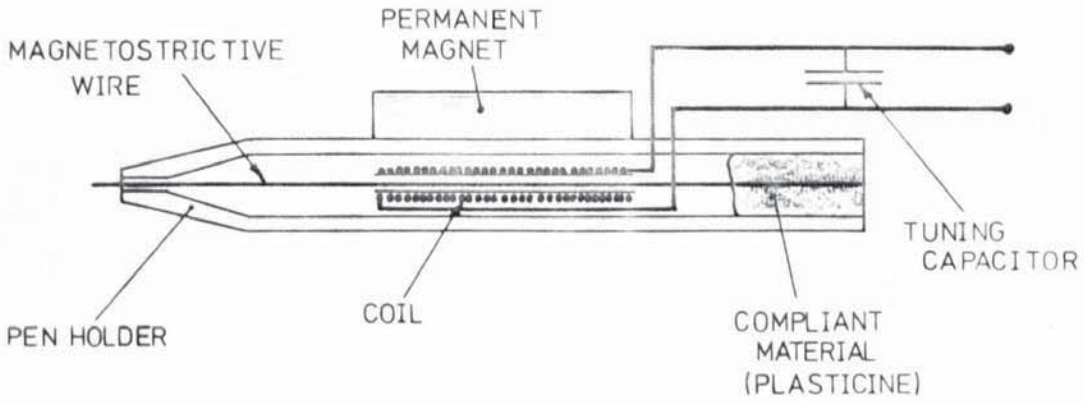

Fig(5·26) - "Macdonald" Probe For High Amplitude Measurement

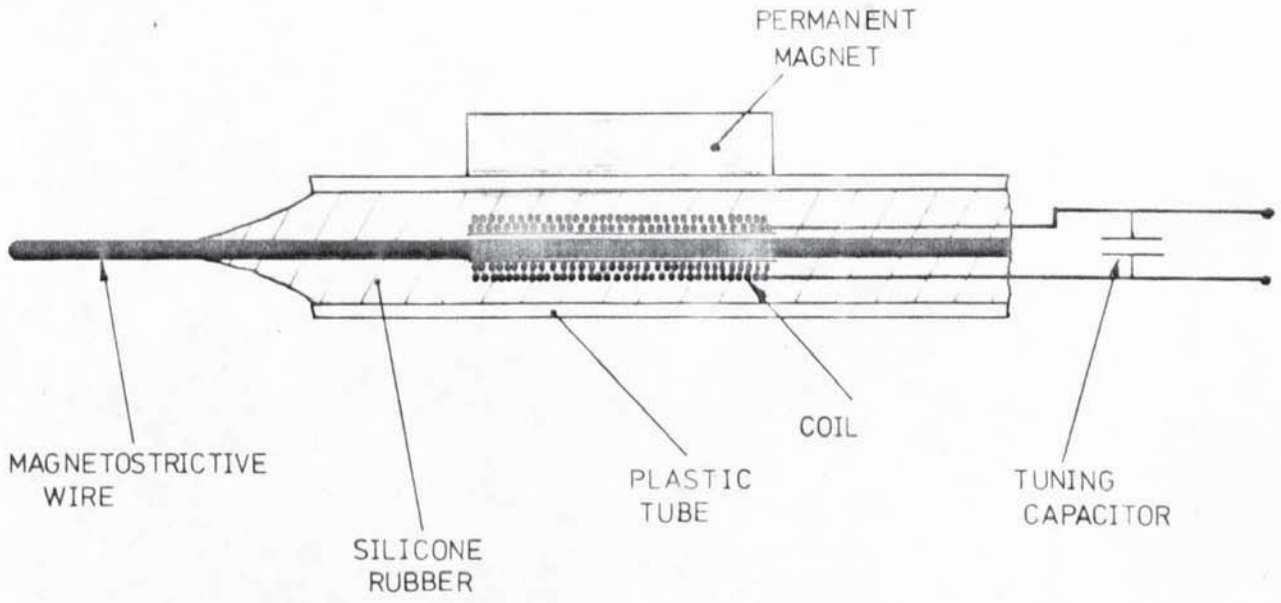

Fig(5·27) - Calibration Of "Macdonald" Probe

Probe Output v. Coil Output

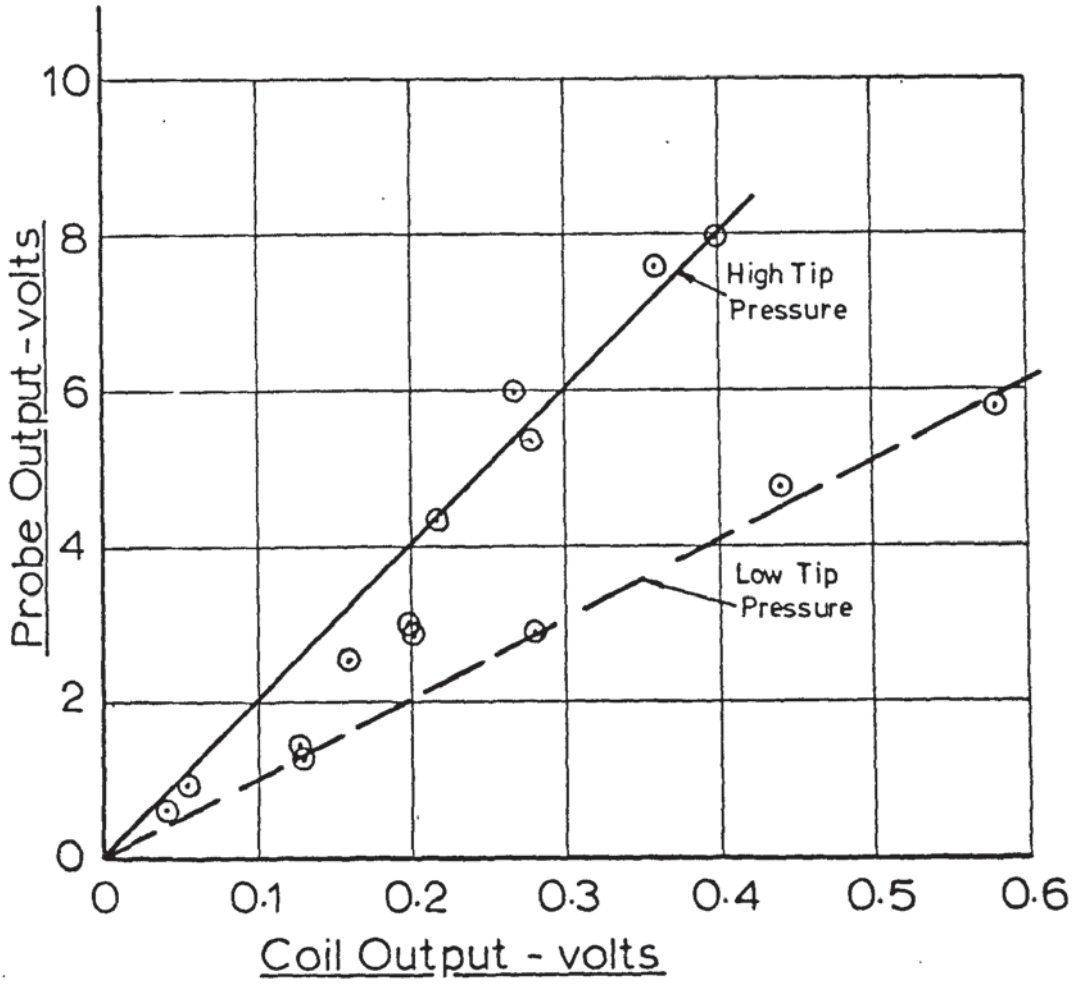

to mounting. The output of the probe, for a given die amplitude, is approximately twenty times that of the horseshoe magnet transducer. This is derived from the direct contact of the magnetostrictive wire which is closely coupled to the coil. The output of the probe therefore has a high signal to noise ratio, and can be used much nearer to the magnetostrictive or piezoelectric transducers used to drive the waveguides than can the magnet coil instruments. For example, the "Macdonald" probe has been used to measure the amplitude of vibration in the throat of a radial resonator. The high level of electrical noise present at the working surface of these devices renders the magnet/coil instruments useless, though the "Distec" can be used in such an environment.

5.2.4) Strain Gauges

It was stated in section 5.2.2. that the Kleesattel type transducer was calibrated against a strain gauge bridge mounted at a stress antinode. The arrangement of the gauges is shown in Figure (5.28) and the associated circuit diagram in Figure (5.29).

The sensitivity of the strain gauge bridge was derived analytically rather than experimentally because of the difficulty in removing the strip from the rig without damaging the strain gauges and wires.

The derivation of the bridge sensitivity is shown below[11].

Referring to Figure (5.29):

$$I_L = \frac{E_{bd}}{R_L + R_B} \qquad (5.1)$$

where R_B, the bridge resistance is given by:

$$R_B = \frac{R_1 R_2}{R_1+R_2} + \frac{R_3 R_4}{R_3+R_4} \qquad (5.2)$$

$$= R_1, \text{ since } R_1 = R_2 = R_3 = R_4$$

R_L is the load resistance, that is the resistance of the indicating instrument.

Fig(5.28)- Layout Of Strain Gauges On Strip For Calibration Of Kleesattel Transducer

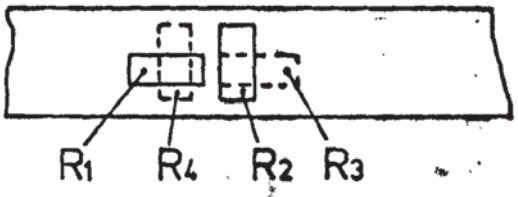

Fig(5.29) - Circuit Diagram For The Strain Gauge Bridge And Indicating Instrument

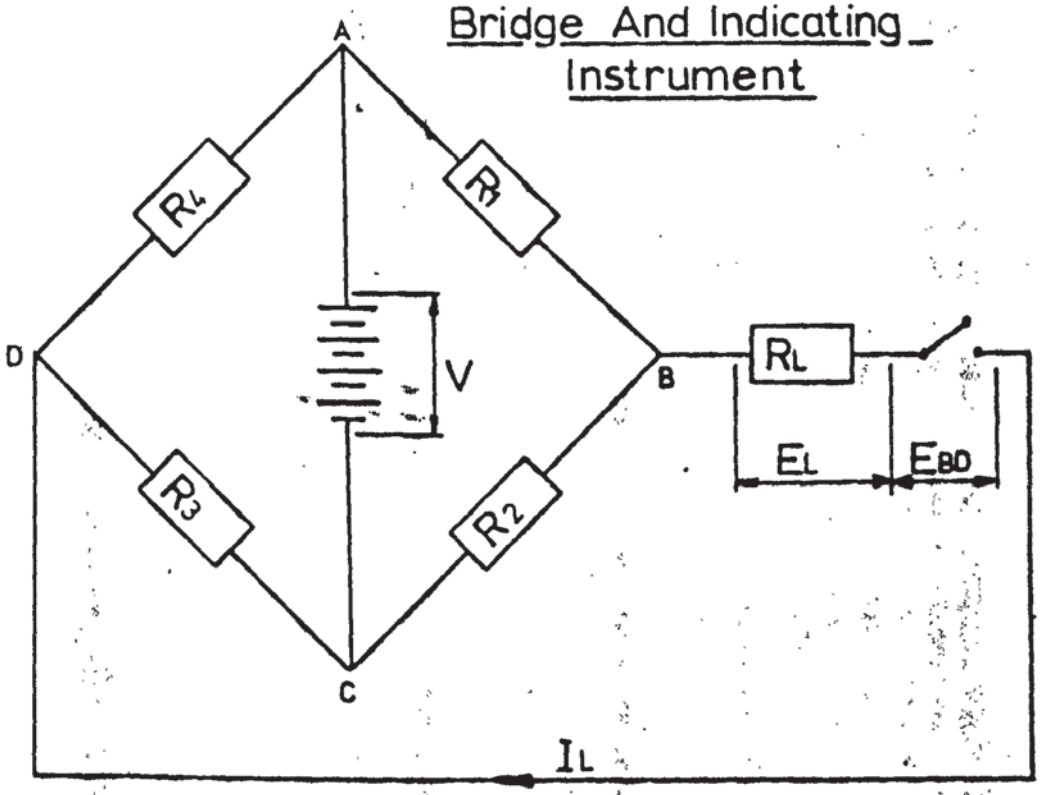

$$\therefore E_L = I_L R_L \qquad (5.3)$$

From Equation (5.1) and Equation (5.2):

$$E_L = E_{bd} \frac{R_L}{R_L + R_B}$$

Now, $\frac{R_L}{R_L+R_B}$ is the factor by which the open circuit potential is reduced by the load resistance. Since the input impedance of an oscilloscope is in the megaohm range and the bridge resistance is 120Ω :

$$\frac{R_L}{R_L + R_B} \rightarrow 1$$

$$\therefore E_L = E_{bd}$$

$$= \frac{FE}{4} (-\Sigma_1 + \Sigma_2 - \Sigma_3 + \Sigma_4)$$

where F is the gauge factor.

For a full wave bridge:

$$\Sigma_1 = \Sigma_3 \text{ and } \Sigma_2 = \Sigma_4 = -\zeta\Sigma_1$$

$$\therefore E_L = \frac{FE}{4} (-\Sigma_1 - \zeta\Sigma_1 - \Sigma_1 - \zeta\Sigma_1)$$

$$= - \frac{FE}{2} (1+\zeta)\Sigma_1$$

The strain gauge bridge consisted of four 120Ω gauges having a gauge factor of 2.15. A voltage of 4v was applied across the bridge from a stabilised power supply. Assuming $\zeta = 0.28$:

$$\therefore E_L = - \frac{2.15 \times 4}{2} (1+0.28)\Sigma_1$$

$$\therefore \Sigma_1 = 0.182 E_L$$

Where E_L is the peak-to-peak voltage registered, on the oscilloscope, since peak-to-peak values were used in the construction of Figure (5.23)

The gauge current is given by:

$$I_g = \frac{1}{2} \frac{E}{Rg} = \frac{4}{2 \times 120} = 16.67 \text{ mA},$$

which is within the capacity of the gauges.

Strain gauges have been used to measure, directly, the dynamic component of strain[12],[13] during tube drawing. This was attempted for the strip drawing tests but was unsuccessful because of the instability of the strip and dies, as with the Kleesattel transducer.

5.2.5) Direct Observation Through a Microscope

Young[27] and Smith [23] have used this technique, with good effect, when calibrating piezocrystals attached to vibrating tools.

A fine line was scribed on a polished area near to the working end of the wave guide. The thickness of the line was measured through a microscope fitted with a micrometer head. This procedure was carried out with and without the wave guide energised, the difference between the two readings was, therefore, equal to twice the vibrational amplitude at that point.

An attempt was made to use this method to measure the vibrational amplitude of the die wave guides. These tests were, however, unsuccessful because the maximum die amplitude was very low. This was later found to be due to the poor performance of the half wavelength wave guide supports; the details of which are given in section 4.2.1.

5.3) Measurement of Mean Draw Speed

The mean draw speed is not related to the rotational velocity of the coiler by a constant factor, since its effective radius increases as drawing proceeds. This implies that it is not feasible to measure strip speed by monitoring the shaft speed of any part of the drive mechanism without correcting for build-up on the coiler, therefore an electro-mechanical pulse generator driven directly from the strip was used, as shown in Plate 3 and, schematically, in Figure (5.30)

The pulse generator consisted of a wheel, running on the strip, with a series of equispaced holes drilled on a common radius. Those holes exposed the light from a 6v bulb as the wheel rotated. The light pulses energised a light activated switch which was placed opposite the bulb on the other side of the disc. This output was passed to a U.V. recorder thus giving a series of marks, the frequency of which was proportional to the mean draw speed.

Now the wheel speed, N, is given by:

$$N = \frac{V_c}{\pi D} \quad \text{rev/min} \quad \text{(see Figure (5.30))}$$

Since there were 5 equispaced holes in the wheel, the pulse frequency, f, is given by:

$$f = 5N = \frac{5\ V_c}{60\pi D} \text{ pulses/sec.}$$

$$\therefore V_c = 12\ \pi\ Df \text{ m/sec}$$

and D = 57.15 mm

$$\therefore V_c = 2.15\ f \text{ m/sec}$$

The pulse frequency is given by:

$$f = \frac{\text{u.v. paper speed (cm/sec)}}{\text{pulse pitch an}}$$

$$= \frac{tp}{p} \text{ pulses/sec}$$

$$\therefore V_c = \frac{2.15\ tp}{p} \text{ m/sec}$$

Fig(5·30)- Method Of Measuring Mean Draw Speed

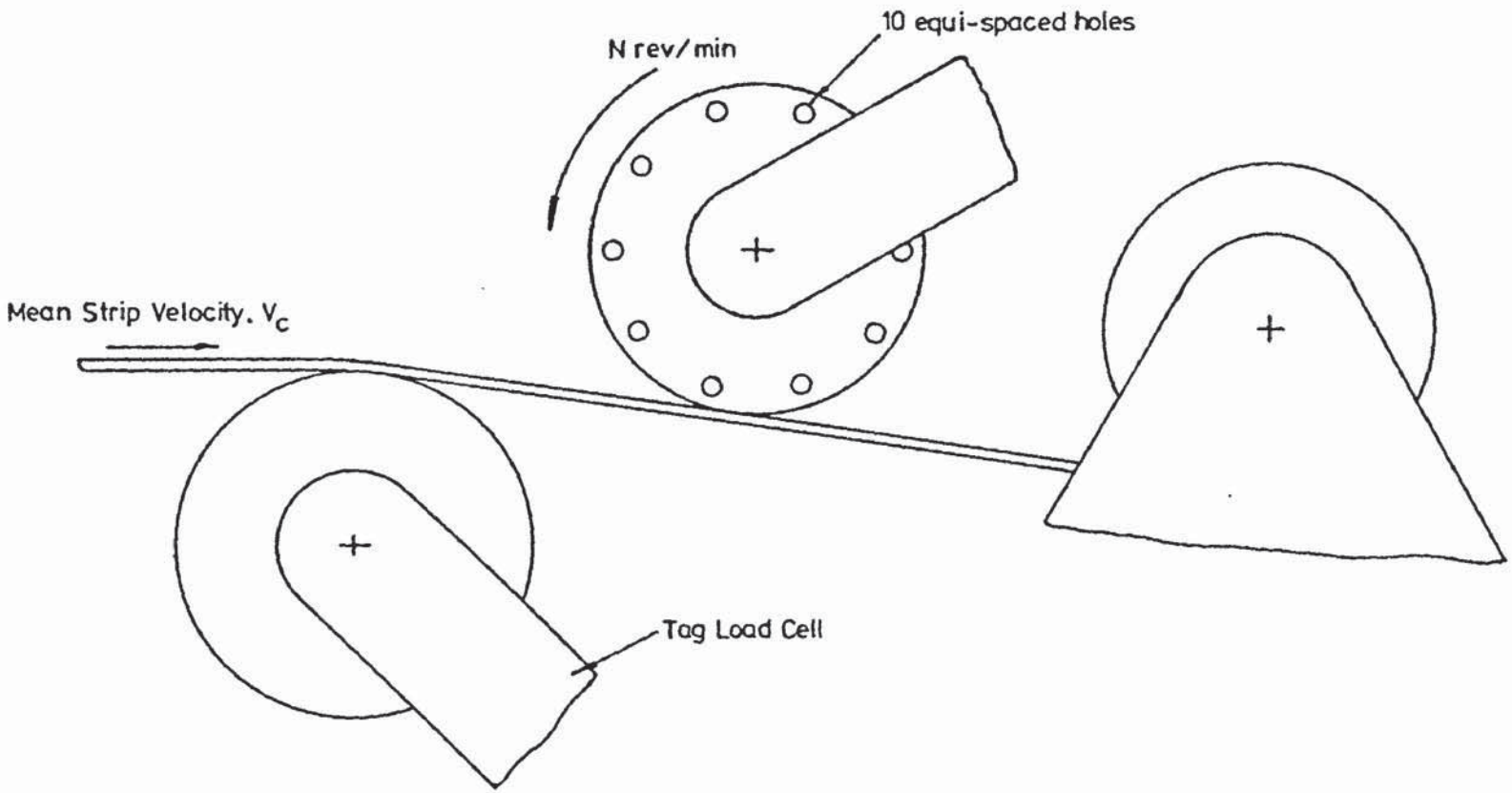

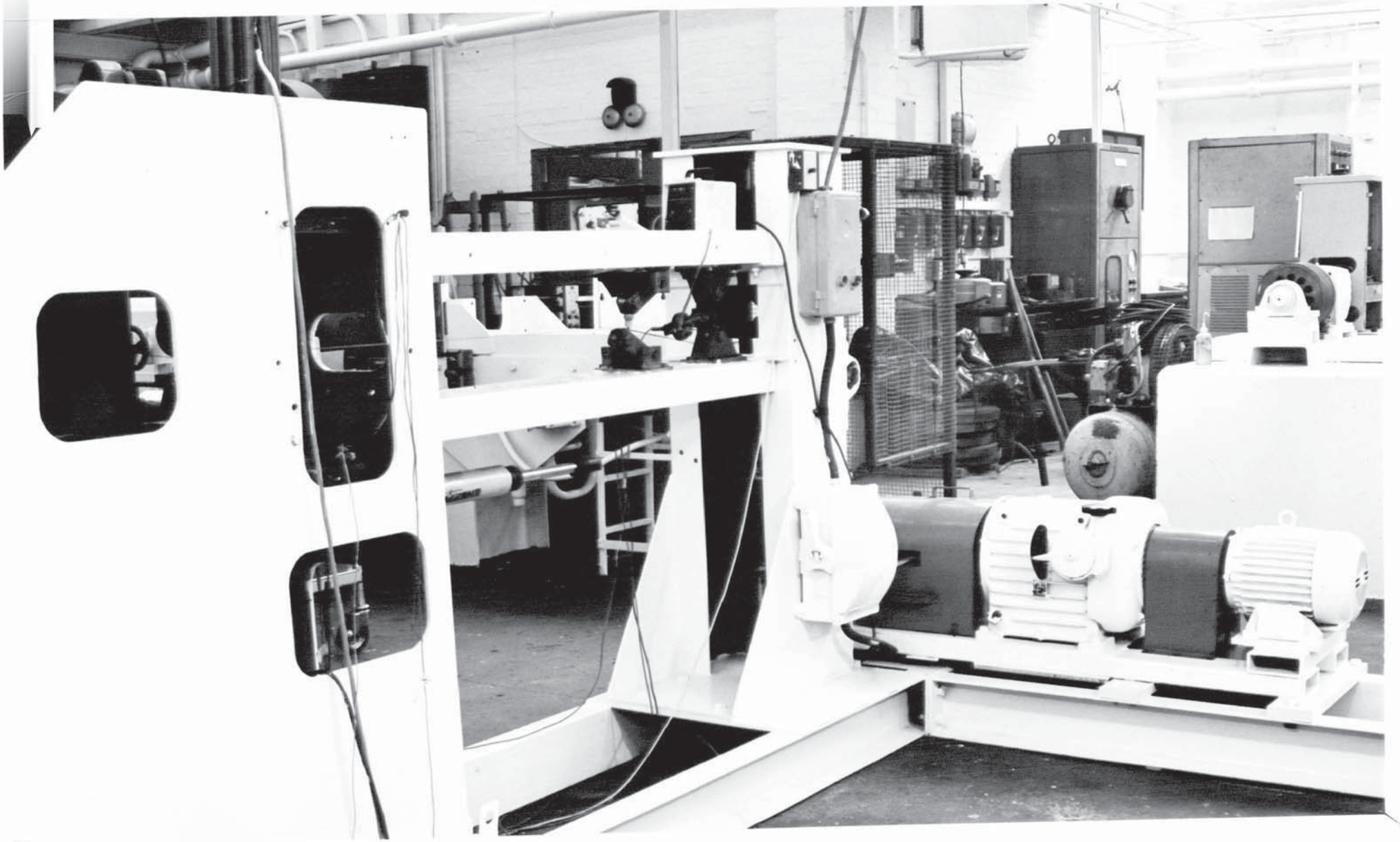

Plate 1 - General View Of The Test Rig_

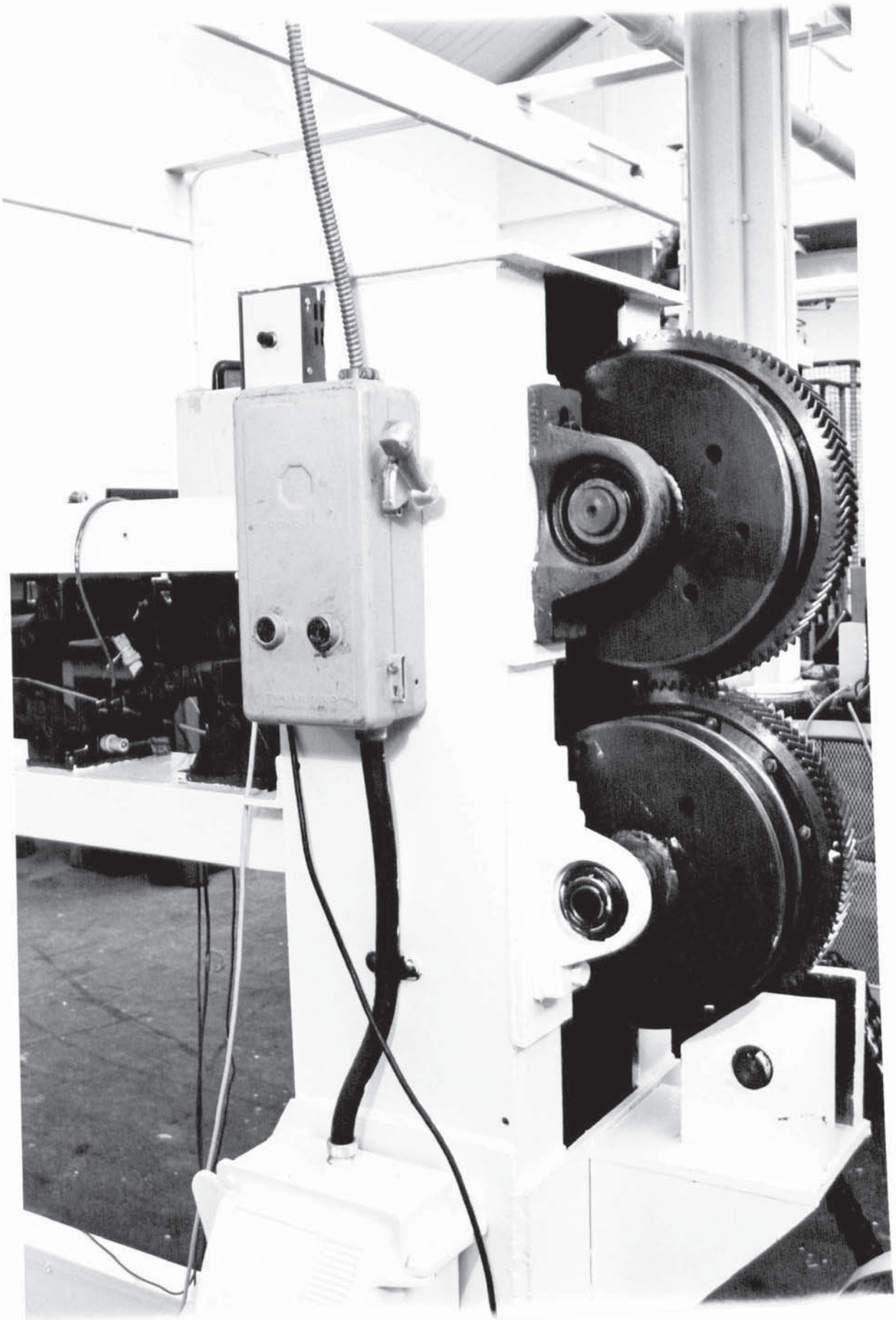

Plate 2 - General View Of The Drive Gear

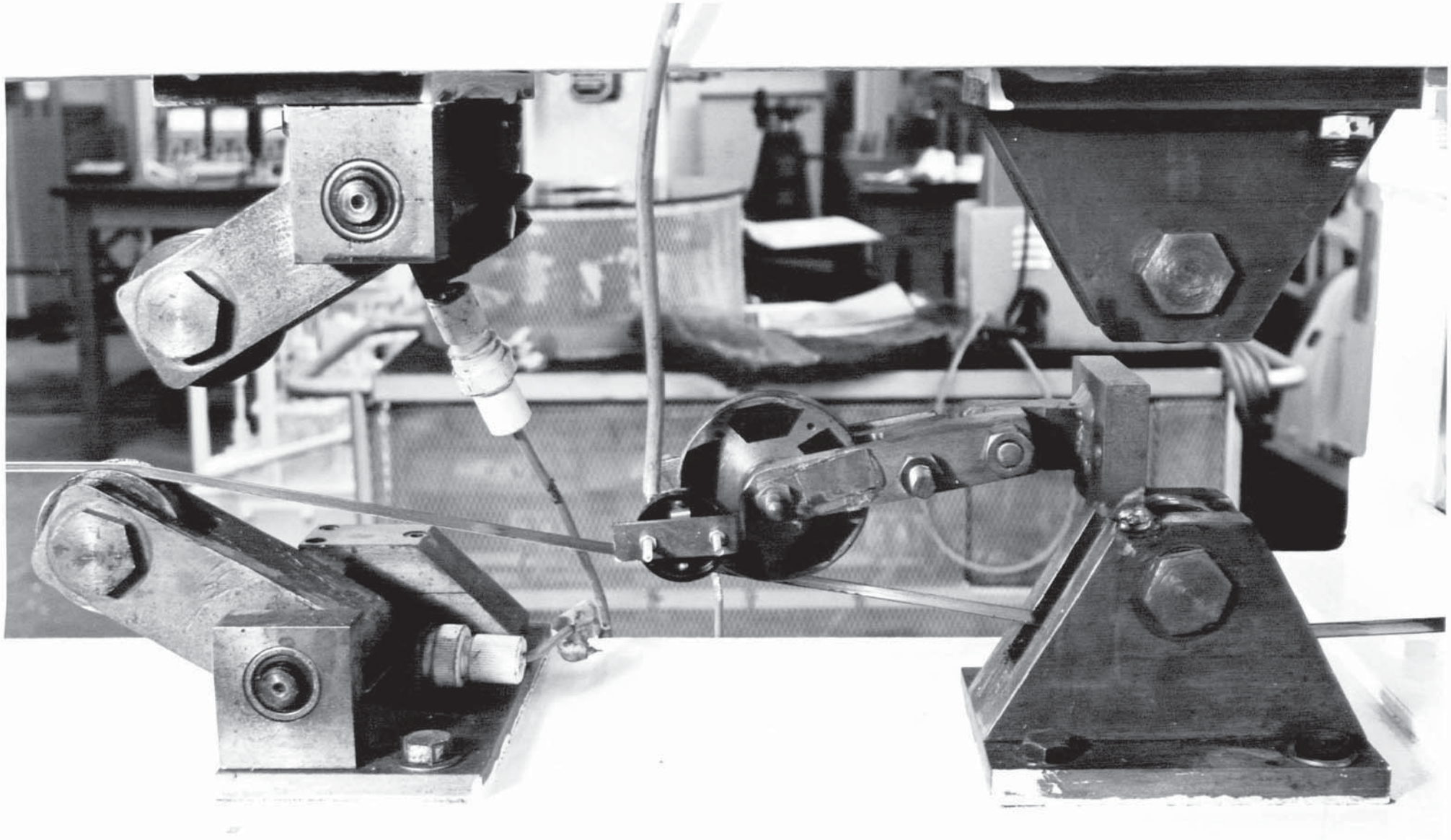

Plate 3 - Tag Load Cell, Guide Rolls, and Pulse Generator

Plate 4 - Die Wave Guides and Strip

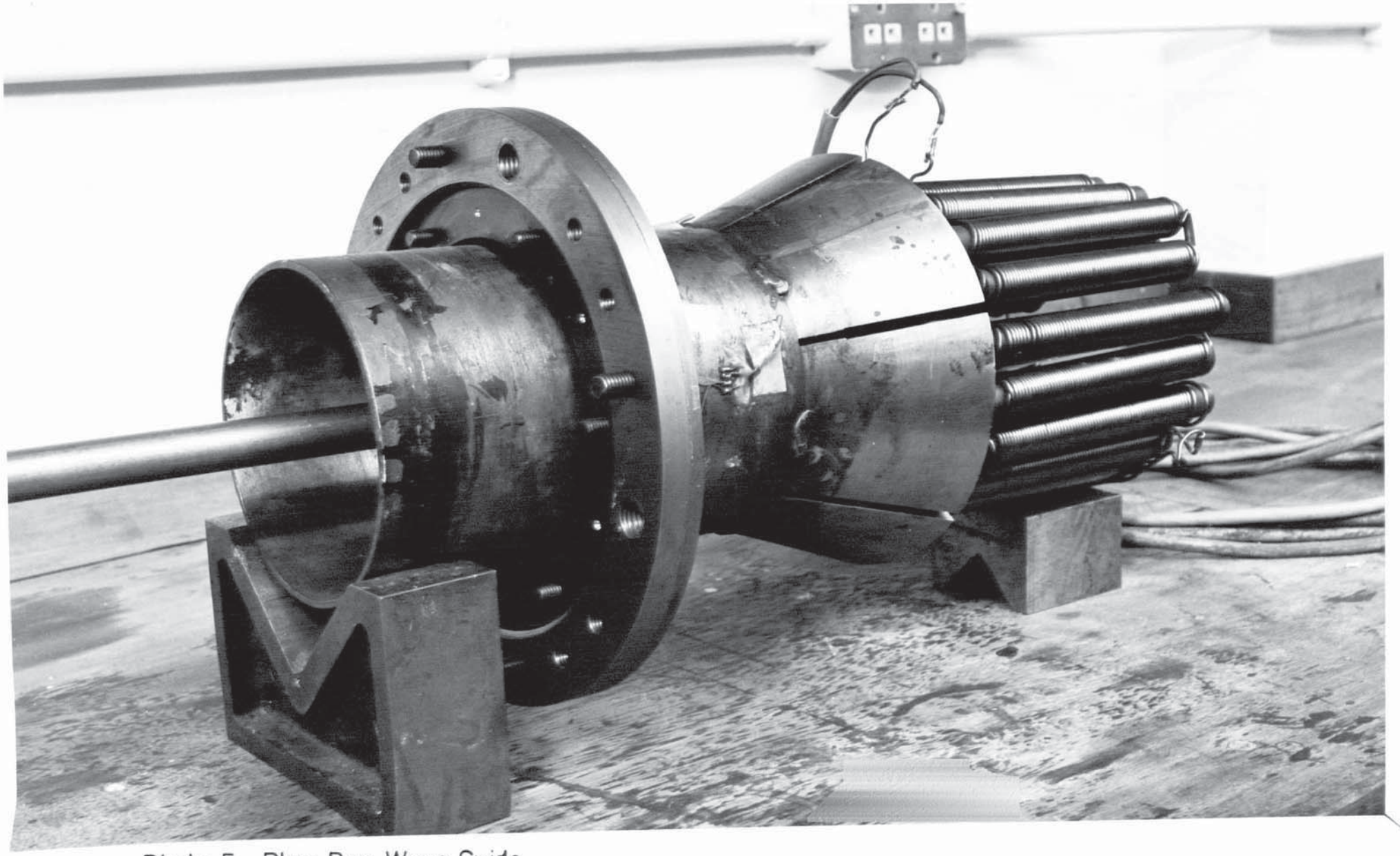

Plate 5 - Plug Bar Wave Guide

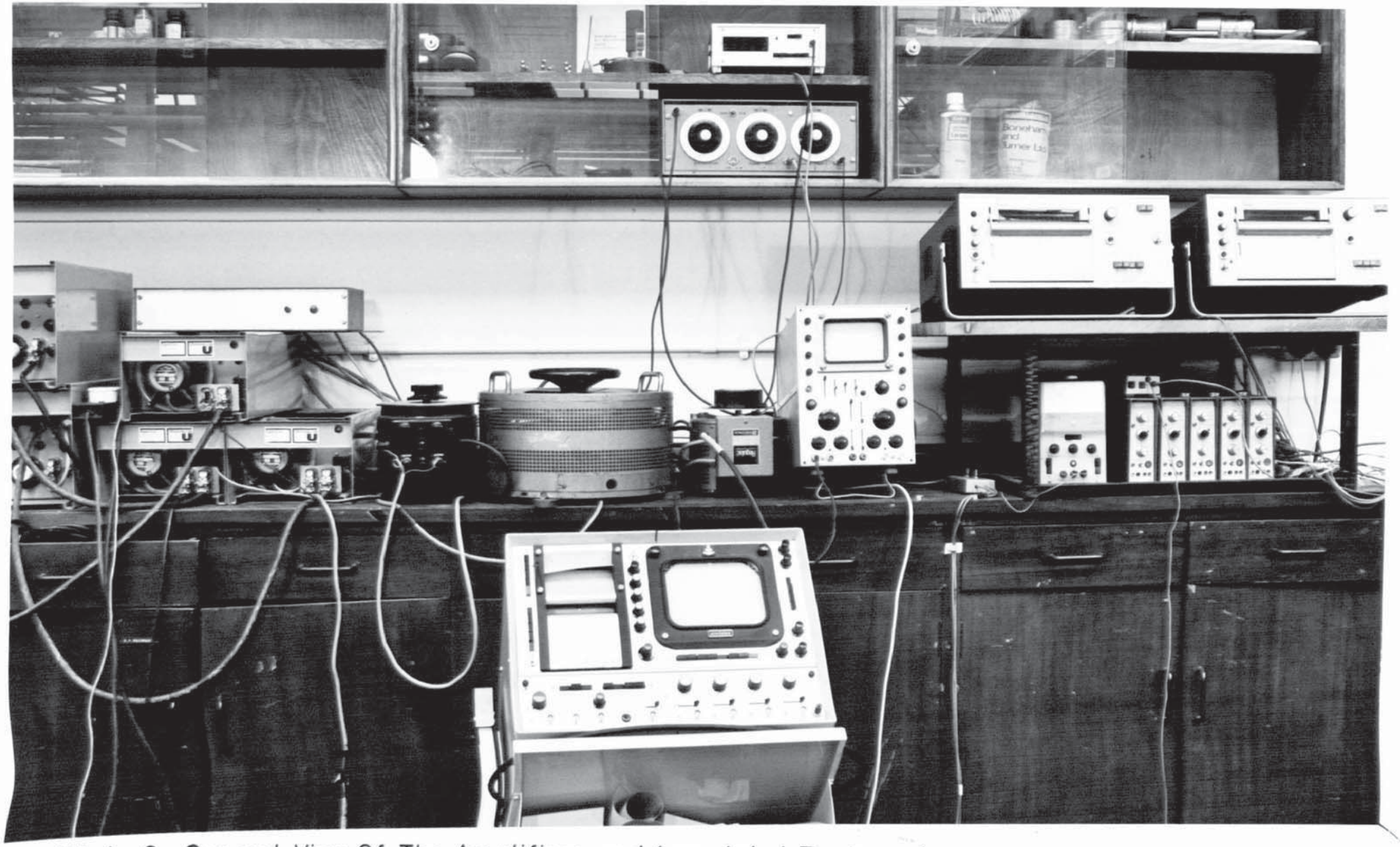

Plate 6 - General View Of The Amplifiers and Associated Equipment

CHAPTER 6: EXPERIMENTAL PROCEDURE

6.1. PREPARATION FOR THE DRAWING TESTS

As already stated in section (4.1), the strip was attached to the coiler by locking it into a slit cut into the drum. The distance between the coiler and dies was such that it was impracticable to swage the strip in a manner similar to that used when drawing tube and wire; neither was it feasible to clamp the dies to the strip as it was being drawn because of difficulties in maintaining a uniform clamping pressure, and, therefore, a uniform die gap. Failure to set a uniform gap between the dies caused the strip to be ejected from the side of the dies even when constrained by the guide rolls.

Attempts were made to indent the strip between two roller bearings mounted in vee blocks, as shown in Figure (6.1). The strip thickness was therefore reduced locally by hammering, which enabled the dies to be clamped into position before inserting the strip from the side of the dies. This gave very variable results; the strip often failed at the indentation before drawing could commence. It also proved difficult to indent the strip to high reductions of area without it shearing.

The most reliable method of loading the strip into the dies proved to be the most obvious; the wave guides were simply clamped together with the strip positioned between the dies. This resulted in symmetric loading of the dies, provided that the bolster plates had been correctly positioned, as described in section (4.1), and, also, the bolts used to clamp the wave guides to the die load cell were tightened in a manner which resulted in uniform indentation of the strip. This was achieved by lightly tightening the bolts to position the wave guide; bolts A and B (see Figure (6.2)) were thus fully clamped in two stages, so indenting the strip; the remaining four bolts were then fully tightened. The wave guides were fully energised, with the strip stationary, to complete the indentation and the bending load on the upper and lower wave guides checked to ensure that they were symmetrically loaded.

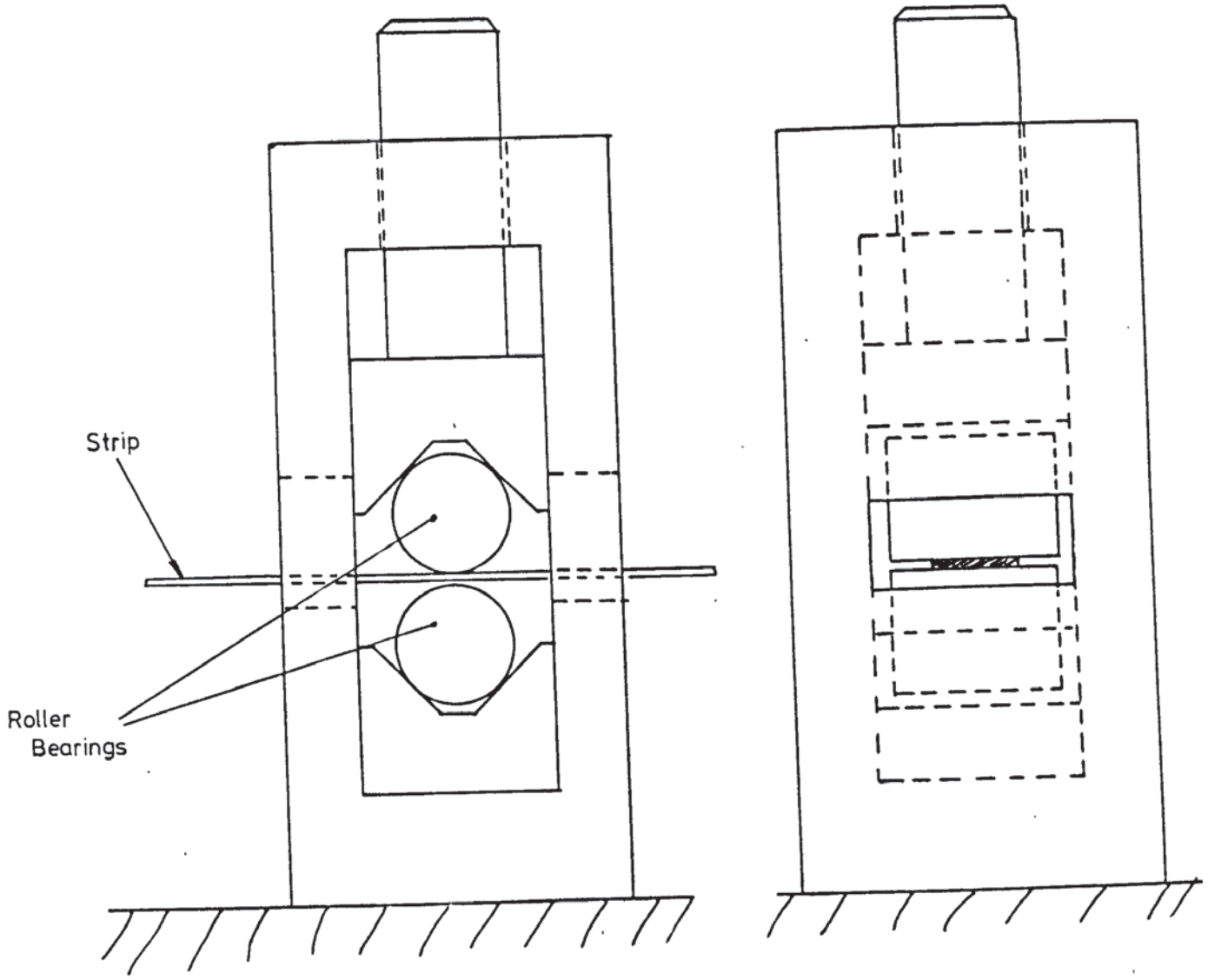

Fig(6.1) - Strip Indenting Tool

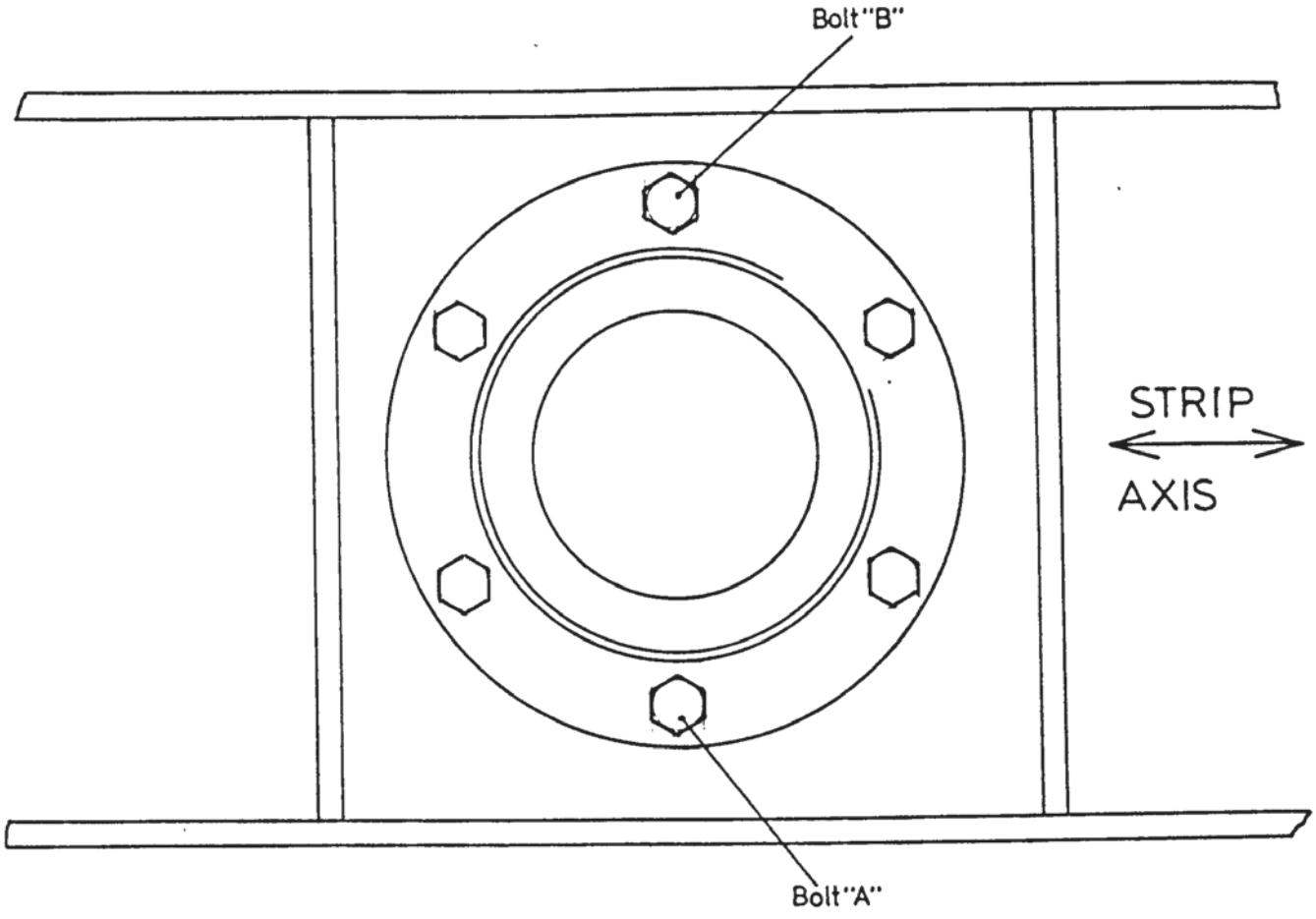

Fig(6.2) - Plan View Of Die Wave Guide

The dies were lubricated before the wave guides were clamped to the die load cell (see section (6.2)).

Preliminary results showed that it was only necessary to record the two components of die load, and die velocity, from one of the wave guides as loading symmetry was maintained throughout the strip-drawing tests. The tube drawing analogue tests were not carried out for reasons given in section (6.3.2.).

6.2. LUBRICATION

The most widely used cold drawing lubricant for mild steel consists of a soap deposited on a phosphate base. It is first necessary to clean the steel by pickling or degreasing, which is immediately followed by a hot dip in a phosphate solution. This produces a chemically bonded phosphate coating on the steel surface. Soap is applied either by drawing the stock through a box, filled with soap powder, sited upstream of the die, or by another hot dip into a soap solution. The former method relies upon mechanical pick-up of the soap on the phosphate coating whilst the latter process results in a chemical bond between the soap and phosphate.

Rod and loosely coiled wire can normally be processed in bulk by the above processes, with satisfactory results, and straight lengths of tube can be processed by dipping into soap solution. Unfortunately, the only suitable methods of treating strip in this manner is to coil it, with gaps between each surface, or to process the coil by passing the strip from one coiler, through the appropriate baths, with allowance for drying, onto another coiler, as shown in Figure (6.3).

The strip used for the drawing tests was supplied with a very light coating of oil. In this condition, it could be stored for a considerable time without significant deterioration of its surface. Some of this strip was coiled into small loosely wound coils and degreased and

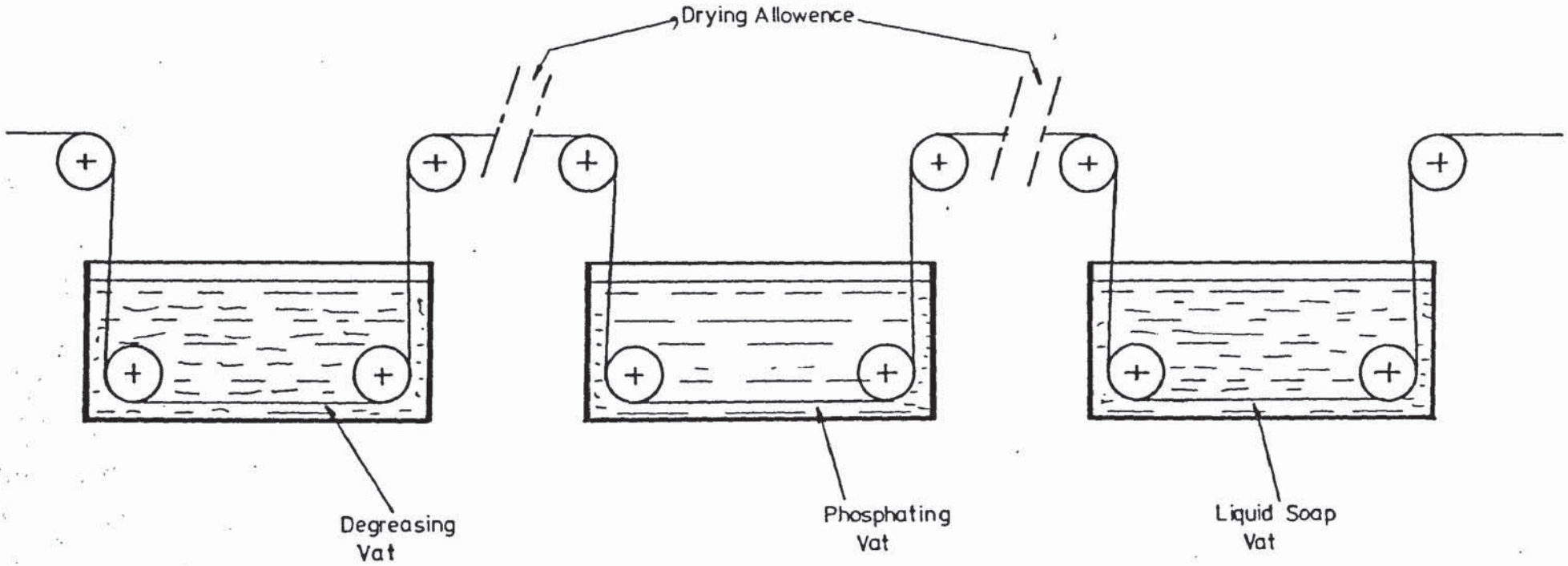

Fig(6.3)- In-Line Arrangement Of Plant For The Soap Lubrication Of Strip

phosphated at a local rod drawing firm. The results were unsatisfactory as the coating was not uniform; the untreated surfaces became very badly corroded. The coil-to coil arrangement was not considered feasible for the relatively small quantities of strip required for the drawing tests, and the soap box method was not used because this too required the strip to be degreased and phosphated prior to drawing.

It was therefore necessary to use a lubricant which could be applied directly to the strip as it was being drawn. Rape oil and molybdenum disulphide grease were found to give unsatisfactory results when used in conjunction with steel dies, even when they were plated, and pick-up was still in evidence, at moderate reductions of area, when molybdenum disulphide grease was used with the tungsten carbide dies. The most satisfactory results were obtained when using the tungsten carbide dies and a special purpose drawing oil produced by Edgar Vaughn Ltd. This oil was marketed under the trade name TD45.

The oil was injected into the die throat with a syringe before the start of each test run. Pick-up only occurred when the drawing conditions were most arduous, that is, at high die amplitudes, high reductions of area and when the draw speed was low. Complete lubrication starvation only occurred when drawing at the limits of reduction with the 2.5^{o} die; under all other conditions a reservoir of lubricant was maintained at the entry of the deformation zone on both sides of the strip, even though no attempt was made to prevent the lubricant leaking from the sides of the dies.

6.3. DRAWING TESTS

6.3.1. STRIP DRAWING

As stated in section (4.1), the gap between the dies was set by clamping shim plates between the wave guide mounting plate and the die load cell. It proved difficult, therefore, to obtain a specific

reduction of area as the smallest change in plate thickness was 0.04 mm (0.001 in) which, at the extremes of reduction of area, represented a relatively large change. Exact repeatability of an output thickness was difficult to obtain after the strip had broken under test. It was for this reason that reductions of area were chosen in an arbitrary manner; the main objects being to determine the limiting reduction of area for a given die angle, draw speed and peak die velocity, and to determine the effect of these variables on the drawing process as a whole by investigating them over the widest possible range.

Drawing tests were carried out using the tungsten carbide dies with TD 45 oil as lubricant. The dies had knife edge profiles with half angles of 2.5^{o}, 5^{o}, 7.5^{o} and 10^{o}. Tests were also carried out with the 7.5 die reground to give a die profile which included a land of approximately 1.5 mm. The land width was arbitrarily chosen to be equal to the contact length along the angled portion of the die at 50% reduction of area. Details of the dies are given in Figure (4.14).

The experimental procedure adopted for the strip drawing tests took two forms; constant power input and constant draw speed. The type of tests attempted initially consisted of setting the H.F. power supply to an arbitrary level, then adjusting the draw speed incrementally, and recording corresponding values, die velocity, tag load, draw speed and the two components of die load. At low reductions of area and high H.F. power input the maximum die velocity was maintained at a sensibly constant level; showing a tendency to reduce with increasing draw speed. Similarly, when the power input was set such that the maximum die velocity could just be maintained at zero draw speed, the die velocity decreased with increasing draw speed. Thus, the electrical energy supplied to the wave guide was not directly related to die amplitude.

Preliminary examination of these results indicated that, for a given die angle, the draw stress was a function of both draw speed and

die velocity, though not directly related to velocity ratio. It was for this reason that constant draw speed tests were carried out in order to examine the effect of a single independent variable, namely, die velocity. At higher reductions of area this type of test was not possible because the slope of the draw stress/die velocity curve increased with increasing reduction of area, that is, the drawing process became increasingly unstable as the conventional draw condition was approached. The results of these tests are given graphically in Chapter 7 and discussed in Chapter 8.

A single test was carried out at constant low draw speed under conventional drawing conditions and then at full H.F. power input. In the latter case the front tension was almost zero, having been carried out at 20.8% reduction of area with the 7.5° knife edge dies. Samples of the strip drawn under these extreme conditions were subjected to plane strain compression tests in order to determine whether or not there was any significant difference in redundant deformation. The results of these tests are given graphically in appendix 1 and are discussed in Chapter 8.

Plane strain compression tests were also carried out on samples from each of the coils of undrawn strip in order to ensure that their mechanical properties were similar. These results are also shown in appendix 1, and the mild steel specification is given in Fig(A1·2)

Tabulated data are shown in appendix 3.

6.3.2. TUBE DRAWING ANALOGUE

The plug wave guide and plug were assembled and fitted to the rear of the draw bench, as shown in Figure (4.8). The plug axis was set parallel to the longitudinal strip axes by adjusting the tie bars, as described in section (4.3.2), lateral parallelism was achieved by rotating the wave guide/plug bar assembly at its nodal support, as shown

in Figure (4.8).

The procedure for setting up these tests was similar to that for the strip drawing tests, except that both the upper and lower wave guides were packed out with shim steel to ensure that the gap between each plug face and die was uniform. The lower wave guide was locked into position and the two pieces of strip loaded into the coilers and guide rolls. The upper wave guide was bolted down, thus indenting both pieces of strip.

As already implied at the end of the introductory chapter, the attempts to carry out the tube-drawing analogue tests were unsuccessful; the plug could not be driven at an amplitude comparable with that of the dies. Also, the change in tuned frequency of the plug bar wave guide, between the loaded and unloaded state, made fine tuning difficult. Control of the phase relationship between the plug and dies also proved inadequate; whether this was due to the low plug amplitude or to transference of the appropriate component of dynamic load to the plug is not clear.

No usable results were taken from these tests.

CHAPTER 7. GRAPHICAL RESULTS

The results obtained during the strip drawing tests are shown graphically in this section and have been arranged in three sections; strip tension, Figures (7.1) to (7.31) ; specific axial thrust, Figures (7.32) to (7.62) ; lateral die pressure, Figures (7.63) to (7.93) . The variation of tuned frequency with die angle and reduction of area is shown in Figure (7.94). Each of the three main sections is arranged in sub-sections in order of die angle with the constant draw speed tests arranged in ascending order of reduction of area; the results of the constant power input tests are shown at the end of each sub-section.

The strip tension was derived from:

$$\sigma_s = \frac{P_s}{t(1-r)b} \qquad (7.1)$$

the specific axial thrust was derived from:

$$\sigma_A = \frac{2P_A}{rtb} \qquad (7.2)$$

and the lateral die pressure was derived from:

$$\sigma_L \qquad \frac{2P_L \tan\alpha}{rtb}$$

where P_s = mean strip load (tag load)

P_A = mean bending load applied to the die load cell

P_L = mean axial load applied to the die load cell

An index of the graphical results is shown in Table (7.1), which enables easy cross-reference to the tabulated data which are shown in Appendix 3 in test number order.

Table (7.1) Index to Results

Figure Number				
Strip tension	Special axial thrust	Lateral die Pressure	Die Angle	Test number and reduction of area
1	32	63	2.5°	039 r = 0.133
2	33	64	2.5	040 r = 0.250
3	34	65	2.5	028 r = 0.267
4	35	66	2.5	029 r = 0.280
5	36	67	2.5	030 r = 0.280
6	37	68	2.5	031-038
7	38	69	5.0	055 r = 0.205
8	39	70	5.0	063 + 065 r = 0.345
9	40	71	5.0	060 + 064 r = 0.364
10	41	72	5.0	061 + 062 r = 0.413
11	42	73	5.0	054 r = 0.442
12	43	74	5.0	055A 056-059
13	44	75	7.5	027
14	45	76	7.5	041
15	45	77	7.5	025
16	47	78	7.5	026
17	48	79	7.5	024
18	49	80	7.5	023
19	50	81	7.5	001-005, 010, 011, 013, 014, 016, 018, 019.
20	51	82	7.5	066 r = 0.187
21	52	83	with-land	069 r = 0.270
22	53	84	7.5	073 r = 0.373
23	54	85	with land	070 r = 0.438
24	55	86	as above	072 r = 0.453
25	56	87	"	066 r = 0.187

Table (7.1) continued

Figure Number				
Strip tension	Special axial thrust	Lateral die Pressure	Die Angle	Test number and reduction of area
26	57	88	7.5^{o} with land	067, 071, 074
27	58	89	10^{o}	053 r = 0.260
28	59	90	10	042 r = 0.263
29	60	91	10	043 r = 0.399
30	61	92	10	044 r = 0.461
31	62	93	10	045 - 052

Fig(7·1) - Mean Strip Tension vs. Peak Die Velocity (α = 2·5°, r=0·133)

[Constant Draw Speed Tests]

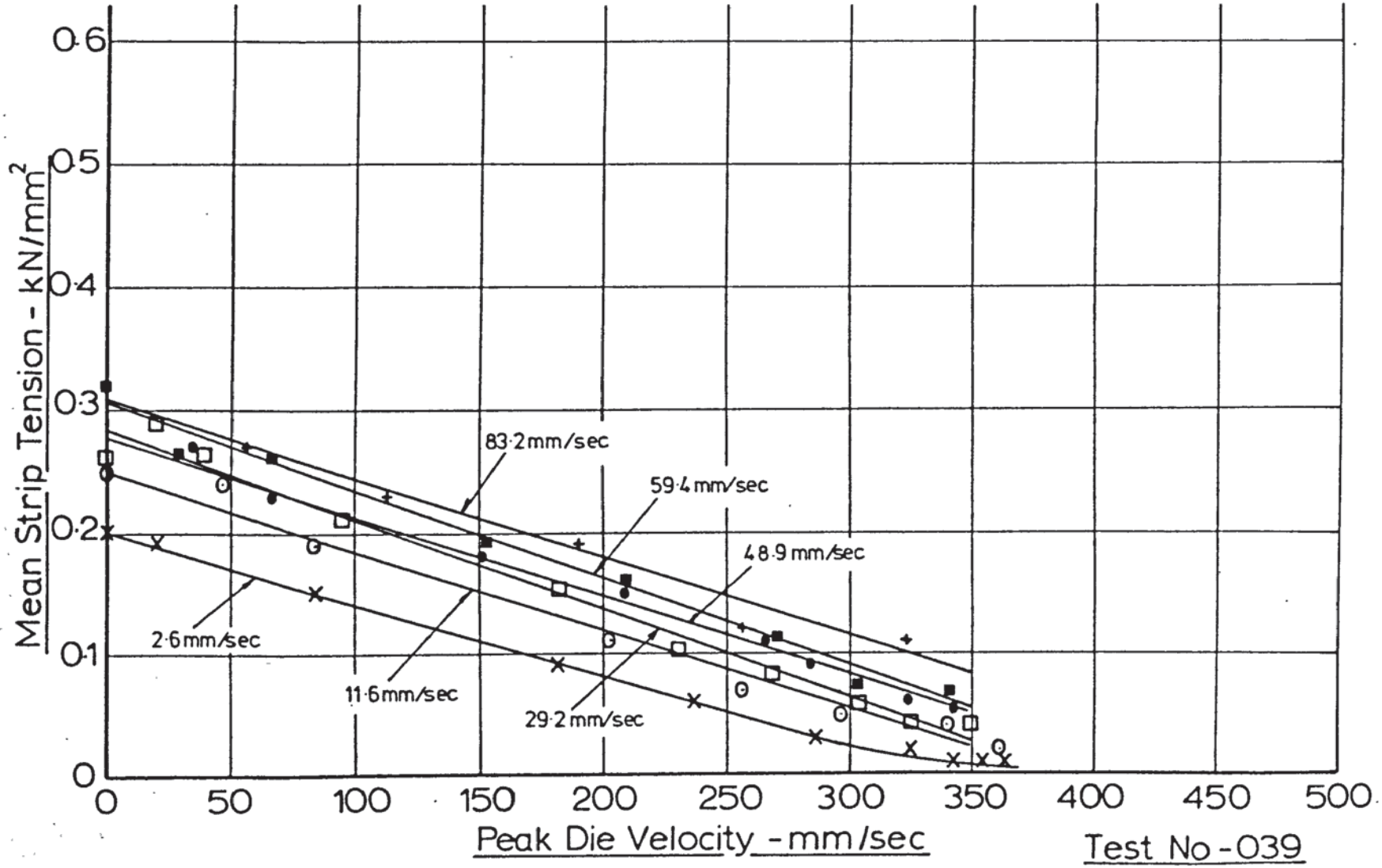

Fig(7·2) - Mean Strip Tension vs. Peak Die Velocity ($\alpha = 2.5°, r = 0.250$)

[Constant Draw Speed Tests]

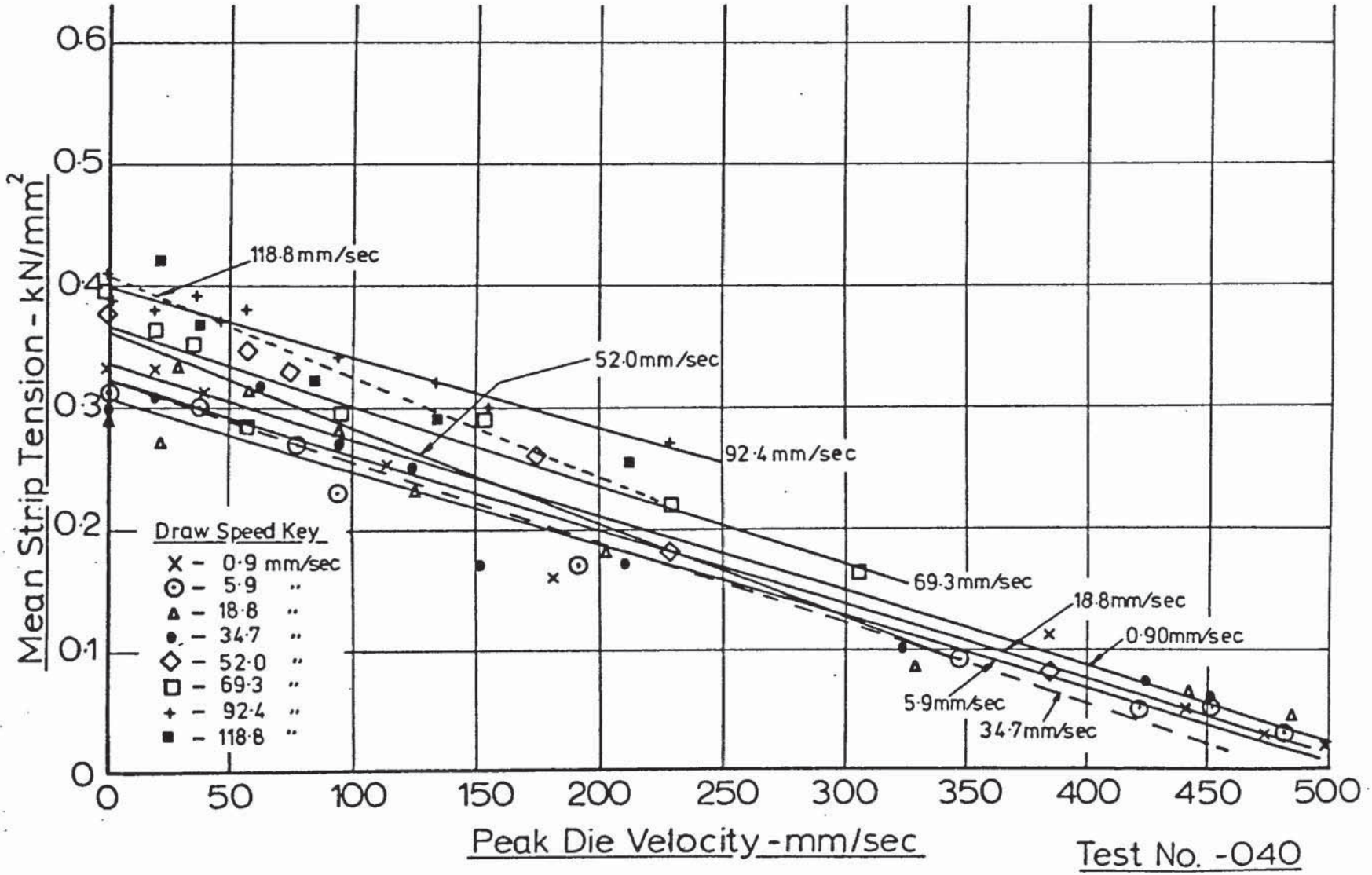

Test No. -040

Fig(7.3)-Mean Strip Tension vs. Peak Die Velocity ($\alpha = 2.5°$, $r = 0.267$)

[Constant Draw Speed Tests]

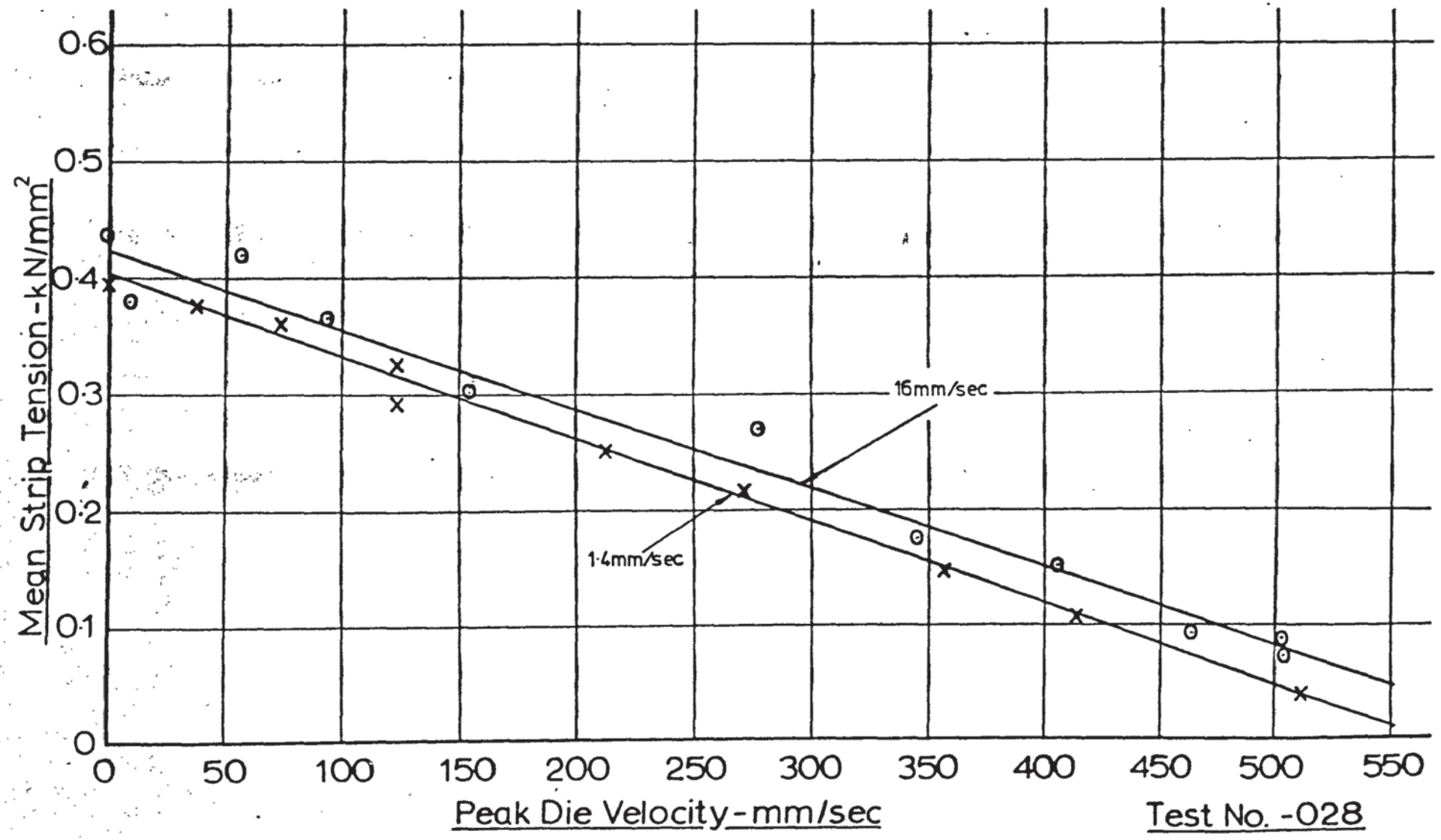

Fig(7.4) - Mean Strip Tension vs. Peak Die Velocity ($\alpha = 2.5°$, $r = 0.280$)

[Draw Speed = 37.0 mm/sec]

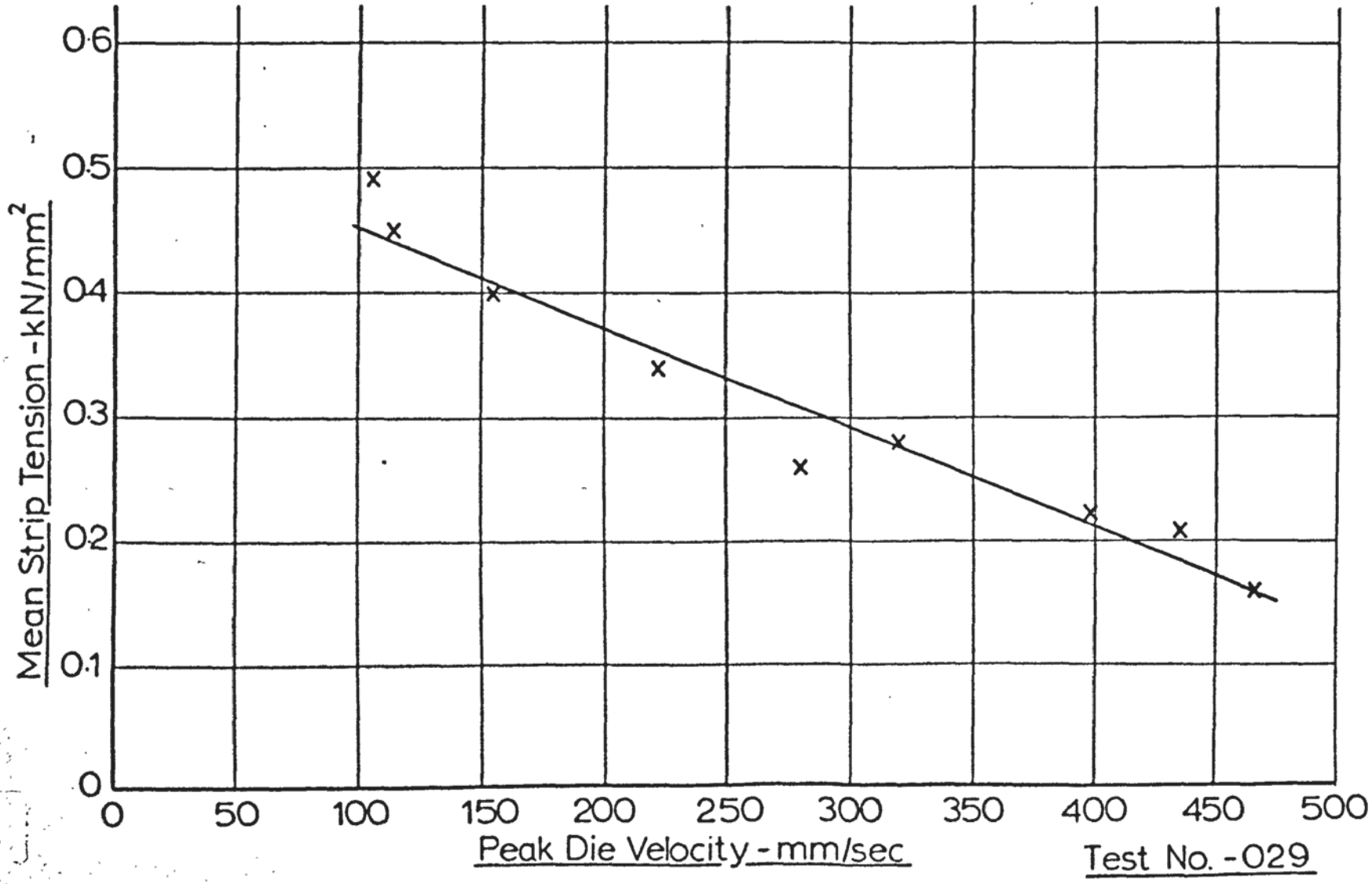

Fig(7.5) - Mean Strip Tension vs. Peak Die Velocity (α=2.5°, r=0.280)

[Arbitrary Power Input And Draw Speed]

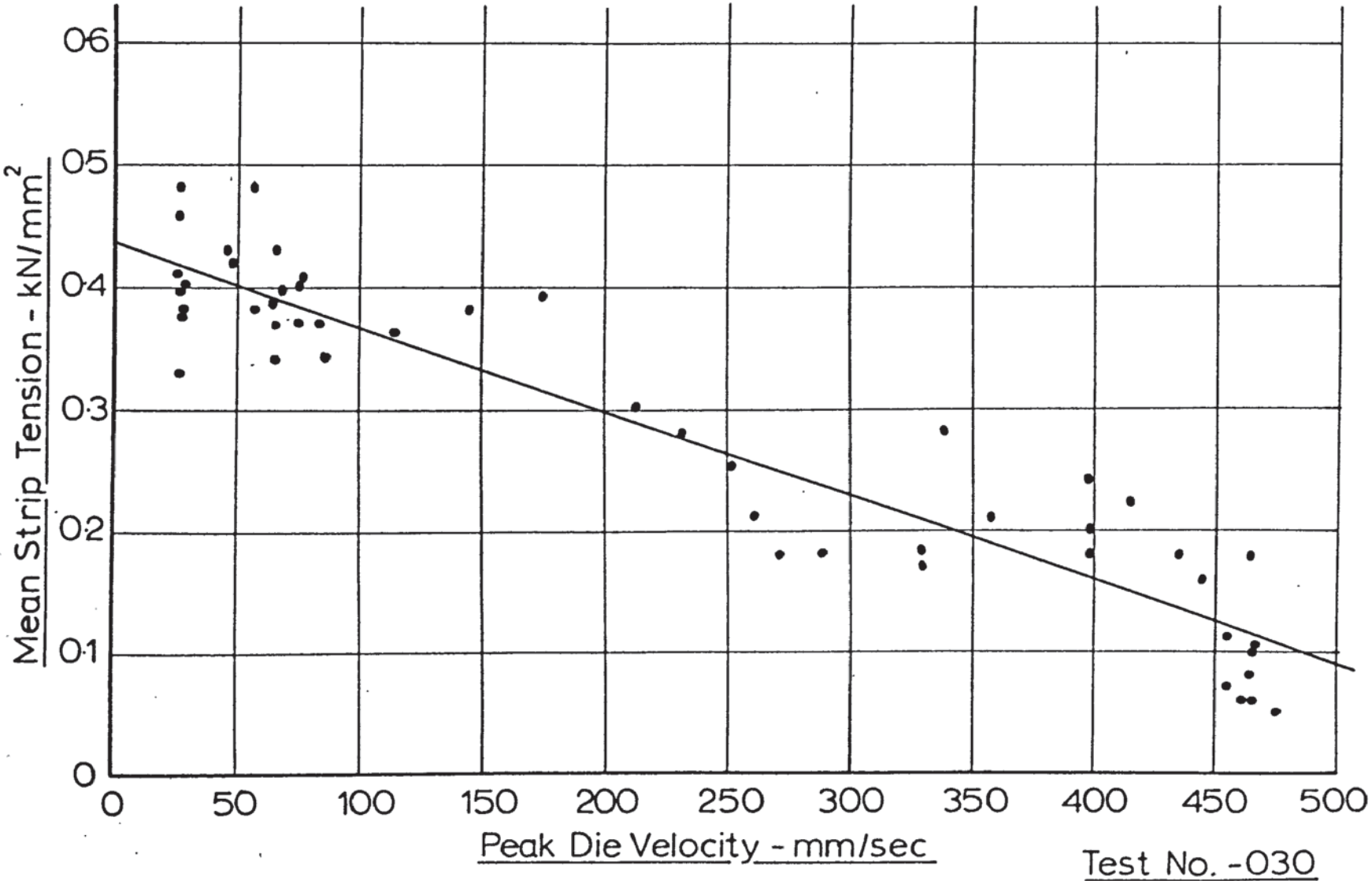

Test No. -030

Fig(7.6) - Mean Strip Tension vs. Peak Die Velocity ($\alpha = 2.5°$)

[Full Power Input - Arbitrary Draw Speed]

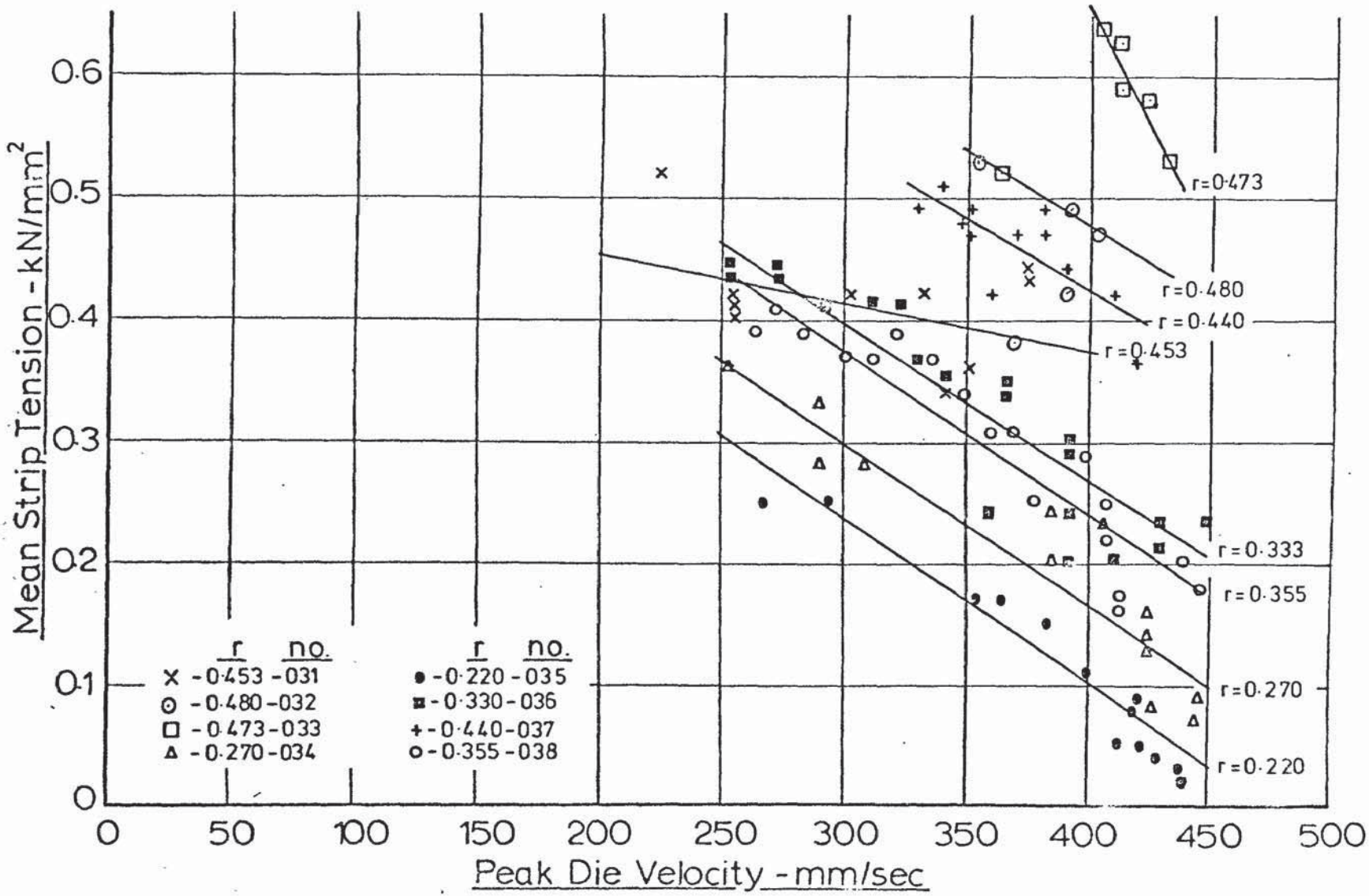

Fig(7.7) - Mean Strip Tension vs. Peak Die Velocity(α=5°, r=0.205)

[Constant Draw Speed Tests]

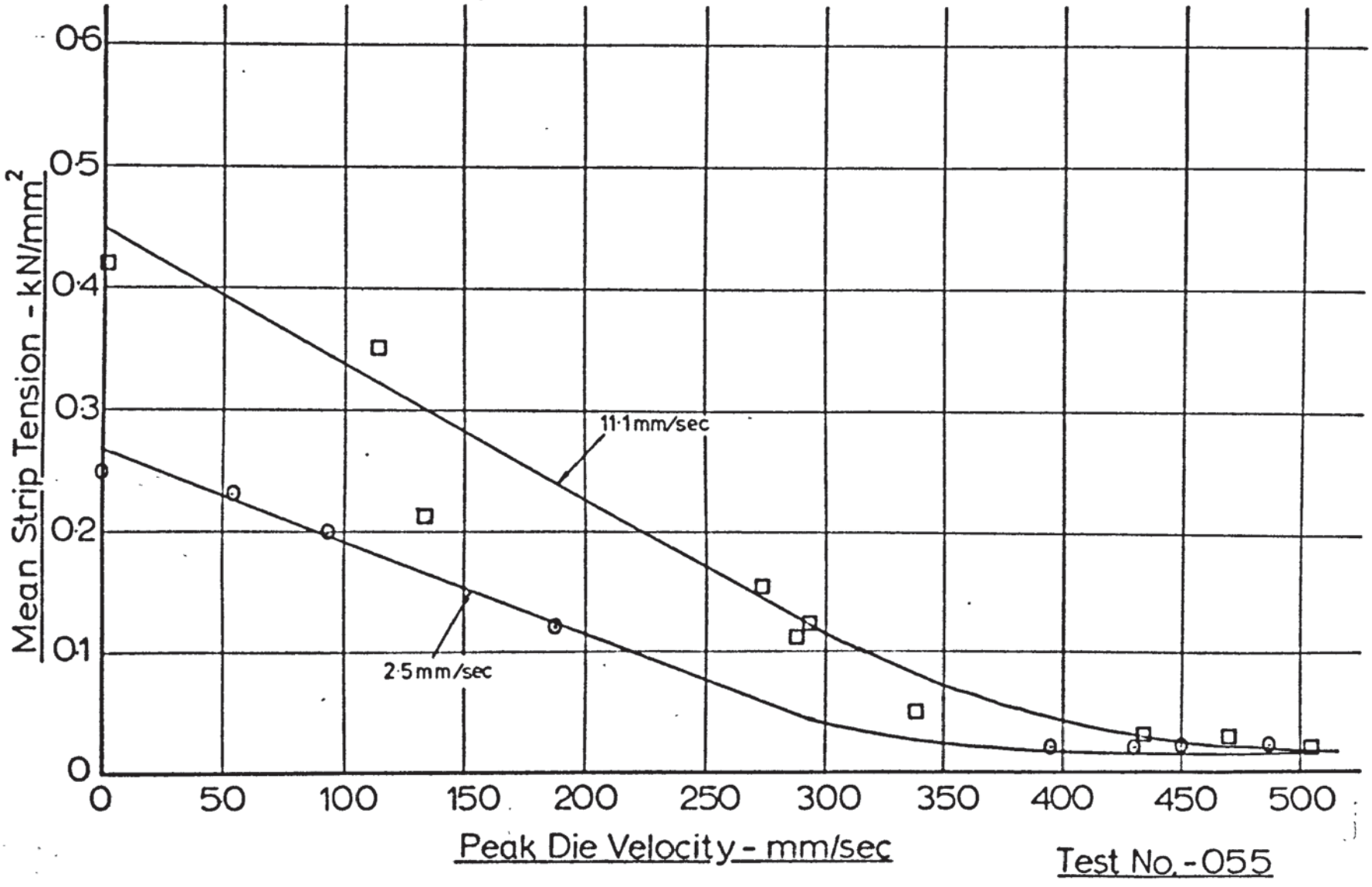

Test No. - 055

Fig(7.8)-Mean Strip Tension vs. Peak Die Velocity($\alpha = 5°$, $r = 0.345$)

[Constant Draw Speed Tests]

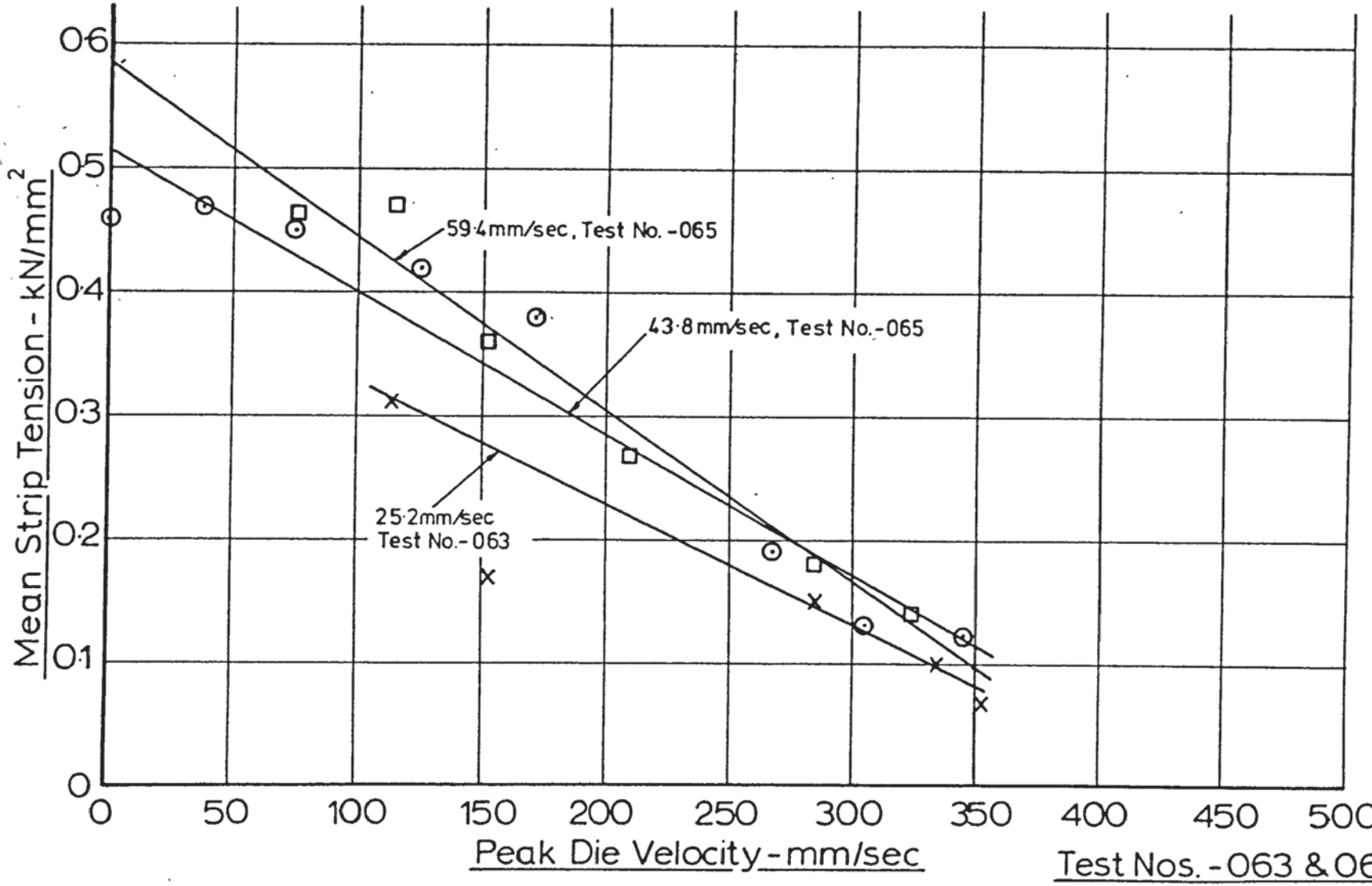

Test Nos. - 063 & 065

Fig(7·9) - Mean Strip Tension vs. Peak Die Velocity($\alpha = 5°$, $r = 0.364$)

[Constant Draw Speed Tests]

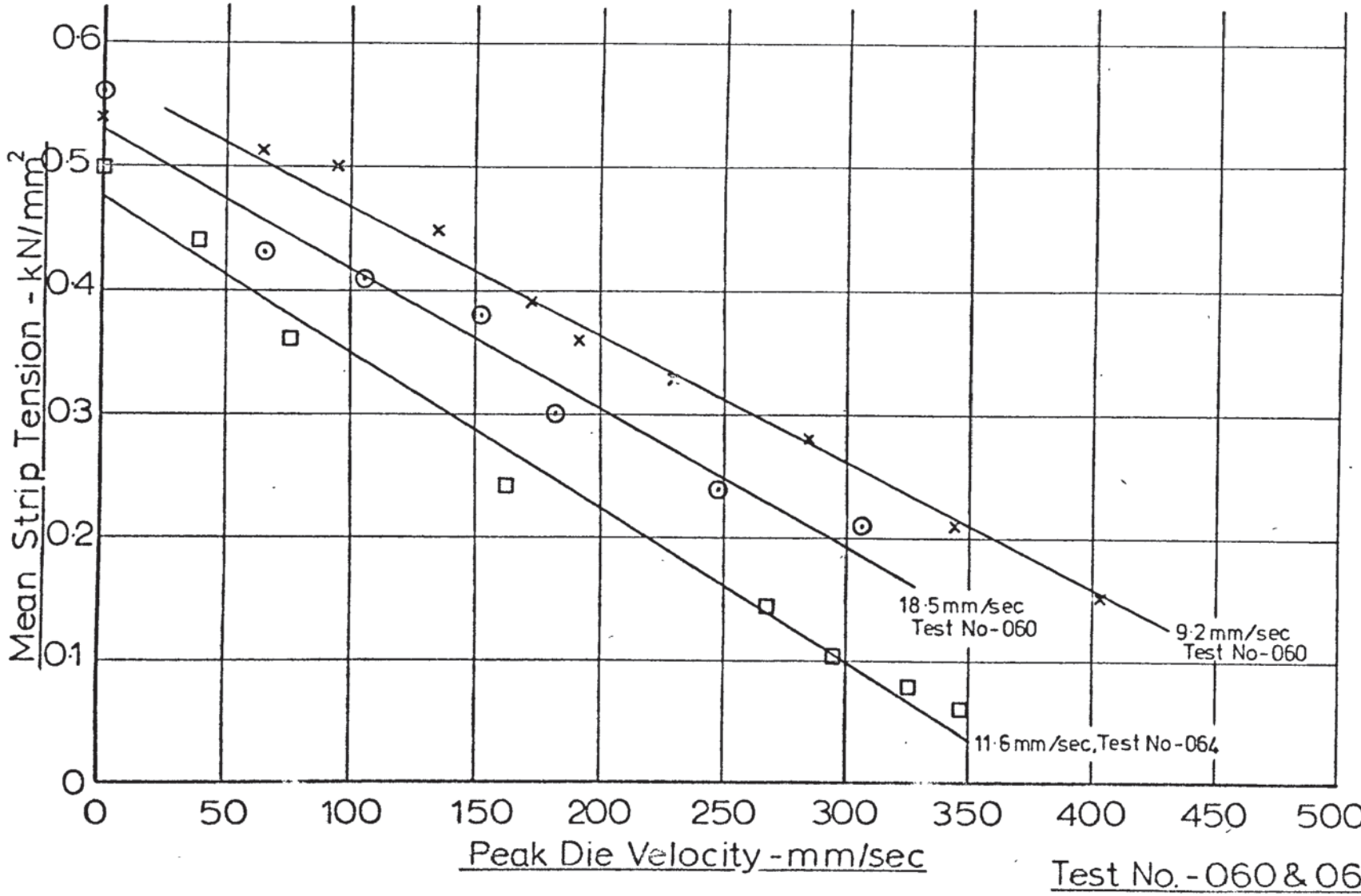

Test No. - 060 & 064

Fig(7·10) - Mean Strip Tension vs. Peak Die Velocity ($\alpha = 5°, r = 0.413$)

[Constant Draw Speed Tests]

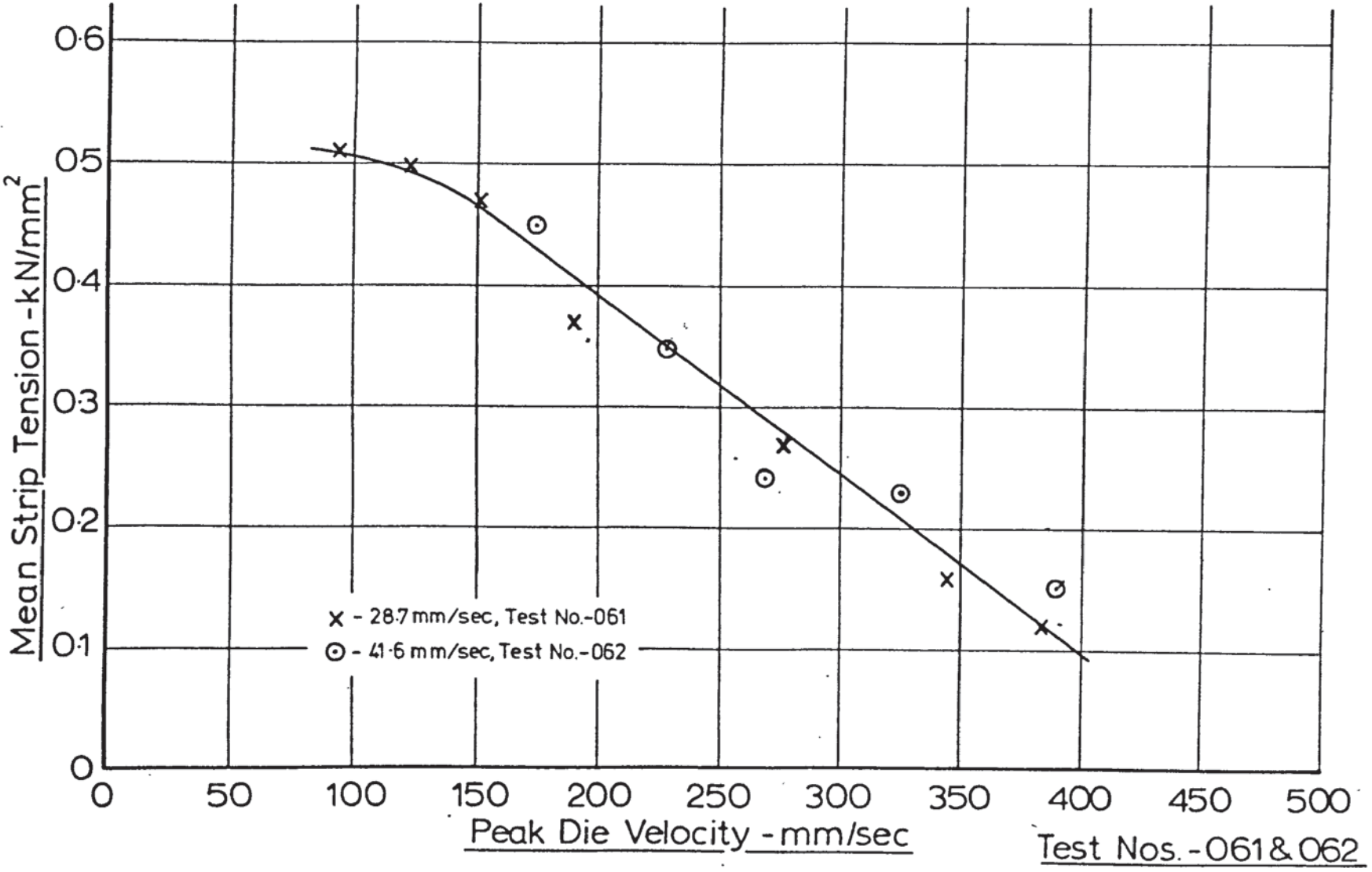

Test Nos. - 061 & 062

Fig(7.11) - Mean Strip Tension vs. Peak Die Velocity(α=5°, r=0.442)

[Draw Speed = 30.8 mm/sec]

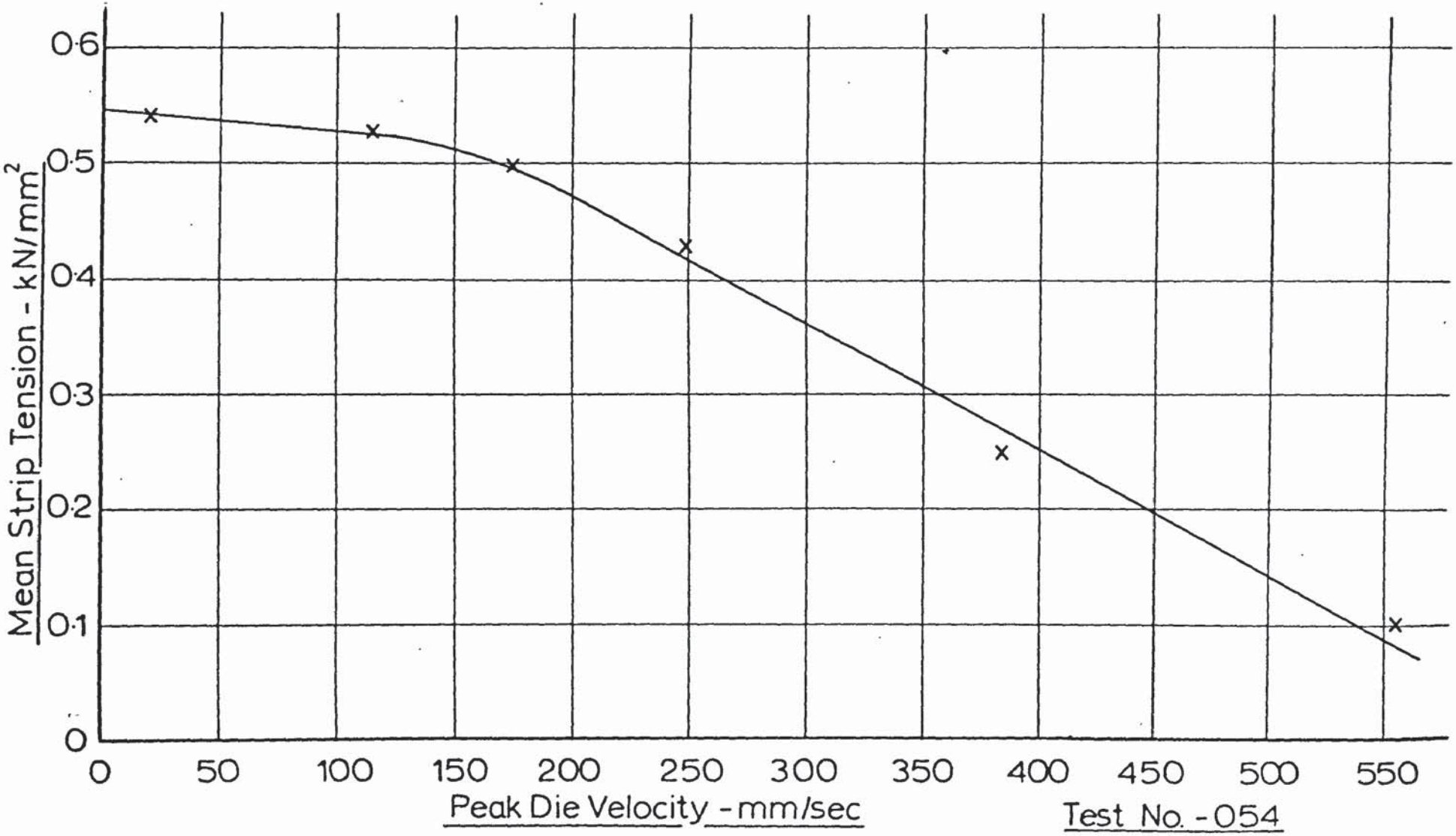

Fig(7·12) - Mean Strip Tension vs. Peak Die Velocity(α= 5°)

[Full Power Input-Arbitrary Draw Speed]

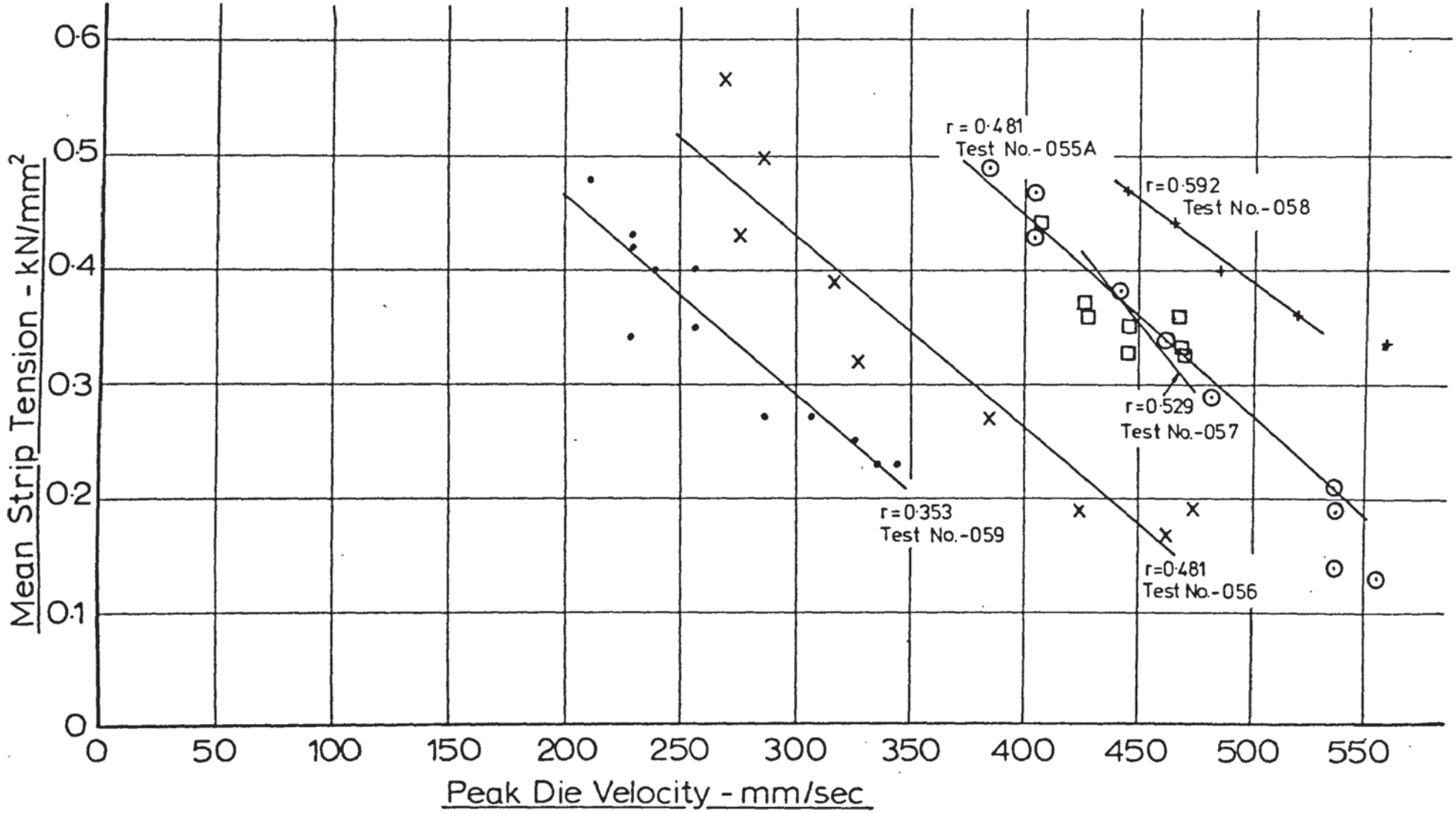

Fig(7·13)-Mean Strip Tension vs. Peak Die Velocity(α=7·5°, r=0·164)

[Constant Draw Speed Tests]

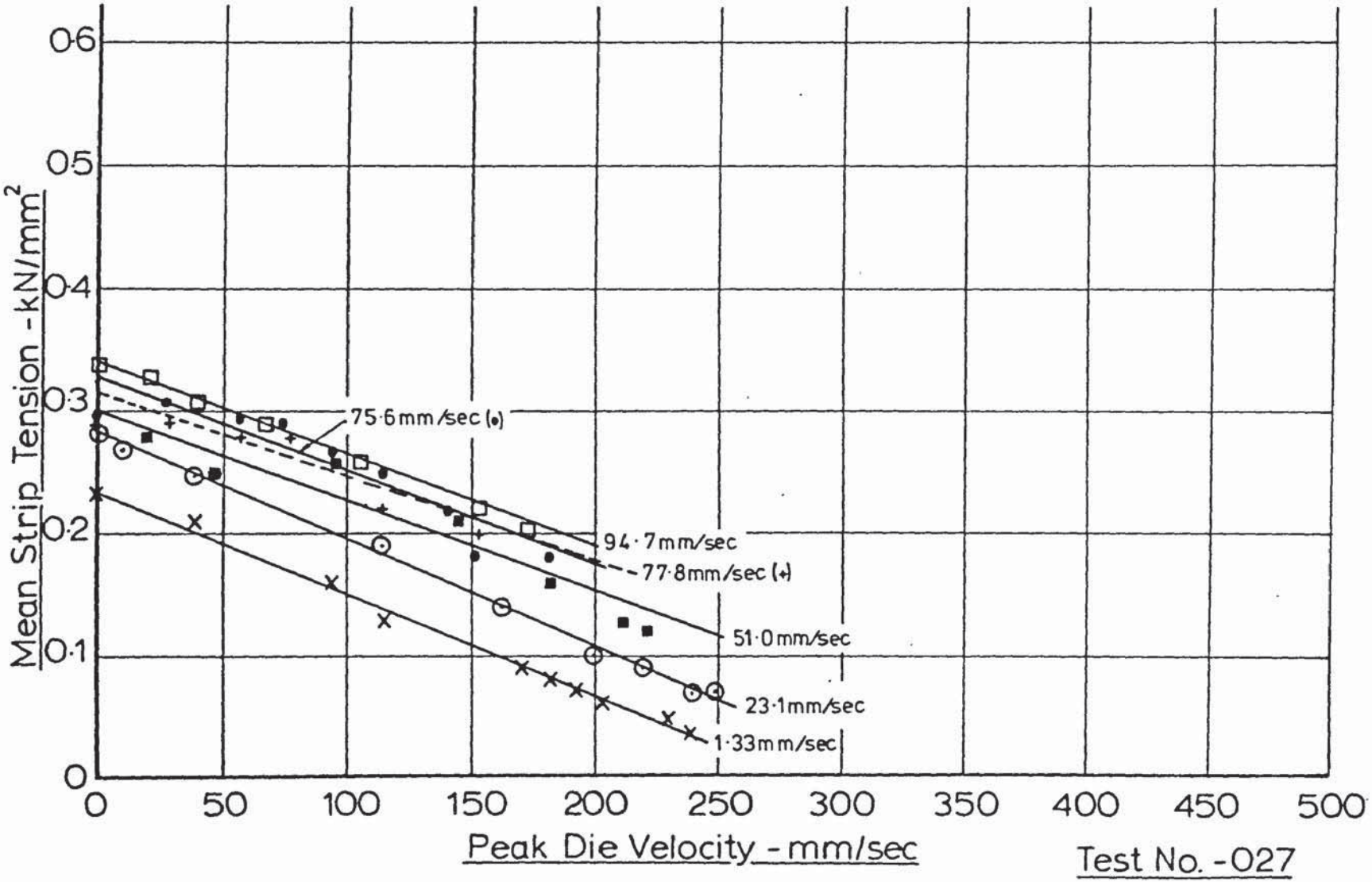

Fig(7.14) - Mean Strip Tension vs. Peak Die Velocity ($\alpha = 7.5°$, $r = 0.267$)

[Constant Draw Speed Tests]

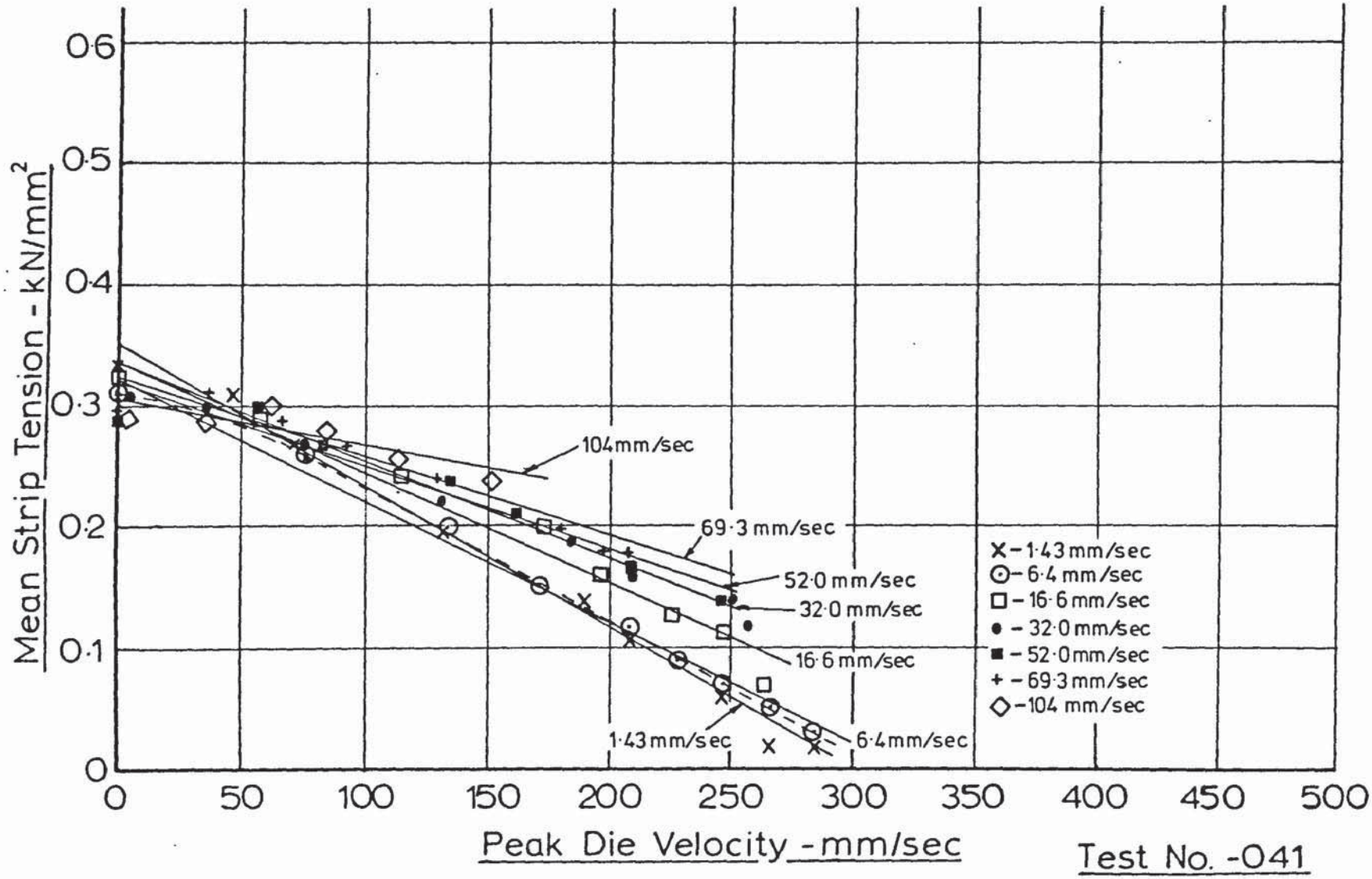

Test No. -041

Fig(7·15)-Mean Strip Tension vs. Peak Die Velocity(α = 7·5°, r=0·307)

[Constant Draw Speed Tests]

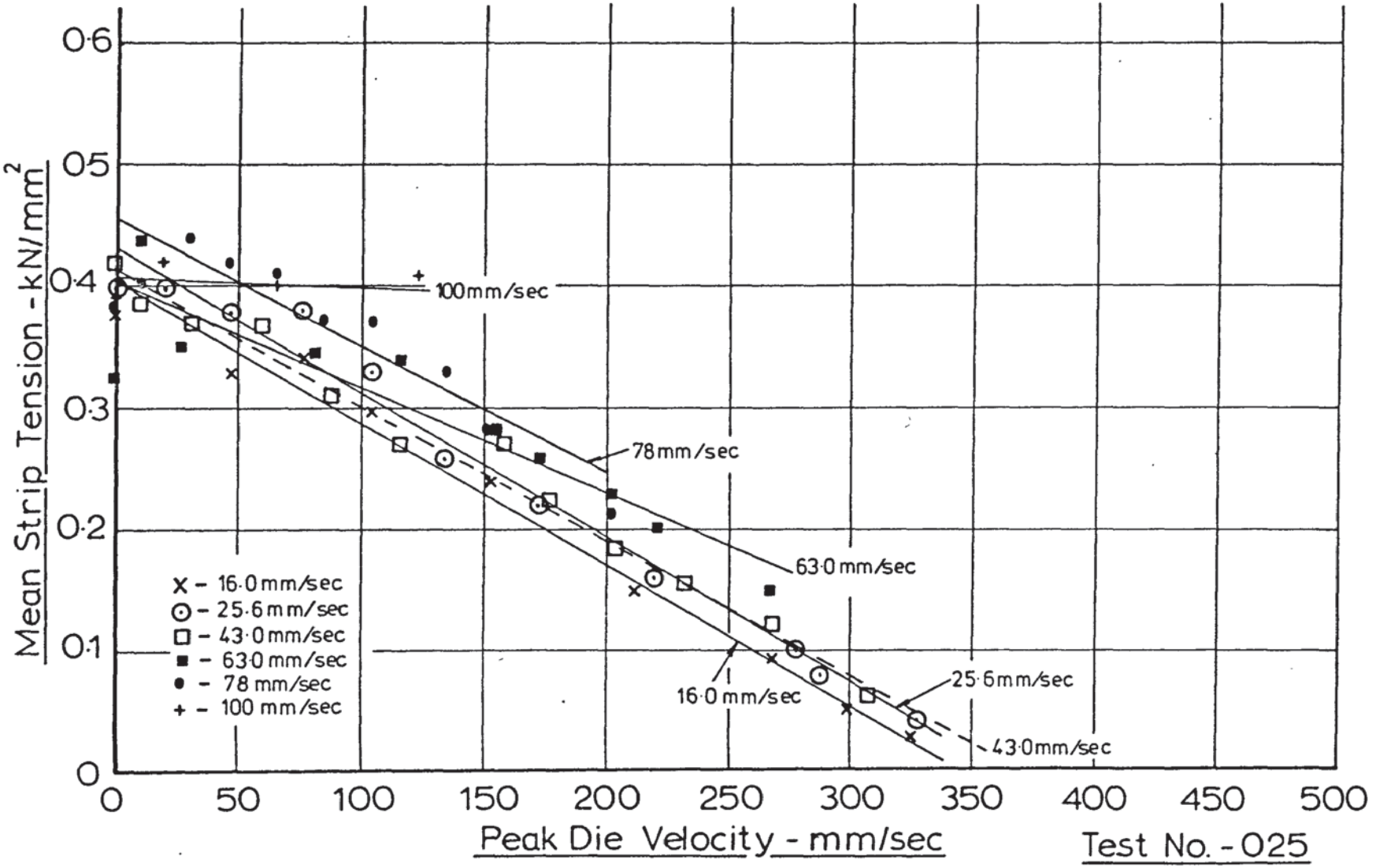

Test No. - 025

Fig(7·16) - Mean Strip Tension vs. Peak Die Velocity($\alpha = 7.5°$, $r = 0.362$)

[Constant Draw Speed Tests]

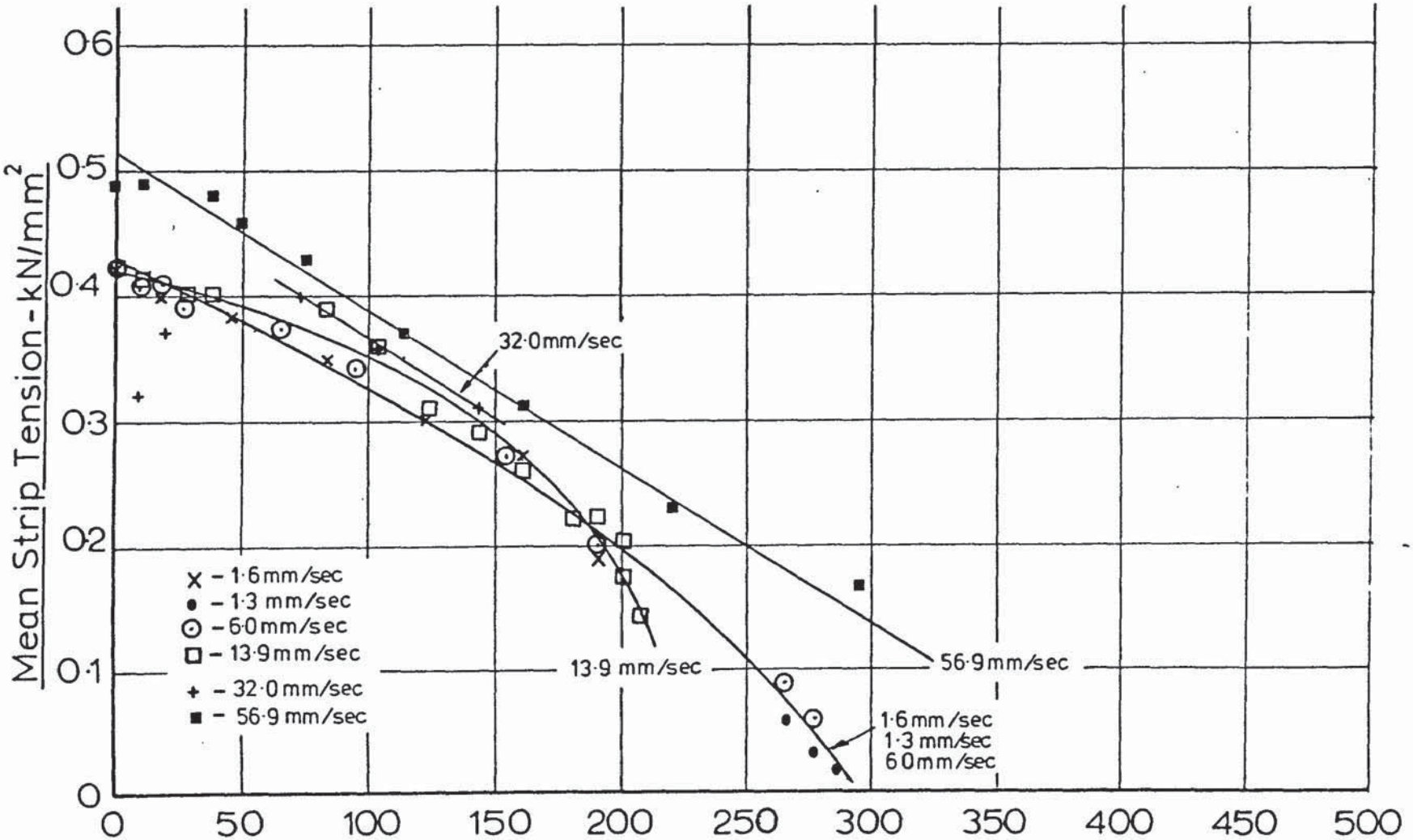

Test No. -026

Fig(7·17) - Mean Strip Tension vs. Peak Die Velocity(α=7·5°, r=0·387)

[Constant Draw Speed Tests]

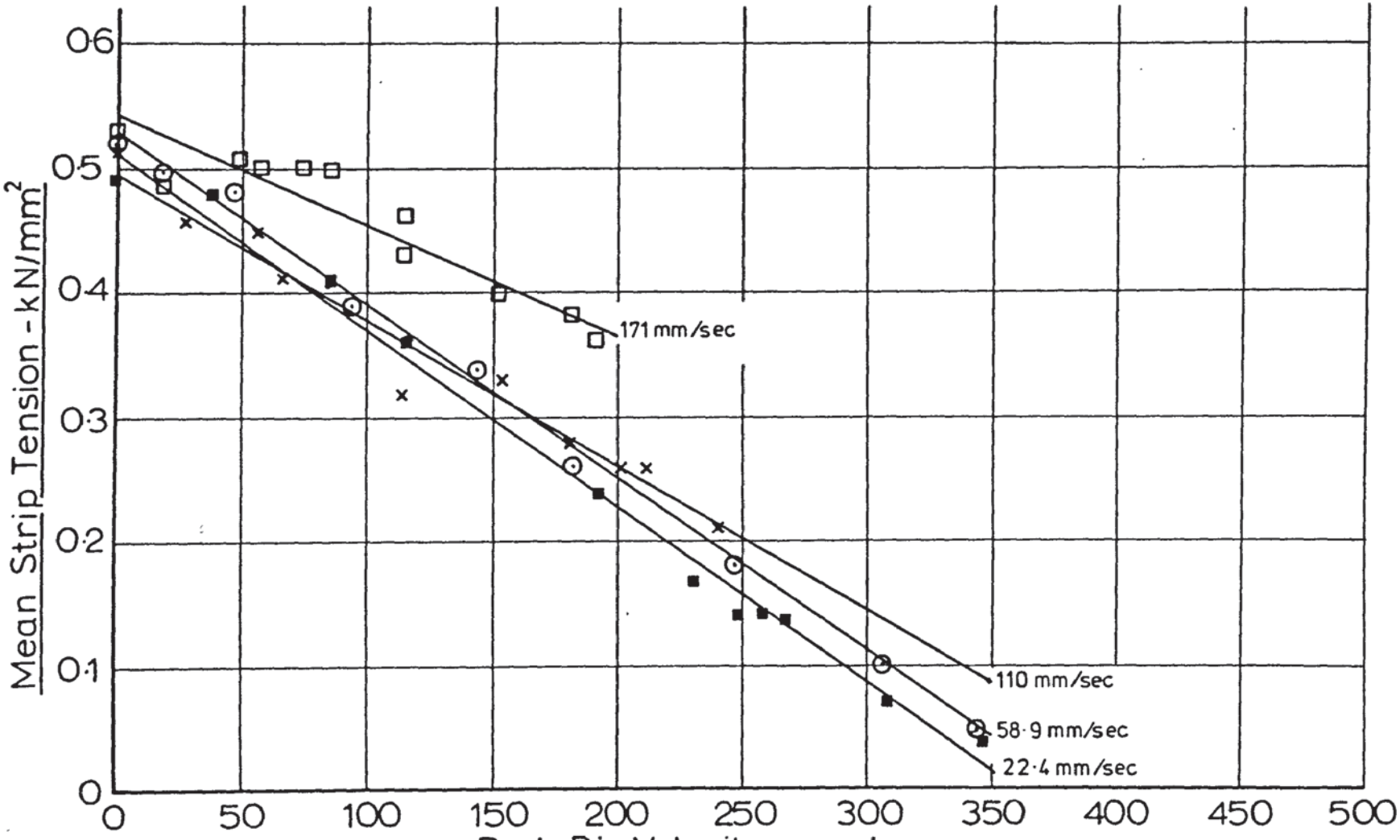

Test No. - 024

Fig(7·18)-Mean Strip Tension vs. Peak Die Veocity(α=7·5°, r=0·440)

[Constant Draw Speed Tests]

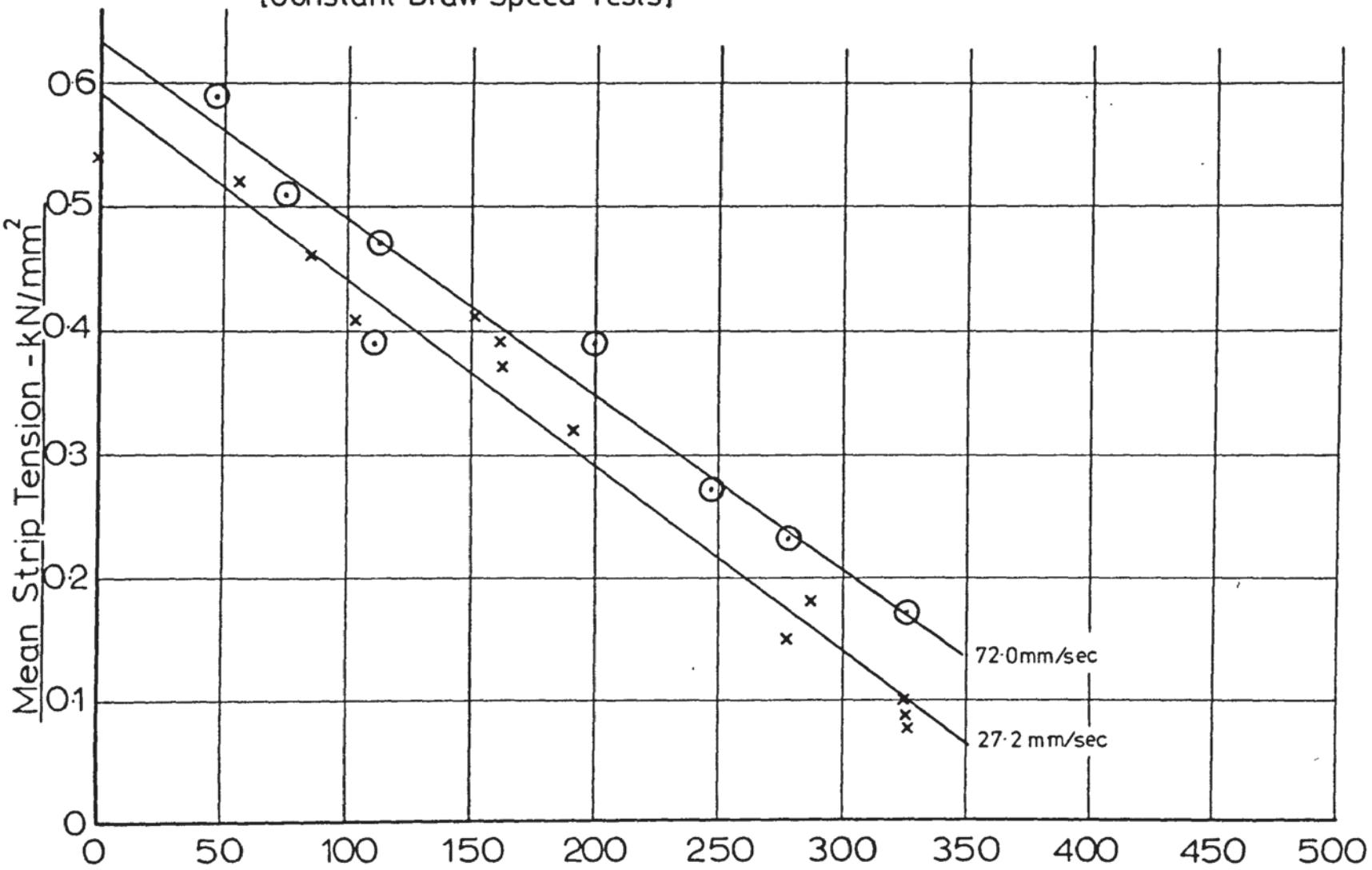

Test No.-023

Fig(7.19)-Mean Strip Tension vs. Peak Die Velocity (α = 7·5°)

[Constant Power Input, Arbitrary]

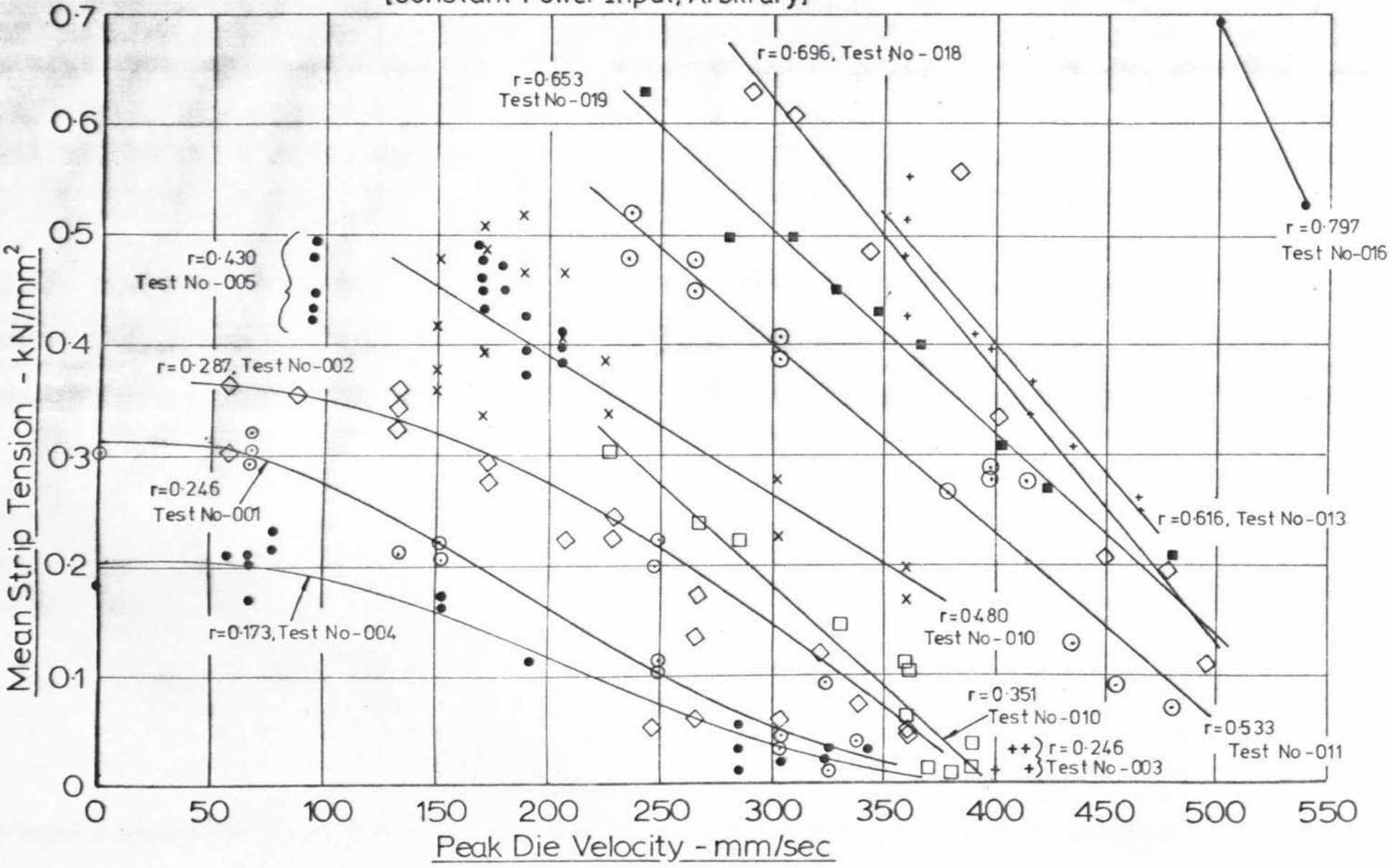

Fig(7·20) - Mean Strip Tension vs. Peak Die Velocity (α = 7·5° with land, r = 0·187)

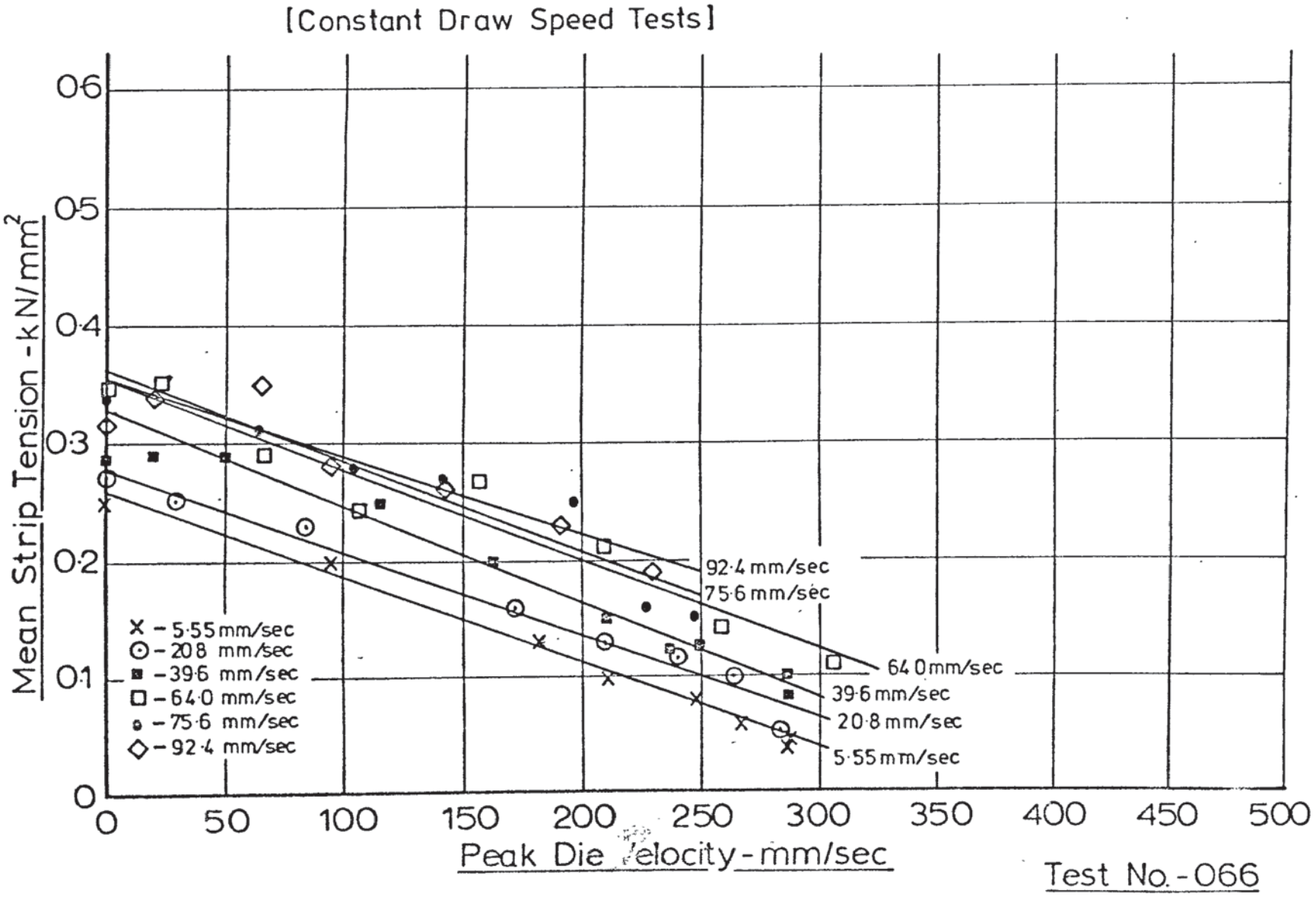

Fig(7·21) - Mean Strip Tension vs. Peak Die Velocity (α = 7·5° with land, r = 0·270)

[Constant Draw Speed Tests]

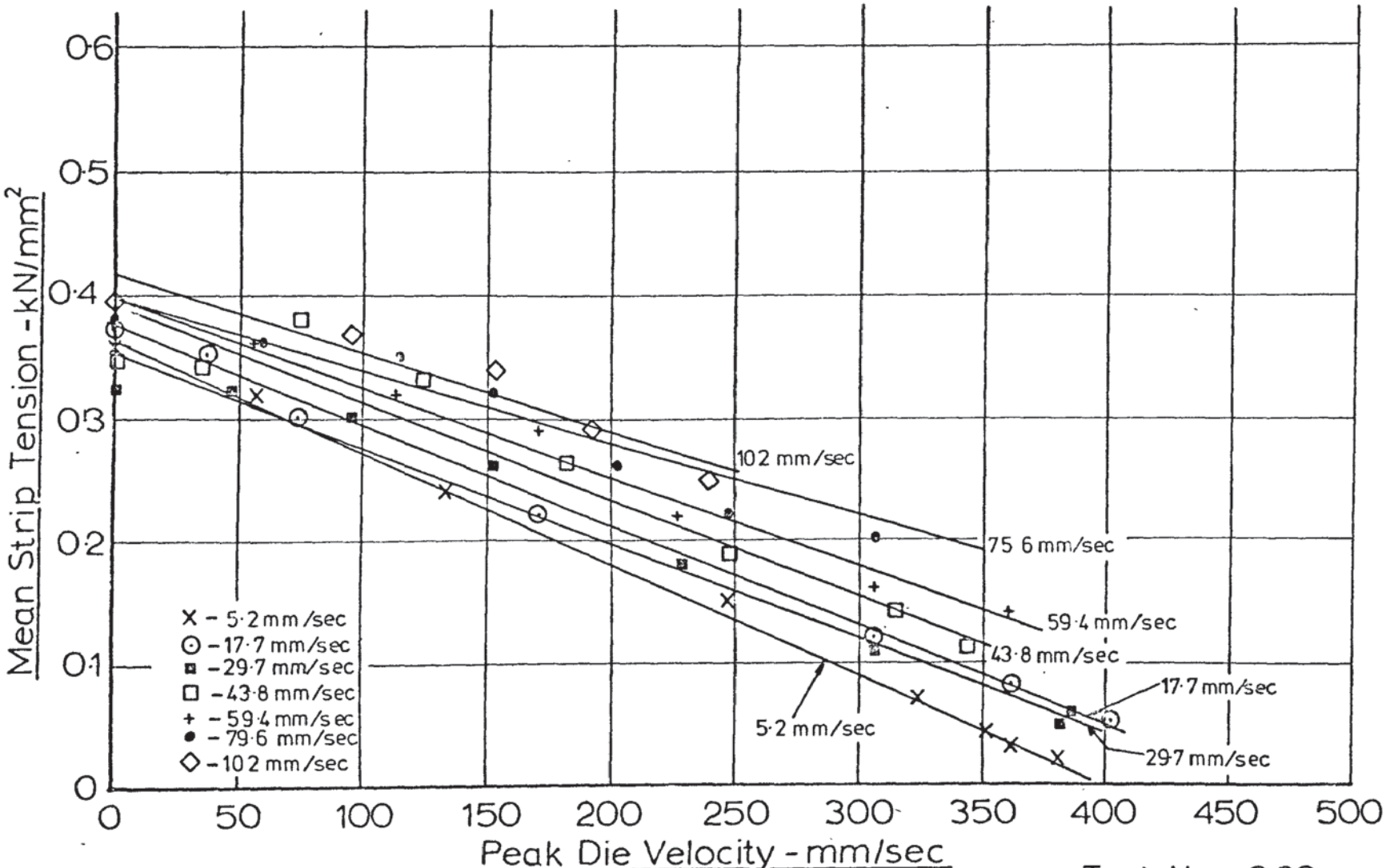

Test No. -069

Fig(7·22) - Mean Strip Tension vs. Peak Die Velocity (α = 7·5° with land, r = 0·373)

[Constant Draw Speed Tests]

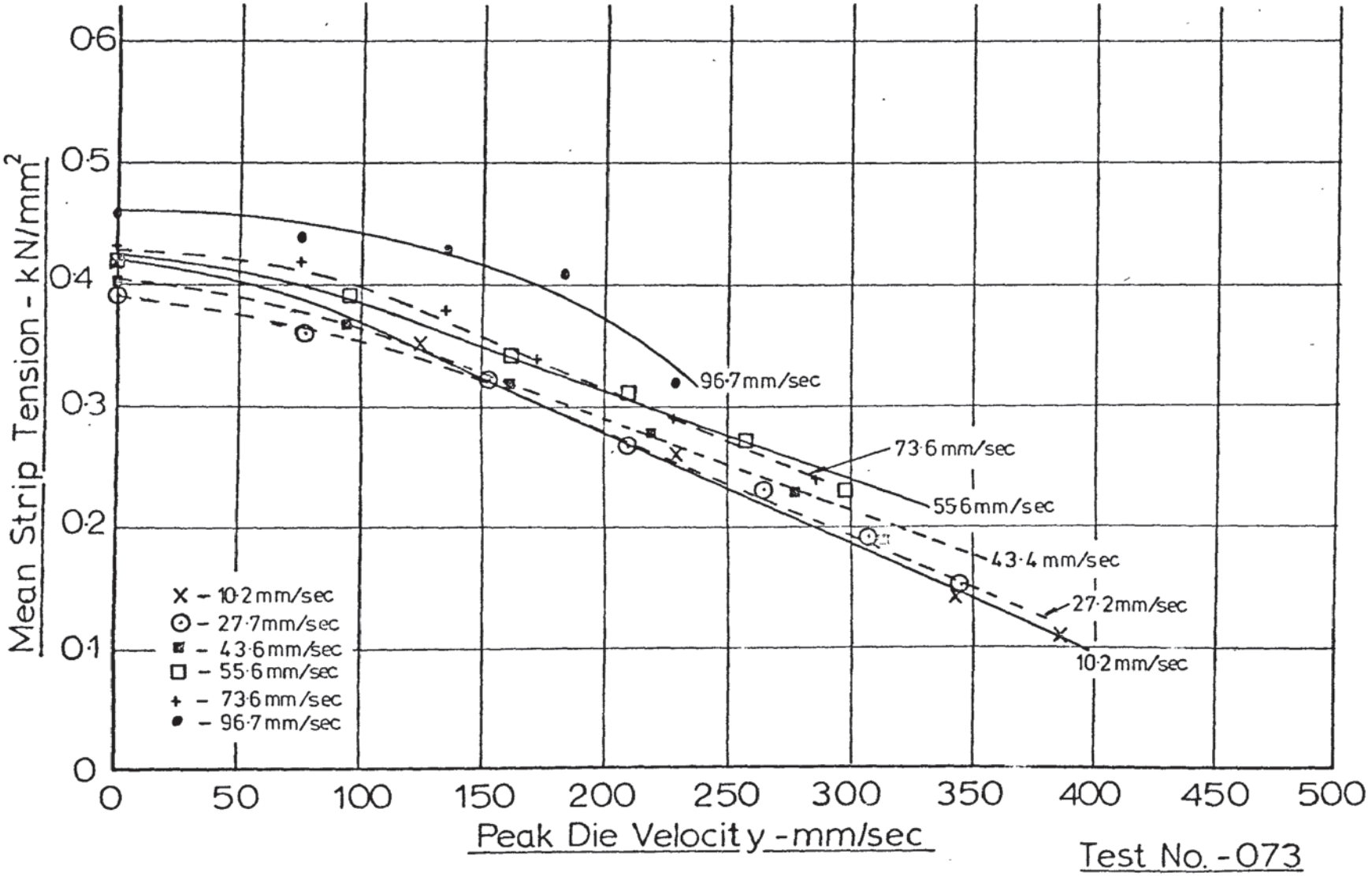

Test No. - 073

Fig(7·23)-Mean Strip Tension vs. Peak Die Velocity (α=7·5° with land, r=0·438)

[Constant Draw Speed Tests]

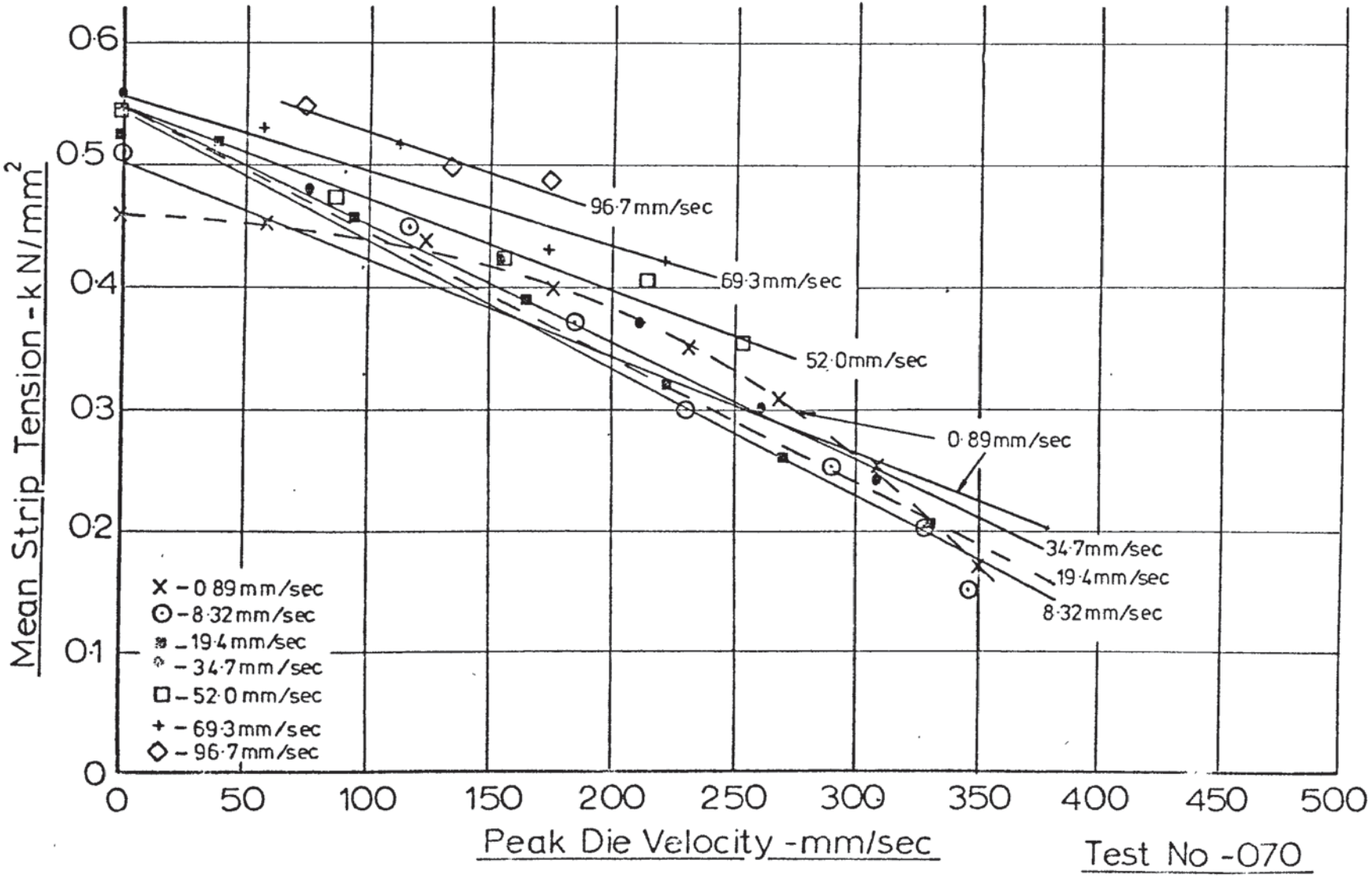

Test No -070

Fig(7·24) - Mean Strip Tension vs. Peak Die Velocity (α = 7·5° with land, r = 0·453)

[Constant Draw Speed Tests]

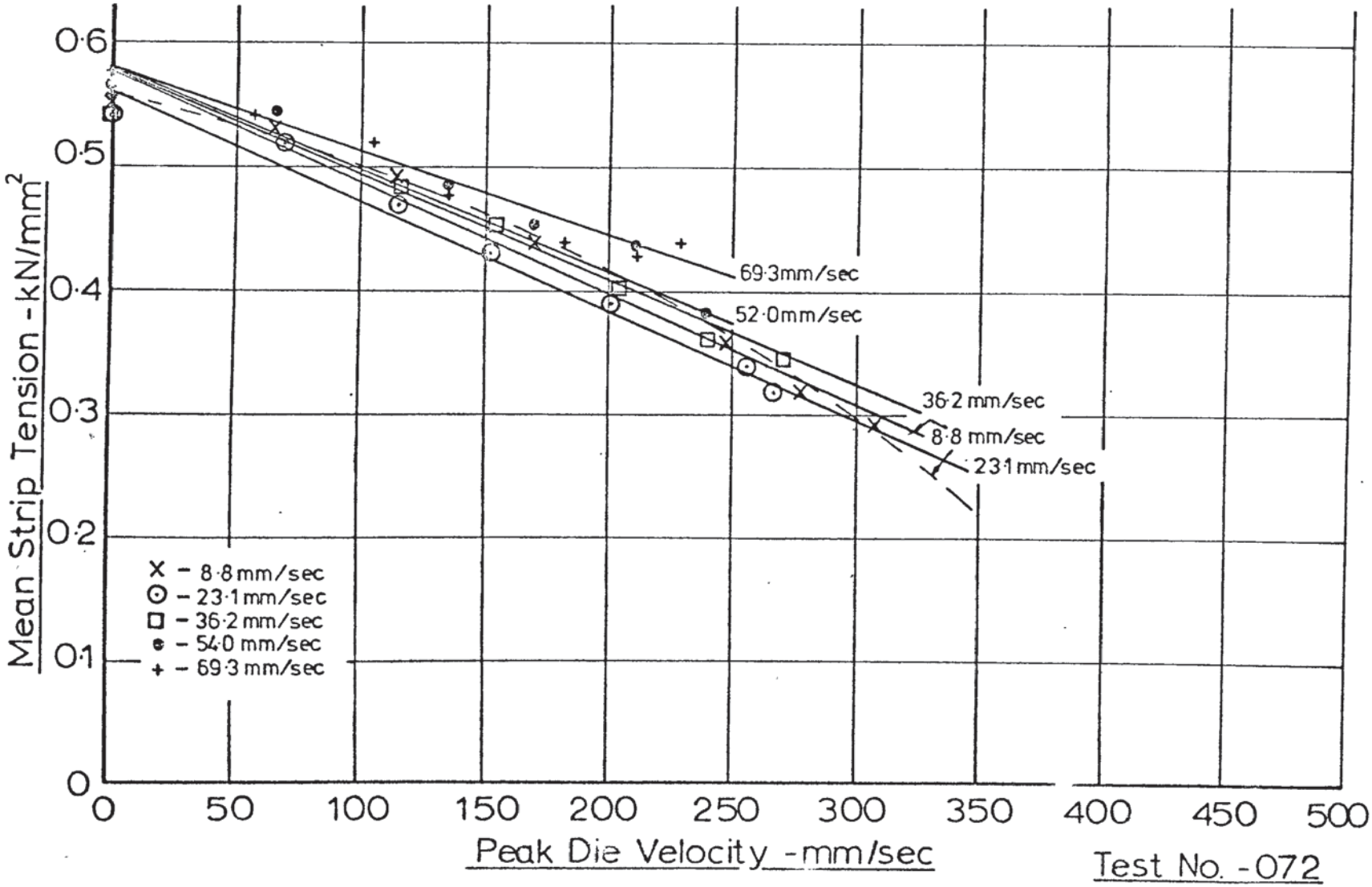

Test No. - 072

Fig(7·26)-Mean Strip Tension vs. Peak Die Velocity(α=7·5° with land)

[Full Power Input]

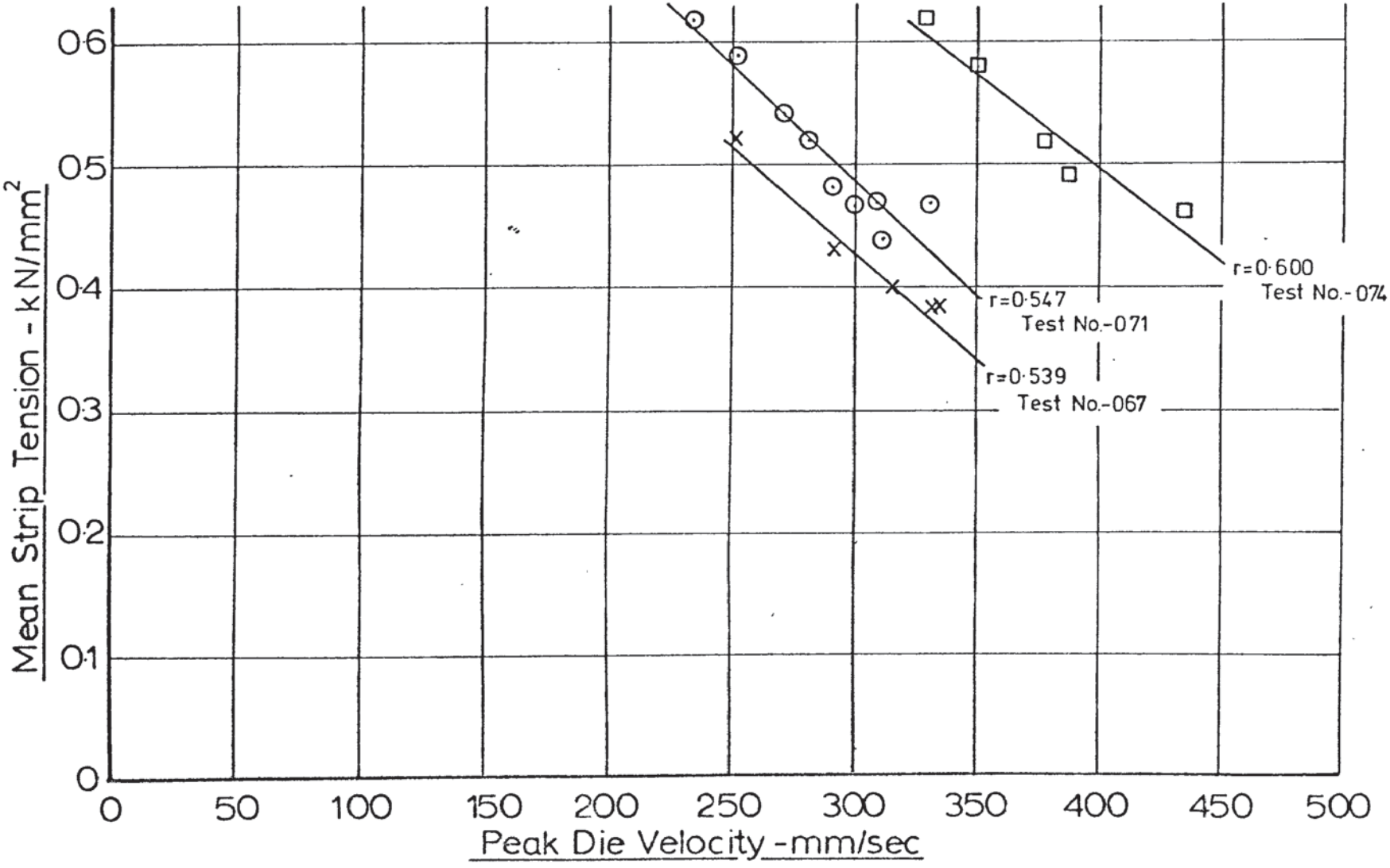

Fig(7·27) - Mean Strip Tension vs. Peak Die Velocity(α=10°, r=0·260)

[Constant Draw Speed Test]

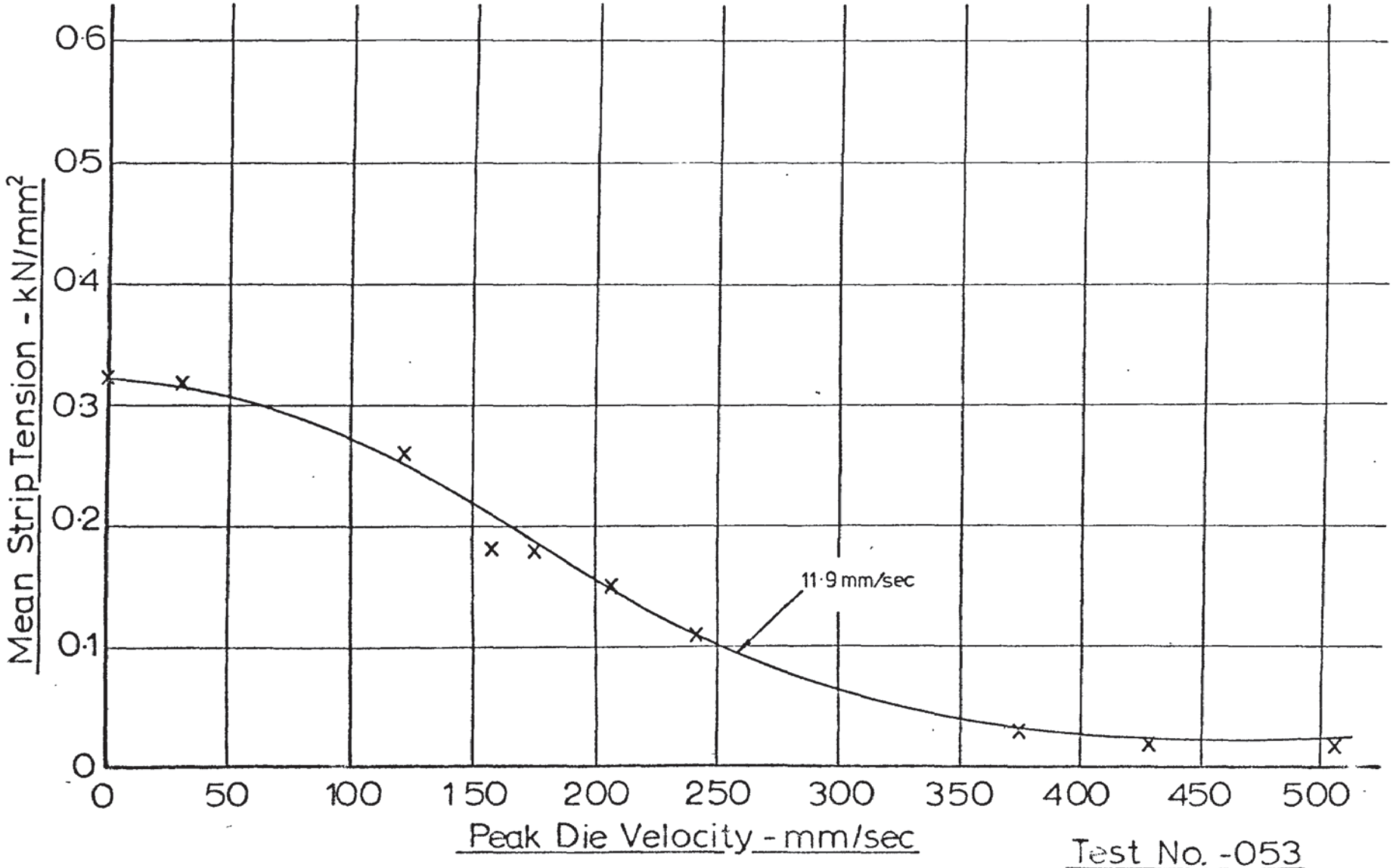

Test No. -053

Fig(7.28)-Mean Strip Tension vs. Peak Die Velocity(α=10°, r=0.263)

[Constant Draw Speed Tests]

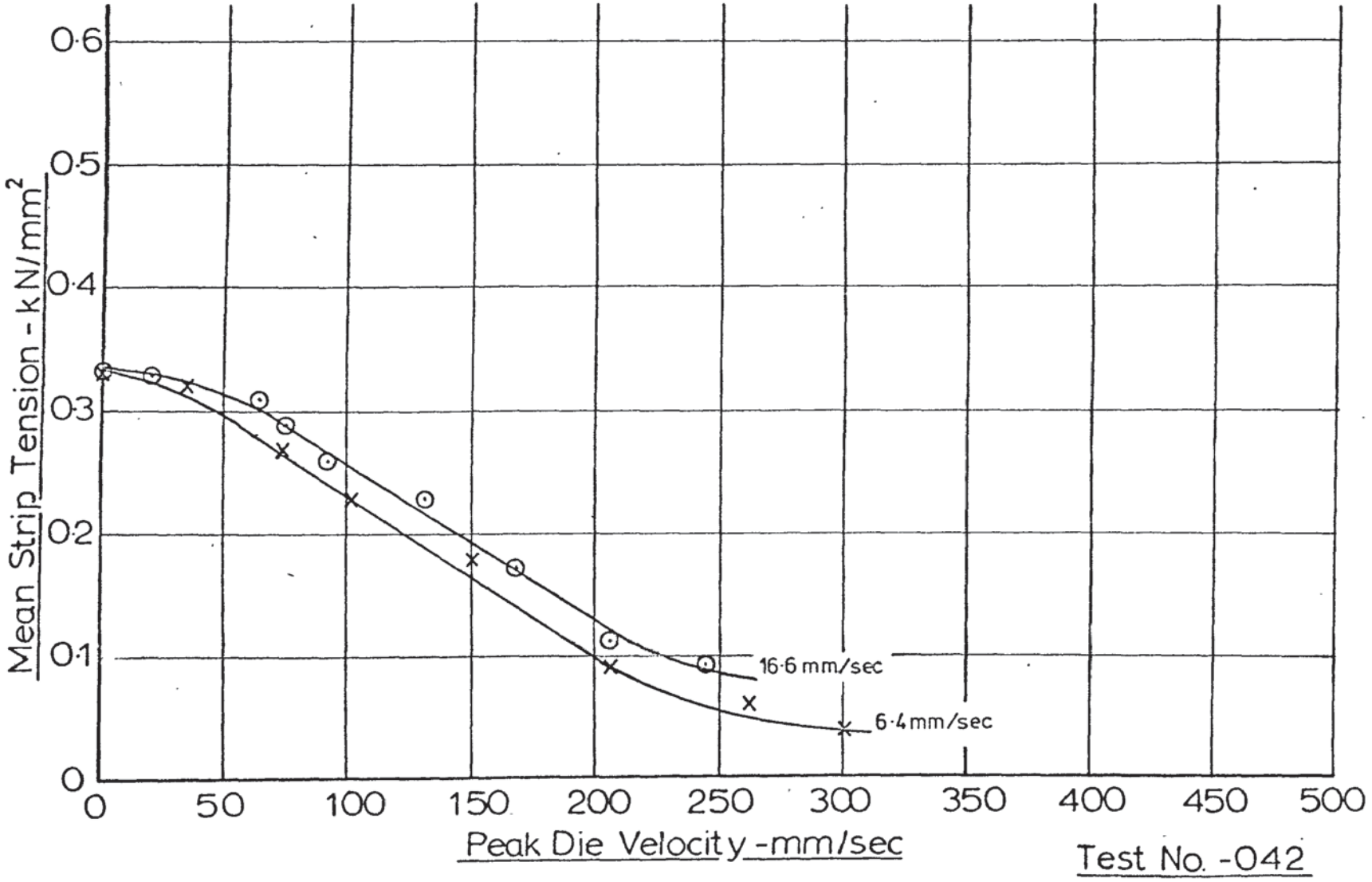

Test No. -042

Fig(7·29) - Mean Strip Tension vs. Peak Die Velocity(α=10°, r=0·399)

[Constant Draw Speed Tests]

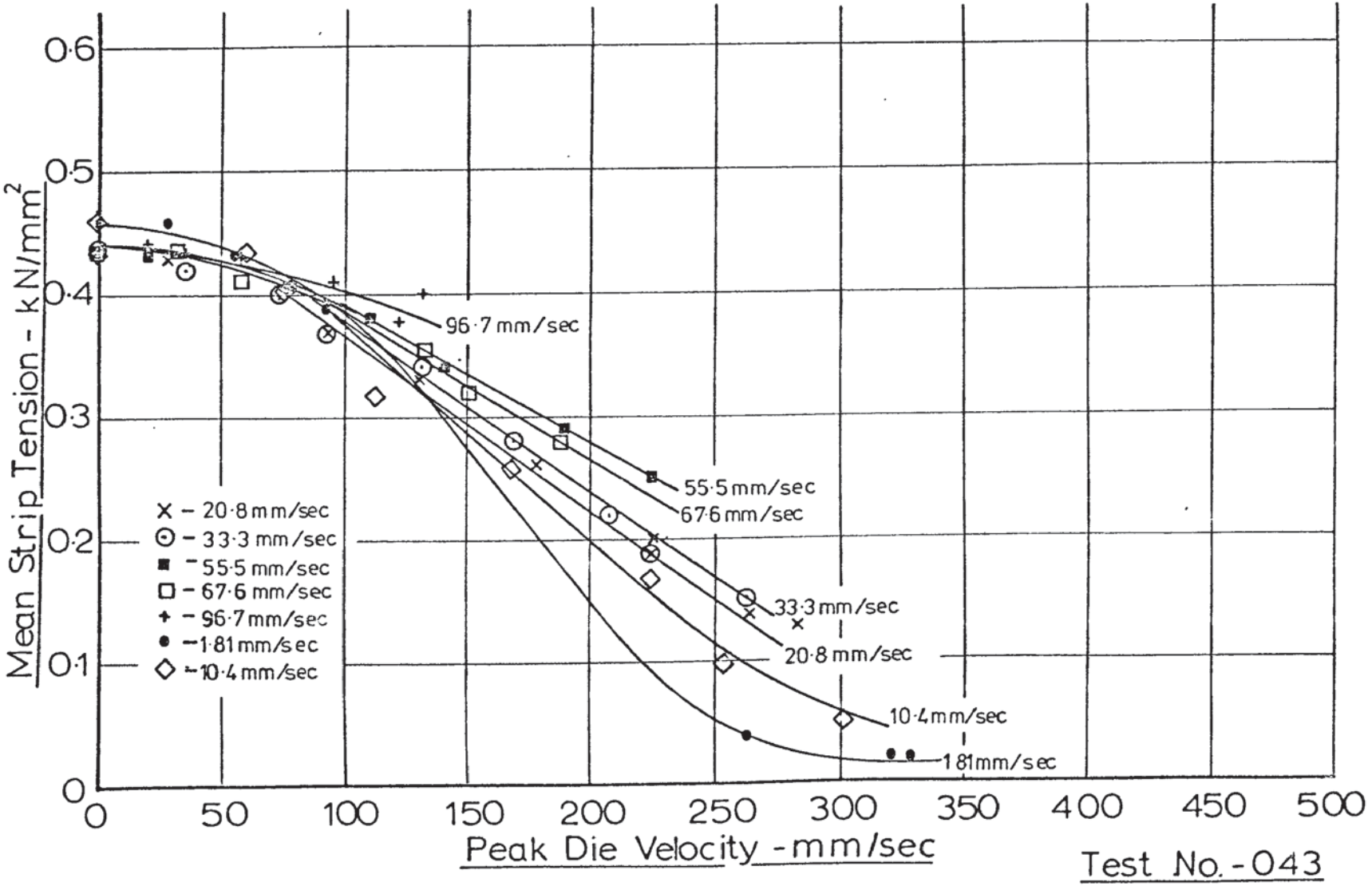

Test No. - 043

Fig(7.30) - Mean Strip Tension vs. Peak Die Velocity(α=10°, r=0.461)

[Constant Draw Speed Tests]

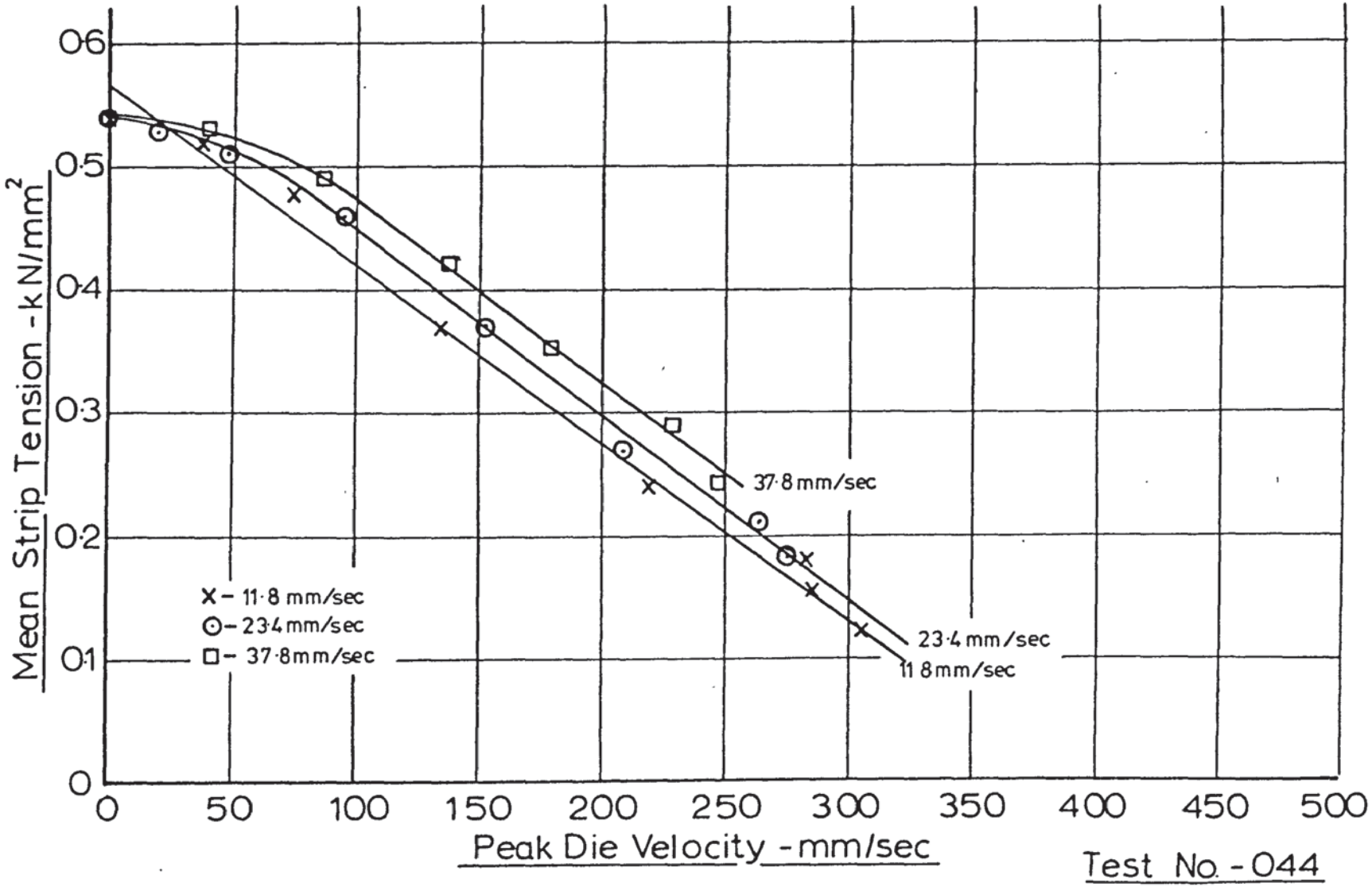

Test No. - 044

Fig(7.31)-Mean Strip Tension vs. Peak Die Velocity(α =10°)

[Arbitrary Draw Speed, Constant Power Input]

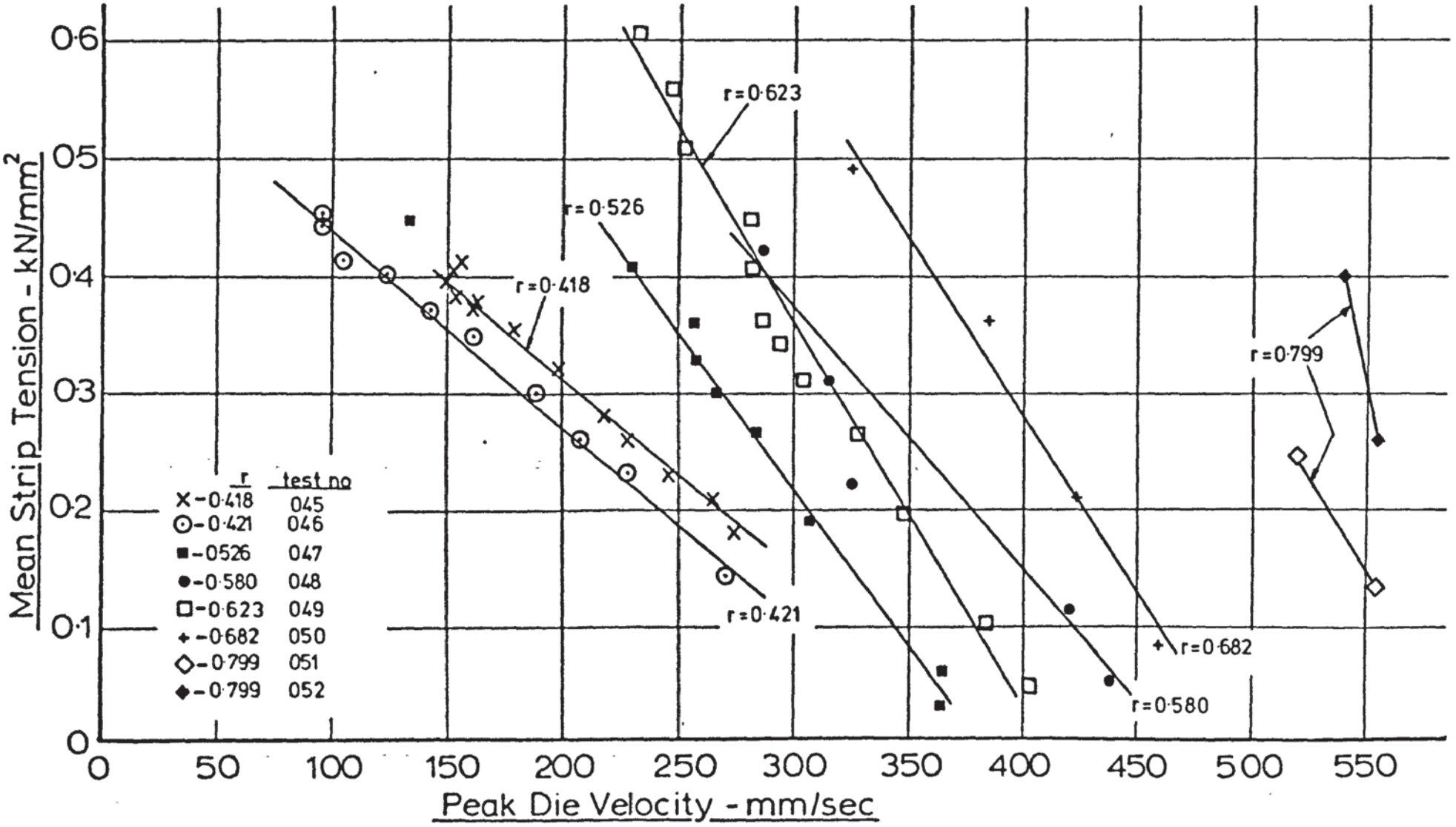

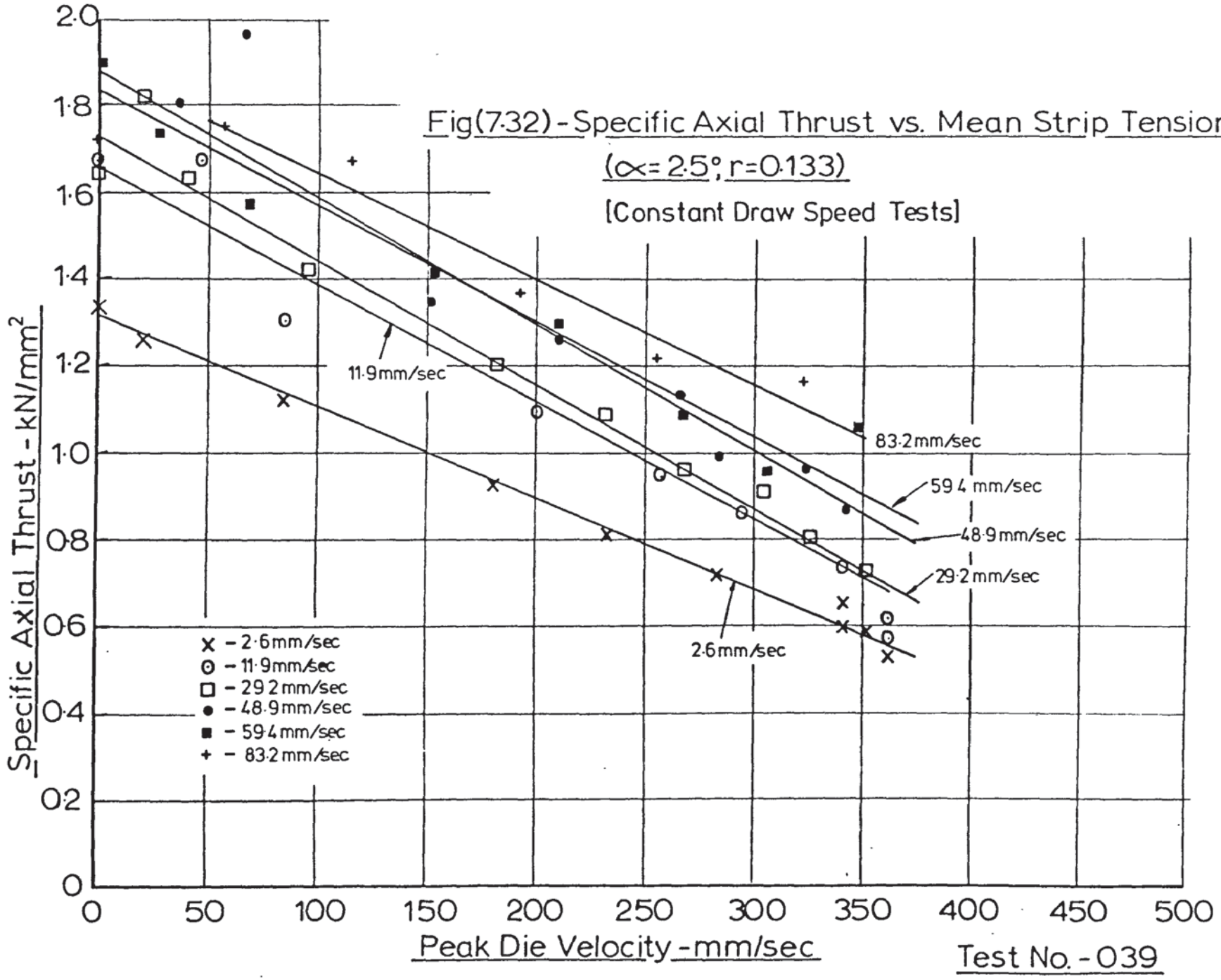
Fig(7.32) - Specific Axial Thrust vs. Mean Strip Tension
(∝= 2.5°, r=0.133)
[Constant Draw Speed Tests]
Specific Axial Thrust - kN/mm²
Peak Die Velocity - mm/sec
Test No. - 039
2.0
1.8
1.6
1.4
1.2
1.0
0.8
0.6
0.4
0.2
0
0
50
100
150
200
250
300
350
400
450
500
11.9mm/sec
83.2mm/sec
59.4 mm/sec
48.9mm/sec
29.2mm/sec
2.6mm/sec
× - 2.6mm/sec
⊙ - 11.9mm/sec
□ - 29.2 mm/sec
● - 48.9mm/sec
■ - 59.4mm/sec
+ - 83.2 mm/sec

Fig(7.33)- Specific Axial Thrust vs. Peak Die Velocity(α= 2.5°, r=0.250)

[Constant Draw Speed Tests]

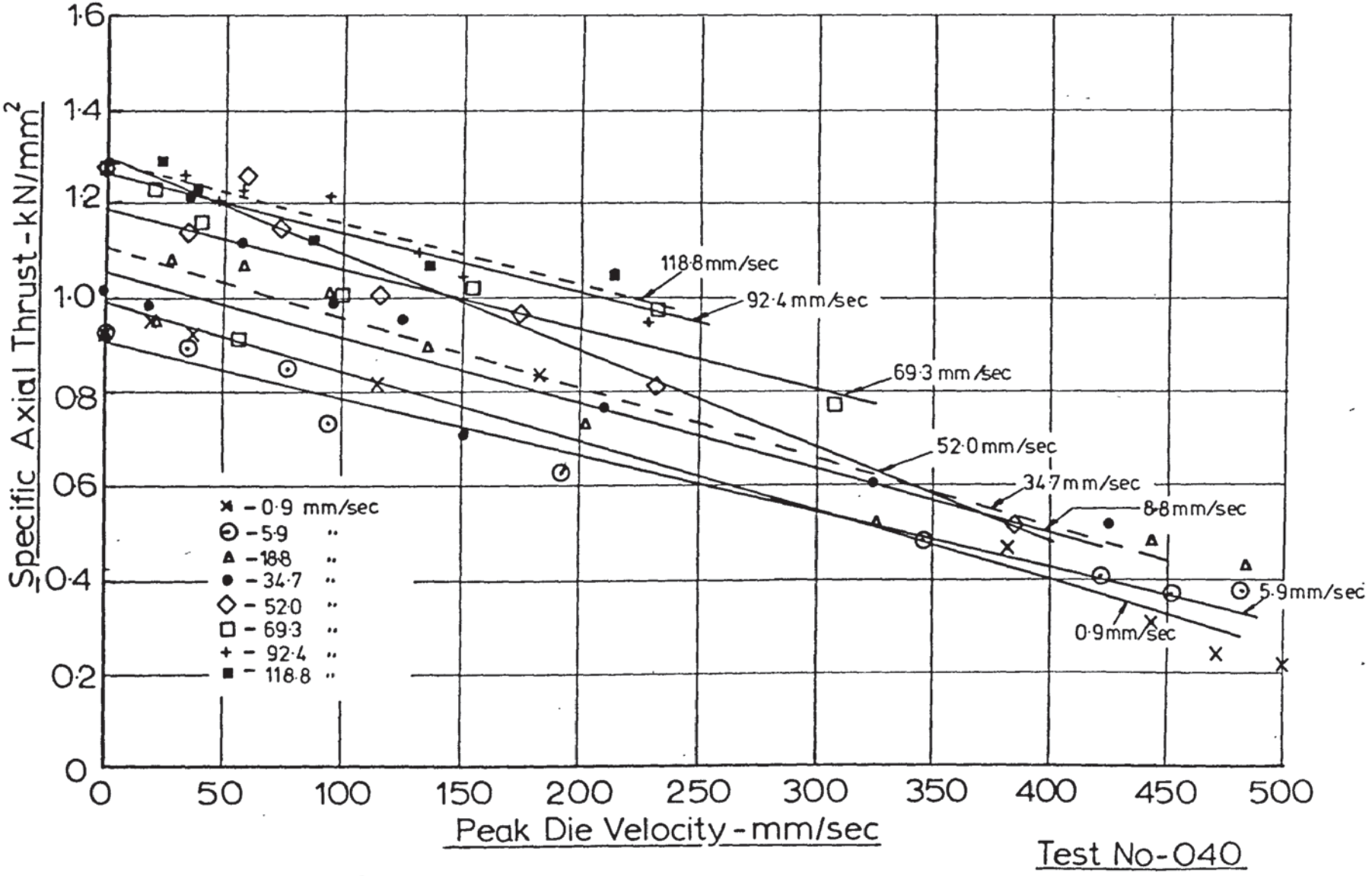

Test No-040

Fig(7·34)-Specific Axial Die Thrust vs. Peak Die Velocity(α=2·5°, r=0·267)

[Constant Draw Speed Tests]

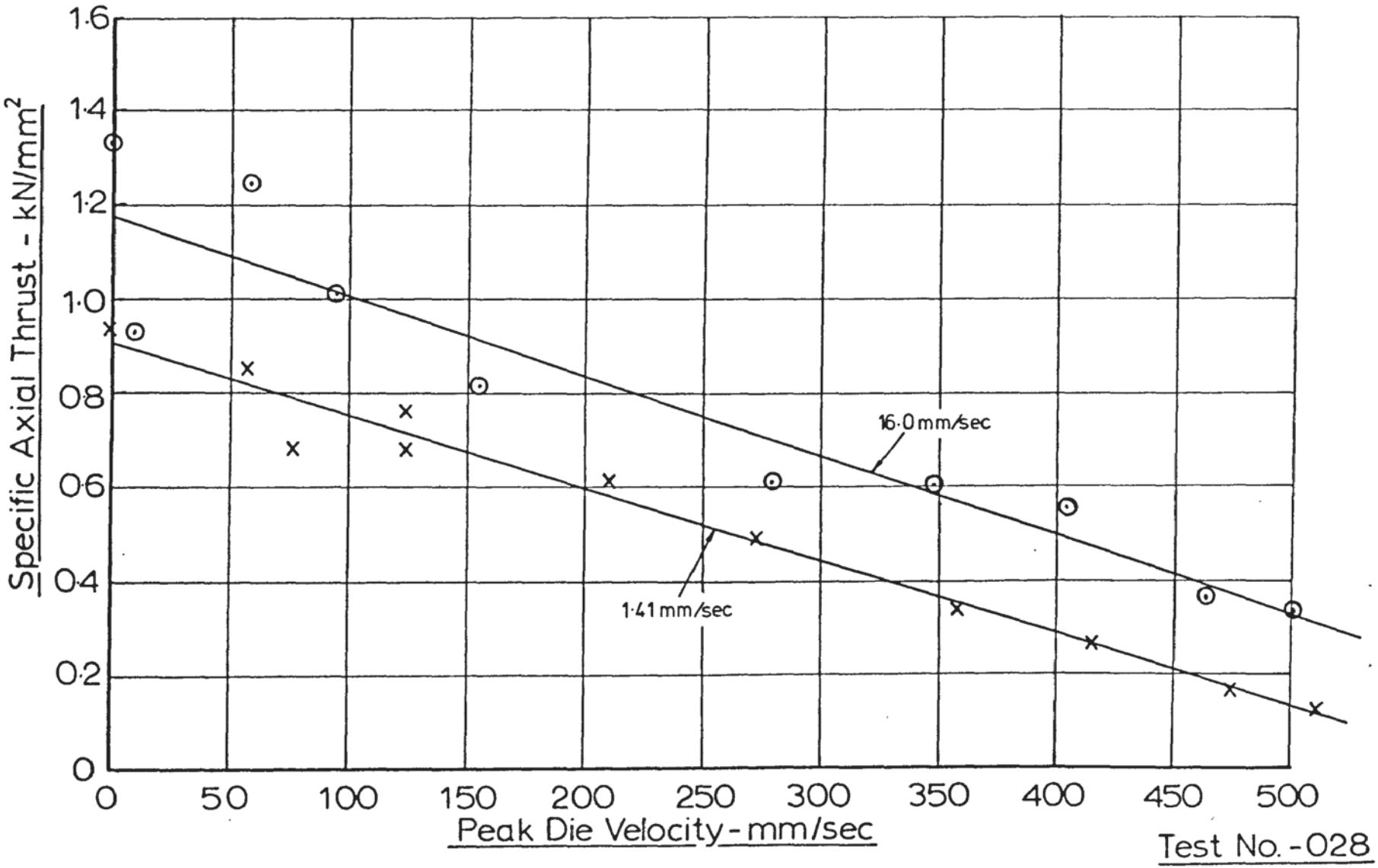

Test No.-028

Fig(7·35) - Specific Axial Thrust vs. Peak Die Velocity (α = 2·5°, r = 0·280)

[Draw Speed = 37·0 mm/sec]

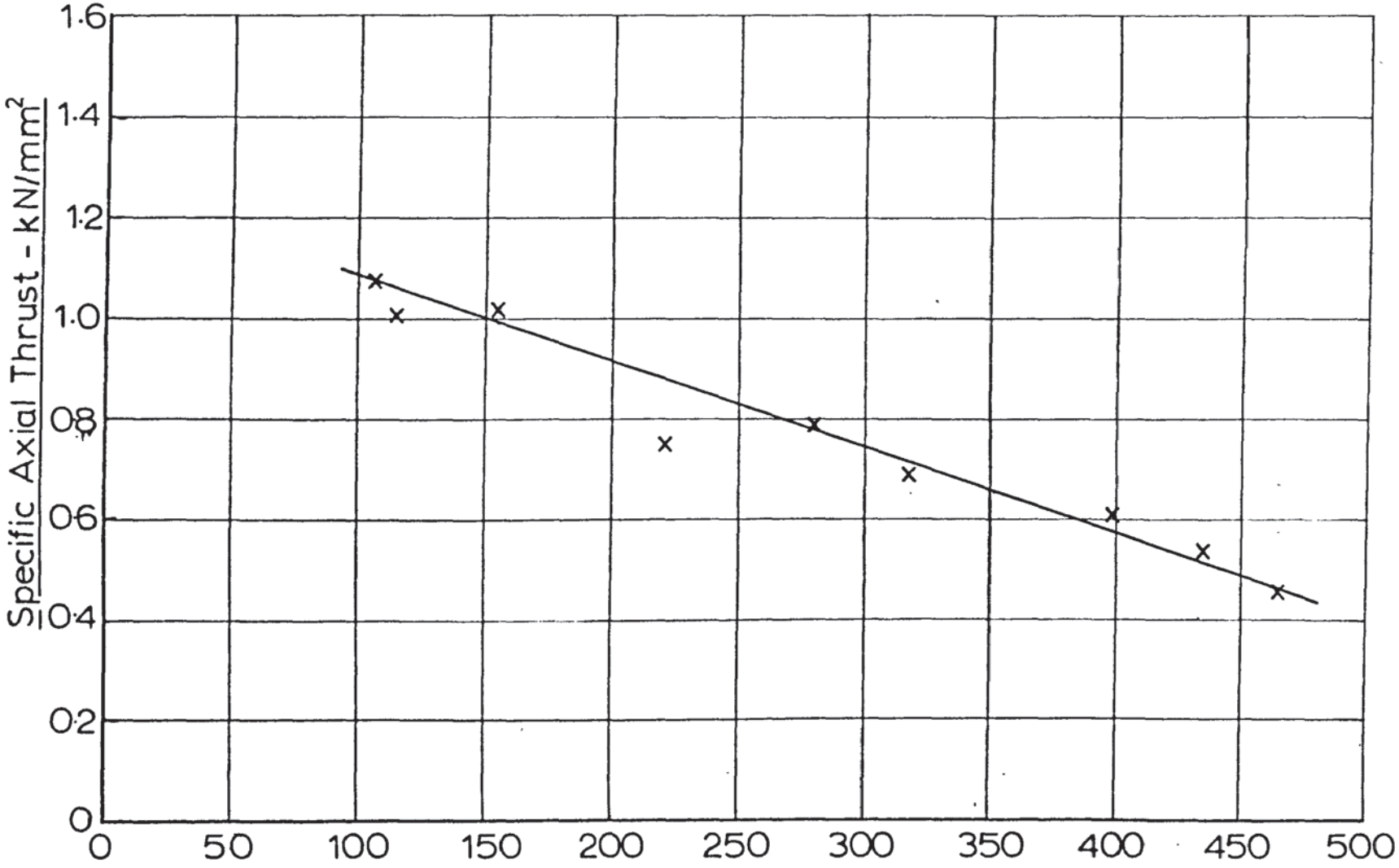

Test No. - 029

Fig(7.36) - Specific Axial Thrust vs. Peak Die Velocity(α=2.5°, r=0.280)

[Arbitrary Power Input And Draw Speed]

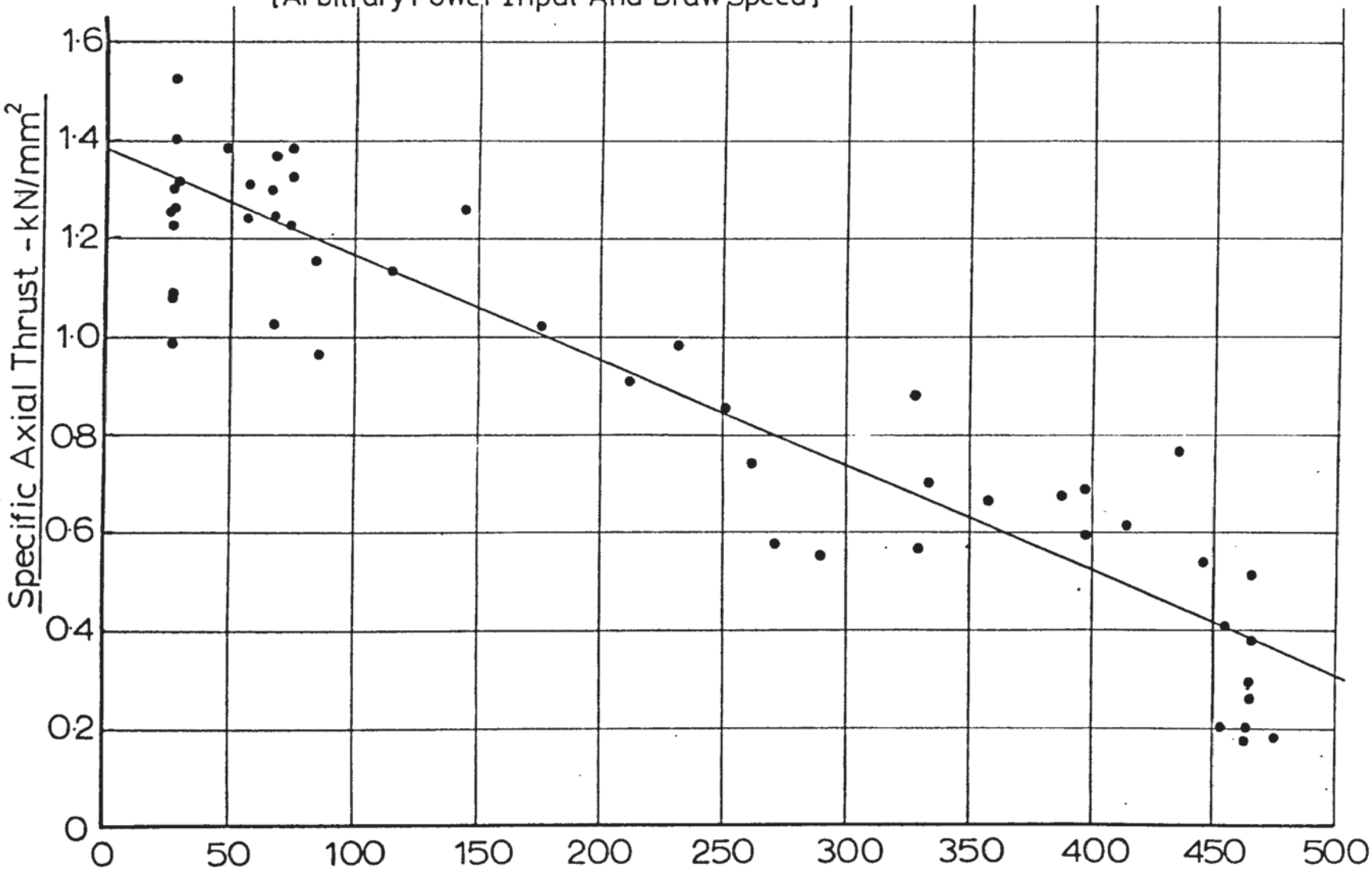

Test No.-030

Fig(7·37)-Specific Axial Thrust vs. Peak Die Velocity($\alpha = 2{\cdot}5°$)

[Full Power Input - Arbitrary Draw Speed]

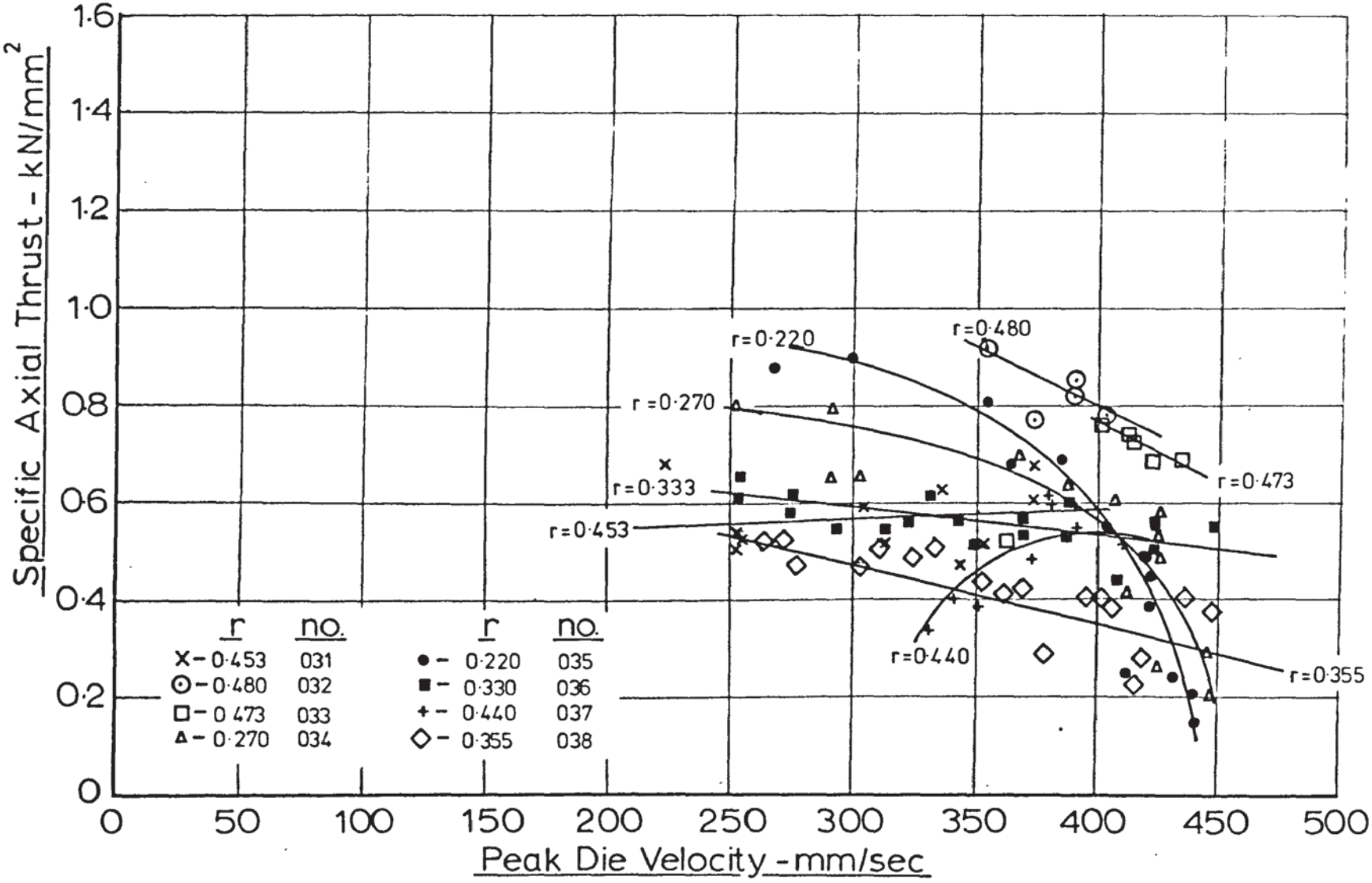

Fig(7·38)-Specific Axial Thrust vs. Mean Strip Tension(α=5°, r=0·205)

[Constant Draw Speed Tests]

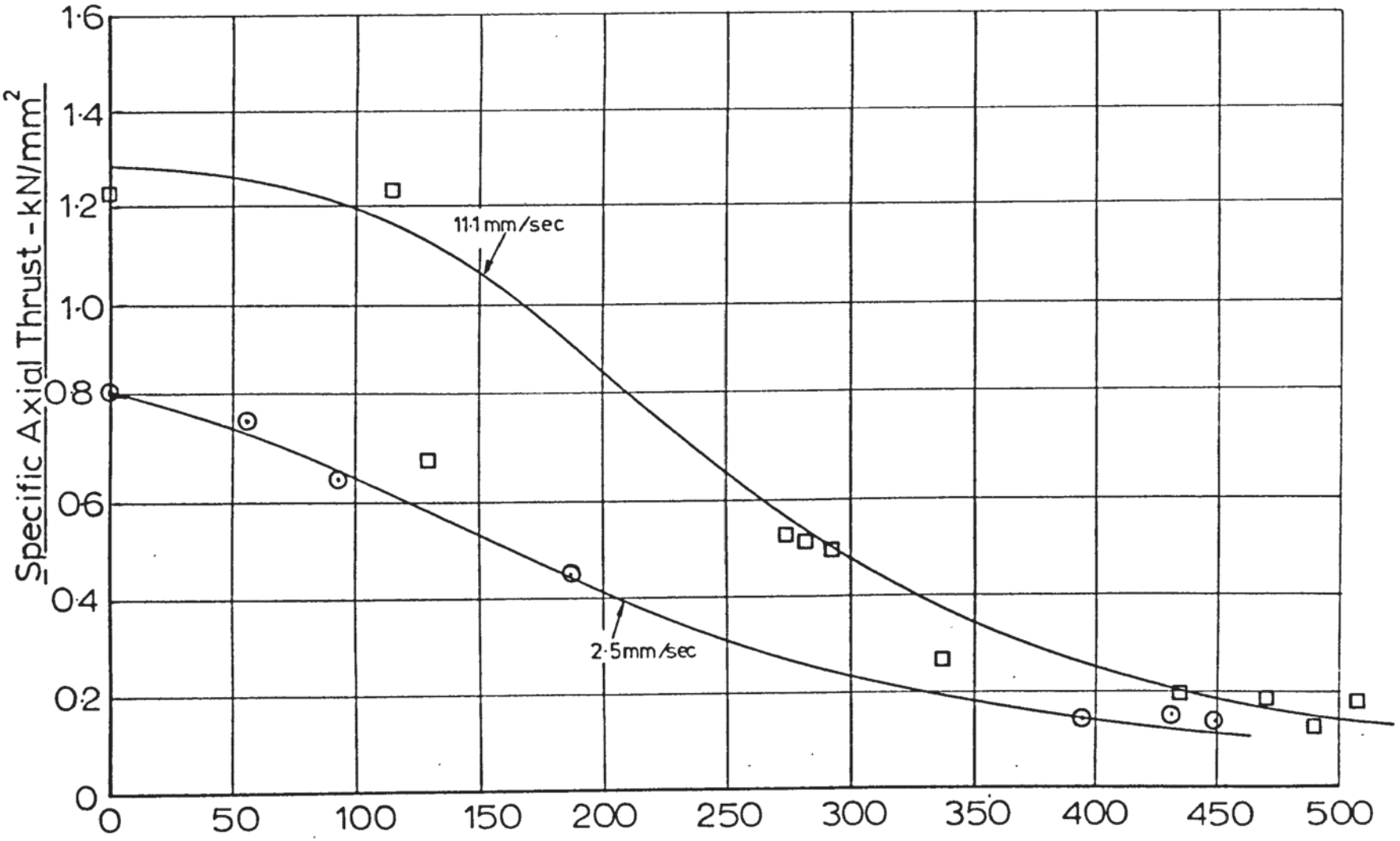

Test No. -055

Fig(7.39)-Specific Axial Thrust vs. Peak Die Velocity(α=5°, r=0.345)

[Constant Draw Speed Tests]

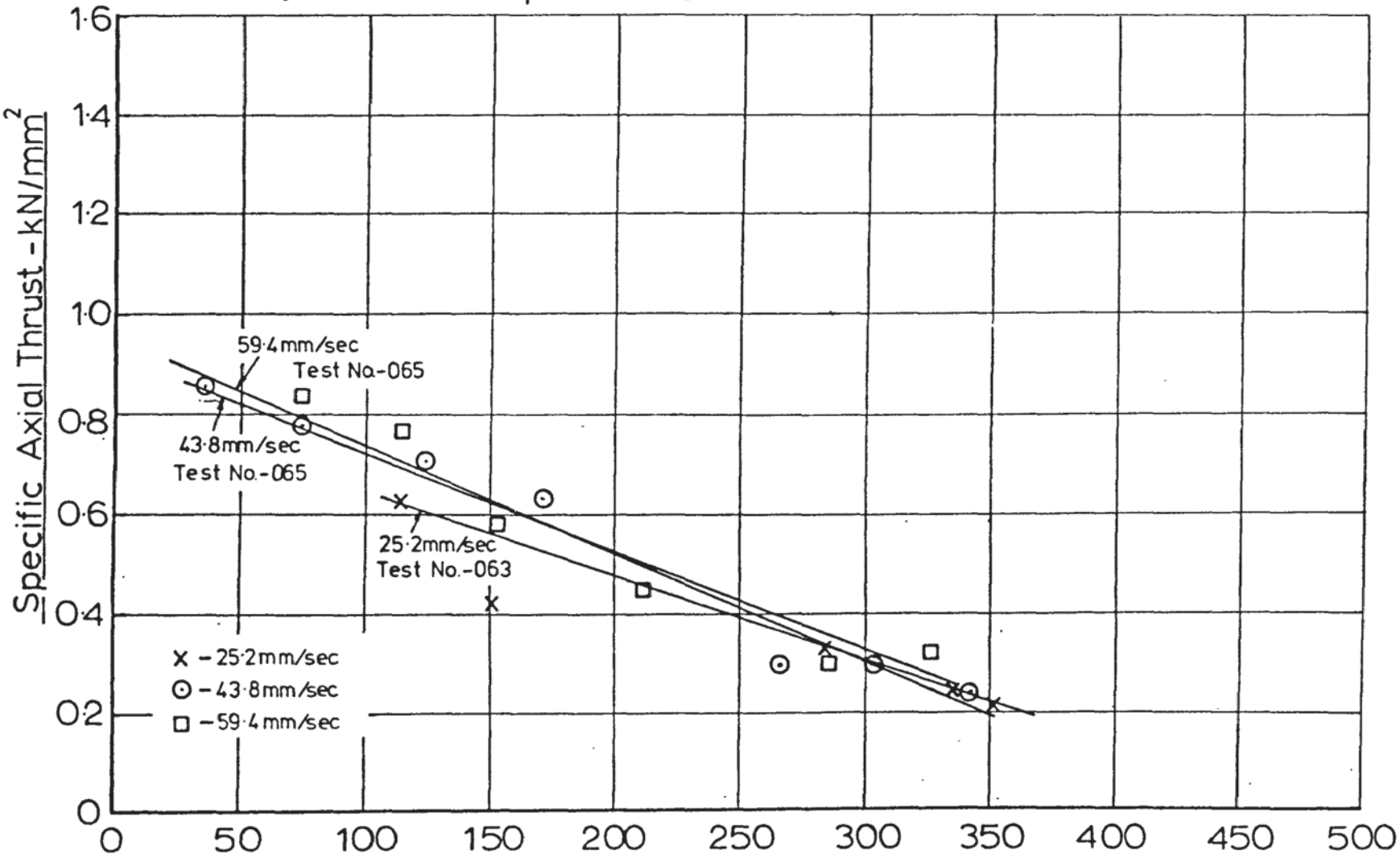

Test Nos.-063&065

Fig(7.40)-Specific Axial Thrust vs. Peak Die Velocity(α=5°, r=0.364)

[Constant Draw Speed Tests]

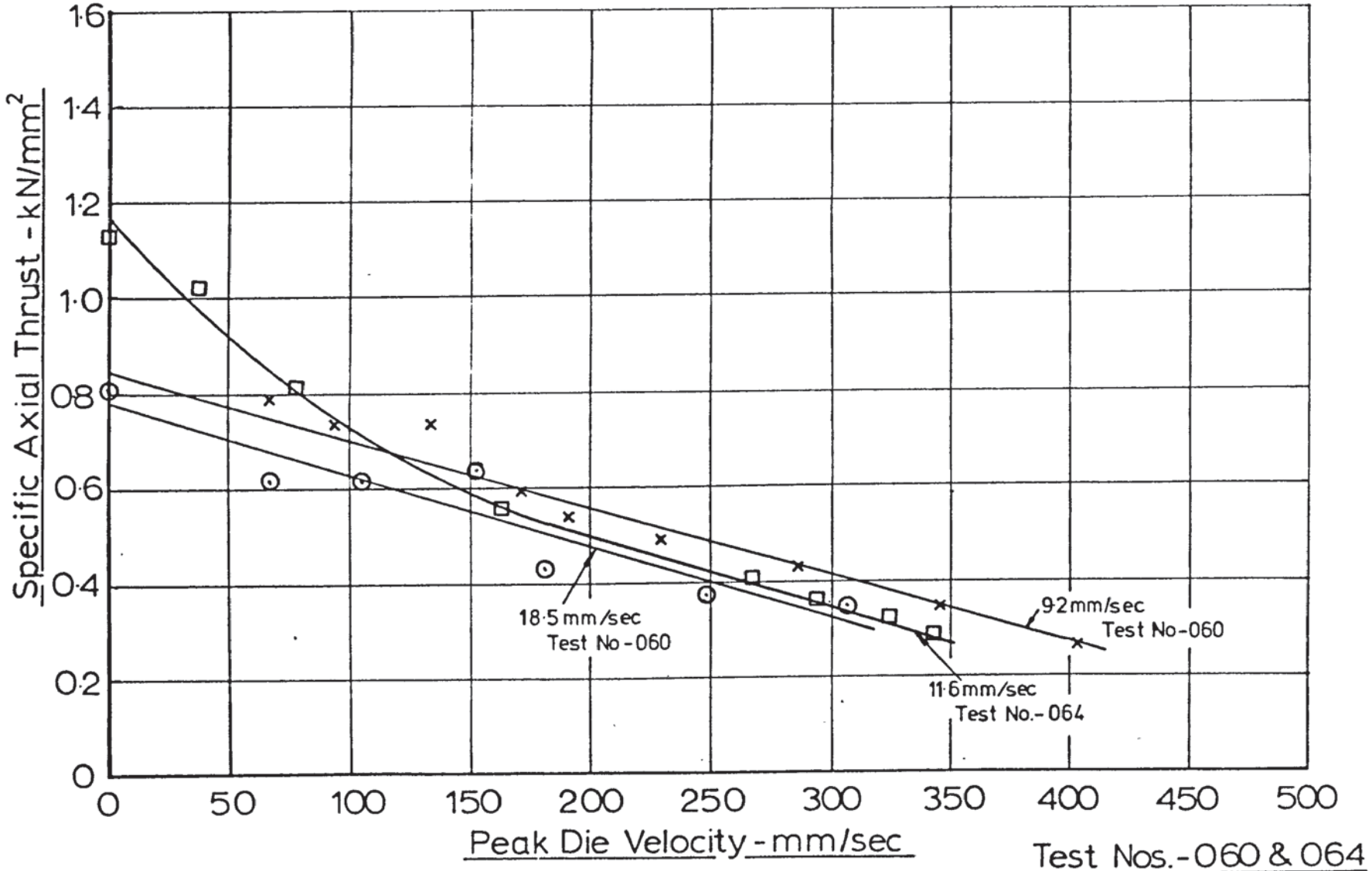

Test Nos.- 060 & 064

Fig(7·41) - Specific Axial Thrust vs. Peak Die Velocity (α=5°, r=0·413)

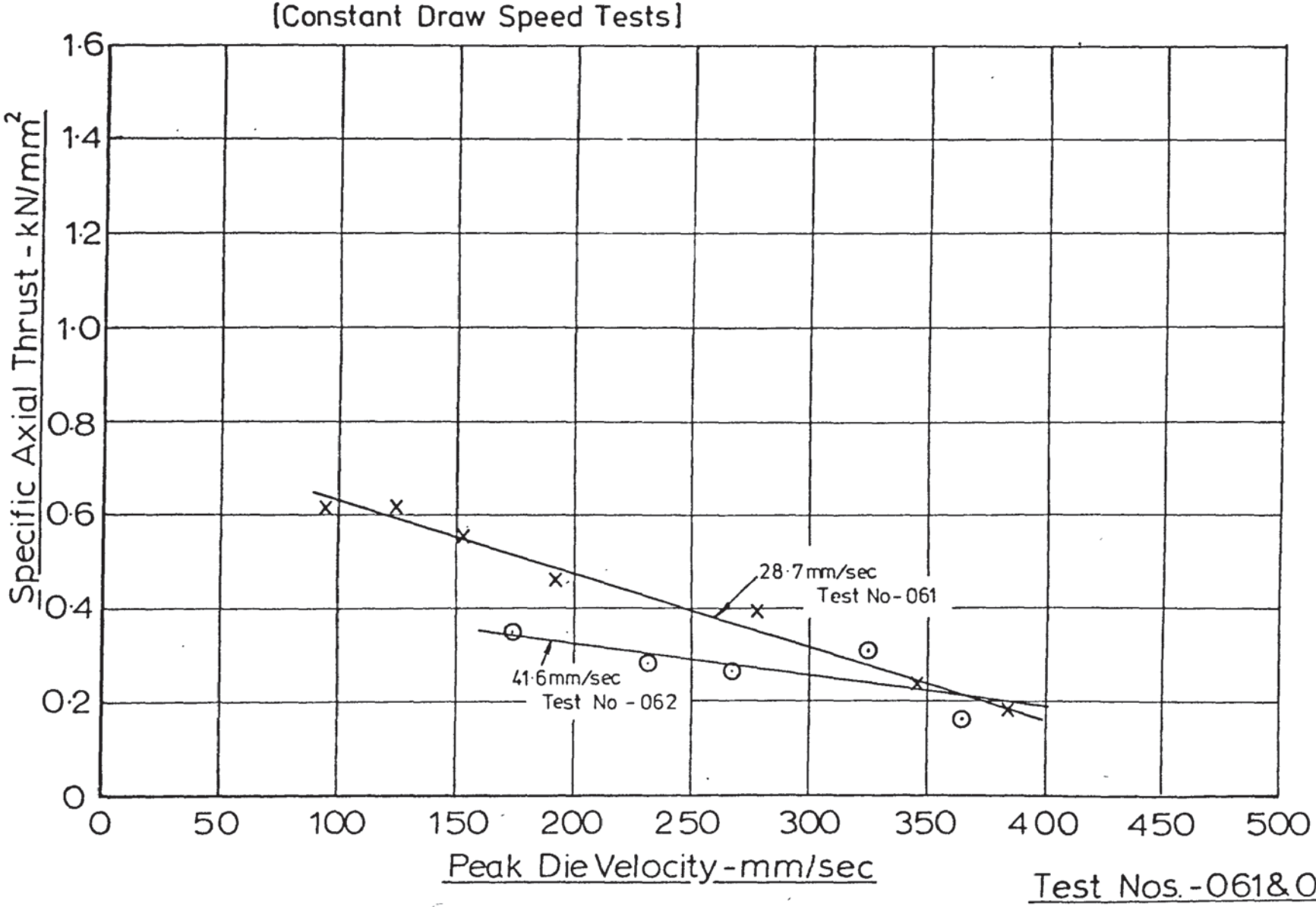

Test Nos. - 061 & 062

Fig(7·42)-Specific Axial Thrust vs. Peak Die Velocity(α=5°, r=0·442)

[Draw Speed=30·8mm/sec]

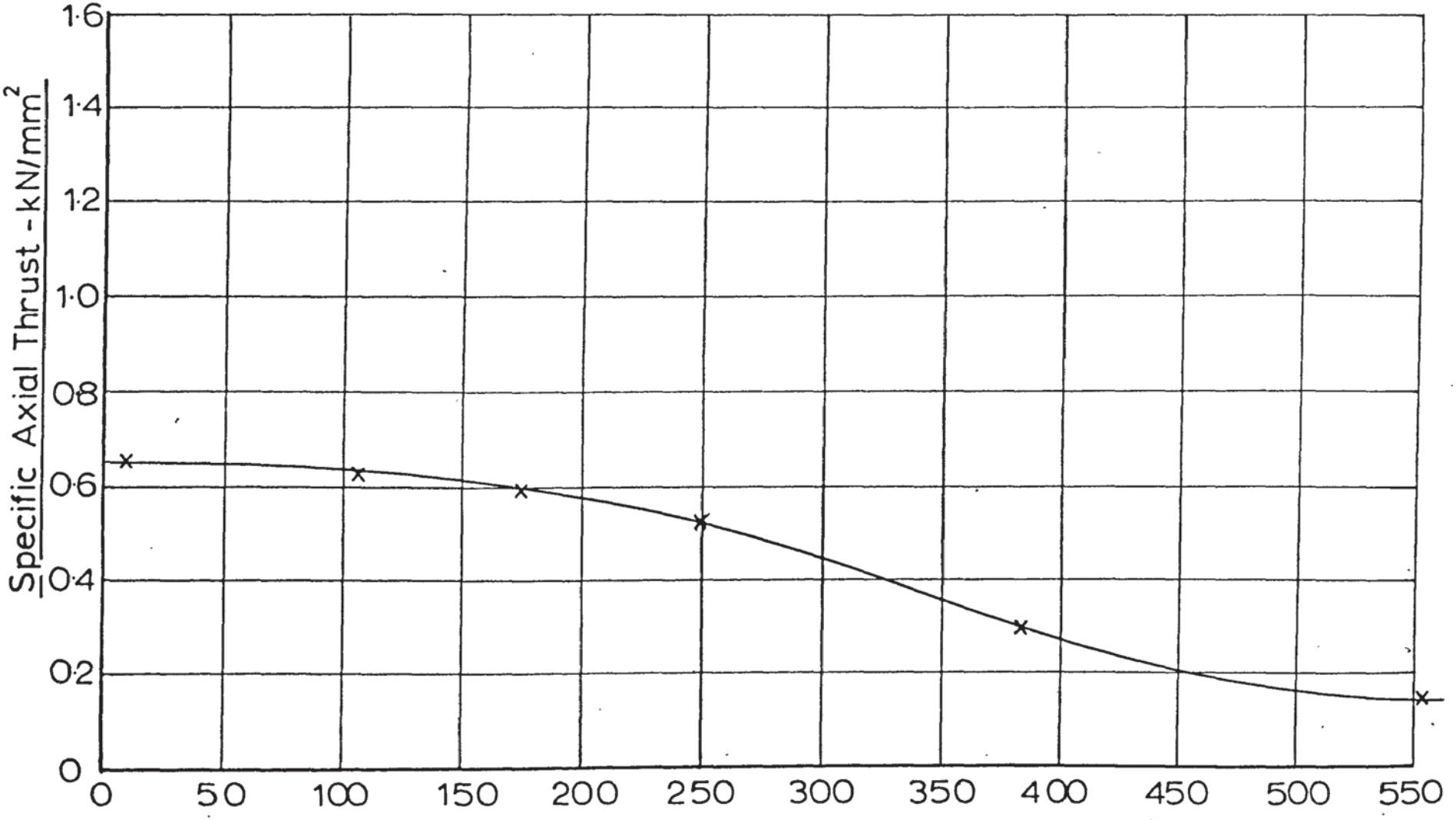

Test No - 054

Fig(7.43)-Specific Axial Thrust vs. Peak Die Velocity($\alpha = 5°$)

[Full Power Input - Arbitrary Draw Speed]

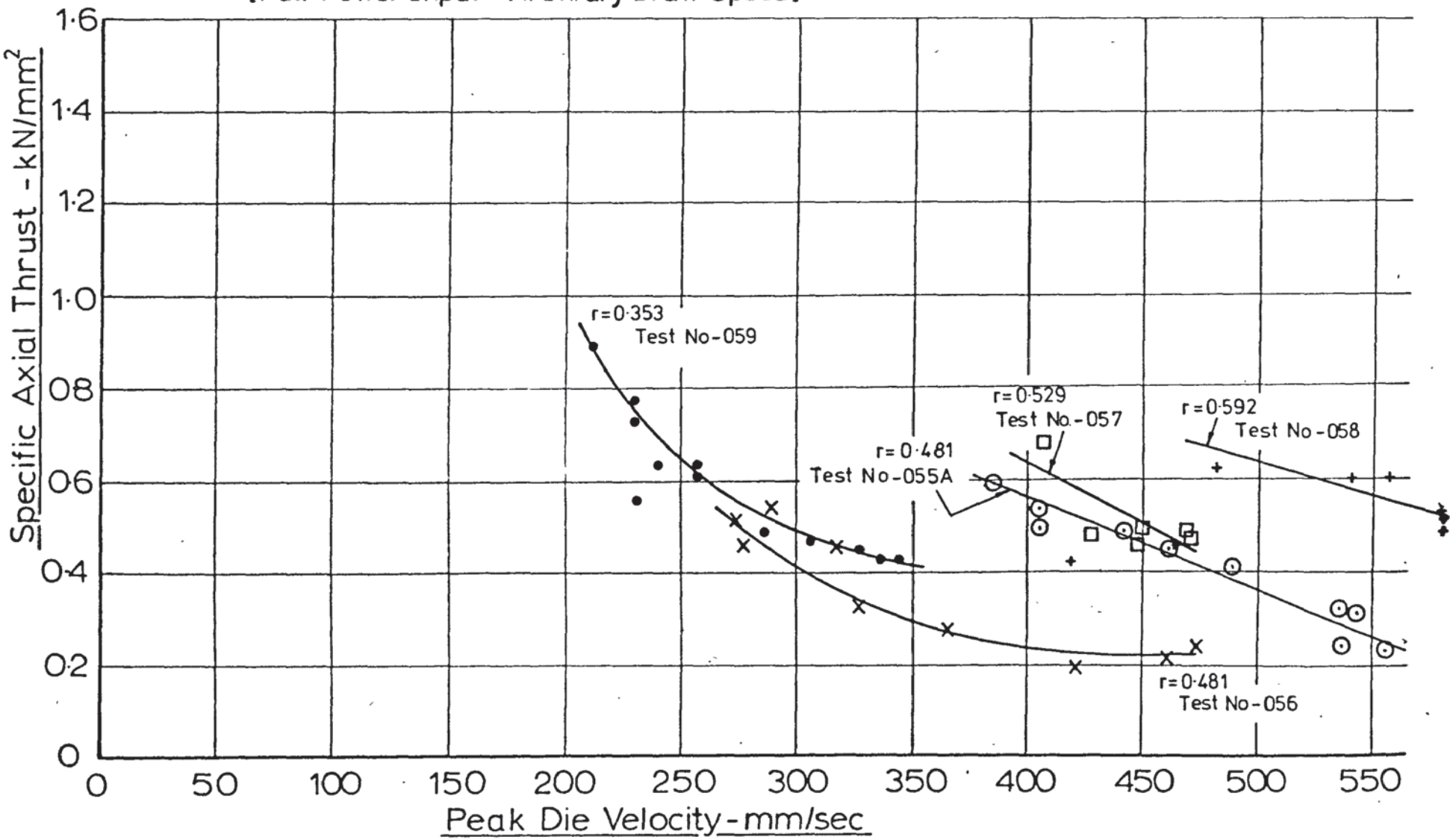

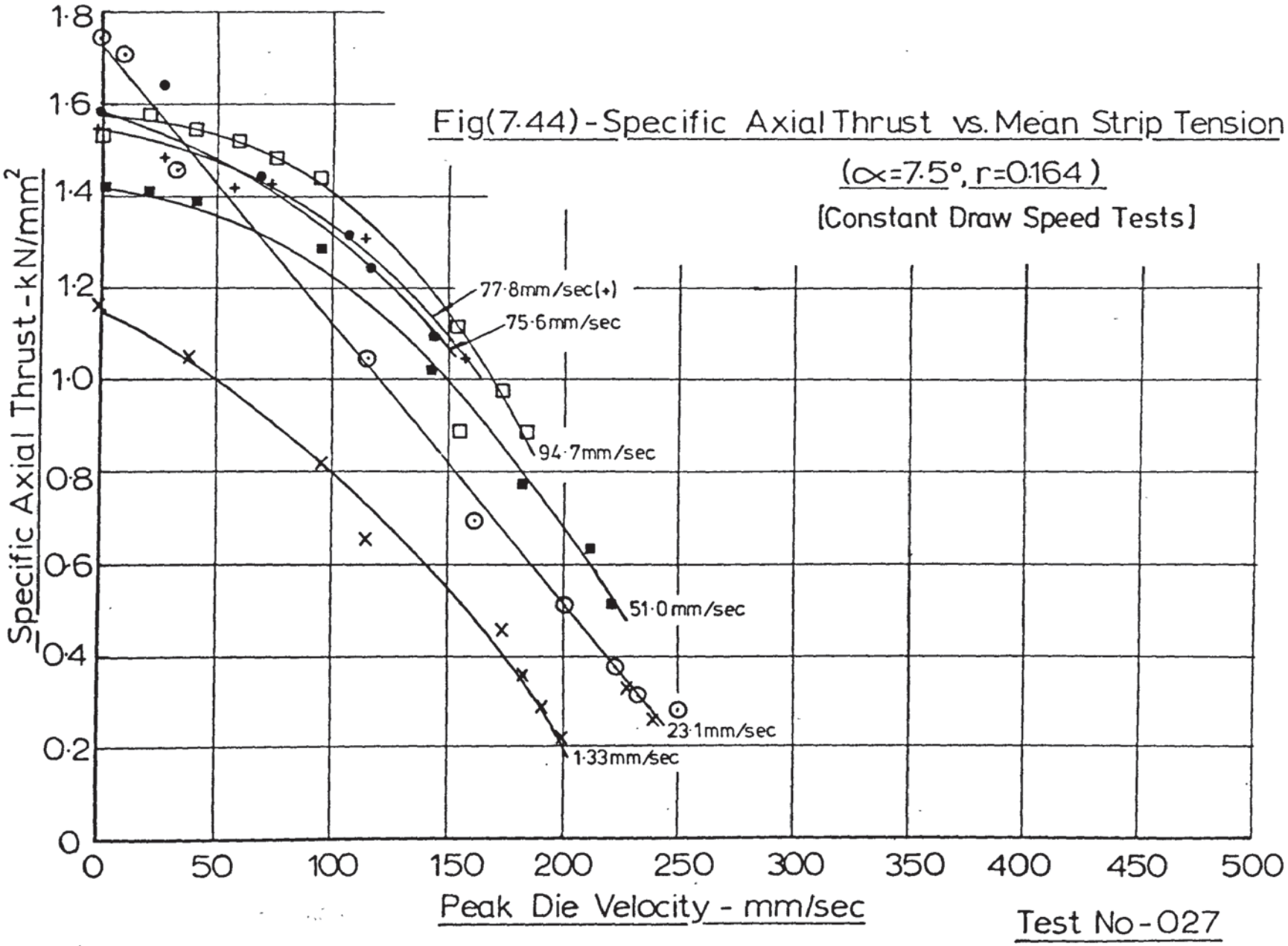

Fig(7.44) - Specific Axial Thrust vs. Mean Strip Tension

(α=7.5°, r=0.164)

[Constant Draw Speed Tests]

Test No - 027

Fig(7·45)-Specific Axial Thrust vs. Peak Die Velocity(α=7·5°; r=0·267)

[Constant Draw Speed Tests]

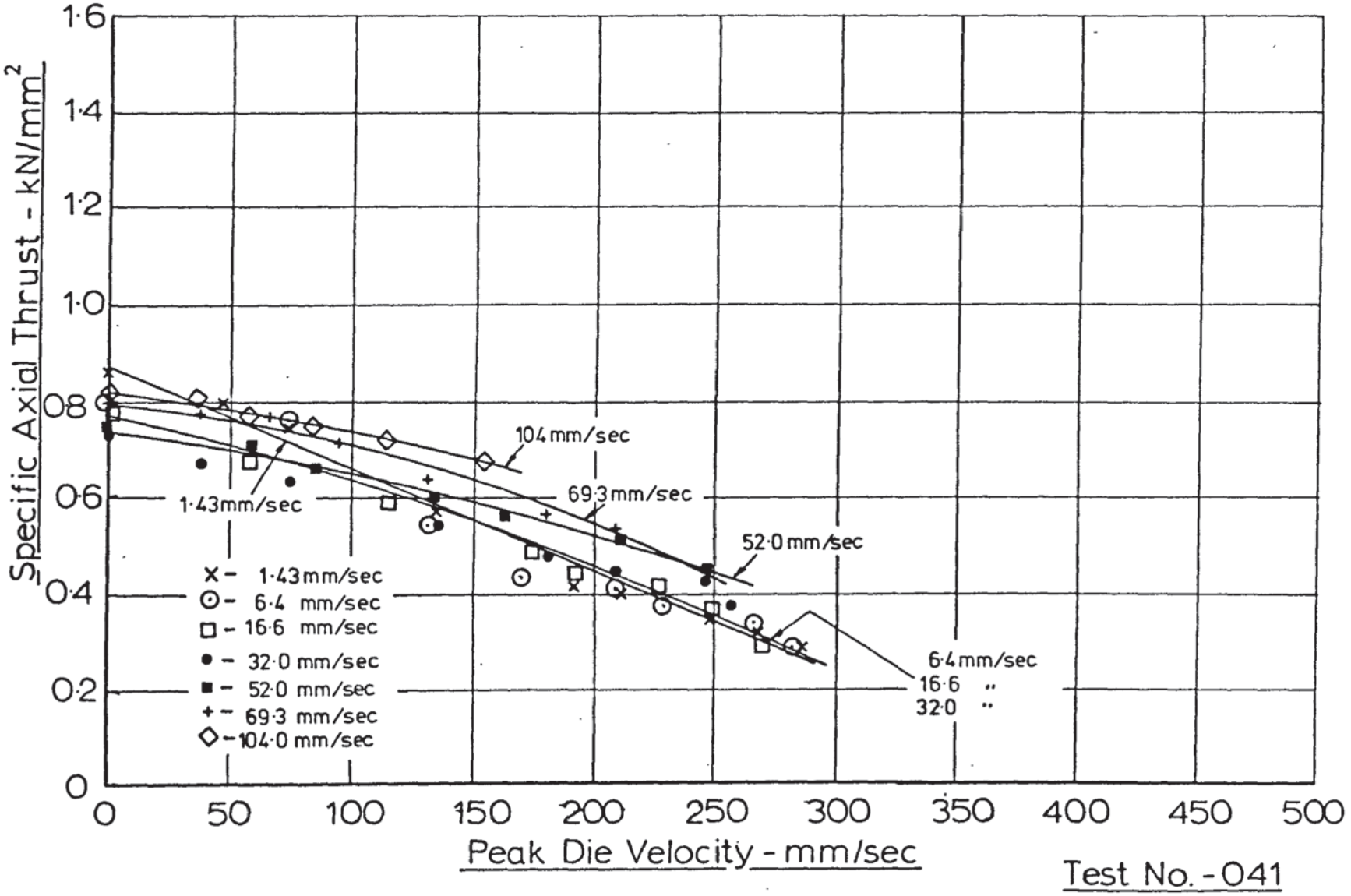

Test No. - 041

Fig(7.46)-Specific Axial Thrust vs. Peak Die Velocity(α=7.5°, r=0.307)

[Constant Draw Speed Tests]

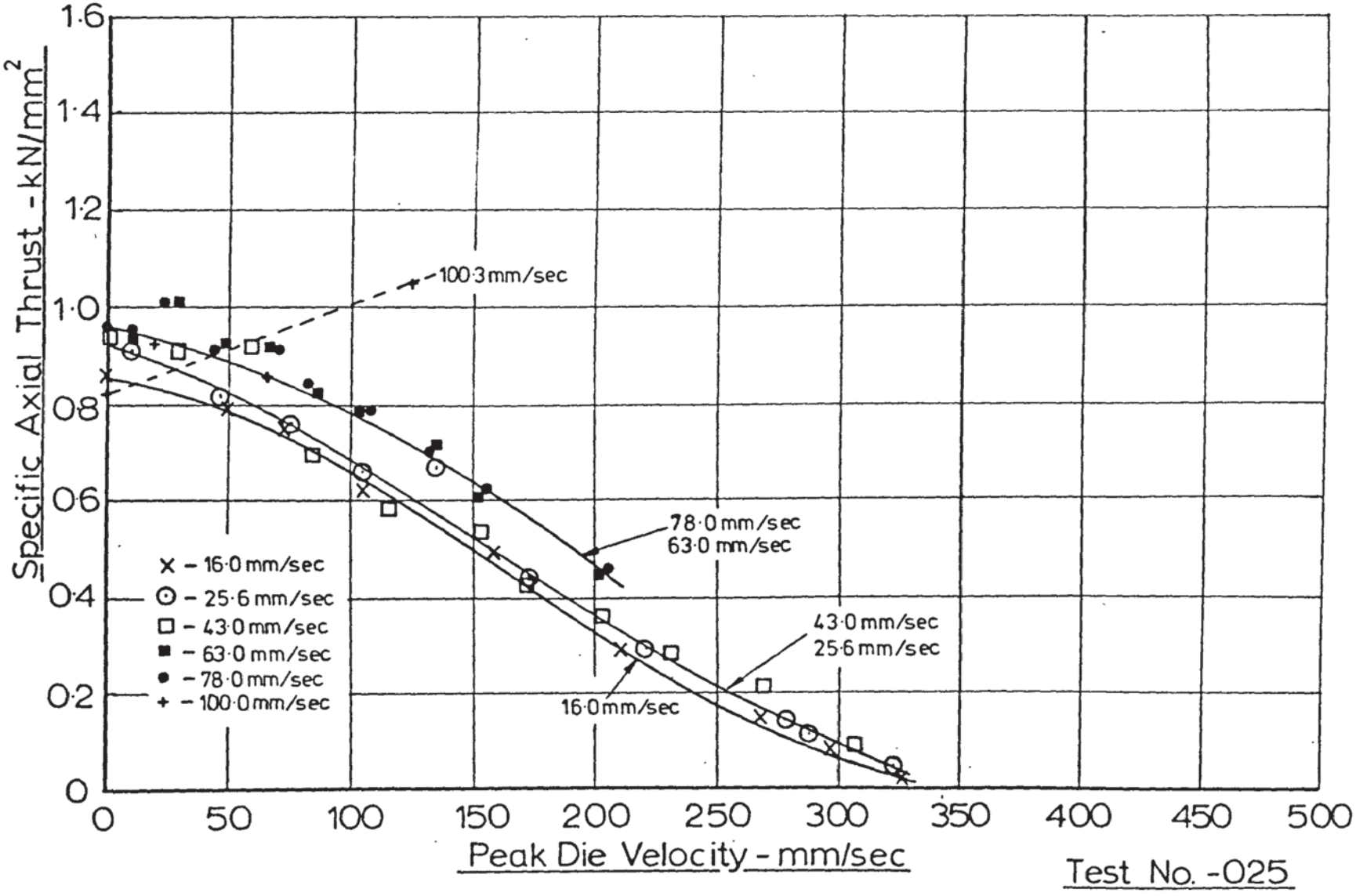

Test No. -025

Fig(7·47) -Specific Axial Thrust vs. Peak Die Velocity(α=7·5°, r=0·368)

[Constant Draw Speed Tests]

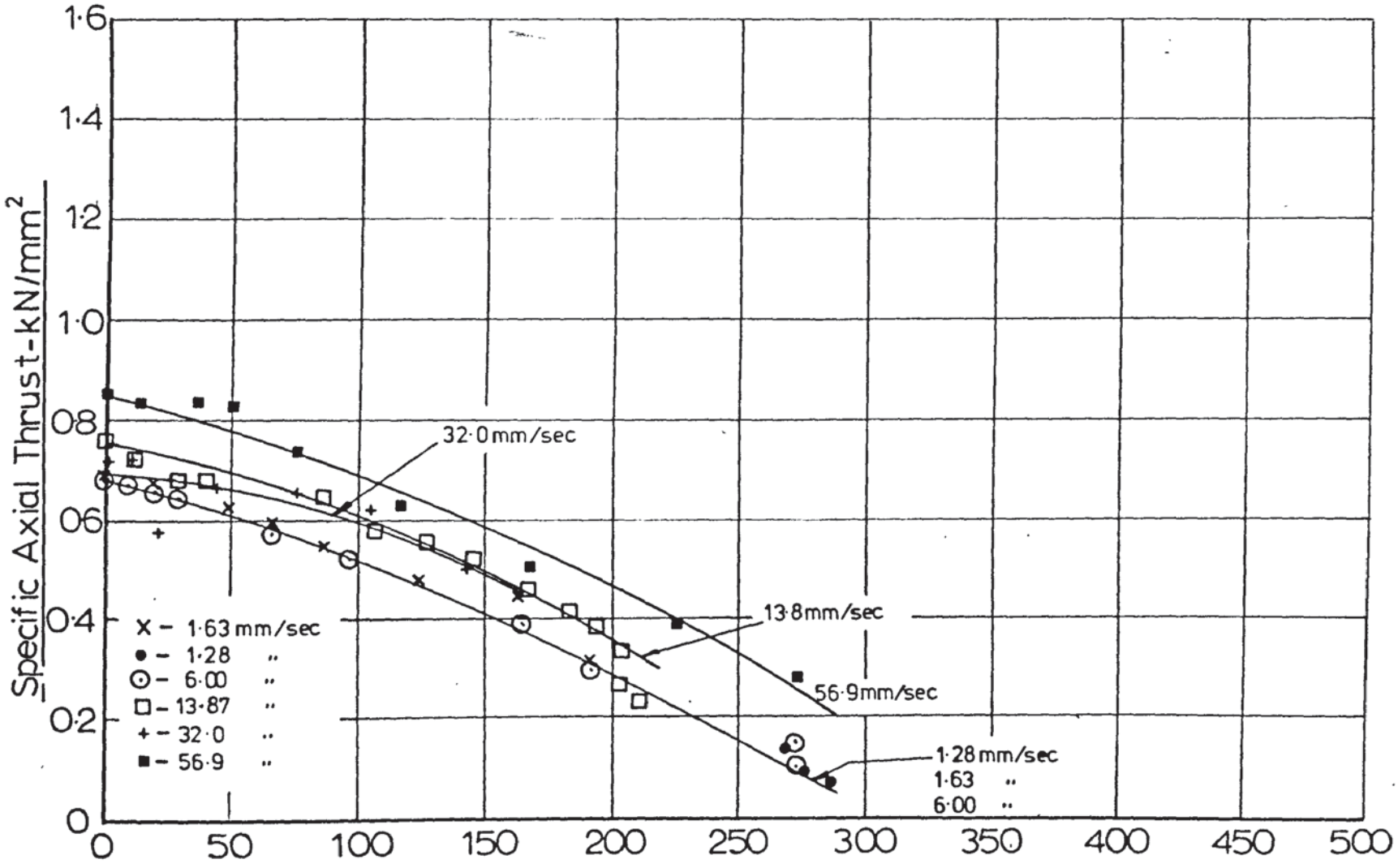

Test No. -026

Fig(7·48)-Specific Axial Thrust vs. Peak Die Velocity(α=7·5°, r=0·387)

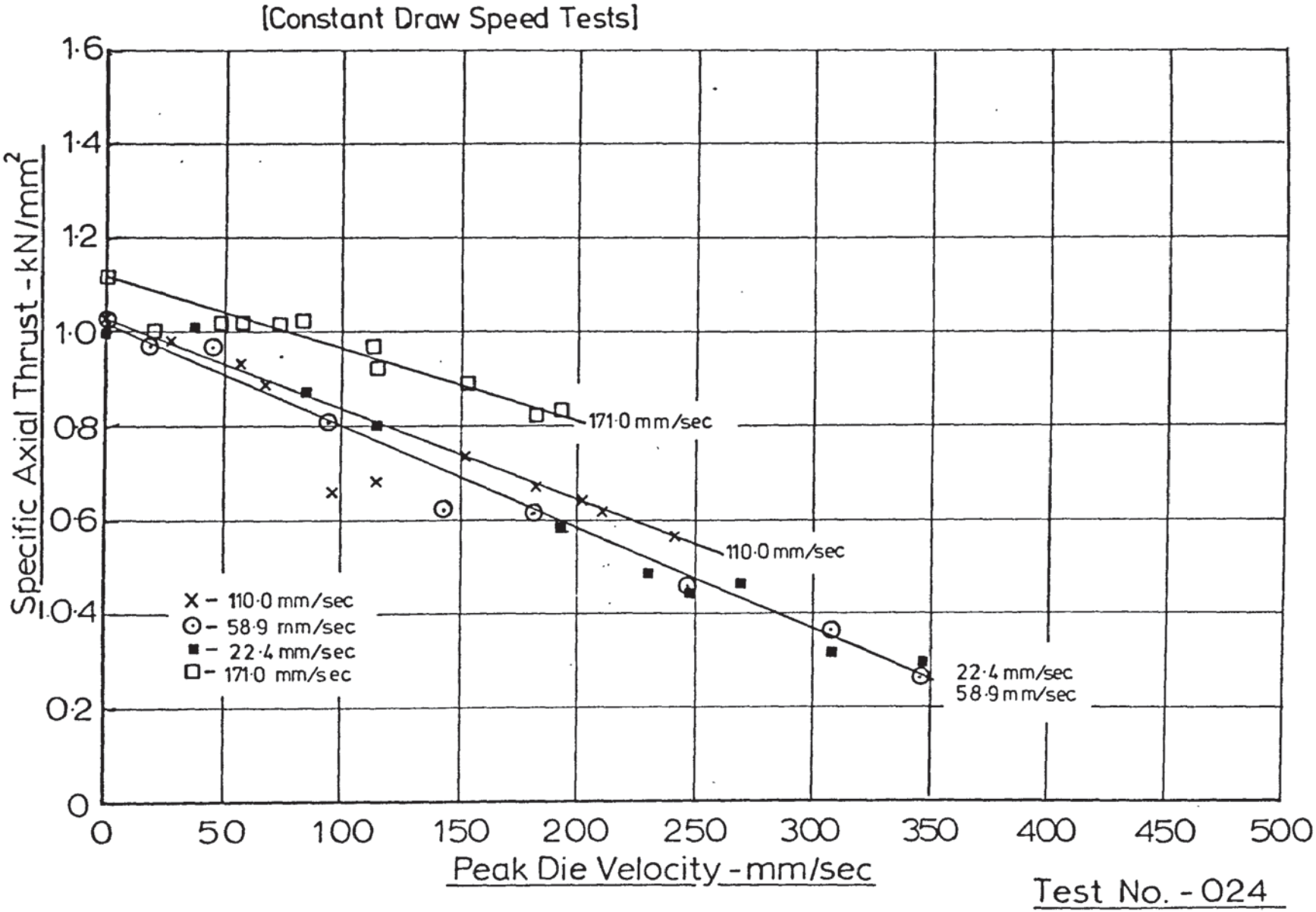

Test No. - 024

Fig(7·49) - Specific Axial Thrust vs. Peak Die Velocity (α=7·5°, r=0·440)

[Constant Draw Speed Tests]

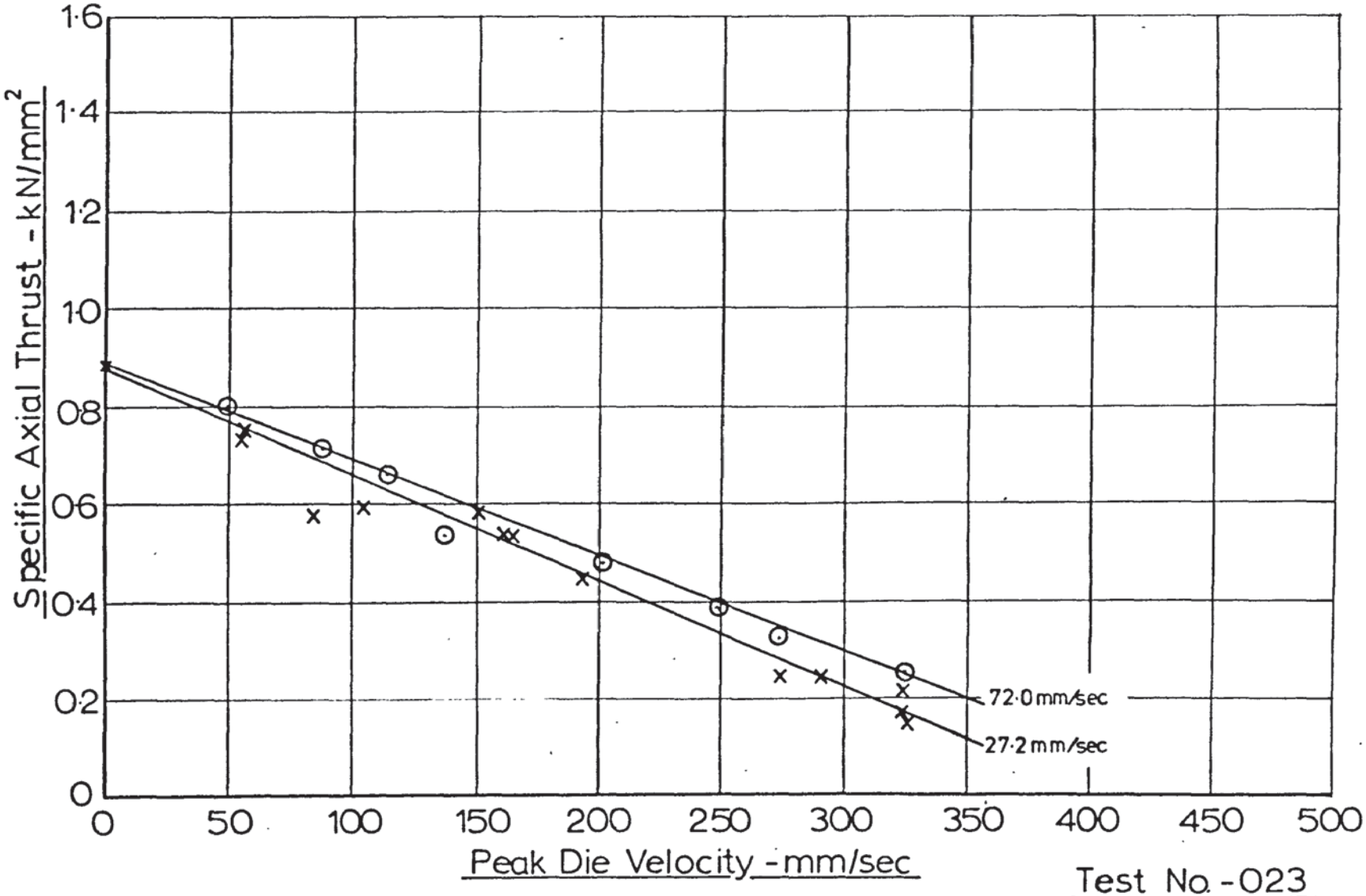

Test No. - 023

Fig(7·50)-Specific Axial Thrust vs. Peak Die Velocity(α= 7·5°)

[Constant Power Input, Arbitrary Draw Speed]

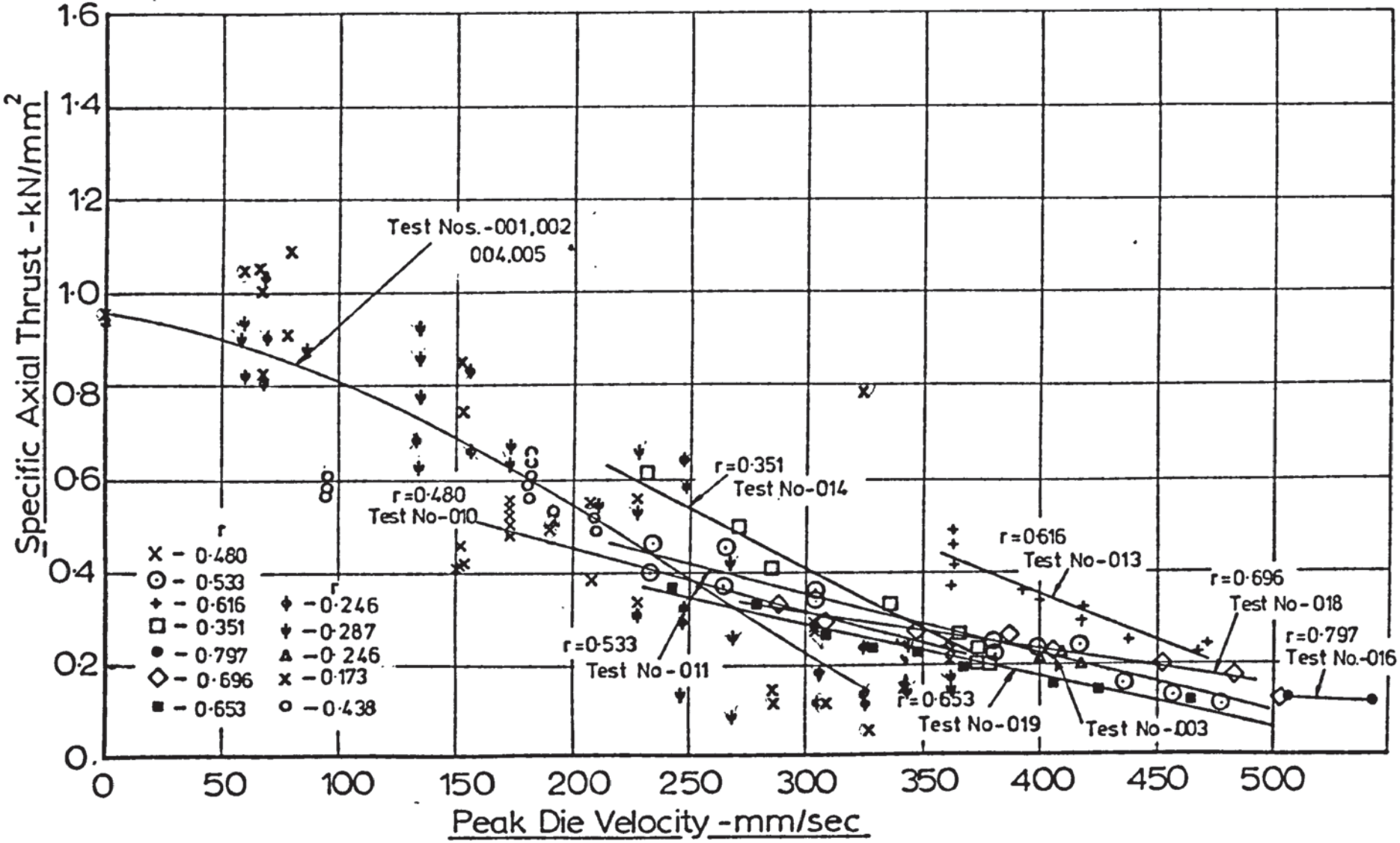

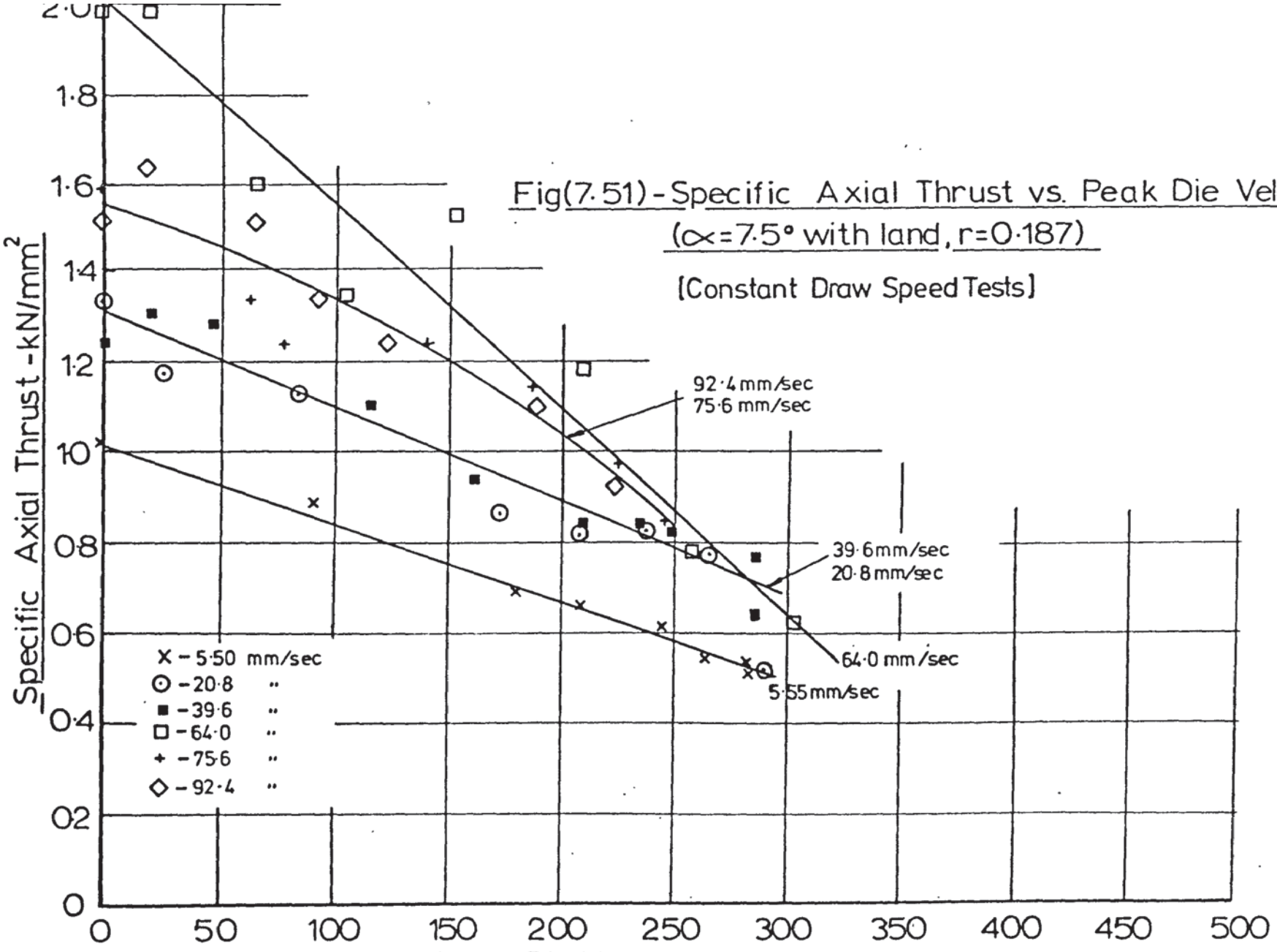

Fig(7·51) - Specific Axial Thrust vs. Peak Die Velocity
(α = 7·5° with land, r = 0·187)

[Constant Draw Speed Tests]

Test No. - 066

Fig(7·52)- Specific Axial Thrust vs. Peak Die Velocity(α=7·5° with land, r=0·270)

[Constant Draw Speed Tests]

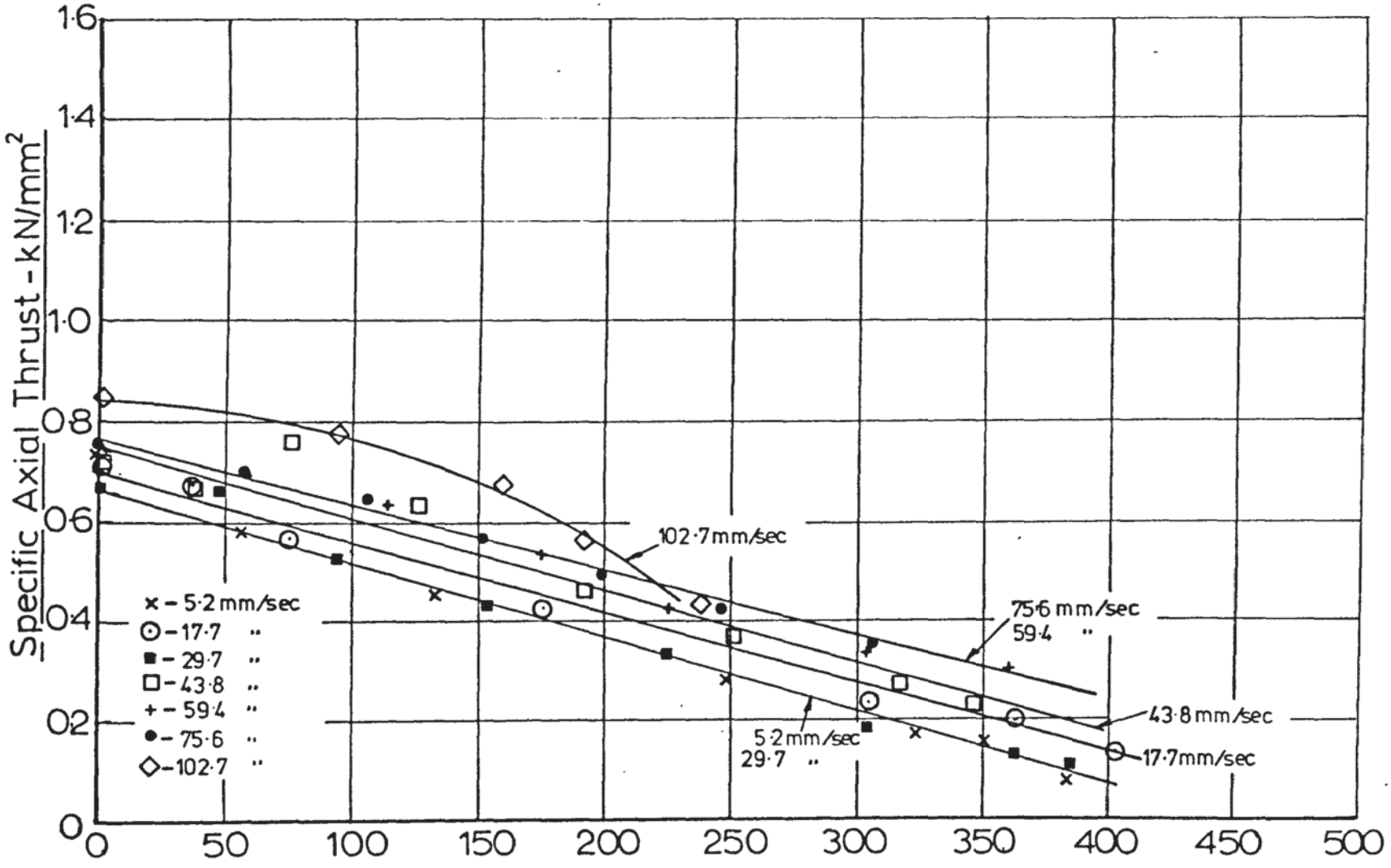

Test No. -069

Fig(7·53) - Specific Axial Thrust vs. Peak Die Velocity(α=7·5°with land, r =0·373)

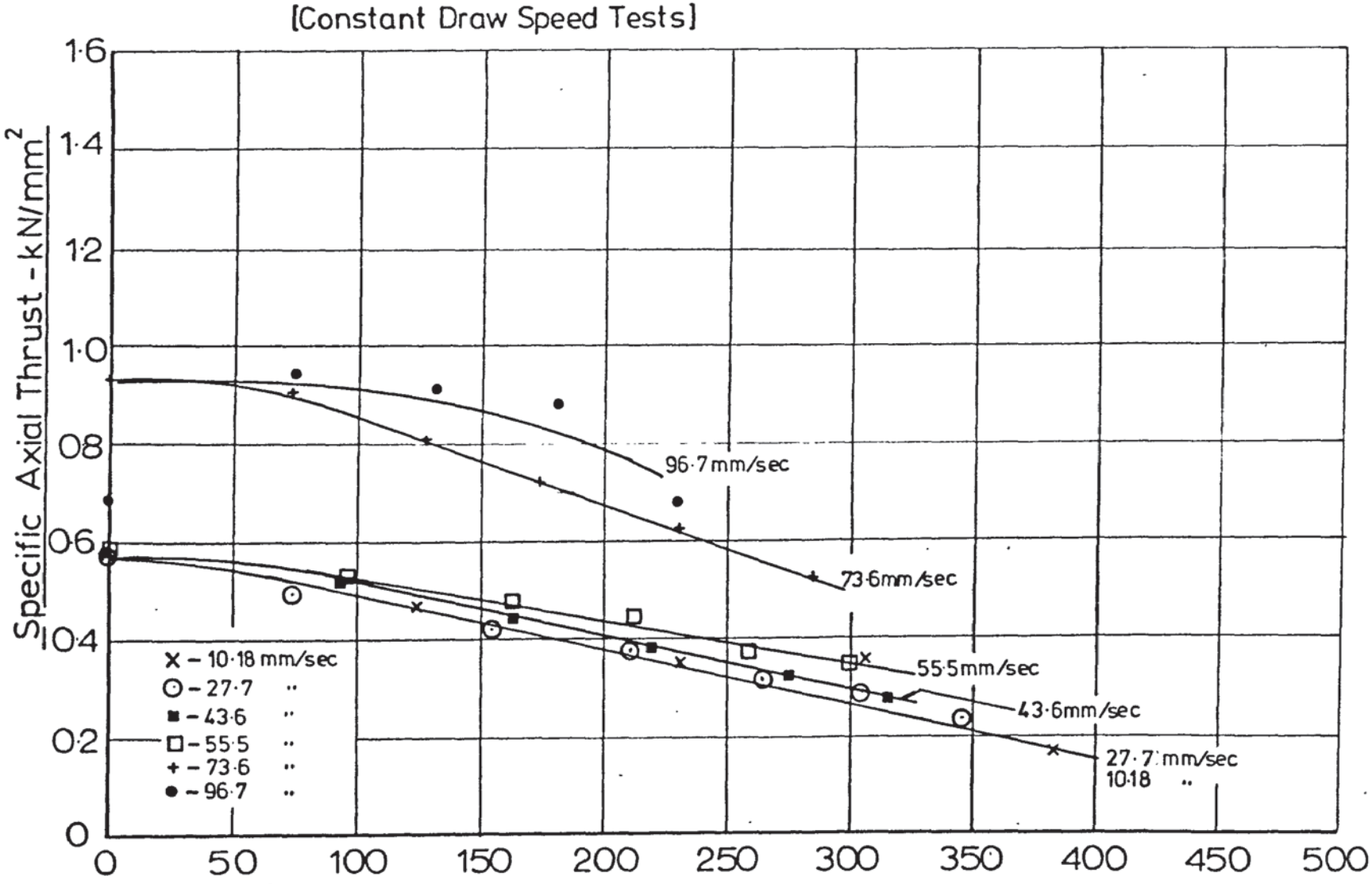

Fig(7.54) - Specific Axial Thrust vs. Peak Die Velocity (α=7.5° with land, r=0.438)

[Constant Draw Speed Tests]

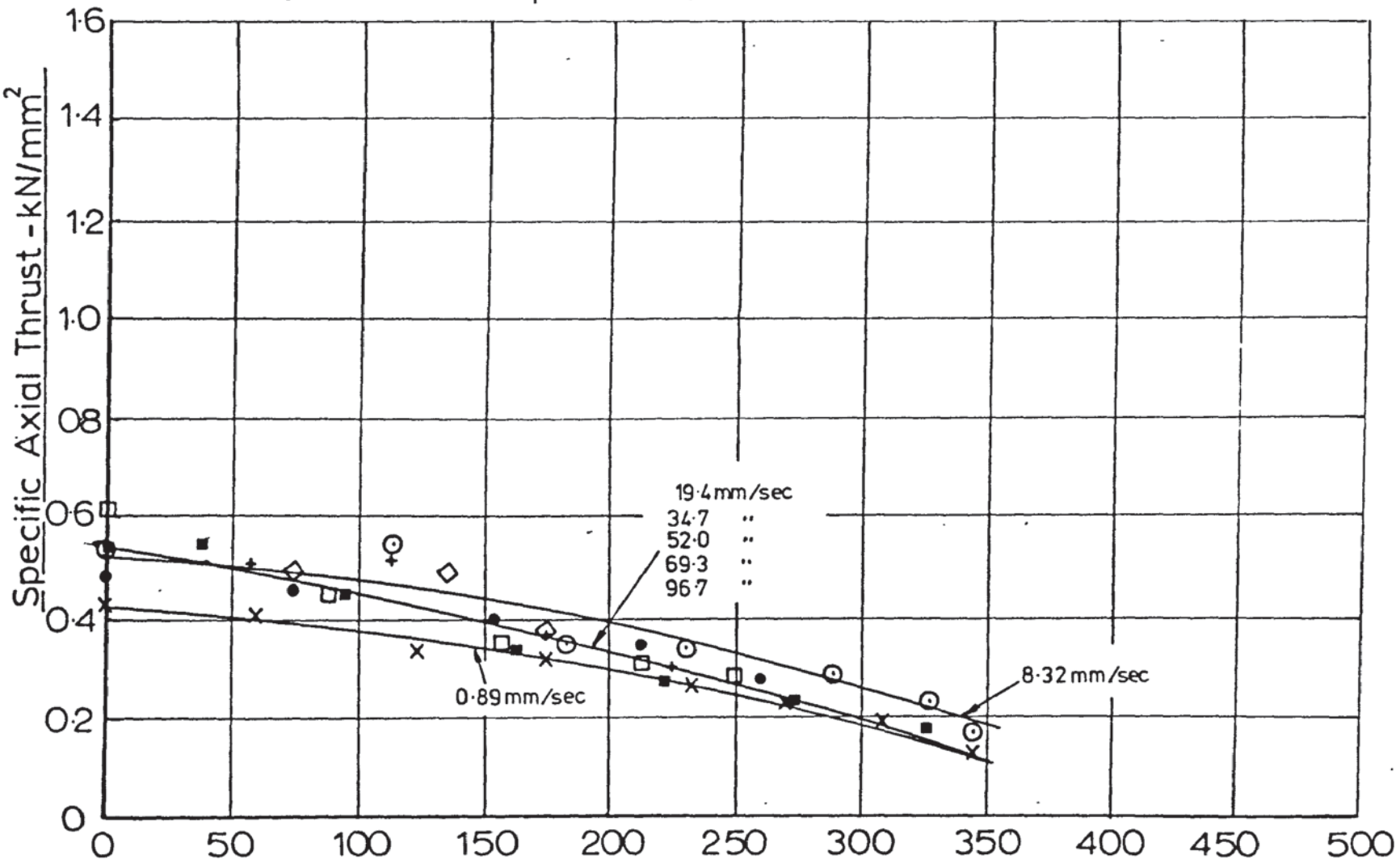

Test No. -070

Fig(7·55) - Specific Axial Thrust vs. Peak Die Velocity (α = 7·5° with land, r = 0·453)

[Constant Draw Speed Tests]

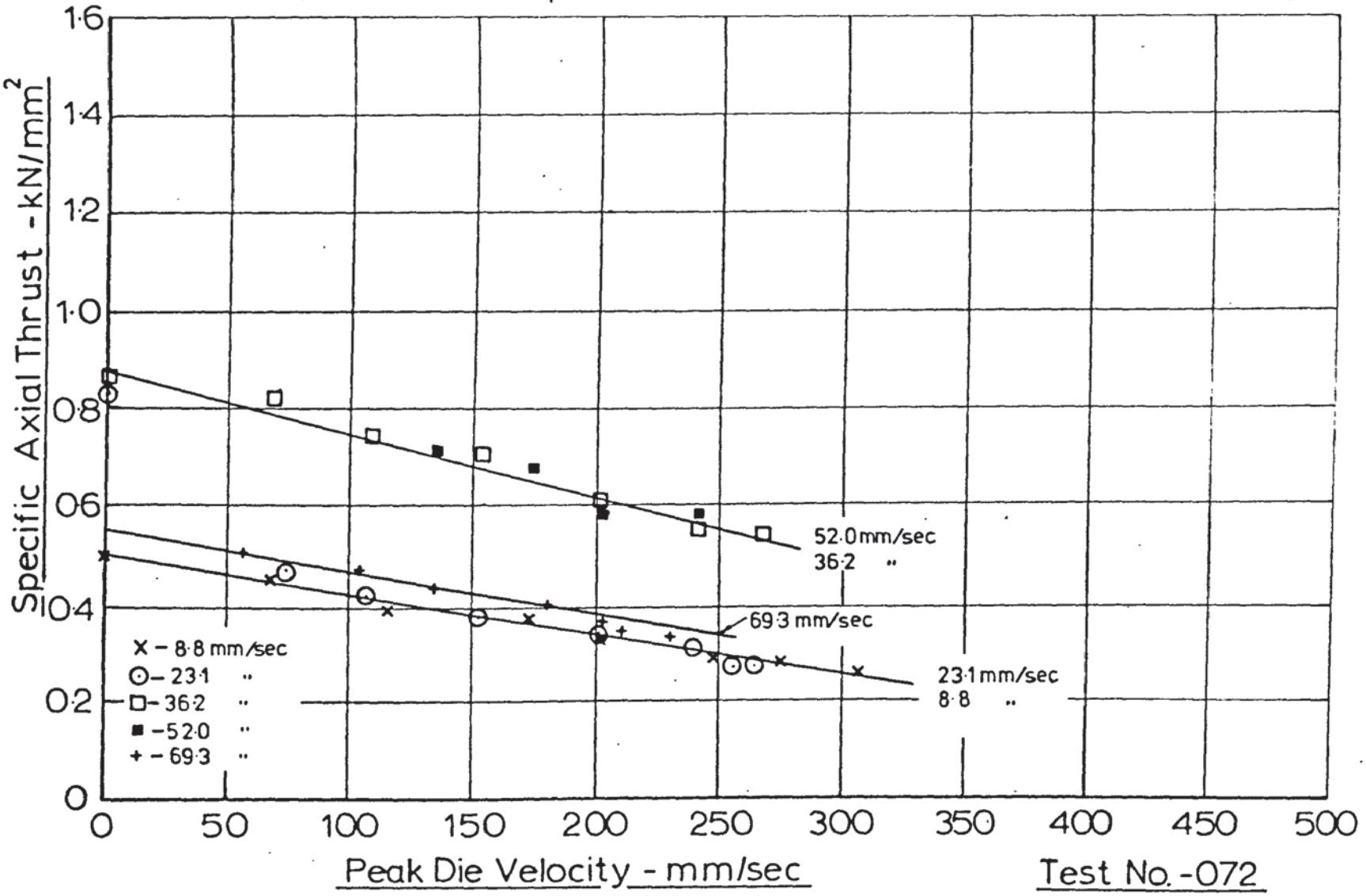

Test No. -072

Fig(7·56) - Specific Axial Thrust vs. Peak Die Velocity(α=7·5°with land, r=0·187)

[Arbitrary Draw Speed, Constant Power Input]

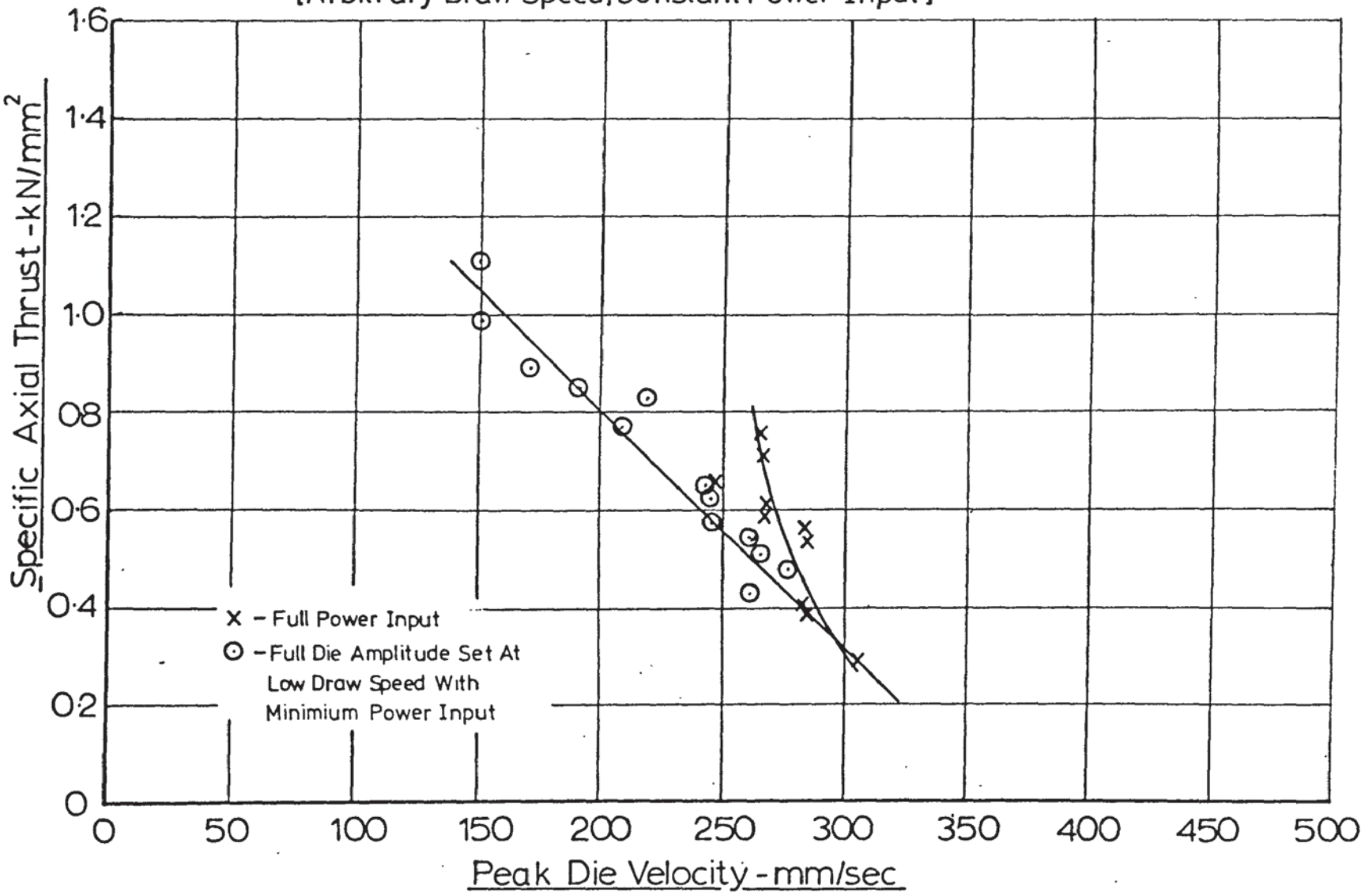

Fig(7·57) - Specific Axial Thrust vs. Peak Die Velocity (α = 7·5°)

[Constant Power Input , Arbitrary Draw Speed]

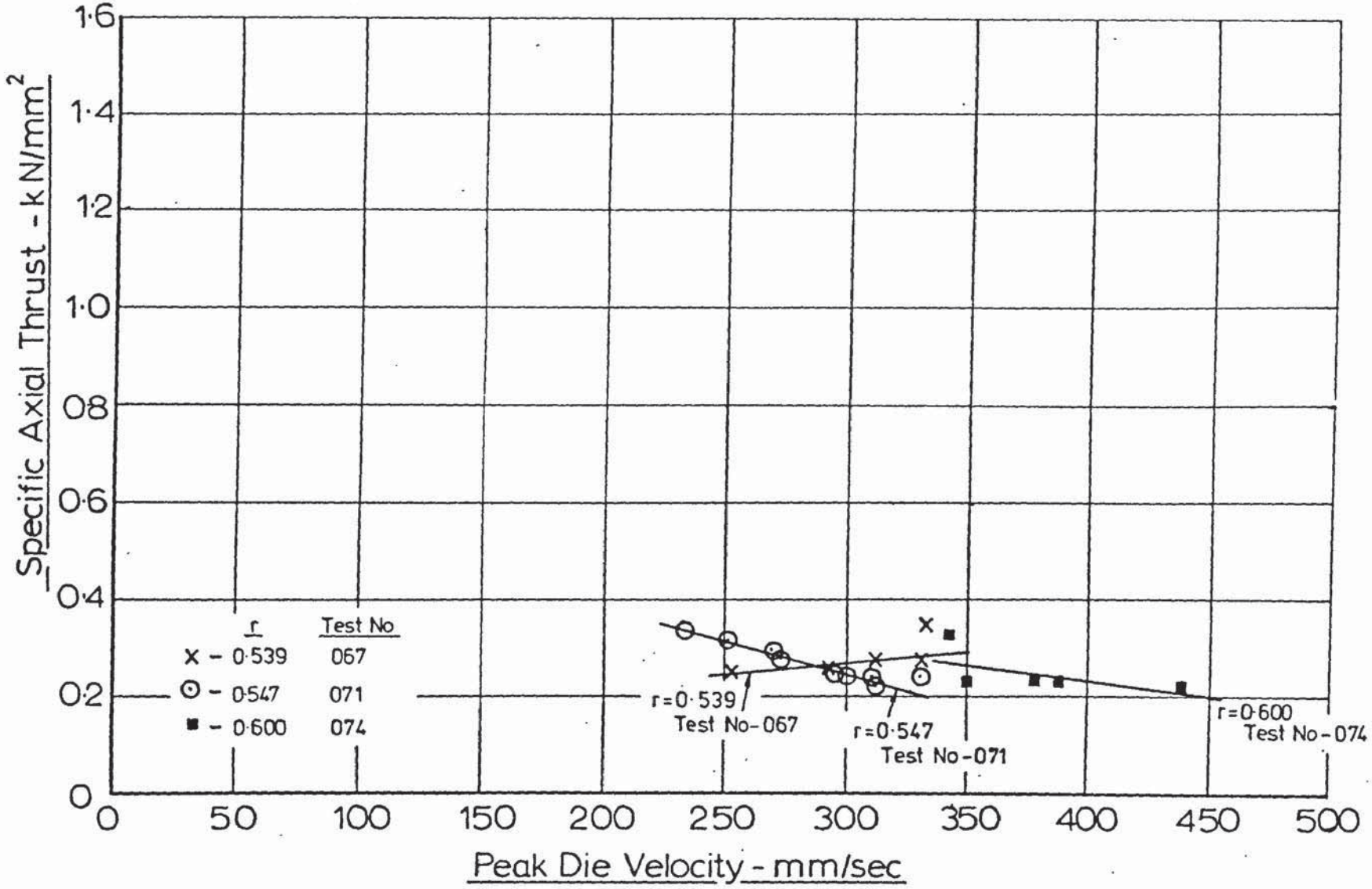

Fig(7·58) - Specific Axial Thrust vs. Peak Die Velocity (α=10°; r=0·260)

[Constant Draw Speed Test]

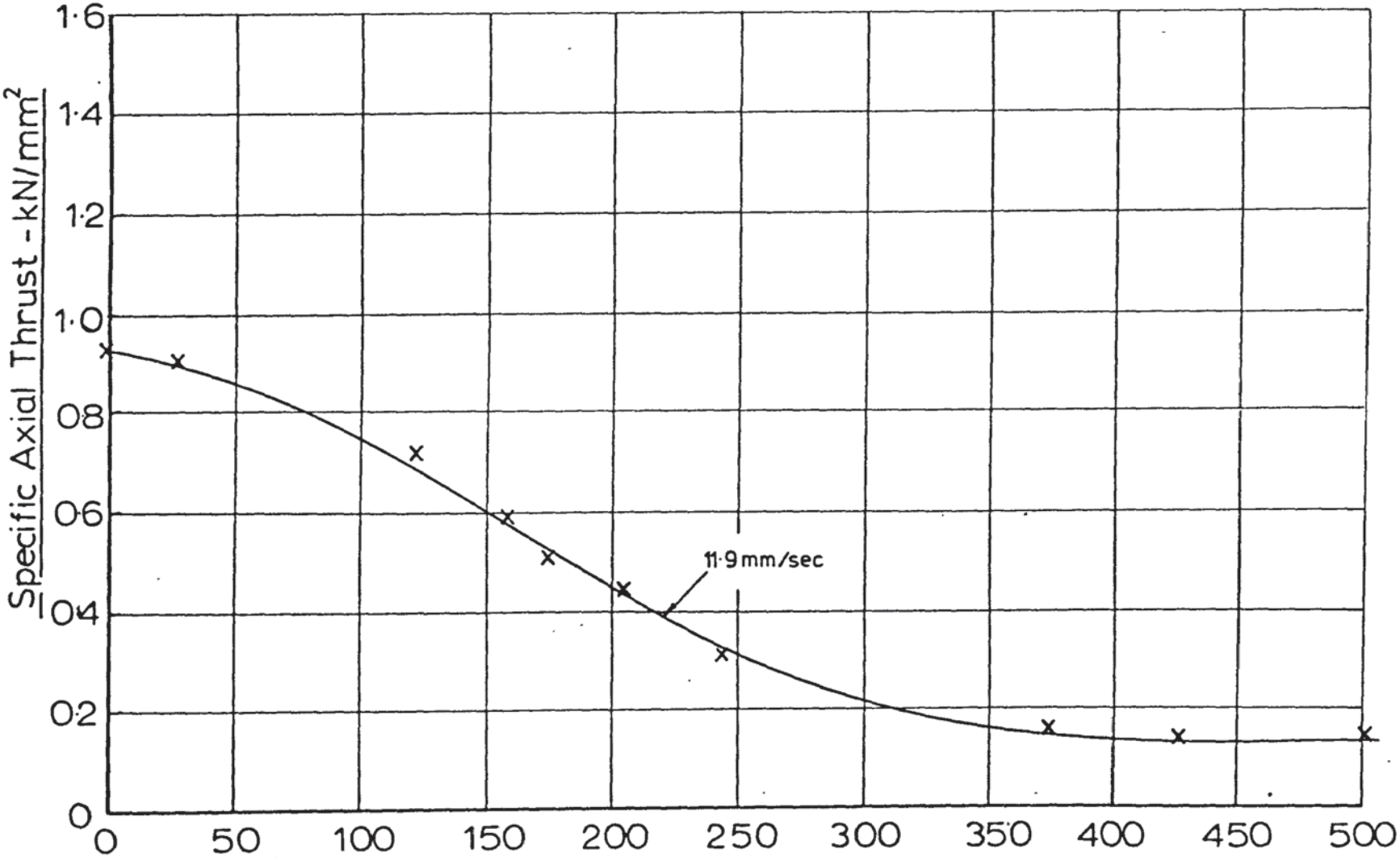

Test No. -053

Fig(7.59) - Specific Axial Thrust vs. Peak Die Velocity (α = 10°, r = 0.263)

[Constant Draw Speed Tests]

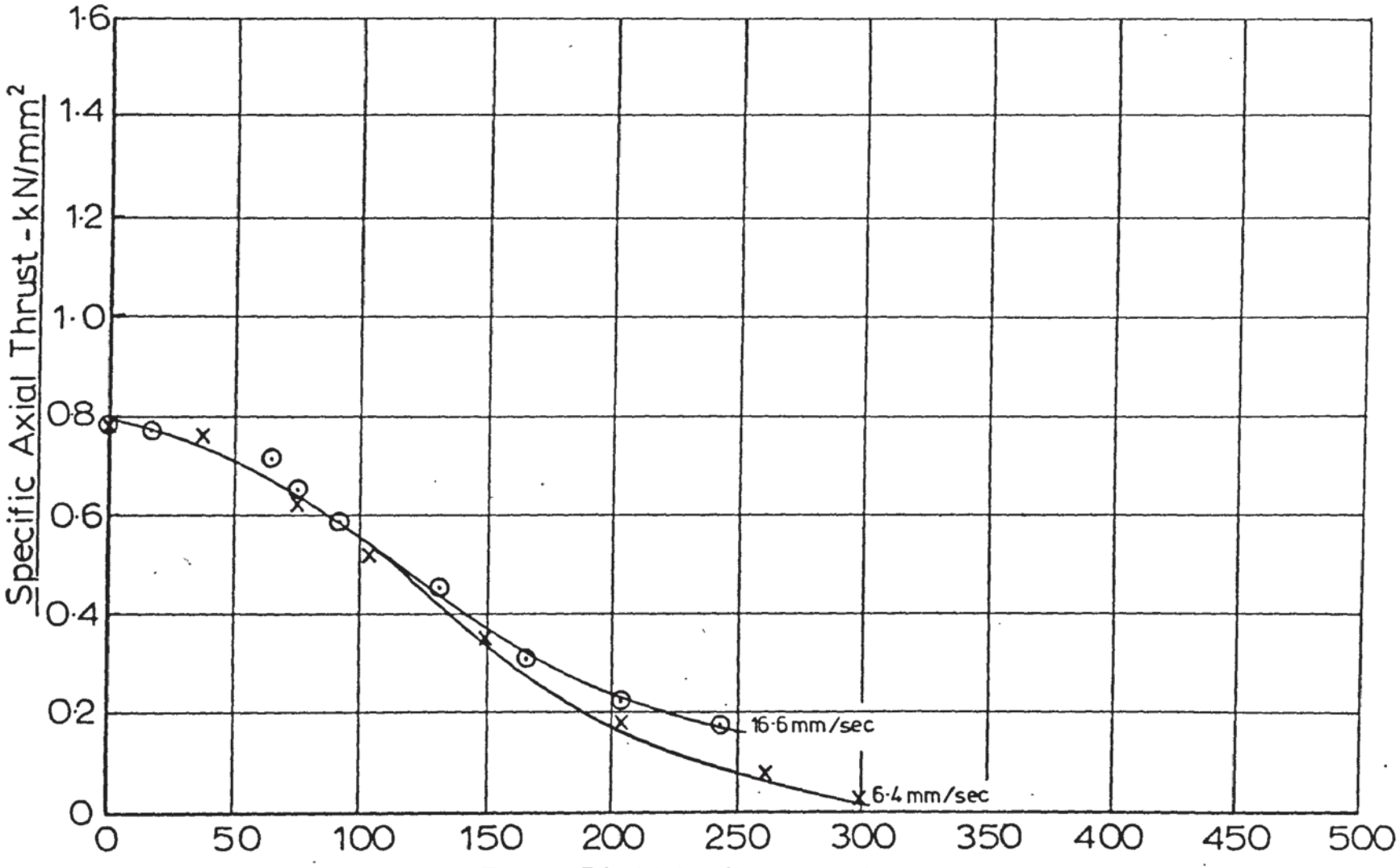

Test No.-042

Fig(7·60) - Specific Axial Thrust vs. Peak Die Velocity (α=10°, r=0·399)

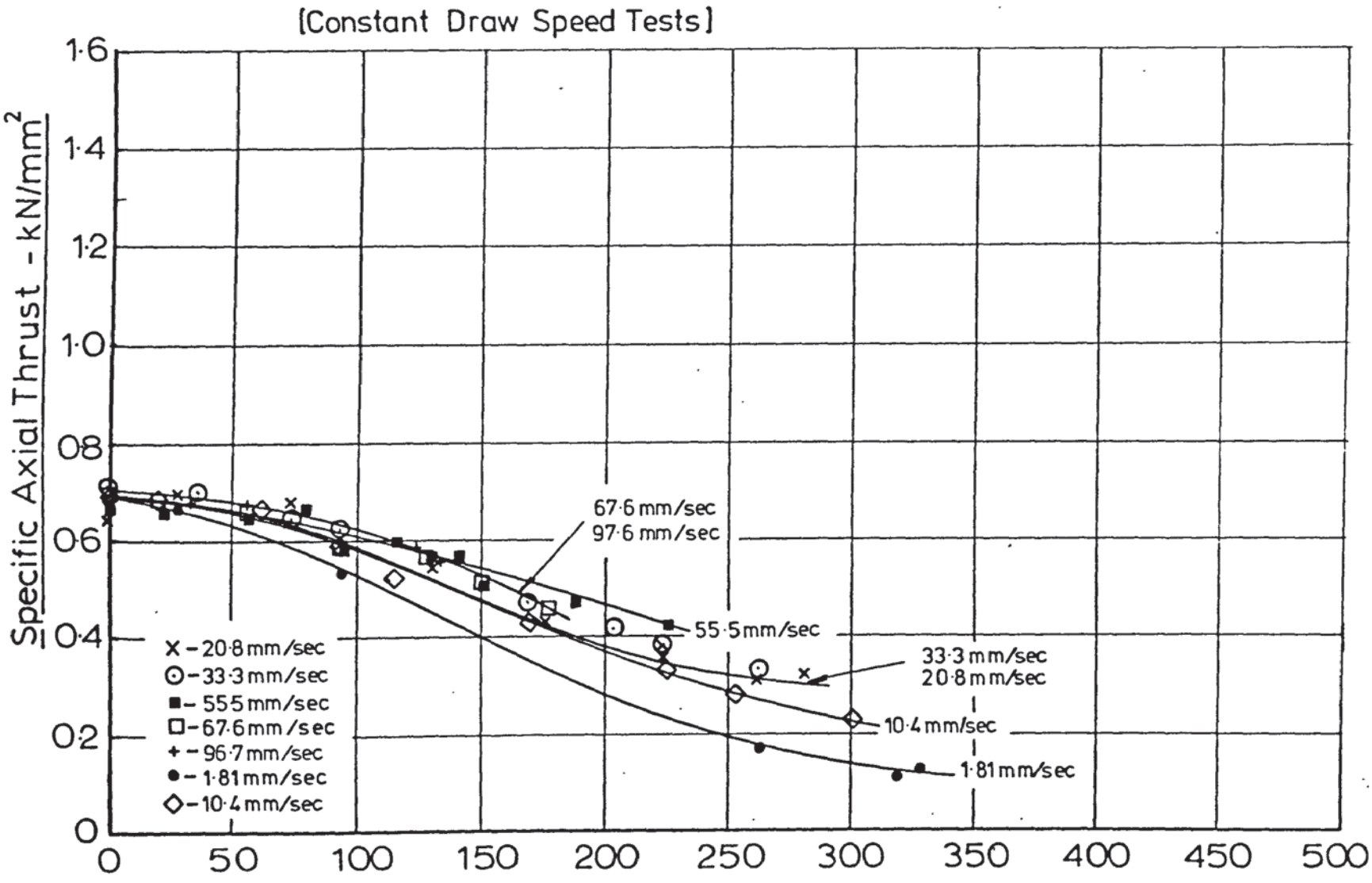

Test No.-043

Fig(7.61)- Specific Axial Thrust vs. Peak Die Velocity (α=10°, r=0.461)

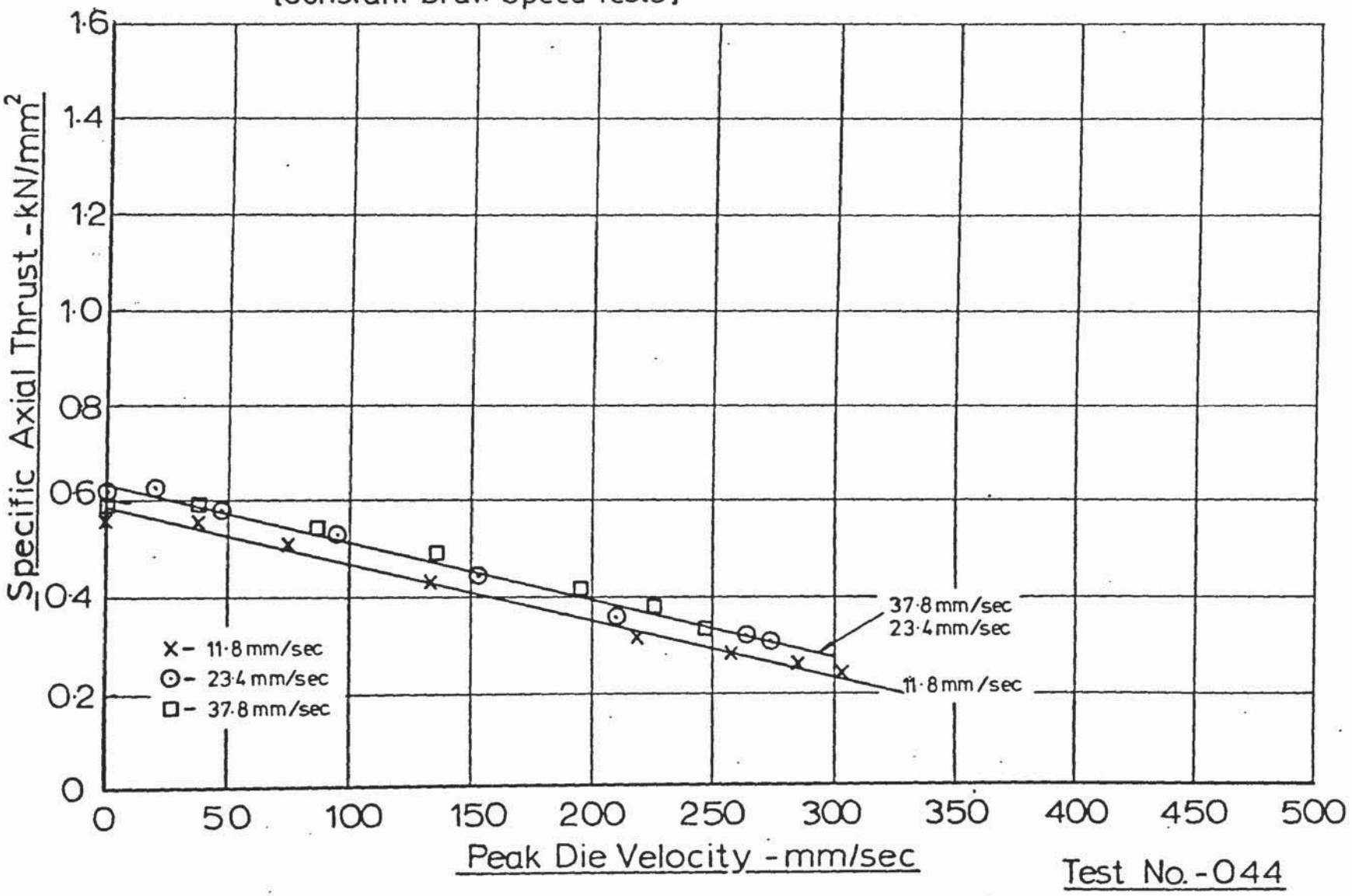

Fig(7·62)-Specific Axial Thrust vs. Peak Die Velocity (α=10°)

[Arbitrary Draw Speed-Full Power Input]

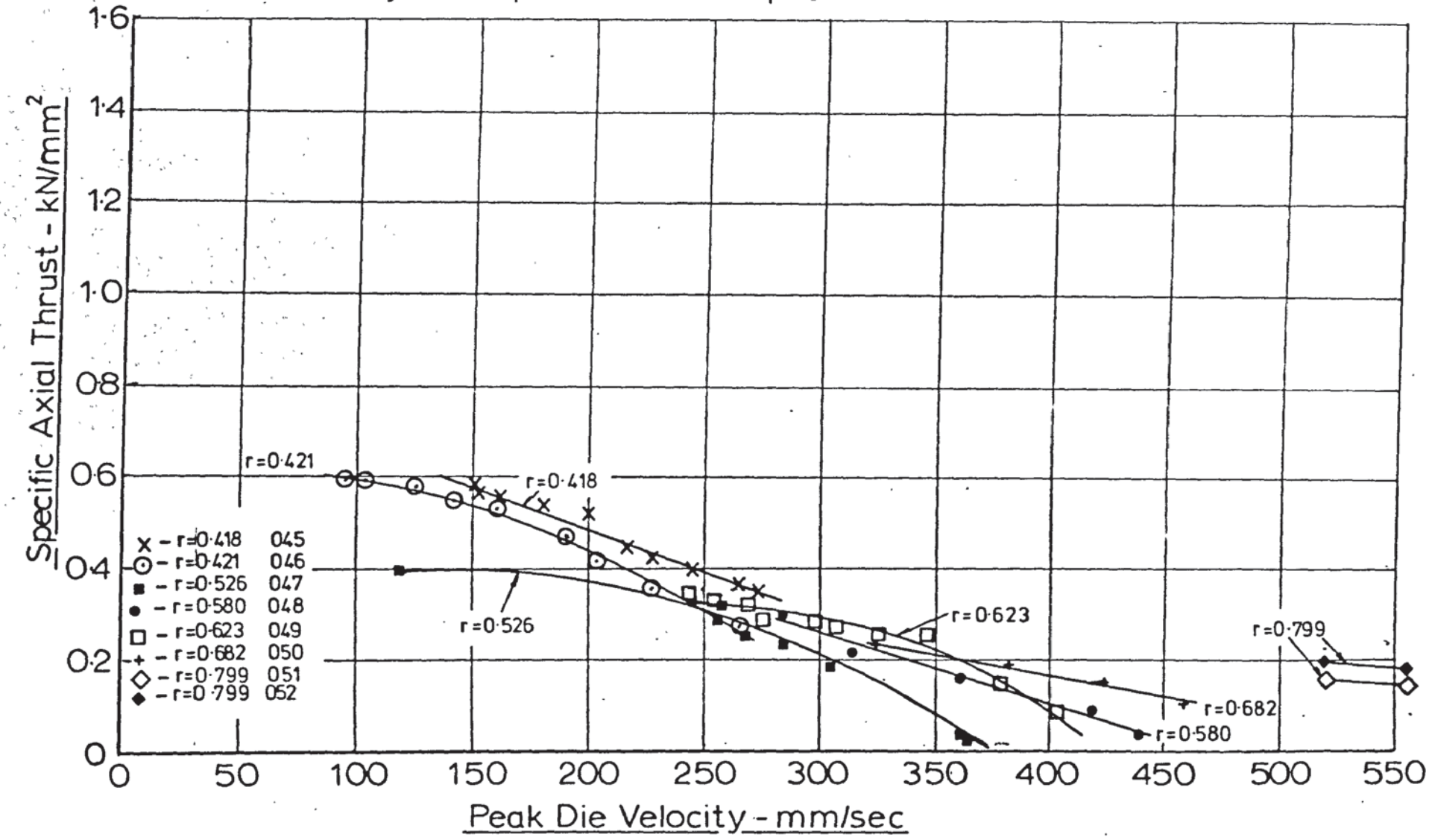

Fig(7·63)- Lateral Die Pressure vs. Peak Die Velocity (α = 2·5°, r = 0·133)

[Constant Draw Speed Tests]

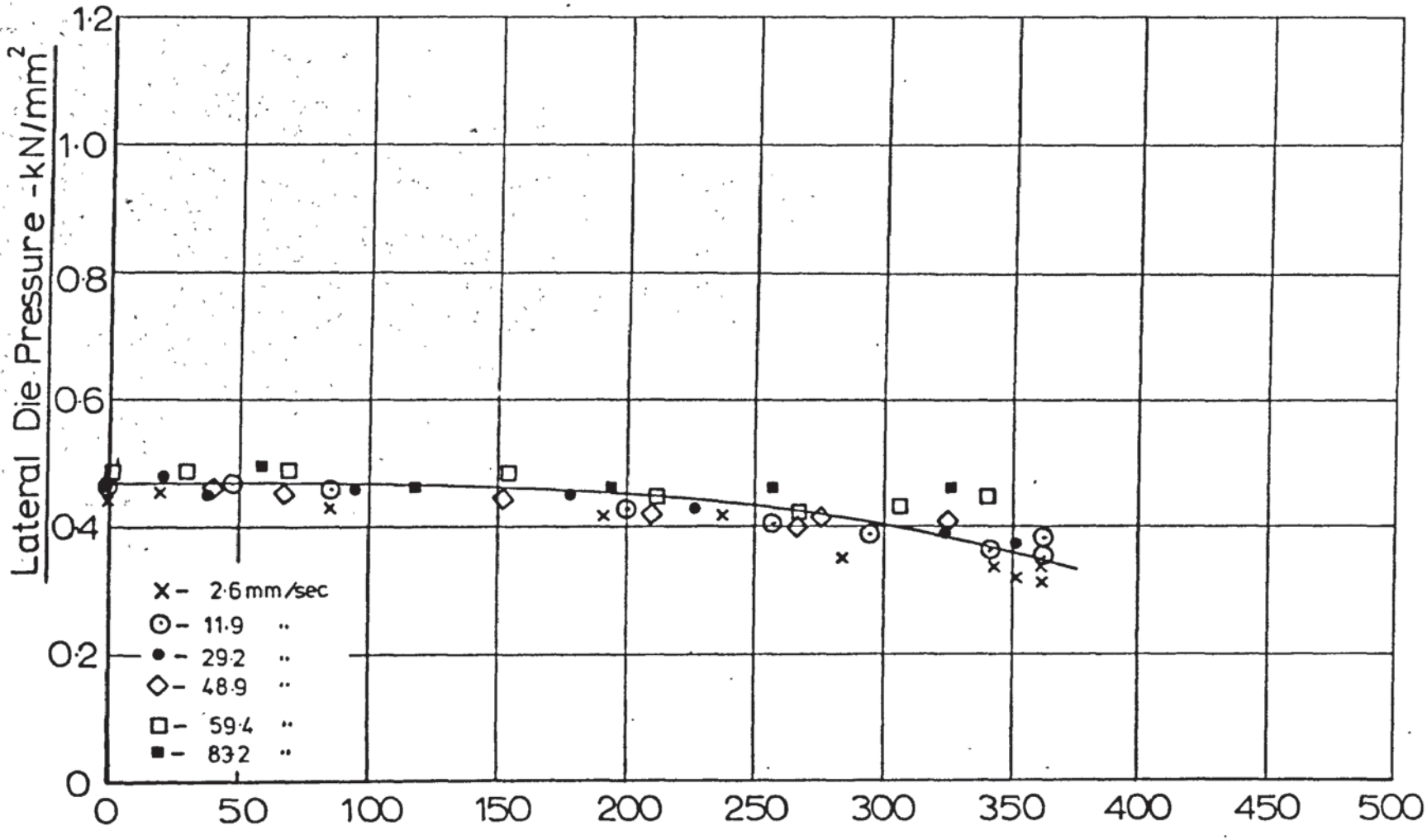

Test No. -039

Fig(7·64) - Lateral Die Pressure vs. Peak Die Velocity (α=2·5°; r=0·250)

[Constant Draw Speed Tests]

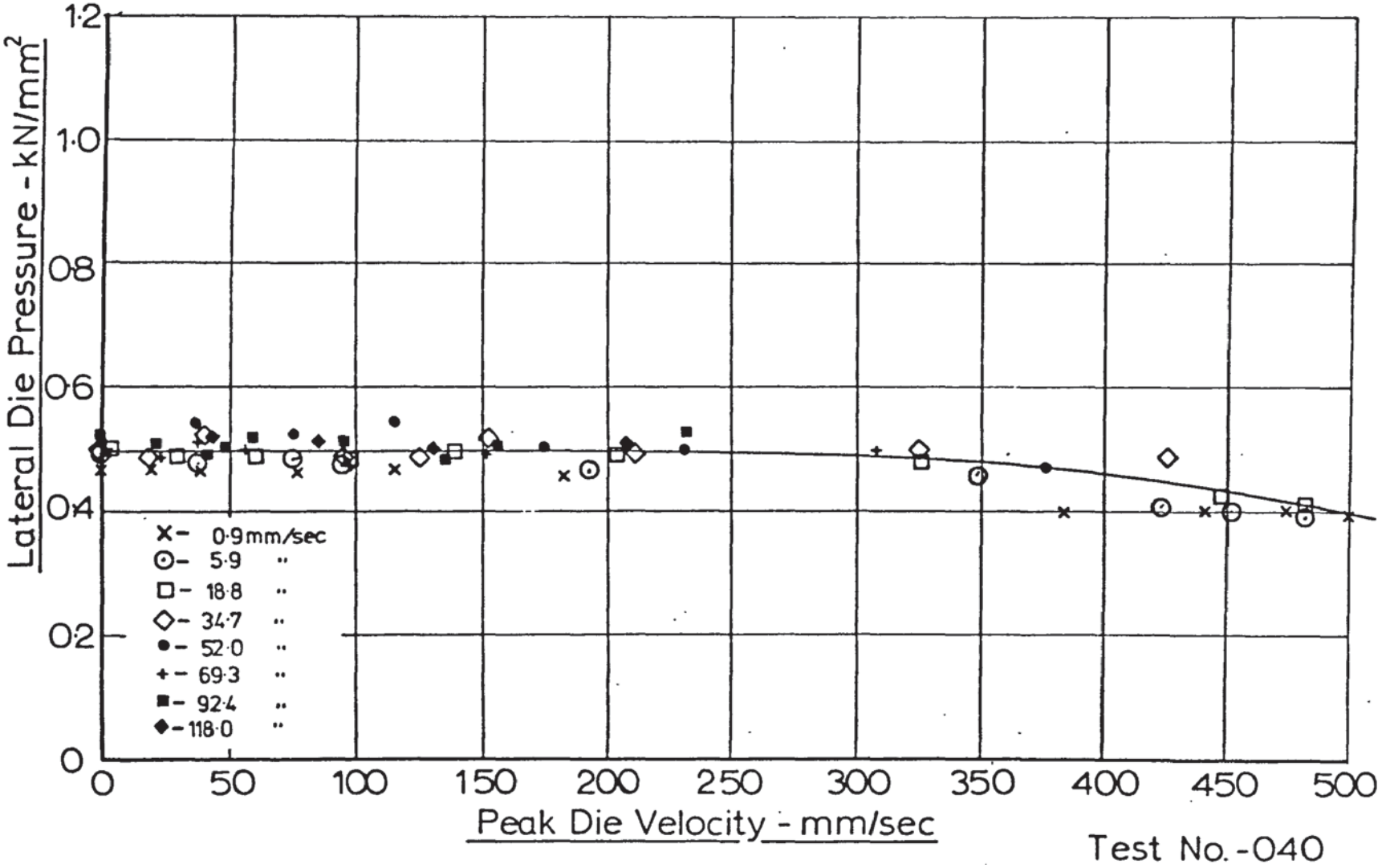

Test No. - 040

Fig(7·65)- Lateral Die Pressure vs. Peak Die Velocity(α=2·5°, r=0·267)

[Constant Draw Speed Tests]

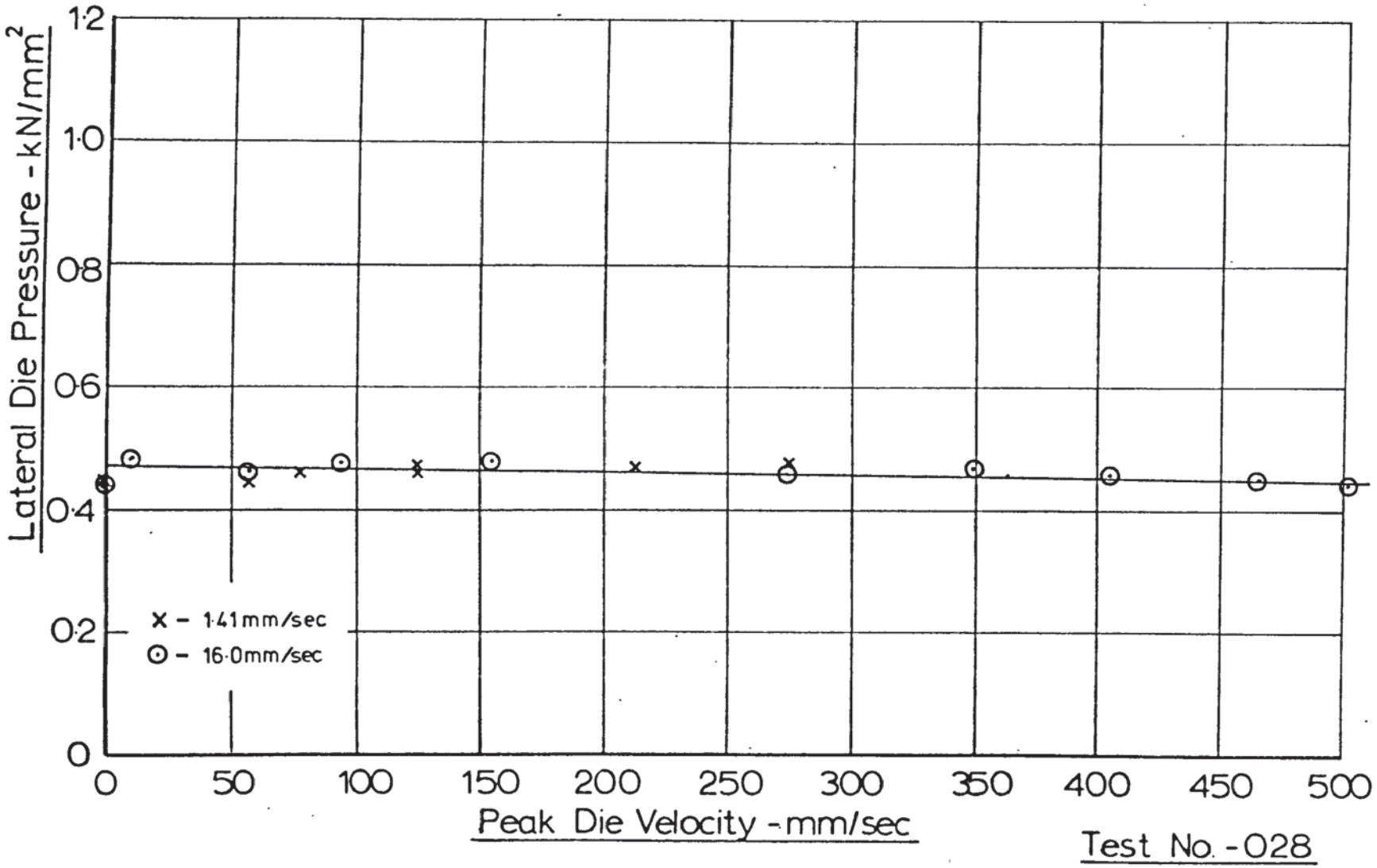

Test No. - 028

Fig(7·66) - Lateral Die Pressure vs. Peak Die Velocity(α= 2·5°; r=0·280)

[Draw Speed = 37·0 mm/sec]

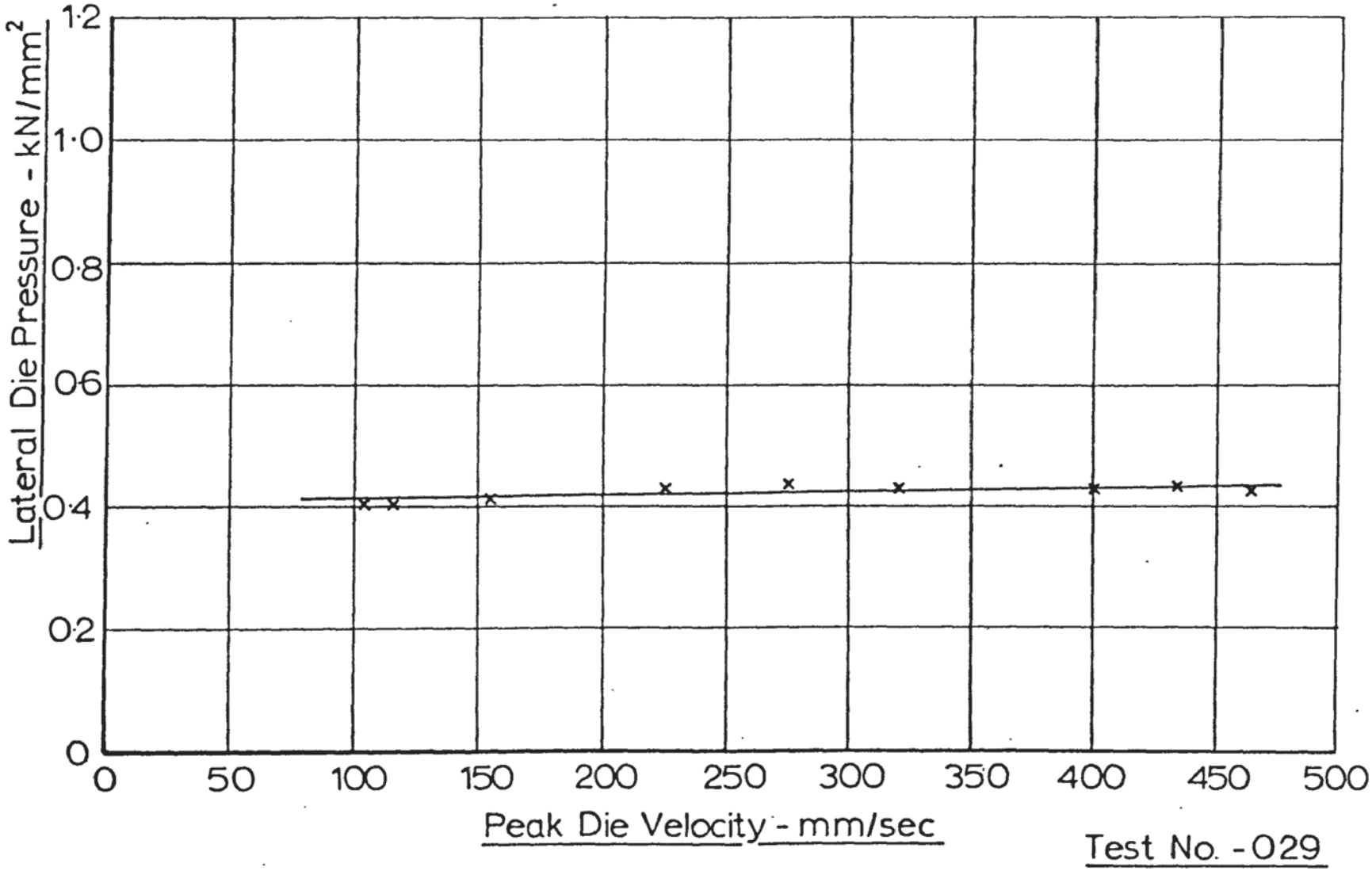

Test No. - 029

Fig(7·67) - Lateral Die Pressure vs. Peak Die Velocity($\alpha = 2·5°$, r=0·280)

[Arbitrary Draw Speed And Power Input]

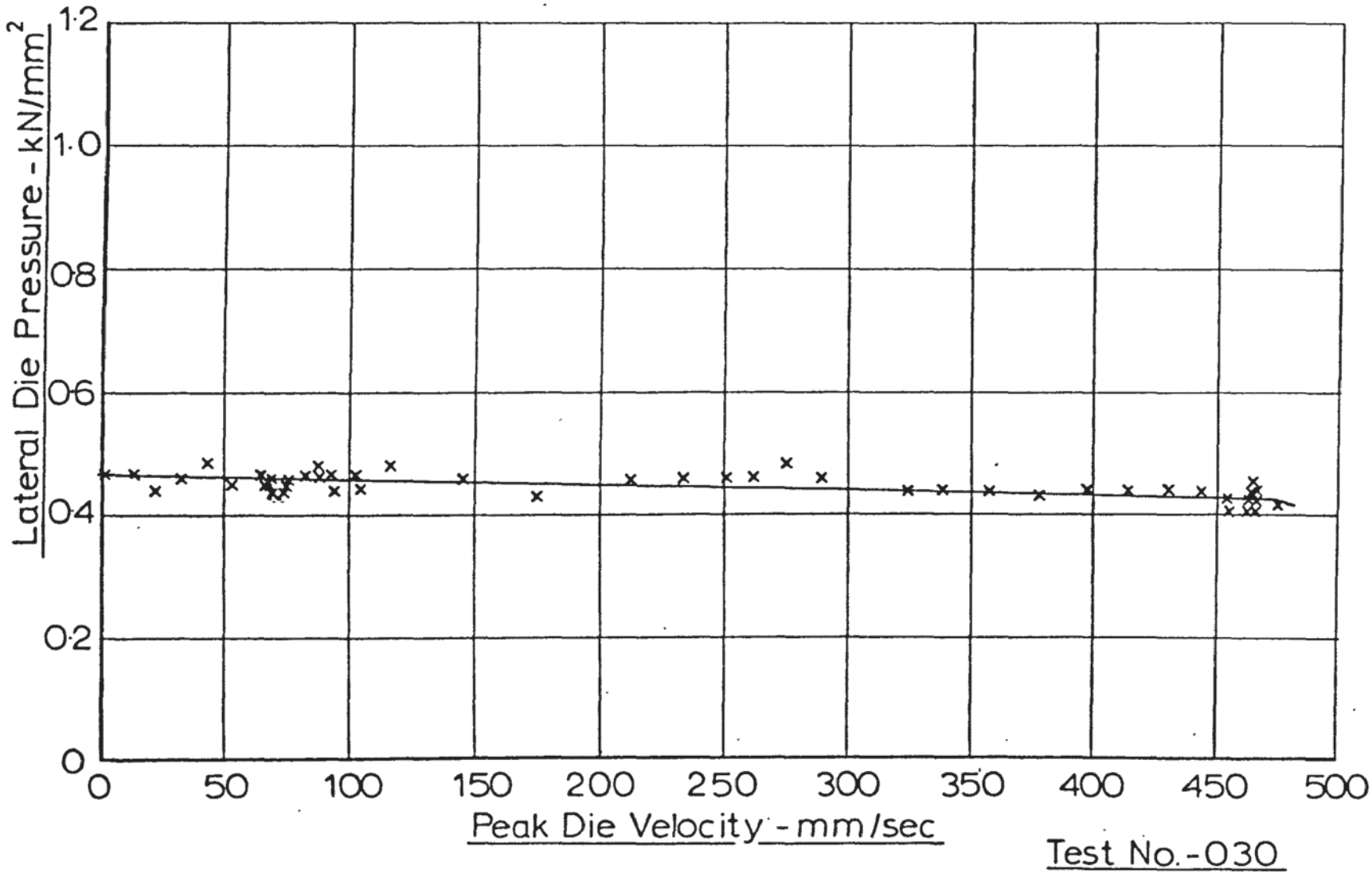

Fig(7·68)-Lateral Die Pressure vs. Peak Die Velocity(α=2·5°)

[Full Power Input, Arbitrary Draw Speed]

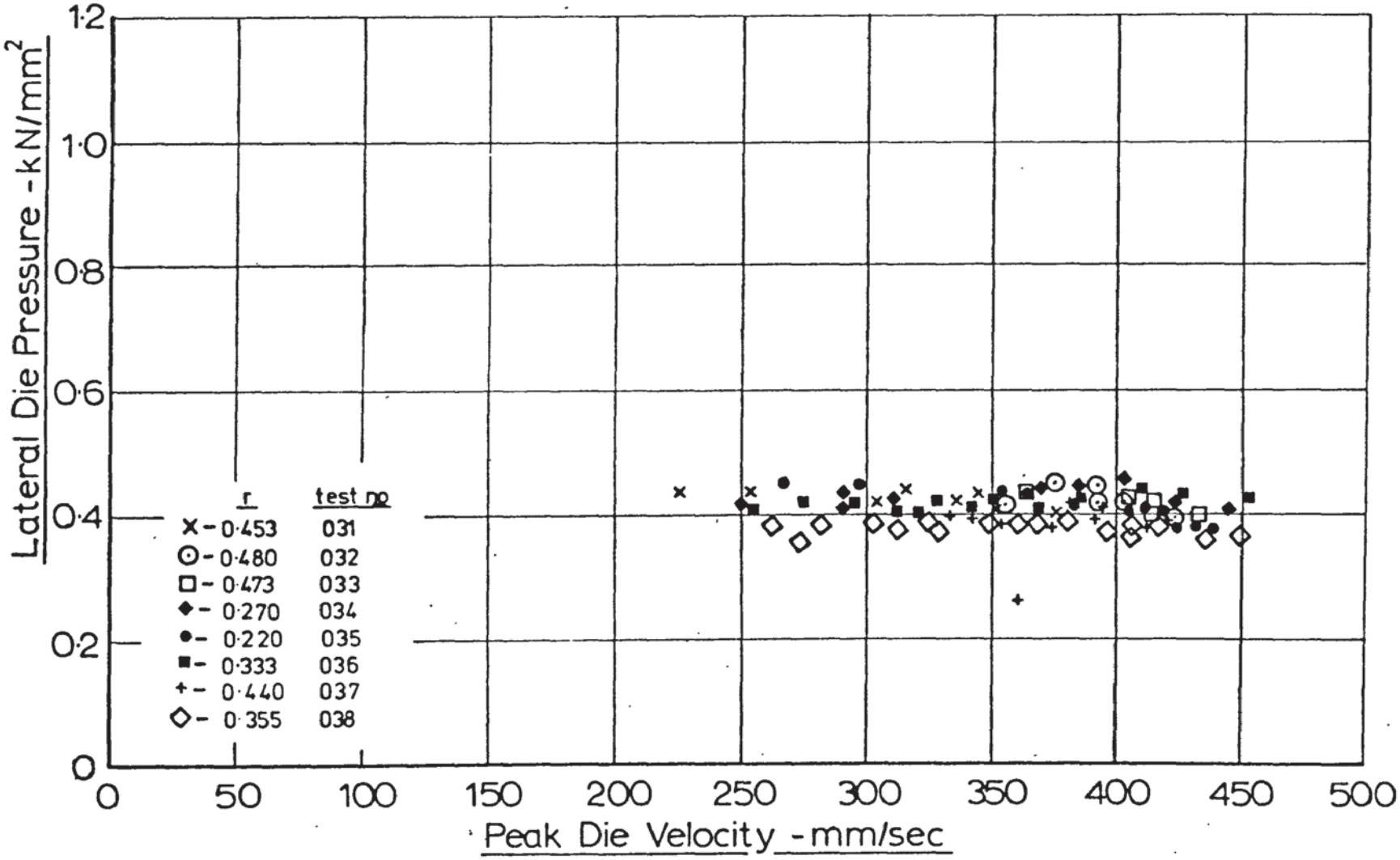

Fig(7·69)- Lateral Die Pressure vs. Peak Die Velocity(α=5°, r=0·205)

[Constant Draw Speed Tests]

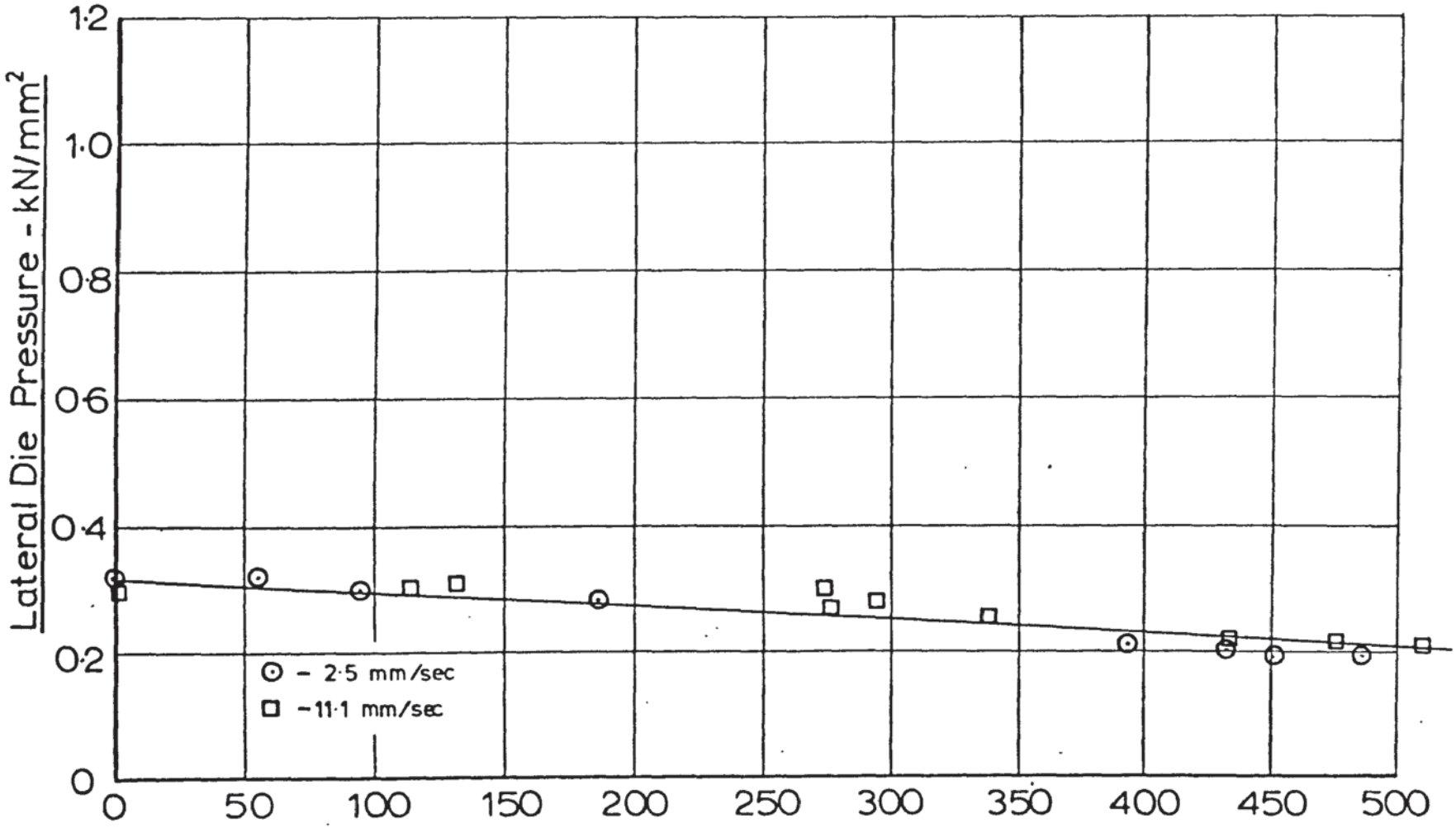

Test No.-055

Fig(7·70) - Lateral Die Pressure vs. Peak Die Velocity ($\alpha = 5°$, $r = 0.345$)

[Constant Draw Speed Tests]

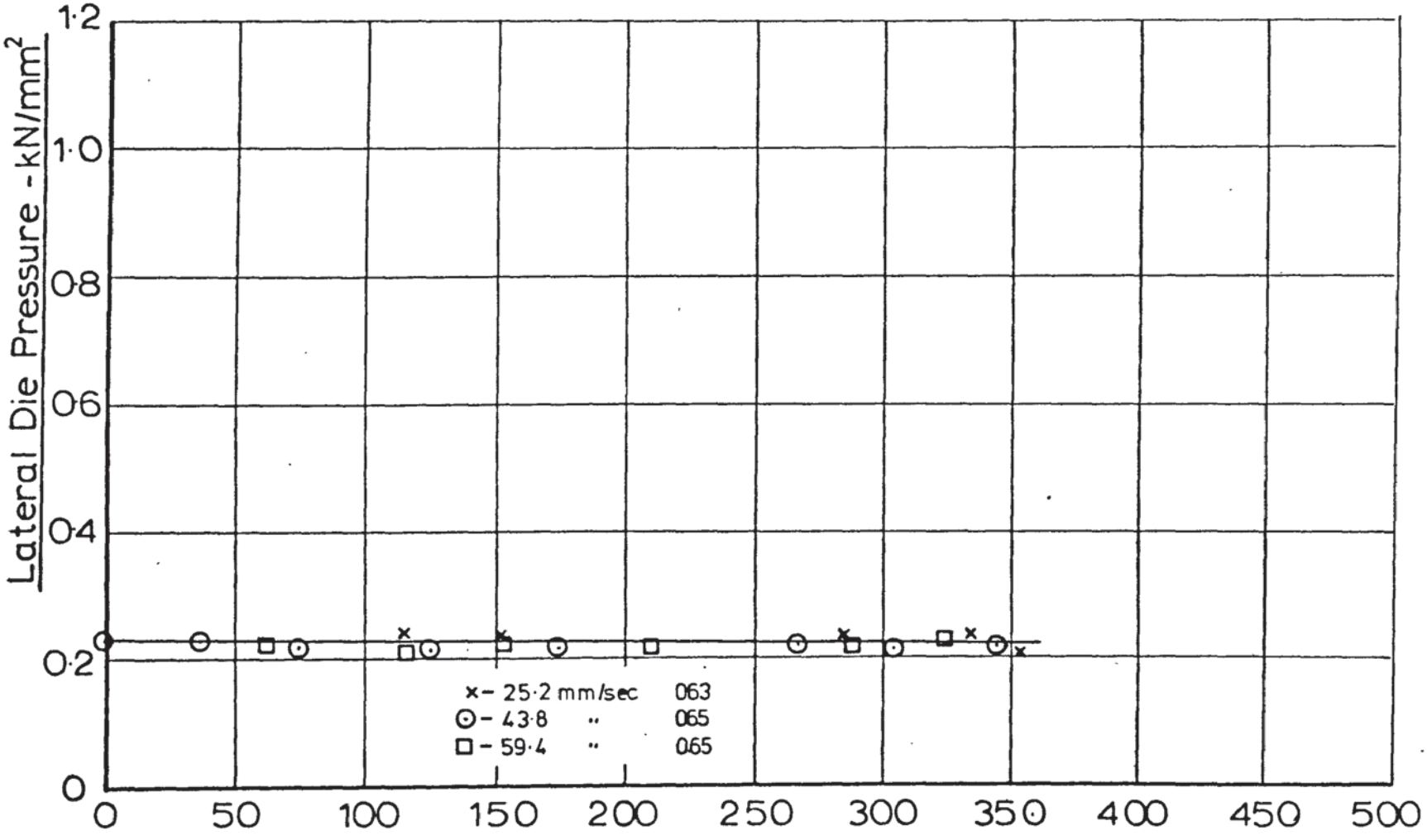

Test Nos. - 063 & 065

Fig(7·71) - Lateral Die Pressure vs. Peak Die Velocity ($\alpha = 5°$, $r = 0.364$)

[Constant Draw Speed Tests]

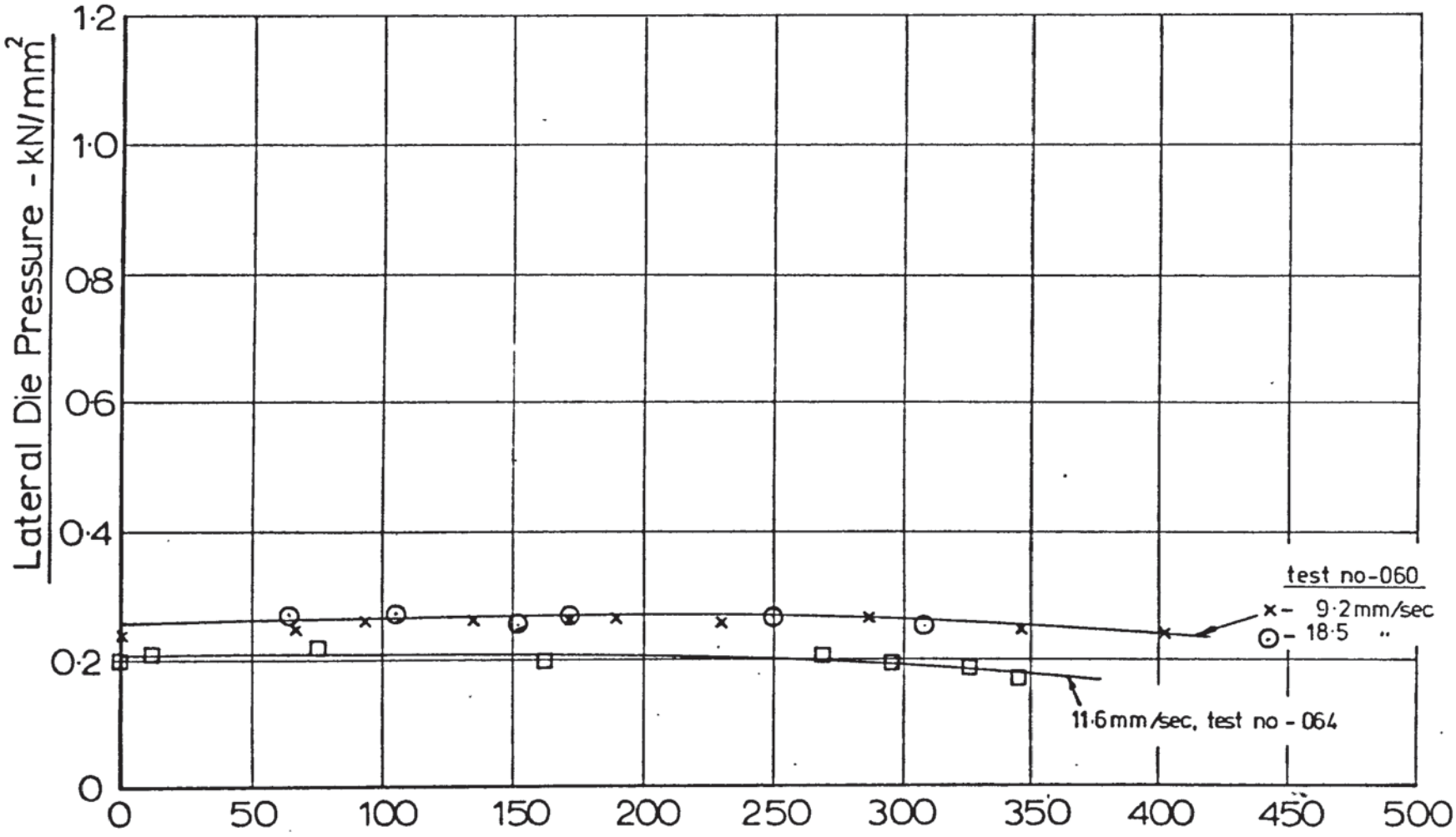

Test Nos. - 060 & 064

Fig(7·72)- Lateral Die Pressure vs. Peak Die Velocity(α=5°, r=0·413)

[Constant Draw Speed Tests]

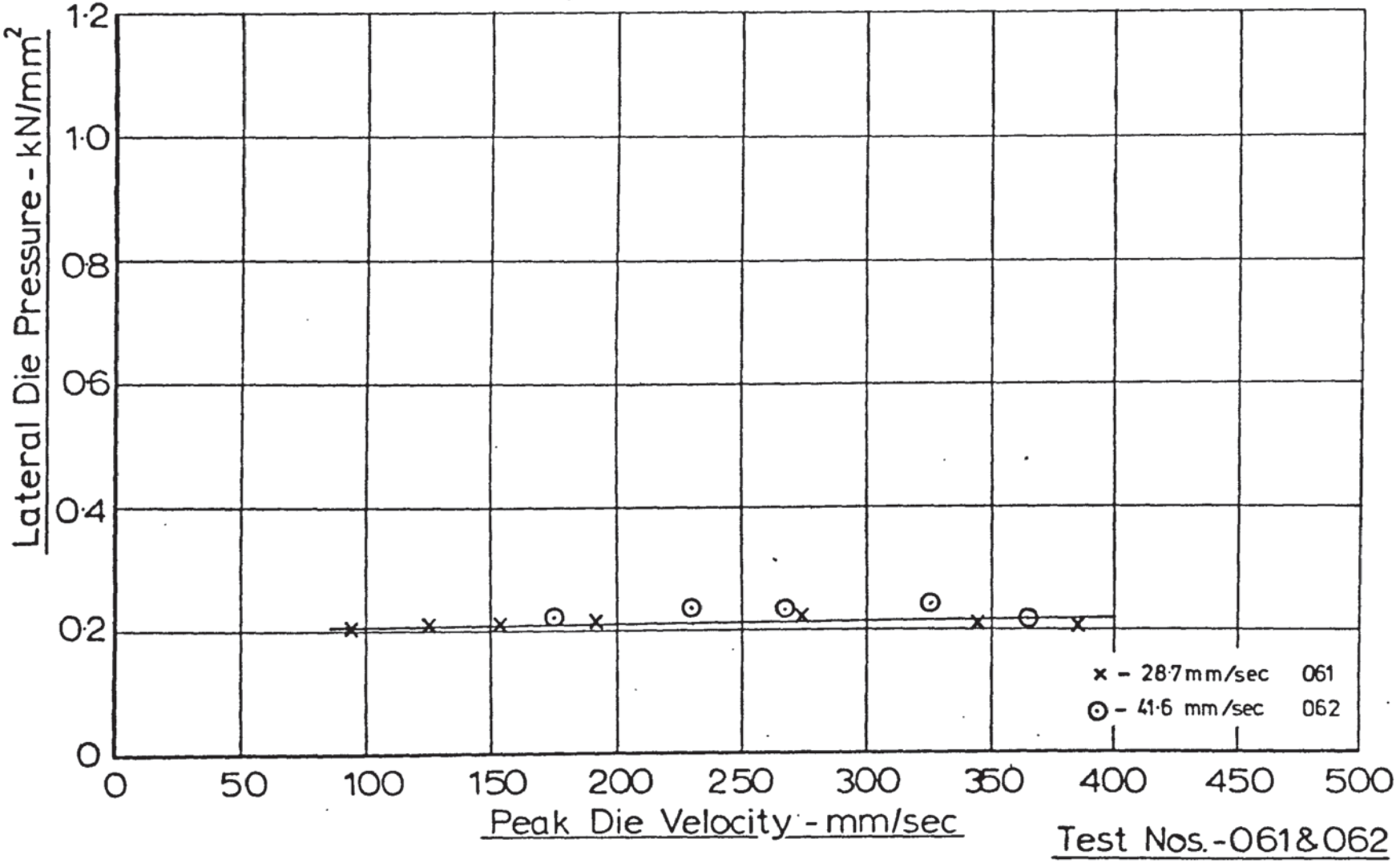

Fig(7·73) - Lateral Die Pressure vs. Peak Die Velocity(α=5°, r=0·442)

[Draw Speed = 30·8mm/sec]

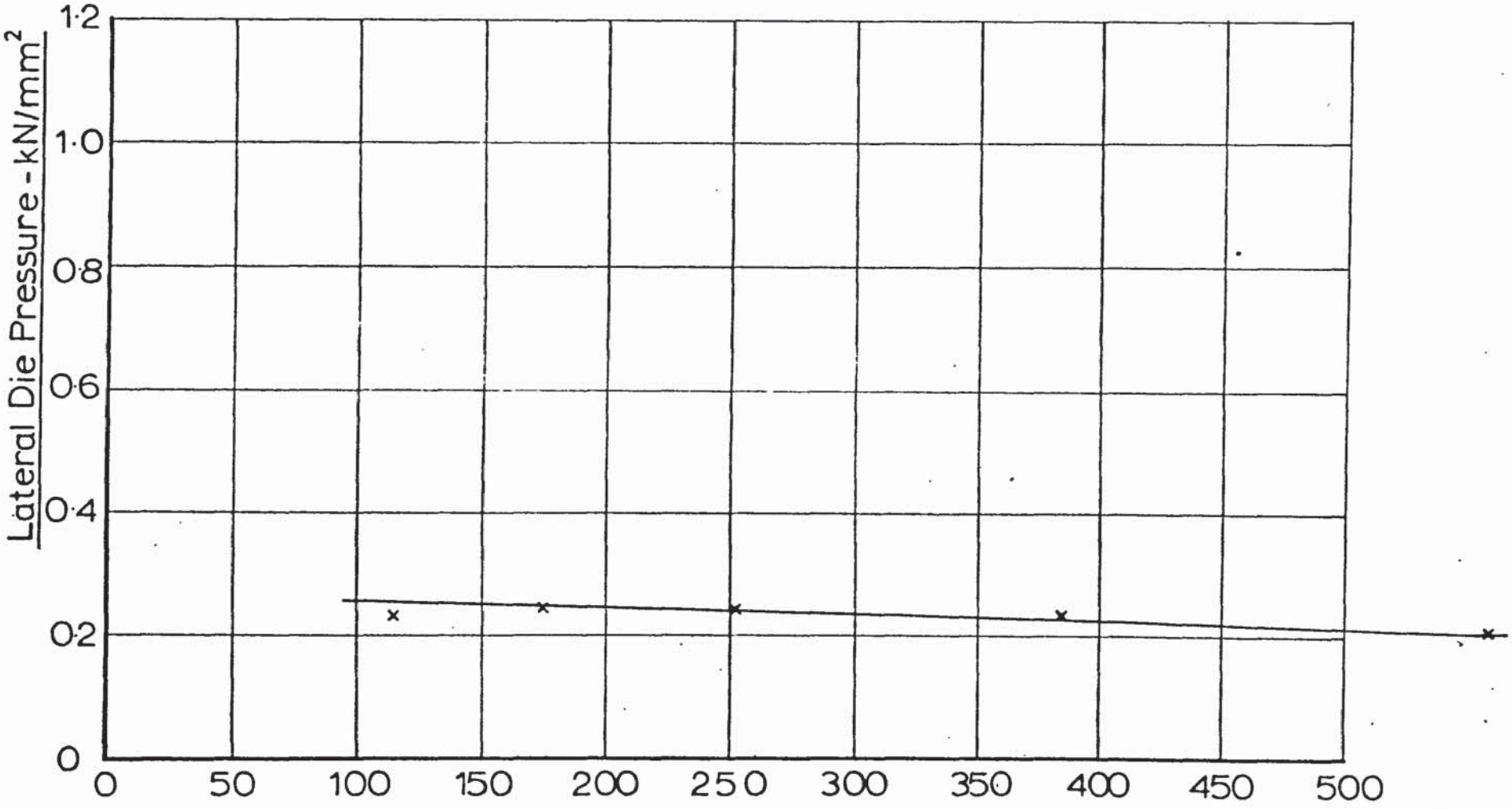

Fig(7·74) - Lateral Die Pressure vs. Peak Die Velocity ($\alpha = 5°$)

[Arbitrary Draw Speed, Constant Power Input]

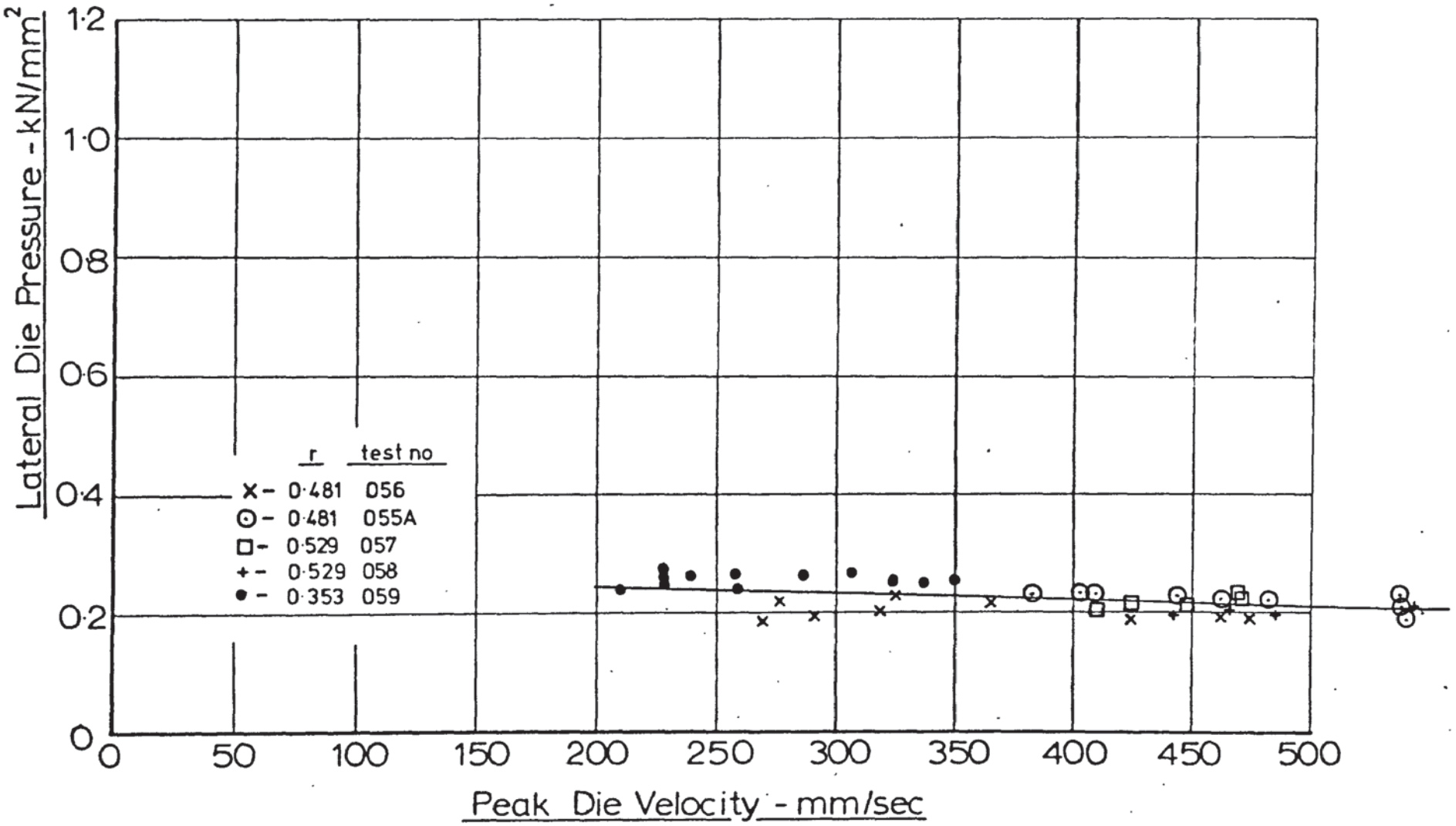

Fig(7.75)-Lateral Die Pressure vs. Peak Die Velocity(α=7.5°, r=0.164)

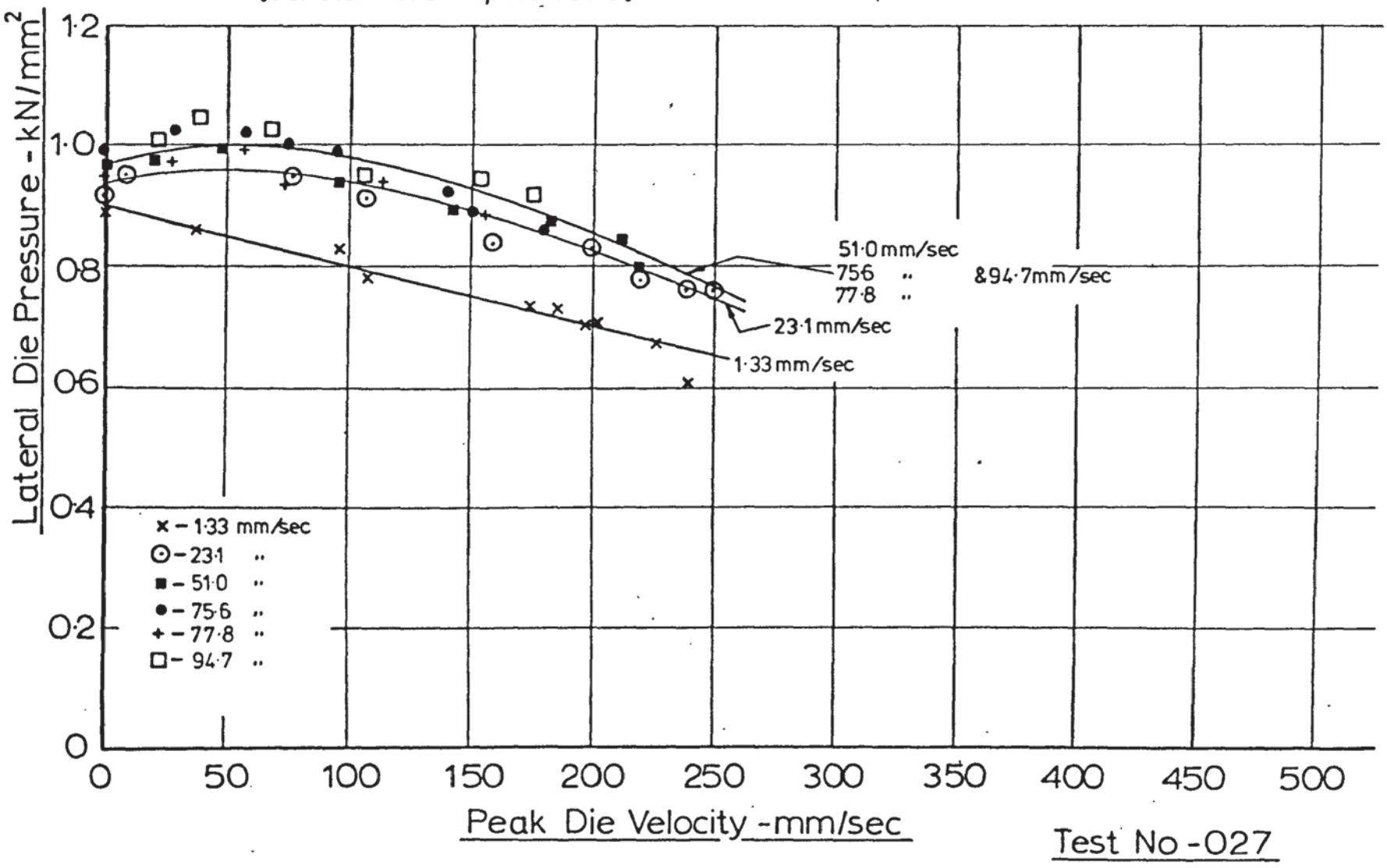

Test No - 027

Fig(7·76)- Lateral Die Pressure vs. Peak Die Velocity(α=7·5°; r=0·267)

[Constant Draw Speed Tests]

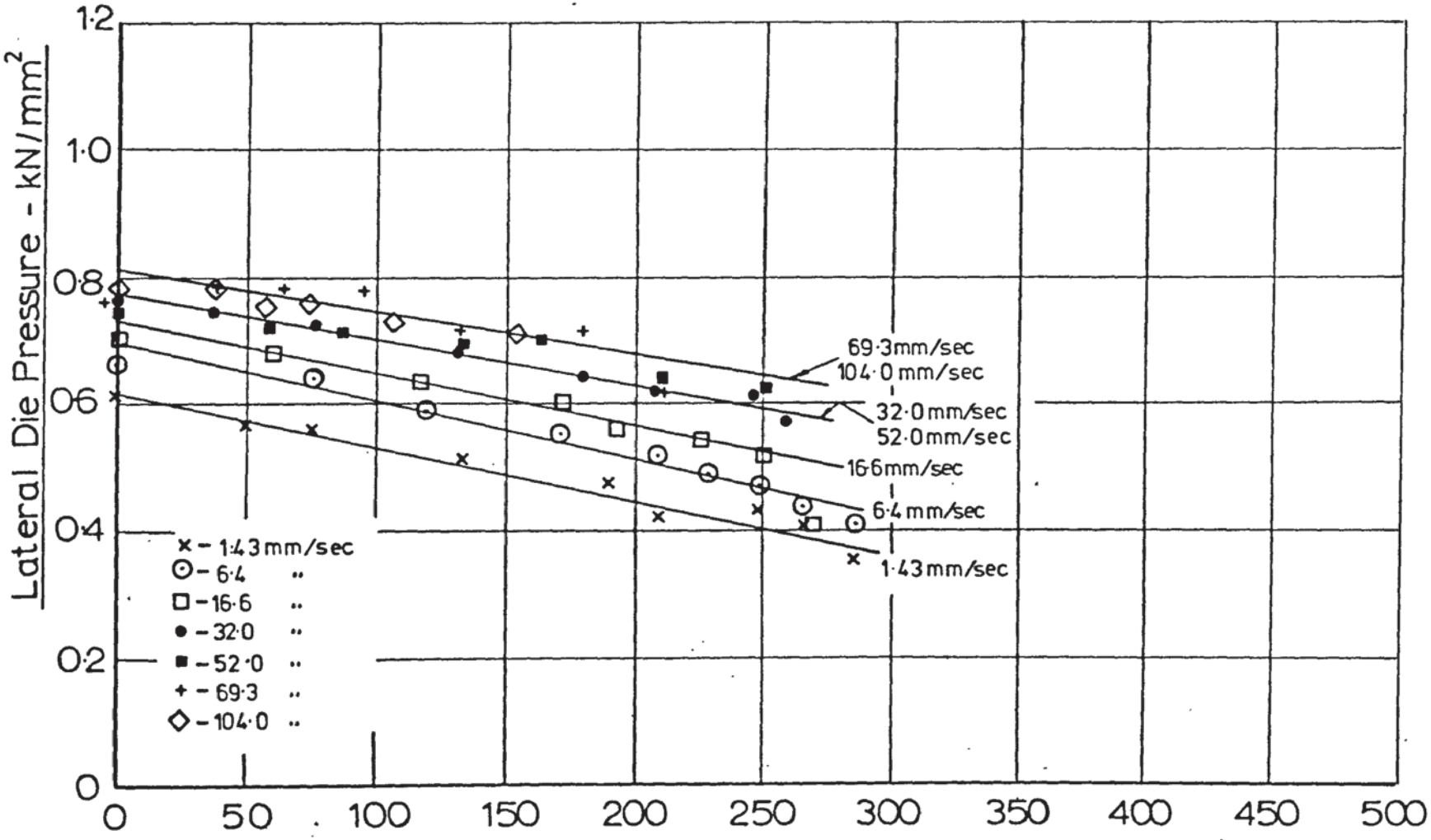

Test No -041

Fig(7·77) - Lateral Die Pressure vs. Peak Die Velocity(α=7·5°, r=0·307)

[Constant Draw Speed Tests]

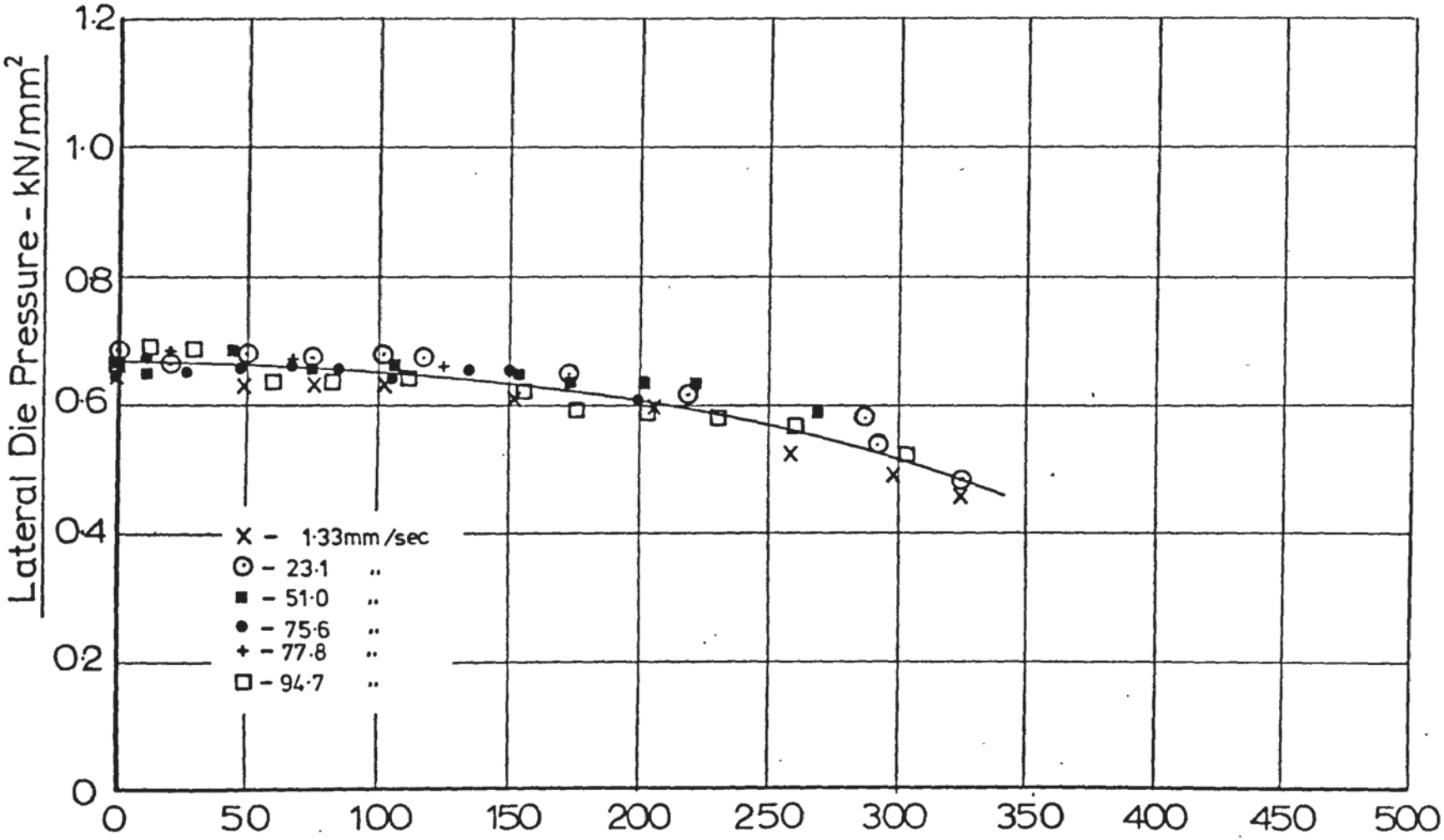

Test No - 025

Fig(7·78)-Lateral Die Pressure vs. Peak Die Velocity(α=7·5°; r=0·368)

[Constant Draw Speed Tests]

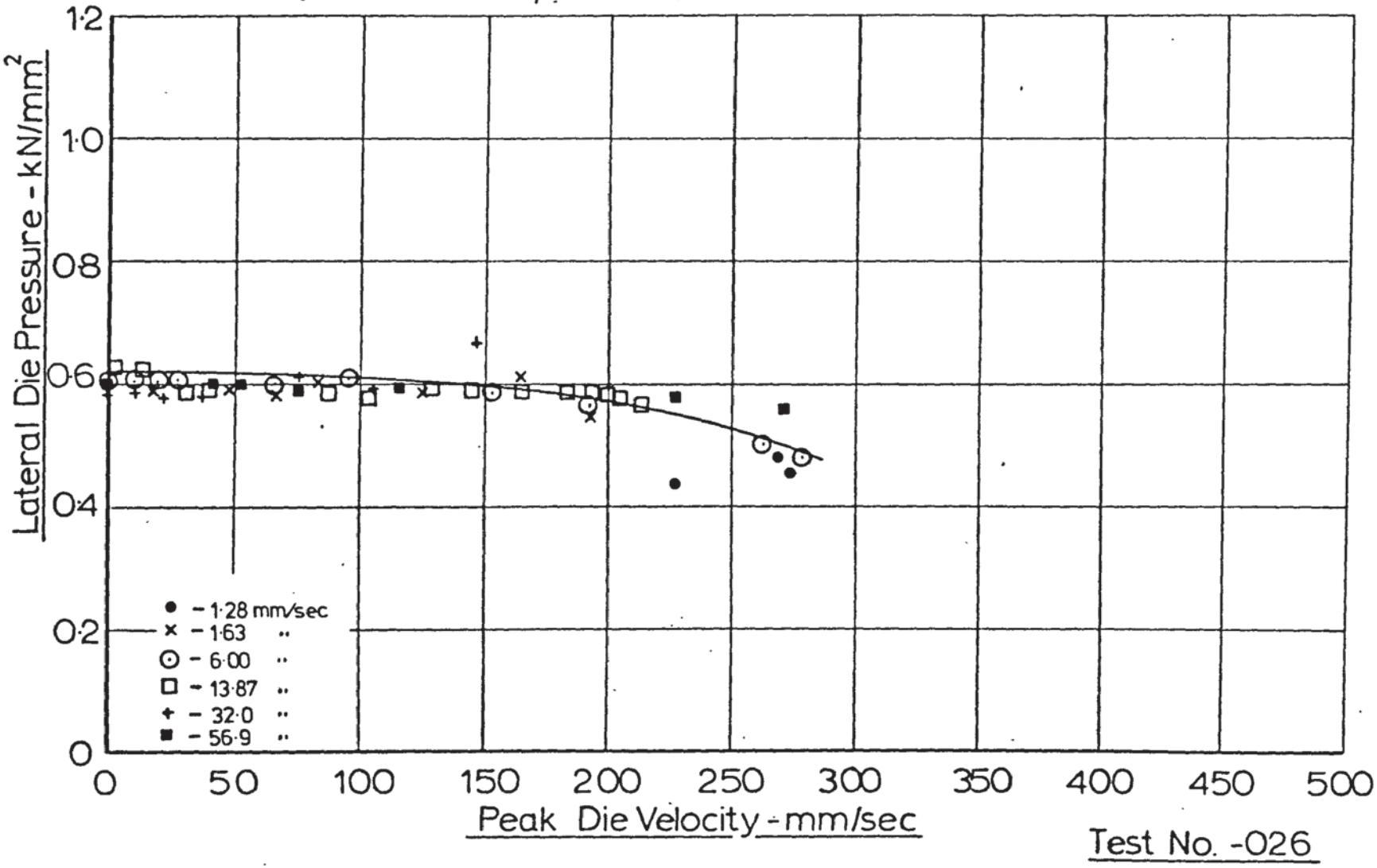

Test No. -026

Fig(7·79)-Lateral Die Pressure vs. Peak Die Velocity(α=7·5°, r=0·387)

[Constant Draw Speed Tests]

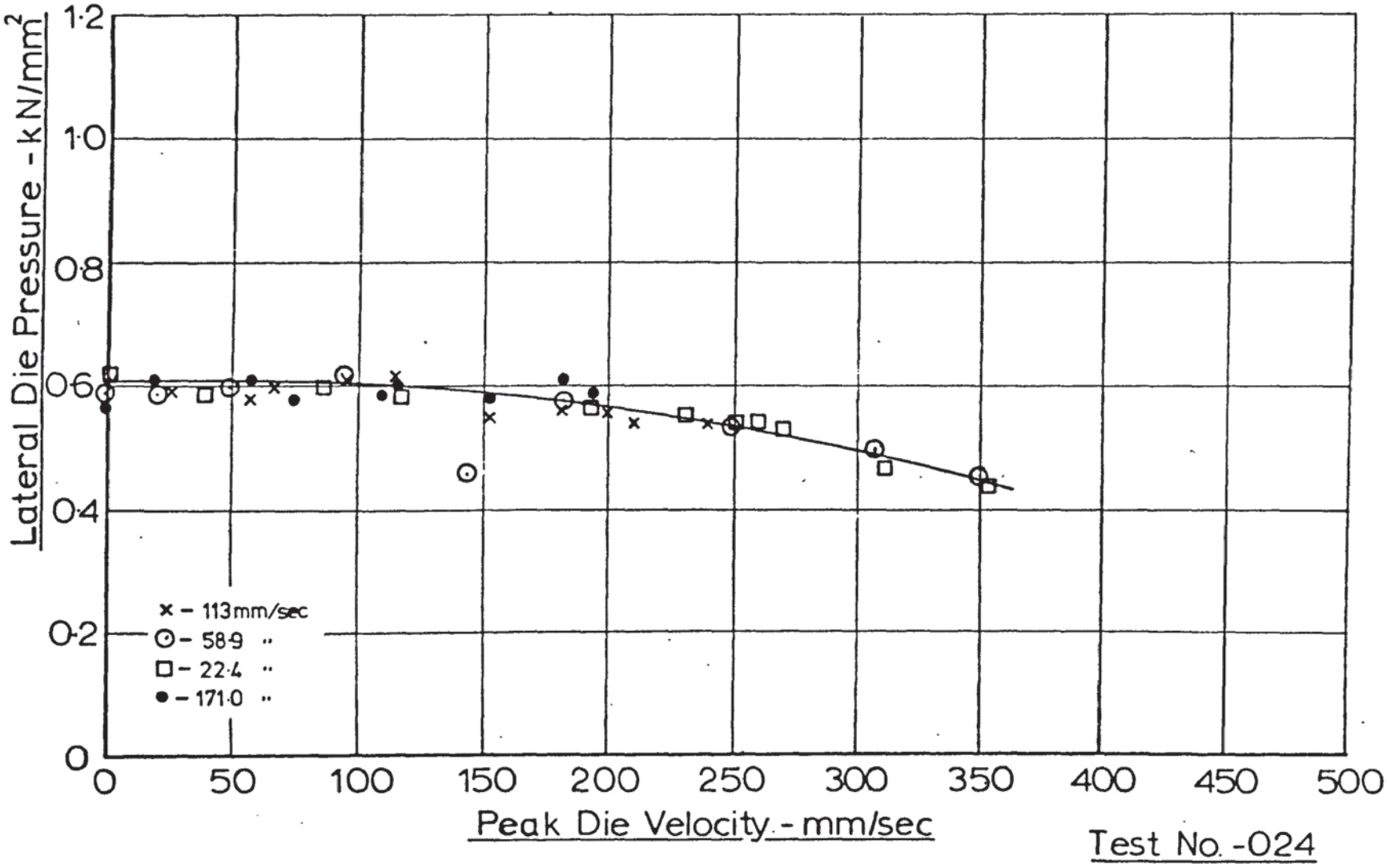

Test No. -024

Fig(7·80) - Lateral Die Pressure vs. Peak Die Velocity (α = 7·5°; r = 0·440)

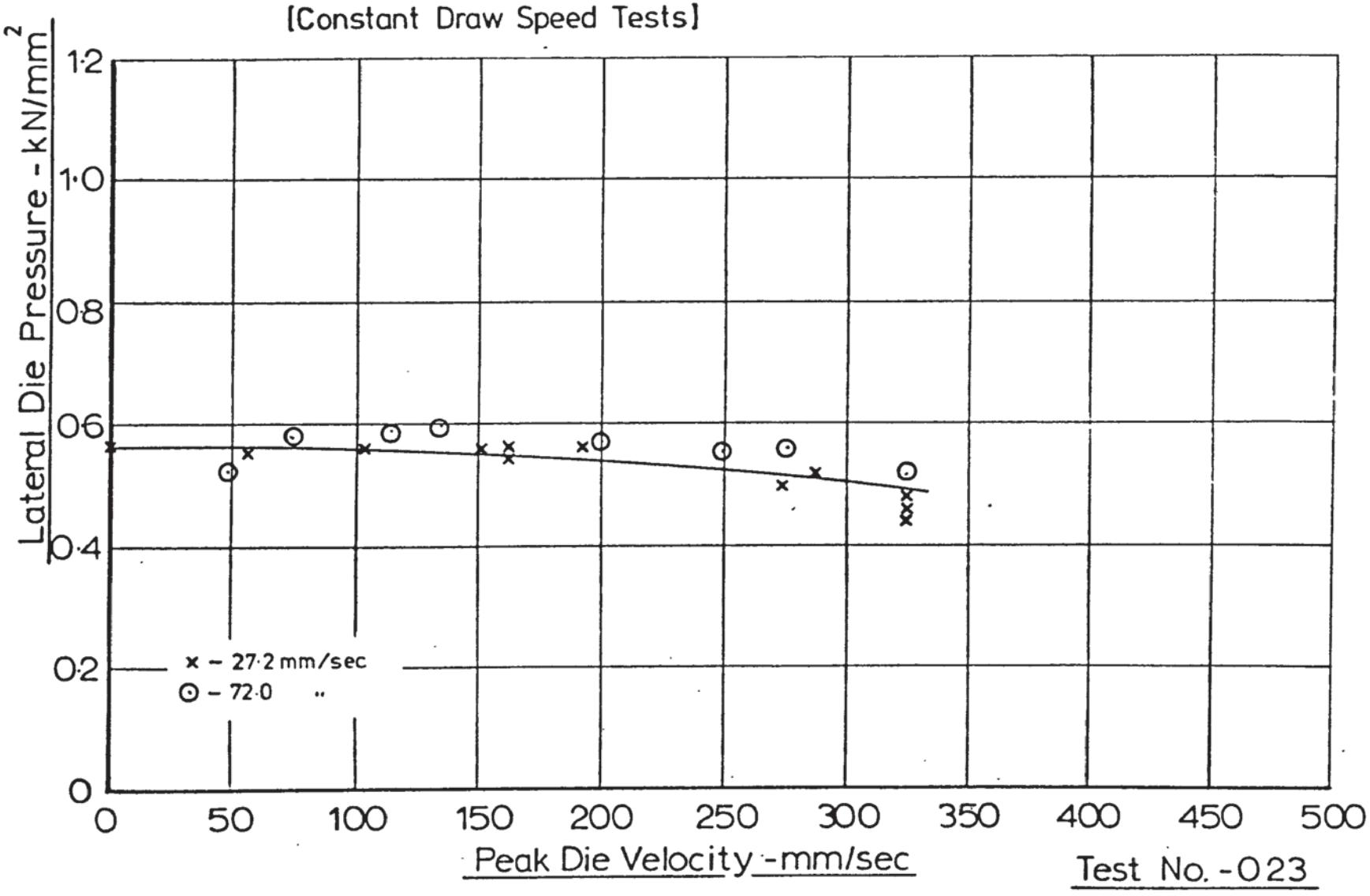

Fig(7·81)- Lateral Die Pressure vs. Peak Die Velocity (α=7·5°)

[Constant Power Input, Arbitrary Draw Speed]

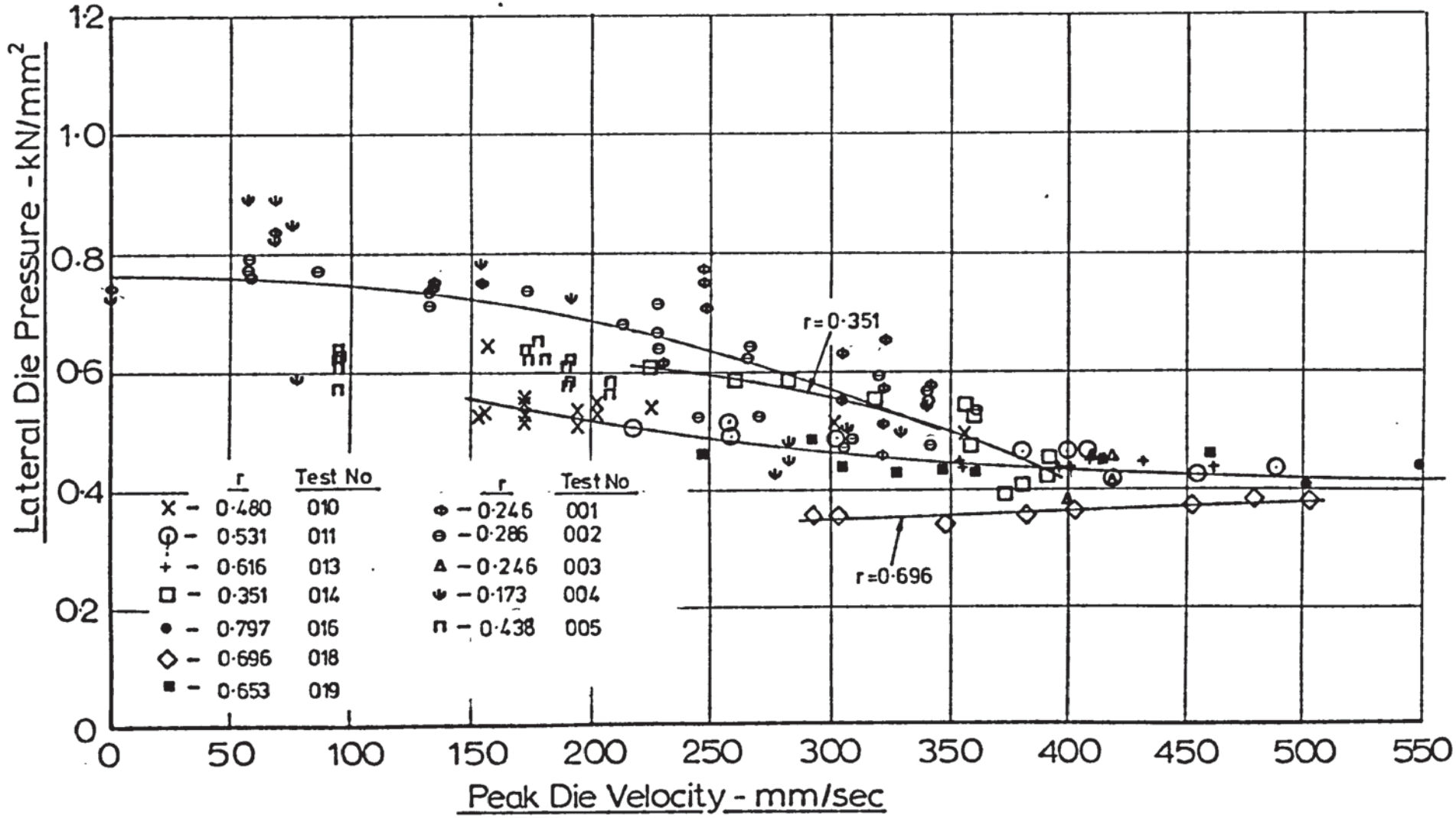

Fig(7.82)-Lateral Die Pressure vs. Peak Die Velocity(α =7.5°with land, r=0.187)

[Constant Draw Speed Tests]

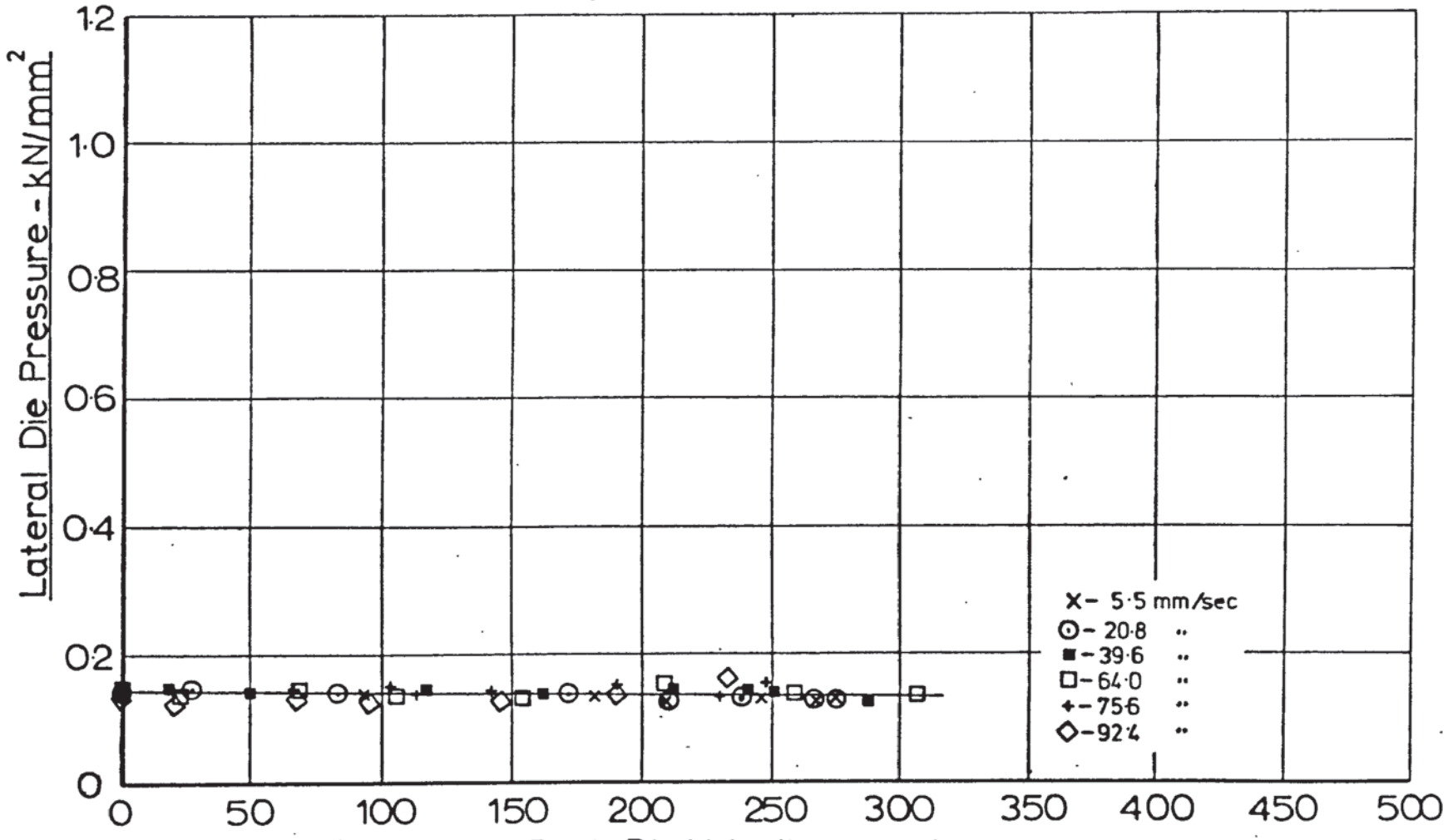

Test No. -066

Fig(7.83) - Lateral Die Pressure vs. Peak Die Velocity (α=7.5° with land, r=0.270)

[Constant Draw Speed Tests]

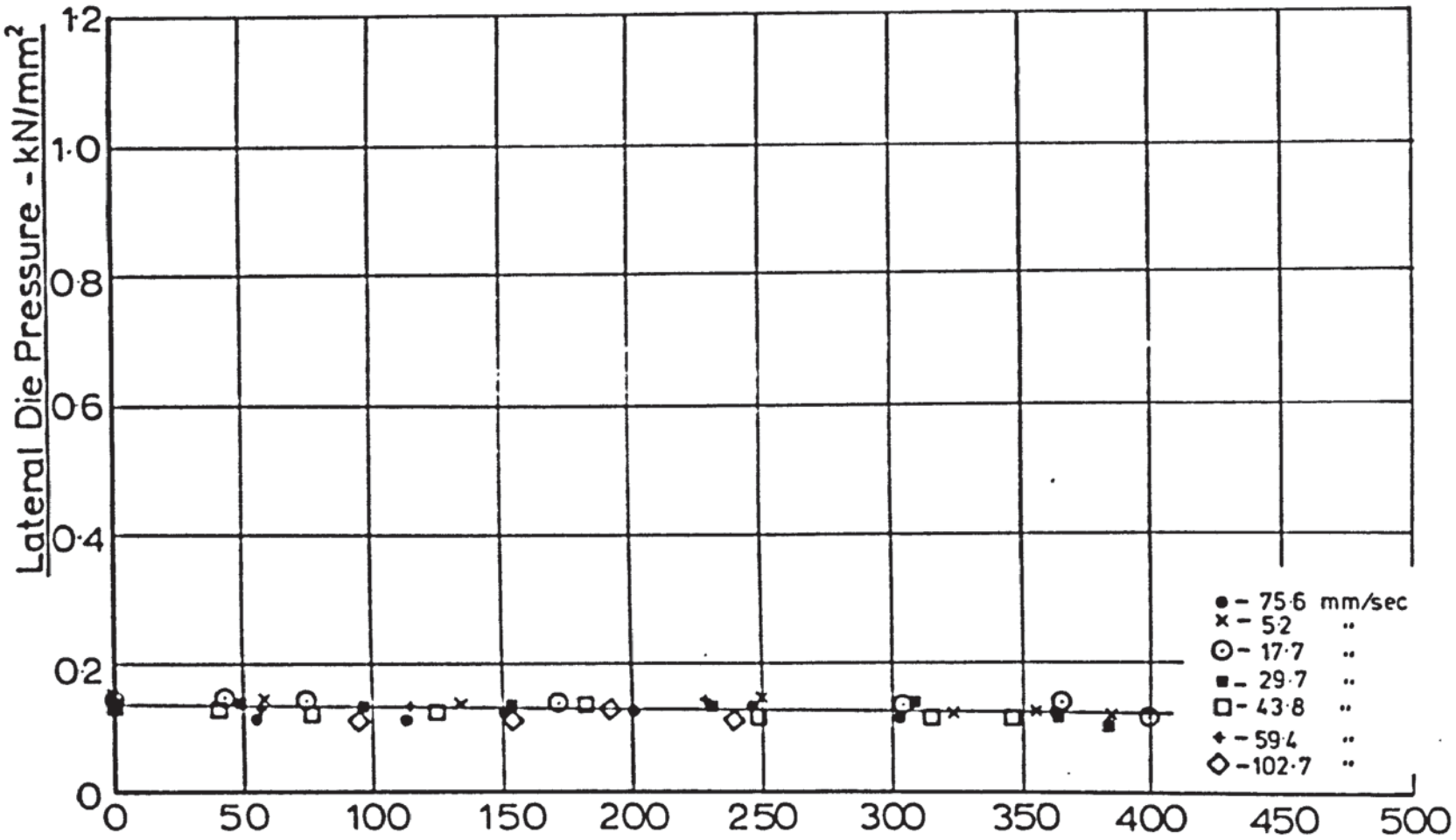

Test No.-069

Fig(7·84)- Lateral Die Pressure vs. Peak Die Velocity(α = 7·5° with land, r = 0·373)

[Constant Draw Speed Tests]

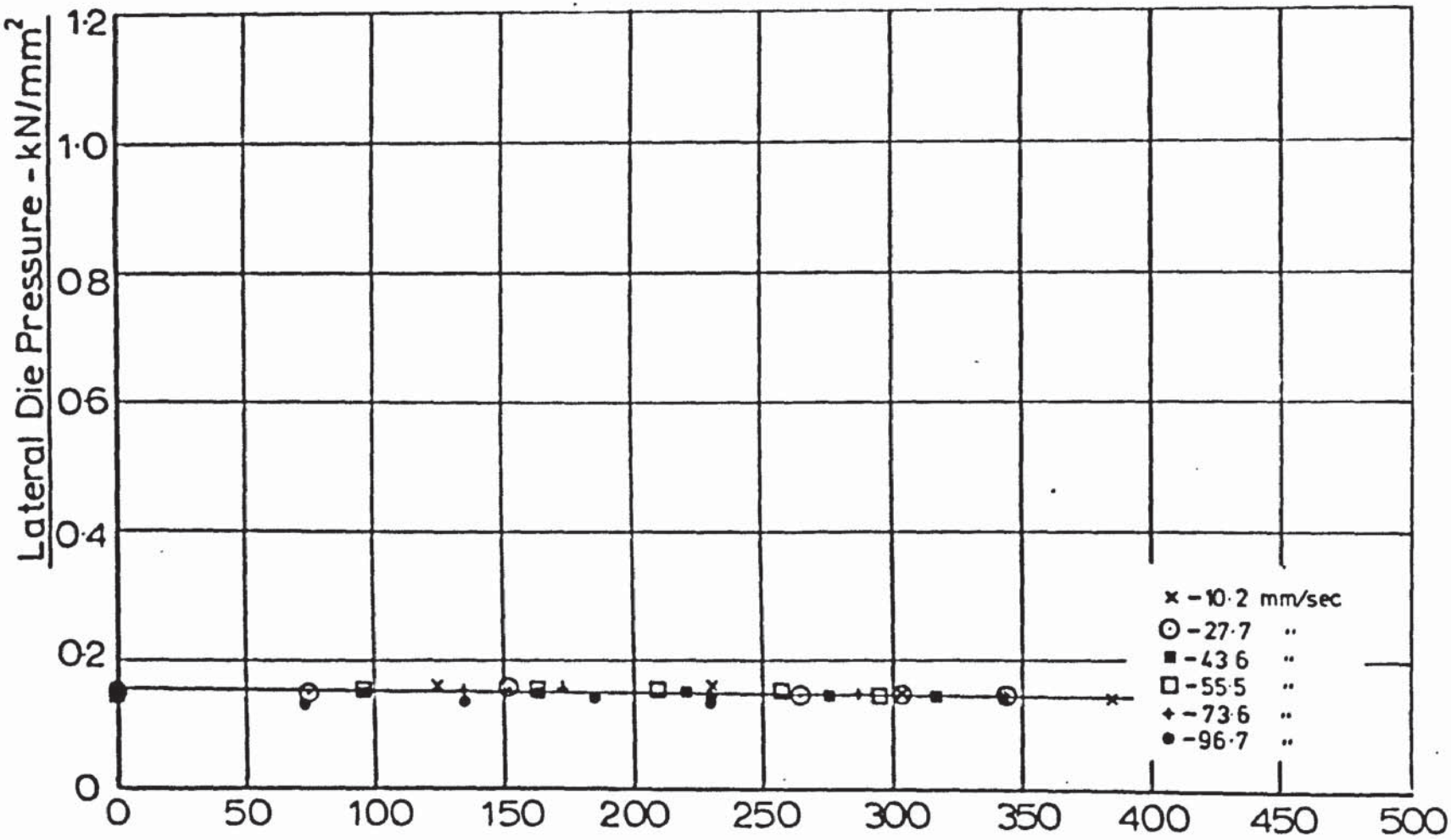

Test No. - 073

Fig(7.85) - Lateral Die Pressure vs. Peak Die Velocity (α = 7.5° with land, r = 0.438)

[Constant Draw Speed Tests]

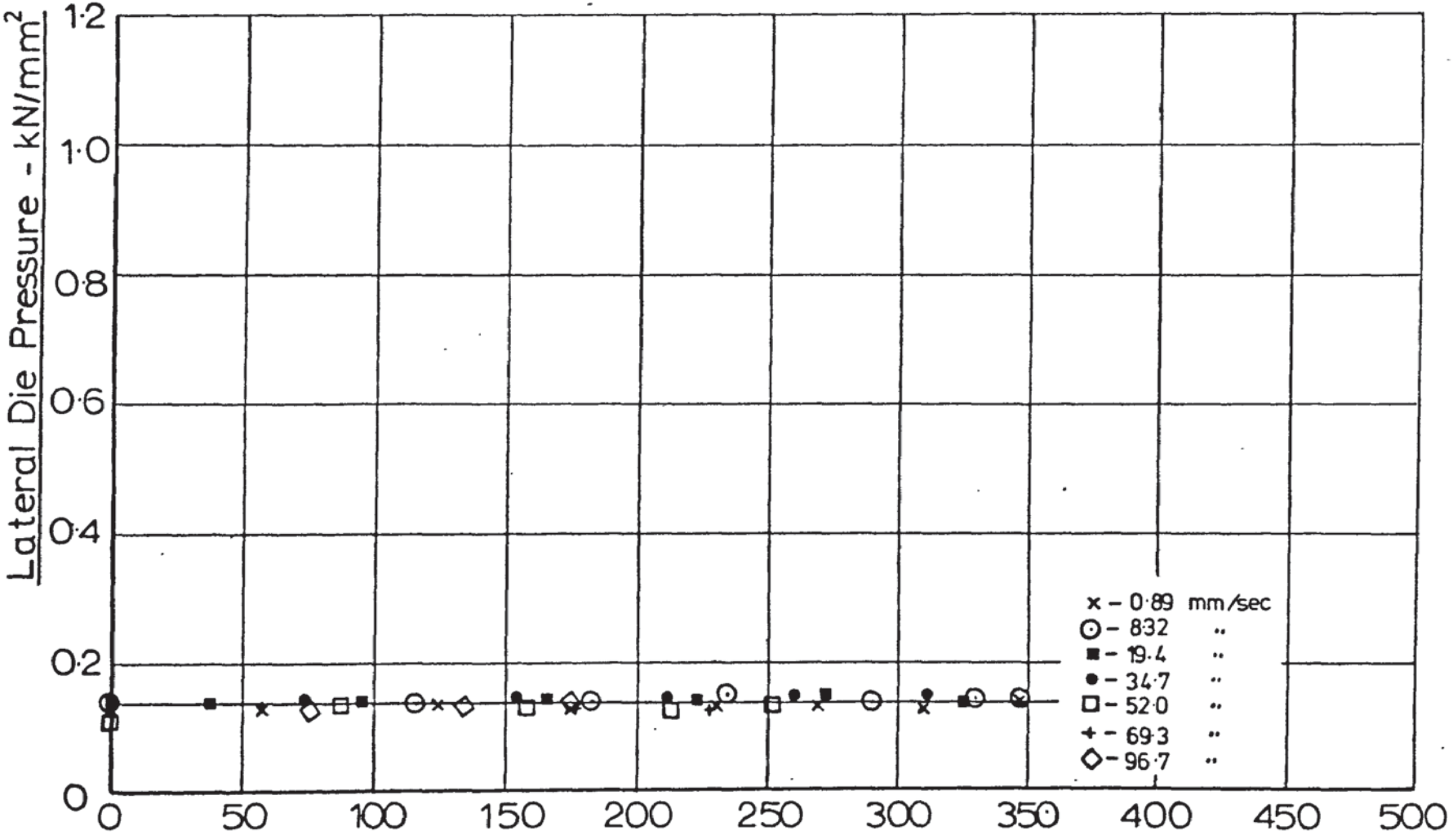

Test No. -070

Fig(7·86) - Lateral Die Pressure vs. Peak Die Velocity(∝=7·5° with land, r=0·453)

[Constant Draw Speed Tests]

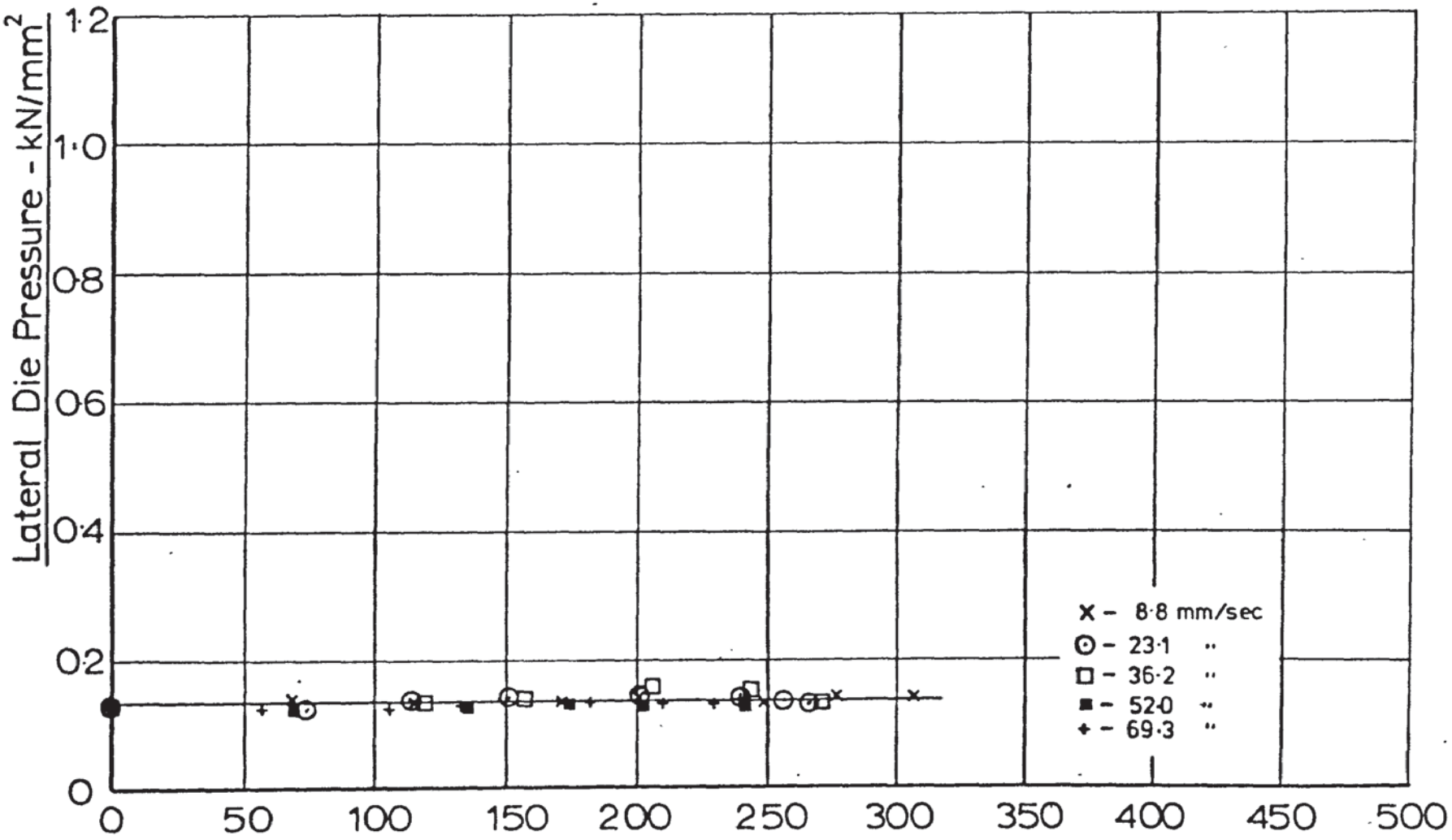

Test No. - 072

Fig(7·87)- Lateral Die Pressure vs. Peak Die Velocity (α=7·5° with land, r=0·187)

[Arbitrary Draw Speed, Constant Power Input]

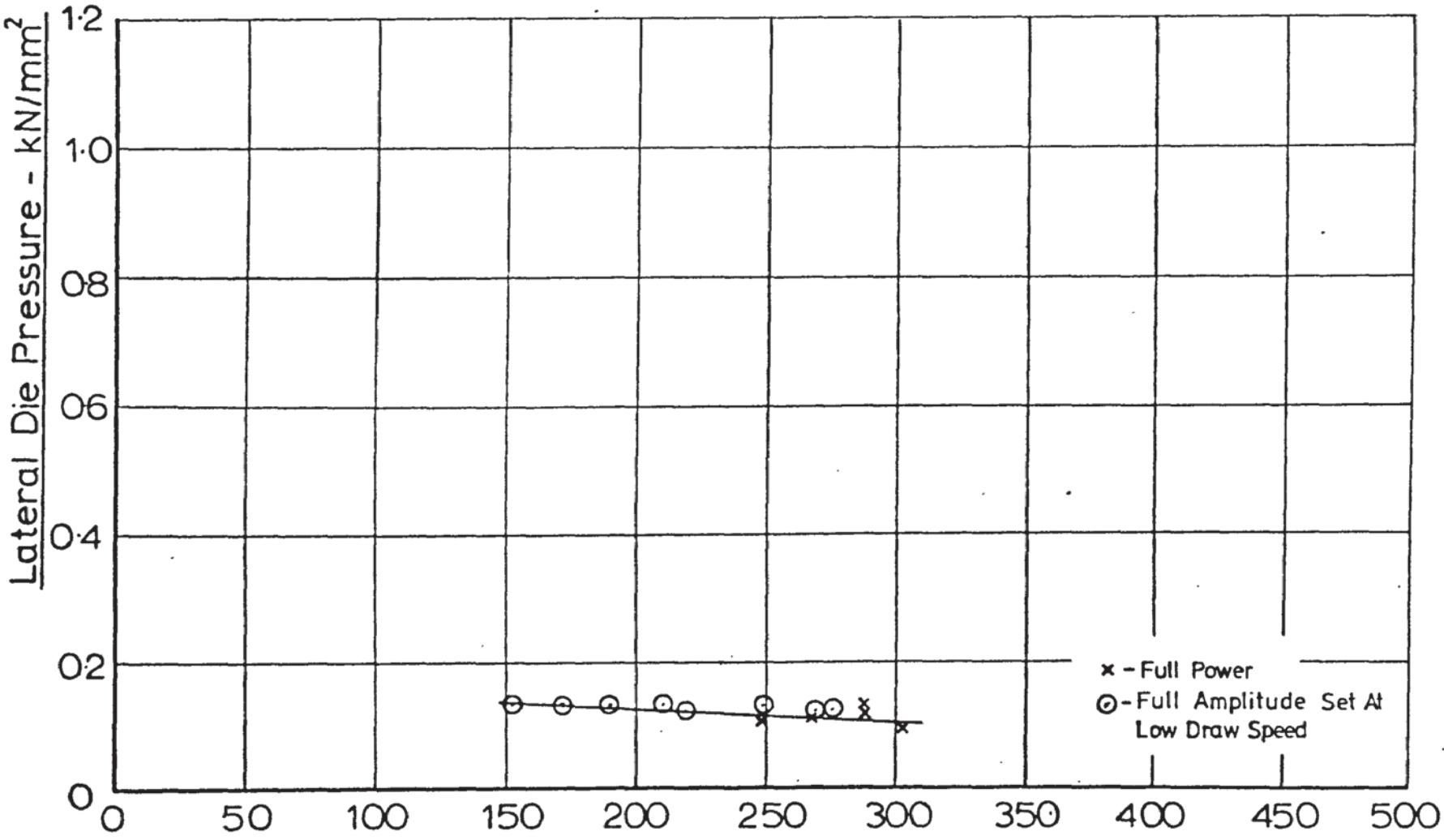

Test No.-066

Fig(7·88)- Lateral Die Pressure vs. Peak Die Velocity(α=7·5° with land)

[Arbitrary Draw Speed, Constant Power Input]

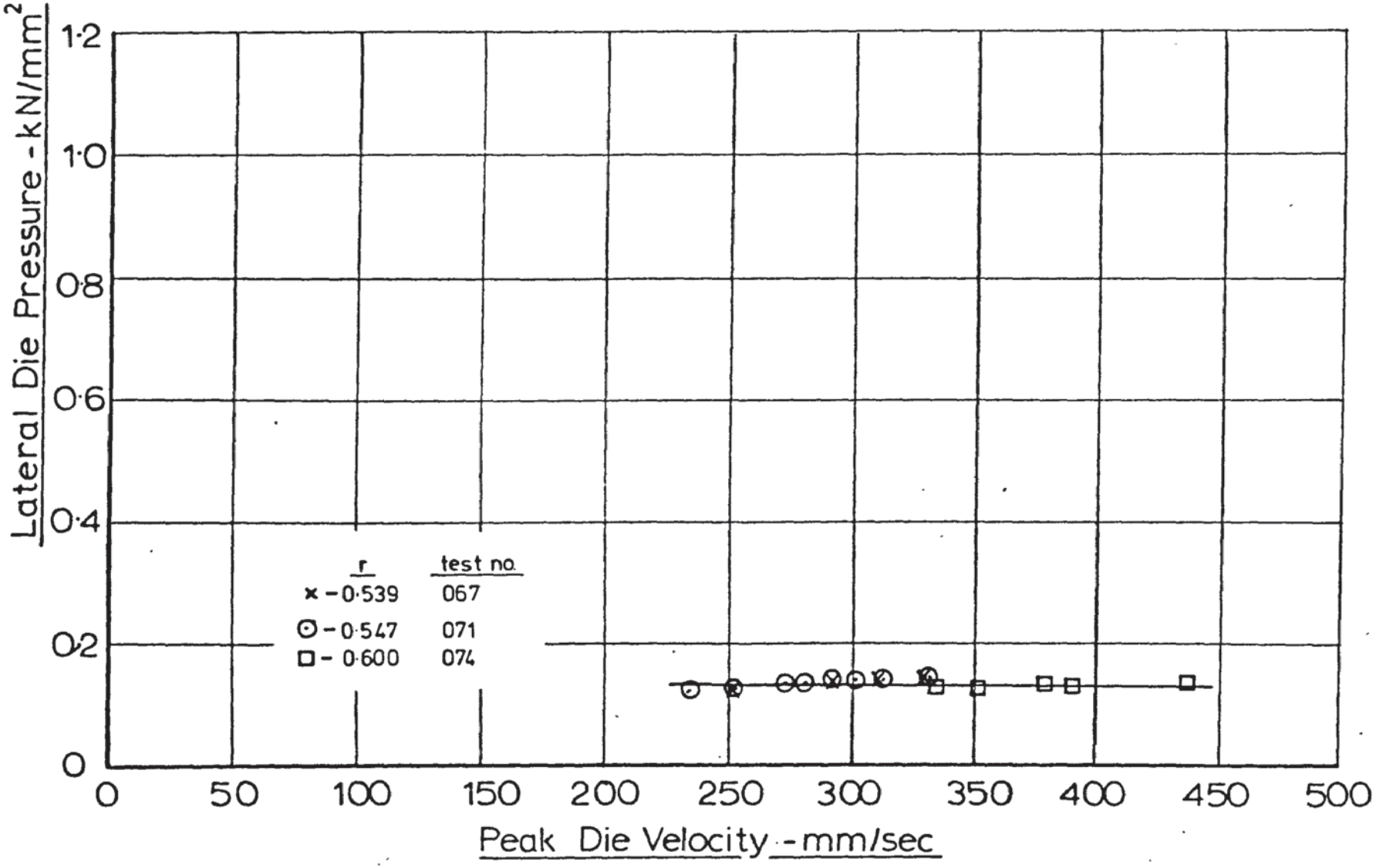

Fig(7·89)- Lateral Die Pressure vs. Peak Die Velocity (α =10°, r =0·260)

[Draw Speed = 11·9mm/sec]

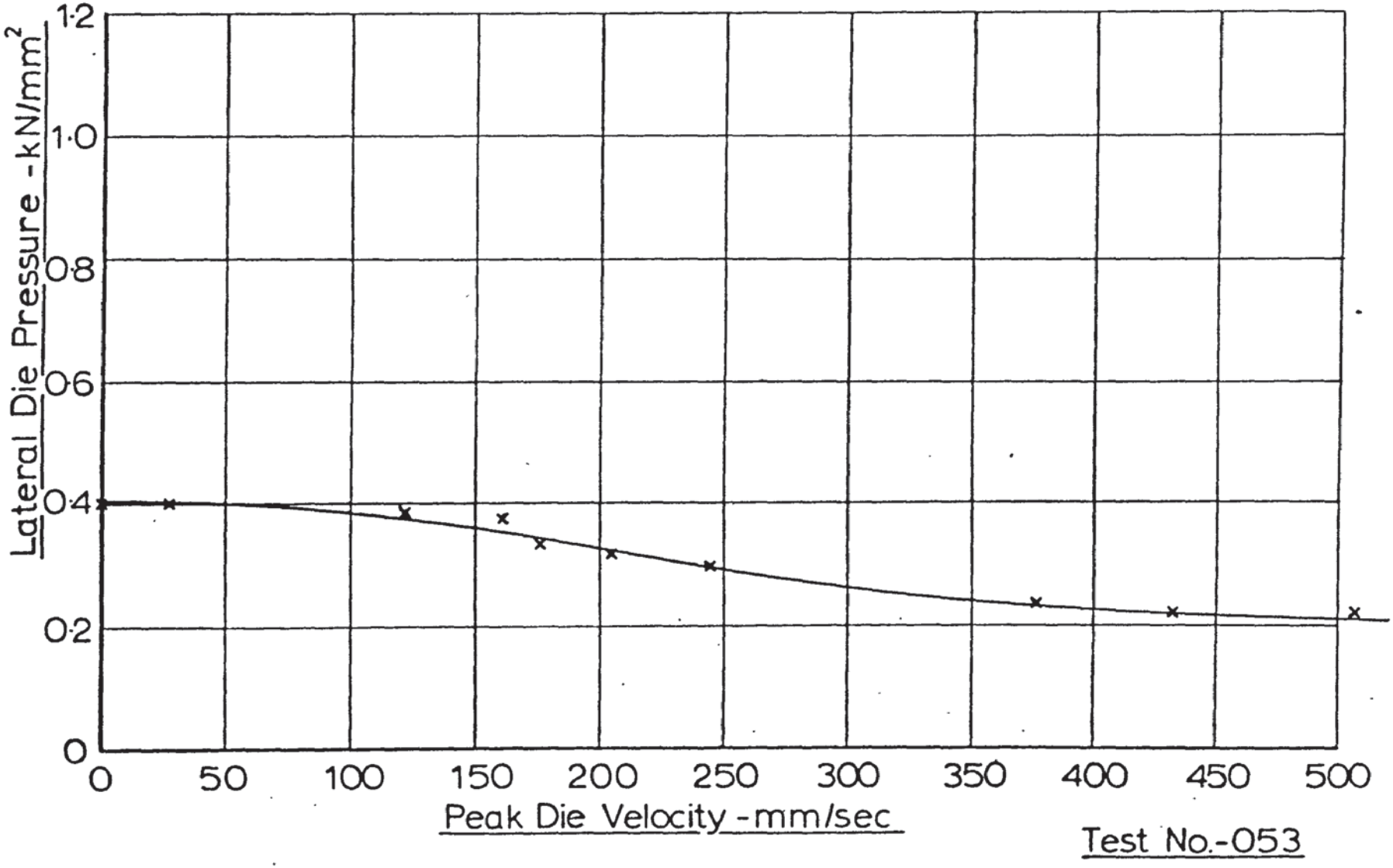

Fig(7·90) - Lateral Die Pressure vs. Peak Die Velocity ($\alpha = 10°$, $r = 0·263$)

[Constant Draw Speed Tests]

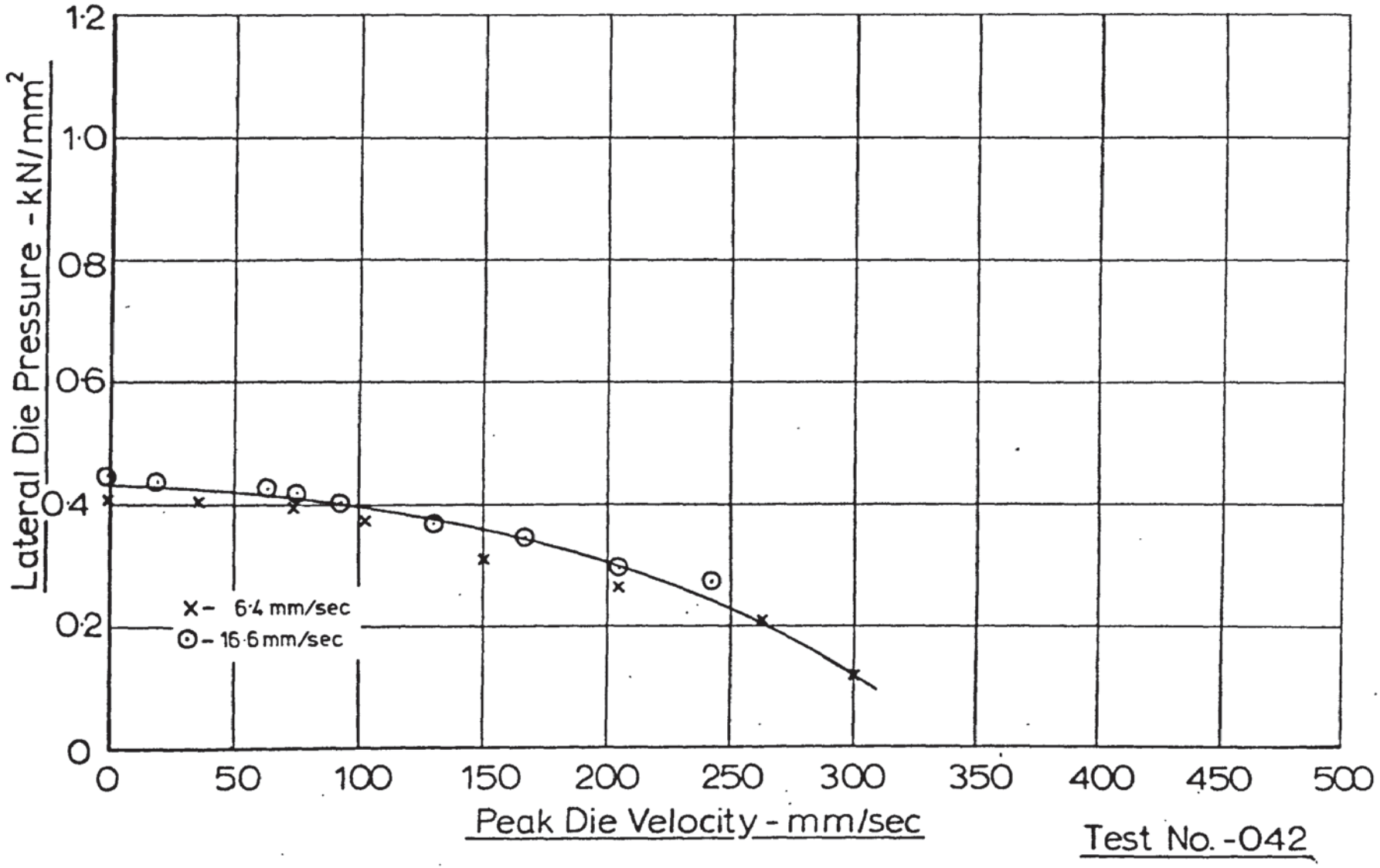

Test No. -042

Fig(7·91)- Lateral Die Pressure vs. Peak Die Velocity(α=10°, r=0·399)

[Constant Draw Speed Tests]

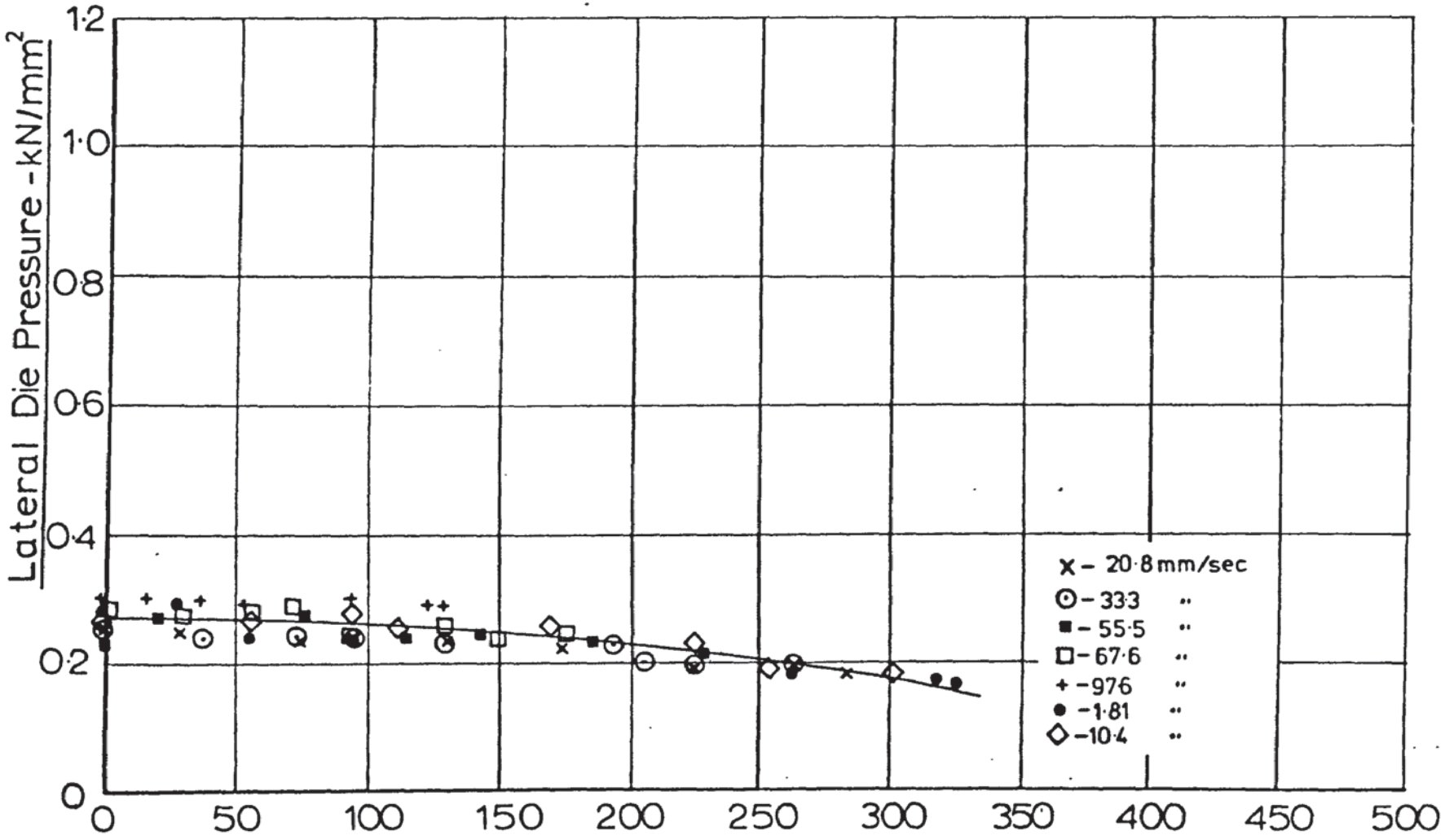

Test No.-043

Fig(7·92)- Lateral Die Pressure vs. Peak Die Velocity($\alpha = 10°$, r = 0·461)

[Constant Draw Speed Tests]

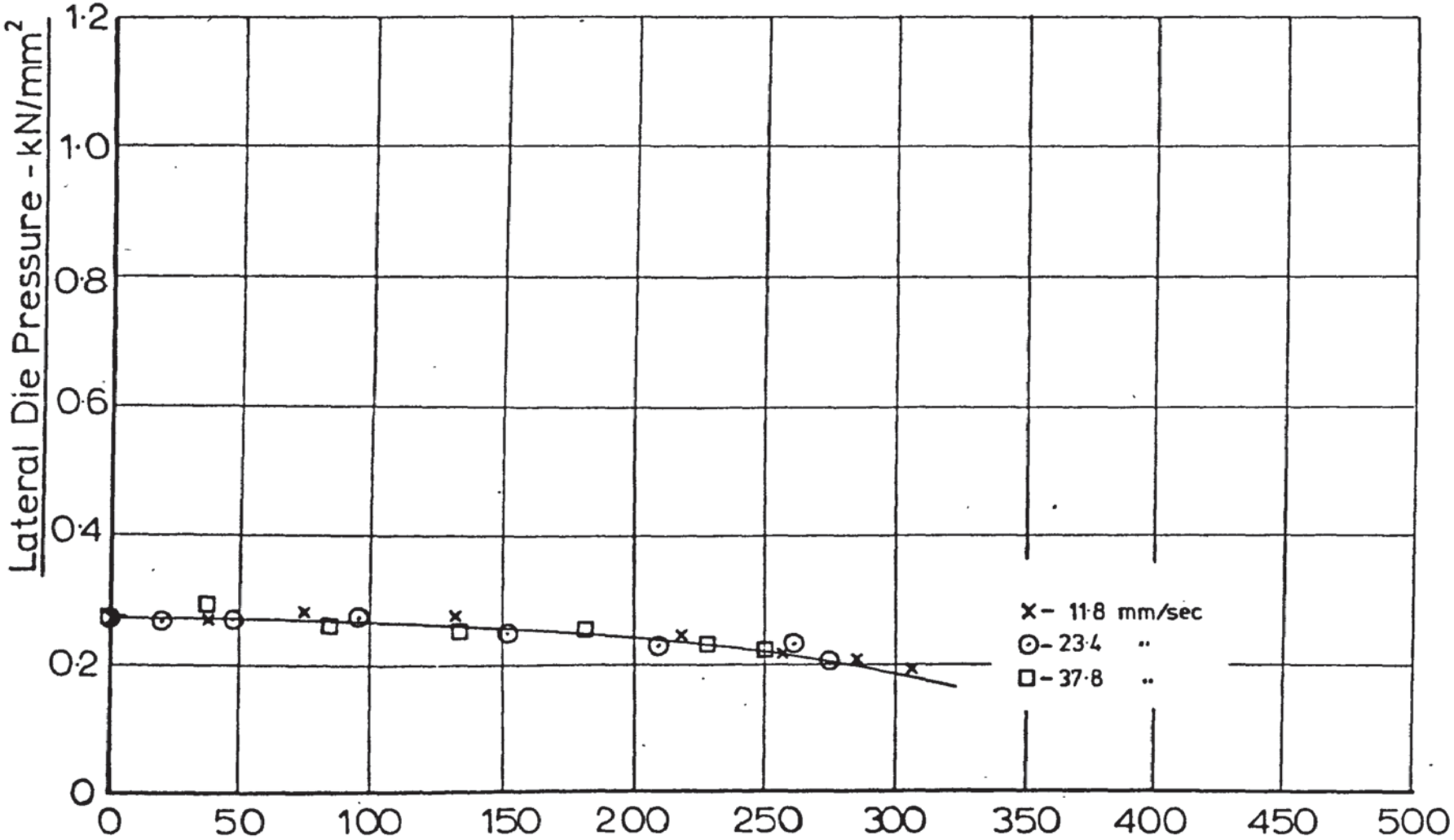

Fig(7·93) - Lateral Die Pressure vs. Peak Die Velocity (α=10°)

[Arbitrary Draw Speed, Constant Power Input]

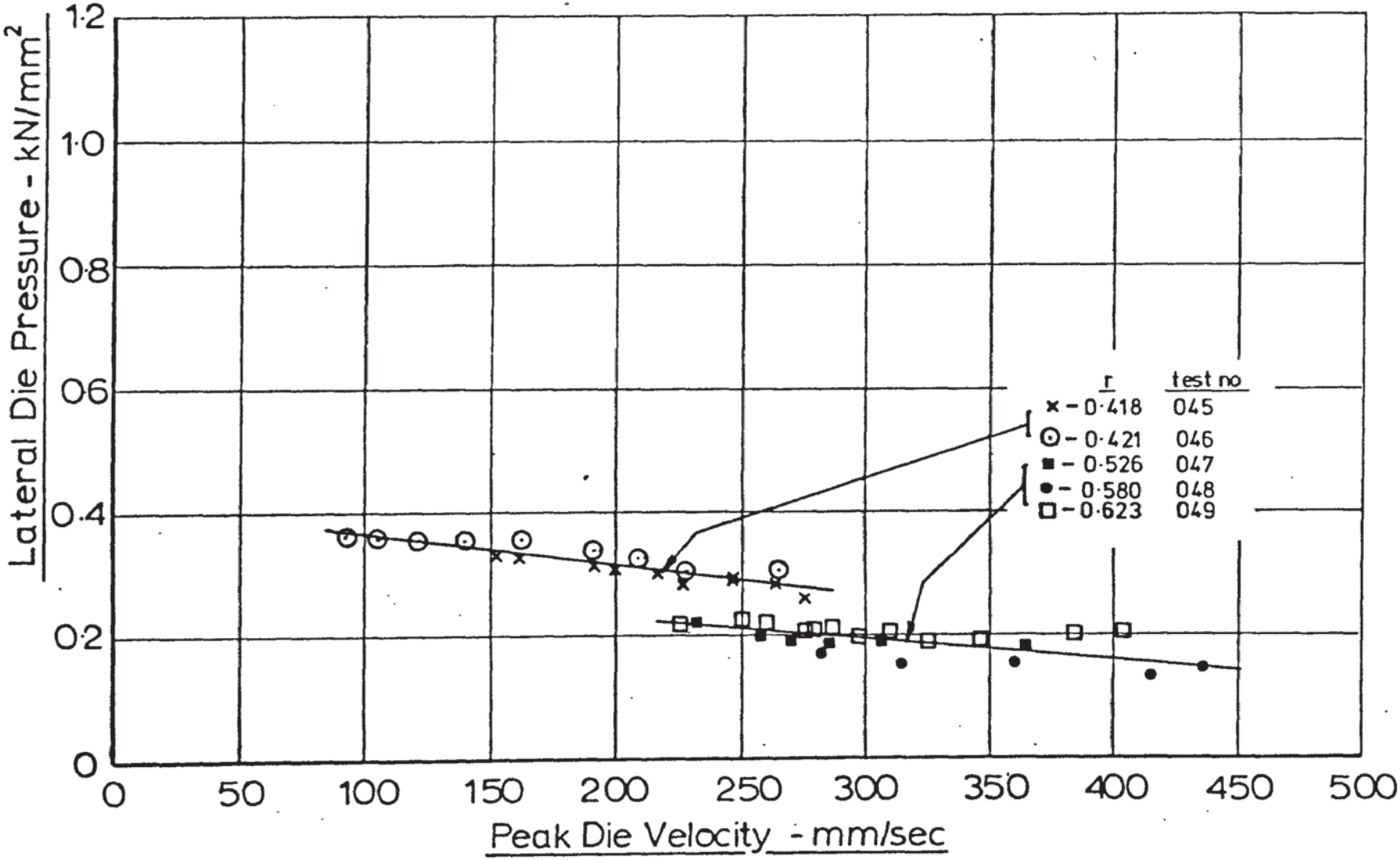

Fig(7.94) -
Variation Of Tuned Frequency With Die Angle And Reduction Of Area

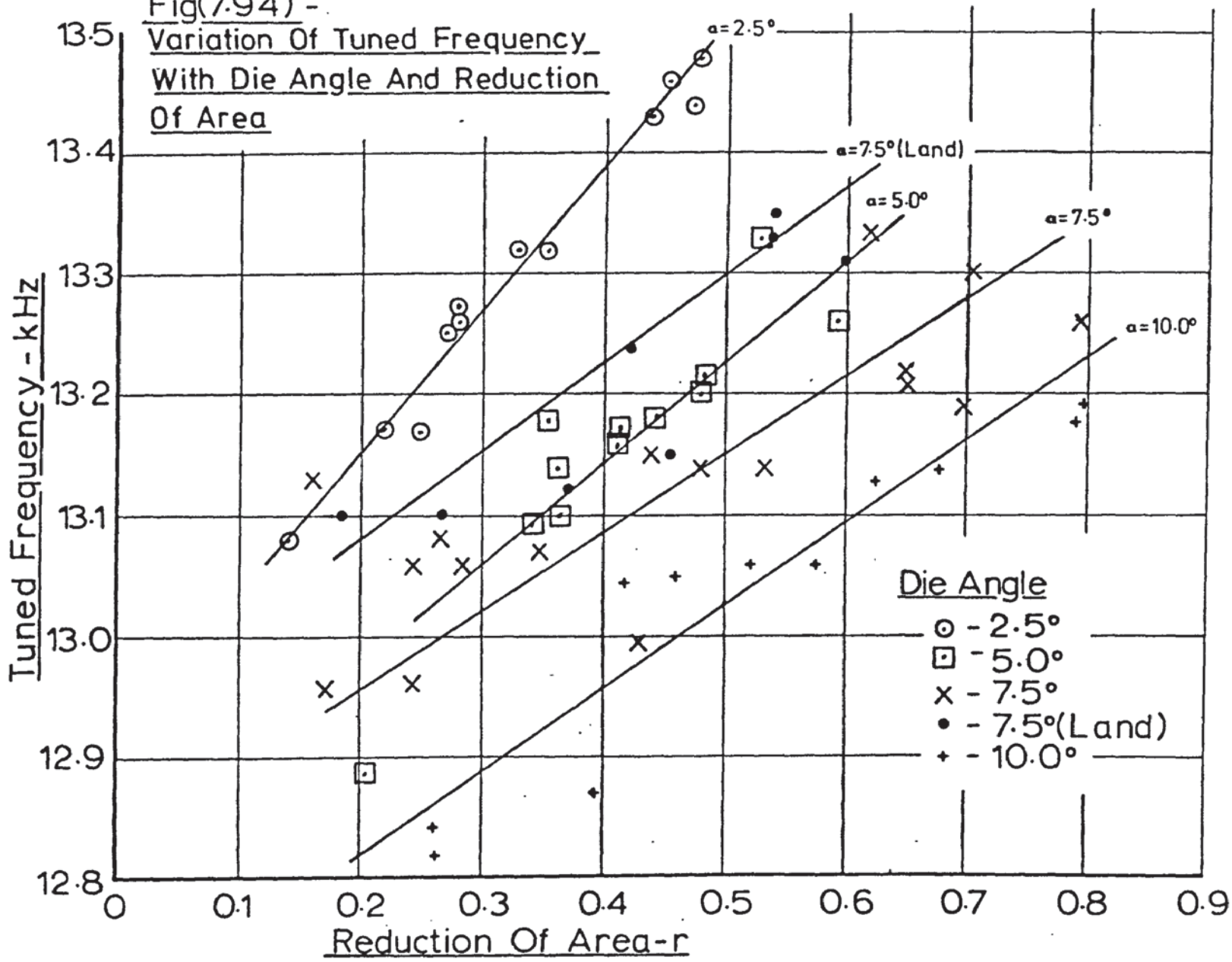

8. DISCUSSION

8.1. DISCUSSION OF RESULTS

Some of the early sets of results are not recorded here either because the strip failed before stable drawing conditions could be established or because the author failed to switch on part of the instrumentation. It was evident from the early sets of usable results that the die and tag loads were, for a given reduction of area and die profile, dependent primarily upon peak die velocity and to a lesser, though significant extent, upon mean draw speed. Many of the tests were carried out at constant draw speed in order that this independent variable could be eliminated. This enabled the effect of draw speed to be determined by obtaining sets of results at different draw speeds. At higher reductions of area, when drawing without ultrasound could not be contemplated, it was necessary to carry out the tests at constant acoustic power input. Some of these tests were carried out at the lower reductions of area in order that comparison could be made with the constant draw speed tests.

The effect of die angle, reduction of area, draw speed, and peak die velocity upon mean strip tension, specific axial thrust and mean die pressure are discussed in section 8.2.

8.1.1. Variation of Tuned Frequency

Before entering into a detailed discussion of the effect of ultrasound upon the strip drawing process it is convenient to discuss the more general effects.

During the early tests it became evident that the tuned frequency was not constant. The effect of the die profile and the reduction of area upon the tuned frequency is shown in Figure (7.94). It can be seen that the tuned frequency increases with reduction of area and, for the knife edged dies, decreases with die angle. The 7.5° die-with-land also tended to

give an increased tuned frequency with respect to the 7.5° knife edged die. No significant change in the tuned frequency could be attributed to a change in the draw speed, that is, the tuned frequency is, sensibly, a function of the geometric configuration of the tool and strip. Thus, an increase in the length of the strip/die interface caused an increase in the tuned frequency. This increase in damping, as would be expected, caused an increase in the natural frequency of the vibratory system. It was found possible to maintain approximately the same maximum peak die velocity throughout the tests.

8.1.2. Failure Modes

As the reduction of area increased the drawing process became increasingly metastable, in fact, the mode of failure of the strip downstream of the die tended to change as the reduction of area was increased. When the reduction of area was less than 50% all failures occurred in a ductile manner, whereas failures occurring at reductions of area in excess of 60% were invariably initiated as a result of fatigue. In the latter case the crack was propagated normal to the strip axis before undergoing a transition to ductile overload failure. These failure modes are illustrated in Figure (8.1), overleaf.

Figures (8.1)(a) and (b) show the ductile failure modes. Figure (8.1)(a) is consistent with failure at relatively low reductions of area; necking was in evidence at one site only. Figure (8.1)(b) shows the type of failure that occurred at somewhat higher reductions of area. In this case necking was very localised and was hardly noticeable across the strip. The single fracture was at approximately 45° to the strip axis with incipient fractures (necking) being propagated from the edge of the strip along the whole of its drawn length, again at 45° to the strip axis.

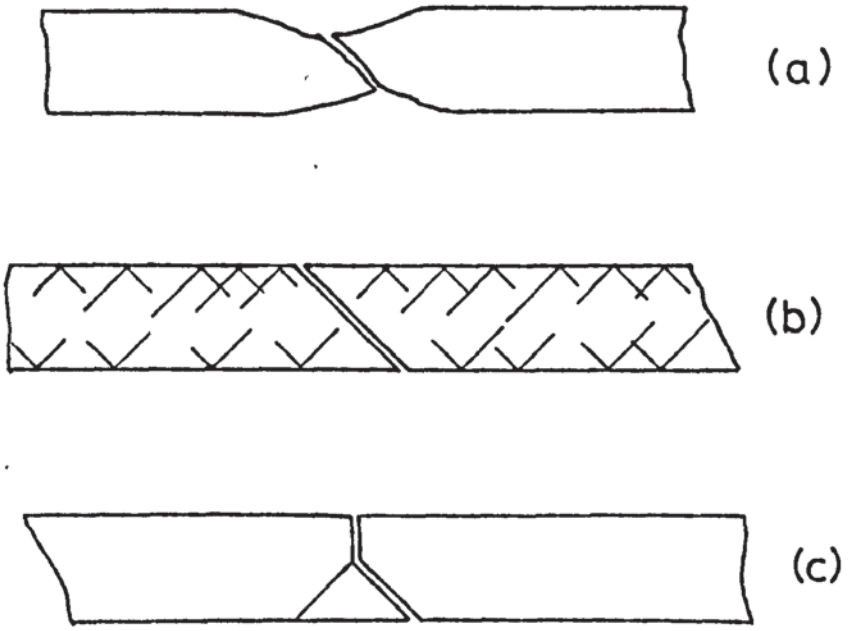

Fig(8.1)- Failure Modes In Ultrasonic Strip Drawing

Figure (8.1)(a) shows the type of fracture consistent with drawing at reductions of area in excess of 60%; a fatigue crack propagated normal to the strip axis followed by transition to overload failure.

The transition between a wholly ductile failure and a fatigue initiated failure occurred at reductions of area between 50% and 60%, irrespective of die angle. The number of cycles to failure reduced with increasing reduction of area.

The condition for producing fatigue failure during strip-drawing is likely to manifest itself as the reduction of area and the draw speed are increased. Both of these factors tend to cause an increase in mean strip tension as shown in Figures (7.1) to (7.31). Dynamic stress amplitude is also likely to increase relative to mean tag load. This is due to the increased rate of strain take-up as draw speed is increased, and to the increased proportion of oscillatory to non-oscillatory work when reduction

of area is increased. That is, increased mean stress and stress amplitude increase the likelihood of fatigue failure.

8.1.3. Performance of the test rig and instrumentation

The test equipment and instrumentation are described in Chapters 4 and 5.

The strain gauge load cells all performed without fault except for drifting, which was not of a high order and was corrected prior to each test run. The method of measuring vibrational amplitude is worth further consideration. It can be seen in Figure (5.23) that the positioning of the "Kleesattel" transducer at a displacement antinode resulted in a different output characteristic from a similar test carried out at a stress anti-node, that is, at the displacement antinode the characteristic became non-linear. The horseshoe magnet transducer - shown in Figure (5.18) - operated in a similar manner to the "Kleesattel" transducer and was placed at a displacement antinode. There was, however, no evidence of non-linearity when the output of the horseshoe magnet transducer was checked against the output of the "Macdonald" probe, when drawing with the 7.5^{o} knife-edged dies. This is not surprising since the direct pressure on the die wave guides due to lateral die pressure, even when using the 2.5^{o} dies, was much less than the dynamic load applied to the strip when calibrating the "Kleesattel" transducer.

As already stated, the frequency response of the load cells and associated equipment was such that only the mean load could be recorded. The whole of the oscillatory load applied to the strip affected the tag load cell; this is not the case with the die load cell. The tuned frequency changes from 12.82 kHz with the 10^{o} dies at low reductions of area to 13.48 kHz with the 2.5^{o} dies at high reductions of area. This change, of approximately 5%, is ten times greater than that necessary to cause complete loss of amplitude when the wave guide was energised without

load and without the die in position. When the dies were positioned and unloaded they tended to flex which damped the amplitude of vibration and increased the tuned frequency. The frequency shift that occurred with variation in loading condition, Figure (7.94), will change the position of the nodal point on the die wave guide. The oscillatory load to which the die load cell was subject varied with loading conditions. That is, no attempt was made to alter the position of the support during the tests from their position set, at approximately 12.8 kHz, when the die wave guide was unloaded.

There was no significant high frequency movement of the dies parallel to the direction of strip motion, though a cyclic stress was induced in the bending load cells.

When using the knife edged dies at lower reductions of area, the surface of the strip was marked with a series of lines parallel to the die throat. These lines were pitched at 1mm or less; the pitch tending to increase with draw speed. At higher reductions of area, when the draw speed was, of necessity, low, this phenomenon was not so noticeable as the lines were pitched closer together and the surface condition of the strip was poor due to pick-up. These marks were not in evidence when the dies with a land were used.

Under conditions of poor lubrication, when using the 7.5^{o} dies at approximately 30% reduction of area at moderate draw speeds, a high amplitude, antiphase, bending mode vibration of the die wave guides was observed. This resulted in slight bending of the strip parallel to the die throat, pitched at approximately 15 mm. This phenomenon could be suppressed by increasing draw speed and improving the lubrication. The results recorded herein were free of this phenomenon, though it did not noticeably affect the process loads.

8.2. VARIATION OF PROCESS LOADS

8.2.1. Mean Strip Tension

The variation of mean strip tension with die angle reduction of area, draw speed and peak die velocity is shown in Figure (7.1) to Figure (7.31) inclusive. As already stated, the mean strip tension tends to increase with draw speed and decrease with peak die velocity. Within the range of die angles used in these tests the mean strip tension also tended to decrease with die angle.

The variation of the strip tension results, at the zero ordinate of peak die velocity, appeared to be rather high in certain cases. This condition corresponds to the conventional draw state which, in the absence of changes in frictional conditions, is independent of draw speed, since cold mild steel is insensitive to strain rate over a very wide range of strain rates.[75] This variation is most in evidence when the die angle is low, for example, when $\alpha = 2.5^{o}$, $r = 0.133$ (figure (7.1)) and $\alpha = 2.5^{o}$, $r = 0.250$ (figure (7.2)), or when the reduction of area is low, for example, at $\alpha = 7.5^{o}$ and $r = 0.187$ (figure (7.20)). Part of this is due to the use of straight lines drawn through each set of data. At some of these extreme conditions the graph would be better represented by a flattening of the curve as the conventional draw condition is approached. This is not the case in Figure (7.2) or Figure (7.20), where spread at the intercept is very uniform. The spread is not so uniform in Figures (7.1) and (7.14). In all of these examples the ratio between the length of the die/strip interface and the volume of the deformation zone is high, since the reduction of area was low. This implies that the proportion of frictional work is high. As the reduction of area and die angle are increased the graphs for the different draw speeds tend to converge to a single point. Increasing reduction of area appears therefore to result in

a stabilisation of frictional conditions. Combined with this is a reduction in the relative importance of the frictional energy, with respect to internal deformation energy, as both die angle and reduction of area are increased.

Attempts were made to use multiple regression of the data, with mean draw stress as a function of both peak die velocity and mean draw speed.

The following forms were used in these regression tests:

$$\bar{\sigma} = A\dot{\xi}V_c^{\,B} + C$$

$$\bar{\sigma} = A\dot{\xi} + BV_c^{\,B} + C$$

$$\bar{\sigma} = A\dot{\xi} + BV_c + C$$

All of these forms were unsuccessful as no clear trend was established. This may have been because the expressions were unrepresentative, or too naive. Alternatively the normal variation of these data could have swamped the effect of draw speed at the higher reductions of area.

The lack of success of this direct approach led to an investigation of the variation of the slopes and intercepts of each test run, whether the tests were of the arbitrary draw speed type or of the constant draw speed type. The data from each test run were subjected to a linear regression test. Some of the graphs resulting from these tests were substantially non-linear near to the coordinate axes; in these cases the slope and intercept were derived subjectively. The slopes, intercepts and correlation coefficients of these data are shown in Appendix (A3.2); the subjectively derived figures are marked with an asterisk, in which case the value given for the correlation coefficient is not valid since it refers to the regression line for the data set.

Constant Draw Speed Tests:- Referring again to Figures (7.1) to (7.31). Tests were carried out with the 2.5^{o} dies over a range of reductions of

area from r = 0.133 to the limiting value of r = 0.473 (Figures (7.1) to (7.6)), though the highest non-oscillatory reduction obtained was r = 0.267 (Figure (7.3)). Figures (7.1) to (7.4) show the results of the constant draw speed tests for the 2.5° dies; all of these tests show a linear relationship between mean strip tension and peak die velocity. The variation of the intercept with draw speed and reduction of area is shown in Figure (8.2).

It can be seen that the variation of intercept is very uniform, which indicates a change in frictional conditions with draw speed. This increase in the value of the intercept with draw speed indicates a break-down in boundary lubrication; the establishment of hydrodynamic lubrication would result in a reduction in draw stress with draw speed. The surface of the strip produced with these dies was highly burnished; the temperature generated at the higher reductions of area was high enough to cause lubricant to vaporise on one occasion.

The variation of the intercepts for the 5° dies is shown in Figure (8.3). It can be seen that the effect of draw speed is much less marked. There is no clear dependence upon this variable, that is, stable frictional conditions were established; there was no obvious excessive temperature rise. Similar data for the 7.5° dies are shown in Figure (8.4). At reductions of area of r = 0.267, r = 0.307 and r = 0.387 the intercept is sensibly independent of draw speed, with a slight tendency to decrease with draw speed. The results at reductions of area of r = 0.163 and r = 0.362 are similar to those for the 5° dies in that the intercept tends to increase with draw speed. The general trend of the intercept to increase with draw speed for the 7.5° with land dies is similar to that for the 2.5° dies, see Figure (8.5). This is probably due to the large land on the die which had no potential to retain the lubricant between the die and the strip. The boundary lubrication film was broken down, as with the 2.5° dies and the strip was similarly burnished, though there was no evidence

of undue temperature rise.

The intercepts for the 10^{o} dies are totally unaffected by draw speed over the speed range used in the tests, as shown in Figure (8.6); this again indicates that frictional conditions were stable. The variation of the virtual intercepts is shown in Figure (8.7).

The variation of the slopes of the regression lines with mean draw speed and peak die velocity for the 2.5^{o}, 5^{o}, 7.5^{o} - with-land, and 10^{o} dies are shown in Figure (8.8) to Figure (8.12) respectively. The results for the 2.5^{o} dies shown in Figure (8.8) give no clear indication of the effect of reduction of area upon the rate of change of strip tension with peak die velocity; these results only range between $r = 0.133$ and $r = 0.280$ so this is, perhaps, not surprising. The slope, between 0 and 60 mm/sec shows a slight tendency to become increasingly negative, then increases. The point (118, 0.83) in Figure (8.8) is derived from the 118 mm/sec test run in Figure (7.2); this result deviates significantly from the other results taken at this reduction of area, therefore the point (118, 0.83) is probably erroneous.

The results for the 5^{o} dies (Figure (8.9)) also indicate that the reduction of area has little effect although there is a general tendency for the slope to become increasingly negative. These results only extended to draw speeds of 60 mm/sec and there was no indication of a minima, as there was with the 2.5^{o} dies.

The results for the 7.5^{o} dies are shown in Figure (8.10). These characteristics differ markedly from those of the 2.5^{o} and 5^{o} dies; the slope becomes less negative as draw speed increases. Reduction of area also has a marked effect; the slope becomes increasingly negative as reduction of area is increased. This trend is continued with the 7.5^{o} with-land and 10^{o} dies as shown in Figure (8.11) and Figure (8.12) respectively, though the effect of reduction of area is not so great.

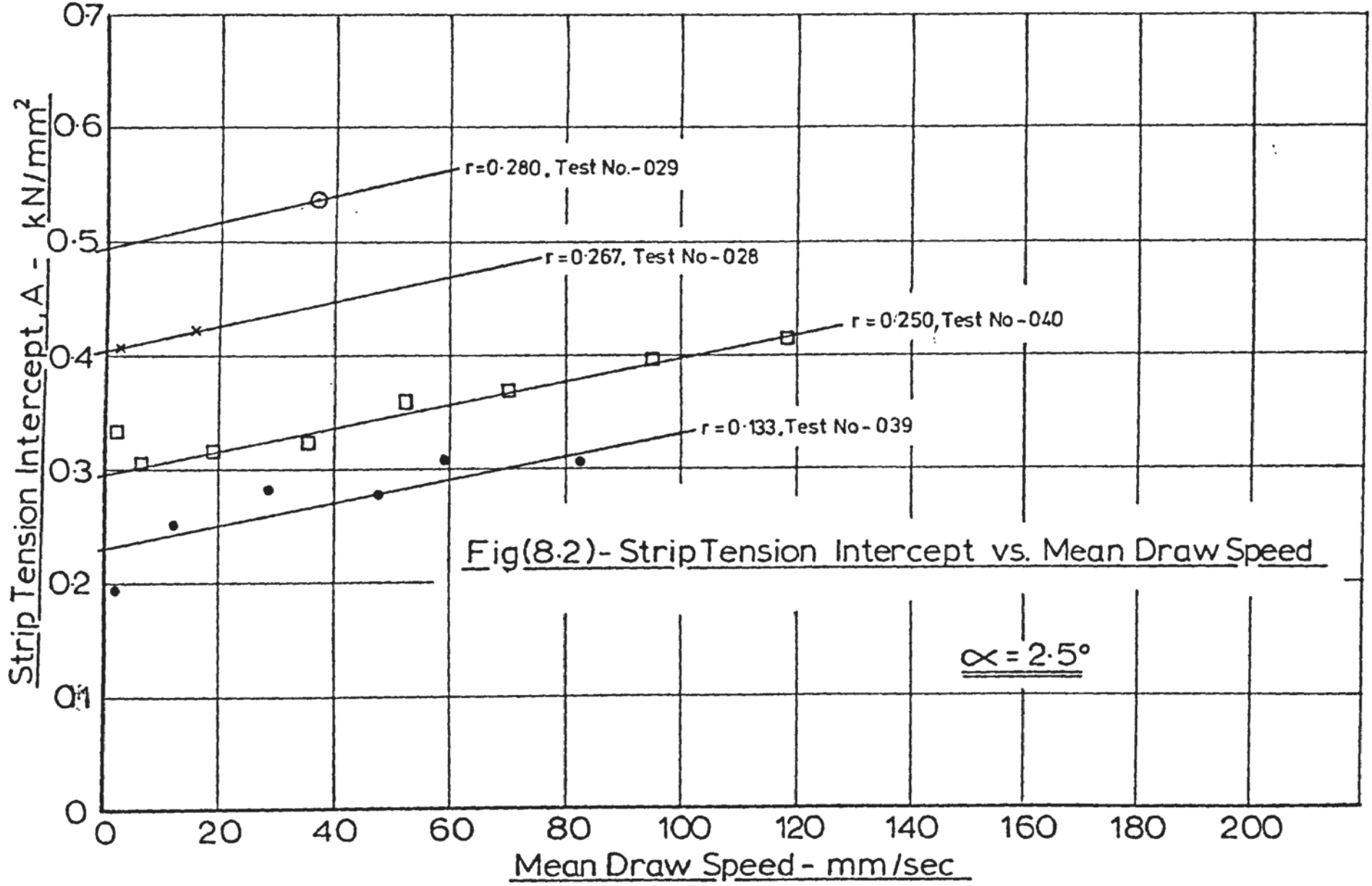

Fig(8·2)- Strip Tension Intercept vs. Mean Draw Speed

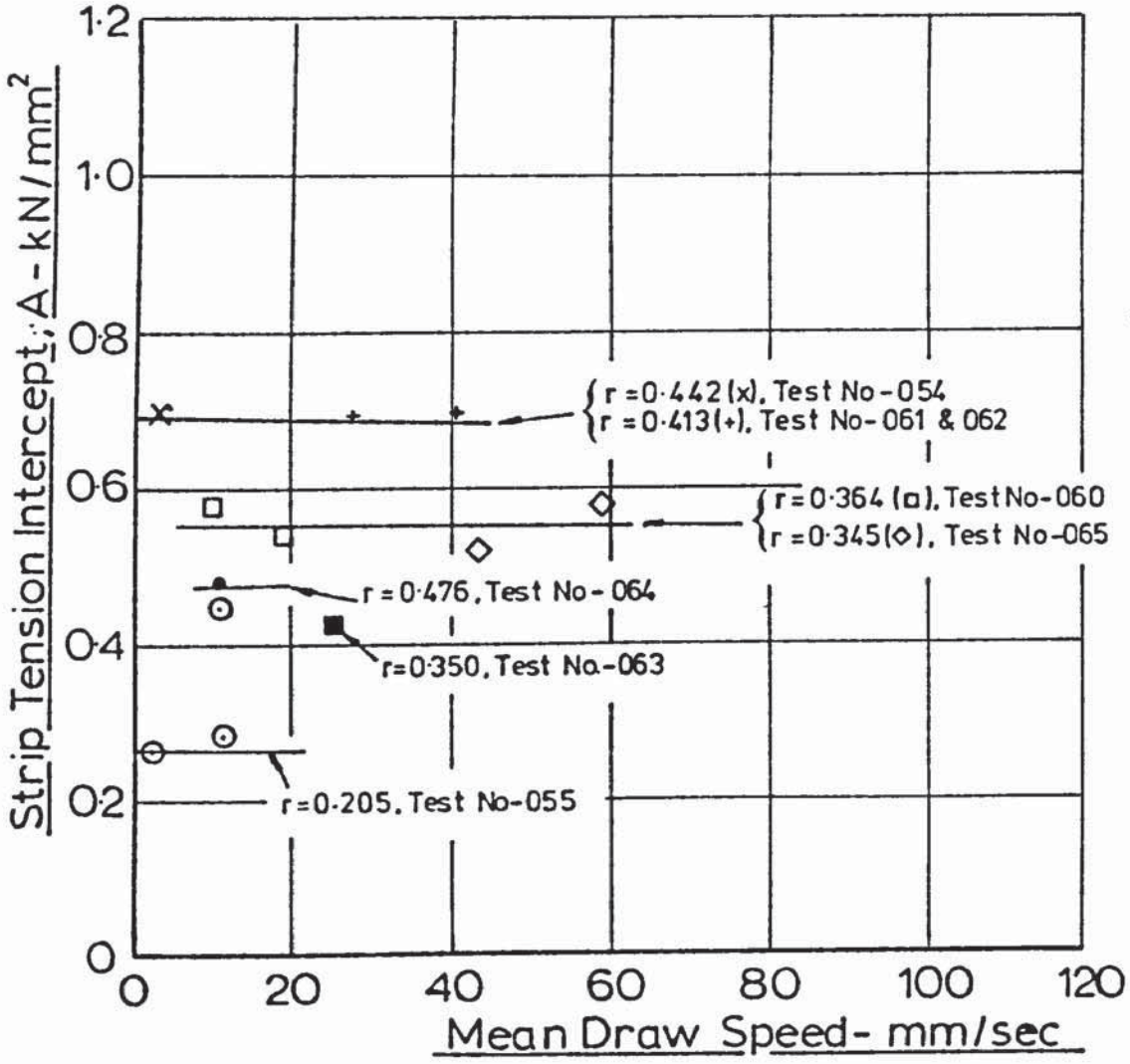

Fig(8·3) - Strip Tension Intercept vs. Mean Draw Speed

$\alpha = 5°$

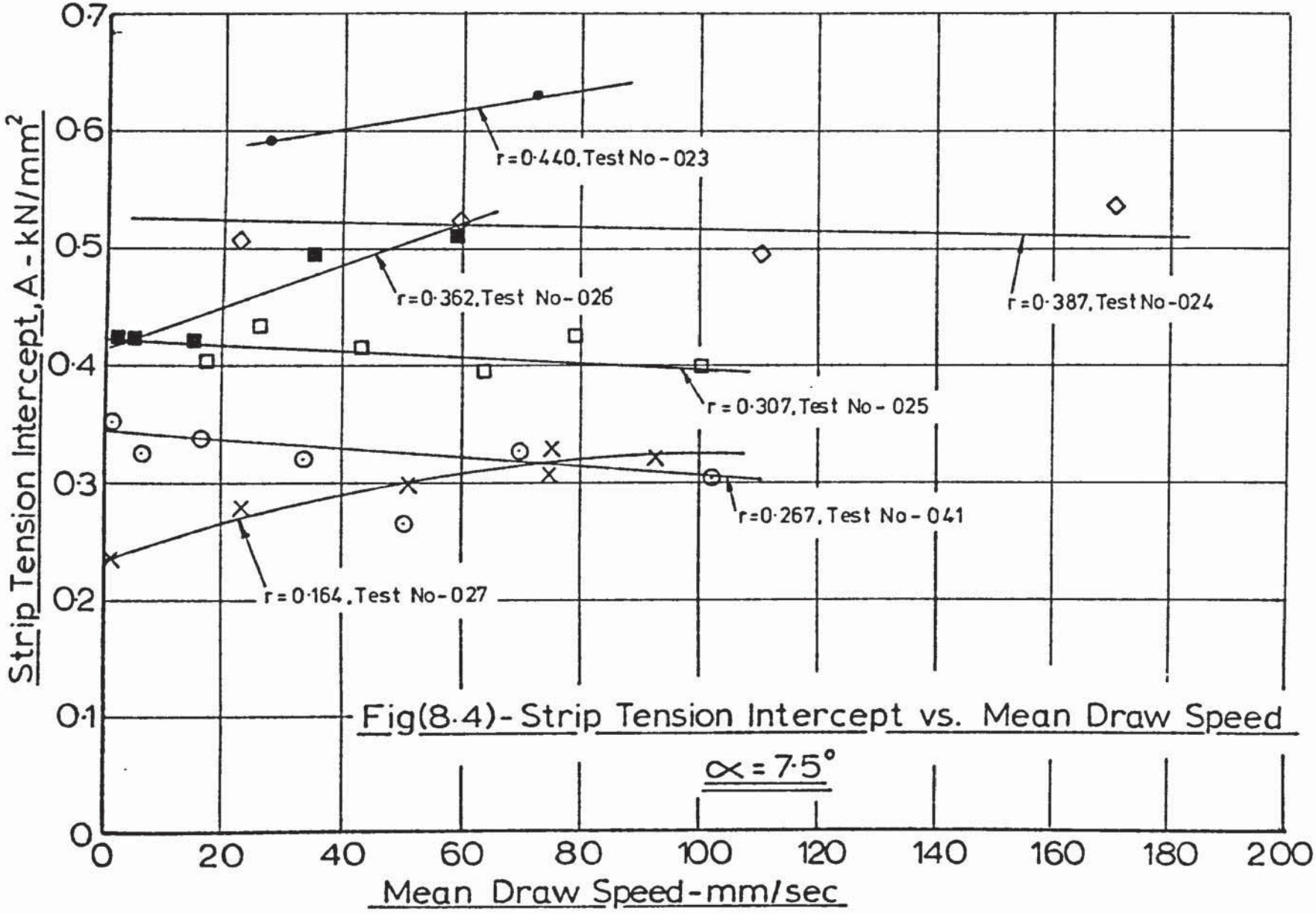

Fig(8·4) - Strip Tension Intercept vs. Mean Draw Speed

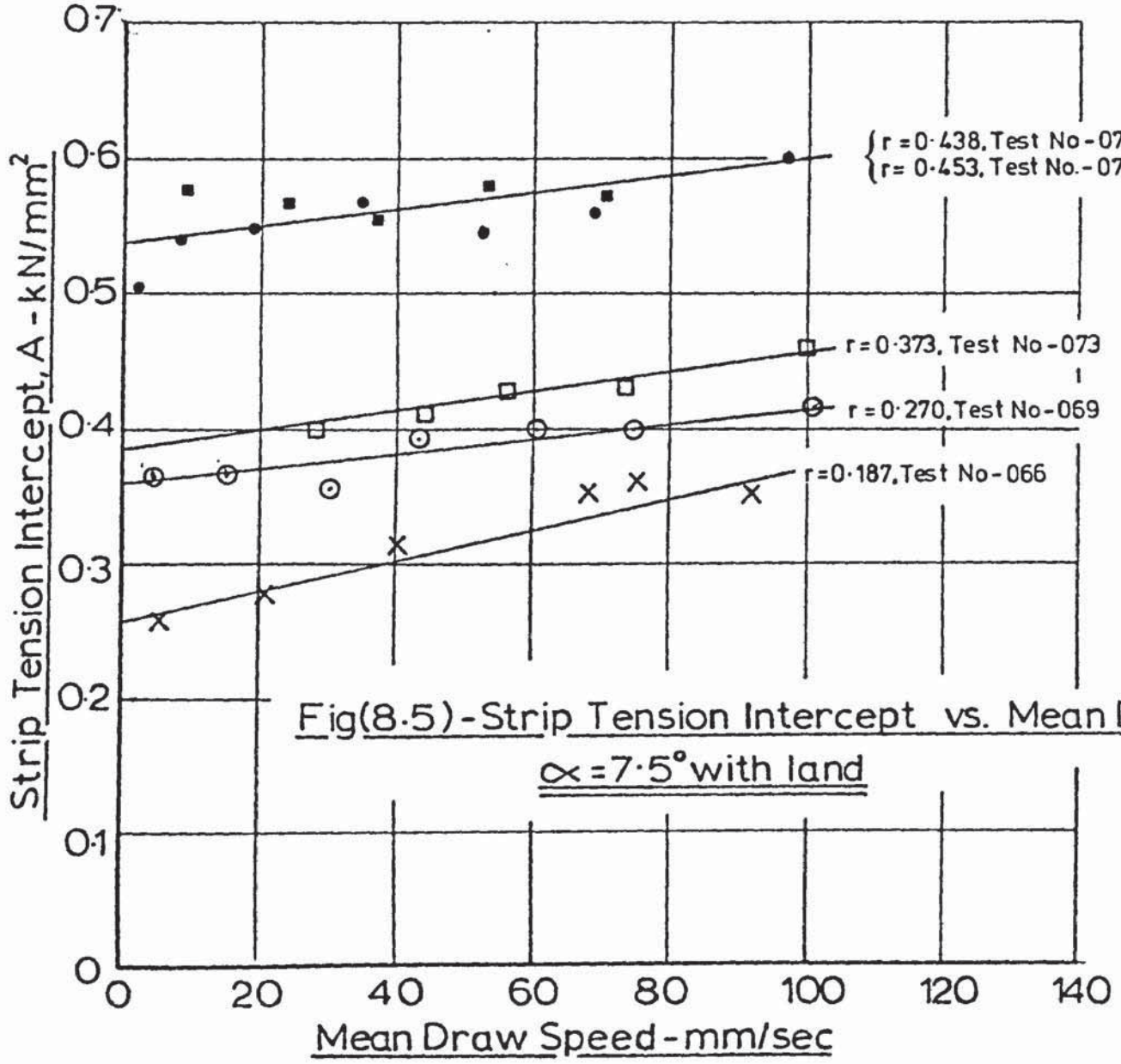

Fig(8.5) - Strip Tension Intercept vs. Mean Draw Speed

$\alpha = 7{\cdot}5°$ with land

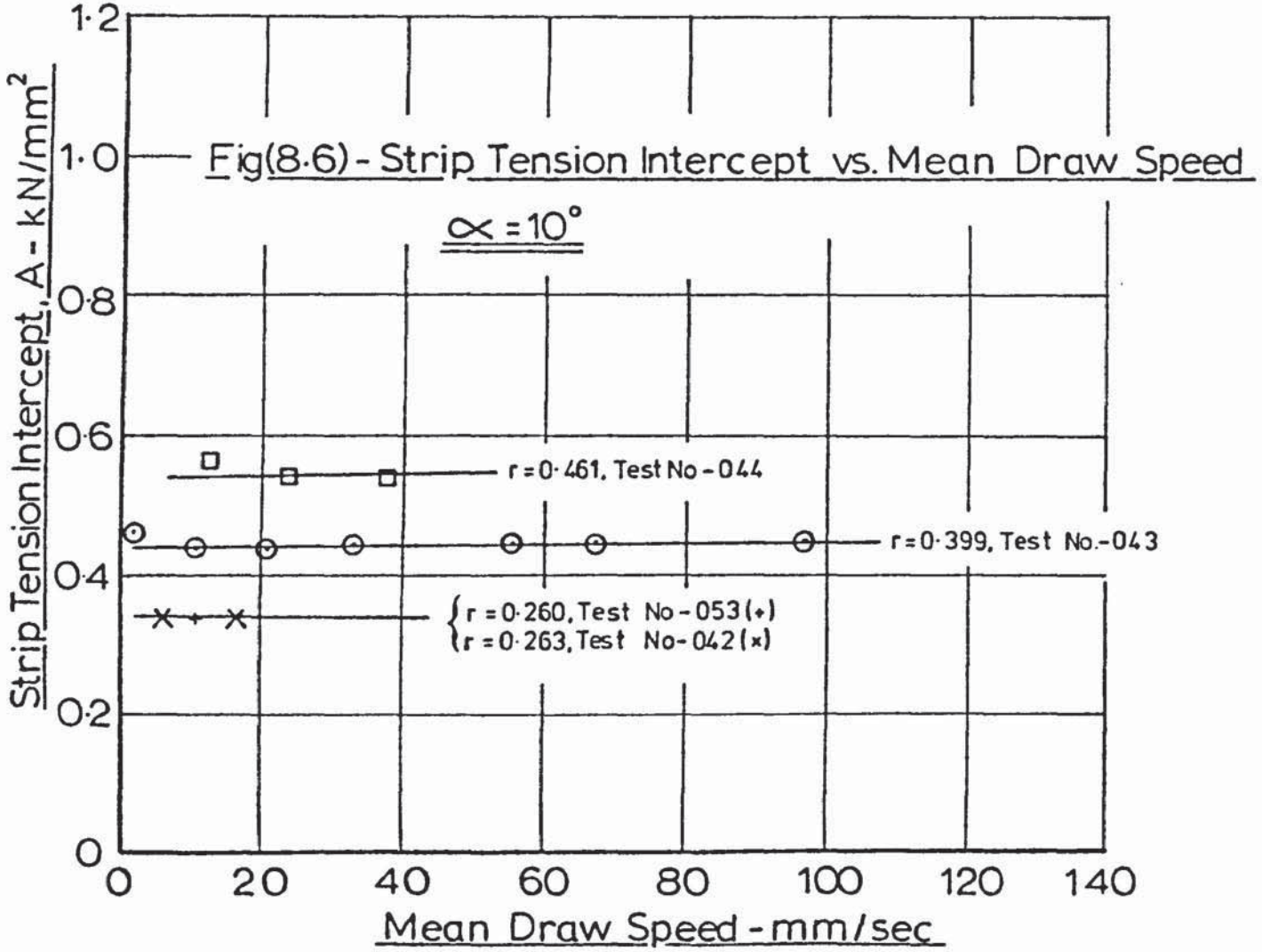
Fig(8.6) - Strip Tension Intercept vs. Mean Draw Speed
∝ = 10°
Strip Tension Intercept, A - kN/mm²
Mean Draw Speed - mm/sec
1·2
1·0
0·8
0·6
0·4
0·2
0
0
20
40
60
80
100
120
140
r = 0·461, Test No - 044
r = 0·399, Test No.-043
r = 0·260, Test No - 053 (+)
r = 0·263, Test No - 042 (×)

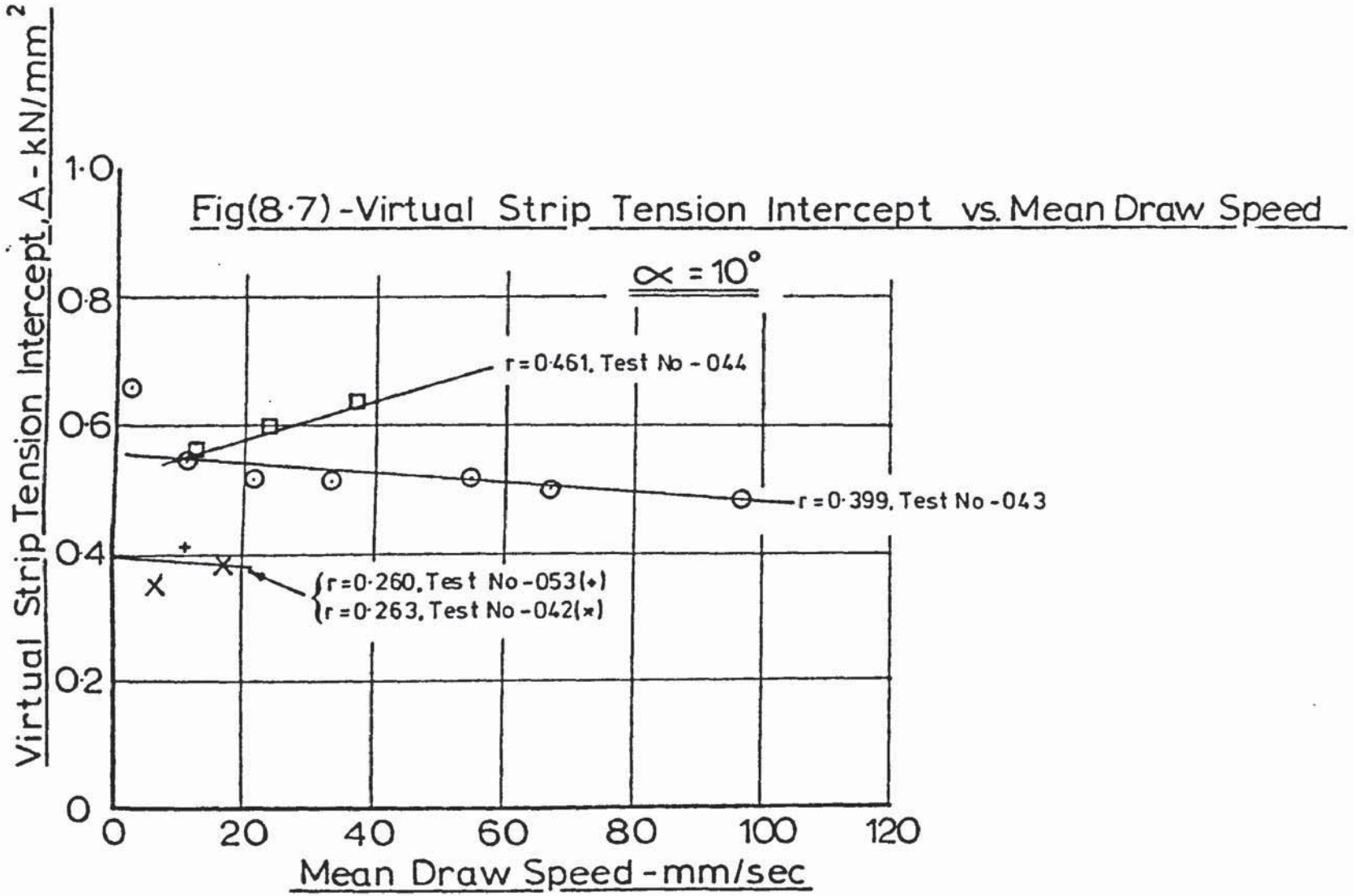

Fig(8·7) - Virtual Strip Tension Intercept vs. Mean Draw Speed

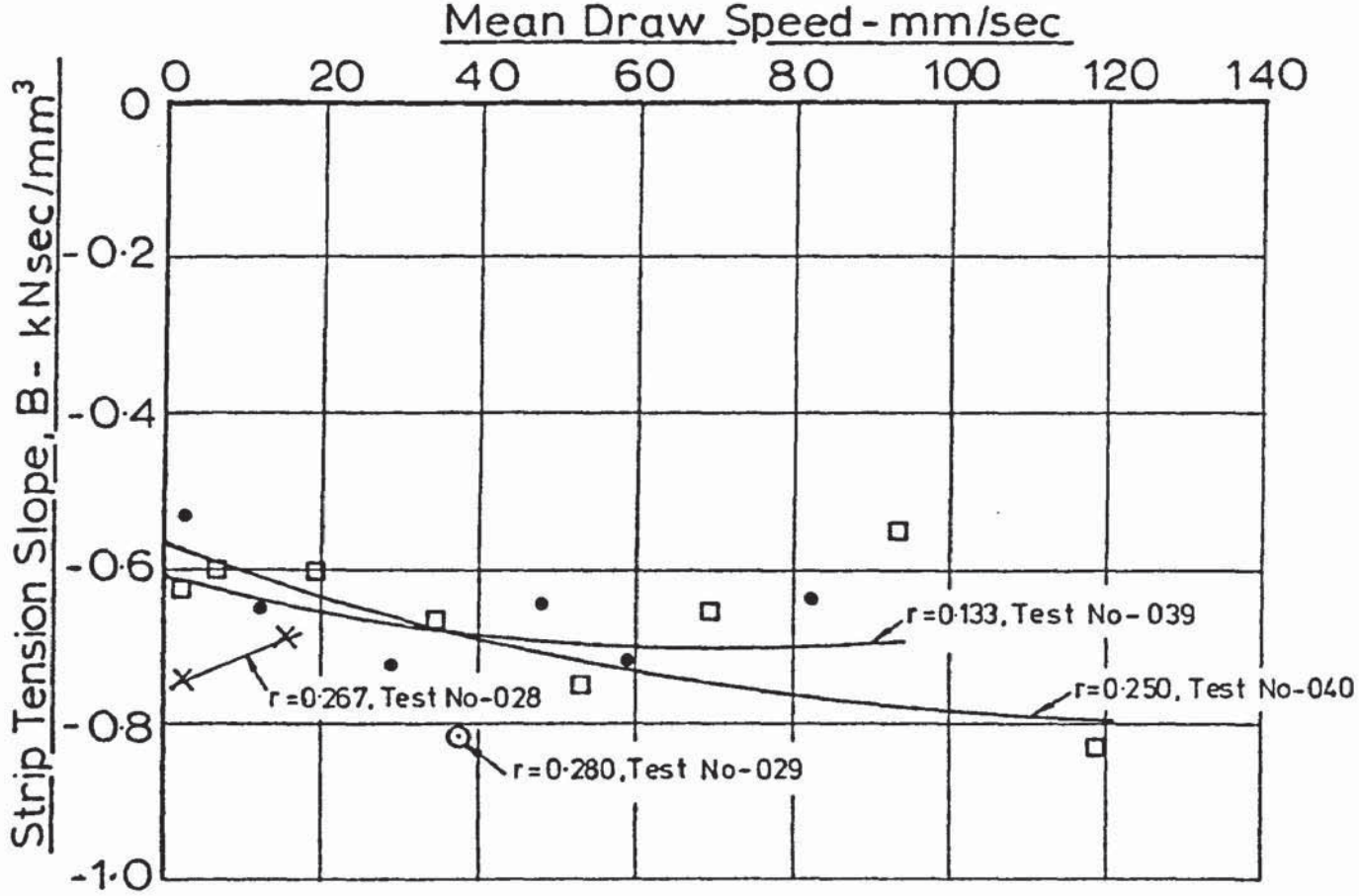

Fig(8·8) - Strip Tension Slope vs. Mean Draw Speed

$\alpha = 2.5°$

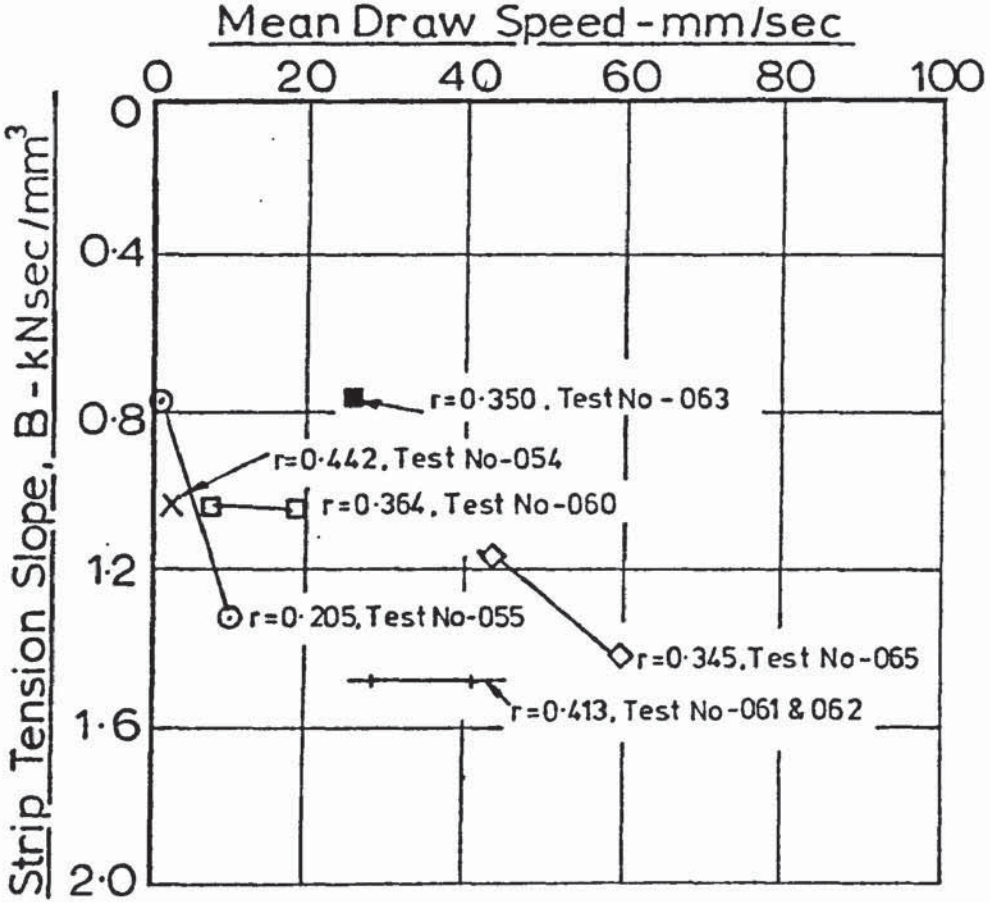

Fig(8.9) - Strip Tension Slope vs. Mean Draw Speed

$\alpha = 5°$

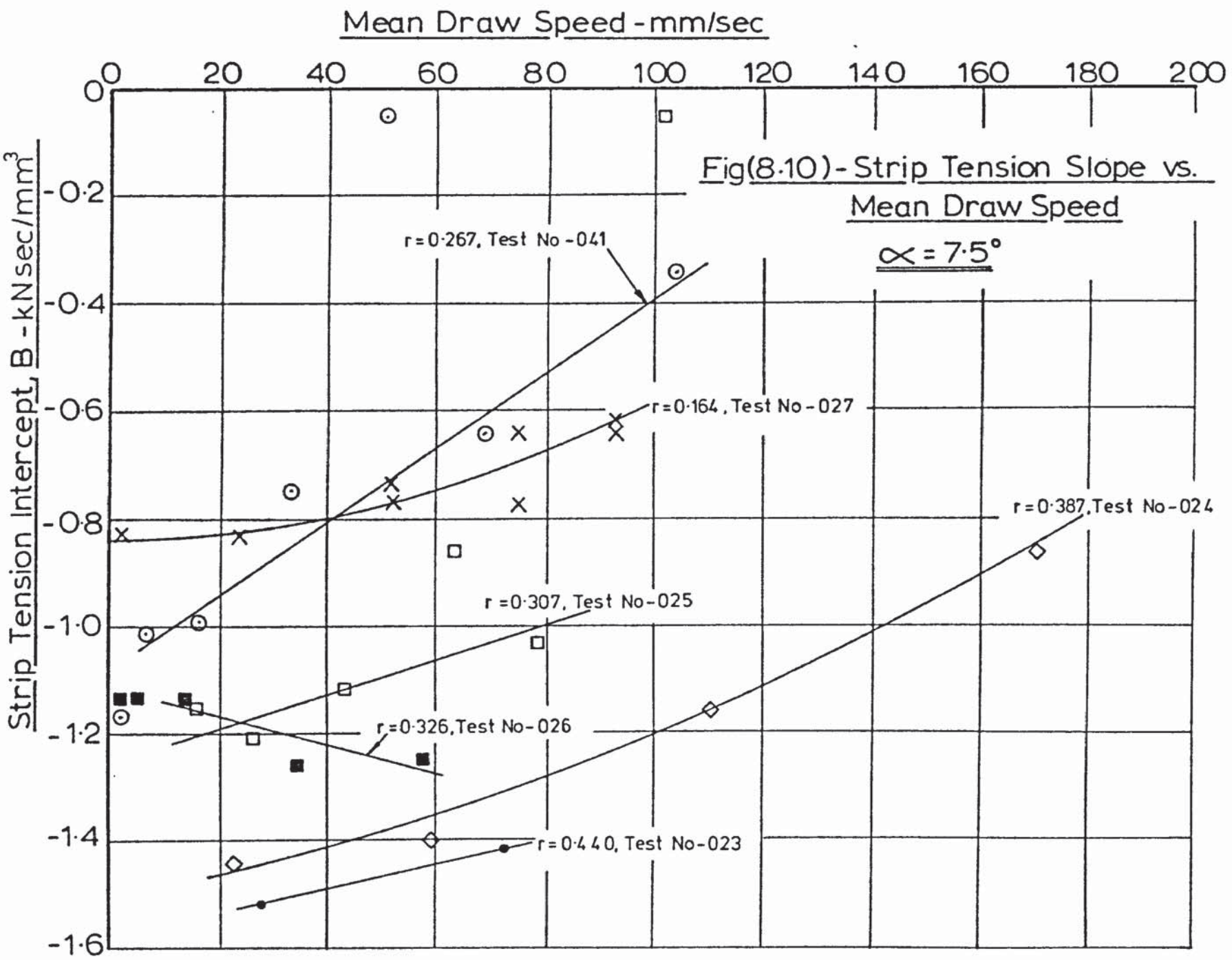
Mean Draw Speed - mm/sec
0
20
40
60
80
100
120
140
160
180
200
Strip Tension Intercept, B - kN sec/mm³
-0·2
-0·4
-0·6
-0·8
-1·0
-1·2
-1·4
-1·6
Fig(8·10) - Strip Tension Slope vs. Mean Draw Speed
∝ = 7·5°
r = 0·267, Test No - 041
r = 0·164, Test No - 027
r = 0·387, Test No - 024
r = 0·307, Test No - 025
r = 0·326, Test No - 026
r = 0·440, Test No - 023

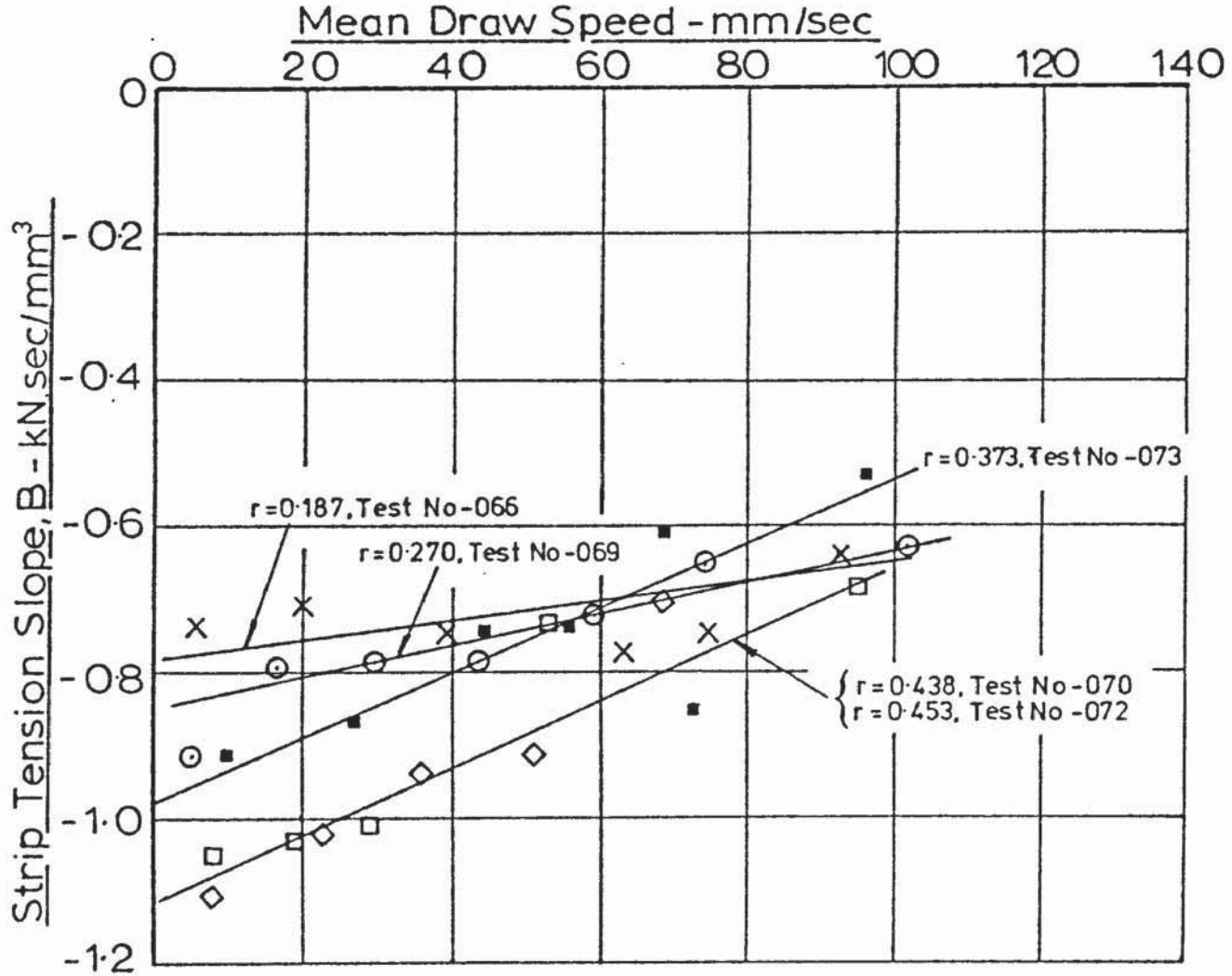

Fig(8·11) - Strip Tension Slope vs. Mean Draw Speed

$\alpha = 7.5°$ with land

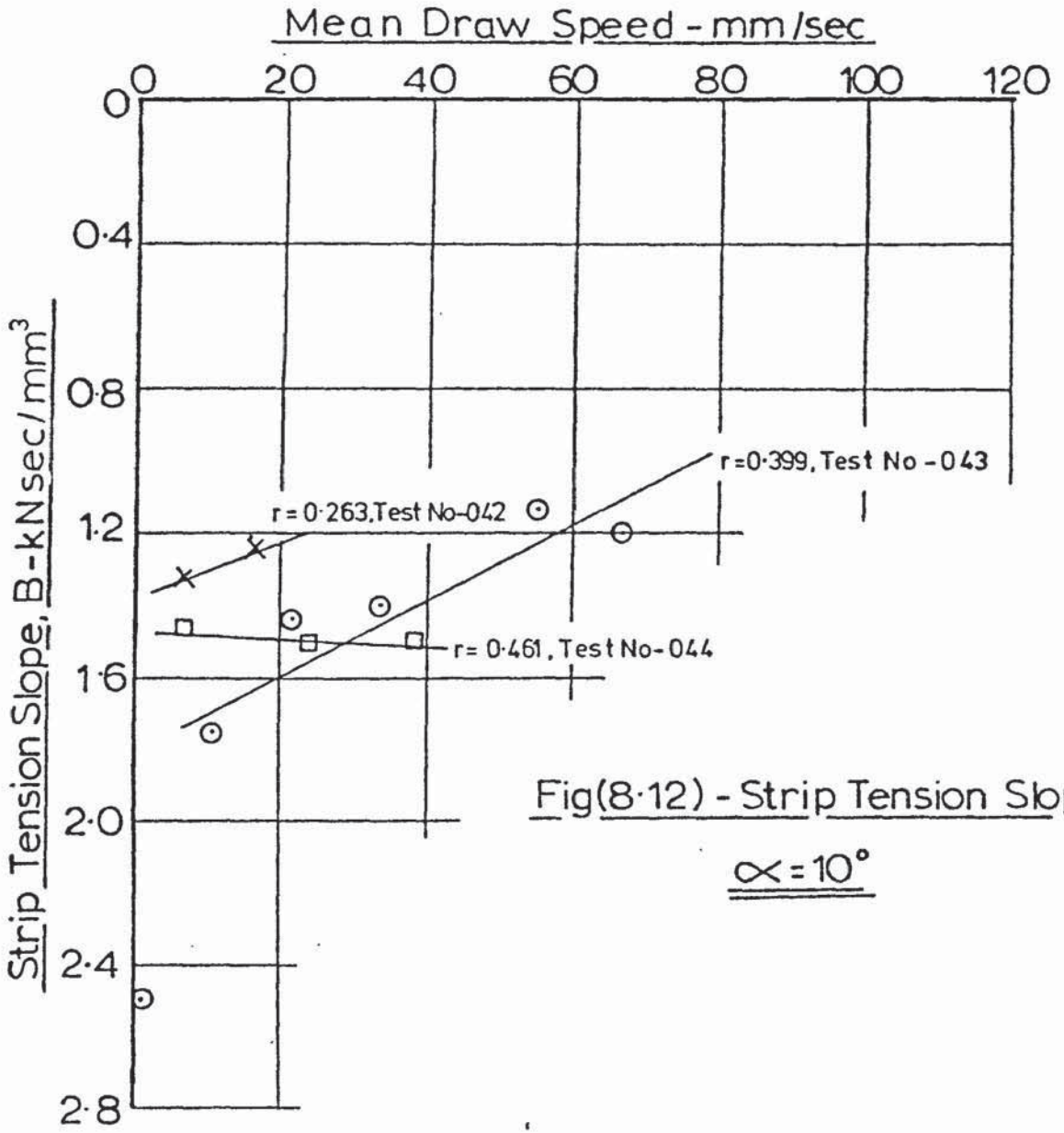

Fig(8·12) - Strip Tension Slope vs. Mean Draw Speed

$\alpha = 10°$

The tendency for the slope to become less negative as the draw speed increased is to be expected since the proportion of the total deformation energy due to pure drawing, for a given die angle and peak die velocity, will increase as mean draw speed increases. Similarly the rate of strain take-up down-stream of the die will increase, causing an increase in mean strip tension. The effect of draw speed appears to be less great when the intercept is subject to change due to increasing friction; for example, by comparing the results for the 2.5^{o} die (Figure (8.2) and Figure (8.8)) with the results for the 7.5^{o} dies (Figure (8.4) and Figure 8.7)). In the latter case the result for the 16% reduction of area tends to confirm this since the test run was clearly affected by the change in frictional conditions (Figure (7.13)), whilst the others were not (Figures (7.14) to (7.19)).

Constant Power Tests: The results of the constant power tests at the higher reductions of area also showed a high degree of linearity between mean strip tension and peak die velocity. At lower reductions of area, for example, $r = 0.280$ (Figure (7.5)), the draw speed was varied over a wide range at various levels of acoustic power input. The regression line drawn through such data is therefore of a slightly different nature from the line drawn through constant draw speed data; the absolute value of the slope and the value of virtual intercept was increased. The reason for this was that, at high reductions of area, the tests were started at low draw speed with full acoustic power input. As the draw speed was increased the peak die velocity decreased. Both of these tendencies increase mean strip tension, therefore the resultant regression line would span a set of constant velocity data.

The effect of allowing mean draw speed to vary is probably not so significant at high reductions of area. This is because the effect of mean draw speed appears to reduce as the reduction of area is increased. Thus, deviation of the slope from that of the constant

draw speed data is generally of a relatively low order. This can be seen by comparing Figures (7.18) and (7.19), test 010 and Figures (7.30) and (7.31) test numbers (045) and (046).

Consolidation Of The Draw Test Data

Figures (8.13) to (8.22) show the five sets of strip tension data extracted from the results of the constant draw speed tests, given in Figures (8.2) to (8.12), and the results of the constant power tests, shown in Appendix A3.2. These graphs show the variation of virtual intercept and slope of the mean strip tension and peak die velocity set against reduction of area and mean draw speed.

The greatest amount of data was collected for the 7.5^{o} dies. There are two main reasons for this. These dies were the first to be used and the the author was, therefore, still gaining experience on the use of the test rig and the manner in which the process loads varied. It also happened that the 7.5^{o} dies gave the most stable drawing conditions; the lower die angles did not yield such high reductions of area and the 10^{o} dies provided so little constraint on the strip that it easily slipped from the sides of the dies. It therefore proved difficult to obtain results over a wide range of draw speeds with the 10^{o} dies, especially at low reductions of area.

Figures (8.23) to (8.27) show the variation of mean strip tension with peak die velocity, reduction of area, and mean draw speed for the various die angles. These figures have been constructed from the relevant graphs of virtual intercept and slope plotted against reduction of area. In the cases where virtual intercept deviates from the actual intercept, or is not reached due to strip failure, the graphs were modified accordingly by reference to the test data shown in Figures (7.1) to (7.31). The term virtual intercept refers to the intercept projected from the straight line portion of the graph.

The aim of constructing the graphs shown in Figures (8.23) to (8.27) is to enable direct comparisons to be made between the various die profiles. This aim has been largely fulfilled although the quality and quantity of these data vary from one set to another. For example, data derived from the tests with the 5^{o} dies were insufficient for the effect of mean draw speed to be established, and the scatter of slope and intercept was of a relatively high order.

The limiting reduction of area at zero peak die velocity increases from approximately 30% with the 2.5^{o} dies to 45% with the 10^{o} dies. This is consistent with the general trend of the results which show an increase in limiting reduction of area with increasing die angle. The extent to which these two factors are interdependent is not clear. The optimal die angle in pure strip drawing and wire drawing is determined by minimising the energy expended upon frictional work and redundant deformation and is dependent also upon reduction of area. The 2.5^{o} dies would only be optimal at low reductions of area whilst the 10^{o} dies would be optimal at reductions of area between 30% and 40%[2][7]. When mandrel drawing through a vibrating die, Biddell[18] used die angles of up to 17^{o} without finding a minimium in the relationship between draw stress, die angle and reduction of area. Ideally, therefore, further tests should be carried out with die angles in excess of 10^{o}, in order to find this relationship for strip drawing through vibrating dies.

The reduction of area that can be achieved without the use of ultrasound, that is, at zero peak die velocity, increases from 0.4 kN/mm^2 at 30% reduction of area with the 2.5^{o} dies to 0.52 kN/mm^2 at 45% reduction of area with the 10^{o} dies. This indicates the shift in optimal die angle with reduction of area. The limiting reduction of area increases from less than 50% with the 2.5^{o} dies to 80% with the 7.5^{o}

and 10^{o} dies though, as already stated, the failure mode changed from ductile overload to fatigue at reductions of area in excess of 60%. These graphs also illustrate the increase in the rate of decrease of mean strip tension with peak die velocity as die angle, reduction of area and mean draw speed are increased.

Fig(8·13) - Strip Tension Intercept vs. Reduction Of Area

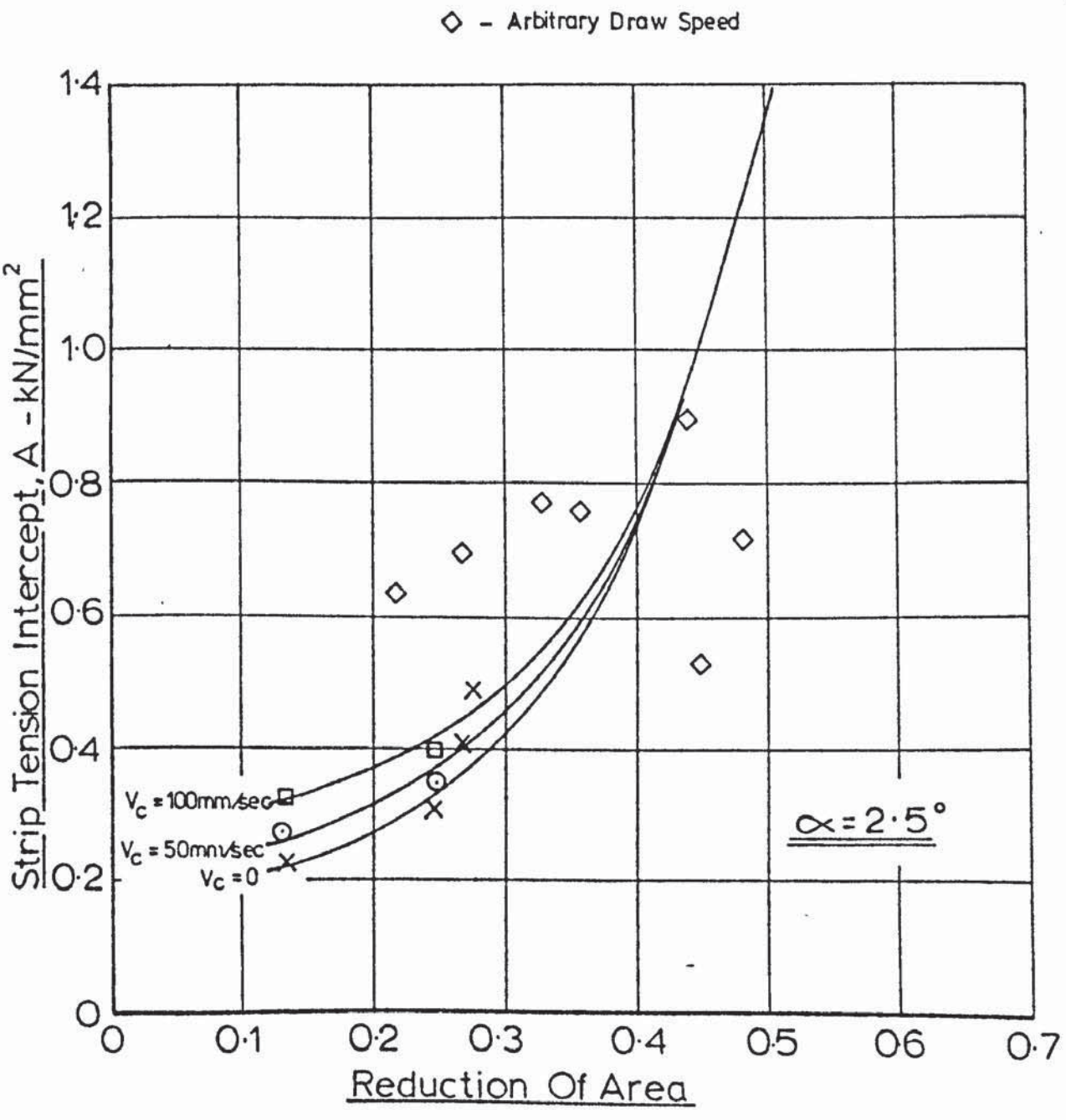

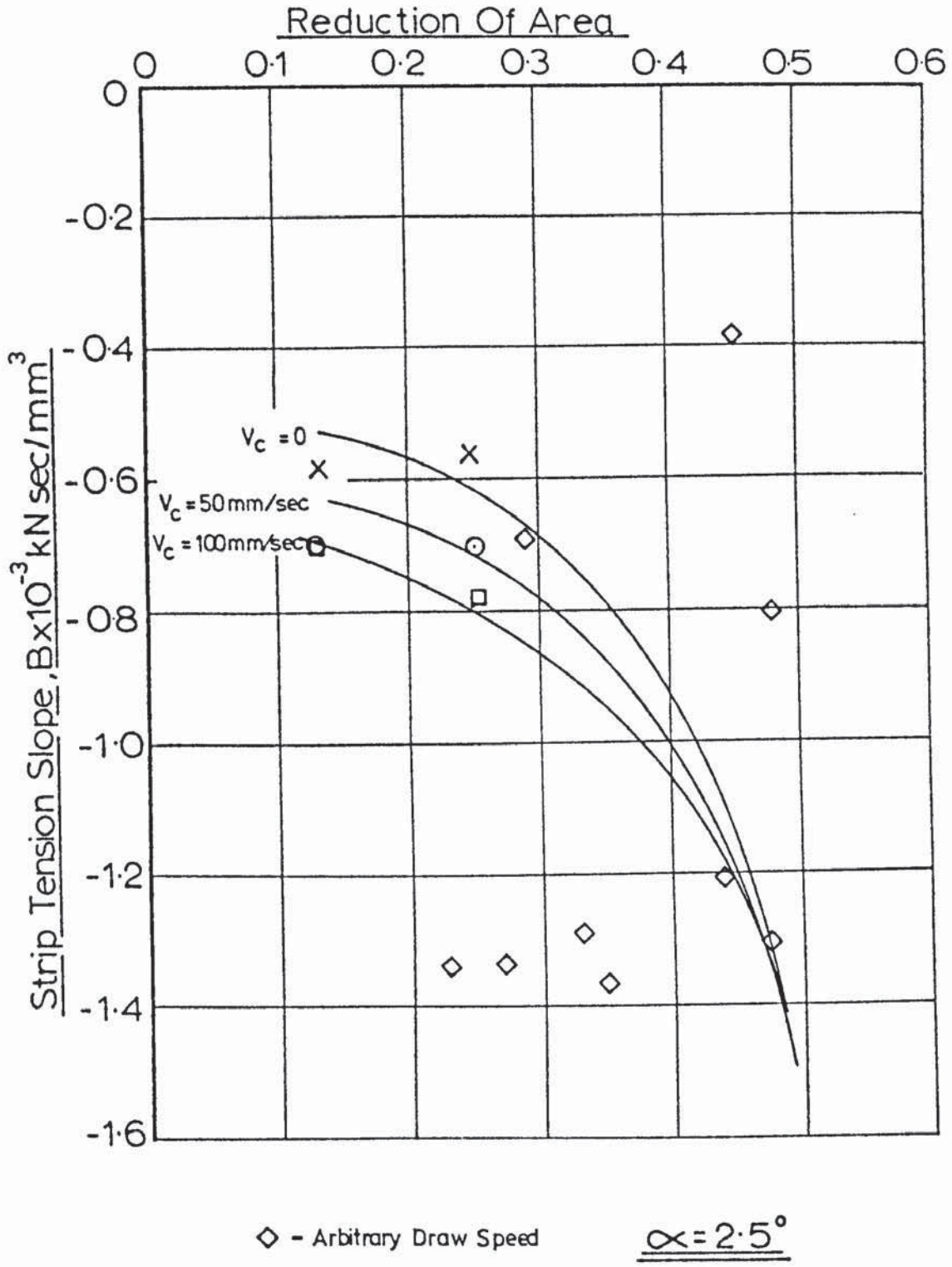

Fig(8·14) - Strip Tension Slope vs. Reduction Of Area

Fig(8·15) - Strip Tension Intercept, A vs. Reduction Of Area

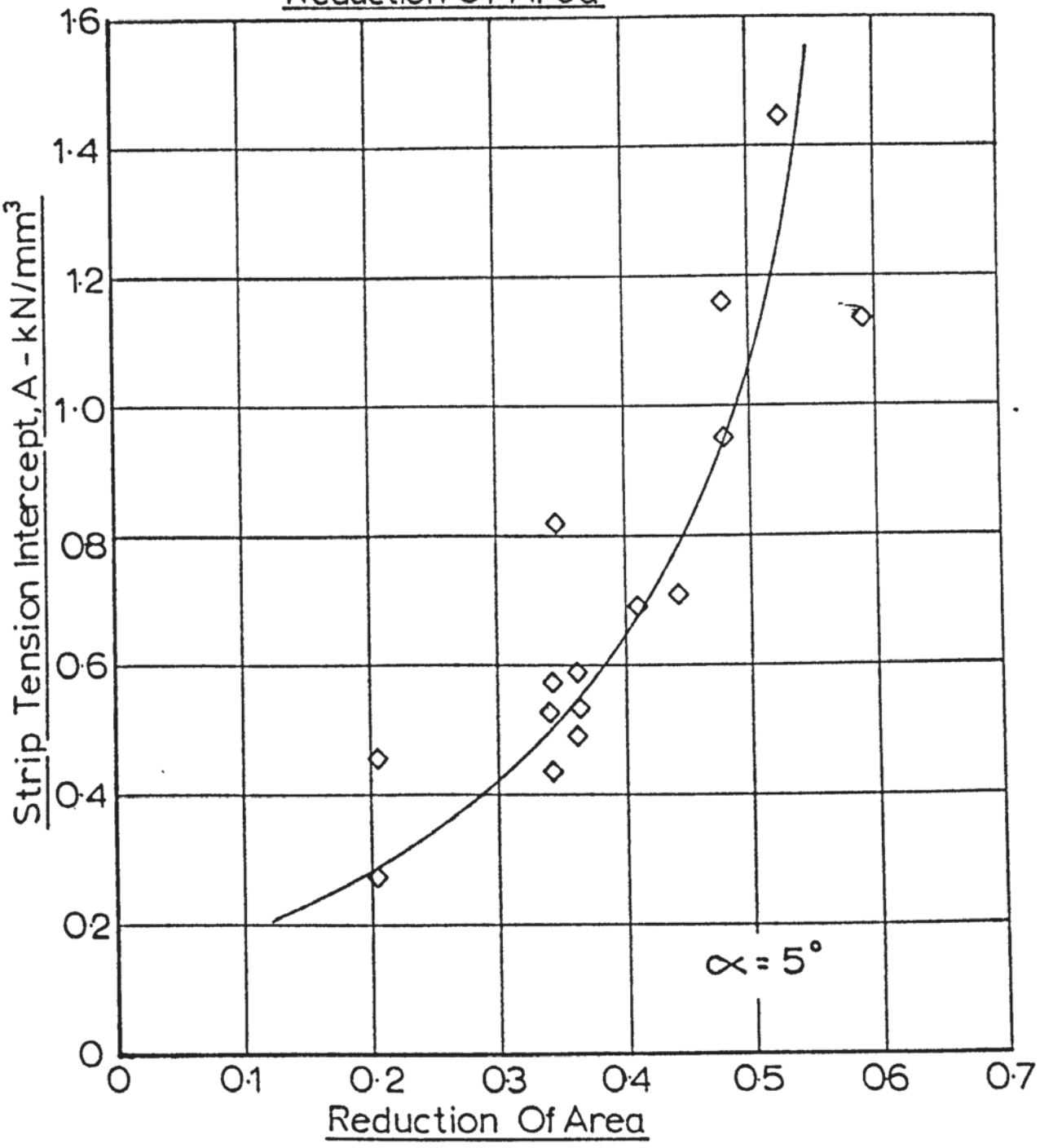

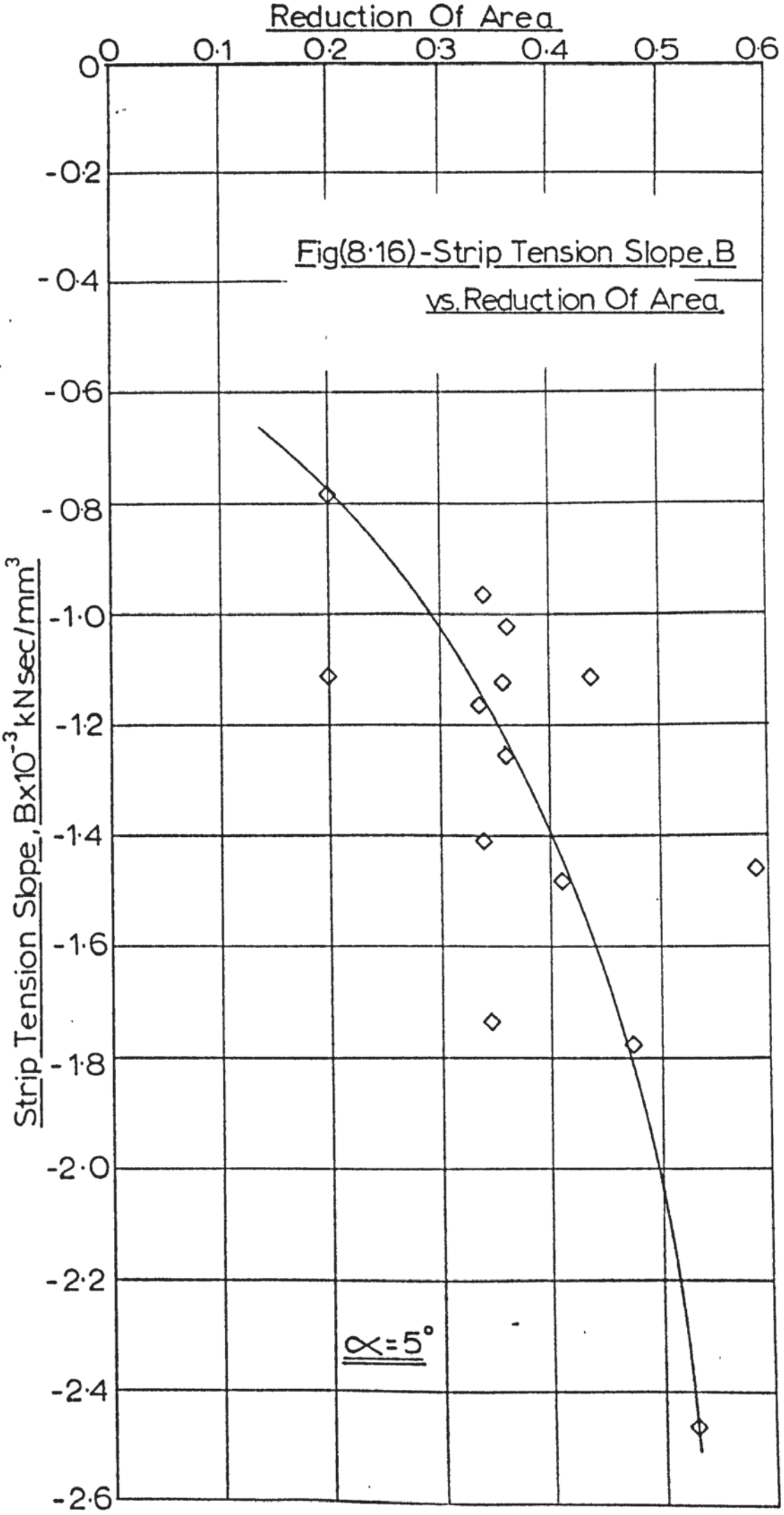
Reduction Of Area
0
0·1
0·2
0·3
0·4
0·5
0·6
-0·2
-0·4
-0·6
-0·8
-1·0
-1·2
-1·4
-1·6
-1·8
-2·0
-2·2
-2·4
-2·6
Strip Tension Slope, $B \times 10^{-3}$ kN sec/mm^3
Fig(8·16)-Strip Tension Slope, B
vs. Reduction Of Area.
$\alpha = 5°$

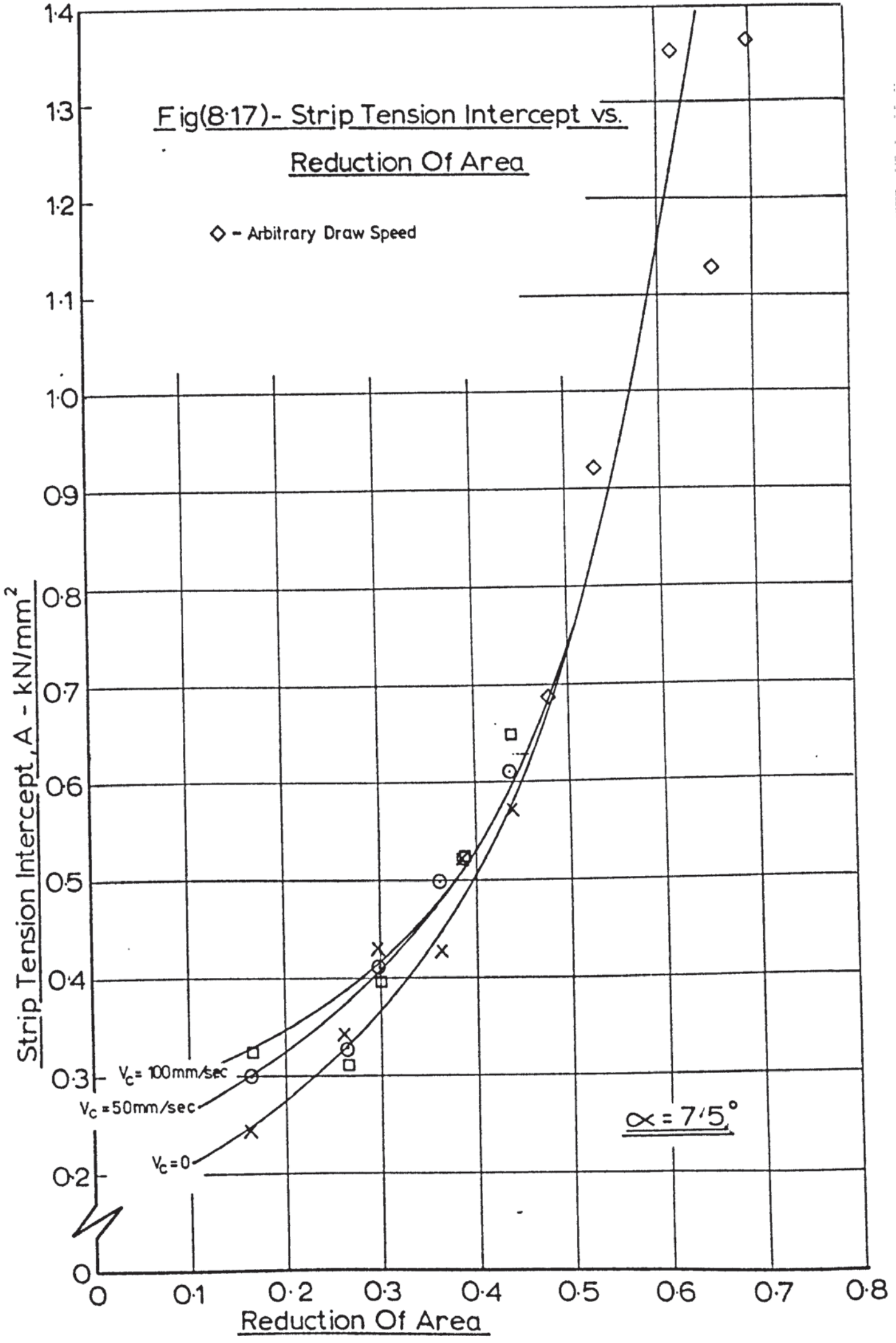
Fig(8·17)- Strip Tension Intercept vs. Reduction Of Area
◇ - Arbitrary Draw Speed
Strip Tension Intercept, A - kN/mm²
Reduction Of Area
1·4
1·3
1·2
1·1
1·0
0·9
0·8
0·7
0·6
0·5
0·4
0·3
0·2
0
0·1
0·2
0·3
0·4
0·5
0·6
0·7
0·8
Vc = 100mm/sec
Vc = 50mm/sec
Vc = 0
∝ = 7·5°

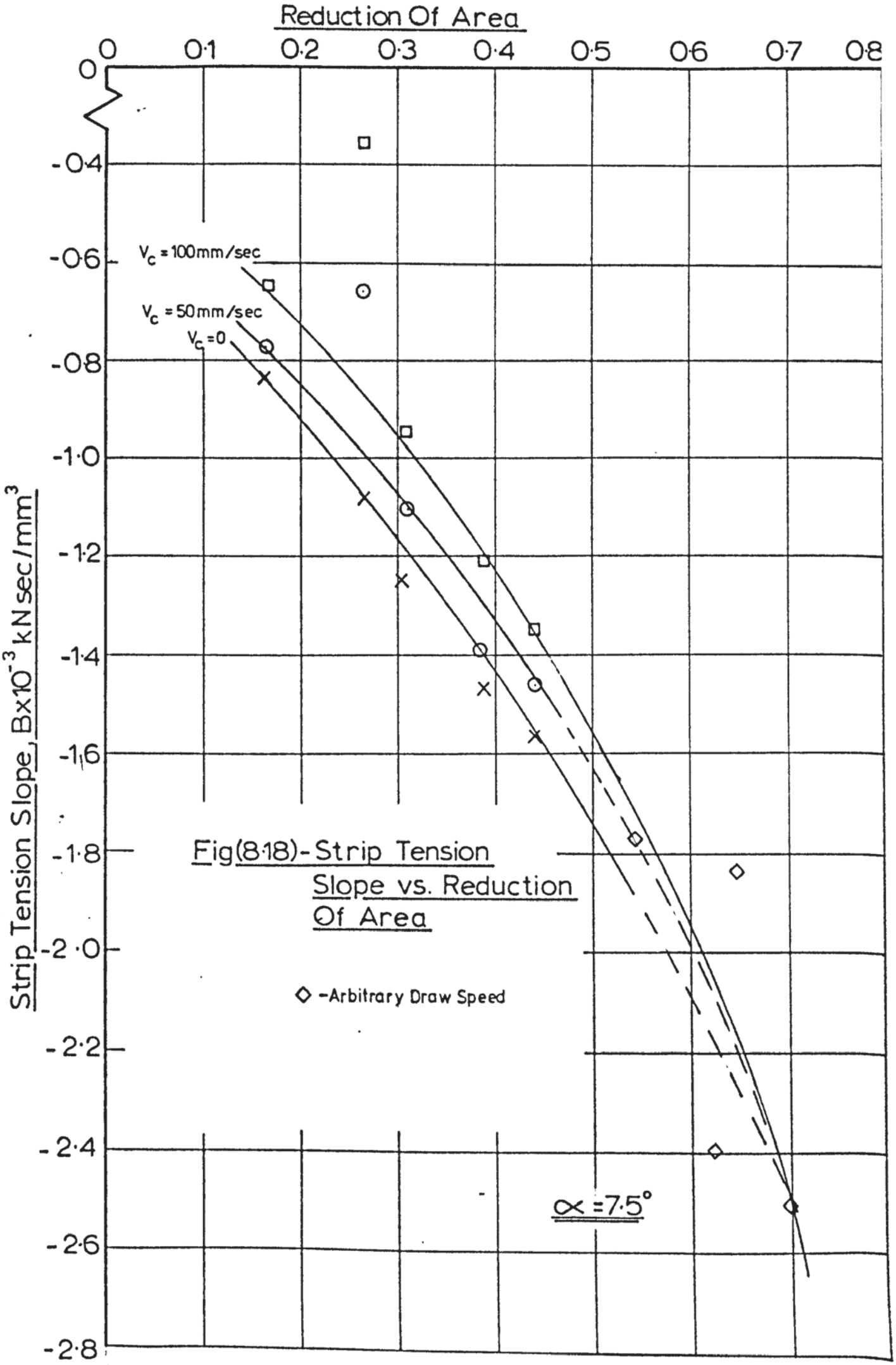

Fig(8·18)- Strip Tension Slope vs. Reduction Of Area

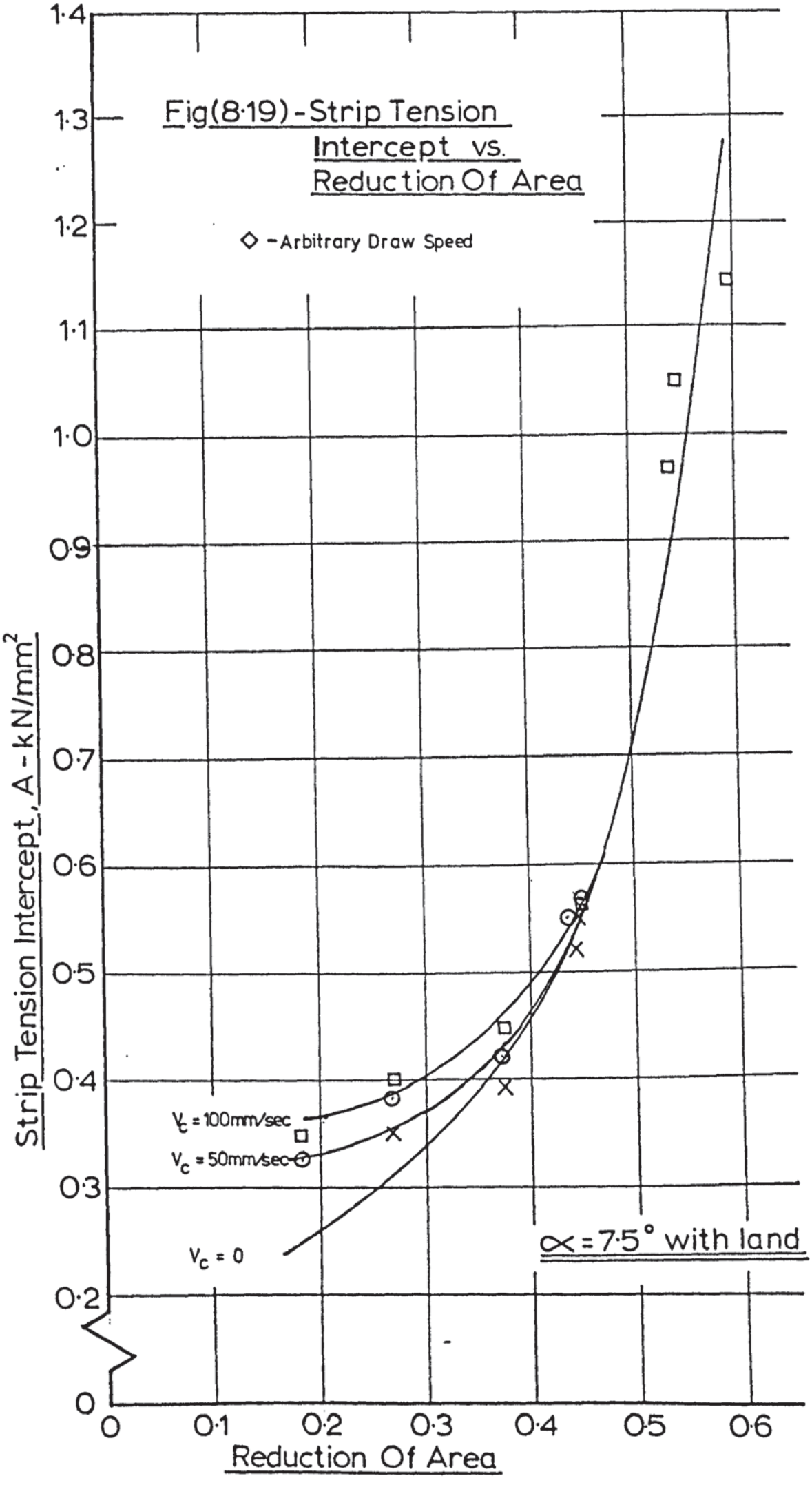
Fig(8·19) - Strip Tension Intercept vs. Reduction Of Area
◇ - Arbitrary Draw Speed
Strip Tension Intercept, A - kN/mm²
Reduction Of Area
V_c = 100mm/sec
V_c = 50mm/sec
V_c = 0
∝ = 7·5° with land
1·4
1·3
1·2
1·1
1·0
0·9
0·8
0·7
0·6
0·5
0·4
0·3
0·2
0
0·1
0·2
0·3
0·4
0·5
0·6

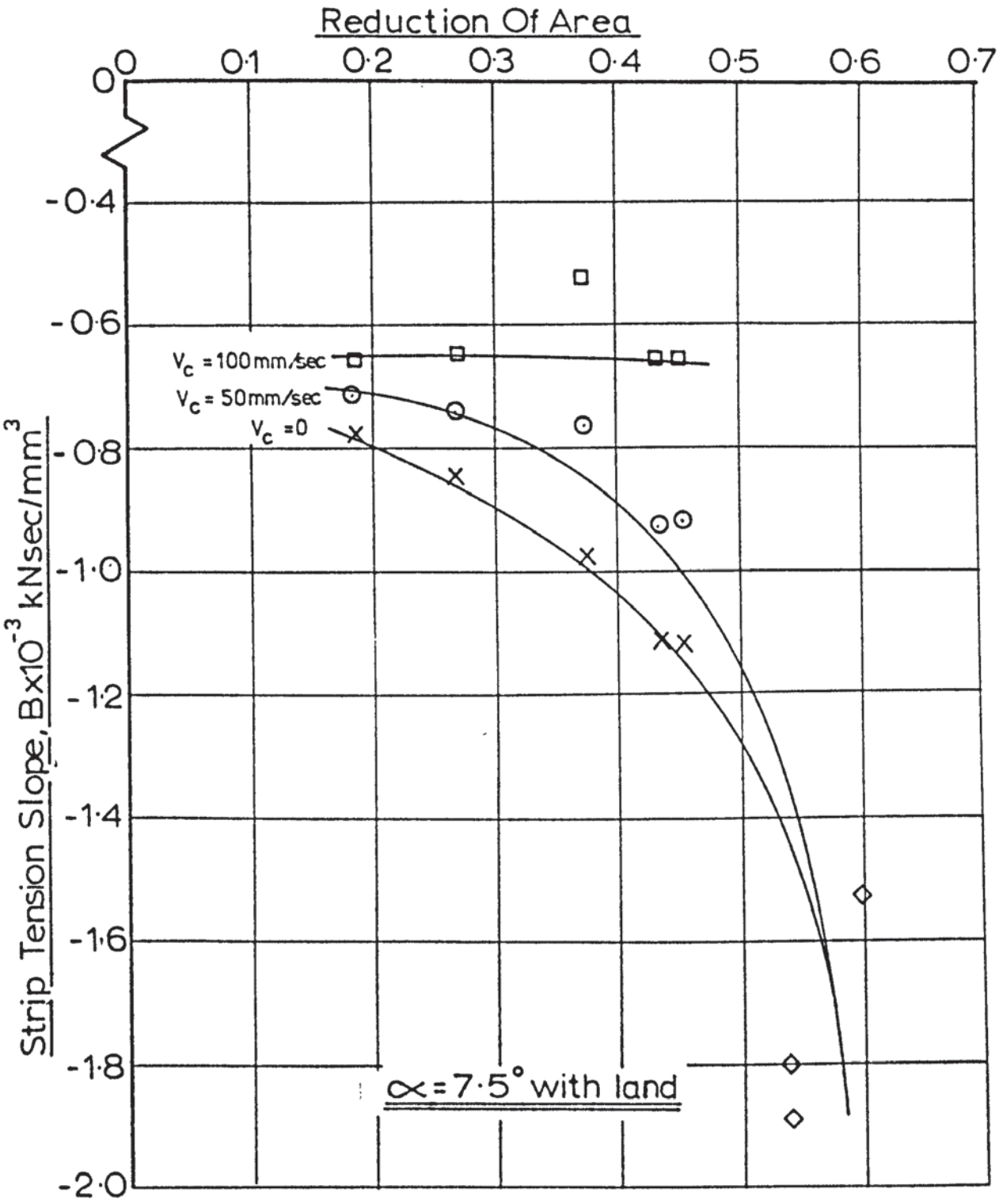

Fig(8·20) - Strip Tension Slope, B vs. Reduction Of Area

◇ - Arbitrary Draw Speed

Fig(8·21)-Strip Tension Intecept, A vs. Reduction Of Area

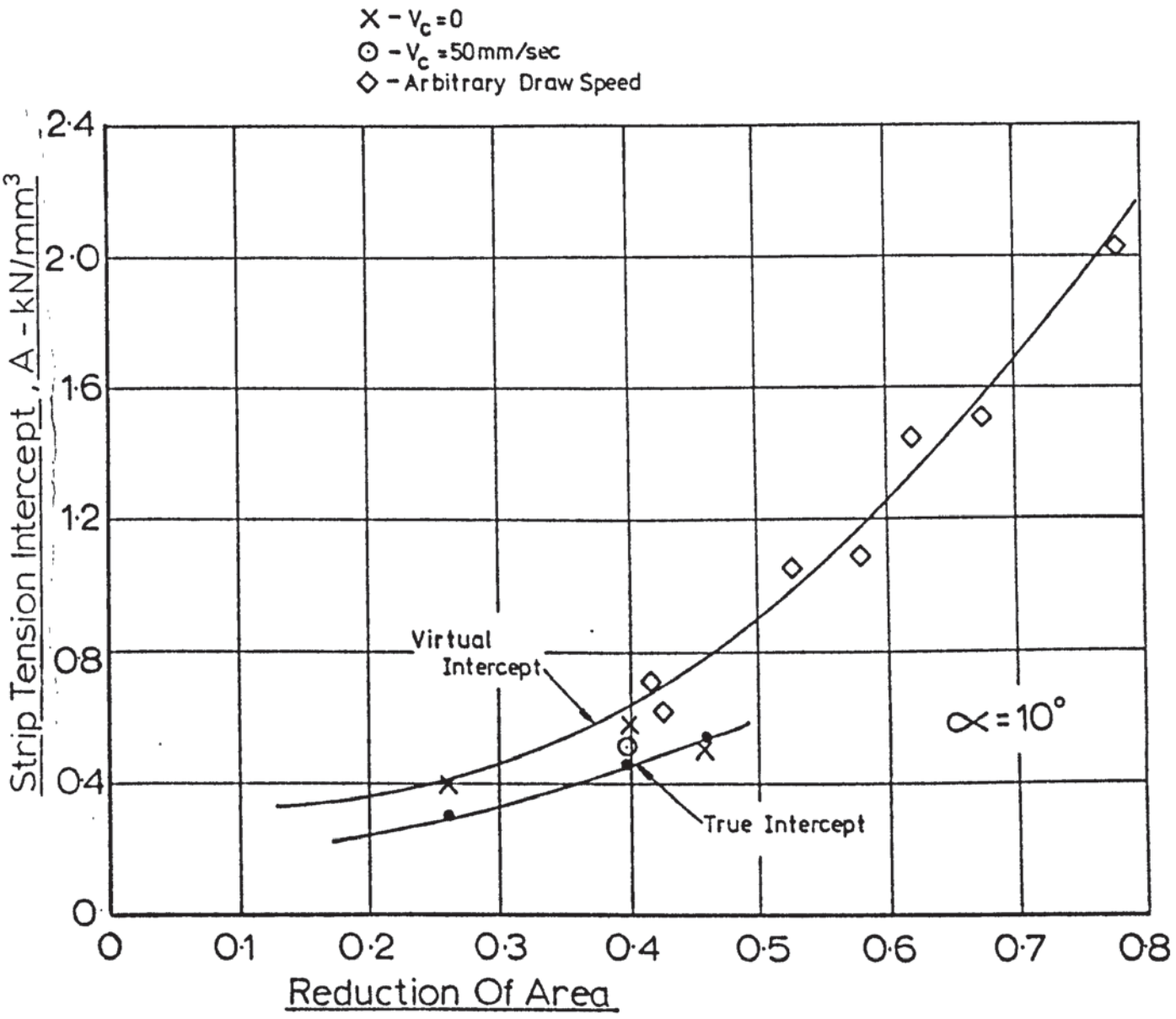

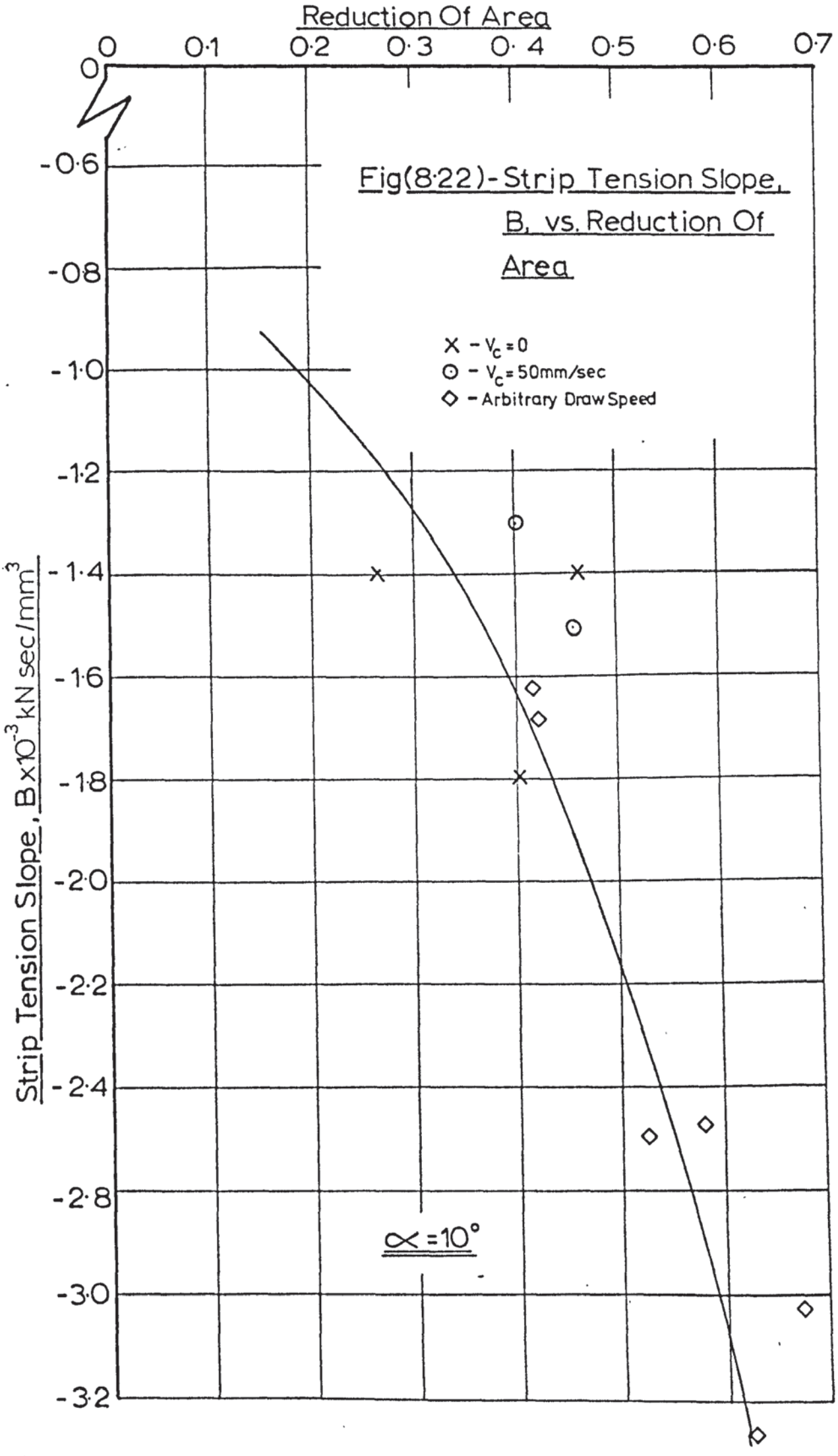
Reduction Of Area
0
0·1
0·2
0·3
0·4
0·5
0·6
0·7
-0·6
-0·8
-1·0
-1·2
-1·4
-1·6
-1·8
-2·0
-2·2
-2·4
-2·8
-3·0
-3·2
Strip Tension Slope, B×10⁻³ kN sec/mm³
Fig(8·22)- Strip Tension Slope, B, vs. Reduction Of Area
× - Vc = 0
⊙ - Vc = 50mm/sec
◇ - Arbitrary Draw Speed
∝ = 10°

Fig(8·23)- Consolidated Data On Mean Strip Tension vs. Peak Die Velocity

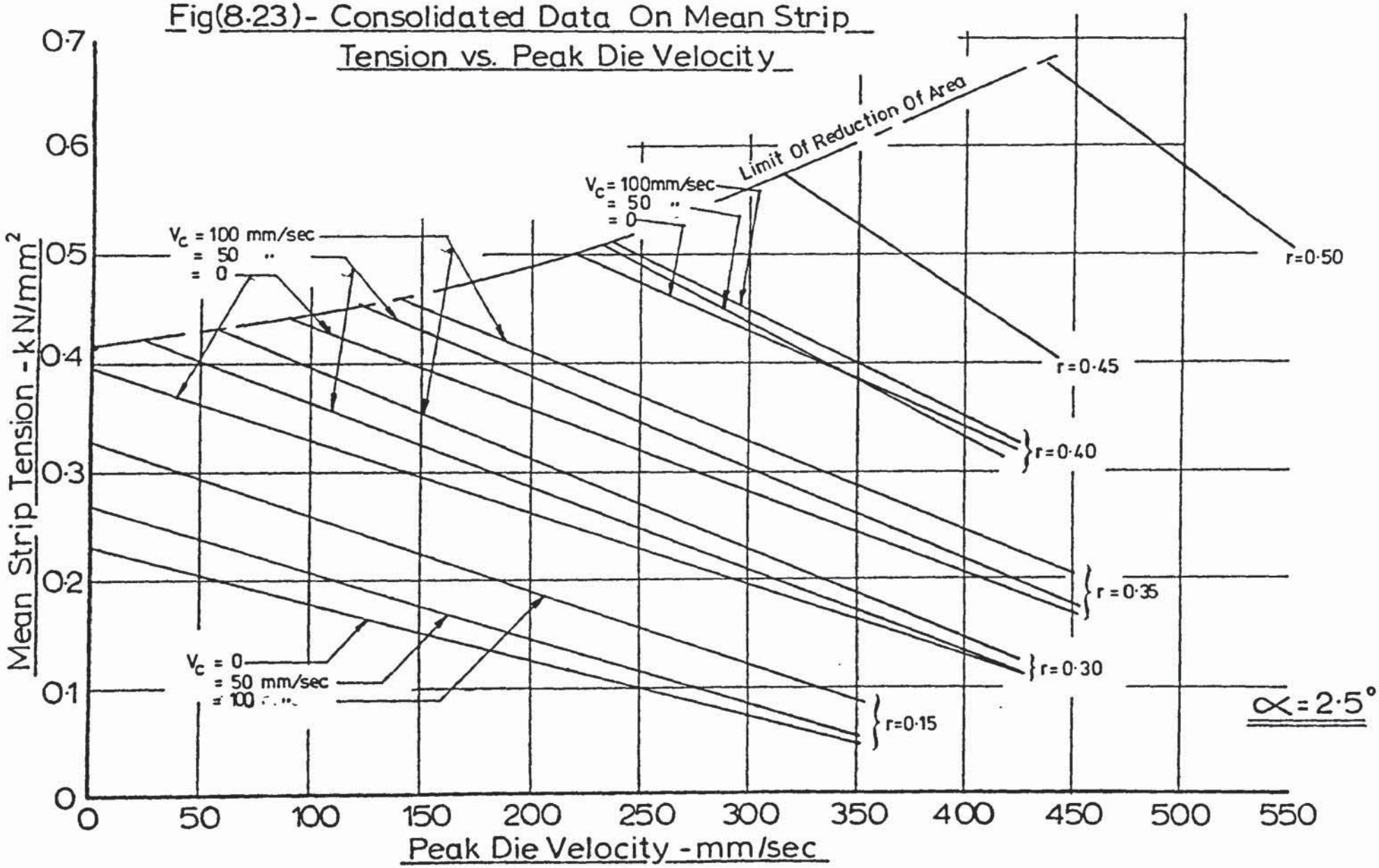

Fig(8·24) - Consolidated Data On Mean Strip Tension vs. Peak Die Velocity

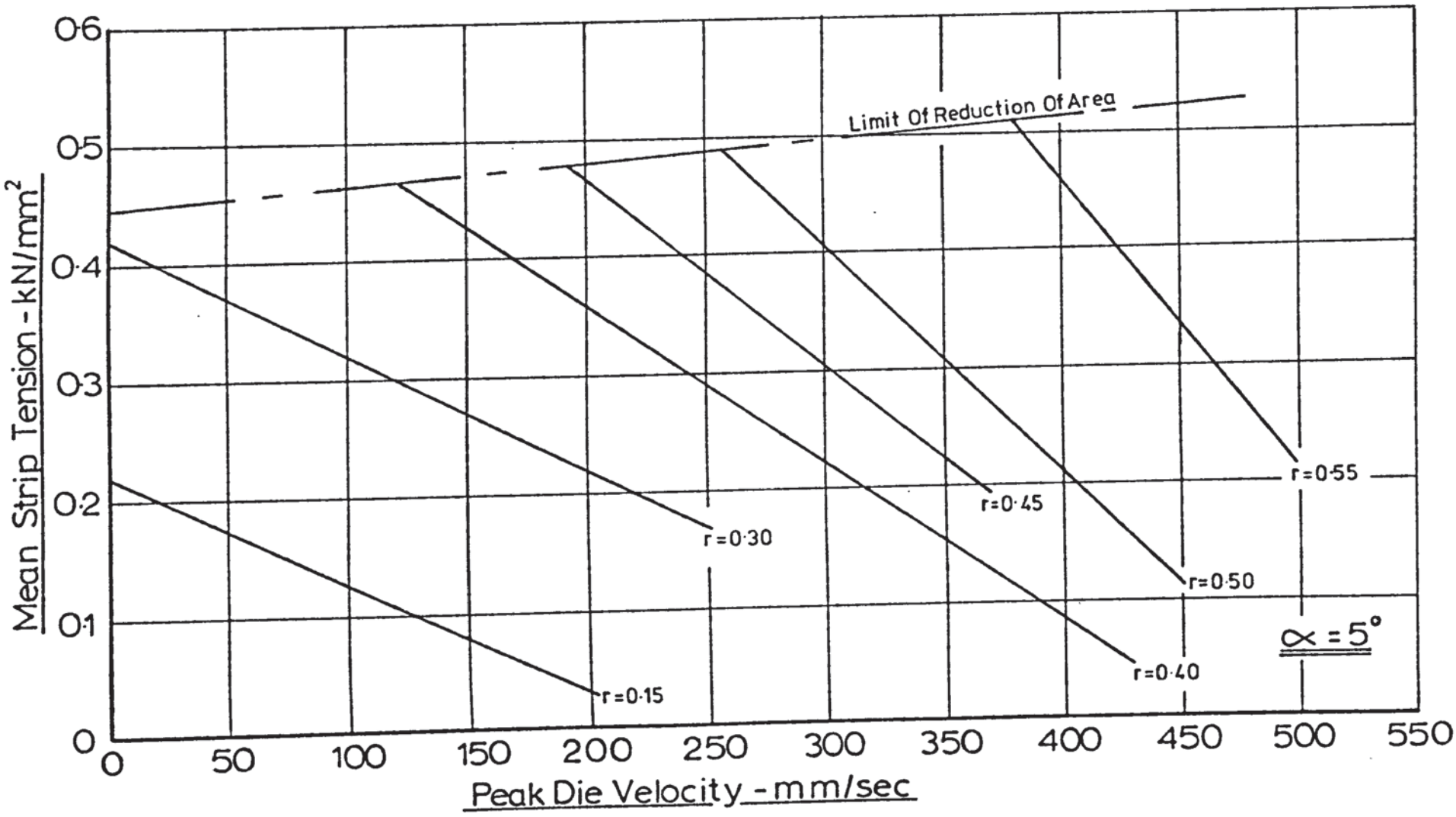

Fig(8·25)-Consolidated Data On Mean Strip Tension vs. Peak Die Velocity

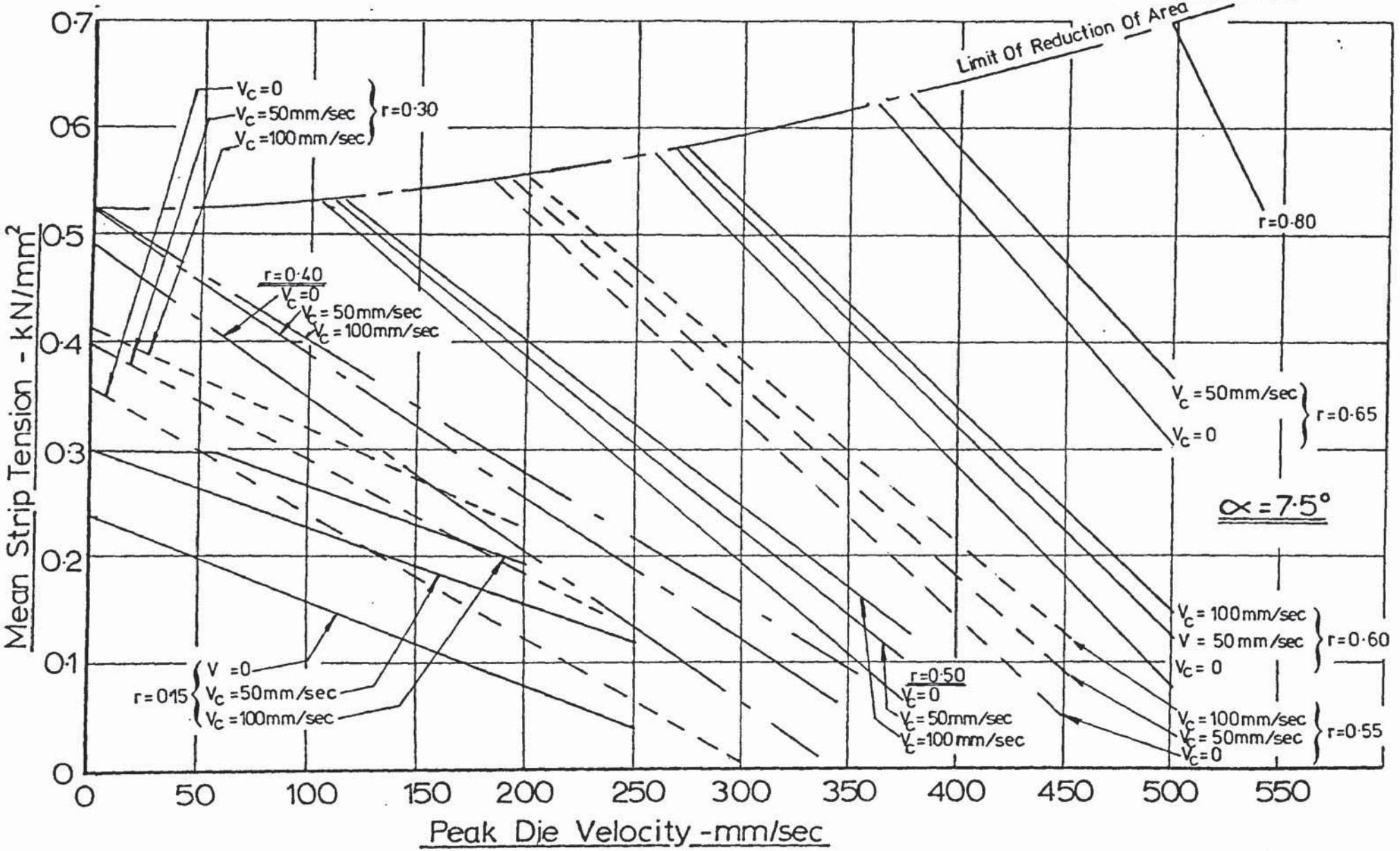

Fig(8·26)-Consolidated Data On Mean Strip vs. Peak Die Velocity

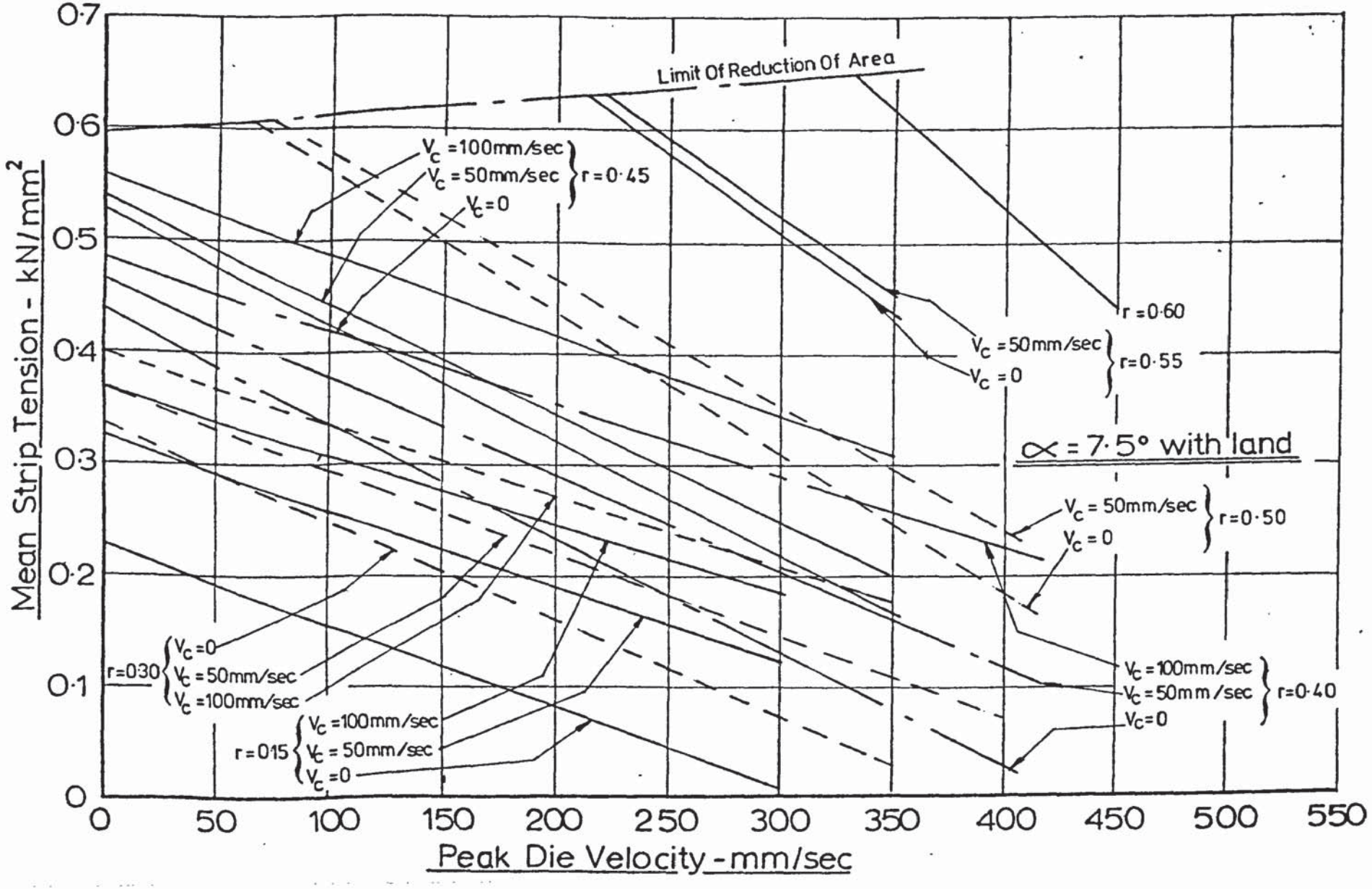

Fig(8·27) - Consolidated Data On Mean Strip Tension vs. Peak Die Velocity

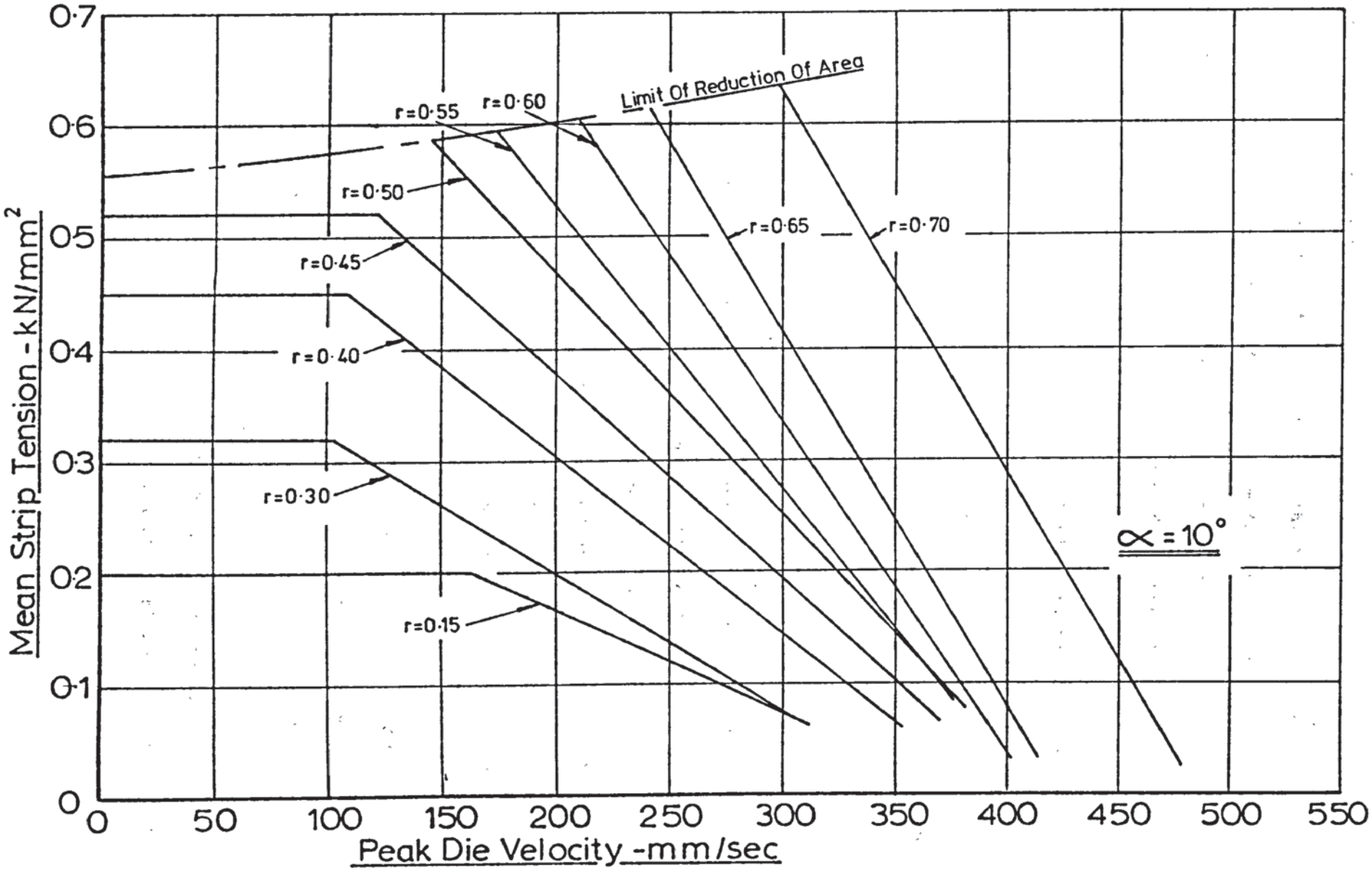

8.2.2. Specific Axial Thrust

The specific axial thrust is defined as the bending load acting upon the die, divided by the projected area over which it is acting.

The variation of the specific axial thrust with die angle, reduction of area, peak die velocity and mean draw speed is shown in Figures (7.32) to (7.63).

The effects of draw speed and peak die velocity are broadly similar to those for the mean strip tension. Specific axial thrust decreases with peak die velocity and tends to increase with mean draw speed. From consideration of force equilibrium, under conventional draw conditions, the tag load will be equal to twice the bending load on the die wave guide. Tag load and bending load at zero peak die velocity correspond to this condition and, as can be seen in appendix A3.1, show good agreement. As the dies are vibrated there will be a change in the frictional conditions and some of the deformation energy will be dissipated by the swaging action, which therefore causes a reduction in strip tension.

At full acoustic power input, moderate reductions of area and low draw speeds the process was converted to one of high frequency swaging in which the strip could be drawn by hand. Thus the front tension can be reduced to a very low level although the bending load on the die wave guides does not fall to such an extent. The reason for this is that the horizontal component of the force required to indent the strip was monitored by the bending load cell and was not transmitted downstream of the deformation zone. Similarly, the nett effect of the frictional loading on the die was monitored by the bending load cell. This force would be balanced by the presence of a neutral plane which resulted in a divided, opposing, friction vector. Similarly, a fully reversed flow of metal within the deformation zone would result in a reversed friction vector. This would reduce bending load on the die rather than add to bending

load, as in the conventional draw case.

Clearly the relationship between the tag load and bending load will vary with the proportion of the deformation attributable to pure drawing and to swaging. This relationship is worthy of further consideration. An indication of the effect of swaging and reversed, or partly reversed, friction vector and superposition is given by the manner in which the bending load on the die, and tag load, deviate from that of the conventional draw condition.

The rate of decrease of bending load with peak die velocity compared with the rate of decrease of tag load, for the various die angles, is shown in Figures (8.12) to (8.16); the ratio:

$$\frac{\text{Slope Of The Tag Load Characteristic}}{\text{Slope Of The Total Bending Load Characteristic}} = \frac{S_b}{S_t}$$

is plotted against mean draw speed for the various reductions of area.

Figure (8.28) shows the variation of the slopes for the 2.5^{o} dies; it can be seen that the value of the ratio of slopes tends to decrease with reduction of area. The scatter with draw speed is high although there is a slight tendency for the ratio S_t/S_b to increase with mean draw speed.

The results for the 5^{o} dies are given in Figure (8.29); the quality and quantity of these data are insufficient for any conclusions to be drawn.

The results for the 7.5^{o} dies are shown in Figure (8.30); with the exception of the test at r = 0.267 (test No. 041), the ratio S_t/S_b increases with reduction of area and decreases as mean draw speed is increased. Thus the trend for the 7.5^{o} die is opposite to that of the 2.5^{o} dies.

Figure (8.31) shows the variation of the slope ratios for the 7.5^{o} with-land dies. The effect of reduction of area is similar to that of the 2.5^{o} dies, that is, the slope ratio decreases as reduction of area

increases, and there is a very marked tendency for this ratio to decrease as mean draw speed is increased.

Only three sets of results are given for the 10^{o} dies, Figure (8.32), two of which span a very small speed range and indicate independence of mean draw speed. The remaining set of results, however, extend over a far greater draw speed range and shows a rapid decrease in the ratio S_t/S_b as draw speed increases. These results indicate that the slope ratio tends to increase with reduction of area in a manner similar to the results for the 7.5^{o} dies.

If the reduction in the front tension occurred purely as a result of a reduction in a frictional constraint which was draw-speed dependent, the slope of the bending load characteristic would decrease at the same rate as the tag load characteristic, that is, $S_t/S_b = 1$. Similarly, a change in the value of coefficient of friction could not change the relationship between the bending load and tag load.

The factors which affect the bending load relative to tag load are:

a) Die angle: Increasing die angle will permit greater transference of the indentation load to a bending mode on the die wave guides. The load required to cause indentation will decrease with increasing die angle because of increased efficiency of deformation due to the change in geometric/frictional conditions.

b) Draw speed: Increasing the draw speed will cause an increase in the proportion of the deformation attributable to pure drawing, and therefore increases mean strip tension. Increasing draw speed will also reduce the tendency for the strip to be rejected from the die, thus enhancing the swaging effect, it is probably this effect that causes the reduction of S_t/S_b with mean draw speed at the higher die angles.

Fig(8·28) - Ratio Of Slopes vs. Mean Draw Speed

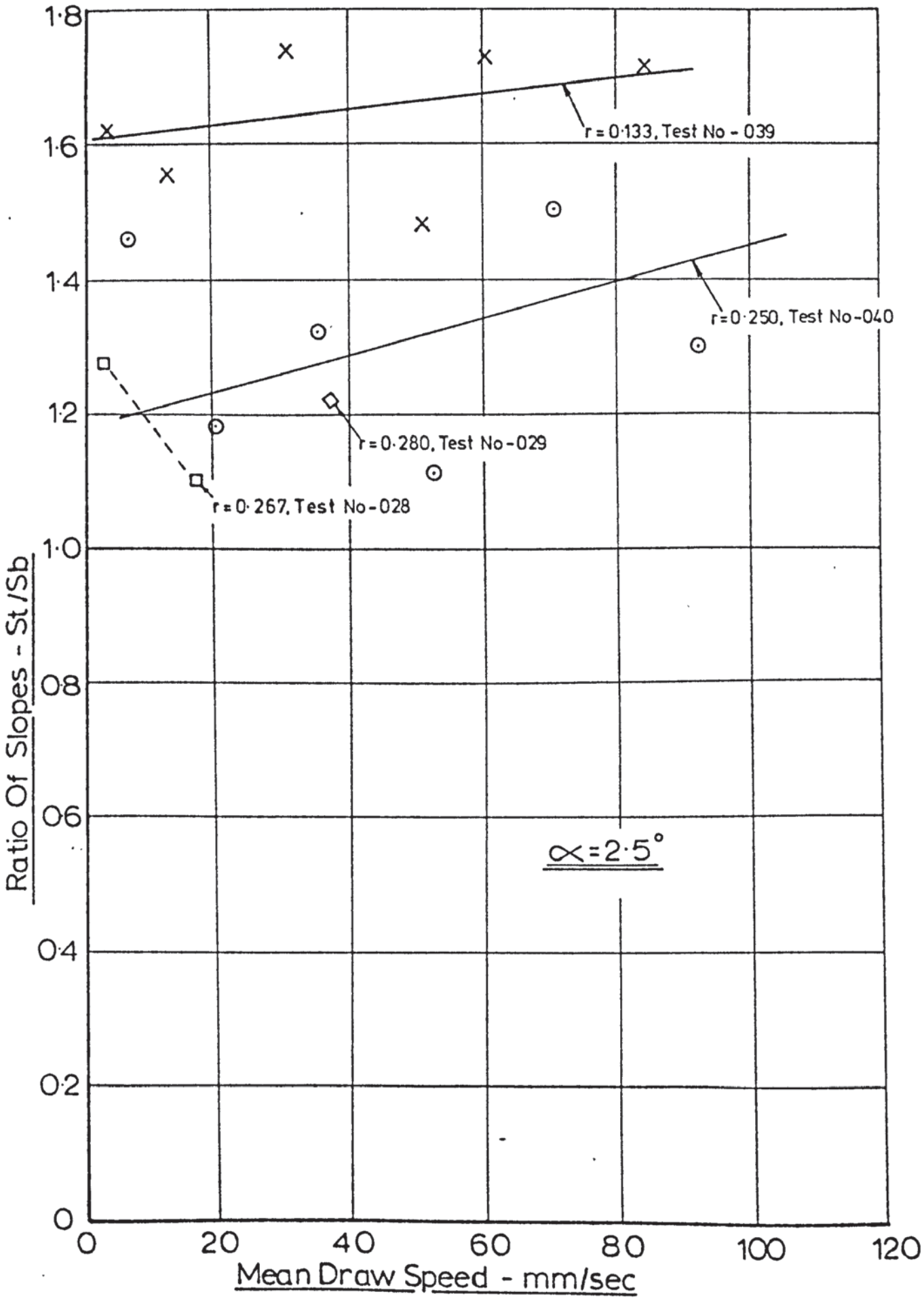

Fig(8·29)-Ratio Of Slopes vs. Mean Draw Speed

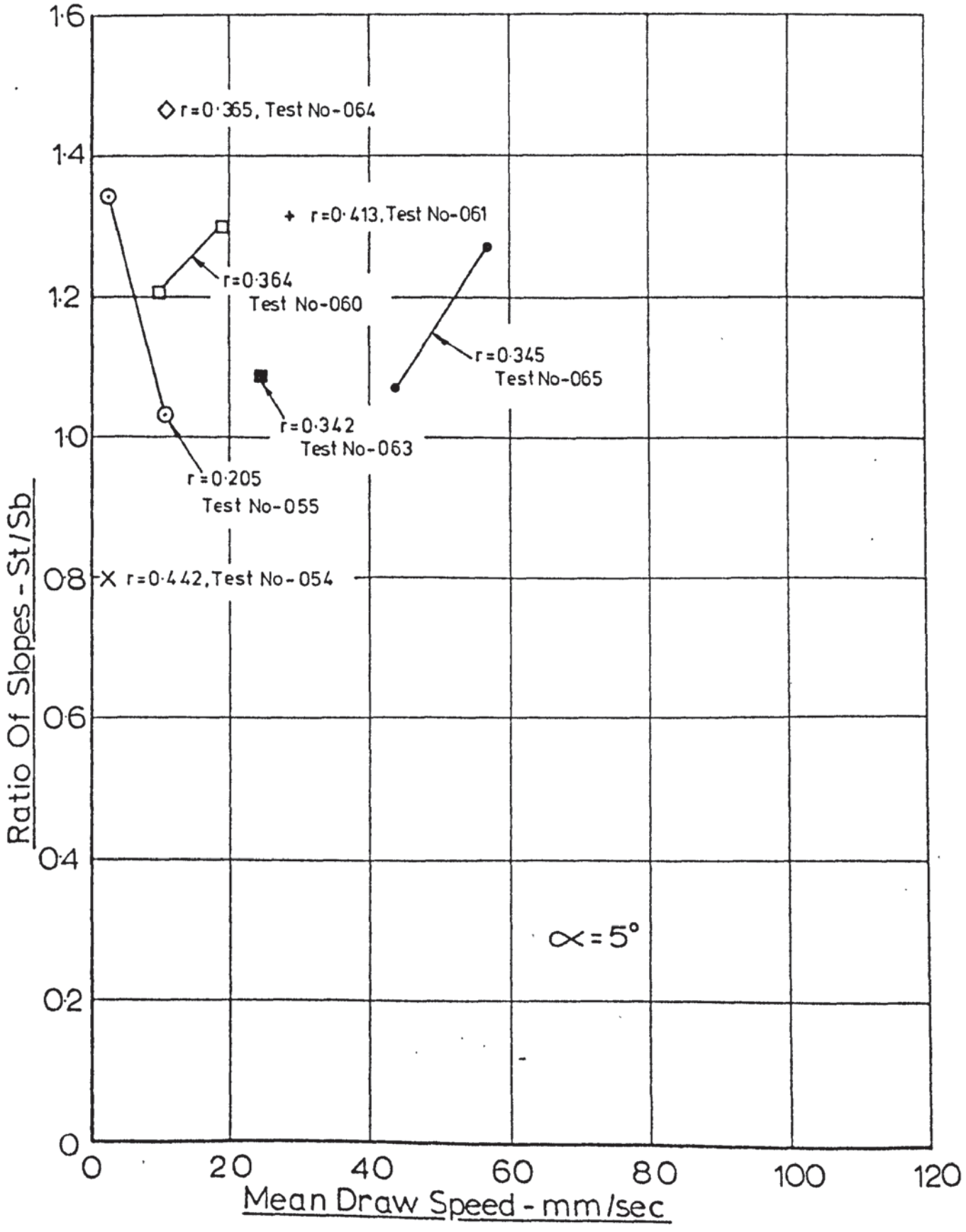

Fig(8·30)-Ratio Of Slopes vs. Mean Draw Speed

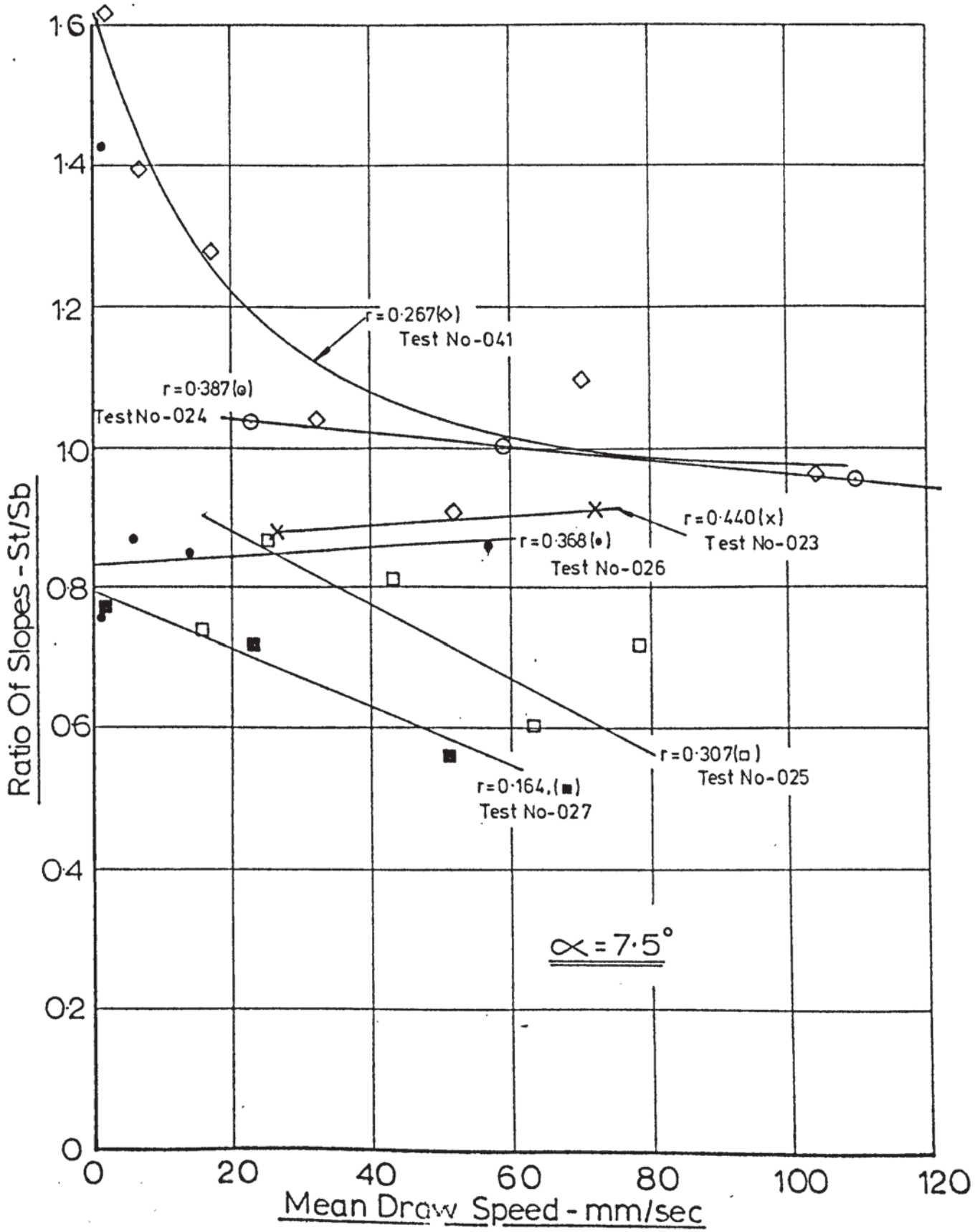

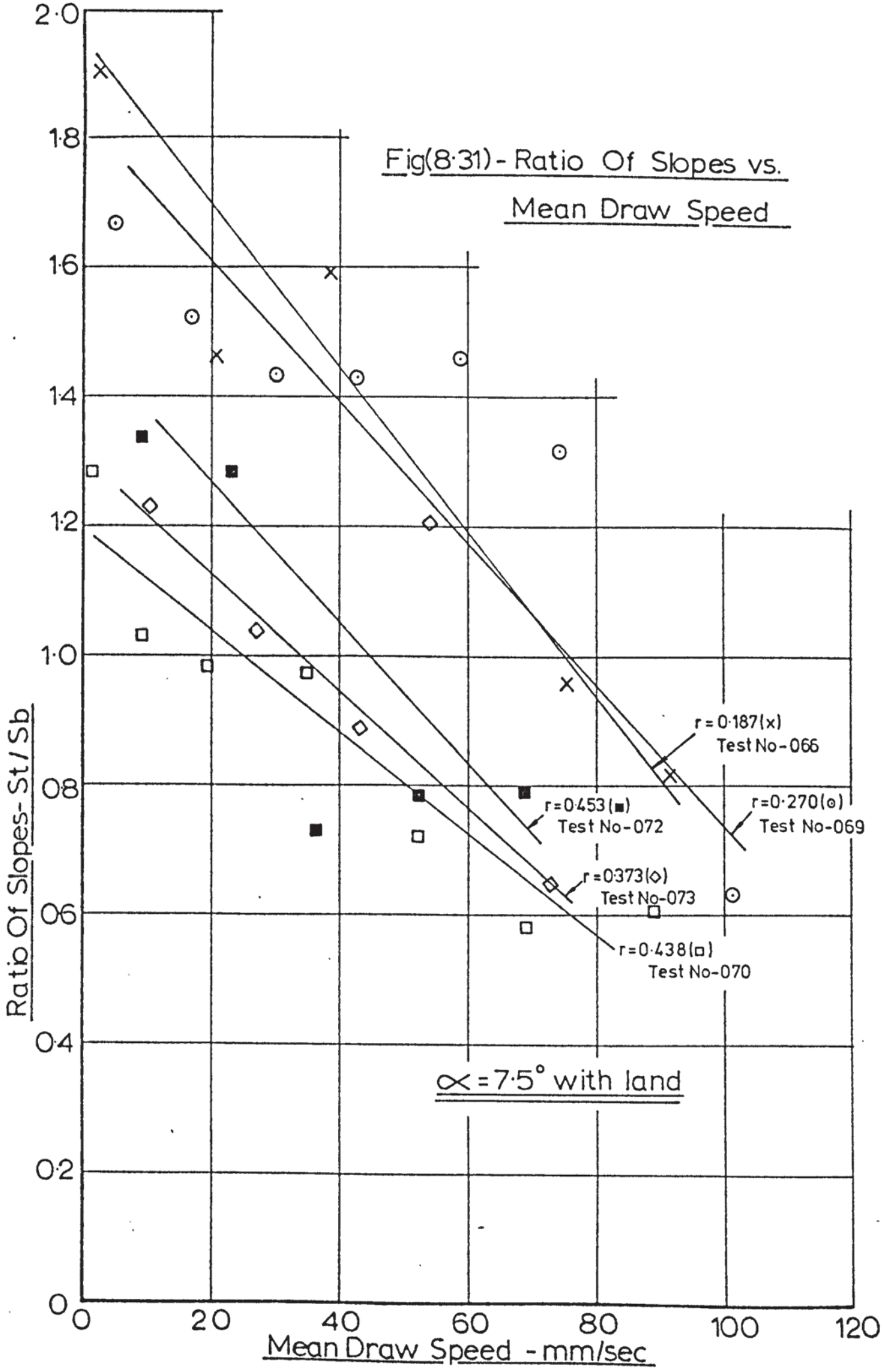
Fig(8·31) - Ratio Of Slopes vs.
Mean Draw Speed
Ratio Of Slopes- St / Sb
Mean Draw Speed - mm/sec
2·0
1·8
1·6
1·4
1·2
1·0
0·8
0·6
0·4
0·2
0
0
20
40
60
80
100
120
r = 0·187 (x)
Test No-066
r=0·453 (■)
Test No-072
r=0·270 (⊙)
Test No-069
r=0373 (◇)
Test No-073
r=0·438 (□)
Test No-070
∝ = 7·5° with land

Fig(8·32)-Ratio Of Slopes vs. Mean Draw Speed

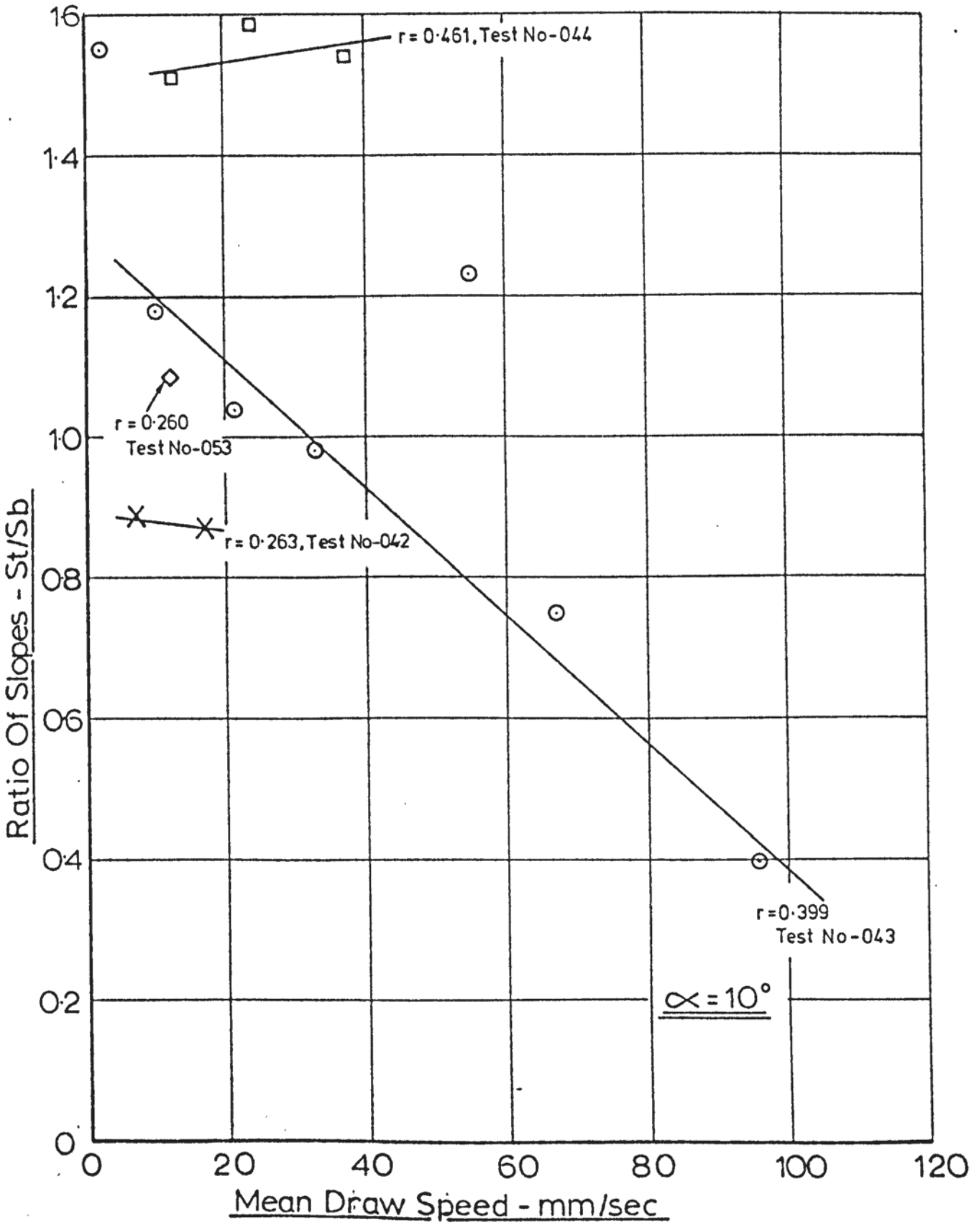

8.2.3. Lateral Die Pressure

The variation of lateral die pressure with die angle, reduction of area, peak die velocity and mean draw speed is shown in Figures (7.63) to (7.93).

The effects of reduction of area and mean draw speed are not, generally, very great. The results for the 2.5^{o} dies are shown in Figures (7.63) to (7.68); there is a very slight tendency for the lateral die pressure to increase with mean draw speed; the points obtained from these draw tests are so close together that drawing individual lines through each data set would be rather confusing. At low reductions of area, Figure (7.63), there is a slight tendency for the lateral die pressure to decrease with peak die velocity; this characteristic flattens as reduction of area is increased and the general level of lateral die pressure falls. The highest indicated lateral die pressure was approximately 0.55 kN/mm^2 at r = 0.250, Figure (7.64), which was reduced to approximately 0.35 kN/mm^2 at r = 0.355, Figure (7.68). The results for the constant acoustic power tests all fall within the band 0.35 kN/mm to 0.45 kN/mm^2.

The indicated lateral die pressure for the 5^{o} dies is shown in Figures (7.69) to (7.74); it can be seen that all of the results fall within a very narrow range, 0.32 kN/mm^2 to 0.20 kN/mm^2. The lowest reduction of area shows the greatest variation with peak die velocity and the effect of mean draw speed is even less marked than with the 2.5 dies.

The results obtained from the 7.5^{o} dies are shown in Figures (7.75) to (7.81). The general level of the lateral die pressure for the 7.5^{o} dies is higher than for both the 2.5^{o} and 5^{o} dies. At low reductions of area the lateral die pressure is, relatively, very high and shows a marked degree of draw speed dependence. Reductions of area in excess

of r = 0.307, Figure (7.77), show a stabilisation of lateral die pressure with some tendency to decrease with peak die velocity.

The constant acoustic power tests for the 7.5° dies, Figure (7.81), also showed some divergence from those of the 2.5° and 5° die tests. The bulk of these results fall upon a common line which shows a decrease in lateral die pressure with peak die velocity whilst the lower reductions of area result in higher values of lateral die pressure.

The results taken with the 7.5° with-land dies are shown in Figures (7.82) to (7.88); it can be seen that, in this case, lateral die pressure is almost totally unaffected by reductions of area, peak die velocity or mean draw speed. The large land, which was taken into account when calculating the area of the die/strip interface, results in a very low reading of the lateral die pressure. The effect of peak die velocity is similar to that of the 2.5° dies.

The results obtained from the 10° dies are shown in Figures (7.80) to (7.93). At the lower reductions of area the level of lateral die pressure falls with peak die velocity. The mean draw speed has little effect on the lateral die pressure, especially as reduction of area was increased.

Apart from the two spurious sets of results, test numbers 027 and 041 the effect of reduction of area is marginal across the whole of the range of die angles used in these tests. The general level of lateral die pressure is therefore dependent upon the die in use. The reason for the relatively high values of the lateral die pressure registered for the 7.5° dies is not clear.

The tendency for the lateral die pressure to decrease with increasing peak die velocity as die angle is increased was probably due to the effects of superposition, that is, the mean load on the die wave guide was lower for high die angles but the dynamic load was greater.

9) CONCLUSIONS

1. The experimental results shown here indicate that real benefits can be derived from augmentation of the drawing process with an oscillatory swaging process.

2. An increase in the reduction of area can be achieved at commercially useful draw speeds; for example, a 50% reduction of area at 150 mm/sec using the 7.5^{o} knife-edged dies.

3. The limiting reduction of area for the various dies is summarised in Table 9.1. These data refer to tests taken at very low draw speed.

Table 9.1: Limiting reduction of area for 2.5^{o}, 5^{o}, 7.5^{o}, 7.5^{o} with-land and 10^{o} dies.

Die Angle	Maximum Reduction of area
2.5^{o}	47%
5.0^{o}	60%
7.5^{o}	80%
7.5^{o} with land	60%
10.0^{o}	80%

4. There is reason to believe that the optimum die angle is in excess of that for conventional strip drawing.

5. The process is critically affected by draw speed; increasing the draw speed results in an increase in mean strip tension.

6. The various mechanisms that operate during ultrasonic metal processing have been discussed briefly in the introductory chapter and, in greater depth, in the literature survey. The extent to which these mechanisms operate during a given process is difficult to establish. This is due to the difficulty of designing experiments in which the effect of individual mechanisms can be measured.

7. The predominant mechanisms operating during the strip drawing process are swaging and superposition, although frictional conditions are also subject to change. Variation in friction coefficient is clearly in evidence, in certain instances, without the application of ultrasound, as already discussed in section (8.2.1). The extent to which the friction coefficient varied with the action of ultrasound could not be established.
8. The theoretical work, shown in Chapter 3 and in reference 70, suggests that swaging cannot be present without modifying the surface conditions. That is, partial or total reversal of the friction vector is a feature of the swaging process.
9. Superposition is, similarly, a feature of the combined drawing/swaging process. It did not prove possible, however, to make direct measurements of the dynamic component of the front tension during these experiments.
10. The dynamic loading to which the drawn strip was subjected was clearly high when reduction of area was high. Under these conditions the strip failed due to fatigue. The transition between overload failure and fatigue failure occurred at reductions of area between 50% and 60% irrespective of the die angle.

10) SUGGESTIONS FOR FURTHER WORK

FURTHER INVESTIGATION OF THE DRAWING PROCESS.

It has been reported that the tube-drawing analogue was not successful, due to difficulty in tuning the plug bar to the die wave guides and the effect of each vibratory system on the other. It is unlikely that further work with these tools would be fruitful without increasing the power available at the deformation zone, that is, by using more efficient generators and power ultrasonic transducers. Therefore a re-design of the tube draw analogue should be made.

The work on bimetal strip drawing is certainly worth further investigation. The reductions of area obtained with the 10^{o} and 7.5^{o} dies was of the order required to achieve bonding between similar metals. This process would be of commercial importance since it could allow small batches of the required metallic combination to be produced economically. At present such strip is produced in large batches from hot rolled stock. Localised, continuous bonding of, say, precious metals to a lower value substrate could also prove feasible.

Further investigation of the strip drawing process under the action of ultrasound is also required. It is necessary to establish the optimum die profile.

The length of the die land should be investigated further to establish its effect upon the process loads and the reduction of area. Further work on the effect of die angle is of primary importance. The work shown in this thesis indicates an increased limiting reduction of area with increasing die angle, though the difference between the 7.5^{o} and 10^{o} dies was not significant. It could be that an optimum die angle exists in this range. It was felt, however, that this limiting reduction of area of 80% was due to the practical difficulty of setting a smaller gap between the dies, rather than to a true limit on the process. It may be worthwhile,

therefore, to carry out tests using thicker strip. This would allow greater reductions of area to be attempted with greater final thicknesses. The greater power drain afforded by the thicker stock could give a better indication of the efficiency of the various die profiles.

Work carried out by Severdenko et al[53] has already indicated that reductions of area in excess of 80% can be obtained when drawing copper and aluminium. Further work should, however, be carried out to establish the general effect of die velocity, draw speed and die profiles on these and other metals.

Difficult-to-draw alloys such as austenitic stainless steel and titanium alloys, exhibit high rates of strain hardening. This could be a positive advantage, if the breakdown of lubrication can be prevented, because of the high value of yield stress attained by the drawn material. That is, the yield stress of the drawn material is higher relative to the mean yield stress of the material within the deformation zone.

The conditions operating during ultrasonic drawing are clearly more arduous than under conventional draw conditions. It is necessary, therefore, to make a systematic study of the effectiveness of the various types of lubricant available. Die wear studies would also be of value, though this may best be carried out as part of an industrially based development programme. Die wear should be monitored whilst commercial production is in operation, and compared with die wear under conventional conditions. It is recommended that tests be carried out transversly vibrating the dies, in antiphase, as in the mode commonly used in ultrasonic welding. It could therefore give a better welded joint if combined with drawing. The swaging effect would be minimised in this case. The effect of friction would therefore be dominant and could lead to a further understanding of the process.

The drawing of section, or round-to-section, combined with swaging should also be invistigated.

INSTRUMENTATION

Further work on the use of the 'Kleesattel' transducer may be of value. This instrument clearly has the potential to measure dynamic stress at the required frequency, as shown in Chapter 5. Under experimental conditions, however, the signal was corrupted by a low frequency vibration. Further work should therefore be directed towards obtaining a 'clean' signal at the driving frequency of the wave guides. This would enable direct measurement of dynamic stress amplitude and thus establish the true level of draw stress attributable to swaging, friction reduction, etc.

MODIFICATIONS TO THE DRAW-BENCH

The primary disadvantage of the draw-bench was the method of adjusting the die gap. This was achieved by use of shim steel placed between the wave guide support and the die load cell. At reductions of area near to the limit for a specific die angle the adjustment of die gap proved difficult. 'An interlocked 'screw-down' mechanism on each side of one of the die bolsters, as used in rolling mills, would enable such adjustments to be made. Strip parallelism could also be controlled directly, without the need for shimming the bolster plate, as described in Chapter 4. Specific strip sizes could also be produced to normal drawing tolerances.

Higher efficiency H.F. drives should be used in line with current practice, that is, that is a change from magnetostrictive drive stacks to piezoelectric. The redsign necessary to incorporate this could also provide for drawing under conditions of full immersion in lubricant.

The development of wave guides for drawing wide strip would also be of use. These would probably take the form of wide exponentional wedges.

The fatigue failures that occurred down-stream of the die could be suppressed by use of drive rolls or a rigid die or rollers. This should be sited down stream of the die, such that the acoustic stress wave is

reflected back towards the deformation zone.

REFERENCES

1. Rowe, G.W. — An Introduction to the Principles of Metalworking. Edward Arnold (1965)

2. Lancaster, P.R. & Rowe, G.W. — Experimental Study of the Influence of Lubrication upon Cold Drawing Under Approximately Plane Strain Conditions at Low Speed. Proc. Instn. Mech. Engrs., Vol, 178, Pt. 1, No. 3, pp 69-89.

3. Rowe, G.W. — Recent Advances in Wire Manufacture. Int. Metall. Revs.

4. Sansome, D.H. — People, Pence and Plasticity. Inaugural Lecture. University of Aston in Birmingham (1975)

5. Tylecote, R.F. — The Solid Phase Welding of Metals. Edward Arnold, London, 1968.

6. Blaha & Langenecker — Naturwissenshaften, 42, 556, 1955.

7. Wistreich — Investigation of the Mechanics of Wire Drawing. Proc. Inst. Mech. Eng. 1955, 169, 654.

8. Herbertz, J. — Non-Contact Electro-Dynamic Measurement on Metallic Vibrators at 20 kHz. Ultrasonics. Oct. 1967, pp 239-240.

9. Calan, N., Sirbu, A. & Dragan, O. — Research on Inductive Transducers for Vibration Measurement. Ultrasonics. March 1976, pp 65-67.

10. Kleesattel, C. — Vibration Sensor Utilizing Eddy Currents Induced in Members Vibrating in the Field of a Magnet. U.S.Patent No. 3,697,867, Oct. 10, 1972.

11. Dove, R.C. & Adams, P.H. — Experimental Stress Analysis and Motion Measurement. Merrill, 1964, pp 83 et seq.

12. Waterhouse, W.J. — Private Communication.

13. Bell, J.F.W. — Private Communication.

14. Avitzur, B. — Metal Forming - Processes and Analysis. McGraw-Hill. 1968.

15. Eaves, A.E. — Unpublished Private Communication.

16. Neubert, M.K.P. — Instrument Transducers. Oxford. 1963.

17. Colloff, N.J. — Private Communication.

18. Biddell, D.C. — Ultrasonic Deep-drawing and Ironing. Private Report to S.R.C., Sept. 1976.

19. Ford, H. & Alexander, J.M. — Advanced Mechanics of Materials. Longman.

20. Irving, C.D. & Cotterill, P. — Redundant Work in Strip Drawing. Metals Technology, May 1975. pp 229-235.

21. Dragan, O. — Cold Drawing of Tubes on an Ultrasonically Activated Plug. Ultrasonics International 1973 Conference Proceedings. pp 254-256.

22. Young, M.J.R. — Ph.D. Thesis. University of Aston in Birmingham. 1973.

23. Smith, A.W. — Ph.D. Thesis. University of Aston in Birmingham. 1977.

24. Winsper, C.E. & Sansome, D.H. — A Review of The Application of Oscillatory Energy to Metals Deforming Plastically. 8th Int. M.T.D.R. Conference. Pergamon. 1967.

25. Eaves, A.E., Smith, A.W. Waterhouse, W.J. & Sansome, D.H. — Review of the Application of Ultrasonic Vibrations to Deforming Metals. Ultrasonics, July 1975. pp 162-9.

26. Schmid, E. — Plasticity of Insonated Metals. Suppl. Trans. Japan Inst. Metals. 1968, Vol. 9, pp 798-804.

27. Winsper, C.E., Dawson, G.R. & Sansome, D.H. — An Introduction to the Mechanics of Oscillatory Metalworking. Metals and Materials. April 1970. pp 158-162.

28. Dawson, G.R., Winsper, C.E. & Sansome, D.H. — Application of High- and Low-Frequency Oscillations to the Plastic Deformation of Metals. Metal Forming. Part 1. August 1970, pp 234-238. Part 2. September 1970, pp 254-261.

29. Biddell, D.C. & Sansome, D.H. — The Development of Oscillatory Metal-drawing Equipment - an Engineer's View. Ultrasonics. Sept. 1974, pp 195-205.

30. Sansome, D.H. — Recent Developments in Oscillatory Metalworking. Engineering. April 1973.

31. Cunningham, J.W. — Effects of Superimposed High-Frequency Vibrations on Deformation Processes. Westinghouse Electrical Corporation.

32. Jones, J.B. — Ultrasonic Metal Deformation Processing. Wire Industry, May 1971, pp 336-341. Abstracted from Proc. CIRP. Int. Conf. on Manufacturing Technology, Sept. 1967.

33. Maropis, N. & Clement, J.C. — Transition between Theory and Practice in Ultrasonic Metal Deformation processing. A.S.M. Tech. Rept. No. C6-26,3,1966, ASM Metals Park, Ohio.

34. Winsper, C.E. & Sansome, D.H. — The Influence of Oscillatory Energy on the Stresses During Plastic Deformation. J. Inst. Metals, 1968, Vol. 96, pp 353-357.

35. Spiers, R.M., Winsper, C.E. & Sansome, D.H. — Direct Extrusion of Metal with Applied Oscillatory Energy. Metal Forming, Oct. 1969, pp 271-277.

36. Petukhov, V.I., Abramov, O.V., Zubko, A.M. & Manegin, Yu. V. — Extrusion of Aluminium in an Ultrasonic Field. Light Age, June, 1973, pp 6-8.

37. Young, M.J.R., Winsper, C.E. & Sansome, D.H. — Radial Mode Vibrators for Oscillatory Metal Forming. Applied Acoustics, 3, 1970, pp 299-307.

38. Smith, A.W., Young, M.J.R. & Sansome, D.H. — Preliminary Results on the Effect of Ultrasonic Vibration on an Analogue of the Deep-Drawing Process. Proc. Ultrasonics Int. Conf. 1973, pp 250-253.

39. Biddell, D.C. & Sansome, D.H. — The Deep-drawing of Cans with Ultrasonic Radial Oscillations Applied to the Die. Proc. Ultrasonics Int. Conf. 1973. pp 56-62.

40. Winsper, C.E. & Sansome D.H. — The Superposition of Longitudinal Sonic Oscillations on the Wire-drawing Process. Proc. Inst. Mech. Eng. 1968-9, Vol. 183, Pt. 1.

41. Winsper, C.E. & Sansome, D.H. — A Study of the Mechanics of Wire Drawing with Superimposed Ultrasonic Stress. 10th Int. M.T.D.R. Conf. pp 553-565. Pergamon.

42. Winsper, C.E. & Sansome, D.H. — Application of Ultrasonic Vibrations to the Plug Drawing of Tube. Metal Forming, March 1971, pp 71-75

43. Severdenko, V.P. — Drawing Titanium Alloy Wires with the Superposition of Ultrasound. Doklady Akad. Nauk Beloruss SSR. 1973, April pp 325-328.

44. Severdenko, V.P., Stepanenko, A.V. & Vinerskii, S.N. — A Study of Various Ultrasonic Drawing Methods. Vesh. Akad. Nauk. Bel. SSR. No. 1, 1971, Ser. Fiz. ekH-Navuk, 100-2.

45. Severdenko, V.P. — Wire Drawing uses Transverse Ultrasonic Vibrations. Doklady Akad. Nauk. Beloruss SSR. June, 1971. pp 499-501.

46. Severdenko, V.P., Stephendnko, A.V. & Vinerskii, S.N. — Effect of Ultrasound on the Drawing of Metals under Conditions of Hydrodynamic Friction. Izv. Akad. Nauk. B. SSR (Fiz-Tekhn) (4), (1970) 92.

47. Vatrushin, L.S. — Efficiency of Drawing in an Ultrasonic Field. Soviet J. Non-Ferrous Metals, 8, 1967, 91.

48. Masao Inoue & Eiji Mori. — Ultrasonic Metal Wire Drawing. 6th Int. Congress on Acoustics. Tokyo, Japan, Aug. 1968, pp 412-417.

49. Samann, K.H. — Wire Drawing With High Frequency Mechanical Vibration. Z. Ind. Fertig, Vol. 61 (1971) pp 672-676.

50. Langenecker, B. & Jones, V.O. — Macrosonic Wire Drawing and Tube Bending. Proc. Ist Int. Symp. High-Power Ultrasonics pp 157-160.

51. Lehfeldt, E. — Wire Drawing with Superimposed Ultrasonic Vibrations. No. 102, Aug. 1969, pp 205-213.

52. Atanasiu, N. — The Wire Drawing Process with Axial Ultrasonic Vibration of the Die. Ultrasonics, March, 1976. pp 69-72.

53. Severdenko, V.P., Stepanenko, A.V. & Kulaga, Ye. N. — Drawing Strip with the aid of Ultrasound. Dokl. Akad. Nauk Bel SSR. 1973, 17, (8), 710-713.

54. Rozner, A.G. — Effect of Ultrasonic Vibration on Coefficient of Friction During Strip Drawing. J. Acoustical Soc. of America, Vol. 49, No. 5. Pt. 1, 1971, 1368-1371.

55. Rozner, A.G. — Effect of Ultrasound on Stresses During Strip Drawing. U.S. Naval Ordnance Laboratory, White Oak, Maryland, 1970.

56. Severdenko, V.P., Stepanenko, A.V., Zayash, I.V. & Ovchinnikov, P.S. — Residual Stresses in Metal Rolled with Application of Ultrasonic Vibrations. Metallovedenie i Termicheskaya Obrabotka Metallov, No. 1, pp 68-69. Jan, 1971.

57. Severdenko, V.P., Stepanenko, A.V. & Zayash, I.V. — Investigation of Strip Rolling with Superimposed Ultrasonic Vibration. Dan B SSR, 13, (10), 1969.

58. Langenecker, B., Jones, V.O. & Illiewich, J. — Metal Forming in Macrosonic Fields. 1st Int. Symp. High-Power Ultrasonics pp 83-87.

59. Mizuno, M. & Kuno, T. — Basic Studies of Plastic Working with Vibration. J.S.M.E., Vol. 16, No. 91, Jan. 1973, pp 40-48.

60 Severdenko, V.P. & Petrenko, V.V. — Effect of Plastic Deformation on Amplitude of Applied Ultrasonic Oscillation. Russian Ultrasonics, 1, (2), (1971), 75.

61. Pohlman, R., & Lehfeldt, E. — Influence of Ultrasonic Vibration on Metallic Friction. Ultrasonics, Oct. 1966, Vol. 4, pp 178-185.

62. Konovalov, G.G. et al. — Reduction of the Forces of Sliding Friction by Introducing Longitudinal Ultrasonic Vibrations Doklady Akad Nauk Beloruss 1973, May, 17, (5), 420-422.

63. Mikmenchan, A.I. & Mashchinov, A.N. — Effect of Ultrasonic Vibrations on Friction Between Solids. Russian Engineering Journal. 1969, Vol. XLIX, No. 1, pp 41-42.

64. Lehfeldt, E. — Internal Friction Effects Produced by Ultrasound in Plastic Deformation of Metallic Materials. V.D.I-Z III, (6). 1969, p 359.

65. Langenecker, B. — Basic concepts and Industrial Applications of Macrosconic Metal Deformation Proc. Ultrasonics Conf. 1971, IPC Science & Technology Press, Guildford (1972) 59.

66. Langenecker, B. — Dislocation Damping in Macrosonic Fields. Proc. 1st Int. High Power Ultrasonics pp 32-35.

67. Langenecker. J.A.M. — Crystal Growth in Macrosonic Fields. Proc. 1st Int. Symp. High-Power Ultrasonics pp 120-123.

68. Gindin, I.A., Neklyudov, I.M., Malik, G.N. & Bolchok, O.I. — The Plastic Strain of Polycrystalline Aluminium under the Infleunce of Ultrasonic Pulses. Soviet Physics - Solid State, Vol. 11, No. 11, May, 1970, pp 2623-2627.

69. Petrukov, V.I., Abramov, O.V., Zubko, A.M. & Kulemin, A.A.V. — Extrusion of Metals with the use of Ultrasonic Radial Vibrations. Kuznecho-Shtampov, 1972, Nov. (11), 14-15.

70. Dawson, G.R. — Ultrasonic Tube Drawing with Floating Plugs. Department of Production Engineering, University of Aston in Birmingham.

71. Ratcliffe, J.F. — Elements of Mathematical Statistics. Oxford University Press, 1967.

72. Green, A.P. — Plane Strain Theories of Drawing. Proc. Instn. Mech. Engrs. Vol. 1974, No. 31, 1960.

73. Hill, R. — Mathematical Theory of Plasticity. Clarendon Press, Oxford (1950).

74. Kachanov, L.M. — Fundamentals of the Theory of Plasticity. MIR Publishers, Moscow, 1974.

75. Ford, H. & Alexander, J.M. — Advanced Mechanics of Materials. Longman, 1972.

76. Johnson, W. & Mellor, P.B. — Plasticity for Mechanical Engineers. Van Nostrand Reinhold Company, London, 1971.

77. Halling, J. & Mitchell, L.A. — Use of Upper-Bound Solutions for Predicting the Pressure for the Plane Strain Extrusion of Materials. J. Mech. Eng. Sco. Vol. 6, No. 3, 1963.

78. Halling, J. & Mitchell, L.A. — An Upper-Bound Solution for Axi-Symmetric Extrusion. Int. J. Mech. Sci. 1965, Vol. 7, pp 277-295.

79. Halling, J. & Mitchell, L.A. — The Solution of Axi-Symmetric Plastic Deformation Problems from Equilibrium Force Diagram Consideration and the Application of the Method to the Extrusion Process. Int. J. Prod. Res. (1965) Vol. 4, No. 2, pp 141-156.

80. Haddow, J.B., Halling, J. & Mitchell, L.A. — Comment and Reply on Ref. 78. Int. J. Mech. Sci., 1966, Vol. 8, p 145.

81. Prager, W. & Hodge, P.G. — Theory of Perfectly Plastic Solids. John Wiley & Sons Ltd., 1961.

82. Westwood, D. & Wallace, J.F. — Upper-bound Values for the Loads on a Rigid-Plastic Body in Plane Strain. J. Mech. Eng. Sci., Vol. 2, No. 3, 1960. pp 178-187.

83. Wistereich, J.G. — The Fundamentals of Wire Drawing. Metall. Revs. 1958, Vol. 3, No. 10, pp 97-142.

84. MacLellan, G.D.S. — A Critical Survey of Wire-Drawing Theory. J. Iron & Steel Inst. March, 1948. pp 347-356..

85. Hill, R. & Tupper, S.J. — A New Theory of The Plastic Deformation in Wire-Drawing. J. Iron & Steel Inst., Aug. 1948. pp 353-359.

86. Green, A.P. & Hill, R. — Calculations on the Influence of Friction and Die Geometry in Sheet Drawing. J. Mech. Phys. Solids, 1952, Vol. 1. pp 31-36.

87. Chung, S.Y. & Swift, H.W. — Cup Drawing from a Flat Blank. Proc. Inst. Mech. Engrs. 1951, 165. pp 199.

88. Blazynski, T.Z. — Tube Drawing Through Straight Tapered and Curved Dies. The Engineer, Jan. 31, 1964. pp 222-224.

89. Rothman, D. & Sansome, D.H. — An Investigation of Rod-Drawing With Die Rotation. Int. Jnl. Mach. Tool Design & Research. Vol. 10. pp 179-192.

90. Chia, H.T. — Ph.D. Thesis. University of Aston in Birmingham. Department of Production Engineering. 1976.

91. Gordon, J.L. & Weinstein, A.S. — A Finite Element Analysis of the Plane Strain Drawing Problem. Proc. 2nd N. Amer. Metal Wks Res. Conf. 1974. pp 194-208.

92. Zienkiewicz, O.C. & Godnoble, P.N. — Flow of Plastic and Visco-Plastic Solids with Special Reference to Extrusion and Forming Processes. Int. J. Num. Methods in Eng., Vol. 8, 1974. pp 3-16.

93. Nayak, G.C. & Zienkiewicz, O.C. — Elasto-Plastic Stress Analysis. A generalisation for various constitutive relations including strain softening. Int. J. Num. Methods.in Eng., Vol. 5, 1972, pp 113-135.

94. Lahoti, G.D. & Kobayashi, S. — On Hill's General Method of Analysis for Metal-working Processes. Int. J. Mech. Sci. 1974, Vol. 16, pp 521-540.

95. Oxley, P. — Note : Allowing for Friction in Estimating Upper Bound Loads. Int. J. Mech. Sci., 1963, Vol. 5, pp 183-184.

96. Wistreich, J.G. — Die Pressure in Plane Strain Drawing: Comparison of Experiment with Theory. J. Mech. Phys. Solids, 1953, Vol. 1. pp 164-171.

97. Male, A.T., DePierre, V. & Saul, G. — The Relative Validity of the Concepts of Friction and Interface Shear Factor for use in Metal Deformation Studies. Trans. A.S.L.E., Vol. 16, 3, 177-184.

98. Bachrach, B.I., & Samanta, S.K. — Plane Strain Sheet and Tube Extrusion Through Cosine-shaped Dies with Friction. Proc. NAMRC II, pp 179-193.

99. Bishop, J.F.W. — On the Effect of Friction on Compression and Indentation Between Flat Dies. J. Mech. Phys. Solids, 1958, Vol. 6, pp 132-144.

100. Shield, R.T. — Plastic Flow in a Converging Conical Channel. J. Mech. Phys. Solds, 1955, Vol. 3, pp 246-258.

101. Johnson, W. & Sowerby, R. — Redundant Deformation Factors and Maximum Reduction in Plane Strain and Axi-symmetric Wire Drawing - 1 A Theoretical Investigation. Annals of C.I.R.P. Vol. XVIX. pp 311-315, 1971.

102. Cristescu, W. & Dragan, O. — Speed Infleuence on Cold Drawing in Ultrasonic Field. Faculty of Mathematics, University of Boucharest/ Metallurgical Research Institute, Bucharest, Romania.

103. Basily, B.B. & Sansome, D.H. — Some Theoretical Considerations for the Direct Drawing of Steel Rod from Round Bar. Int. J. Mech. Sc. Vol. 18, pp 201-208.

104. Bennett, D.F. — Private Communication. Bendix Industrial Brushes Ltd.

105. Vaidyanath, K.R., Nicholas, M.G. & Milner, D.R. — Pressure Welding by Rolling. British Welding Journal, Jan. 1969. pp 13-28.

ACKNOWLEDGEMENTS

The author would like to extend his thanks to the Head of the Department of Production Technology and Production Management for permission to undertake this research programme, and to the Science Research Council for financial support over a three year period.

The author would also like to thank Professor D.H. Sansome for his assistance and encouragement whilst supervising this project, and Dr. J.F.W. Bell, of the Department of Electrical Engineering, for assistance with certain aspects of the instrumentation.

Further, the author wishes to acknowledge the assistance of Mr. G.M. Jones, Mr. E. Langton, Mr.A.F. Scott and other members of the technical staff, for their assistance with the construction, and maintenance of the test equipment.

APPENDIX 1: Plane Strain Compression Tests

The plane strain compression test was developed to give a yield stress curve which results from a loading condition similar to that pertaining in such operations as strip rolling, strip drawing, and the drawing of thin walled tubes. This allows a realistic comparison between process loads and yield stress to be made.

This test[1][19] consists of indenting a strip of width, w and initial thickness, ho, with a pair of platens of breadth b. The ratio w:b should be at least 6:1 in order that plane strain conditions can be maintained (see Fig.(A1.1))

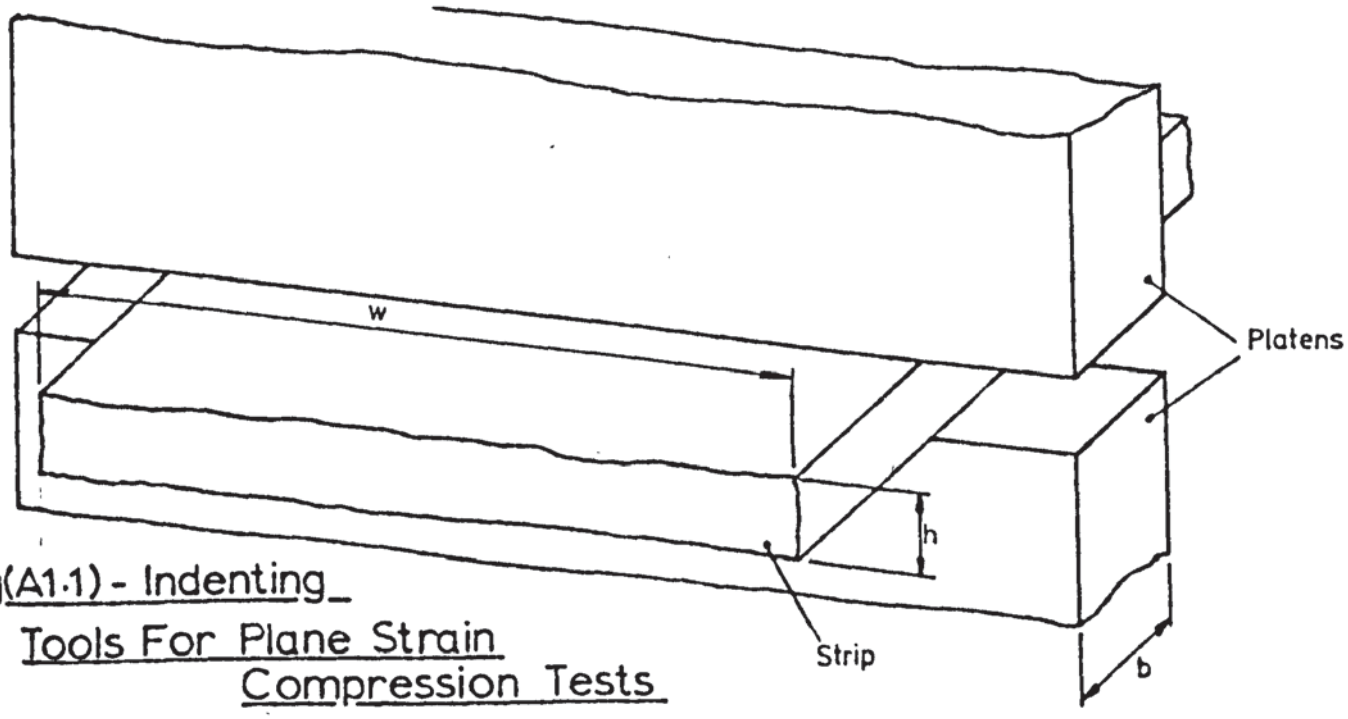

Fig(A1.1) - Indenting Tools For Plane Strain Compression Tests

Samples of strip were taken from each of the coils of strip used in the drawing tests and plane strain compression tests were carried out on each sample. The strip was successively indented and corresponding values of load and resulting strip thickness and breadth were noted. The indenting platens were mounted in a special sub-press and loaded in an Avery testing machine. These platens were changed, as required, in order to maintain the ratio b/h within, or near, the range 4 to 2. This is necessary, in the case of thick strip, to ensure that plane strain conditions apply and, in the case of a thin strip, to ensure that the frictional

constraint at the strip/platen interface does not contribute, appreciably, to the indentation load. It is for this latter reason that the strip is indented in small increments and relubricated, with molybdenum disulphide in this case, before further loading.

Figure (A1.2) shows the results of those tests. It can be seen that there were no significant differences in the properties of the test material.

Similar tests were carried out on two samples of strip which had been predrawn through the 7.5^{o} dies at 20.8% reduction of area. One sample had been drawn by conventional means and the other at full ultrasonic power input, which, at this reduction of area, results in practically zero front tension. Both samples had been drawn at the same coiler speed. It can be seen in Figure (A1.2) that there was no significant difference in the final properties of the material, and that there was no detectable redundant work. The work of Irving and Cotterill[20] indicate a redundant work factor, for mild steel, of 1.01 for a 5^{o} semi-angle die and 1.07 for a 15^{o} semi-angle die.

A.1.1.) Determination of Mean Yield Stress

Let the plane strain yield stress be described by the function:

$\sigma = f(\Sigma)$ where Σ is the natural strain resulting in the true stress, σ.

The mean yield stress in the interval

$(0,\Sigma_t)$ is therefore given by:

$$\bar{\sigma} = \frac{1}{\Sigma_t} \int_0^{\Sigma_t} f(\Sigma) d\,\Sigma$$

$$= \frac{1}{\Sigma_t} \left\{ \text{Area under the curve between 0 and } \Sigma_t \right\}$$

The area under the yield stress curve for the undrawn material, shown in Figure (A1.2), is derived as follows. The area under the 'knee' of the curve, in the interval $\Sigma \varepsilon (0,0.2)$ was determined by counting the squares it

Fig(A1.2) - Plane Strain Compression Test Results From Each Coil

Of The Test Results

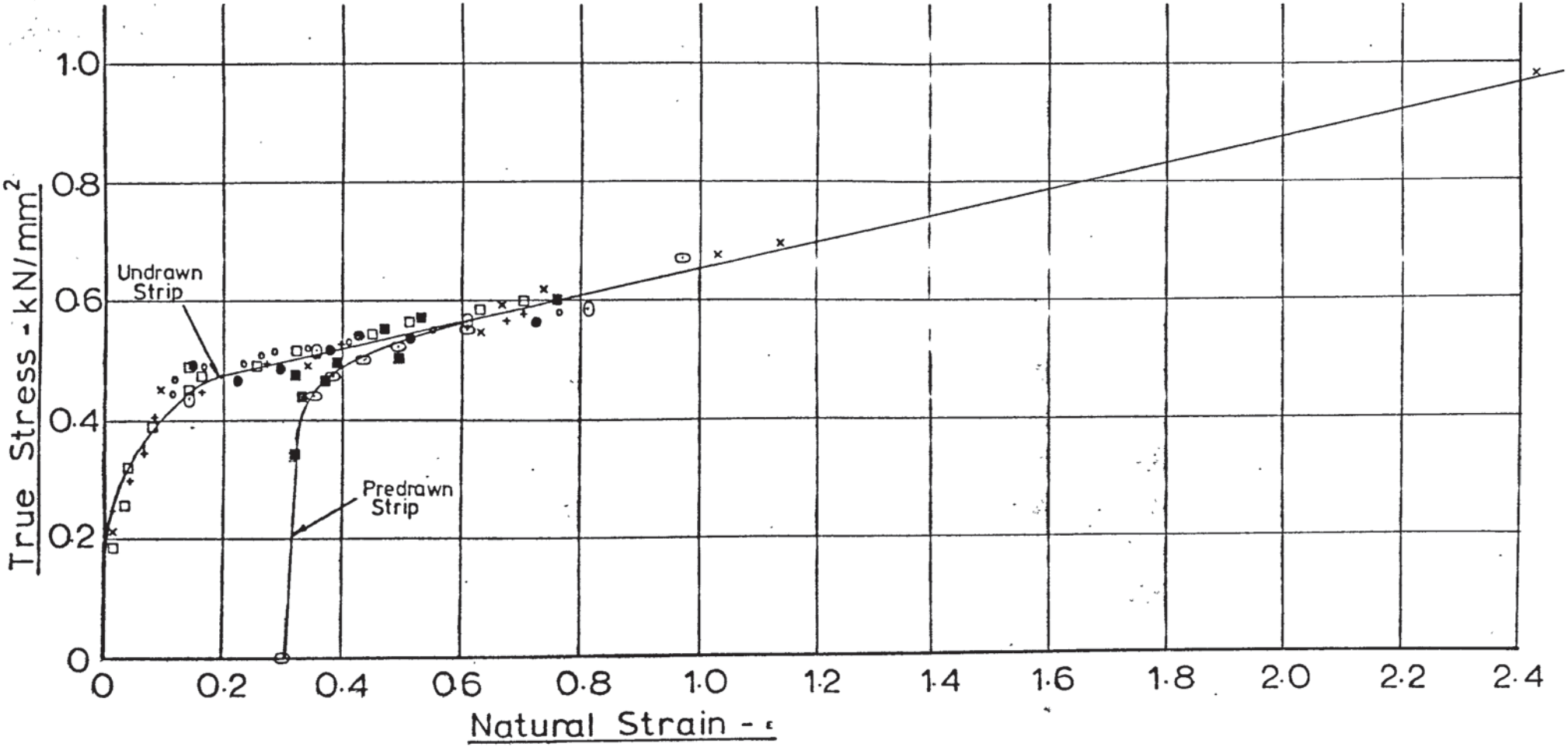

□ - Undrawn Strip, Last Coil, α = 7·5° with land

× - " " " , " "

+ - " " " , α = 7·5°

• - " " " , α = 2·5°

θ - " " " , α = 10·0°

● - " " " , α = 5·0°

■ - Predrawn With Ultrasonics

⊙ - Predrawn Conventionally

Material – Mild Steel (C – 0·05, Mn – 0·37, S – 0·02)

encloses on graph paper, for example:

Interval	Area-kN/mm^2
(0,0.05)	0.0102
(0,0.10)	0.0288
(0,0.20)	0.0732

The area under the curve for $\Sigma > 0.2$ can be considered as the area under the 'knee' plus a parallelogram bounded by the ordinates $\sigma = f(0.2)$ and $\sigma = f(\Sigma_t)$. That is, the area:

$$A_\sigma = 0.0732 + \frac{\left[\sigma_{\Sigma=0.2} + \sigma_{\Sigma=\Sigma_t}\right]}{2}\left[\Sigma_t - 0.2\right]$$

for $\Sigma_t \geqslant 0.2$

$$\sigma = f(\Sigma) = 0.225\Sigma_t + 0.43 \text{ kN/mm}^2$$

$$\therefore A\sigma = 0.0732 + \frac{\left|0.48 + 0.225\Sigma_t + 0.43\right|}{2}\left|\Sigma_t - 0.2\right|$$

$$= 0.1125\Sigma_t^2 + 0.4295\Sigma_t - 0.0178$$

$\therefore$ The mean yield stress in the interval $\Sigma = (0,\Sigma_t)$ for $\Sigma > 0.2$

$$\therefore \bar{\sigma} = \frac{A\sigma}{\Sigma_t} = \frac{0.1125\Sigma_t^2 + 0.4295\Sigma_t - 0.0178}{\Sigma_t}$$

The relationship between the nominal draw strain, Σ_t, and the mean draw stress, $\bar{\sigma}$, for reductions proceeding from the undrawn stock to Σ_t is shown in Figure (A1.3).

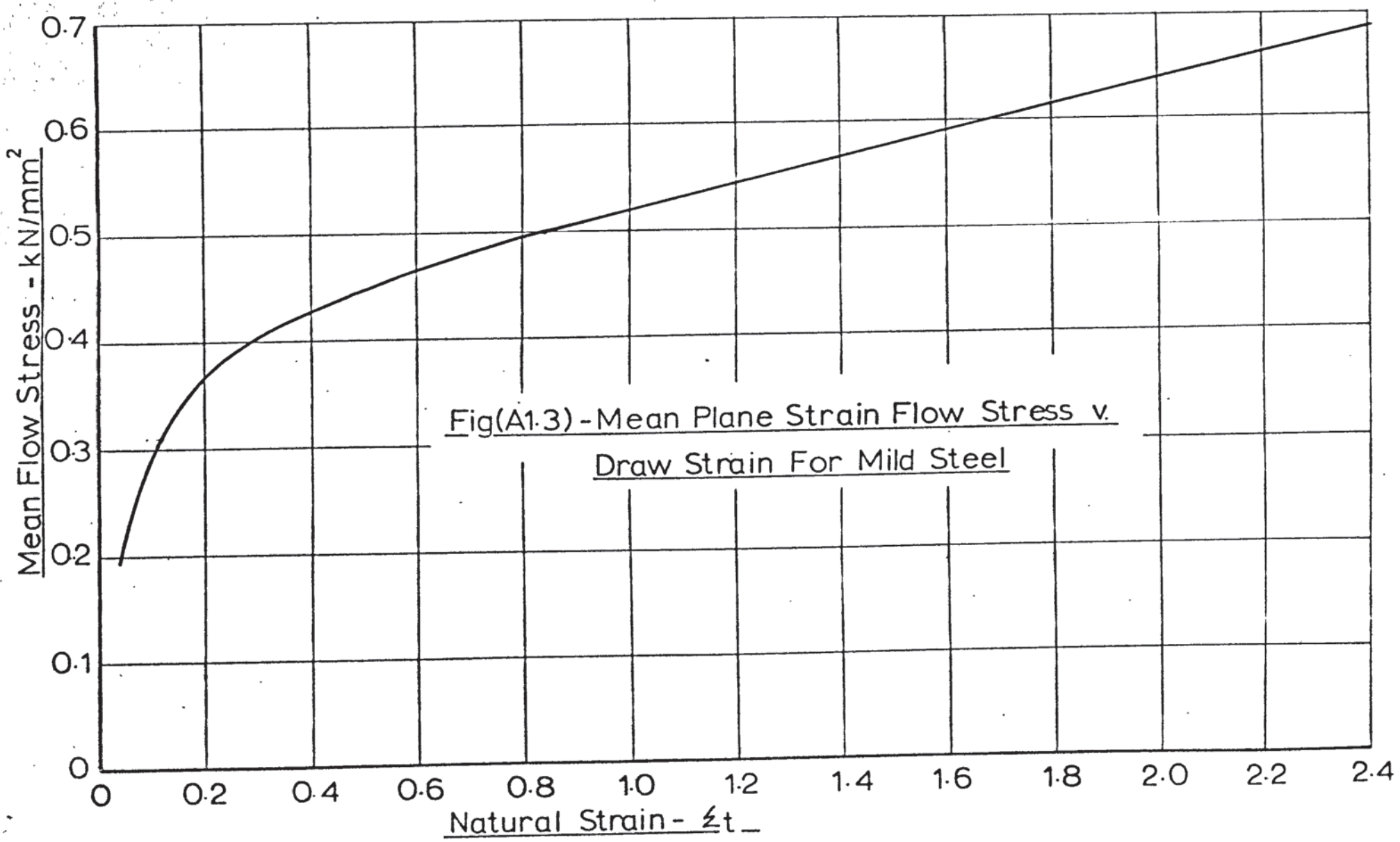

Fig(A1.3) - Mean Plane Strain Flow Stress v. Draw Strain For Mild Steel

APPENDIX 2: Bimetal Strip Drawing

Bimetal strip is usually produced by welding together plates of the required combination and hot rolling to reductions in excess of 70%. This produces the required interfacial bonding prior to any cold finishing passes.

It is important to generate a large increase in the length of the bimetal interface in a single pass. This requirement for a high initial reduction, more than any other factor, favours rolling as a method of producing bimetal strip. The reason for this is that interfacial oxide films are extensively disrupted by large axial strains allowing intimate metallic contact which enables metal diffusion between the two metals to procede. Temperature and pressure both play a part in the diffusion process though temperature affects the rate of diffusion to a far greater extent than does the pressure and hence the metals are heated prior to rolling. The theoretical background to this process is discussed in section A2.1. It is sufficient to state here, that an interfacial extension in excess of 60% is normally required before a full bond strength is obtained[105]. The early work in wire and tube drawing under the action of ultrasound indicated that reductions of area consistent with such extensions could be obtained without the need for pre-heating, thus enabling, for instance, combinations including precious metals to be processed in small batches with minimal waste.

A2.1) Theoretical Background[5]

In order to achieve welding between metal surfaces in the solid state it is necessary to obtain intimate contact between the metal surfaces. The normal cohesive forces are generally minimised by oxide films and these must therefore be removed or broken-up before welds can be initiated.

The process procedes in the following manner; in the first stage of deformation surface matching is achieved. This can occur at low overall

levels of deformation, though localised deformation of surface imperfections may be of a relatively high order. Bonding occurs between the oxide films on the metal surfaces which deform thereafter, in most metals, as a single film. As the oxide is brittle relative to the base metal, the interfacial oxide film breaks-up as deformation procedes and the pure or oxide free metal is extruded through the gaps in the oxide layers. The break-up of the oxide film, in aluminium, occurs, typically, at 40% reduction of area. The pressure required to extrude the metal through the gaps in the fragmented oxide film increases with film thickness, though the initiation of welds occur at reductions of area little greater than that required to break-up oxide film. Such welds are unstable and can be broken by elastic recovery upon the release of the deformation load, that is a further reduction is required to establish a permanent metallic bond. The extension of the metal interface consistent with a 70% reduction of area is, typically, necessary to achieve the mechanical properties of the parent metals.

In order to produce conditions compatible with the production of bimetal strip the mating surfaces must be free of contamination and with minimal oxide film. Wire brushing just prior to welding further improves weldability because of the disturbance of the oxide films and the exposure of the new surfaces which are chemically active.

A2.2) Design of the Apparatus

A generalised layout of the apparatus for bimetal strip drawing is shown in Figure (A2.1). Strip of the required combination is loaded onto the feed coils and fed over the guide rolls into an ultrasonic cleaning bath. This removes surface contamination prior to wire brushing. The power drawn during wire brushing is typically 30 watts per cm width of strip,[104] therefore a suitable drive system was designed. The brushes were mounted as close to the inlet of the die throat as possible in order to minimise

Fig(A2·1) - Bimetal Strip Drawing

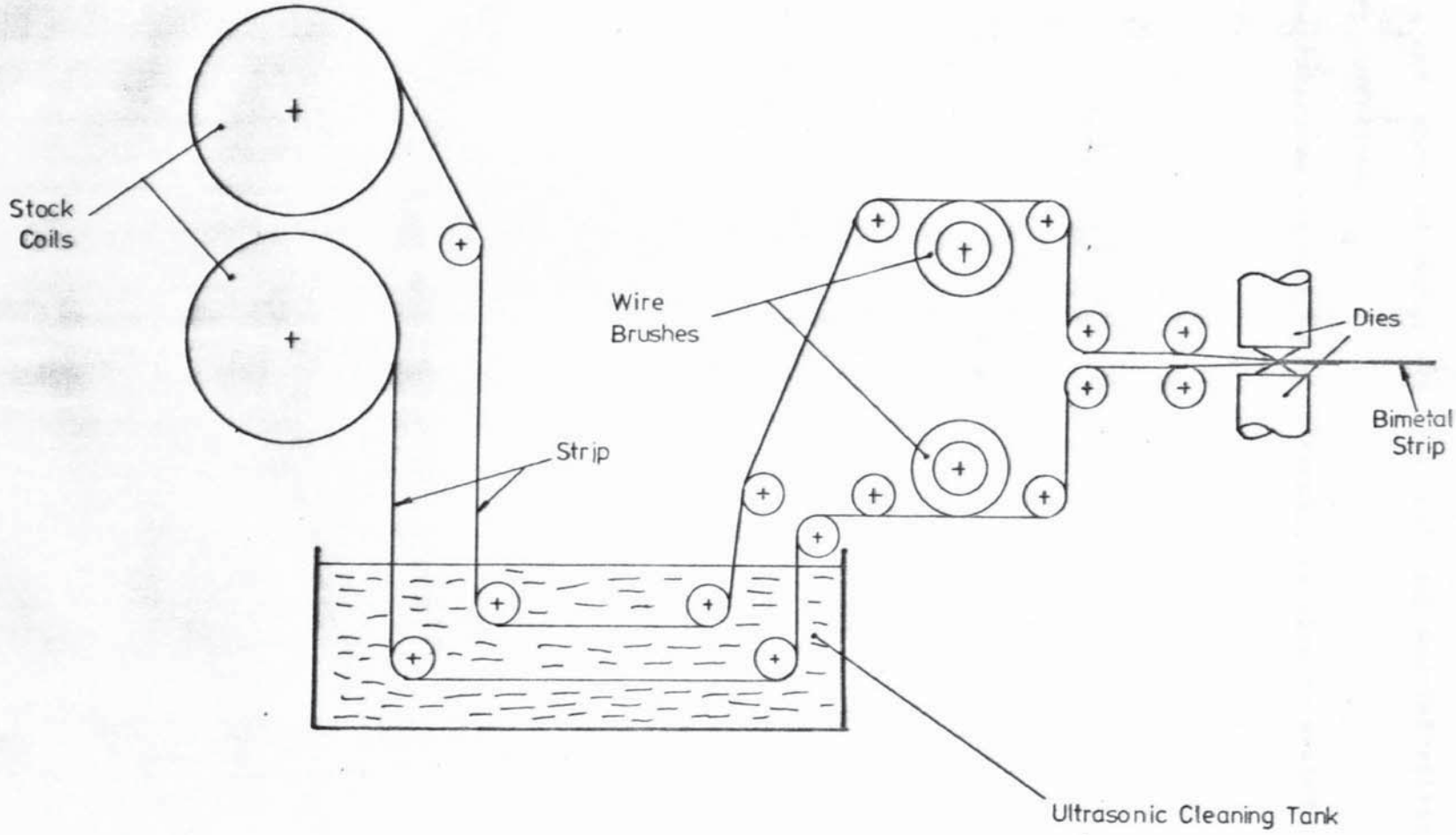

oxide build-up after brushing, by minimising the time the fresh surfaces were exposed to the air. It was intended to use the same tooling as in the strip drawing and, also, to design and make tools for Steckel rolling under oscillatory conditions.

Part of this apparatus was manufactured though, as already stated, it was never used.

APPENDIX 3: TABULATED DATA

A3.1. Draw test data

A3.2. Results of the regression tests

$\alpha = 7.5°$, r = 0.246, f = 13.06 kHz — Test No - 001

MEAN DRAW SPEED mm/sec	PEAK DIE VELOCITY mm/sec	Mean Loads - kN			Specific Loads - kN/mm^2		
		TAG	BENDING	DIE	DRAW STRESS	SPECIFIC AXIAL	LATERAL DIE
0.6	323	0.06	0.14	4.01	0.01	0.12	0.46
3.9	323	0.18	0.14	4.39	0.03	0.12	0.51
8.8	323	0.22	0.16	4.97	0.03	0.14	0.57
12.6	342	0.28	0.19	5.06	0.04	0.16	0.58
24.0	323	0.64	0.28	5.63	0.09	0.25	0.65
24.0	323	0.64	0.33	5.63	0.09	0.29	0.65
37.2	247	1.39	0.66	6.68	0.20	0.58	0.77
37.2	247	1.51	0.73	6.49	0.22	0.64	0.75
1.2	304	0.18	0.13	4.78	0.03	0.11	0.55
6.0	304	0.30	0.20	5.44	0.04	0.18	0.63
16.0	247	0.72	0.36	6.11	0.10	0.32	0.71
16.0	247	0.80	0.41	6.11	0.11	0.36	0.71
29.2	152	1.64	0.75	6.49	0.23	0.66	0.75
29.2	152	1.51	0.95	6.49	0.22	0.83	0.75
3.6	228	0.52	0.33	5.35	0.07	0.29	0.62
14.3	113	1.49	0.78	6.49	0.21	0.68	0.75
37.1	66.7	2.25	1.18	7.26	0.32	1.03	0.84
37.1	66.7	2.09	1.03	7.26	0.30	0.90	0.84
37.1	66.7	2.01	0.91	7.26	0.29	0.80	0.84
—	0	2.07	1.06	6.30	0.30	0.93	0.73

$\alpha = 7.5$, r = 0.287, f = 13.06 kHz — Test No - 002

MEAN DRAW SPEED mm/sec	PEAK DIE VELOCITY mm/sec	Mean Loads - kN			Specific Loads - kN/mm^2		
		TAG	BENDING	DIE	DRAW STRESS	SPECIFIC AXIAL	LATERAL DIE
0.5	342	0.24	0.16	4.87	0.04	0.12	0.48
2.4	361	0.28	0.18	5.16	0.04	0.14	0.51
5.9	361	0.34	0.23	5.16	0.05	0.17	0.51
10.1	342	0.44	0.28	5.54	0.07	0.21	0.55
13.3	342	0.48	0.21	5.73	0.07	0.16	0.57
13.3	342	0.48	0.30	5.73	0.07	0.23	0.57
21.7	323	0.80	036	6.11	0.12	0.27	0.60
27.5	266	1.09	0.54	6.49	0.17	0.41	0.64
35.9	228	1.61	0.71	6.88	0.24	0.53	0.68
35.9	228	1.41	0.88	7.25	0.22	0.66	0.72
35.9	228	1.53	0.83	7.25	0.24	0.62	0.72
1.5	304	0.24	0.25	4.97	0.04	0.18	0.49
5.8	304	0.42	0.33	5.73	0.06	0.25	0.57
13.5	266	0.84	0.45	6.30	0.13	0.25	0.62
21.7	209	1.49	0.73	7.07	0.22	0.55	0.70

$\alpha = 7.5°$, $r = 0.287$, $f = 13.06$ kHz — Test No - 002 cont.

MEAN DRAW SPEED mm/sec	PEAK DIE VELOCITY mm/sec	Mean Loads - kN			Specific Loads - kN/mm^2		
		TAG	BENDING	DIE	DRAW STRESS	SPECIFIC AXIAL	LATERAL DIE
—	171	1.76	0.85	7.45	0.27	0.64	0.74
30.6	171	1.87	0.90	7.45	0.29	0.68	0.74
35.9	133	2.37	1.25	7.64	0.36	0.94	0.76
35.1	133	2.21	1.16	7.26	0.34	0.87	0.72
35.1	133	2.09	1.05	7.64	0.85	0.79	0.76
—	247	0.36	0.19	5.35	0.32	0.14	0.53
—	266	0.40	0.13	5.35	0.05	0.09	0.53
8.0	133	1.73	0.83	7.45	0.06	0.62	0.74
16.5	85.7	2.25	1.16	7.83	0.27	0.87	0.77
22.9	57.1	2.37	1.23	7.64	0.35	0.92	0.76
29.5	57.1	2.37	1.21	7.83	0.36	0.91	0.77
41.3	57.1	1.97	1.08	8.02	0.30	0.81	0.79
41.3	57.1	2.41	1.23	8.02	0.37	0.92	0.79

$\alpha = 7.5°$, $r = 0.246$, $f = 12.9$ kHz — Test No - 003

MEAN DRAW SPEED mm/sec	PEAK DIE VELOCITY mm/sec	Mean Loads - kN			Specific Loads - kN/mm^2		
		TAG	BENDING	DIE	DRAW STRESS	SPECIFIC AXIAL	LATERAL DIE
0.4	419	0.04	0.23	3.63	0.01	0.20	0.42
0.5	400	0.04	0.24	3.25	0.01	0.21	0.38
1.7	419	0.08	0.23	3.63	0.01	0.20	0.42
4.4	419	0.18	0.23	4.01	0.03	0.20	0.46
7.2	410	0.24	0.25	4.01	0.03	0.22	0.46

α = 7·5°, r = 0·173, f = 12·96 kHz — Test No - 004

MEAN DRAW SPEED mm/sec	PEAK DIE VELOCITY mm/sec	Mean Loads - kN			Specific Loads - kN/mm²		
		TAG	BENDING	DIE	DRAW STRESS	SPECIFIC AXIAL	LATERAL DIE
3·5	286	0·10	0·10	2·67	0·01	0·12	0·43
8·6	305	0·16	0·10	3·25	0·02	0·12	0·52
11·1	286	0·26	0·13	3·44	0·03	0·16	0·55
18·4	286	0·36	0·14	3·63	0·05	0·17	0·58
25·1	191	0·90	0·40	4·58	0·12	0·50	0·73
36·1	152	1·37	0·68	4·97	0·18	0·85	0·79
36·1	152	1·29	0·60	4·97	0·17	0·75	0·79
SMALL	324	0·16	0·63	3·25	0·02	0·79	0·52
2·2	324	0·20	0·08	3·25	0·03	0·09	0·52
4·6	343	0·26	0·10	3·44	0·03	0·12	0·55
5·5	66·9	1·32	0·65	5·16	0·17	0·81	0·82
10·9	76·4	1·75	0·73	3·63	0·23	0·91	0·58
16·6	76·4	1·57	0·88	5·35	0·21	1·09	0·85
21·9	66·9	1·53	0·81	5·54	0·20	1·01	0·89
28·6	66·9	1·61	0·86	5·54	0·21	1·07	0·89
41·5	57·3	1·57	0·85	5·54	0·21	1·05	0·89
?	0	1·41	0·75	4·58	0·18	0·94	0·73

α = 7·5°, r = 0·438, f = 12·95 kHz — Test No - 005

MEAN DRAW SPEED mm/sec	PEAK DIE VELOCITY mm/sec	Mean Loads - kN			Specific Loads - kN/mm²		
		TAG	BENDING	DIE	DRAW STRESS	SPECIFIC AXIAL	LATERAL DIE
0·5	209	2·01	1·05	9·17	0·39	0·52	0·59
1·3	209	2·09	1·10	9·17	0·41	0·54	0·59
3·6	209	2·05	1·05	9·07	0·40	0·52	0·59
5·6	209	1·89	0·98	8·98	0·37	0·48	0·58
5·6	190	1·89	0·98	8·98	0·37	0·48	0·58
9·4	190	1·89	0·96	9·17	0·37	0·47	0·59
11·5	190	2·01	1·00	9·36	0·39	0·49	0·61
14·9	190	2·01	1·00	9·55	0·39	0·49	0·62
14·9	190	2·13	1·10	9·55	0·42	0·54	0·62
18·2	181	2·33	1·25	9·55	0·45	0·61	0·62
18·2	181	2·41	1·35	9·55	0·47	0·66	0·62
21·8	171	2·29	1·18	9·93	0·45	0·58	0·64
21·8	171	2·45	1·23	9·93	0·48	0·61	0·64
25·2	171	2·37	1·26	9·55	0·46	0·62	0·62
25·2	171	2·29	1·16	9·55	0·45	0·57	0·62
31·5	171	2·21	1·28	9·55	0·43	0·63	0·62
38·0	171	2·49	1·33	9·74	0·49	0·66	0·63
38·0	171	2·49	1·33	9·74	0·49	0·66	0·63
1·3	95·4	2·45	1·15	9·74	0·48	0·57	0·63

$\alpha = 7.5°$, $r = 0.438$, $f = 12.95$ kHz — Test No - 005 CONT.

MEAN DRAW SPEED mm/sec	PEAK DIE VELOCITY mm/sec	Mean Loads - kN			Specific Loads - kN/mm^2		
		TAG	BENDING	DIE	DRAW STRESS	SPECIFIC AXIAL	LATERAL DIE
3.1	95.4	2.45	1.15	9.74	0.48	0.57	0.63
5.3	95.4	2.47	1.20	9.83	0.48	0.59	0.64
7.8	95.4	2.53	1.23	9.83	0.49	0.61	0.64
11.2	95.4	2.21	1.25	8.78	0.43	0.62	0.57
17.2	95.4	2.27	1.20	9.55	0.44	0.59	0.62
23.4	95.4	2.21	1.18	9.74	0.43	0.58	0.63
34.1	95.4	2.17	1.18	8.98	0.42	0.58	0.58

$\alpha = 7.5°$, $r = 0.480$, $f = 13.14$ kHz — Test No - 010

MEAN DRAW SPEED mm/sec	PEAK DIE VELOCITY mm/sec	Mean Loads - kN			Specific Loads - kN/mm^2		
		TAG	BENDING	DIE	DRAW STRESS	SPECIFIC AXIAL	LATERAL DIE
3.2	362	0.84	0.49	8.40	0.17	0.21	0.48
7.4	362	0.96	0.53	8.69	0.20	0.23	0.49
15.0	305	1.13	0.59	8.78	0.23	0.26	0.50
26.9	305	1.36	0.68	9.16	0.28	0.29	0.52
29.0	228	1.65	0.78	9.55	0.34	0.33	0.54
29.0	228	1.89	1.27	9.55	0.39	0.55	0.54
50.3	209	1.96	0.88	9.74	0.41	0.38	0.55
50.3	209	2.25	1.24	9.26	0.47	0.54	0.53
62.8	190	2.29	1.12	9.55	0.47	0.48	0.54
62.8	190	2.49	1.22	8.97	0.52	0.53	0.51
72.5	171	1.93	1.25	9.07	0.40	0.54	0.52
72.5	171	1.65	1.07	9.93	0.34	0.46	0.56
88.7	171	2.45	1.22	9.74	0.51	0.53	0.55
88.7	171	2.37	1.14	9.74	0.49	0.49	0.55
101	152	2.33	0.96	8.88	0.48	0.41	0.51
101	152	1.84	0.96	11.27	0.38	0.41	0.64
121	152	1.76	1.04	9.17	0.36	0.45	0.52
121	152	2.05	0.96	9.17	0.42	0.41	0.52

$\alpha = 7.5°$, r 0.533, f = 13.14 kHz — Test No - 011

MEAN DRAW SPEED mm/sec	PEAK DIE VELOCITY mm/sec	Mean Loads - kN			Specific Loads - kN/mm^2		
		TAG	BENDING	DIE	DRAW STRESS	SPECIFIC AXIAL	LATERAL DIE
6.0	477	0.34	0.31	8.31	0.07	0.12	0.43
11.4	457	0.44	0.34	8.12	0.09	0.32	0.42
17.9	438	0.60	0.39	8.02	0.13	0.15	0.41
32.8	419	1.26	0.62	8.98	028	0.24	0.46
47.1	400	1.32	0.61	8.98	0.29	0.24	0.46
47.1	400	1.24	061	8.98	0.28	0.24	0.46
68.5	381	1.21	0.55	8.98	0.27	021	0.46
68.5	381	1.21	0.61	8.98	0.27	0.24	0.46
107.	305	1.74	0.86	9.65	039	0.33	0.49
107	305	1.84	0.94	9.65	0.41	0.37	0.49
125	267	2.13	1.14	9.55	0.48	0.44	0.49
125	267	2.01	0.93	9.93	0.45	036	0.51
150	238	2.33	1.17	9.74	0.52	046	0.53
150	238	2.13	1.03	9.74	0.48	040	0.50

$\alpha = 7.5°$, r = 0.616, f = 13.32 kHz — Test No - 013

MEAN DRAW SPEED mm/sec	PEAK DIE VELOCITY mm/sec	Mean Loads - kN			Specific Loads - kN/mm^2		
		TAG	BENDING	DIE	DRAW STRESS	SPECIFIC AXIAL	LATERAL DIE
4.2	467	0.94	0.66	9.93	0.25	0.22	0.44
5.0	467	1.00	0.68	10.03	0.26	0.23	0.44
7.6	438	1.17	0.73	9.93	0.31	0.25	0.44
11.5	419	1.29	0.86	9.84	0.34	0.29	0.44
15.6	419	1.41	0.94	9.74	0.37	0.32	0.43
19.3	400	1.53	0.99	9.74	0.40	0.33	0.43
17.4	391	1.56	1.05	9.74	0.41	0.35	0.43
28.2	362	1.65	1.09	9.74	0.43	0.37	0.43
40.8	362	1.85	1.20	9.93	0.49	0.40	0.44
45.8	362	1.97	1.35	9.93	0.52	0.45	0.44
52.4	362	2.15	1.47	9.64	0.56	0.49	0.43

$\alpha = 7.5$, $r = 0.351$, $f = 13.07$ kHz — Test No - 014

MEAN DRAW SPEED mm/sec	PEAK DIE VELOCITY mm/sec	Mean Loads - kN			Specific Loads - kN/mm^2		
		TAG	BENDING	DIE	DRAW STRESS	SPECIFIC AXIAL	LATERAL DIE
<2.8	381	0.04	0.35	5.15	0.01	0.21	0.40
2.8	372	0.08	0.36	5.06	0.01	0.21	0.39
10.8	381	0.12	0.39	5.34	0.02	0.23	0.42
17.1	381	0.24	0.39	5.73	0.04	0.23	0.45
34.2	362	0.40	0.42	6.02	0.07	0.25	0.47
51.3	362	0.64	0.42	6.67	0.10	0.25	0.52
59.8	362	0.66	0.39	6.88	0.11	0.23	0.54
79.8	333	0.92	0.54	7.07	0.15	0.32	0.55
102.6	286	1.36	0.70	7.45	0.22	0.41	0.58
119.7	267	1.49	0.83	7.45	0.24	0.49	0.58
179.5	228	1.88	1.04	7.83	0.31	0.61	0.61

$\alpha = 7.5$, $r = 0.797$, $f = 13.26$ kHz — Test No - 016

MEAN DRAW SPEED mm/sec	PEAK DIE VELOCITY mm/sec	Mean Loads - kN			Specific Loads - kN/mm^2		
		TAG	BENDING	DIE	DRAW STRESS	SPECIFIC AXIAL	LATERAL DIE
4.0	542	1.01	0.52/0.36	13.56	0.53	0.13/0.09	0.43
7.2	503	1.33	0.52/0.36	12.61	0.70	0.13/0.08	0.40

$\alpha = 7.5$, $r = 0.696$, $f = 13.19$ kHz — Test No - 018

MEAN DRAW SPEED mm/sec	PEAK DIE VELOCITY mm/sec	Mean Loads - kN			Specific Loads - kN/mm^2		
		TAG	BENDING	DIE	DRAW STRESS	SPECIFIC AXIAL	LATERAL DIE
2.2	501	0.32	0.44	9.74	0.11	0.13	0.38
5.8	481	0.60	0.59	9.36	0.20	0.18	0.37
10.3	452	0.64	0.65	9.17	0.21	0.19	0.36
19.9	404	1.00	0.73	8.98	0.34	0.22	0.35
29.9	385	1.67	0.75	8.79	0.56	0.22	0.35
44.9	346	1.47	0.87	8.79	0.49	0.26	0.35
59.8	308	1.81	0.99	8.79	0.61	0.30	0.35
71.8	289	1.89	1.09	8.79	0.63	0.32	0.35

α = 7.5°, = 0.653, f = 13.21 kHz Test No - 019

MEAN DRAW SPEED mm/sec	PEAK DIE VELOCITY mm/sec	Mean Loads - kN			Specific Loads - kN/mm²		
		TAG	BENDING	DIE	DRAW STRESS	SPECIFIC AXIAL	LATERAL DIE
3.0	463	0.72	0.36	10.67	0.21	0.11	0.45
4.0	463	0.74	0.36	10.79	0.21	0.11	0.45
6.0	424	0.93	0.44	10.51	0.27	0.14	0.44
12.8	405	1.07	0.49	10.22	0.31	0.16	0.43
22.3	366	1.39	0.62	10.12	0.40	0.20	0.42
33.2	347	1.48	0.70	10.31	0.43	0.22	0.43
44.5	328	1.53	0.78	10.12	0.45	0.25	0.42
61.9	308	1.73	0.86	10.31	0.50	0.27	0.43
73.3	279	1.73	1.00	11.56	0.50	0.32	0.48
83.5	241	2.17	1.16	10.70	0.63	0.37	0.45

α = 7.5°, r = 0.440, f = 13.15 kHz Test No - 023

MEAN DRAW SPEED mm/sec	PEAK DIE VELOCITY mm/sec	Mean Loads - kN			Specific Loads - kN/mm²		
		TAG	BENDING	DIE	DRAW STRESS	SPECIFIC AXIAL	LATERAL DIE
27.2	326	0.44	0.44	7.45	0.08	0.21	0.46
27.2	278	0.78	0.52	8.02	0.15	0.25	0.50
25.3	163	1.95	1.14	8.79	0.37	0.54	0.55
26.4	153	2.17	1.20	8.98	0.41	0.57	0.56
26.4	86	2.43	1.22	9.16	0.46	0.58	0.57
26.4	57	2.77	1.61	8.79	0.52	0.76	0.55
26.4	0	2.89	1.86	9.17	0.54	0.88	0.57
26.4	57	2.77	1.56	8.79	0.52	0.74	0.55
27.2	105	2.21	1.25	8.98	0.41	0.59	0.56
27.2	163	2.09	1.14	9.17	0.39	0.54	0.57
27.2	192	1.73	0.94	8.98	0.32	0.44	0.56
27.6	288	0.96	0.52	8.40	0.18	0.25	0.52
27.6	326	0.56	0.33	7.74	0.10	0.16	0.48
27.6	326	0.44	0.31	7.45	0.08	0.15	0.46
27.6	326	0.48	0.39	7.07	0.09	0.18	0.44
70.4	326	0.92	0.53	8.40	0.17	0.25	0.52
71.8	278	1.21	0.68	8.98	0.23	0.32	0.56
71.8	249	1.45	0.81	8.97	0.27	0.38	0.56
73.3	134	2.09	1.13	9.74	0.39	0.53	0.60
71.8	201	1.85	1.01	9.17	0.39	0.48	0.57
73.3	115	2.53	1.38	9.55	0.47	0.65	0.59
71.8	77	2.71	1.52	9.36	0.51	0.72	0.58
71.8	48	3.13	1.69	8.60	0.59	0.80	0.53

$\alpha = 7.5°$, $r = 0.387$, $f = -$ kHz Test No - 024

MEAN DRAW SPEED mm/sec	PEAK DIE VELOCITY mm/sec	Mean Loads - kN			Specific Loads - kN/mm^2		
		TAG	BENDING	DIE	DRAW STRESS	SPECIFIC AXIAL	LATERAL DIE
108	211	1.51	1.14	7.54	0.26	0.61	0.53
108	240	1.25	1.03	7.54	0.21	0.55	0.53
110	201	1.53	1.19	7.83	0.26	0.64	0.55
110	182	1.65	1.25	7.93	0.28	0.67	0.56
115	153	1.93	1.38	7.83	0.33	0.74	0.55
113	115	1.85	1.26	8.59	0.32	0.68	0.61
112	96.1	2.21	1.24	8.50	0.38	0.66	0.60
115	67.3	2.37	1.65	8.40	0.41	0.86	0.59
115	57.7	2.61	1.72	8.21	0.45	0.92	0.58
117	28.8	2.69	1.76	8.40	0.46	0.94	0.59
58.9	0	3.06	1.90	8.40	0.52	1.02	0.59
58.9	19.2	2.93	1.82	8.40	0.50	0.97	0.59
58.9	48.1	2.81	1.82	8.49	0.48	0.97	0.60
58.9	96.1	2.29	1.50	8.49	0.39	0.80	0.62
58.9	144	2.01	1.14	6.49	0.34	0.61	0.46
58.9	182	1.51	1.13	8.11	0.26	0.60	0.57
57.9	249	1.03	0.86	7.45	0.18	0.46	0.53
57.4	307	0.60	0.68	6.97	0.10	0.36	0.49
56.5	346	0.32	0.47	6.30	0.05	0.25	0.44
22.4	346	0.24	0.55	6.21	0.04	0.29	0.44
22.4	307	0.34	0.60	6.49	0.06	0.32	0.46
22.4	269	0.80	0.85	7.45	0.14	0.46	0.53
22.4	259	0.84	0.85	7.64	0.14	0.46	0.54
22.4	249	0.82	0.83	7.54	0.14	0.44	0.53
22.4	230	1.00	0.85	7.83	0.17	0.46	0.55
22.4	192	1.41	1.09	8.02	0.24	0.58	0.57
22.4	115	2.13	1.55	8.40	0.36	0.83	0.59
22.4	86.5	2.41	1.63	8.60	0.41	0.87	0.60
22.4	38.5	2.83	1.92	8.40	0.48	1.03	0.59
22.4	0	2.89	1.87	8.60	0.49	1.09	0.61
171	0	3.10	2.08	8.12	0.53	1.11	0.57
171	19.2	2.85	1.87	8.69	0.49	1.00	0.61
171	48.1	2.97	1.98	8.40	0.51	1.06	0.59
171	86.5	2.91	1.95	8.40	0.50	1.04	0.59
171	115	2.73	1.82	8.31	0.46	0.97	0.59
171	182	2.21	1.51	8.60	0.38	0.81	0.61
171	57.6	2.93	1.90	8.60	0.50	1.02	0.61
171	76.9	2.93	1.92	8.21	0.50	1.03	0.58

α = 7.5° r = 0.387, f = — kHz Test No - 024 CONT

MEAN DRAW SPEED mm/sec	PEAK DIE VELOCITY mm/sec	Mean Loads - kN			Specific Loads - kN/mm²		
		TAG	BENDING	DIE	DRAW STRESS	SPECIFIC AXIAL	LATERAL DIE
171	115	2.51	1.72	8.60	0.43	0.92	0.61
171	153	2.31	1.66	8.21	0.40	0.89	0.58
171	192	2.13	1.53	8.40	0.36	0.82	0.59

α = 7.5°, r = 0.307, f = — kHz Test No - 025

MEAN DRAW SPEED mm/sec	PEAK DIE VELOCITY mm/sec	Mean Loads - kN			Specific Loads - kN/mm²		
		TAG	BENDING	DIE	DRAW STRESS	SPECIFIC AXIAL	LATERAL DIE
14.9	326	0.18	0.03	5.16	0.03	0.02	0.46
14.9	297	0.30	0.09	5.54	0.05	0.06	0.49
15.1	268	0.60	0.22	5.92	0.09	0.15	0.53
15.1	211	0.96	0.43	6.78	0.15	0.29	0.60
16.0	153	1.61	0.73	6.88	0.24	0.49	0.61
16.0	105	1.95	0.92	7.07	0.30	0.62	0.63
16.6	76.7	2.21	1.11	7.07	0.34	0.75	0.63
16.0	48.0	2.19	1.17	7.07	0.33	0.79	0.63
16.3	0	2.49	1.25	7.25	0.38	0.84	0.64
—	—	—	—	—	—	—	—
24.8	0	2.61	1.42	7.64	0.40	0.96	0.68
25.2	19.2	2.65	1.38	7.54	0.40	0.93	0.67
25.2	47.9	2.49	1.19	7.64	0.38	0.80	0.68
24.8	76.7	2.49	1.17	7.64	0.38	0.79	0.68
25.2	105	2.17	0.98	7.64	0.33	0.66	0.68
25.6	134	1.69	1.01	7.64	0.26	0.68	0.68
25.2	172	1.45	0.65	7.35	0.22	0.44	0.65
25.6	220	1.05	0.44	6.97	0.16	0.30	0.62
25.6	278	0.68	0.20	6.59	0.10	0.14	0.58
25.6	287	0.52	0.17	6.11	0.08	0.12	0.54
25.6	326	0.24	0.05	5.44	0.04	0.03	0.48
—	—	—	—	—	—	—	—
43.1	306	0.40	0.14	5.73	0.06	0.09	0.51
43.1	268	0.78	0.30	6.30	0.12	0.20	0.56
43.8	230	1.00	0.40	6.49	0.15	0.27	0.58
43.8	201	1.17	0.53	6.69	0.18	0.36	0.59
44.9	172	1.45	0.63	6.69	0.22	0.43	0.59
43.1	153	1.81	0.78	6.87	0.27	0.53	0.61
43.8	115	1.81	0.86	7.26	0.27	0.58	0.65
45.0	86.3	2.07	1.04	7.25	0.31	0.70	0.64
45.0	57.6	2.47	1.36	7.25	0.37	0.92	0.64
44.0	28.8	2.47	1.34	7.64	0.37	0.90	0.68

α = 7.5°, r = 0.307, f = — kHz Test No - 025 CONT

MEAN DRAW SPEED mm/sec	PEAK DIE VELOCITY mm/sec	Mean Loads - kN			Specific Loads - kN/mm^2		
		TAG	BENDING	DIE	DRAW STRESS	SPECIFIC AXIAL	LATERAL DIE
44.8	9.6	2.55	1.38	7.64	0.39	0.93	0.68
45.0	0	2.77	1.38	7.49	0.42	0.93	0.66
—	—	—	—	—	—	—	—
59.4	0	2.21	1.12	7.45	0.33	0.76	0.66
59.4	9.6	2.89	1.35	7.26	0.44	0.91	0.65
61.2	48.0	2.33	1.14	7.83	0.35	0.77	0.69
61.6	76.7	2.25	1.09	7.45	0.34	0.74	0.66
61.6	115	2.21	1.07	7.45	0.33	0.72	0.66
64.0	153	1.83	0.87	7.26	0.28	0.59	0.64
64.0	172	1.75	0.79	7.07	0.26	0.53	0.63
64.0	201	1.51	0.65	7.07	0.23	0.44	0.63
64.0	220	1.33	0.53	6.97	0.20	0.36	0.62
64.0	268	1.00	0.38	6.69	0.15	0.26	0.59
—	—	—	—	—	—	—	—
79.2	201	1.41	0.68	6.88	0.21	0.46	0.61
79.2	153	1.83	0.89	7.26	0.28	0.60	0.65
77.0	134	2.15	1.05	7.45	0.33	0.71	0.66
81.6	105	2.45	1.18	7.26	0.37	0.80	0.65
77.8	86.3	2.43	1.21	7.45	0.37	0.82	0.66
81.6	67.1	2.71	1.37	7.45	0.41	0.93	0.66
84.9	48.0	2.77	1.37	7.54	0.42	0.93	0.67
75.6	28.8	2.91	1.52	7.35	0.44	1.03	0.65
80.8	9.6	2.67	1.38	7.64	0.40	0.93	0.68
83.2	0	2.75	1.37	7.16	0.42	0.93	0.64
—	—	—	—	—	—	—	—
100	0	2.57	1.22	7.64	0.39	0.82	0.68
100	19.2	2.79	1.37	7.64	0.42	0.93	0.68
100	67.1	2.65	1.26	7.45	0.40	0.84	0.66
100	124	2.69	1.56	7.45	0.41	1.05	0.66
—							—

$\alpha = 7.5°$, r = 0.368, f = – kHz Test No - 026

MEAN DRAW SPEED mm/sec	PEAK DIE VELOCITY mm/sec	Mean Loads - kN			Specific Loads - kN/mm^2		
		TAG	BENDING	DIE	DRAW STRESS	SPECIFIC AXIAL	LATERAL DIE
1.28	228	0.12	0.13	5.92	0.02	0.07	0.44
1.28	278	0.18	0.17	6.21	0.03	0.10	0.46
1.28	269	0.34	0.26	6.49	0.06	0.15	0.48
2.05	192	1.15	0.56	7.45	0.19	0.32	0.55
1.89	163	1.64	0.77	7.83	0.27	0.43	0.58
1.81	124	1.83	0.83	7.93	0.30	0.47	0.59
1.75	86.5	2.13	0.98	8.02	0.35	0.55	0.59
1.63	67.3	2.25	1.05	8.02	0.37	0.59	0.59
1.57	48.1	2.31	1.11	7.93	0.38	0.63	0.59
1.57	19.2	2.45	1.20	8.02	0.40	0.68	0.59
1.57	0	2.55	1.24	8.02	0.42	0.70	0.59
5.37	0	2.59	1.21	8.21	0.42	0.68	0.61
6.16	9.6	2.51	1.20	8.21	0.41	0.68	0.61
5.74	19.2	2.51	1.18	8.21	0.41	0.66	0.61
5.94	28.8	2.39	1.14	8.21	0.39	0.64	0.61
5.94	67.3	2.25	1.03	8.12	0.37	0.58	0.60
5.94	96.1	2.05	0.94	8.21	0.34	0.53	0.61
5.94	153	1.58	0.70	7.93	0.26	0.39	0.59
6.16	192	1.21	0.53	7.54	0.20	0.30	0.56
5.94	269	0.56	0.25	6.78	0.09	0.14	0.50
5.94	278	0.36	0.18	6.50	0.06	0.10	0.48
13.8	211	0.88	0.42	7.64	0.14	0.24	0.57
12.8	201	1.04	0.48	7.83	0.17	0.27	0.58
13.9	201	1.21	0.60	7.83	0.20	0.34	0.58
13.9	192	1.37	0.70	7.83	0.22	0.39	0.58
13.9	182	1.49	0.75	8.02	0.22	0.42	0.59
13.9	163	1.57	0.83	8.02	0.26	0.47	0.59
13.9	144	1.77	0.92	8.02	0.29	0.52	0.59
13.9	124	1.91	0.99	8.02	0.31	0.56	0.59
13.9	105	2.21	1.04	7.83	0.36	0.59	0.58
13.9	86.5	2.37	1.16	7.83	0.39	0.65	0.58
13.9	38.5	2.43	1.22	8.02	0.40	0.69	0.59
13.9	28.8	2.41	1.22	8.02	0.40	0.69	0.59
13.9	9.6	2.49	1.27	8.21	0.41	0.72	0.61
13.9	0	2.57	1.34	8.21	0.42	0.75	0.61
32.0	0	1.97	1.09	8.02	0.32	0.61	0.59
32.0	9.6	1.99	1.11	8.02	0.32	0.63	0.59

$\alpha = 7.5°$, r = 0.307, f = ~ kHz — Test No - 026 cont.

MEAN DRAW SPEED mm/sec	PEAK DIE VELOCITY mm/sec	Mean Loads - kN			Specific Loads - kN/mm^2		
		TAG	BENDING	DIE	DRAW STRESS	SPECIFIC AXIAL	LATERAL DIE
32.0	19.2	2.25	1.04	7.83	0.37	0.59	0.58
32.0	38.5	2.41	1.20	8.02	0.40	0.68	0.59
32.0	76.9	2.45	1.17	8.21	0.40	0.66	0.61
32.0	105	2.21	1.10	8.02	0.36	0.62	0.59
32.0	144	1.89	0.91	8.98	0.31	0.51	0.67
—	—	—	—	—	—	—	—
57.0	269	1.05	0.53	7.64	0.17	0.30	0.57
57.0	221	1.41	0.70	7.83	0.23	0.39	0.58
57.0	163	1.89	0.90	8.12	0.31	0.51	0.60
57.0	115	2.25	1.11	8.02	0.37	0.63	0.59
57.0	76.9	2.61	1.30	8.02	0.43	0.73	0.59
57.0	48.1	2.81	1.48	8.02	0.46	0.83	0.59
57.0	38.5	2.93	1.51	8.02	0.48	0.85	0.59
57.0	9.6	2.97	1.51	8.02	0.49	0.85	0.59
57.0	0	2.97	1.56	8.02	0.49	0.88	0.59

$\alpha = 7.5°$, r = 0.164, f = 13.13 kHz — Test No - 027

MEAN DRAW SPEED mm/sec	PEAK DIE VELOCITY mm/sec	Mean Loads - kN			Specific Loads - kN/mm^2		
		TAG	BENDING	DIE	DRAW STRESS	SPECIFIC AXIAL	LATERAL DIE
1.33	0	1.75	0.92	5.35	0.23	1.16	0.89
1.33	38.4	1.59	0.83	5.16	0.21	1.05	0.86
1.33	95.9	1.21	0.64	4.97	0.16	0.81	0.83
1.33	115	1.00	0.52	4.68	0.13	0.66	0.78
1.33	172	0.72	0.35	4.39	0.09	0.44	0.73
1.33	182	0.64	0.29	4.39	0.08	0.37	0.73
1.33	191	0.52	0.23	4.20	0.07	0.29	0.70
1.33	201	0.46	0.17	4.20	0.06	0.22	0.70
1.33	230	0.40	0.26	4.01	0.05	0.33	0.67
1.33	239	0.33	0.21	3.63	0.04	0.27	0.60
—	—	—	—	—	—	—	—
23.1	0	2.13	1.38	5.54	0.28	1.74	0.92
23.1	9.6	2.09	1.35	5.73	0.27	1.71	0.95
23.1	38.4	1.93	1.11	5.73	0.25	1.40	0.95
23.1	115	1.45	0.83	5.44	0.19	1.05	0.91
23.1	163	1.05	0.55	5.06	0.14	0.70	0.84
23.1	201	0.80	0.40	4.97	0.10	0.51	0.83
23.1	220	0.68	0.30	4.68	0.09	0.38	0.78
23.1	239	0.56	0.25	4.58	0.07	0.32	0.76
23.1	249	0.52	0.22	4.58	0.07	0.28	0.76

$\alpha = 7.5°$, $r = 0.164$, $f = 13.13$ kHz — Test No - 027 CONT.

MEAN DRAW SPEED mm/sec	PEAK DIE VELOCITY mm/sec	Mean Loads - kN			Specific Loads - kN/mm^2		
		TAG	BENDING	DIE	DRAW STRESS	SPECIFIC AXIAL	LATERAL DIE
51.0	0	2.15	1.12	5.83	0.28	1.42	0.97
51.0	19.2	2.15	1.12	5.83	0.28	1.42	0.97
51.0	48.0	2.00	1.10	6.02	0.25	1.39	1.00
51.0	95.9	2.03	1.01	5.64	0.26	1.28	0.94
51.0	143	1.61	0.81	5.35	0.21	1.02	0.89
51.0	182	1.27	0.61	5.25	0.16	0.77	0.87
51.0	211	0.97	0.49	5.06	0.13	0.62	0.84
51.0	220	0.95	0.40	4.78	0.12	0.51	0.80
92.4	0	2.39	1.20	8.79	0.31	1.52	1.46
92.4	19.2	2.43	1.25	6.21	0.31	1.58	1.03
92.4	38.4	2.33	1.22	6.30	0.30	1.54	1.05
92.4	67.1	2.11	1.14	6.21	0.27	1.44	1.03
92.4	105	2.07	1.04	5.73	0.27	1.31	0.95
92.4	153	1.67	0.88	5.73	0.22	1.11	0.95
92.4	172	1.55	0.78	5.54	0.20	0.99	0.92
75.6	182	1.41	0.70	5.16	0.18	0.88	0.86
75.6	153	1.41	0.70	5.35	0.18	0.88	0.89
75.6	143	1.69	0.86	5.54	0.22	1.09	0.92
75.6	115	1.95	0.98	5.73	0.25	1.24	0.95
75.6	95.9	2.11	1.14	5.92	0.27	1.44	0.99
75.6	76.7	2.21	1.17	6.02	0.29	1.48	1.00
75.6	57.6	2.27	1.20	6.11	0.29	1.52	1.02
75.6	28.8	2.41	1.30	6.11	0.31	1.64	1.02
75.6	0	2.33	1.25	5.92	0.30	1.58	0.99
77.8	0	2.25	1.22	5.73	0.29	1.54	0.95
77.8	28.8	2.25	1.18	5.83	0.29	1.49	0.97
77.8	57.6	2.15	1.12	5.92	0.28	1.42	0.99
77.8	76.7	2.13	1.12	5.63	0.28	1.42	0.94
77.8	115	1.69	1.04	5.73	0.22	1.31	0.95
77.8	153	1.49	0.83	5.35	0.20	1.05	0.89

$\alpha = 2.5°$, r = 0.267, f = 13.26 kHz — Test No - 028

MEAN DRAW SPEED mm/sec	PEAK DIE VELOCITY mm/sec	Mean Loads - kN			Specific Loads - kN/mm^2		
		TAG	BENDING	DIE	DRAW STRESS	SPECIFIC AXIAL	LATERAL DIE
1.41	513	0.28	0.16	12.42	0.04	0.12	0.42
1.41	474	0.48	0.22	12.80	0.07	0.17	0.43
1.41	416	0.74	0.33	13.08	0.11	0.26	0.44
1.41	358	1.00	0.43	13.27	0.14	0.33	0.45
1.41	271	1.49	0.64	13.75	0.21	0.50	0.47
1.41	213	1.75	0.78	13.75	0.25	0.61	0.47
1.41	127	2.03	0.88	13.75	0.29	0.68	0.47
1.41	125	2.27	0.98	13.66	0.33	0.76	0.46
1.41	77.5	2.51	0.88	13.56	0.36	0.68	0.46
1.41	58.1	2.63	1.11	13.37	0.38	0.86	0.45
1.41	0	2.77	1.20	13.37	0.40	0.93	0.45
15.9	0	3.05	1.72	13.37	0.44	1.33	0.45
16.0	9.7	2.65	1.20	14.33	0.38	0.93	0.49
16.0	58.1	2.94	1.61	13.50	0.42	1.25	0.46
16.0	96.9	2.45	1.30	14.13	0.35	1.01	0.48
16.0	154	2.09	1.04	14.13	0.30	0.81	0.48
16.0	280	1.89	0.98	13.56	0.27	0.61	0.46
16.0	348	1.21	0.75	13.94	0.17	0.58	0.47
16.0	406	1.05	0.72	13.56	0.15	0.56	0.46
16.0	464	0.64	0.47	13.37	0.09	0.37	0.45
16.0	506	0.52	0.43	12.99	0.08	0.33	0.44
16.0	503	0.60	0.43	12.89	0.09	0.33	0.44

$\alpha = 2.5°$, r = 0.280, f = 13.26 kHz — Test No - 029

MEAN DRAW SPEED mm/sec	PEAK DIE VELOCITY mm/sec	Mean Loads - kN			Specific Loads - kN/mm^2		
		TAG	BENDING	DIE	DRAW STRESS	SPECIFIC AXIAL	LATERAL DIE
34.7	434	1.09	0.61	12.99	0.21	0.54	0.43
36.2	397	1.47	0.73	13.27	0.22	0.61	0.43
36.2	319	1.53	0.83	13.37	0.28	0.70	0.43
37.8	280	1.93	0.94	13.37	0.26	0.80	0.44
37.8	222	1.75	1.08	13.75	0.34	0.77	0.43
37.8	154	2.33	1.05	13.18	0.40	1.03	0.41
39.6	116	2.78	1.39	12.70	0.45	1.02	0.40
39.6	106	3.06	1.38	12.42	0.49	1.15	0.40
33.3	464	3.36	1.56	12.22	0.16	0.45	0.42

$\alpha = 2.5°$, $r = 0.280$, $f = 13.26$ kHz — Test No - 030

MEAN DRAW SPEED mm/sec	PEAK DIE VELOCITY mm/sec	Mean Loads - kN			Specific Loads - kN/mm^2		
		TAG	BENDING	DIE	DRAW STRESS	SPECIFIC AXIAL	LATERAL DIE
3.5	475	0.36	0.21	12.61	0.05	0.16	0.41
7.9	463	0.40	0.21	12.70	0.06	0.16	0.41
11.9	465	0.44	0.25	12.80	0.06	0.19	0.41
15.1	455	0.48	0.26	12.80	0.07	0.19	0.41
18.5	465	0.72	0.51	13.00	0.10	0.38	0.42
21.5	455	0.78	0.55	13.18	0.11	0.41	0.43
23.8	465	0.58	0.35	13.37	0.08	0.26	0.43
27.7	465	0.68	0.39	13.94	0.10	0.29	0.45
29.7	465	1.21	0.70	13.56	0.18	0.52	0.44
33.3	445	1.11	0.72	13.56	0.16	0.53	0.44
37.8	436	1.21	1.03	13.56	0.18	0.76	0.44
45.5	416	1.51	0.83	13.47	0.22	0.61	0.44
49.8	397	1.21	0.81	13.56	0.18	0.60	0.44
60.3	397	1.37	0.94	13.56	0.20	0.70	0.44
59.4	387	1.65	0.91	13.37	0.24	0.67	0.43
68.8	358	1.45	0.90	13.75	0.21	0.67	0.44
78.5	339	1.89	0.95	13.56	0.28	0.70	0.44
94.5	329	2.25	1.18	13.66	0.17	0.87	0.44
3.4	329	1.17	0.75	13.56	0.18	0.56	0.44
7.6	290	1.21	0.74	14.13	0.18	0.55	0.46
15.1	271	1.25	0.78	14.71	0.18	0.58	0.48
18.5	261	1.47	1.01	14.13	0.21	0.75	0.46
33.3	252	1.69	1.17	14.13	0.25	0.87	0.46
39.6	232	1.93	1.33	14.13	0.28	0.98	0.46
52.0	213	2.05	1.22	14.13	0.30	0.90	0.46
59.4	174	2.69	1.46	13.37	0.39	1.08	0.43
83.2	145	2.61	1.72	14.13	0.38	1.27	0.46
138	116	2.49	1.53	14.71	0.36	1.13	0.48
7.6	87	2.31	1.30	14.71	0.34	0.96	0.48
13.9	77	2.57	1.65	14.31	0.37	1.22	0.46
20.8	87	2.57	1.59	14.31	0.37	1.18	0.46
27.7	77	2.73	1.81	13.75	0.40	1.34	0.44
33.3	77	2.73	1.86	13.56	0.40	1.38	0.44
37.8	67	2.33	1.40	14.33	0.34	1.04	0.46
41.6	67	2.57	1.68	13.94	0.37	1.24	0.45
46.2	67	2.67	1.76	13.75	0.39	1.30	0.44
58.6	67	2.65	1.66	13.94	0.39	1.23	0.45
67	69.3	2.93	1.87	13.75	0.43	1.38	0.44
58	69.3	2.61	1.68	14.52	0.38	1.24	0.47
58	83.2	3.26	1.79	14.52	0.48	1.32	0.47
48	92.4	2.97	1.87	14.52	0.43	1.38	0.47

α = 2·5°, r = 0·280, f = 13·26 kHz — Test No - 030 cont

MEAN DRAW SPEED mm/sec	PEAK DIE VELOCITY mm/sec	Mean Loads - kN			Specific Loads - kN/mm²		
		TAG	BENDING	DIE	DRAW STRESS	SPECIFIC AXIAL	LATERAL DIE
48	103	2·89	1·87	14·33	0·42	1·38	0·46
29	3·9	2·61	1·47	14·42	0·38	1·09	0·47
29	11·9	2·57	1·46	14·42	0·37	1·08	0·47
29	20·8	2·77	1·78	13·85	0·40	1·32	0·44
29	33·3	2·59	1·72	14·33	0·38	1·27	0·46
29	41·6	2·29	1·35	15·09	0·33	0·99	0·49
29	52·0	2·71	1·76	13·94	0·40	1·30	0·45
29	69·3	2·81	1·70	13·94	0·41	1·26	0·45
29	77·8	3·14	1·90	14·04	0·46	1·41	0·45
29	94·5	2·73	2·07	13·56	0·40	1·53	0·44
29	104	3·26	1·65	13·75	0·48	1·22	0·44

α = 2·5°, r = 0·453, f = 13·46 kHz — Test No - 031

MEAN DRAW SPEED mm/sec	PEAK DIE VELOCITY mm/sec	Mean Loads - kN			Specific Loads - kN/mm²		
		TAG	BENDING	DIE	DRAW STRESS	SPECIFIC AXIAL	LATERAL DIE
1.4	373	2.25	1.47	19.9	0·43	0.67	0·40
3·5	373	2.27	1·29	20.3	0·44	0·59	0·40
9·8	353	1·89	1·12	21·0	0·36	0·51	0·42
19·2	344	1·75	1·04	21·6	0·34	0·48	0·43
28·9	334	2·17	1·39	21·0	0·42	0·64	0·42
34·7	314	1·89	1·13	22·2	0·36	0·52	0·44
46·2	304	2·21	1·38	21·2	0·42	0·60	0·42
55·5	255	2·09	1·11	21·6	0·40	0·51	0·43
66·6	255	2·13	1·12	21·6	0·41	0·51	0·43
77·0	255	2·17	1·11	22·2	0·42	0·51	0·44
89·5	226	2·71	1·47	21·4	0·52	0·67	0·43

α = 2·5°, r = 0·480, f = 13·48 kHz — Test No - 032

MEAN DRAW SPEED mm/sec	PEAK DIE VELOCITY mm/sec	Mean Loads - kN			Specific Loads - kN/mm²		
		TAG	BENDING	DIE	DRAW STRESS	SPECIFIC AXIAL	LATERAL DIE
0·9	403	2·33	1·79	22·07	0·47	0·77	0·42
5·7	393	2·41	1·89	22·43	0·49	0·82	0·42
13·9	393	2·09	1·85	23·42	0·42	0·80	0·44
19·5	374	1·89	1·76	23·82	0·38	0·76	0·45
23·8	354	2·61	2·13	21·84	0·53	0·92	0·45

$\alpha = 2.5°$, r = 0.473, f = 13.44 kHz Test No - 033

MEAN DRAW SPEED mm/sec	PEAK DIE VELOCITY mm/sec	Mean Loads - kN			Specific Loads - kN/mm^2		
		TAG	BENDING	DIE	DRAW STRESS	SPECIFIC AXIAL	LATERAL DIE
1.2	431	2.61	1.56	20.64	0.53	0.68	0.40
3.0	422	2.85	1.56	20.84	0.58	0.68	0.40
5.7	412	2.93	1.61	21.04	0.59	0.71	0.40
11.9	412	3.12	1.69	21.84	0.63	0.74	0.42
16.6	402	3.18	1.77	22.23	0.64	0.78	0.43
23.8	363	2.59	1.35	23.03	0.52	0.60	0.44

$\alpha = 2.5°$, r = 0.270, f = 13.25 kHz Test No - 034

MEAN DRAW SPEED mm/sec	PEAK DIE VELOCITY mm/sec	Mean Loads - kN			Specific Loads - kN/mm^2		
		TAG	BENDING	DIE	DRAW STRESS	SPECIFIC AXIAL	LATERAL DIE
1.1	445	0.50	0.25	12.31	0.07	0.19	0.41
3.4	425	0.56	0.34	12.31	0.08	0.26	0.41
7.6	445	0.64	0.39	12.51	0.09	0.30	0.42
11.9	425	0.96	0.69	12.70	0.14	0.53	0.43
15.1	425	0.92	0.64	12.90	0.13	0.49	0.43
20.9	425	1.13	0.75	13.10	0.16	0.58	0.44
25.2	406	1.55	0.78	13.30	0.23	0.60	0.45
31.1	387	1.37	0.81	13.50	0.20	0.62	0.45
37.8	367	1.67	0.91	13.10	0.24	0.70	0.44
46.2	309	1.91	0.86	12.70	0.28	0.66	0.43
59.4	290	1.93	0.85	13.10	0.28	0.65	0.44
75.6	290	2.29	1.03	12.31	0.33	0.79	0.41
92.4	251	2.45	1.04	12.51	0.36	0.80	0.42

$\alpha = 2.5°$, $r = 0.220$, $f = 13.17$ kHz — Test No - 035

MEAN DRAW SPEED mm/sec	PEAK DIE VELOCITY mm/sec	Mean Loads - kN			Specific Loads - kN/mm^2		
		TAG	BENDING	DIE	DRAW STRESS	SPECIFIC AXIAL	LATERAL DIE
1.5	442	0.18	0.17	9.33	0.02	0.16	0.38
1.8	442	0.22	0.22	9.33	0.03	0.21	0.38
4.4	432	0.26	0.26	9.53	0.04	0.25	0.39
6.7	413	0.36	0.26	9.93	0.05	0.25	0.41
7.6	423	0.40	0.42	9.33	0.05	0.40	0.38
13.9	423	0.58	0.48	9.93	0.08	0.45	0.41
20.8	423	0.66	0.53	10.12	0.09	0.50	0.42
27.7	404	0.84	0.60	10.32	0.11	0.57	0.42
41.6	384	1.13	0.73	10.72	0.15	0.69	0.44
58.2	365	1.29	0.74	10.72	0.17	0.70	0.44
61.6	355	1.29	0.87	10.72	0.17	0.82	0.44
77.8	298	1.83	0.96	10.92	0.25	0.90	0.45
92.4	269	1.89	0.94	10.92	0.25	0.89	0.45

$\alpha = 2.5°$, $r = 0.333$, $f = 13.32$ kHz — Test No - 036

MEAN DRAW SPEED mm/sec	PEAK DIE VELOCITY mm/sec	Mean Loads - kN			Specific Loads - kN/mm^2		
		TAG	BENDING	DIE	DRAW STRESS	SPECIFIC AXIAL	LATERAL DIE
1.1	447	1.45	0.87	15.48	0.23	0.54	0.42
3.6	423	1.45	0.86	15.88	0.23	0.54	0.43
8.3	428	1.31	0.78	15.48	0.21	0.49	0.42
13.9	408	1.25	0.70	15.88	0.20	0.44	0.43
18.5	389	1.25	0.99	15.88	0.20	0.62	0.43
23.1	389	1.93	0.99	15.48	0.30	0.62	0.42
24.6	389	1.85	0.86	15.48	0.29	0.54	0.42
29.7	389	2.17	0.86	15.48	0.34	0.54	0.42
33.3	369	2.13	0.90	15.48	0.34	0.56	0.42
37.8	369	2.21	0.80	15.48	0.35	0.55	0.42
41.6	350	2.17	0.81	15.61	0.34	0.50	0.43
44.3	340	2.25	0.90	15.98	0.35	0.56	0.42
46.2	380	2.37	0.99	15.48	0.37	0.62	0.42
52.7	321	2.61	0.90	14.69	0.41	0.56	0.40
58.6	311	2.57	0.88	15.09	0.41	0.55	0.41
66.6	291	2.61	0.91	15.48	0.41	0.57	0.42
72.8	272	2.71	0.92	15.28	0.43	0.57	0.42
78.5	272	2.79	0.95	15.28	0.44	0.60	0.42
83.2	252	2.75	1.00	15.28	0.43	0.62	0.42
91.4	252	2.79	1.11	15.09	0.44	0.69	0.41

$\alpha = 2.5°$, r = 0.440, f = 13.43 kHz Test No - 037

MEAN DRAW SPEED mm/sec	PEAK DIE VELOCITY mm/sec	Mean Loads - kN			Specific Loads - kN/mm^2		
		TAG	BENDING	DIE	DRAW STRESS	SPECIFIC AXIAL	LATERAL DIE
1.1	421	1.95	1.09	18.86	0.37	0.51	0.39
3.0	412	2.25	1.09	18.66	0.42	0.51	0.38
7.6	392	2.23	1.18	19.06	0.42	0.56	0.39
16.6	382	2.49	1.33	20.25	0.47	0.63	0.42
23.8	392	2.33	1.27	19.85	0.44	0.60	0.41
29.7	382	2.59	1.30	20.45	0.49	0.61	0.42
32.0	372	2.53	1.04	19.06	0.47	0.49	0.39
37.8	362	2.25	0.83	12.70	0.42	0.39	0.26
43.8	353	2.61	0.87	19.06	0.49	0.41	0.39
52.0	353	2.49	0.81	19.06	0.47	0.38	0.39
59.4	343	2.73	0.87	19.45	0.51	0.41	0.40
66.6	333	2.61	0.73	19.25	0.49	0.34	0.40

$\alpha = 2.5°$, r = 0.355, f = 13.32 kHz Test No - 038

MEAN DRAW SPEED mm/sec	PEAK DIE VELOCITY mm/sec	Mean Loads - kN			Specific Loads - kN/mm^2		
		TAG	BENDING	DIE	DRAW STRESS	SPECIFIC AXIAL	LATERAL DIE
1.4	447	1.11	0.64	14.69	0.18	0.37	0.37
3.8	437	1.25	0.61	14.49	0.20	0.36	0.37
9.2	428	1.05	0.43	15.09	0.17	0.25	0.39
12.8	418	0.96	0.39	15.28	0.16	0.23	0.39
18.5	408	1.35	0.68	15.48	0.22	0.40	0.39
23.8	408	1.35	0.62	14.69	0.22	0.36	0.37
27.7	408	1.53	0.56	14.89	0.25	0.33	0.38
33.3	398	1.81	0.69	14.89	0.29	0.40	0.38
41.6	379	1.49	0.51	15.68	0.24	0.30	0.40
46.2	369	1.91	0.72	15.09	0.31	0.42	0.39
51.7	360	1.93	0.69	15.28	0.31	0.40	0.39
55.5	350	2.13	0.72	15.09	0.34	0.42	0.39
59.4	330	2.29	0.86	14.69	0.37	0.50	0.37
69.3	321	2.45	0.85	15.28	0.39	0.50	0.39
75.6	311	2.29	0.90	15.28	0.37	0.53	0.39
75.6	301	2.29	0.81	15.09	0.37	0.47	0.39
83.2	282	2.41	0.83	14.89	0.39	0.48	0.38
87.6	262	2.41	0.90	15.09	0.39	0.53	0.39
92.4	272	2.57	0.91	14.29	0.41	0.53	0.36

$\alpha = 2.5°$, $r = 0.133$, $f = 13.08$ kHz Test No - 039

MEAN DRAW SPEED mm/sec	PEAK DIE VELOCITY mm/sec	Mean Loads - kN			Specific Loads - kN/mm^2		
		TAG	BENDING	DIE	DRAW STRESS	SPECIFIC AXIAL	LATERAL DIE
28	363	0.08	0.34	4.96	0.01	0.53	0.34
27	363	0.08	0.35	4.57	0.01	0.55	0.31
27	353	0.10	0.38	4.76	0.01	0.59	0.32
26	343	0.12	0.39	4.96	0.01	0.61	0.34
26	342	0.18	0.42	5.16	0.02	0.65	0.35
26	286	0.28	0.46	5.16	0.03	0.72	0.35
25	238	0.46	0.52	5.96	0.06	0.81	0.41
25	181	0.74	0.59	5.96	0.09	0.92	0.41
23	86.0	1.27	0.72	6.35	0.15	1.12	0.43
23	19.1	1.61	0.83	6.55	0.19	1.29	0.45
23	0	1.65	0.86	6.55	0.20	1.34	0.45
11.9	363	0.14	0.36	5.16	0.03	0.56	0.35
11.9	363	0.16	0.39	5.56	0.02	0.61	0.38
11.9	343	0.30	0.48	5.36	0.04	0.75	0.37
11.9	296	0.40	0.55	5.75	0.05	0.86	0.39
11.9	257	0.60	0.61	5.96	0.07	0.95	0.41
11.9	200	0.92	0.70	6.35	0.11	1.09	0.43
11.9	86.0	1.57	0.88	6.75	0.19	1.37	0.46
11.9	47.8	1.95	1.08	6.95	0.24	1.68	0.47
11.9	0	2.09	1.07	6.75	0.25	1.67	0.46
29.2	353	0.30	0.47	5.36	0.04	0.73	0.37
29.2	324	0.32	0.51	5.76	0.04	0.80	0.39
29.2	305	0.48	0.57	6.15	0.06	0.89	0.42
29.2	267	0.62	0.61	6.35	0.08	0.95	0.43
29.2	229	0.86	0.70	6.35	0.10	1.09	0.43
29.2	181	1.21	0.77	6.55	0.15	1.20	0.45
29.2	95.6	1.75	0.91	6.75	0.21	1.42	0.46
29.2	38.2	2.13	1.05	6.55	0.26	1.64	0.45
29.2	19.1	2.41	1.17	6.95	0.29	1.82	0.47
29.2	0	2.15	1.05	6.75	0.26	1.64	0.46
48.9	343	0.40	0.56	5.36	0.05	0.87	0.37
48.9	324	0.50	0.62	5.96	0.06	0.97	0.41
48.9	286	0.70	0.64	6.15	0.09	0.99	0.42
48.9	267	0.90	0.73	5.96	0.11	1.14	0.41
48.9	210	1.21	0.81	6.35	0.15	1.26	0.43
48.9	152	1.49	0.86	6.55	0.18	1.34	0.45
48.9	66.9	1.93	1.27	6.75	0.23	1.98	0.46
48.9	38.0	2.25	1.16	6.75	0.27	1.81	0.46
48.9	0	2.17	1.08	6.95	0.26	1.68	0.47

$\alpha = 2.5°$, r = 0.133, f = 13.08 kHz — Test No - 039 cont.

MEAN DRAW SPEED mm/sec	PEAK DIE VELOCITY mm/sec	Mean Loads - kN			Specific Loads - kN/mm^2		
		TAG	BENDING	DIE	DRAW STRESS	SPECIFIC AXIAL	LATERAL DIE
59.4	343	0.60	0.68	6.55	0.07	1.06	0.45
59.4	305	0.60	0.62	6.35	0.07	0.97	0.43
59.4	267	0.94	0.70	6.35	0.11	1.09	0.43
59.4	210	1.29	0.83	6.55	0.16	1.29	0.45
59.4	152	1.55	0.88	7.15	0.19	1.37	0.49
59.4	66.9	2.17	1.01	7.15	0.26	1.57	0.49
59.4	28.7	2.15	1.11	7.15	0.26	1.73	0.49
59.4	0	2.63	1.27	7.15	0.32	1.98	0.49
83.2	324	0.88	0.75	6.75	0.11	1.17	0.46
83.2	257	0.96	0.78	6.75	0.12	1.22	0.46
83.2	191	1.53	0.88	6.75	0.19	1.37	0.46
83.2	114	1.93	1.08	6.75	0.23	1.68	0.46
83.2	57.3	2.21	1.12	7.34	0.27	1.74	0.50

$\alpha = 2.5°$, r = 0.250, f = 13.17 kHz — Test No - 040

MEAN DRAW SPEED mm/sec	PEAK DIE VELOCITY mm/sec	Mean Loads - kN			Specific Loads - kN/mm^2		
		TAG	BENDING	DIE	DRAW STRESS	SPECIFIC AXIAL	LATERAL DIE
0.9	500	0.12	0.27	10.72	0.02	0.22	0.39
0.9	471	0.20	0.29	11.12	0.03	0.24	0.40
0.9	442	0.38	0.38	11.12	0.05	0.32	0.40
0.9	384	0.80	0.57	11.12	0.11	0.47	0.40
0.9	182	1.85	1.01	12.31	0.26	0.84	0.45
0.9	115	1.81	0.98	12.70	0.25	0.81	0.46
0.9	77.0	1.99	1.04	12.70	0.27	0.86	0.46
0.9	38.5	2.25	1.12	12.70	0.31	0.93	0.46
0.9	19.2	2.37	1.14	12.70	0.33	0.95	0.46
0.9	6	2.37	1.13	12.70	0.33	0.94	0.46
5.9	481	0.24	0.42	10.72	0.03	0.35	0.39
5.9	452	0.28	0.44	10.92	0.04	0.37	0.40
5.9	423	0.36	0.49	11.31	0.05	0.41	0.41
5.9	346	0.68	0.59	12.70	0.09	0.49	0.46
5.9	192	1.27	0.75	13.10	0.17	0.62	0.47
5.9	96.2	1.65	0.90	13.30	0.23	0.72	0.48
5.9	76.9	1.97	1.03	13.30	0.27	0.85	0.48
5.9	38.5	2.15	1.09	13.30	0.30	0.90	0.48
5.9	0	2.27	1.12	13.50	0.31	0.93	0.49

$\alpha = 2.5°$, $r = 0.250$, $f = 13.17$ kHz Test No - 040

MEAN DRAW SPEED mm/sec	PEAK DIE VELOCITY mm/sec	Mean Loads - kN			Specific Loads - kN/mm^2		
		TAG	BENDING	DIE	DRAW STRESS	SPECIFIC AXIAL	LATERAL DIE
18.8	481	0.28	0.52	11.12	0.04	0.43	0.40
18.8	442	0.40	0.57	11.91	0.06	0.47	0.43
18.8	327	0.60	0.61	13.30	0.08	0.51	0.48
18.8	202	1.33	0.87	13.50	0.18	0.72	0.49
18.8	134	1.69	1.08	13.50	0.23	0.90	0.49
18.8	96.2	2.01	1.24	13.30	0.28	1.05	0.49
18.8	57.7	2.25	1.30	13.30	0.31	1.08	0.49
18.8	28.9	2.37	1.30	13.30	0.33	1.08	0.49
18.8	19.2	1.93	1.16	13.90	0.27	0.96	0.50
18.8	0	2.09	1.13	13.90	0.29	0.94	0.50
— —	— —	— —	— —	— —	— —	— —	— —
34.7	423	0.52	0.62	13.50	0.07	0.51	0.49
34.7	327	0.72	0.70	13.90	0.10	0.58	0.50
34.7	211	1.27	0.91	13.90	0.17	0.75	0.50
34.7	153	12.7	0.86	14.29	0.17	0.71	0.52
34.7	125	17.3	1.14	13.50	0.24	0.95	0.49
34.7	96.2	19.3	1.20	13.50	0.27	1.00	0.49
34.7	57.7	2.25	1.34	13.90	0.31	1.11	0.50
34.7	38.5	2.53	1.46	14.69	0.35	1.21	0.53
34.7	19.2	2.21	1.20	13.50	0.31	0.99	0.49
34.7	0	2.17	1.22	13.90	0.30	1.01	0.50
— —	— —	— —	— —	— —	— —	— —	— —
52.0	384	0.56	0.62	13.10	0.16	0.78	0.50
52.0	231	1.29	0.99	13.90	0.22	0.98	0.50
52.0	173	1.89	1.17	13.90	0.29	1.01	0.49
52.0	115	1.33	1.26	14.90	0.29	1.00	0.49
52.0	76.9	2.41	1.40	14.29	0.28	0.90	0.50
52.0	57.7	2.55	1.53	15.29	0.35	1.15	0.50
52.0	38.5	2.21	1.37	14.89	0.36	1.23	0.49
52.0	0	2.77	1.56	13.50	0.39	1.29	0.47
—	— —	— —	— —	— —	— —	— —	— —
69.3	307	1.17	0.94	13.70	0.16	0.78	0.50
69.3	230	1.61	1.18	13.90	0.22	0.98	0.50
69.3	153	2.09	1.22	13.50	0.29	1.01	0.49
69.3	96.2	2.09	1.21	13.50	0.29	1.00	0.49
69.3	57.7	2.01	1.09	13.90	0.28	0.90	0.50
69.3	38.5	2.53	1.39	13.90	0.35	1.15	0.50
69.3	19.2	2.61	1.48	13.50	0.36	1.23	0.49
69.3	0	2.85	1.56	13.10	0.39	1.29	0.47
— —	— —	— —	— —	— —	— —	— —	— —
92.4	230	1.93	1.20	14.30	0.27	0.99	0.52

$\alpha = 2.5°$, r = 0.250, f = 13.17 kHz — Test No - 040

MEAN DRAW SPEED mm/sec	PEAK DIE VELOCITY mm/sec	Mean Loads - kN			Specific Loads - kN/mm^2		
		TAG	BENDING	DIE	DRAW STRESS	SPECIFIC AXIAL	LATERAL DIE
92.4	153	2.15	1.24	13.90	0.30	1.03	0.50
92.4	134	2.33	1.30	13.50	0.32	1.08	0.49
92.4	96.2	2.45	1.46	13.90	0.34	1.21	0.50
92.4	57.7	2.77	1.48	13.70	0.38	1.23	0.50
92.4	48.1	2.65	1.43	13.90	0.37	1.19	0.50
92.4	38.5	2.81	1.51	13.50	0.39	1.25	0.49
92.4	19.2	2.77	1.51	13.90	0.38	1.25	0.50
92.4	0	2.81	1.51	13.90	0.39	1.25	0.50
118	211	1.81	1.25	13.90	0.25	1.04	0.50
118	134	2.09	1.30	13.90	0.29	1.08	0.50
118	86.6	2.33	1.33	14.30	0.32	1.10	0.52
118	38.5	2.71	1.48	14.30	0.37	1.23	0.52
118	19.2	3.02	1.55	14.30	0.42	1.28	0.52

$\alpha = 7.5°$, r = 0.267, f = 13.08 kHz — Test No - 041

MEAN DRAW SPEED mm/sec	PEAK DIE VELOCITY mm/sec	Mean Loads - kN			Specific Loads - kN/mm^2		
		TAG	BENDING	DIE	DRAW STRESS	SPECIFIC AXIAL	LATERAL DIE
1.43	286	0.12	0.38	3.63	0.02	0.30	0.37
1.43	267	0.16	0.39	4.01	0.02	0.30	0.41
1.43	248	0.44	0.44	4.20	0.06	0.34	0.43
1.24	210	0.76	0.48	4.11	0.11	0.37	0.42
1.24	191	1.01	0.53	4.58	0.14	0.41	0.47
1.24	133	1.41	0.72	4.97	0.20	0.56	0.51
1.24	76.4	1.89	0.95	5.44	0.27	0.74	0.56
1.24	47.8	2.13	1.03	5.54	0.31	0.80	0.57
1.24	0	2.33	1.12	5.92	0.33	0.87	0.61
6.4	286	0.24	0.36	4.01	0.03	0.28	0.41
6.4	267	0.36	0.42	4.30	0.05	0.33	0.44
6.4	248	0.50	0.43	4.58	0.07	0.33	0.47
6.4	229	0.66	0.48	4.78	0.09	0.37	0.49
6.4	210	0.84	0.52	5.06	0.12	0.40	0.52
6.4	171	1.07	0.56	5.35	0.15	0.44	0.55
6.4	133	1.37	0.65	5.73	0.20	0.50	0.59
6.4	76	1.81	0.87	6.30	0.26	0.68	0.64
6.4	0	2.19	1.03	6.59	0.31	0.80	0.67
16.6	267	0.52	0.38	4.01	0.07	0.29	0.41

α = 7.5°, r = 0.267, f = 13.08 kHz — Test No - 041 CONT

MEAN DRAW SPEED mm/sec	PEAK DIE VELOCITY mm/sec	Mean Loads - kN			Specific Loads - kN/mm^2		
		TAG	BENDING	DIE	DRAW STRESS	SPECIFIC AXIAL	LATERAL DIE
16.6	248	0.76	0.47	5.16	0.11	0.37	0.53
16.6	229	0.92	0.52	5.35	0.13	0.40	0.54
16.6	191	1.09	0.57	5.54	0.16	0.44	0.57
16.6	171	1.37	0.64	5.83	0.20	0.50	0.60
16.6	114	1.65	0.75	6.30	0.24	0.58	0.64
16.6	57.3	2.01	0.87	6.69	0.29	0.68	0.68
16.6	0	2.25	0.98	6.97	0.32	0.76	0.71
32.0	257	0.84	0.49	5.54	0.12	0.38	0.57
32.0	248	0.96	0.55	5.92	0.14	0.43	0.61
32.0	210	1.13	0.59	6.11	0.16	0.46	0.62
32.0	181	1.33	0.62	6.30	0.19	0.48	0.64
32.0	133	1.61	0.69	6.69	0.23	0.54	0.68
32.0	76.4	1.89	0.82	7.07	0.27	0.64	0.72
32.0	38.2	2.07	0.88	7.26	0.30	0.68	0.74
32.0	0	2.19	0.95	7.45	0.31	0.74	0.76
52.0	248	1.01	0.57	6.11	0.41	0.44	0.62
52.0	210	1.21	0.65	6.30	0.17	0.50	0.64
52.0	162	1.49	0.73	6.88	0.21	0.57	0.70
52.0	133	1.69	0.77	6.88	0.24	0.60	0.70
52.0	86.0	1.89	0.86	7.07	0.27	0.67	0.72
52.0	57.3	2.01	0.91	7.07	0.29	0.71	0.72
52.0	0	2.05	0.94	7.35	0.29	0.73	0.75
69.3	210	1.25	0.68	6.49	0.18	0.53	0.63
69.3	181	1.41	0.73	6.97	0.20	0.57	0.71
69.3	133	1.69	0.82	6.97	0.24	0.64	0.71
69.3	95.6	1.89	0.92	7.64	0.27	0.71	0.78
69.3	66.9	2.05	0.98	7.64	0.29	0.76	0.78
69.3	38.2	2.13	1.00	7.64	0.31	0.78	0.78
693	0	2.09	1.00	7.45	0.30	0.78	0.76
104	152	1.65	0.87	7.07	0.24	0.68	0.72
104	114	1.85	0.94	7.26	0.26	0.73	0.74
104	66.0	1.97	0.96	7.45	0.28	0.75	0.76
104	57.3	2.01	0.99	7.45	0.29	0.77	0.76
104	38.2	2.05	1.04	7.64	0.29	0.81	0.78
104	0	2.05	1.04	7.64	0.29	0.81	0.78

$\alpha = 10°$, r = 0.263, f = 12.84 kHz — Test No - 042

MEAN DRAW SPEED mm/sec	PEAK DIE VELOCITY mm/sec	Mean Loads - kN			Specific Loads - kN/mm²		
		TAG	BENDING	DIE	DRAW STRESS	SPECIFIC AXIAL	LATERAL DIE
6.4	300	0.28	0.03	1.43	0.04	0.02	0.12
6.4	262	0.40	0.10	1.53	0.06	0.08	0.21
6.4	206	0.66	0.23	1.91	0.09	0.18	0.27
6.4	150	1.29	0.44	2.20	0.18	0.35	0.31
6.4	103	1.65	0.65	2.67	0.23	0.51	0.37
6.4	75.0	1.93	0.79	2.87	0.27	0.62	0.40
6.4	37.5	2.25	0.96	2.96	0.32	0.76	0.41
6.4	0	2.37	0.99	2.96	0.33	0.78	0.41
16.6	243	0.64	0.23	1.91	0.09	0.18	0.27
16.6	206	0.80	0.29	2.10	0.11	0.23	0.29
16.6	168	1.21	0.40	2.48	0.17	0.32	0.35
16.6	131	1.61	0.59	2.67	0.23	0.47	0.37
16.6	93.8	1.85	0.72	2.87	0.26	0.57	0.40
16.6	75.0	2.09	0.82	2.96	0.29	0.65	0.41
16.6	65.7	2.23	0.91	3.06	0.31	0.72	0.43
16.6	18.8	2.33	0.99	3.15	0.33	0.78	0.44
16.6	0	2.33	0.98	3.15	0.33	0.77	0.44

$\alpha = 10°$, r = 0.399, f = 12.81 kHz — Test No - 043

MEAN DRAW SPEED mm/sec	PEAK DIE VELOCITY mm/sec	Mean Loads - kN			Specific Loads - kN/mm²		
		TAG	BENDING	DIE	DRAW STRESS	SPECIFIC AXIAL	LATERAL DIE
20.8	0	2.53	1.24	3.06	0.43	0.64	0.28
20.8	225	1.13	0.74	2.20	0.19	0.38	0.20
20.8	282	0.74	0.62	1.91	0.13	0.32	0.18
20.8	263	0.84	0.60	2.10	0.14	0.31	0.19
20.8	225	1.15	0.70	2.30	0.20	0.36	0.21
20.8	178	1.49	0.83	2.48	0.26	0.43	0.23
20.8	131	1.91	1.05	2.58	0.33	0.55	0.24
20.8	94.0	2.17	1.16	2.67	0.37	0.60	0.24
20.8	75.2	2.41	1.29	2.67	0.41	0.67	0.24
20.8	28.2	2.53	1.33	2.77	0.43	0.69	0.25
20.8	0	2.55	1.35	2.87	0.44	0.70	0.26
27.7	263	0.86	0.62	2.10	0.15	0.32	0.19
33.3	225	1.09	0.72	2.20	0.19	0.37	0.20
33.3	206	1.31	0.78	2.20	0.22	0.41	0.20
33.3	169	1.65	0.92	2.48	0.28	0.48	0.23
33.3	131	2.01	1.07	2.48	0.34	0.56	0.23
33.3	94.0	2.19	1.18	2.67	0.37	0.61	0.24

$\alpha = 10°$, $r = 0.394$, $f = 12.87$ kHz — Test No - 043 CONT.

MEAN DRAW SPEED mm/sec	PEAK DIE VELOCITY mm/sec	Mean Loads - kN			Specific Loads - kN/mm^2		
		TAG	BENDING	DIE	DRAW STRESS	SPECIFIC AXIAL	LATERAL DIE
33.3	75.2	2.35	1.25	2.58	0.40	0.65	0.24
33.3	37.6	2.45	1.34	2.67	0.42	0.70	0.24
33.3	0	2.53	1.37	2.77	0.43	0.71	0.25
55.5	225	1.46	0.82	2.39	0.25	0.43	0.22
55.5	188	1.69	0.91	2.48	0.29	0.47	0.23
55.5	141	2.01	1.07	2.58	0.34	0.56	0.24
55.5	112	2.21	1.14	2.58	0.38	0.59	0.24
55.5	75.2	2.41	1.26	2.96	0.41	0.65	0.27
55.5	18.8	2.55	1.34	2.96	0.44	0.70	0.27
55.5	0	2.49	1.33	2.58	0.43	0.69	0.24
67.3	188	1.65	0.88	2.58	0.28	0.46	0.24
67.3	150	1.89	0.98	2.67	0.32	0.51	0.24
67.3	131	2.07	1.03	2.87	0.35	0.54	0.26
67.3	94.0	2.27	1.13	3.06	0.39	0.59	0.28
67.3	56.4	2.41	1.26	3.06	0.41	0.65	0.28
67.3	28.2	2.49	1.30	3.06	0.43	0.68	0.28
67.3	0	2.53	1.30	3.06	0.43	0.68	0.28
96.7	131	2.33	1.05	3.15	0.40	0.55	0.29
96.7	122	2.23	1.11	3.15	0.38	0.58	0.29
96.7	94.0	2.39	1.16	3.25	0.41	0.60	0.30
96.7	56.4	2.51	1.26	3.15	0.43	0.65	0.29
96.7	37.6	2.53	1.26	3.25	0.43	0.65	0.30
96.7	18.8	2.55	1.30	3.25	0.44	0.68	0.30
96.7	0	2.55	1.29	3.25	0.44	0.67	0.30
1.8	329	0.12	0.29	1.72	0.02	0.15	0.16
1.8	319	0.12	0.23	1.81	0.02	0.12	0.17
1.8	263	0.22	0.33	1.91	0.04	0.18	0.18
1.8	94.0	2.25	1.05	2.67	0.39	0.55	0.24
1.8	56.4	2.49	1.25	2.67	0.43	0.65	0.24
1.8	28.2	2.69	1.35	3.06	0.46	0.70	0.28
1.8	0	2.77	1.40	3.15	0.47	0.73	0.29
10.4	300	0.28	0.46	1.91	0.05	0.24	0.18
10.4	253	0.60	0.55	2.10	0.10	0.29	0.19
10.4	225	0.98	0.65	2.48	0.17	0.34	0.23
10.4	169	1.53	0.86	2.77	0.26	0.45	0.25
10.4	112	1.89	1.01	2.77	0.32	0.52	0.25

$\alpha = 10°$, r = 0.399, f = 12.87kHz — Test No - 043 CONT.

MEAN DRAW SPEED mm/sec	PEAK DIE VELOCITY mm/sec	Mean Loads - kN			Specific Loads - kN/mm^2		
		TAG	BENDING	DIE	DRAW STRESS	SPECIFIC AXIAL	LATERAL DIE
10.4	94.0	22.5	1.16	3.06	0.39	0.60	0.28
10.4	56.4	2.49	1.29	3.06	0.43	0.67	0.28
10.4	0	2.73	1.39	3.15	0.47	0.72	0.29

$\alpha = 10°$, r = 0.461, f = 13.05kHz — Test No - 044

MEAN DRAW SPEED mm/sec	PEAK DIE VELOCITY mm/sec	Mean Loads - kN			Specific Loads - kN/mm^2		
		TAG	BENDING	DIE	DRAW STRESS	SPECIFIC AXIAL	LATERAL DIE
11.9	305	0.64	0.55	2.39	0.12	0.25	0.19
11.9	285	0.78	0.59	2.48	0.15	0.27	0.20
11.9	257	0.94	0.62	2.67	0.18	0.28	0.21
11.9	219	1.25	0.70	3.06	0.24	0.32	0.24
11.9	133	1.95	0.92	3.44	0.37	0.41	0.27
11.9	76.3	2.49	1.13	3.53	0.48	0.51	0.28
11.9	38.1	2.71	1.25	3.44	0.52	0.56	0.27
11.9	0	2.81	1.30	3.53	0.54	0.58	0.28
23.4	276	0.96	0.65	2.48	0.18	0.29	0.20
23.4	266	1.08	0.72	2.87	0.21	0.32	0.23
23.4	209	1.38	0.82	2.87	0.27	0.37	0.23
23.4	152	1.91	0.98	3.15	0.37	0.44	0.25
23.4	95.3	2.39	1.18	3.44	0.46	0.53	0.27
23.4	47.7	2.67	1.31	3.44	0.51	0.59	0.27
23.4	19.1	2.77	1.37	3.44	0.53	0.62	0.27
23.4	0	2.79	1.35	3.44	0.54	0.61	0.27
37.8	247	1.23	0.73	2.77	0.24	0.33	0.22
37.8	228	1.49	0.84	2.87	0.29	0.38	0.23
37.8	181	1.83	0.94	3.15	0.35	0.42	0.25
37.8	133	2.19	1.09	3.25	0.42	0.49	0.26
37.8	85.8	2.55	1.20	3.44	0.49	0.54	0.27
37.8	38.1	2.75	1.30	3.63	0.53	0.58	0.29
37.8	0	2.81	1.33	3.63	0.54	0.60	0.28

$\alpha = 10°$, r=0.418, f=13.05kHz — Test No - 045

MEAN DRAW SPEED mm/sec	PEAK DIE VELOCITY mm/sec	Mean Loads - kN			Specific Loads - kN/mm^2		
		TAG	BENDING	DIE	DRAW STRESS	SPECIFIC AXIAL	LATERAL DIE
20.8	276	1.01	0.70	2.96	0.18	0.35	0.26
27.7	266	1.17	0.73	3.15	0.21	0.36	0.28
33.3	241	1.29	0.79	3.34	0.23	0.39	0.29
41.6	247	1.29	0.79	3.15	0.23	0.39	0.28
47.5	228	1.49	0.86	3.15	0.26	0.43	0.28
52.0	219	1.61	0.91	3.44	0.28	0.45	0.30
64.0	200	1.81	1.03	3.53	0.32	0.51	0.31
70.5	181	1.99	1.07	3.63	0.35	0.53	0.32
75.6	162	2.09	1.11	3.72	0.37	0.55	0.33
97.9	153	2.17	1.14	3.82	0.38	0.57	0.33
100.2	153	2.25	1.16	3.82	0.40	0.58	0.33
100.2	153	2.25	1.16	3.82	0.40	0.58	0.33

$\alpha = 10°$, r=0.421, f=13.05kHz — Test No - 046

MEAN DRAW SPEED mm/sec	PEAK DIE VELOCITY mm/sec	Mean Loads - kN			Specific Loads - kN/mm^2		
		TAG	BENDING	DIE	DRAW STRESS	SPECIFIC AXIAL	LATERAL DIE
2.2	267	0.80	0.56	3.44	0.14	0.28	0.30
8.3	228	1.27	0.75	3.44	0.23	0.37	0.30
20.8	209	1.47	0.83	3.63	0.26	0.41	0.32
33.3	191	1.69	0.94	3.82	0.30	0.46	0.33
36.9	162	1.97	1.09	4.11	0.35	0.54	0.36
46.5	142	2.09	1.13	4.11	0.37	0.56	0.36
62.3	123	2.23	1.18	4.11	0.40	0.58	0.36
71.1	104	2.31	1.22	4.20	0.41	0.60	0.36
77.8	95.3	2.47	1.31	4.20	0.44	0.65	0.36
80.1	95.3	2.51	1.31	4.20	0.45	0.65	0.36
88.5	95.3	2.49	1.30	4.20	0.45	0.64	0.36

$\alpha = 10°$, r = 0.526, f = 13.06 kHz — Test No - 047

MEAN DRAW SPEED mm/sec	PEAK DIE VELOCITY mm/sec	Mean Loads - kN			Specific Loads - kN/mm^2		
		TAG	BENDING	DIE	DRAW STRESS	SPECIFIC AXIAL	LATERAL DIE
1.3	362	0.12	0.03	2.48	0.03	0.01	0.17
5.7	362	0.28	0.10	2.58	0.06	0.04	0.18
13.9	305	0.88	0.49	2.67	0.19	0.19	0.19
20.8	286	1.23	0.61	2.77	0.27	0.24	0.19
27.7	267	1.37	0.64	2.77	0.30	0.25	0.19
33.3	257	1.51	0.72	2.87	0.33	0.28	0.20
41.6	257	1.69	0.79	2.96	0.36	0.31	0.21
46.2	229	1.89	0.90	3.15	0.41	0.36	0.22
55.5	134	2.09	1.01	—	0.45	0.40	—

$\alpha = 10°$, r = 0.580, f = 13.06 kHz — Test No - 048

MEAN DRAW SPEED mm/sec	PEAK DIE VELOCITY mm/sec	Mean Loads - kN			Specific Loads - kN/mm^2		
		TAG	BENDING	DIE	DRAW STRESS	SPECIFIC AXIAL	LATERAL DIE
11.1	438	0.20	0.10	2.19	0.05	0.04	0.14
16.6	419	0.44	0.27	2.10	0.11	0.10	0.13
27.7	362	0.90	0.46	2.29	0.22	0.16	0.14
33.3	314	1.25	0.57	2.39	0.31	0.20	0.15
41.6	286	1.67	0.83	2.39	0.42	0.30	0.15

$\alpha = 10°$, r = 0.623, f = 13.13 kHz — Test No - 049

MEAN DRAW SPEED mm/sec	PEAK DIE VELOCITY mm/sec	Mean Loads - kN			Specific Loads - kN/mm^2		
		TAG	BENDING	DIE	DRAW STRESS	SPECIFIC AXIAL	LATERAL DIE
1.3	402	0.16	0.26	3.44	0.04	0.09	0.20
4.2	383	0.38	0.46	3.34	0.10	0.15	0.20
9.2	345	0.70	0.68	3.25	0.19	0.23	0.19
13.9	326	0.96	0.75	3.25	0.26	0.25	0.19
18.5	306	1.13	0.81	3.25	0.31	0.27	0.19
23.8	297	1.25	0.83	3.25	0.34	0.28	0.19
27.7	387	1.31	0.82	3.34	0.36	0.27	0.20
27.7	278	1.51	0.86	3.44	0.41	0.29	0.20
33.3	278	1.67	0.94	3.44	0.45	0.31	0.20
41.6	258	1.89	1.04	3.53	0.51	0.35	0.21
41.6	249	2.05	1.13	3.72	0.56	0.38	0.22
55.5	230	2.25	1.25	3.72	0.61	0.42	0.22

$\alpha = 10$, $r = 0.682$, $f = 13.14$ kHz — Test No - 050

MEAN DRAW SPEED mm/sec	PEAK DIE VELOCITY mm/sec	Mean Loads - kN			Specific Loads - kN/mm^2		
		TAG	BENDING	DIE	DRAW STRESS	SPECIFIC AXIAL	LATERAL DIE
—	460	0.16	0.39	2.77	0.05	—	—
3.47	460	0.24	0.39	2.87	0.08	—	—
8.3	422	0.64	0.47	2.67	0.21	—	—
13.9	384	1.11	0.57	2.39	0.36	—	—
18.5	326	1.53	0.72	2.48	0.49	—	—

$\alpha = 10°$, $r = 0.779$, $f = 13.18$ kHz — Test No - 051

MEAN DRAW SPEED mm/sec	PEAK DIE VELOCITY mm/sec	Mean Loads - kN			Specific Loads - kN/mm^2		
		TAG	BENDING	DIE	DRAW STRESS	SPECIFIC AXIAL	LATERAL DIE
1.7	558	0.28	0.55	4.30	0.13	—	—
3.5	519	0.52	0.62	4.01	0.24	—	—

$\alpha = 10°$, $r = 0.779$, $f = 13.19$ kHz — Test No - 052

MEAN DRAW SPEED mm/sec	PEAK DIE VELOCITY mm/sec	Mean Loads - kN			Specific Loads - kN/mm^2		
		TAG	BENDING	DIE	DRAW STRESS	SPECIFIC AXIAL	LATERAL DIE
1.3	558	0.56	0.68	4.29	0.26	—	—
3.0	539	0.86	0.78	5.73	0.40	—	—
—	—	1.29	0.91	—	0.60	—	—

$\alpha = 10°$, $r = 0.260$, $f = 12.82$ kHz — Test No - 053

MEAN DRAW SPEED mm/sec	PEAK DIE VELOCITY mm/sec	Mean Loads - kN			Specific Loads - kN/mm^2		
		TAG	BENDING	DIE	DRAW STRESS	SPECIFIC AXIAL	LATERAL DIE
11.9	505	0.16	0.18	1.53	0.02	0.14	0.22
11.9	431	0.18	0.18	1.53	0.02	0.14	0.22
11.9	375	0.22	0.21	1.72	0.03	0.17	0.24
11.9	244	0.78	0.39	2.10	0.11	0.31	0.30
11.9	206	1.09	0.55	2.29	0.15	0.44	0.32
11.9	177	1.31	0.65	2.48	0.18	0.52	0.34
11.9	159	1.31	0.75	2.67	0.18	0.60	0.38
11.9	121	1.85	0.91	2.67	0.26	0.73	0.38
11.9	28.1	2.29	1.14	2.87	0.32	0.91	0.40
11.9.	0	2.35	1.17	2.87	0.32	0.93	0.40

$\alpha = 5°$, r = 0.442, f = 13.18 kHz — Test No - 054

MEAN DRAW SPEED mm/sec	PEAK DIE VELOCITY mm/sec	Mean Loads - kN			Specific Loads - kN/mm^2		
		TAG	BENDING	DIE	DRAW STRESS	SPECIFIC AXIAL	LATERAL DIE
3.1	654	0.24	0.23	9.52	0.04	0.11	0.19
3.1	596	0.36	0.25	9.94	0.07	0.12	0.20
3.1	558	0.54	0.30	10.33	0.10	0.14	0.20
3.1	385	1.37	0.62	11.52	0.25	0.29	0.23
3.1	250	2.37	1.12	12.30	0.43	0.53	0.23
3.1	173	2.73	1.26	12.30	0.50	0.59	0.24
3.1	115	2.89	1.34	11.52	0.53	0.63	0.23
3.1	19.3	2.97	1.37	—	0.54	0.64	—

$\alpha = 5°$, r = 0.205, f = 12.88 kHz — Test No - 055

MEAN DRAW SPEED mm/sec	PEAK DIE VELOCITY mm/sec	Mean Loads - kN			Specific Loads - kN/mm^2		
		TAG	BENDING	DIE	DRAW STRESS	SPECIFIC AXIAL	LATERAL DIE
2.5	489	0.12	0.12	4.55	0.02	0.12	0.19
2.5	451	0.14	0.13	4.36	0.02	0.13	0.19
2.5	433	0.12	0.14	4.76	0.02	0.14	0.20
2.2	395	0.16	0.14	4.95	0.02	0.14	0.21
2.1	188	0.93	0.44	6.55	0.12	0.45	0.28
2.1	94.1	1.59	0.65	7.15	0.20	0.66	0.30
1.9	56.5	1.89	0.77	7.55	0.23	0.78	0.32
1.9	0	1.97	0.82	7.55	0.25	0.83	0.32
—	—	—	—	—	—	—	—
11.1	508	0.18	0.17	4.97	0.02	0.17	0.21
11.1	470	0.20	0.18	4.97	0.03	0.18	0.21
11.1	432	0.22	0.18	4.97	0.03	0.18	0.21
11.1	338	0.38	0.26	5.76	0.05	0.26	0.25
11.1	131	1.69	0.69	7.34	0.21	0.70	0.31
11.1	282	0.90	0.51	6.36	0.11	0.52	0.27
11.1	291	0.98	0.49	6.55	0.12	0.50	0.28
11.1	272	1.21	0.52	7.15	0.15	0.53	0.30
11.1	112	2.75	1.22	7.15	0.35	1.23	0.30
11.1	0	3.30	1.22	7.15	0.42	1.23	0.30

$\alpha = 5°$, r=0.529, f=13.33 kHz — Test No - 057

MEAN DRAW SPEED mm/sec	PEAK DIE VELOCITY mm/sec	Mean Loads - kN			Specific Loads - kN/mm^2		
		TAG	BENDING	DIE	DRAW STRESS	SPECIFIC AXIAL	LATERAL DIE
1.3	467	1.53	1.14	13.09	0.33	0.45	0.22
1.3	467	1.63	1.22	12.69	0.36	0.48	0.21
3.9	467	1.53	1.14	13.09	0.33	0.45	0.22
7.2	448	1.49	1.09	12.69	0.33	0.43	0.21
11.9	448	1.51	1.13	12.51	0.33	0.44	0.21
16.6	448	1.61	1.17	12.51	0.35	0.46	0.21
23.8	429	1.65	1.20	12.69	0.36	0.47	0.21
30.8	429	1.67	1.20	13.09	0.37	0.47	0.22
37.8	409	2.45	1.77	11.91	0.54	0.69	0.20

$\alpha = 5°$, r=0.592, f=13.26 kHz — Test No - 058

MEAN DRAW SPEED mm/sec	PEAK DIE VELOCITY mm/sec	Mean Loads - kN			Specific Loads - kN/mm^2		
		TAG	BENDING	DIE	DRAW STRESS	SPECIFIC AXIAL	LATERAL DIE
1.4	581	0.84	1.37	14.30	0.21	0.48	0.21
1.4	581	0.96	1.44	13.69	0.24	0.50	0.20
2.1	581	1.15	1.47	13.49	0.29	0.51	0.20
3.1	561	1.33	1.70	13.09	0.34	0.60	0.19
6.9	542	1.43	1.69	12.69	0.36	0.59	0.19
12.8	484	1.57	1.74	12.91	0.40	0.61	0.19
18.5	464	1.75	1.33	13.31	0.44	0.47	0.20
24.8	445	1.85	1.22	12.91	0.47	0.43	0.20

$\alpha = 5°$, r=0.353, f=13.18 kHz — Test No - 059

MEAN DRAW SPEED mm/sec	PEAK DIE VELOCITY mm/sec	Mean Loads - kN			Specific Loads - kN/mm^2		
		TAG	BENDING	DIE	DRAW STRESS	SPECIFIC AXIAL	LATERAL DIE
16.6	346	1.41	0.72	9.94	0.23	0.42	0.25
21.9	337	1.43	0.72	9.94	0.23	0.42	0.25
25.6	327	1.55	0.75	10.12	0.25	0.44	0.25
31.2	308	1.65	0.79	10.33	0.27	0.46	0.26
33.3	288	1.69	0.82	10.33	0.27	0.48	0.26
41.6	259	2.15	1.09	10.52	0.35	0.64	0.26
51.0	259	2.45	1.03	9.73	0.40	0.61	0.24
55.	240	2.49	1.07	10.52	0.40	0.63	0.26
62.6	231	2.07	0.94	9.94	0.34	0.55	0.25
69.3	231	2.67	1.24	10.73	0.43	0.73	0.27
83.2	231	2.57	1.31	10.52	0.42	0.77	0.26
89.5	211	2.95	1.53	9.73	0.48	0.90	0.24

$\alpha = 5°$, r=0.364, f=13.14 kHz — Test No - 060

MEAN DRAW SPEED mm/sec	PEAK DIE VELOCITY mm/sec	Mean Loads - kN			Specific Loads - kN/mm^2		
		TAG	BENDING	DIE	DRAW STRESS	SPECIFIC AXIAL	LATERAL DIE
9.2	403	0.92	0.47	9.73	0.15	0.27	0.23
9.2	345	1.29	0.60	10.12	0.21	0.34	0.24
9.2	287	1.69	0.77	10.73	0.28	0.44	0.26
9.2	230	2.01	0.87	10.91	0.33	0.50	0.26
9.2	191	2.19	0.94	10.91	0.36	0.54	0.26
9.2	172	2.37	1.04	10.73	0.39	0.59	0.26
9.2	134	2.75	1.30	10.73	0.45	0.74	0.26
9.2	96.0	3.04	1.30	10.73	0.50	0.74	0.26
9.2	67.2	3.14	1.39	10.33	0.51	0.79	0.25
9.2	0	3.30	1.37	10.33	0.54	0.78	0.25
18.5	307	1.31	0.60	10.52	0.21	0.34	0.25
18.5	250	1.49	0.65	10.73	0.24	0.37	0.26
18.5	182	1.81	0.77	11.12	0.30	0.44	0.27
18.5	153	2.29	1.11	10.73	0.38	0.63	0.26
18.5	106	2.47	1.07	11.12	0.41	0.61	0.27
18.5	67.2	2.61	1.08	11.12	0.43	0.62	0.27
18.5	0	3.40	1.42	—	0.56	0.81	—

$\alpha = 5°$, r=0.413, f=13.16 kHz — Test No - 061

MEAN DRAW SPEED mm/sec	PEAK DIE VELOCITY mm/sec	Mean Loads - kN			Specific Loads - kN/mm^2		
		TAG	BENDING	DIE	DRAW STRESS	SPECIFIC AXIAL	LATERAL DIE
28.7	384	0.66	0.35	9.52	0.12	0.18	0.20
28.7	346	0.90	0.47	10.12	0.16	0.24	0.21
28.7	278	1.53	0.78	10.33	0.27	0.39	0.22
28.7	192	2.07	0.91	10.52	0.37	0.46	0.22
28.7	153	2.63	1.09	10.12	0.47	0.55	0.21
28.7	96.1	2.83	1.20	9.73	0.51	0.60	0.21
28.7	124	2.79	1.22	9.94	0.50	0.61	0.21

$\alpha = 5°$, r=0.413, f=13.16kHz — Test No - 062

MEAN DRAW SPEED mm/sec	PEAK DIE VELOCITY mm/sec	Mean Loads - kN			Specific Loads - kN/mm^2		
		TAG	BENDING	DIE	DRAW STRESS	SPECIFIC AXIAL	LATERAL DIE
41.6	365	0.84	0.33	10.52	0.15	0.17	0.22
41.6	327	1.29	0.60	11.31	0.23	0.30	0.24
41.6	269	1.37	0.53	11.52	0.24	0.27	0.24
41.6	230	1.93	0.56	11.31	0.35	0.28	0.24
41.6	173	2.51	0.68	10.33	0.45	0.34	0.22

$\alpha = 5°$, r=0.342, f=13.09kHz — Test No - 063

MEAN DRAW SPEED mm/sec	PEAK DIE VELOCITY mm/sec	Mean Loads - kN			Specific Loads - kN/mm^2		
		TAG	BENDING	DIE	DRAW STRESS	SPECIFIC AXIAL	LATERAL DIE
25.2	353	0.46	0.34	7.73	0.07	0.21	0.20
25.2	334	0.66	0.40	8.94	0.10	0.24	0.23
25.2	286	0.94	0.53	8.94	0.15	0.32	0.23
25.2	153	1.09	0.69	9.12	0.17	0.42	0.23
25.2	115	1.95	1.03	9.52	0.31	0.62	0.24

$\alpha = 5°$, r=0.365, f=13.10kHz — Test No - 064

MEAN DRAW SPEED mm/sec	PEAK DIE VELOCITY mm/sec	Mean Loads - kN			Specific Loads - kN/mm^2		
		TAG	BENDING	DIE	DRAW STRESS	SPECIFIC AXIAL	LATERAL DIE
11.6	344	0.34	0.48	7.15	0.06	0.27	0.17
11.6	325	0.46	0.56	7.73	0.08	0.32	0.19
11.6	296	0.60	0.64	7.73	0.10	0.36	0.19
11.6	268	0.86	0.72	8.72	0.14	0.41	0.21
11.6	162	1.41	0.96	8.54	0.24	0.55	0.20
11.6	76.6	2.15	1.43	9.33	0.36	0.81	0.22
11.6	8.3	2.61	1.81	8.94	0.44	1.03	0.21
11.6	0	2.99	2.01	8.73	0.51	1.14	0.21

$\alpha = 5°$, r=0.345, f=13.09 kHz — Test No - 065

MEAN DRAW SPEED mm/sec	PEAK DIE VELOCITY mm/sec	Mean Loads - kN			Specific Loads - kN/mm^2		
		TAG	BENDING	DIE	DRAW STRESS	SPECIFIC AXIAL	LATERAL DIE
43.8	344	0.76	0.58	8.33	0.12	0.23	0.21
43.8	305	0.78	0.47	8.33	0.13	0.28	0.21
43.8	268	1.17	0.48	8.54	0.19	0.29	0.22
43.8	172	2.31	1.05	8.54	0.38	0.63	0.22
43.8	124	2.61	1.18	8.73	0.42	0.71	0.22
43.8	76.5	2.75	1.29	8.73	0.45	0.78	0.22
43.8	38.3	2.91	1.43	8.93	0.47	0.86	0.23
43.8	0	2.81	1.27	8.93	0.46	0.76	0.23
59.4	325	0.86	0.53	8.54	0.14	0.32	0.22
59.4	286	1.09	0.48	8.54	0.18	0.29	0.22
59.4	210	1.67	0.73	8.54	0.27	0.44	0.22
59.4	153	2.19	0.95	8.54	0.36	0.57	0.22
59.4	114	2.87	1.27	8.73	0.47	0.76	0.22
59.4	76.5	2.83	1.37	8.54	0.46	0.82	0.22

$\alpha = 7.5°$ WITHLAND, r=0.187, f=13.10 kHz — Test No - 066

MEAN DRAW SPEED mm/sec	PEAK DIE VELOCITY mm/sec	Mean Loads - kN			Specific Loads - kN/mm^2		
		TAG	BENDING	DIE	DRAW STRESS	SPECIFIC AXIAL	LATERAL DIE
5.2	306	0.16	0.26	2.48	0.02	0.29	0.095
10.4	287	0.32	0.34	2.87	0.04	0.38	0.110
16.6	287	0.36	0.34	2.87	0.05	0.38	0.110
27.7	287	0.50	0.36	2.96	0.06	0.40	0.113
29.7	287	0.62	0.47	3.06	0.08	0.52	0.117
41.6	287	0.70.	0.47	3.06	0.09	0.52	0.117
52.0	287	0.80	0.49	2.87	0.10	0.54	0.110
59.4	267	0.86	0.55	3.06	0.11	0.61	0.117
64.0	267	0.86	0.53	3.06	0.11	0.59	0.117
75.6	248	1.07	0.60	2.87	0.14	0.67	0.110
83.2	267	1.15	0.64	3.34	0.15	0.71	0.128
94.5	267	1.35	0.69	3.25	0.17	0.77	0.125
4.3	267	0.64	0.49	3.06	0.08	0.54	0.117
8.3	267	0.56	0.42	2.96	0.07	0.47	0.113
13.9	267	0.66	0.46	3.25	0.09	0.51	0.125
20.8	277	0.64	0.43	3.25	0.08	0.48	0.125
33.3	248	0.86	0.52	3.25	0.11	0.58	0.125
41.6	248	1.01	0.57	3.15	0.13	0.63	0.121
48.9	248	1.07	0.60	3.25	0.14	0.67	0.125

$\alpha = 7.5°$ WITH LAND, $r = 0.187$, $f = 13.10$kHz — Test No - Oldo CONT.

MEAN DRAW SPEED mm/sec	PEAK DIE VELOCITY mm/sec	Mean Loads - kN			Specific Loads - kN/mm^2		
		TAG	BENDING	DIE	DRAW STRESS	SPECIFIC AXIAL	LATERAL DIE
55.5	220	1.45	0.75	3.25	0.19	0.83	0.125
69.3	210	1.33	0.69	3.44	0.17	0.77	0.132
75.6	191	1.41	0.78	3.44	0.18	0.86	0.132
83.2	172	1.61	0.81	3.53	0.21	0.90	0.135
89.5	153	2.05	0.99	3.53	0.26	1.10	0.135
96.7	153	1.81	0.90	3.53	0.23	0.99	0.135
5.6	287	0.32	0.46	2.96	0.04	0.51	0.113
5.6	287	0.36	0.47	2.87	0.05	0.52	0.110
5.6	267	0.44	0.48	3.15	0.06	0.53	0.120
5.6	248	0.62	0.55	3.15	0.08	0.61	0.120
5.6	210	0.78	0.59	3.34	0.10	0.65	0.128
5.6	181	1.01	0.62	3.34	0.13	0.69	0.128
5.6	95.7	1.57	0.79	3.72	0.20	0.88	0.142
5.6	0	1.97	0.92	3.82	0.25	1.02	0.146
20.8	287	0.38	0.46	3.06	0.05	0.51	0.117
20.8	267	0.78	0.70	3.06	0.10	0.78	0.117
20.8	239	0.92	0.74	3.25	0.12	0.82	0.125
20.8	210	1.05	0.73	3.25	0.13	0.81	0.125
20.8	172	1.21	0.78	3.63	0.16	0.86	0.139
20.8	86.1	1.75	1.03	3.63	0.23	1.14	0.139
20.8	28.7	1.93	1.07	3.82	0.25	1.19	0.146
20.8	0	2.11	1.24	3.82	0.27	1.37	0.146
39.6	287	0.58	0.57	3.06	0.08	0.63	0.117
39.6	287	0.78	0.69	3.15	0.10	0.77	0.121
39.6	248	1.01	0.74	3.34	0.13	0.82	0.128
39.6	239	0.96	0.72	3.34	0.12	0.80	0.128
39.6	210	1.15	0.77	3.44	0.15	0.85	0.132
39.6	162	1.55	0.83	3.44	0.20	0.92	0.132
39.6	114	1.93	0.99	3.63	0.25	1.10	0.139
39.6	47.9	2.21	1.16	3.63	0.29	1.29	0.139
39.6	1.1	2.27	1.18	3.63	0.29	1.31	0.139
39.6	0	2.21	1.12	3.63	0.29	1.24	0.139
64.0	306	0.84	0.55	3.44	0.11	0.61	0.131
64.0	258	1.07	0.69	3.34	0.14	0.77	0.128
64.0	210	1.65	1.07	3.34	0.21	1.19	0.128
64.0	153	2.11	1.37	3.34	0.27	1.52	0.128
64.0	105	1.85	1.20	3.44	0.24	1.33	0.132

$\alpha = 7.5°$ WITH LAND, $r = 0.187$, $f = 13.10$ kHz — Test No - 066 CONT.

MEAN DRAW SPEED mm/sec	PEAK DIE VELOCITY mm/sec	Mean Loads - kN			Specific Loads - kN/mm^2		
		TAG	BENDING	DIE	DRAW STRESS	SPECIFIC AXIAL	LATERAL DIE
64.0	67.0	2.21	1.43	3.63	0.29	1.58	0.139
64.0	19.1	2.71	1.76	3.63	0.35	1.95	0.139
64.0	0	2.71	1.76	3.63	0.35	1.95	0.135
75.6	248	1.17	0.78	3.34	0.15	0.86	0.128
75.6	230	1.25.	0.86	3.44	0.16	0.95	0.132
75.6	191	1.91	1.05	3.82	0.25	1.16	0.146
75.6	143	2.09	1.11	3.82	0.27	1.23	0.146
75.6	105	2.17	1.12	3.72	0.28	1.24	0.143
75.6	67.0	2.37	1.20	3.63	0.31	1.33	0.139
75.6	0	2.65	1.42	3.63	0.34	1.57	0.139
92.4	230	1.49	0.83	3.44	0.19	0.92	0.131
92.4	191	1.77	0.99	3.44	0.23	1.10	0.131
92.4	144	2.01	1.12	3.44	0.26	1.24	0.131
92.4	95.7	2.17	1.21	3.44	0.28	1.34	0.131
92.4	67.0	2.69	1.37	3.63	0.35	1.52	0.139
92.4	19.1	2.61	1.47	3.63	0.34	1.63	0.139
92.4	0	2.51	1.37	3.63	0.32	1.52	0.139

$\alpha = 7.5°$ WITH LAND, $r = 0.539$, $f = 13.33$ kHz — Test No - 067

MEAN DRAW SPEED mm/sec	PEAK DIE VELOCITY mm/sec	Mean Loads - kN			Specific Loads - kN/mm^2		
		TAG	BENDING	DIE	DRAW STRESS	SPECIFIC AXIAL	LATERAL DIE
1.5	331	1.67	0.91	5.54	0.38	0.35	0.141
6.9	331	1.71	0.74	5.54	0.38	0.28	0.141
13.9	312	1.79	0.73	5.54	0.40	0.28	0.141
27.7	292	1.89	0.69	5.54	0.43	0.27	0.141
41.6	253	2.33	0.70	5.06	0.52	0.27	0.129

$\alpha = 7.5°$ WITHLAND, $r = 0.270$, $f = 13.10$ kHz Test No - 069

MEAN DRAW SPEED mm/sec	PEAK DIE VELOCITY mm/sec	Mean Loads - kN			Specific Loads - kN/mm^2		
		TAG	BENDING	DIE	DRAW STRESS	SPECIFIC AXIAL	LATERAL DIE
5.2	383	0.16	0.13	3.34	0.02	0.10	0.114
5.2	364	0.20	0.18	3.53	0.03	0.14	0.121
5.2	354	0.28	0.20	3.44	0.04	0.15	0.118
5.2	325	0.48	0.22	3.44	0.07	0.17	0.118
5.2	249	1.01	0.36	4.01	0.15	0.28	0.137
5.2	134	1.65.	0.59	4.01	0.24	0.45	0.137
5.2	57.4	2.17	0.75	4.20	0.32	0.58	0.144
5.2	0	2.45	0.96	4.20	0.36	0.74	0.144.
17.7	402	0.34	0.17	3.25	0.05	0.13	0.111
17.7	364	0.54	0.26	3.82	0.08	0.20	0.131
17.7	306	0.84	0.31	3.82	0.12	0.24	0.131
17.7	172	1.49	0.55	4.20	0.22	0.42	0.144
17.7	76.6	2.05	0.73	4.20	0.30	0.56	0144
17.7	38.3	2.37	0.86	4.20	0.35	0.66	0.144
17.7	0	2.45	0.91	4.01	0.36	0.70	0.137
29.7	382	0.36	0.13	3.15	0.05	0.22	0.114
29.7	363	0.40	0.14	3.25	0.06	0.27	0.118
29.7	306	0.76	0.25	3.72	0.11	0.36	0.124
29.7	229	1.27	0.43	3.82	0.18	0.47	0.131
29.7	153	1.77	0.57	3.82	0.26	0.64	0.124
29.7	95.7	2.09	0.70	3.92	0.30	0.76	0.124
29.7	47.9	2.17	0.90	3.92	0.32	0.67	0.127
29.7	0	2.21	0.78	4.11	0.32	0.65	0.144
43.8	344	0.74	0.29	3.34	0.11	0.22	0.114
43.8	315	0.94	0.35	3.44	0.14	0.27	0.118
43.8	248	1.23	0.47	3.63	0.18	0.36	0.124
43.8	181	1.77	0.61	3.82	0.26	0.47	0.131
43.8	124	2.29	0.83	3.63	0.33	0.64	0.124
43.8	76.6	2.57	0.99	3.63	0.38	0.76	0.124
43.8	38.3	2.33	0.87	3.72	0.34	0.67	0.127
43.8	0	2.41	0.85	4.20	0.35	0.65	0.144
59.4	363	0.96	0.38	3.63	0.14	0.29	0.124
59.4	306	1.09	0.42	3.82	0.16	0.32	0.131
59.4	230	1.53	0.51	4.01	0.22	0.39	0.137
59.4	172	2.01	0.68	4.01	0.29	0.52	0.137
59.4	114	2.19	0.81	3.63	0.32	0.62	0.137
59.4	57.4	2.49	0.91	3.63	0.36	0.69	0.124

$\alpha = 7.5°$ WITH LAND, $r = 0.270$, $f = 13.10$ kHz — Test No - 069 CONT

MEAN DRAW SPEED mm/sec	PEAK DIE VELOCITY mm/sec	Mean Loads - kN			Specific Loads - kN/mm^2		
		TAG	BENDING	DIE	DRAW STRESS	SPECIFIC AXIAL	LATERAL DIE
59.4	0	2.57	0.92	3.63	0.38	0.71	0.124
---	---	---	---	---	---	---	---
75.6	306	1.37	0.48	3.63	0.20	0.37	0.124
75.6	248	1.53	0.55	3.82	0.22	0.42	0.131
75.6	201	1.79	0.62	3.82	0.26	0.48	0.131
75.6	153	2.19	0.77	3.82	0.32	0.59	0.131
75.6	114	2.39	0.85	3.53	0.35	0.65	0.121
75.6	57.4	2.45	0.91	3.63	0.36	0.70	0.124
75.6	0	2.57	0.98	4.01	0.38	0.75	0.137
---	---	---	---	---	---	---	---
102	239	1.73	0.60	3.72	0.25	0.46	0.127
102	191	2.01	0.73	3.72	0.29	0.56	0.127
102	153	2.33	0.88	3.63	0.34	0.68	0.124
102	95.7	2.53	1.01	3.92	0.37	0.78	0.134
102	0	2.73	1.09	4.20	0.40	0.84	0.144

$\alpha = 7.5°$ WITH LAND, $r = 0.438$, $f = 13.24$ kHz — Test No - 070

MEAN DRAW SPEED mm/sec	PEAK DIE VELOCITY mm/sec	Mean Loads - kN			Specific Loads - kN/mm^2		
		TAG	BENDING	DIE	DRAW STRESS	SPECIFIC AXIAL	LATERAL DIE
0.9	348	0.90	0.27	4.58	0.17	0.13	0.129
0.9	309	1.35	0.39	4.49	0.25	0.18	0.126
0.9	270	1.69	0.47	4.58	0.31	0.22	0.129
0.9	232	1.93	0.53	4.68	0.35	0.25	0.132
0.9	174	2.21	0.64	4.68	0.40	0.30	0.132
0.9	125	2.39	0.75	4.78	0.44	0.36	0.135
0.9	58	2.45	0.86	4.78	0.45	0.41	0.135
0.9	0	2.53	0.90	4.78	0.46	0.43	0.135
---	---	---	---	---	---	---	---
8.3	348	0.84	0.23	4.78	0.15	0.17	0.135
8.3	328	1.09	0.34	4.97	0.20	0.22	0.140
8.3	290	1.37	0.42	4.97	0.25	0.27	0.140
8.3	232	1.65	0.49	4.97	0.30	0.33	0.140
8.3	183	2.01	0.59	5.06	0.37	0.45	0.142
8.3	116	2.45	0.73	5.06	0.45	0.55	0.142
8.3	0	2.79	0.96	4.97	0.51	0.53	0.140
---	---	---	---	---	---	---	---
19.4	324	1.11	0.35	4.97	0.20	0.17	0.140
19.4	270	1.41	0.47	5.06	0.26	0.22	0.142

$\alpha = 7.5°$ WITH LAND, $r = 0.438$, $f = 13.24$ kHz Test No - 070 CONT

MEAN DRAW SPEED mm/sec	PEAK DIE VELOCITY mm/sec	Mean Loads - kN			Specific Loads - kN/mm^2		
		TAG	BENDING	DIE	DRAW STRESS	SPECIFIC AXIAL	LATERAL DIE
19.4	222	1.77	0.57	5.06	0.32	0.27	0.142
19.4	164	2.15	0.70	5.16	0.39	0.33	0.145
19.4	96.7	2.51	0.94	4.97	0.46	0.45	0.140
19.4	38.7	2.85	1.17	4.87	0.52	0.55	0.137
19.4	0	2.81	1.11	4.97	0.52	0.53	0.140
34.7	309	1.29	0.39	5.16	0.24	0.18	0.145
34.7	261	1.63	0.56	5.16	0.30	0.27	0.145
34.7	212	2.01	0.70	5.16	0.37	0.33	0.145
34.7	154	2.31	0.83	5.16	0.42	0.39	0.145
34.7	77.4	2.63	0.99	5.16	0.48	0.47	0.145
34.7	0	3.06	1.42	4.78	0.56	0.67	0.155
52.0	251	1.93	0.59	4.78	0.35	0.28	0.135
52.0	212	2.21	0.62	4.87	0.40	0.29	0.137
52.0	154	2.29	0.78	4.87	0.42	0.37	0.137
52.0	87.0	2.57	0.96	4.97	0.47	0.45	0.140
52.0	0	3.02	1.30	4.20	0.55	0.62	0.118
69.3	222	2.29	0.66	4.97	0.42	0.31	0.140
69.3	174	2.37	0.78	4.87	0.43	0.37	0.137
69.3	116	2.83	1.12	4.58	0.52	0.53	0.129
69.3	58.0	2.91	1.07	4.58	0.53	0.51	0.129
69.3	0	2.93	1.07	4.68	0.54	0.51	0.132
96.7	174	2.67	0.81	4.58	0.38	0.38	0.129
96.7	135	2.73	1.04	4.58	0.49	0.49	0.129
96.7	77.4	2.99	0.95	4.58	0.45	0.45	0.129

$\alpha = 7.5°$ WITH LANDS, $r = 0.547$, $f = 13.35$ kHz — Test No - 071

MEAN DRAW SPEED mm/sec	PEAK DIE VELOCITY mm/sec	Mean Loads - kN			Specific Loads - kN/mm^2		
		TAG	BENDING	DIE	DRAW STRESS	SPECIFIC AXIAL	LATERAL DIE
1.2	312	1.91	0.60	5.73	0.44	0.23	0.145
5.9	331	2.03	0.65	5.73	0.47	0.25	0.145
13.9	312	2.01	0.62	5.73	0.47	0.24	0.145
22.2	302	2.03	0.65	5.63	0.47	0.25	0.142
25.6	292	2.07	0.65	5.54	0.48	0.25	0.140
33.3	282	2.23	0.72	5.44	0.52	0.27	0.137
41.6	273	2.33	0.74	5.35	0.54	0.28	0.135
51.0	253	2.55	0.82	5.16	0.59	0.31	0.130
55.5	234	2.67	0.87	4.97	0.62	033	0.125

$\alpha = 7.5°$ WITH LANDS, $r = 0.453$, $f = 13.15$ kHz — Test No - 072

MEAN DRAW SPEED mm/sec	PEAK DIE VELOCITY mm/sec	Mean Loads - kN			Specific Loads - kN/mm^2		
		TAG	BENDING	DIE	DRAW STRESS	SPECIFIC AXIAL	LATERAL DIE
8.8	307	1.51	0.55	5.25	0.29	0.25	0.132
8.8	278	1.69	0.60	5.35	0.32	0.27	0.135
8.8	249	1.85	0.62	5.35	0.36	0.28	0.135
8.8	201	2.09	0.72	5.35	0.40	0.33	0.135
8.8	172	2.31	0.81	5.35	0.44	0.37	0.135
8.8	115	2.53	0.87	5.35	0.49	0.40	0.135
8.8	67.2	2.77	1.00	5.16	0.53	0.46	0.130
8.8	0	2.87	1.09	5.25	0.55	0.50	0.132
23.1	268	1.67	0.59	5.16	0.32	0.27	0.130
23.1	259	1.79	0.61	5.16	0.34	0.28	0.130
23.1	240	1.85	0.68	5.25	0.36	0.31	0.132
23.1	201	2.03	0.73	5.35	0.39	0.33	0.135
23.1	163	2.25	0.81	5.35	0.43	0.37	0.135
23.1	115	2.47	0.91	5.35	0.47	0.42	0.135
23.1	76.9	2.69	1.05	5.16	0.52	0.48	0.130
23.1	0	2.79	1.81	5.35	0.54	0.83	0.135
36.2	269	1.79	1.16	5.16	0.34	054	0.130
36.2	240	1.89	1.22	5.40	0.36	0.56	0.136
36.2	202	2.09	1.35	5.44	0.40	0.62	0.137
36.2	154	2.33	1.51	5.44	0.45	0.69	0.137
36.2	115	2.51	1.63	5.35	0.48	0.75	0.135
362	0	2.83	1.83	5.16	0.54	0.84	0.130

$\alpha = 7.5°$ WITH LAND, r = 0.453, f = 13.15 kHz — Test No - 072 CONT

MEAN DRAW SPEED mm/sec	PEAK DIE VELOCITY mm/sec	Mean Loads - kN			Specific Loads - kN/mm²		
		TAG	BENDING	DIE	DRAW STRESS	SPECIFIC AXIAL	LATERAL DIE
36.2	269	1.79	1.16	5.16	0.34	0.54	0.130
36.2	240	1.89	1.22	5.40	0.36	0.56	0.136
36.2	202	2.09	1.35	5.44	0.40	0.62	0.137
36.2	154	2.33	1.51	5.44	0.45	0.69	0.137
36.2	115	2.51	1.63	5.35	0.48	0.75	0.135
36.2	0	2.83	1.83	5.16	0.54	0.84	0.130
52.0	240	1.97	1.27	5.25	0.38	0.58	0.132
52.0	202	2.01	1.30	5.25	0.39	0.60	0.132
52.0	173	2.33	1.51	5.25	0.45	0.69	0.132
52.0	135	2.49	1.61	5.16	0.48	0.74	0.130
52.0	67.2	2.79	1.81	4.97	0.54	0.83	0.125
52.0	0	2.89	1.87	4.97	0.56	0.86	0.125
69.3	211	2.25	0.82	5.16	0.43	0.38	0.130
69.3	230	2.27	0.70	5.16	0.44	0.32	0.130
69.3	211	2.23	0.81	5.06	0.43	0.37	0.128
69.3	182	2.31	0.86	5.16	0.44	0.39	0.130
69.3	134	2.51	0.94	5.06	0.48	0.43	0.128
69.3	105	2.71	1.03	4.87	052	0.47	0.122
69.3	57.6	2.81	1.11	4.78	0.54	0.51	0.121
69.3	0	2.91	1.12	4.87	0.56	0.51	0.123

$\alpha = 7.5°$ WITH LAND, r = 0.373, f = 13.12 kHz — Test No - 073

MEAN DRAW SPEED mm/sec	PEAK DIE VELOCITY mm/sec	Mean Loads - kN			Specific Loads - kN/mm²		
		TAG	BENDING	DIE	DRAW STRESS	SPECIFIC AXIAL	LATERAL DIE
10.2	384	0.66	0.30	4.49	0.11	0.17	0.136
10.2	345	0.86	0.38	4.58	0.14	0.21	0.138
10.2	306	1.15	0.70	4.87	0.19	0.39	0.147
10.2	230	1.55	0.62	5.16	0.26	0.34	0.151
10.2	124	2.09	0.83	5.16	0.35	0.46	0.156
10.2	0	2.53	1.01	5.16	042	0.56	0.156
27.7	345	0.90	0.40	4.49	0.15	0.22	0.135
27.7	306	1.11	0.51	4.78	0.19	0.28	0.144
27.7	264	1.35	0.56	4.78	0.23	0.31	0.144
27.7	210	1.59	0.66	4.97	0.27	0.37	0.150
27.7	153	1.91	0.77	5.06	0.32	0.43	0.153

$\alpha = {}^{7.5°}_{\text{WITH CANS}}$, r=0.373, f=13.12 kHz Test No - 073 CONT

MEAN DRAW SPEED mm/sec	PEAK DIE VELOCITY mm/sec	Mean Loads - kN			Specific Loads - kN/mm^2		
		TAG	BENDING	DIE	DRAW STRESS	SPECIFIC AXIAL	LATERAL DIE
27.7	76.7	2.17	0.90	4.97	0.36	0.50	0.150
27.7	0	2.35	1.50	4.97	0.39	0.56	0.150
43.6	316	1.15	0.49	4.58	0.19	0.27	0.138
43.6	277	1.39	0.59	4.78	0.23	0.33	0.144
43.6	220	1.65	0.69	4.97	0.28	0.38	0.150
43.6	162	1.93	0.78	4.97	0.32	0.43	0.150
43.6	95.8	2.21	0.94	4.97	0.37	0.52	0.150
43.6	0	2.41	0.99	5.06	0.40	0.55	0.153
55.5	297	1.37	0.60	4.78	0.23	0.33	0.144
55.5	258	1.59	0.66	4.97	0.27	0.37	0.150
55.5	210	1.85	0.79	4.97	0.31	0.44	0.150
55.5	162	2.01	0.85	4.97	0.34	0.47	0.150
55.5	95.8	2.33	0.95	4.97	0.39	0.53	0.150
55.5	0	2.49	1.03	4.97	0.42	0.57	0.150
73.6	287	1.45	0.94	4.87	0.24	0.52	0.147
73.6	230	1.75	1.13	4.87	0.29	0.63	0.147
73.6	172	2.01	1.30	4.97	0.34	0.72	0.150
73.6	134	2.25	1.46	4.97	0.38	0.81	0.150
73.6	76.7	2.53	1.64	4.97	0.42	0.91	0.150
73.6	0	2.57	1.66	5.16	0.43	0.92	0.156
96.7	230	1.89	1.22	4.78	0.32	0.68	0.144
96.7	182	2.43	1.57	4.58	0.41	0.87	0.138
96.7	134	2.55	1.65	4.57	0.43	0.92	0.138
96.7	76.7	2.63	1.70	4.78	0.44	0.94	0.144
96.7	0	2.77	1.24	4.87	0.46	0.69	0.147

$\alpha = {}^{7.50}_{\text{UNCLAD}}$, r=0.680, f=13.31 kHz Test No - 074

MEAN DRAW SPEED mm/sec	PEAK DIE VELOCITY mm/sec	Mean Loads - kN			Specific Loads - kN/mm^2		
		TAG	BENDING	DIE	DRAW STRESS	SPECIFIC AXIAL	LATERAL DIE
3·3	437	1·75	0·60	5·92	0·46	0·20	0·142
10·4	389	1·87	0·65	5·63	0·49	0·22	0·135
15·1	379	1·97	0·65	5·54	0·52	0·22	0·133
20·8	350	2·19	0·68	5·35	0·58	0·23	0·128
23·8	331	2·37	0·70	5 16	0·62	0 24	0·124

Appendix A3.2

Results of the Regression Tests

$\alpha = 2.5°$

Test Number	Reduction Of Area, r.	Mean Draw Speed, mm/sec	STRIP TENSION		BENDING LOAD		Correlation Coefficient r_c	$\frac{S_t}{S_b}$
			A-KN/mm^2	B-KN/mm^2 x10^{-3}	A-KN/mm^2	B-KN x10^{-3}		
028	0.267	1.41	0.407	-0.720	0.90	1.55	0.996	1.28
"	"	16.0	0.424	-0.684	1.18	1.70	0.986	1.10
029	0.280	37.0	0.539	-0.818	1.25	1.70	0.975	1.22
030	0.280	ARBITRARY	0.435	-0.690	—	—	0.942	—
031	0.280	"	0.529	-0.384	—	—	0.415	—
032	0.453	"	0.762	-0.793	—	—	0.262	—
033	0.480	"	0.378	-1.29	—	—	0.241	—
034	0.473	"	0.702	-1.34	—	—	0.940	—
035	0.270	"	0.657	-1.36	—	—	0.964	—
036	0.220	"	0.788	-1.29	—	—	0.919	—
037	0.333	"	0.902	-1.20	—	—	0.789	—
038	0.440	"	0.793	-1.38	—	—	0.944	—
039	0.133	2.6	0.195	-0.53	1.33	2.13	0.995	1.62
"	"	11.88	0.252	-0.65	1.65	2.73	0.993	1.55
"	"	24.19	0.281	-0.73	1.73	2.73	0.991	1.74
"	"	48.94	0.277	-0.65	1.88	2.87	0.993	1.48
"	"	59.42	0.303	-0.71	1.83	2.67	0.990	1.73
"	"	83.19	0.304	-0.63	1.88	2.40	0.984	1.71
040	0.250	0.92	0.336	-0.63	NON-LINEAR		0.992	—
"	"	5.94	0.306	-0.60	0.90	1.23	0.993	1.46
"	"	18.78	0.314	-0.60	1.05	1.52	0.971	1.18
"	"	34.66	0.325	-0.66	1.10	1.50	0.954	1.32
"	"	51.99	0.360	-0.75	1.30	2.03	0.913	1.11
"	"	69.33	0.367	-0.66	1.20	1.30	0.951	1.52
"	"	92.43	0.399	-0.57	1.28	1.32	0.978	1.30
"	"	118.8	0.411	-0.83	1.30	1.32	0.961	1.89
—								—

$\alpha = 5.0°$

Test Number	Reduction Of Area, r.	Mean Draw Speed, mm/sec	STRIP TENSION		BENDING LOAD		Correlation Coefficient r_c	$\frac{S_t}{S_b}$
			A-KN/mm^2	B-KN/mm^2 $\times 10^{-3}$	A-KN/mm^2	B-KN$\times 10^{-3}$		
054	0.442	3.08	0.695*	1.10*	0.95*	1.73*	0.998	0.80
055	0.205	11.09	0.445*	1.11*	1.30*	4.14*	0.46	1.03
"	"	2.5	0.265*	0.78*	0.88*	2.26*	0.985	1.34
055A	0.481	ARBITRARY	—	—	—	—	0.984	—
056	0.481	"	—	—	—	—	0.933	—
057	0.529	"	—	—	—	—	0.750	—
058	0.592	"	—	—	—	—	0.933	—
059	0.352	"	—	—	—	—	0.935	—
060	0.364	9.24	0.571	1.04	0.85	1.50	0.992	1.21
"	"	18.49	0.533	1.12	0.78	1.50	0.981	1.30
061	0.413	28.69	0.690*	1.44	0.78	1.55	0.995	1.32
062	"	41.60	0.690*	1.44	0.45	0.65	0.968	3.14
063	0.342	25.20	0.425*	0.99*	1.20	1.74*	0.897	1.09
064	0.365	11.55	0.476	1.27	0.80*	1.50*	0.994	1.47
065	0.345	43.78	0.519	1.13*	0.93*	2.01*	0.966	1.07
"	"	59.42	0.587	1.42*	0.95*	2.13*	0.984	1.27

$\alpha = 7.5°$

Test Number	Reduction Of Area, r.	Mean Draw Speed, mm/sec	STRIP TENSION A-KN/mm²	STRIP TENSION B-KN/mm² $\times 10^{-3}$	BENDING LOAD A-KN/mm²	BENDING LOAD B-KN $\times 10^{-3}$	Correlation Coefficient r_c	$\frac{S_t}{S_b}$
001	0.246	ARBITRARY	—	—	—	—	—	—
002	0.287	"	—	—	—	—	—	—
003	0.246	"	—	—	—	—	—	—
004	0.173	"	—	—	—	—	—	—
005	0.438	"	—	—	—	—	—	—
010	0.480	"	—	—	—	—	0.782	—
011	0.533	"	—	—	—	—	0.968	—
013	0.616	"	—	—	—	—	0.950	—
014	0.351	"	—	—	—	—	0.971	—
016	0.297	"	TWO POINT DATA SET		—	—	—	—
018	0.696	"	—	—	—	—	0.957	—
019	0.653	"	—	—	—	—	0.992	—
023	0.440	27.2	0.60	1.52	0.90	2.19	0.988	0.88
"	"	72.0	0.63	1.42	0.90	1.97	0.981	0.91
024	0.387	110.0	0.49	1.16	1.03	1.93	0.981	0.95
"	"	58.9	0.53	1.39	1.03	2.20	0.998	1.00
"	"	22.4	0.52	1.44	1.03	2.20	0.995	1.04
"	"	171	0.54	0.86	1.10	1.54	0.939	0.88
025	0.307	16.0	0.40	1.15	0.83*	3.58*	0.992	0.74
"	"	25.6	0.43	1.20	0.93*	3.13*	0.990	0.87
"	"	43.0	0.41	1.12	0.93*	3.13*	0.993	0.81
"	"	63.0	0.40	0.85	0.95*	3.21*	0.928	0.60
"	"	78.0	0.45	1.03	0.95*	3.21*	0.928	0.72
"	"	100.2	0.40	0.06	TWO POINT DATA SET		0.267	—
026	0.362	1.28	0.62	2.08	0.70*	2.56*	0.961	1.43
"	"	1.63	0.43	1.10	0.70*	2.56*	0.977	0.76
"	"	5.94	0.44	1.27	0.70*	2.56*	0.992	0.87
"	"	13.9	0.45	1.23	0.75*	2.56*	0.961	0.85
"	"	32.0	0.36	0.03	0.70*	2.56*	0.043	—
"	"	56.9	0.52	1.25	0.85*	2.56*	0.995	0.86
027	0.164	1.33	0.23	0.83	1.15*	5.52	0.996	0.77
"	"	23.11	0.28	0.87	1.75	6.14	0.999	0.72
"	"	51.04	0.30	0.74	1.41.	6.80	0.963	0.56
"	"	92.43	0.32	0.64	NON-LINEAR		0.975	—
"	"	75.63	0.33	0.78	— "	—	0.933	—
"	"	77.75	0.31	0.65	— "	—	0.925	—

$\alpha = 7.5°$ CONTINUED

Test Number	Reduction Of Area, r.	Mean Draw Speed, mm/sec	STRIP TENSION		BENDING LOAD		Correlation Coefficient r_c	$\frac{S_t}{S_b}$
			A-KN/mm^2	B-KN/mm^2 $\times 10^{-3}$	A-KN/mm^2	B-KN.$\times 10^{-3}$		
041	0.267	1.43	0.352	1.17	0.78*	1.98*	0.993	1.62
"	"	6.4	0.325	1.01	0.78*	1.98*	0.996	1.40
"	"	16.6	0.337	0.92	0.78*	1.98*	0.988	1.28
"	"	32.0	0.32	0.75	0.78*	1.98*	0.995	1.04
"	"	52.0	0.26	0.53	0.79*	1.60*	0.061	0.91
"	"	69.3	0.32	0.64	0.79*	1.60*	0.969	1.10
"	"	104.0	0.30	0.35	0.82*	1.60*	0.915	0.96

$\alpha = 7.5°$ WITH LAND

Test Number	Reduction Of Area, r.	Mean Draw Speed, mm/sec	STRIP TENSION		BENDING LOAD		Correlation Coefficient r_c	$\frac{S_t}{S_b}$
			A-KN/mm^2	B-KN/mm^2 $\times 10^{-3}$	A-KN/mm^2	B-KN $\times 10^{-3}$		
066	0.187	ARBITRARY	0.80	2.52	—	—	0.831	—
"	"	"	0.45	1.34	—	—	0.965	—
"	"	5.5	0.26	0.74	1.00	1.69	0.996	1.89
"	"	20.08	0.28	0.70	1.33	2.08	0.986	1.47
"	"	39.6	0.31	0.76	1.33	2.08	0.985	1.58
"	"	63.9	0.35	0.77	2.55	4.44	0.971	0.76
"	"	75.6	0.36	0.76	1.58*	3.45*	0.947	0.96
"	"	92.4	0.35	0.64	1.58*	3.45*	0.926	0.80
067	0.539	ARBITRARY			—	—	0.986	—
069	0.270	5.20	0.37	0.91	0.63	1.47	0.999	1.67
"	"	17.7	0.37	0.79	0.70	1.40	0.998	1.52
"	"	29.7	0.35	0.78	0.63	1.47	0.987	1.43
"	"	43.8	0.39	0.78	0.75	1.46	0.958	1.44
"	"	59.4	0.39	0.72	0.76	1.33	0.990	1.46
"	"	75.6	0.40	0.65	0.76	1.33	0.970	1.32
"	"	102.7	0.42	0.63	1.13*	2.70	0.960	0.63
070	0.438	0.89	0.51	0.80	0.43	0.80	0.938	1.28
"	"	8.33	0.54	1.04	0.50	1.29	0.985	1.03
"	"	19.4	0.55	1.03	0.52	1.34	0.993	0.99
"	"	34.7	0.57	1.01	0.52	1.34	0.995	0.97
"	"	52.0	0.54	0.75	0.52	1.34	0.990	0.72
"	"	69.3	0.56	0.61	0.52	1.34	0.925	0.52
"	"	96.7	0.60	0.64	0.52	1.34	0.968	0.61
071	0.547	ARBITRARY			—	—	0.943	—
072	0.453	8.76	0.58	0.89	0.50	0.80	0.987	1.34
"	"	23.1	0.56	0.85	0.50	0.80	0.987	1.28
"	"	36.2	0.55	0.77	0.87	1.27	0.987	0.73
"	"	52.0	0.58	0.82	0.87	1.27	0.973	0.78
"	"	69.3	0.57	0.63	0.55	0.96	0.975	0.79
073	0.373	10.2	0.44	0.83	0.55*	1.13	0.993	1.23
"	"	27.2	0.41	0.70	0.55*	1.13	0.988	1.04
"	"	43.4	0.42	0.67	0.55*	1.25	0.984	0.90
"	"	55.5	0.44	0.64	0.55*	0.88	0.983	1.22
"	"	73.6	0.46	0.70	0.93*	1.80	0.972	0.65
"	"	96.7	0.48	0.53	NON-LINEAR		0.866	—
074	0.600	ARBITRARY	—	—	—	—	0.943	—

$\alpha = 10°$

Test Number	Reduction Of Area, r.	Mean Draw Speed, mm/sec	STRIP TENSION		BENDING LOAD		Correlation Coefficient r_c	$\frac{S_t}{S_b}$
			A-KN/mm^2	B-KN/mm^2 $\times 10^{-3}$	A-KN/mm^2	B-KN $\times 10^{-3}$		
042	0.263	6.4	0.33*	1.31*	0.78*	4.13*	0990	0.88
"	"	16.64	0.33*	1.28*	0.78*	4.13	0.982	0.87
043	0.399	20.80	0.44	1.45*	0.70*	2.11	0.987	1.04
"	"	33.28	"	1.37*	"	2.11	0982	0.98
"	"	55.46	"	1.12*	"	1.50	0.974	1.24
"	"	67.63	"	1.21*	"	2.43	0.973	0.75
"	"	96.33	"	0.65*	"	2.43	0.931	0.40
"	"	1.81	"	2.57*	"	2.49	0.989	1.55
"	"	10.40	"	1.74*	"	2.22	0.992	1.18
044	0.461	11.88	0.54*	1.45*	0.58	1.12	0.996	1.51
"	"	23.37	"	1.52*	0.61	"	0.994	1.59
"	"	37.81	"	1.48*	0.61	"	0.986	1.54
045	0.418	ARBITRARY	—	—	—	—	0996	—
046	0.421	"	—	—	—	—	0.993	—
047	0.526	"	—	—	—	—	—	—
048	0.580	"	—	—	—	—	—	—
049	0.623	"	—	—	—	—	—	—
053	0.260	11.9	0.32*	1.26*	0.94*	3.28*	0.968	1.09
051 + 052	0.799	ARBITRARY		TWO POINT DATA SETS.			—	—
050	0.682	"	—	—	—	—	—	—

APPENDIX 4) EQUILIBRIUM ANALYSIS FORDRAWING THROUGH VIBRATING DIES

Dawson[70], in his analysis of wire drawing with radially vibrating dies used the following relationship:

Volume flow rate into die = volume flow rate our of die - rate of decrease of deformation zone

that is,

Flow rate into the die - Flow rate out of die = Rate of change of deformation zone volume.

Dawson analysed the wire drawing process in a similar manner to the following plane strain (strip-drawing) analysis.

Referring to Figure (A4.1):

$$= \frac{(h_s + dh + h_s)}{2} b\,dx + \xi\, b dx$$

$$= \frac{2\,h_s\, b\, dx}{2} + \xi b\, dx$$

where $\xi = \xi_m \sin \omega t$

$$\therefore \quad \frac{d\,Vol}{dt} = \frac{d\ \xi m \sin \omega t\ b\ dx}{dt}$$

$$= \omega \xi m \cos \omega t\ b\ dx$$

$$= \dot{\xi}\ dx\ b$$

and $dx = \cot \alpha dh$

From the flow rate equation

$$(V + dv)\ (h + dh)\ b - V\ hb = \dot{\xi} dx\ b$$

$$\therefore \quad V\ dh + h\ dv = \dot{\xi}\ \cot \alpha\ dh$$

$$\therefore \quad -\frac{dh}{h} = \frac{dv}{V - \xi \cot \alpha}$$

Applying limits and noting that $V_n = 0$

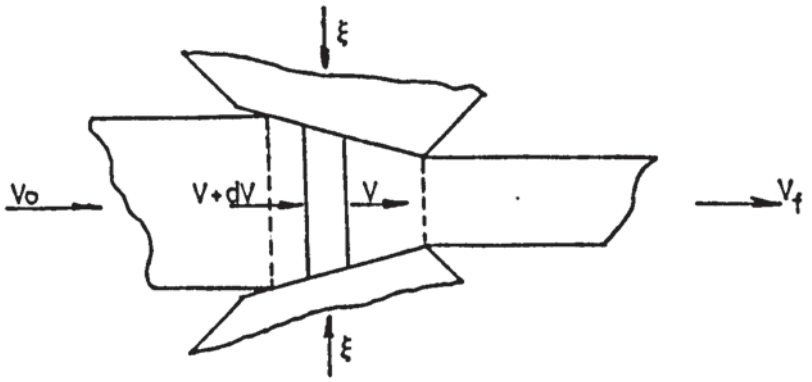

Fig(A4·1) - Instantaneous Velocity Conditions During Deformation

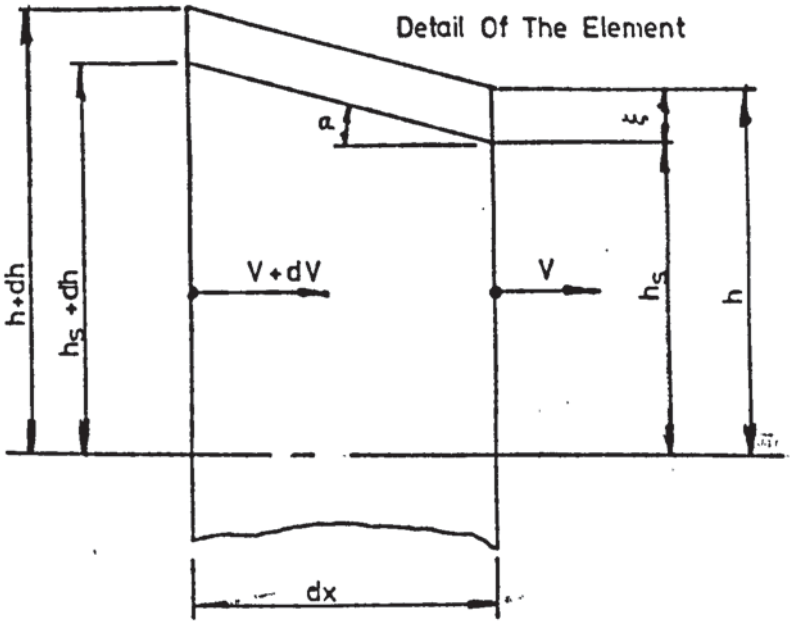

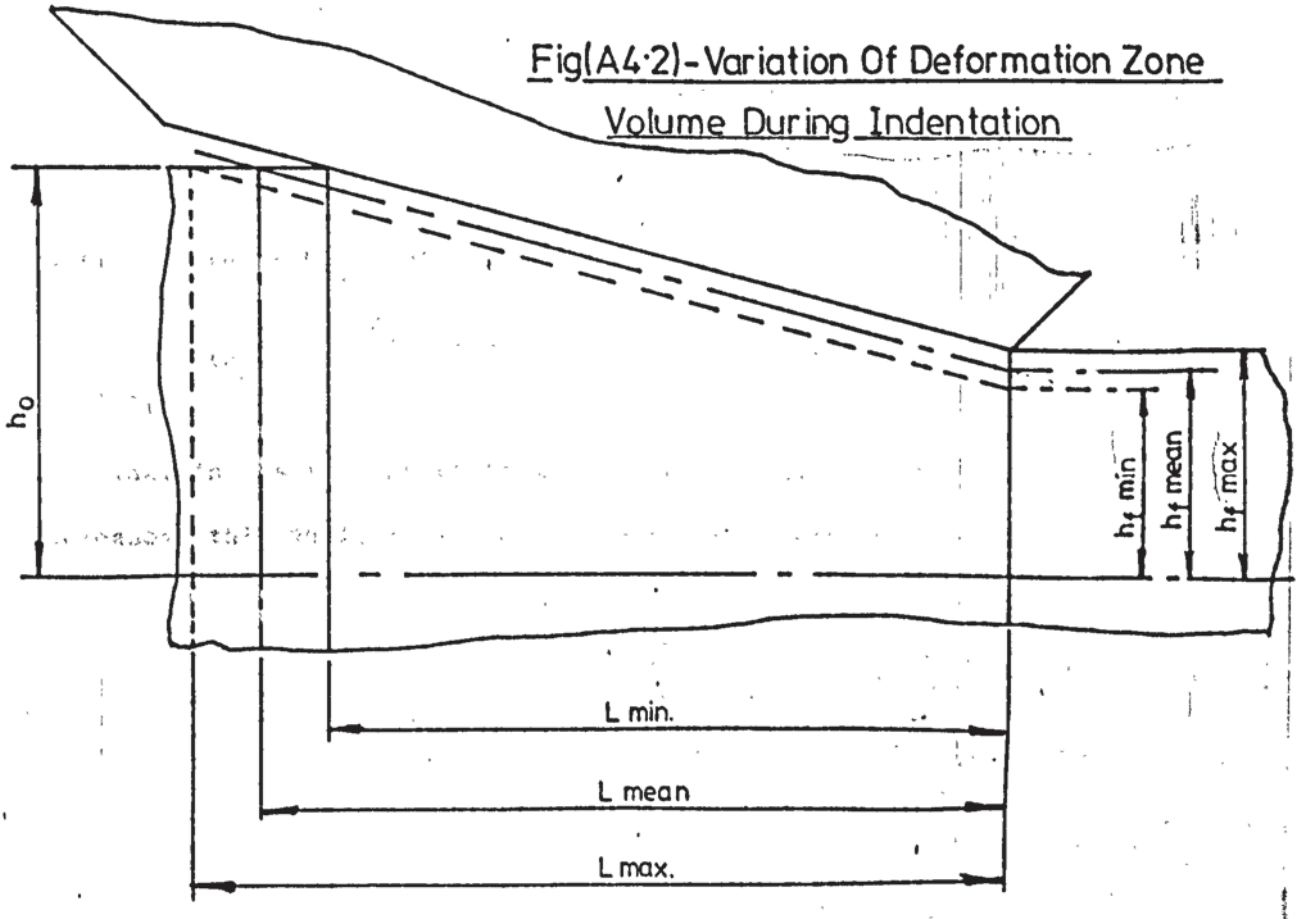

Fig(A4·2) - Variation Of Deformation Zone Volume During Indentation

$$\left[- \ln h \right]_{h_n}^{h_o} = \left[\ln (V - \dot{\xi} \cot\alpha) \right]_{V_n}^{V_o}$$

$$\therefore \quad \frac{h_n}{h_o} = \frac{\dot{\xi}\cot\alpha - V_o}{\dot{\xi} \cot\alpha}$$

Similarly:

$$\frac{h_n}{h_o} = \frac{\dot{\xi}\cot\alpha - V_f}{\dot{\xi} \cot\alpha}$$

The velocity, V_f, in this case, is due to both the indentation and the drawing velocity fields. It is also implied that the deformation zone volume decreases and the indentation phase proceeds, which is not the case.

Referring to Figure (A4.2), with instantaneous values denoted by suffix, i:

Volume of deformation zone:

$$= \frac{(h_o + hf_i)\ L_i\ b}{2}$$

where $L_i = (h_o - hf_i) \cot\alpha$

$$\therefore \quad \dot{Vol}_i = \frac{(h_o^2 - hf_i^2) \cot \alpha b}{2}$$

That is, as the indentation proceeds the deformation zone volume increases: this analysis was not carried any further.